The Definitive All-Sky Observational Study Of Accretion Disc Physics In Galactic Black Hole X-ray Binaries

by

Bailey Elizabeth Tetarenko

A thesis submitted in partial fulfillment of the requirements for the degree of

Master of Science

Department of Physics
University of Alberta

Abstract

Stellar mass black holes (BHs) accreting in binary systems provide valuable insight into how binary systems evolve and how mass is transferred via accretion. Although in recent years a canonical picture of the outburst evolution in black hole X-ray binaries (BHXRBs) has emerged (Fender and Gallo, 2014), these systems actually exhibit a wide range of unorthodox behaviour as well. Using today's more sensitive all-sky X-ray instruments, which have made an in-depth exploration of the X-ray Universe possible, we have the ability to classify the range of behaviours exhibited by these accreting BHs.

Taking advantage of these resources, we have established a comprehensive database of BH (and BH candidate) XRB activity over the last 18 years as revealed by the Swift Burst Alert Telescope (BAT), Monitor of All-Sky X-ray Image (MAXI) telescope, Rossi X-ray Timing Explorer (RXTE), and the INTErnational Gamma-ray Astrophysics Laboratory (INTEGRAL). As a result we have detected 90 outbursts occurring in 43 transient BHXRBs, tracked the long-term behaviour of 9 persistent BHXRBs, and estimate that the current suite of instruments in space can detect $\sim$ 6–12 transient outbursts every year, more than a factor of two larger than with RXTE alone.

Perhaps our most noteworthy result comes in the discovery that, despite the

prevailing opinion, the outbursts undergone by BHXRBs that do not complete the canonical pattern (i.e., those that fail to transition to the soft accretion states) make up $\sim 50\%$ of all outbursts occurring in transient BHXRBs in the past 18 years. Interestingly enough, we find that these "failed" outbursts are not just limited to the transient systems but are also exhibited by a fair number of persistently accreting systems in the form of long continuous periods spent in the hard state. This "failed" behaviour being neither a rare nor recent phenomena, challenges the standard paradigm (Fender et al., 2004, 2009; Fender and Gallo, 2014) for accretion behaviour in both transient and persistent BHXRBs.

The questions that remain are, "what ramifications do the larger number of these "failed" outbursts have on the mass-transfer history of the Galactic BHXRB population" and "what observational parameters best probe the degree to which this behaviour impacts the population as a whole". In this thesis we present the detailed findings of our database making use of X-ray hardness, luminosity, disc fraction, and mass-transfer rate to probe canonical and anomalous outburst behaviour exhibited by BHXRBs, its impact on the physical observables of individual systems alone, and the universal properties of the population as a whole. We show that enumerating the frequency at which outbursts occur and quantitatively classifying the wide range of behaviour exhibited during outburst is critical to furthering our understanding of the physical mechanisms driving mass-accretion in BHXRBs and a key step toward filling in the many gaps in our knowledge of how BHXRBs form, accrete, and evolve.

Preface

This thesis is original work by Bailey Tetarenko. Note that the data analyzed in this thesis is publicly available online.

"Learn from yesterday, live for today, hope for tomorrow. The important thing is to not stop questioning."

Albert Einstein

Acknowledgements

First and foremost to my supervisor, Greg, for introducing me to the field of X-ray astronomy, having the immeasurable patience to put up with my incessant question asking and near constant presence in his office, and most importantly for helping me climb the numerous brick walls we ran into along the way.

Secondly, to a similar effect, I also owe a debt of gratitude to Craig, for making sure our statistics were sound and sharing his seemingly infinite knowledge of the BH literature, and Erik, for introducing me to the wonderful world of MCMC.

Thirdly, to my family who has offered a near continuous flow of support and understanding over the years. Specifically, to my Mom (i.e. the corrector of my non-existent grammatical skills and inability to use commas correctly) who is and will always remain my first proofreader, to my Dad, whose never-ending inquiries into the world of astronomy have served to make me more comfortable talking to those who are actually in the field, and to my sister, may our constant bickering always lead to solved problems and fruitful results.

Lastly, to Ben and Sophie, the only two who have the ability to get me to stop exclusively living in my own head, for reminding me (on a daily basis) that I am a human being who, in addition to having a constant need to work, requires food, sleep and occasional sunlight.

Contents

List of Tables

List of Figures

List of Abbreviations

ADAF	Advection Dominated Accretion Flow
ADIOS	Advection Dominated Inflow/Outflow Solution
AGN	Active Galactic Nuclei
ASM	All-Sky Monitor
ATel	Astronomer's Telegram
BeXB	Be/X-ray Binary
BH	Black Hole
BHC	Black Hole Candidate
BHXRB	Black Hole X-ray Binary
CDAF	Convection Dominated Accretion Flow
DIM	Disc Instability Model
FRED	Fast Rise Exponential Decay
GR	General Relativity
HCS	Hard Comptonized State
HID	Hard Intensity Diagram
HIMS	Hard Intermediate State
HMXB	High Mass X-ray Binary
HMXBCAT	High Mass X-ray Binary Catalog
HSS	High Soft State
IMS	Intermediate State
IR	Infrared
ISAF	Ion Supported Accretion Flow
ISCO	Innermost Stable Circular Orbit
ISS	International Space Station
ISM	Interstellar Medium
JDAF	Jet Dominated Accretion Flow
K	Kelvin
keV	kilo-electron volt
kpc	kilo-parsec

ksec	kilo-second
LHAF	Luminous Hot Accretion Flow
LHS	Low Hard State
LMXB	Low Mass X-ray Binary
LMXBCAT	Low Mass X-ray Binary Catalog
MCMC	Markov Chain Monte-Carlo
MHD	Magnetohydrodynamic
MDAF	Magnetically Dominated Accretion Flow
MRI	Magneto-Rotational Instability
NS	Neutron Star
NSL	Non-Stellar Luminosity
PDF	Probability Density Function
QPO	Quasi-Periodic Oscillations
RLO	Roche Lobe Overflow
SDS	Soft Disc-Dominated State
SFXT	Supergiant Fast X-ray Transient
SGXB	Supergiant X-ray Binary
SIMS	Soft Intermediate State
SPL	Steep Power Law State
SXT	Soft X-ray Transient
UV	Ultraviolet
VFXT	Very Faint X-ray Transient
VHS	Very High State
XLF	X-ray Luminosity Function
XRB	X-ray Binary
XRN	X-ray Novae

Chapter 1

Accretion Flows in Astrophysical Systems

1.1 Introduction to Black Hole X-Ray Binaries

Since their discovery almost 50 years ago, stellar mass black holes (BHs) existing in accreting binary systems have provided both unique insights into the astrophysics occurring during the end stages of stellar evolution (Psaltis, 2006) and ample opportunity to resolve important outstanding questions in high energy astrophysics and relativity, such as the physics of accretion.

In the late 1960's, X-ray detectors discovered an unforeseen population of luminous Galactic X-ray sources. The large energies and short timescale of variability in these systems, termed X-Ray Binaries (XRBs), suggested that they were composed of an interacting binary system where X-rays are produced by material accreting from a companion star onto a compact object (Casares, 2006).

Through the launch of X-Ray satellites, such as the Rossi X-ray Timing Explorer (RXTE), BeppoSAX, XMM-Newton, CHANDRA X-Ray Observatory, INTErnational Gamma-Ray Astrophysics Laboratory (INTEGRAL), Swift X-ray Observatory and Monitor of All-Sky Image (MAXI) Telescope, access to large amounts of X-Ray observations have placed observational constraints on accretion flows in strong gravity and have allowed for further theoretical understanding of these sys-

tems (Psaltis, 2006). As a consequence of the development of a variety of different models of the changing nature and geometry of accretion flows created over the last few decades in an effort to understand the wide variety and variability of emission observed from these systems, we now have an emerging picture explaining much of the behaviour seen from BHXRBs (Done et al., 2007).

However, despite the advances made in the field, much of the physics causing the temporal evolution observed in BHXRBs remains unexplained. Being able to enumerate the frequency of outbursts occurring and quantitatively classify the wide range of behaviours exhibited during outburst by these types of systems is critical to furthering our understanding of the physical mechanisms driving mass accretion in BHXRBs. In addition, such work would be a key step toward filling in the myriad of gaps in our knowledge of how they form, accrete and evolve.

Furthermore, understanding BH accretion has wide physical and astronomical applications (Done et al., 2007). Accretion is not simply limited to binary systems, but is also a central process among astronomical objects ranging from protoplanetary discs around young stellar objects to supermassive black holes at the centres of galaxies (McClintock and Remillard, 2006). Moreover, as these binary systems act as Galactic analogs to supermassive black holes, which appear to play a pivotal role in galaxy formation (Frolov and Zelnikov, 2011), their study has broad impact.

1.1.1 Binary Composition and Mass-Transfer

BHXRBs are composed of an interacting binary system involving a BH primary, paired with a non-degenerate secondary companion star (Remillard and McClintock, 2006). Due to angular momentum, this material does not flow directly onto the compact object, rather it forms a differentially rotating disc around the BH known as an accretion disc (Casares, 2006). A portion of this inward falling material may also be transferred outward in the form of a relativistic plasma jet (Remillard and McClintock, 2006) or an accretion disc wind (Lee et al., 2002; Miller et al., 2004, 2006d,c; Diaz Trigo et al., 2011).

Historically, these systems have been divided into two classes, the Low Mass X-ray Binaries (LMXBs) and the High Mass X-ray Binaries (HMXBs), where the

nomenclature refers to the mass of the companion star (Psaltis, 2006). The particular class of the system is what typically governs the mass-transfer process and the overall environment in the vicinity of the compact object (White et al., 1995).

In LMXB systems, mass transfer will occur when the companion, with a mass $M_2 \ll M_{\rm BH}$ and spectral type A or later (White et al., 1995), fills its critical gravitational potential lobe, the Roche lobe. In this case, the material is transferred onto the accretion disc around the compact object through the inner Lagrangian point L_1, in turn powering the source of X-ray emission (see Figure 1.1). This process is known as Roche Lobe Overflow (RLO) (Psaltis, 2006).

These types of systems are often transient, cycling between periods of quiescence and outburst. The very nature of this pattern is dependent upon the mass accretion rate onto the BH (Tanaka and Lewin, 1995). Quiescence is characterized by long periods of time during which a BHXRB is exceptionally faint, usually on the order of $10^{30} - 10^{33}\,{\rm erg\,s^{-1}}$, and very little material is transferred from the accretion disc onto the compact object. This period of inactivity can last anywhere from a few months to decades.

The transition to outburst occurs as a consequence of instabilities, both thermal and viscous in nature, developing in the accretion disc (see Section 1.4 for a detailed discussion) causing increased mass transfer onto the BH, and leading to bright X-ray emission (McClintock and Remillard, 2006). The fact that we can observe this transient behaviour on short timescales (days to weeks) makes XRB systems ideal proxies of accretion physics. As transients spend most of their time in quiescence at low luminosities their long-term mass transfer rates are usually very low, on the order of $\sim 10^{-10} M_\odot\,{\rm yr^{-1}}$ (King, 1995).

HMXB systems harbour a massive companion of spectral type O or B with a mass $M_2 \geq M_{\rm BH}$ which (typically) under-fills its Roche lobe. They can be split into two subcategories; supergiant companions, those which have evolved away from the main sequence, and Be star companions, which are non-supergiant, fast rotating B-type stars characterized by spectral emission lines (hence the "e" in the spectral type). These emission lines originate from a circumstellar disc that is fed by material expelled from the star (King, 1995; Reig, 2011). For a recent review on the

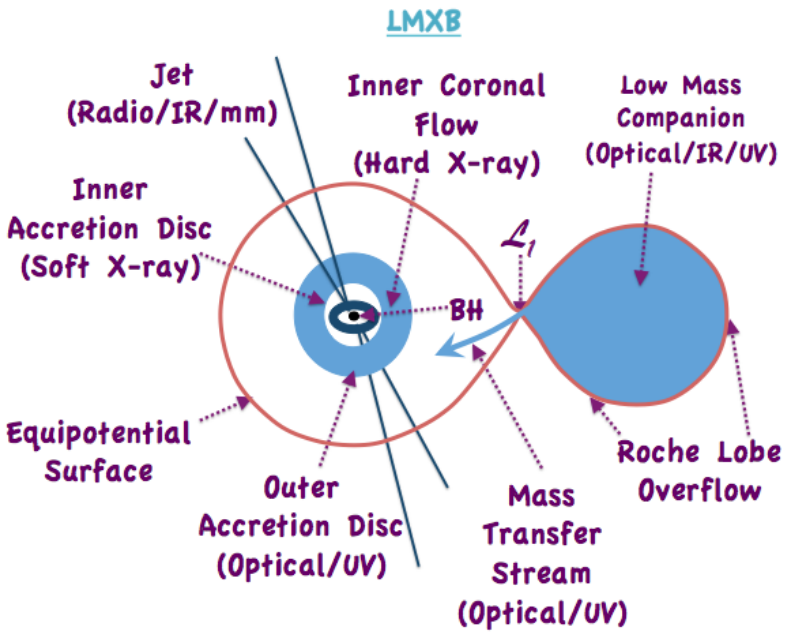

Figure 1.1: Schematic diagram of the mass-transfer mechanism (i.e., RLO), system components and emission regions in LMXBs. Figure adapted from Tauris and van den Heuval (2006).

observational characteristics of Be/X-ray binaries (BeXBs) see Reig (2011).

In the Supergiant X-ray Binaries (SGXBs) the compact object captures mass from the stellar wind of the companion star (Psaltis, 2006). This process is far less efficient than RLO as the mass can leave the companion star in all directions, not just in the direction of the BH, and has enough kinetic energy to escape the system except where it passes near the compact object (King, 1995). The massive companion drives a strong stellar wind that can remove up to $10^{-6} M_{\odot} \mathrm{yr}^{-1}$. The BH then has the ability to capture a sufficient enough portion of this wind to power the X-ray source (see Figure 1.2) (Psaltis, 2006). As a result, these SGXBs are persistent X-ray sources, meaning they spend most of their time in an X-ray bright ("outburst") state (King, 1995).

In contrast, the mass loss of Be stars is anisotropic. At the poles the wind has a low density and high velocity, similar to the supergiant wind but with a lower mass loss rate. At the equator, mass loss is highly variable, with the wind density being high and the velocity low (van Paradijs and McClintock, 1995). As a result, BeXBs

are usually transient in nature, where outbursts are normally associated with the compact object either passing close to or completely through the circumstellar disc (see Figure 1.2) (Okazaki and Negueruela, 2001; Charles and Coe, 2006). Here the conversion of the in-falling matter's kinetic energy into radiation powers the X-ray emission (Reig, 2011).

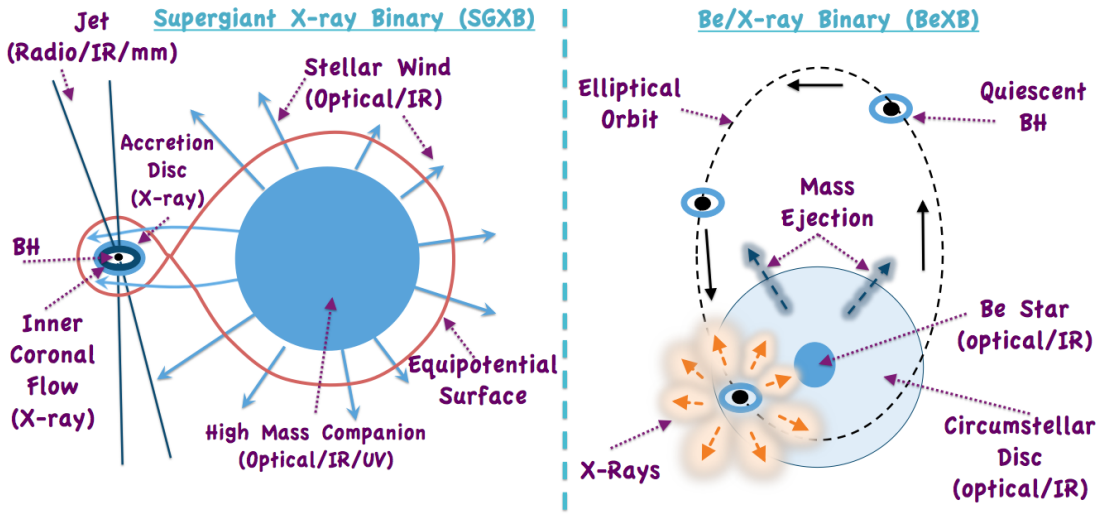

Figure 1.2: Schematic diagram of the mass-transfer mechanisms, system components and emission regions in the two subclasses of High-Mass X-ray Binaries (HMXBs), Super-Giant X-ray Binaries (SGXBs) (left) and Be/X-ray Binaries (BeXBs) (right). Figure adapted from Tauris and van den Heuval (2006).

Each mode of mass transfer, whether it be stellar wind dominated in the case of HMXBs or RLO in LMXBs, produces specific observational properties across multi-wavelength regimes (Charles and Coe, 2006). Thus, probing BHXRB systems at different wavelengths allows us to study separate components of the system.

X-ray studies, in which we observe emission from the inner coronal flow and inner accretion disc, allow us to discern the nature of the compact object and its properties (McClintock and Remillard, 2006). Optical, Infrared (IR) and Ultraviolet (UV) observations permit detailed studies of the companion and outer accretion disc and thus provide information pertaining to the orbital parameters of the system (Charles and Coe, 2006). While observing the system in the radio, IR and mm regimes give us insight into the inner workings of the relativistic jets and their connection to the

accretion flow (Fender, 2006).

1.1.2 Quiescent Activity

In Quiescence, transient XRBs are an invaluable resource for research into the orbital parameters of the system and therefore the mass of the compact object (Charles and Coe, 2006). An observational quantity of particular interest is the mass function,

$$f(M) = \frac{P_{\rm orb} K_2^3}{2\pi G}, \tag{1.1}$$

which corresponds to the minimum allowable mass of the primary (Remillard and McClintock, 2006). The two quantities on the right, $P_{\rm orb}$ the orbital period of the system, and K_2 the half-amplitude of the radial velocity curve of the companion, are observables that can be obtained from optical/IR spectroscopy (Charles and Coe, 2006).

To determine the mass function $f(M)$, and in turn the mass of the primary $M_{\rm BH}$, we also require additional constraints on the mass ratio q and the inclination i. First, in an interacting binary system the secondary must co-rotate with the primary. This results in an observed rotational velocity (Wade and Horne, 1998),

$$v_{\rm rot} \sin(i) = \frac{2\pi R_2}{P_{\rm orb}} \sin(i) \tag{1.2}$$

and radial velocity (Shahbaz et al., 1994a),

$$K_2 = \frac{2\pi a \sin(i)}{P_{\rm orb}} \left[\frac{q}{1+q}\right] \tag{1.3}$$

for the companion star, where v_{rot} is the true rotational velocity, which can be measured by observing line broadening in high-resolution spectra, and R_2 is the radius of the star (Shahbaz et al., 1994a).

Second, in the case of LMXBs, the companion must also be Roche lobe filling (Charles and Coe, 2006). Therefore, we need an idea of the geometry of this critical surface, specifically its dependence on the mass ratio q and the orbital separation a. As the lobes are not spherical, their size can instead be characterized by the radius of

a sphere having the same volume as the lobe, a quantity that unfortunately can only be solved for numerically (Frank et al., 2002). However, an approximate analytical formula (Eggleton, 1983), which works for all values of q,

$$\frac{R_2}{a} = \frac{0.49q^{2/3}}{0.6q^{2/3} + \ln(1 + q^{1/3})}, \tag{1.4}$$

can be used. Although, more often than not, a simplified relation by Paczynski (1971),

$$\frac{R_2}{a} = \frac{0.46}{(1 + q)^{1/3}} \tag{1.5}$$

valid only for $0.1 \lesssim q \lesssim 0.8$, is employed for its comprehensibility.

Third, the gravitational and centrifugal forces at the companion star about the centre of mass of the binary system can be combined to yield (Shahbaz et al., 1994a),

$$\frac{GM_1}{a} = \frac{K_2^2}{\sin^2(i)}\left[\frac{1 + q}{q}\right]. \tag{1.6}$$

Making use of 1.2 through 1.6, we can derive a value for q, and in turn $M_{\rm BH}$, in terms of observable parameters. To derive q we can first solve 1.3 for a,

$$a = \frac{K_2 P_{\rm orb}}{2\pi \sin(i)}\left[\frac{1 + q}{q}\right] \tag{1.7}$$

then combine the result with Equations 1.2 and 1.5 to yield,

$$v_{\rm rot} \sin(i) = K_2\left[0.46\frac{(1 + q)^{2/3}}{q}\right], \tag{1.8}$$

therefore allowing a value of q to be derived, given a measured v_{rot}.

To solve for $M_{\rm BH}$, we combine Equation 1.3 and 1.6 yielding,

$$\frac{P_{\rm orb}K_2^3}{2\pi G} = M_{\rm BH} \sin^3(i)\left[\frac{q}{1 + q}\right]^2. \tag{1.9}$$

Given the original definition of $q = M_{\rm BH}/M_2$ Equation 1.9 becomes,

$$\frac{P_{\rm orb}K_2^3}{2\pi G} = \frac{M_{\rm BH}^3 \sin^3(i)}{(M_{\rm BH} + M_2)^2}, \tag{1.10}$$

yielding the familiar form of the mass function.

The only remaining unknown is the inclination, i. Typically i is measured by analyzing ellipsoidal variability, due to gravitational distortion of the companion star, in the observed photometric light curve.

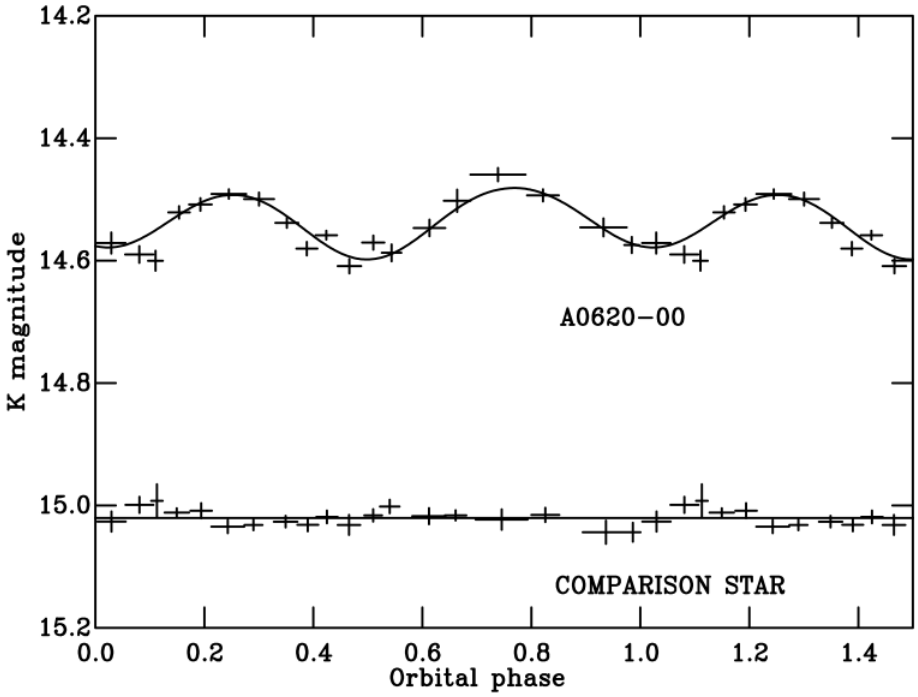

Figure 1.3: The IR light curve of BHXRB 1A 0620−00 demonstrating the classical double-humped ellipsoidal variations (Shahbaz et al., 1994a).

As the star, which fills its Roche lobe, orbits the BH both the projected surface area and average temperature along the observer's line of sight vary resulting in the characteristic double peaks in the light curve, which have an amplitude dependent upon i, known as ellipsoidal variations (see Figures 1.3 and 1.4) (Charles and Coe, 2006; Kreidberg et al., 2012). In face on systems, where $i = 0°$, no ellipsoidal variations are detected. While in edge on systems, where $i = 90°$, the maximum amplitude of variation is observed as a result of the geometry maximizing the changes in the projected surface area of the star with orbital phase (Kreidberg et al., 2012).

The simplest and most commonly used model to analyze ellipsoidal variability

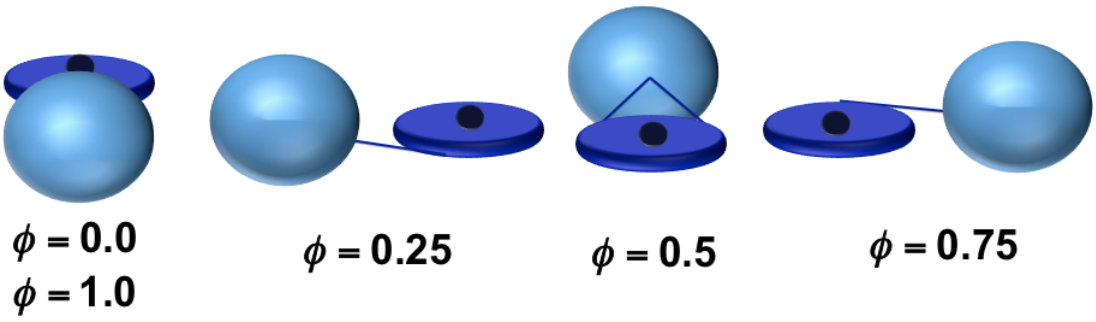

Figure 1.4: The orientation of the system with respect to orbital phase ϕ. Figure adapted from Orosz and Bailyn (1997).

in photometric light curves, referred to as the "star-only" model, works under the assumption that sources of light not due to the star, particularly in the IR, are negligible (Martin et al., 1995; Greene et al., 2001; Gelino and Harrison, 2003). However, it has been observed that non-stellar flux can contribute a significant fraction of the total flux of the system at both optical (Zurita et al., 2002; Orosz et al., 2004; Cantrell et al., 2010) and IR (Hynes et al., 2005; Gelino et al., 2010) wavelengths.

As a result, knowledge of the ratio of non-stellar flux to total flux, denoted as the NSL fraction, is critical to an accurate inclination measurement. One can obtain the NSL fraction by subtracting a template stellar spectrum from the observed spectrum (Marsh et al., 1994). However, the situation is further complicated by the fact that several sources can contribute to the NSL fraction, such as the accretion disc, hotspots on the disc, and the jet, which can all vary on timescales smaller than the orbital period itself resulting in a distortion of the shape of the light curve (Cantrell et al., 2010).

Measurements of orbital inclination are by far the largest source of systematic error involved in estimating the mass of the BH primary. An accurate inclination measurement requires fitting the light curve, which has a consistent shape and known NSL fraction, with a model which includes disc and hotspot parameters (Kreidberg et al., 2012). Fortunately, Kreidberg et al. (2012) recently published a study in which they characterize the systematic error, caused by the effects discussed above, for 16 BHXRB systems and compare inclination estimates in the literature with the most

probable value of inclination in these systems.

In particular, they build on the study of 1A 0620−00 quiescent light curves by Cantrell et al. (2008), who define two separate states existent in the quiescent optical light curves,

- Passive: displaying minimum aperiodic variability, resulting in a stable light curve shape over short timescales; and
- Active: brighter, bluer and more variable than the passive state, possibly as a result of increased accretion activity.

We have made extensive use of this study in determining the orbital parameters used in our analysis (see Chapter 2).

1.1.3 Outburst Behaviour

X-Ray spectral observations of BHXRBs in outburst have revealed two predominant sources of emission, each producing separate spectral components. Thermal emission, observed at low energies, produces a modified disc black body type spectrum[1], while the higher energy emission observed suggests the presence of a separate source of emission, producing a smooth hard comptonized spectrum extending up to relatively high energies (Mayer and Pringle, 2007).

Low Energy (Thermal) Emission:

The thermal emission observed, via direct soft photons from the accretion disc (see Figure 1.5), is due to black body radiation. Black body radiation is a type of thermal radiation that arises when matter is in thermal equilibrium. The specific intensity of this radiation is dependent only on the temperature T of the matter. The flux (energy emitted per unit time per unit area) of a black body source is given by the Stefan-Boltzmann Law (Rybicki and Lightman, 1985),

$$F_{\mathrm{BB}} = \sigma_{\mathrm{SB}} T^4 \tag{1.11}$$

where σ_{SB} is the Stefan-Boltzmann constant.

[1] A superposition of black body components from disc annuli at different temperatures.

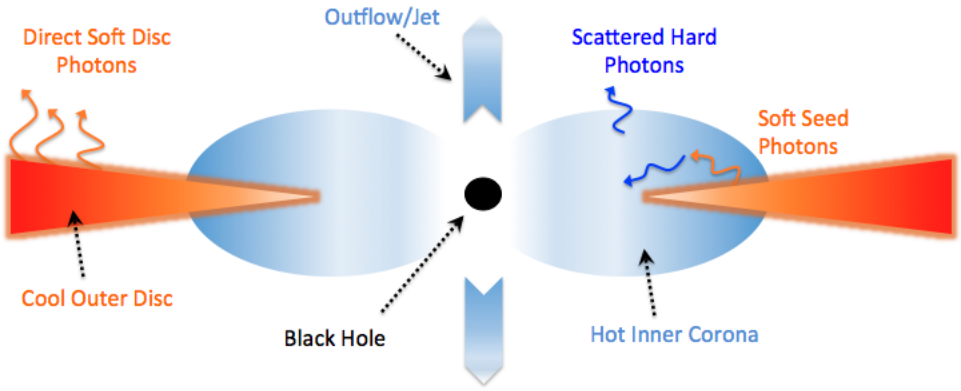

Figure 1.5: Sources of emission during outburst in a BHXRB. Figure adapted from Zdziarski et al. (2004).

High Energy Emission:

The high energy emission in BHXRBs is created via Compton Scattering, where the soft disc photons are up-scattered by the high energy electrons in the hot inner coronal flow (see Figure 1.5). Compton scattering is essentially an energy exchange process occurring between a photon and an electron (Done et al., 2007). For an incoming photon of energy ϵ_{in}, hitting a stationary electron, the scattered photon energy ϵ_{out}, is as follows,

$$\epsilon_{out} = \frac{\epsilon_{in}}{1 + (\epsilon_{in}/m_e c^2)(1 - \cos\theta)}, \tag{1.12}$$

where θ represents the photon scattering angle (Bradt, 2008). Overall, Equation 1.12 tells us that the particle, whether it be the incident photon or the electron, with the most energy will share its energy with the other (Done et al., 2007).

Now consider a situation involving moving electrons, a process often referred to as Inverse Compton or up-scattering. In a collision, the more energetic electrons will give energy to the photons. If we assume the photons and electrons are distributed isotropically, and the incoming photon energy is much less than the electron rest mass energy (i.e., $\epsilon_{in} << m_e c^2$), we can obtain the scattered photon energy averaged over all directions to be,

$$\epsilon_{out} = \frac{4}{3}\gamma^2 \epsilon_{in}, \tag{1.13}$$

where γ is the Lorentz factor of the electrons.

If the electrons have a thermal (Maxwellian) distribution, they are non-relativistic $\gamma \simeq 1$, yielding small electron velocities and $\beta^2 = 3kT_e/m_e c^2 = 3\Theta$, where we define the electron temperature as Θ. Because we are in the Thompson scattering regime, the net energy gain for photons can be shown to be,

$$\frac{\Delta\epsilon}{\epsilon} = \frac{4kT_e - \epsilon_{in}}{m_e c^2}. \tag{1.14}$$

Photons can only interact with electrons through collision. An electron has a cross section, σ_T, for interaction with a photon. Therefore, the average photon should interact if one or more electrons are within a volume with length L (path length) and cross-sectional area σ_T. The optical depth, τ_e, is defined as the number of electrons within this volume such that,

$$\tau_e = N_e L \sigma_T, \tag{1.15}$$

where N_e is the volume density of electrons. For optically thick material of $\tau_e >> 1$, photons will do a random walk to escape, yielding the number of scatterings equal to τ_e^2. For optically thin material of $\tau_e < 1$, the average number of scatterings can be shown to equal τ_e (Bradt, 2008) .

Thus, starting with photons of initial energy $\epsilon_{in} << 4kT_e$, only a fraction τ will be scattered in optically thin material, to an energy obtained from Equation 1.14 to be,

$$\epsilon_{out,1} = (1 + 4\Theta)\epsilon_{in}. \tag{1.16}$$

These scattered photons can be scattered N times until they reach the limit of the electron energy, 3Θ. After N scatterings, the photons will have an energy,

$$\epsilon_{out,N} = (1 + 4\Theta)^N \epsilon_{in} \sim 3\Theta. \tag{1.17}$$

Both the energy boost, as demonstrated in Equations 1.16 and 1.17, and the fraction of photons scattered, as Comptonizaton conserves photon number, is constant, yielding a power law $\propto \epsilon^{-\Gamma}$ (see Figure 1.6a).

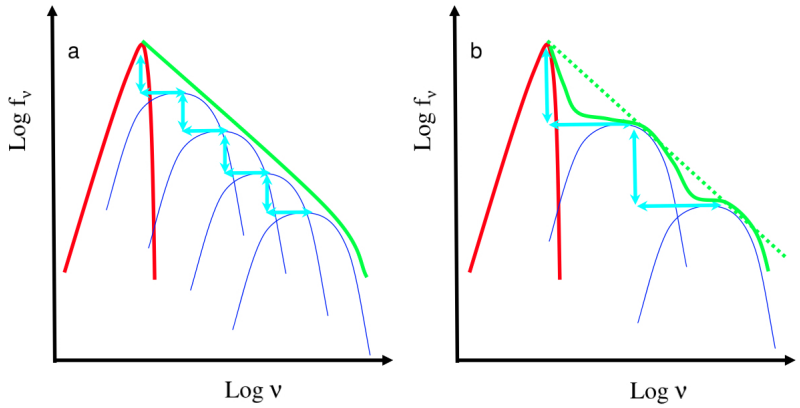

Figure 1.6: a) For an optically thin material ($\tau \lesssim 1$), the spectrum is built up from repeated thermal (Maxwellian) up-scatterings. Here, a fraction τ of the seed photons (red line) are boosted. These boosted photons form the seed photons for the next scattering and so forth. Each scattering order (blue lines) is shifted by the same amount, yielding a power law (green line); b) A power law of the same index can be obtained with a lower τ and a higher Θ. Although, the larger separation between scattering orders (blue lines) will yield a bumpy spectrum (green line). Figure from Done (2010).

This power-law ranges from the initial photon energy ϵ_{in}, to the electron energy 3Θ, where the spectrum exhibits a cutoff. The spectral index,

$$\alpha = \Gamma - 1 = \frac{\ln \tau}{\ln(1 + 4\Theta)} \tag{1.18}$$

is determined by both the electron temperature Θ and the optical depth τ. Because multiple values of Θ and τ may yield the same Γ, there exists a constraint stating that τ must not be too small and Θ must not be too large to yield a smooth power-law (see Figure 1.6b) (Done, 2010).

If instead, we have a non-thermal (power-law) distribution of electrons such that, $N(\gamma) \propto \gamma^{-p}$, ranging from $\gamma = 1$ to γ_{max}, then energies can be relativistic ($\gamma >> 1$). From Equation 1.13, the energy of the seed photon is increased by a factor $\sim \gamma^2$ due

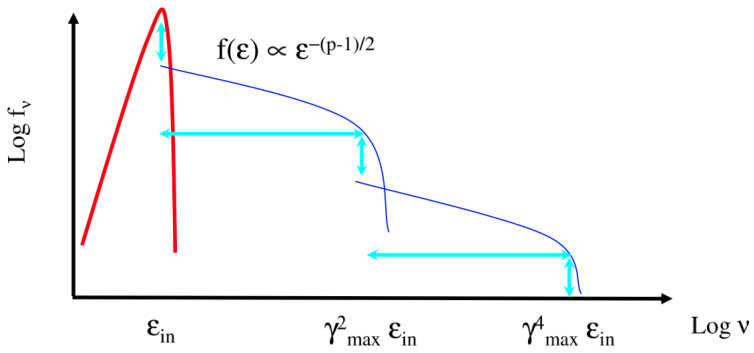

Figure 1.7: For non-thermal up-scattering, the seed photons (red line) will form a power law distribution from one scattering order (blue line) due to the large energy boost involved from relativistic electrons. Figure from Done (2010).

to up-scattering, with each factor of γ attributed to doppler shift transformations. Therefore, the comptonized spectrum will range from ϵ_{in} to $\gamma^2_{max}\epsilon_{in}$, forming a power-law from a single scattering order (see Figure 1.7). Using the fact that the rate at which the electrons lose energy is equal to the rate at which the photons gain energy, the power law index of the photon spectrum can be calculated to be,

$$\alpha = \frac{(p-1)}{2}. \tag{1.19}$$

The electrons in the optically thin region intercept only a fraction τ of the seed photons from the disc, scattering them to energies $\propto \gamma^2\epsilon_{in}$. These photons can then be scattered again to energies $\propto \gamma^4\epsilon_{in}$. Due to relativistic electrons ($\gamma >> 1$) being involved, the energy boost is so large that the scattered photons of energy ϵ_{out}, will hit the limit of the electron energy γ_{max}, within a few scattering orders yielding the spectrum shown in Figure 1.7.

1.2 Theoretical Stable Accretion Flow Models

The past four decades have offered a multitude of discoveries involving the physics of accreting astrophysical objects. Efforts to model accretion flows beginning in the early 1970's and continuing for the next two decades for the most part were associ-

ated with endeavours based on two restrictive assumptions. Firstly, accretion flows were losing angular momentum at high rates thought to be proportional to pressure due to some unknown process (Shakura and Sunyaev, 1972). Such an assumption stemmed from the fact that microscopic viscosity proved to be an insufficient mechanism to explain the observed high mass accretion rates existent in some sources (Pringle, 1981). Secondly, radiation processes were highly efficient suggesting cool, geometrically thin accretion discs (Psaltis, 2006).

It was not until the early 1990's that a multitude of sophisticated and distinct theories would emerge. Such theories were inspired by two major discoveries (Psaltis, 2006). The first, the notion of an efficient mechanism for angular momentum transport, the Magneto-Rotational Instability (MRI) (Balbus and Hawley, 1991), spurring complex numerical simulations and vigorous research efforts. The second, the concept of stable, inefficient accretion flows, termed Advection Dominated Accretion Flows (ADAFs) (Narayan and Yi, 1994).

Currently there are two types of theoretical stable accretion flow models accepted; a cool, geometrically thin, optically thick disc and a hot, geometrically thick, optically thin inner coronal flow (Done et al., 2007). The following Section provides a detailed analysis of the structure and emission mechanisms in each accretion flow model, as well as a way in which to connect them.

1.2.1 Shakura-Sunayev Thin Disc

In binary systems, which undergo mass transfer, we have seen that it is the very fact that this accreting material has sufficient angular momentum that allows for the formation of an accretion disc around the compact object. To examine the detailed physics involved in this accretion disc we must begin with an assumption. The thin disc approximation, first developed by Shakura and Sunyaev (1972), allows us to regard the accretion disc as a two-dimensional gas flow on the basis that many close binary systems show disc flow is confined very close to the orbital plane (Frank et al., 2002).

Therefore, working in cylindrical coordinates (R, ϕ, z), matter, which moves with an angular velocity Ω around the compact object of mass M, will lie very close to

the plane $z = 0$. If we assume this matter moves in a Keplarian orbit, the angular velocity takes the following form,

$$\Omega = \Omega_{\rm K}(R) = \left[\frac{GM}{R^3}\right]^{1/2} \tag{1.20}$$

and the circular velocity is then,

$$v_\phi = R\Omega_{\rm K}(R). \tag{1.21}$$

In addition to angular and circular velocity, the gas also possesses a radial velocity[2], denoted v_R. As a result, this disc can be characterized by a surface density $\Sigma(R, t)$, the mass per unit surface area of the disc.

If we consider a disc annulus lying between R and $R + \Delta R$, the rate of change of the total mass, $2\pi R\Delta R\Sigma$, and total angular momentum, $2\pi R\Delta R\Sigma R^2\Omega$, is governed by the net flow from adjacent annuli. Thus, given the above assumptions, the equations for conservation of mass and angular momentum transported in the disc are as follows,

$$R\frac{\partial \Sigma}{\partial t} + \frac{\partial}{\partial R}\left[R\Sigma v_R\right] = 0 \tag{1.22}$$

$$R\frac{\partial}{\partial t}\left[\Sigma R^2\Omega\right] + \frac{\partial}{\partial R}\left[R\Sigma v_R R^2\Omega\right] = \frac{1}{2\pi}\frac{\partial G}{\partial R}, \tag{1.23}$$

where $G(R, t)$ is the viscous torque, parametrized by

$$G(R, t) = 2\pi R\nu\Sigma R^2\Omega', \tag{1.24}$$

Ω' denotes the derivative with respect to r and ν represents the viscosity[3].

Combining Equations 1.22, 1.23 and 1.24 results in the basic equation determin-

[2]In general, this radial velocity is a function of both radius and time allowing for analysis of time-varying situations (Frank et al., 2002).

[3]Shakura and Sunyaev (1972) originally parametrized the viscosity with the α-prescription, which states that $\nu = \alpha c_s H$, where c_s represents the speed of sound and H is disc height.

ing the time evolution of surface density in a Keplarian disc,

$$\frac{\partial \Sigma}{\partial t} = \frac{3}{R}\frac{\partial}{\partial R}\left[R^{1/2}\frac{\partial}{\partial R}(\nu \Sigma R^{1/2})\right]. \tag{1.25}$$

Given a known solution, using equations 1.23 and 1.24, one can obtain the functional form of v_R,

$$v_R = -\frac{3}{\Sigma R^{1/2}}\frac{\partial}{\partial R}\left[\nu \Sigma R^{1/2}\right]. \tag{1.26}$$

In many situations, the system's external conditions, such as mass-transfer rate, change on timescales much longer than the timescales needed to change the radial structure of the disc[4], allowing the problem to be simplified further with the assumption that the disc has a steady state structure (Frank et al., 2002). Setting $\partial/\partial t = 0$ in both conservation equations (1.22 and 1.23) will yield the mass flux (or mass-transfer rate) at any point in the disc,

$$\dot{M} = 2\pi R \Sigma(-v_R) \tag{1.27}$$

and in turn the surface density distribution,

$$\nu \Sigma = \frac{\dot{M}}{3\pi}\left[1 - \left(\frac{R_{in}}{R}\right)^{1/2}\right], \tag{1.28}$$

where v_R is given by equation 1.26 and R_{in} denotes the innermost annulus radius.

Because the annulus is in equilibrium, the flux emerging, assumed to be radiated locally with no advection present, must equal the rate at which energy is deposited within the annulus from viscous dissipation due to viscous stresses (now thought to originate from the MRI; see Section 1.4.2) that convert gravitational potential energy to heat (Done et al., 2007).

In the case of an optically thick accretion disc, photons scatter (off electrons) many times causing the particles to share their kinetic energies and come into thermal equilibrium. Therefore, we expect the flux emerging from the annulus to be that

[4]Changes to the radial structure of a thin disc can be be shown to occur on timescales proportional to the viscous timescale, $t_{\rm visc} \sim R^2/\nu$ (Frank et al., 2002).

of a black body (Equation 1.11) characterized by an effective temperature, $T_{\rm eff}(r)$. Equating the viscous dissipation rate to the black body flux yields the temperature profile of a steady state, optically thick, geometrically thin accretion disc,

$$T_{\rm eff}^4(r) = \frac{3GM\dot{M}}{8\pi\sigma_{SB}r^3}\left[1-\left(\frac{R_{in}}{R}\right)^{1/2}\right]. \tag{1.29}$$

Overall, as the functional form of Equation 1.29 illustrates, the emission from the entire accretion disc will be made up of the sum of black body components emitted from each annulus. As the radius of the annuli decrease, a black body component will exhibit larger luminosities due to stronger gravity and larger temperatures due to larger luminosity being dissipated over a smaller area (Done et al., 2007). The peak temperature and luminosity correspond to an annulus at radius R_{in}, the Innermost Stable Circular Orbit (ISCO) in General Relativity (GR) (Frank et al., 2002).

It is important to note that the Shakura-Sunyaev solution above assumes the mass transfer rate $\dot{M}$ is constant with radius. This is actually not true as accretion discs are subject to instabilities (see Section 1.4) (Done et al., 2007). In addition, for a more realistic treatment, other radiative and relativistic effects must be accounted for. For example, for each annuli to be a true black body, the disc would have to be optically thick to absorption at all frequencies. Because free-free absorption drops as a function of frequency, the high energy photons will be unlikely to thermalize, creating a modified black body characterized by an effective temperature which is a factor larger than the true black body. In addition, emission from each annuli will be smeared out due to special and general relativistic effects arising from the rapid rotation of the emitting material (disc) in a strong gravitational field (Done, 2010).

1.2.2 Radiatively Inefficient Accretion Flow

The hot, inner coronal flow, in contrast to the accretion disc flow, is geometrically thick (Done, 2010)[5]. In geometrically thick flows, pressure forces due to gas pressure,

[5]The viscous timescale of the disc can be written in terms of the dynamical (orbital) timescale around a Schwarzschild BH ($t_{dyn} = 4.5(m/10)(r/6)^{3/2}$ ms, given an $mM_\odot$ BH at some number of gravitational radii, r (Frank et al., 2002)) as follows, $t_{visc} \sim$

become important (Shapiro et al., 1976; Ichimaru, 1977; Narayan and Yi, 1994), implying that the flow must be hot with protons close to the virial temperature $T \sim 10^{12}K$. In addition, observational data require the electrons to also be hot in order to produce the high energy emission via up-scattering (i.e., if spectra exhibits Compton rollover at $\sim$ 100 keV , $T_e \sim 10^9$K). To satisfy these two different temperature requirements, the structure of the flow must take the form of a two-temperature plasma (Done et al., 2007).

This two temperature behaviour, referred to as an Ion-Supported Accretion Flow (ISAF) (Rees et al., 1982), happens in cases where the plasma is not very dense. Here, electrons that are far more efficient radiators than protons, will lose energy more rapidly. In addition, the protons will acquire most of the gravitational energy, as they are more massive. Thus, even if the electrons and protons are heated at the same rate in this plasma, the proton temperature will still be larger provided they do not interact enough to thermalize, in turn implying that the flow must have a low optical depth (Shapiro et al., 1976; Ichimaru, 1977; Narayan and Yi, 1994). Due to the fact that this plasma is optically thin, it will produce the observed radiation via Comptonization (as described in Section 1.1.3) (Done et al., 2007).

In addition, this flow is radiatively inefficient because the protons, which are the receivers of the gravitational energy, are not able to transfer their energy to the electrons before they fall into the BH, resulting in the majority of the accretion energy getting lost to the BH and therefore a low radiative efficiency (Spruit, 2014).

Originally the detailed properties of this flow were described assuming no advection was present (Shapiro et al., 1976). However, both Ichimaru (Ichimaru, 1977) and Rees (Rees et al., 1982) came to realize the importance of the advection of gravitational energy by the protons in these types of two temperature plasmas, leading to the development of the Advection Dominated Accretion Flow (ADAF) model, which allowed for advection, as a cooling process, in the ISAF model (Narayan and Yi, 1994).

$\alpha^{-1}(H/R)^{-2}t_{dyn}$. If we take $\alpha = 0.1$, as found from modelling variability in the disc (King et al., 2007), typical fluctuations seen in power density spectra of the high energy emission that give $t_{visc} = 0.05s$ and the t_{dyn} for a 10 $M_\odot$ BH at $6R_g$ of 0.005s, we find that $H/R \sim 1$ (i.e., geometrically thick (Done, 2010)).

To present a simple picture of ADAFs, we follow Narayan and Yi (1994), beginning with the basic equations for conservation of mass, radial momentum, angular momentum and energy for a steady axisymmetric rotating accretion flow,

$$\rho R H v = \text{constant} \tag{1.30}$$

$$v\frac{dv}{dR} - (\Omega^2 - \Omega_K^2)R = -\frac{1}{\rho}\frac{d}{dR}(\rho c_s^2) \tag{1.31}$$

$$\rho R H v \frac{d(\Omega R^2)}{dR} = -\frac{1}{dR}\left[\nu\rho R^3 H \frac{d\Omega}{dR}\right] \tag{1.32}$$

$$\rho v T \frac{ds}{dR} = q^+ - q^-, \tag{1.33}$$

where R is the central radius from the compact object, ρ is the gas density, H is the thickness of the flow, v is the radial velocity, Ω is the angular velocity, Ω_K is the Keplarian angular velocity (as defined in Equation 1.20), c_s is the sound speed, ν is the viscosity, T is the temperature of the gas, and s is the specific entropy of the gas.

Defining,

$$q^+ = \nu\rho R^2 \left[\frac{d\Omega}{dR}\right]^2 \tag{1.34}$$

as the viscous dissipation rate per unit volume, q^- as the radiative cooling rate per volume, and

$$q^{adv} = \rho v T \frac{ds}{dR} \tag{1.35}$$

as the radial advection rate per volume, the energy equation (Equation 1.33) can be written in the form,

$$q^{adv} = q^+ - q^- = f q^+ \tag{1.36}$$

allowing us to define the advection fraction, f (Yi, 1999). If we assume f is constant, then the accretion flow can be completely described using the conservation equations and the viscosity prescription[6], in terms of four variables; surface density[7], the speed of sound, radial velocity and angular velocity (Frank et al., 2002). Thus, this classical ADAF solution is self-similar, operating on the assumption that a single value of the

[6]viscosity prescription: $\nu = \alpha c_s^2/\Omega_K$

[7]Surface density can be expressed in terms of thickness of flow and gas density, $\Sigma = 2H\rho$.

advected fraction is valid at all radii and that advection is only a cooling process.

We have now established a detailed account of both the structure and emission mechanisms of the two separate accretions flows: a cool, geometrically thin, optically thick disc and a hot, geometrically thick, optically thin inner coronal flow (Done et al., 2007). To complete the picture we must also be able to connect them. The mechanism responsible for this is called the evaporation instability (Liu et al., 1999; Rozanaska and Czerny, 2000; Mayer and Pringle, 2007). If the cool disc is in thermal contact with the hot flow, heat conduction will be present between the two, leading to either,

- evaporation of the cool disc into the hot flow or;

- condensation of the hot flow onto the cool disc.

At this point in our discussion we must caution the reader. While ADAFs are the most well known solution, the hot flow is thought to be more complex. As a result, numerous other research efforts into the structure of this flow have followed Narayan and Yi (1994), including, but not limited to, Yuan (2001) who applied these solutions to high luminosity situations, known as Luminous Hot Accretion Flows (LHAFs), and a multitude of theories involving other physical processes such as convection (Convection Dominated Accretion Flows (CDAFs; Abramowicz and Igumenshchev (2001))), magnetic fields (Magnetically Dominated Accretion Flow (MDAFs; Meier (2005))), winds (Advection Dominated Inflow/Outflow Solution (ADIOS; Blandford and Begelman (1999))) and jets (Jet Dominated Accretion Flows (JDAFs; Falke et al. (2004))). In the end though, what we really need to fully explore the complex properties of these flows are complete Magneto-Hydrodynamic (MHD) simulations in full GR, including radiative cooling[8], allowing us to accomplish what these pure analytical models do not have the full ability to do (Done, 2010).

[8]These are beyond current computational capacities.

1.3 A Quantitative Four-State Description for Active Accretion

During an outburst of a BHXRB, notable variations in spectral and timing properties are observed[9], allowing a number of different accretion states to be defined. The particular state a system is in at any given time is dependent upon the rate at which the mass transfers onto the BH.

The existence of X-Ray accretion states first became known in the early 1970's when Tananbaum et. al. observed a global spectral change in Cygnus X−1. A transition from a low energy (soft) spectrum to a high energy (hard) spectrum lasting less than one month revealed a decrease in source intensity by a factor of 4 in the soft X-rays (2–6 keV) and an increase of a factor of 2, accompanied by radio source detection, in the hard X-rays (10–20 keV) (Remillard and McClintock, 2006).

The bi-model state behaviour exhibited in Cygnus X−1 would be shown to occur in numerous other sources, including 1A 0620−00 (Belloni, 2009). This observational pattern led to a two-state classification, (i) a "Low Hard State" (LHS) usually observed when the source was fainter, associated with a dominant power law component[10] with a hard photon index of $\Gamma \sim 1.5 - 1.7$ and a high energy cutoff ~ 100 keV, and an accompanying radio source; and (ii) a "High Soft State" (HSS) generally observed when the source was brighter, associated with a dominant soft thermal disc

[9]This work will mainly focus on the spectral properties observed. Timing, which is beyond the scope of this work, involves tracking millisecond variability existing within the accretion disc and has been linked to major behavioural changes occurring during state transitions (McClintock and Remillard, 2006).

[10]This component can be written in terms of differential photon number density (i.e., photons $\mathrm{cm}^{-2}\mathrm{s}^{-1}\mathrm{keV}^{-1}$) as $N(E) = N_0 E^{-\Gamma}$ where Γ is photon index or in terms of the energy flux as $F(E) = EN(E) = N_0 E^{-(\Gamma-1)} = N_0 E^{-\alpha}$ where $\alpha = \Gamma - 1$ represents the energy index. As power-law spectra often span multiple decades in energy they are plotted in logarithmic space in $\log E$, resulting in the number of photons per bin being represented by $N(E)dE = N(E)EdE/E = EN(E)d\log E = F(E)d\log E$. As a result plotting $F(E)$ with respect to $\log E$ will show the number of photons rather than a flux. Applying the same concept to the energy flux, the energy per bin becomes $F(E)dE = F(E)EdE/E = EF(E)d\log E$. Thus, plotting $\log EF(E)$ (i.e., $\nu F(\nu)$) with respect to $\log E$ depicts what energy the source luminosity peaks at. As a result, $\Gamma < 2$ (hard spectra) will peak at high energies, $\Gamma > 2$ (soft spectra) will peak at low energies and $\Gamma = 2$ indicates equal power per decade of energy.

component, a weak power-law tail with no detectable cutoff and no radio detection (Remillard and McClintock, 2006).

The launch of the *Ginga* Satellite (1987) would bring the discovery of new X-Ray transients and corresponding follow-up observations. Among them, being the bright transients GS 1124−684 (Miyamoto et al., 1993) and GX 339−4 (Miyamoto et al., 1991), whose discovery and subsequent analysis would lead to the identification of an additional spectral behaviour.

Occurring at high fractions of Eddington[11], this behaviour was aptly named the "very high state" (VHS) (Belloni, 2009). In addition to the increase in luminosity, the spectrum in this state was observed to be softer than that of the LHS. The softening of the spectrum was due to two effects happening simultaneously; the appearance of a significant thermal disc component and the steepening of the hard power-law component to a photon index of $\Gamma \sim 2.0 - 2.5$ (Capitanio et al., 2009a). Evidence of the VHS (also commonly known as the Steep Power-law (SPL) state) is not just limited to a few cases, but can be seen in the brightest phases of many BHXRBs, including GX 339−4 (McClintock and Remillard, 2006; Motta et al., 2009), GRS 1915+105 (Done et al., 2004; Reig et al., 2003), GRO J1655−40 (Kubota et al., 2001; McClintock and Remillard, 2006; Brocksopp et al., 2006; Dunn et al., 2009), 4U 1543−475 (Park et al., 2004), H1743−322 (McClintock et al., 2009; Chen et al., 2010), and XTE J1550−564 (Miller et al., 2001b; Rodriguez et al., 2003; McClintock and Remillard, 2006).

In fact, further observations of GS 1124−684 (Done and Kubota, 2006) and GX 339−4 (Miyamoto et al., 1991) led to the realization that the X-Ray states of BHXRBs exhibit hysteresis. That is, observed properties of the SPL/VHS were seen to occur at varying luminosities in the same source (Done et al., 2007).

Such a revelation led to yet another proposed behaviour, the Intermediate State (IMS) (Belloni, 2009). Often the IMS is split into two separate states, the Hard

[11]The Eddington limit (under the assumption of steady spherically symmetric accretion of material composed of mainly hydrogen) is defined as the luminosity at which the outward radiation pressure (which pushes electron-proton pairs outward) balances the inward gravitational force (acting on each pair). The Eddington luminosity can be parametrized in terms of mass as follows, $L_{\rm edd} \approxeq 1.3 \times 10^{38}(M/M_{\odot})\mathrm{ergs}^{-1}$.

Intermediate State (HIMS) and the Soft Intermediate State (SIMS). The differences between these two states is established mostly with timing parameters (Homan and Belloni, 2005) as well as the ejection of relativistic jets (associated with the HIMS to SIMS transition) (Capitanio et al., 2009a; Miller-Jones et al., 2012). It is common for the SPL/VHS to be treated as part of the IMS due to their similar spectral characteristics (Belloni et al., 1996; Gierlinski and Newton, 2006).

Despite these efforts, the scarce amount of information available prior to 1995 made it difficult to form a coherent picture of outburst evolution in BHXRBs (Belloni, 2009). This changed with the launch of X-Ray satellites with unparalleled capabilities like RXTE (1995), BeppoSAX (1996), XMM-Newton (1999), CHANDRA (1999), INTEGRAL (2002), SWIFT (2004), and MAXI (2009), which have challenged, and continue to challenge, the prevailing views of X-ray accretion states in BHXRBs with the vast database of observations they provide (Done et al., 2007).

The generally accepted paradigm of outburst evolution involves the system cycling through a pattern of hard (dominated by comptonized emission) and soft (dominated by thermal emission) states, where the rise in luminosity at the start of outbursts occurs in the hard state, while much of the outburst's peak and decline occurs in the soft state (see Figure 1.8). As discussed above, the observed luminosity of the reverse transition (soft-hard) is always lower than that of the forward transition (hard-soft).

This basic canonical pattern (often referred to as the "turtlehead" or "q-track" in a Hardness-Intensity Diagram (HID)) has been modelled after numerous outbursts of GX 339−4 (Zdziarski et al., 2004; Fender et al., 2004; Belloni et al., 2005; Homan and Belloni, 2005; Del Santo et al., 2008; Belloni, 2009; Motta et al., 2009; Corbel et al., 2013; Debnath et al., 2013b) and can be observed in a multitude of other sources (Capitanio et al., 2009a) including, but not limited to H 1743−322 (Zhou et al., 2013; Chen et al., 2010), GRO 1655−40 (Tomsick et al., 1999; Brocksopp et al., 2006), 4U 1543−475 (Park et al., 2004), XTE J2012+381 (Campana et al., 2001), MAXI J1659−152 (Kuulkers et al., 2013), and GRS 1739−278 (Borozdin and Trudolyubov, 2000).

Before proceeding with our discussion of each individual accretion state we must

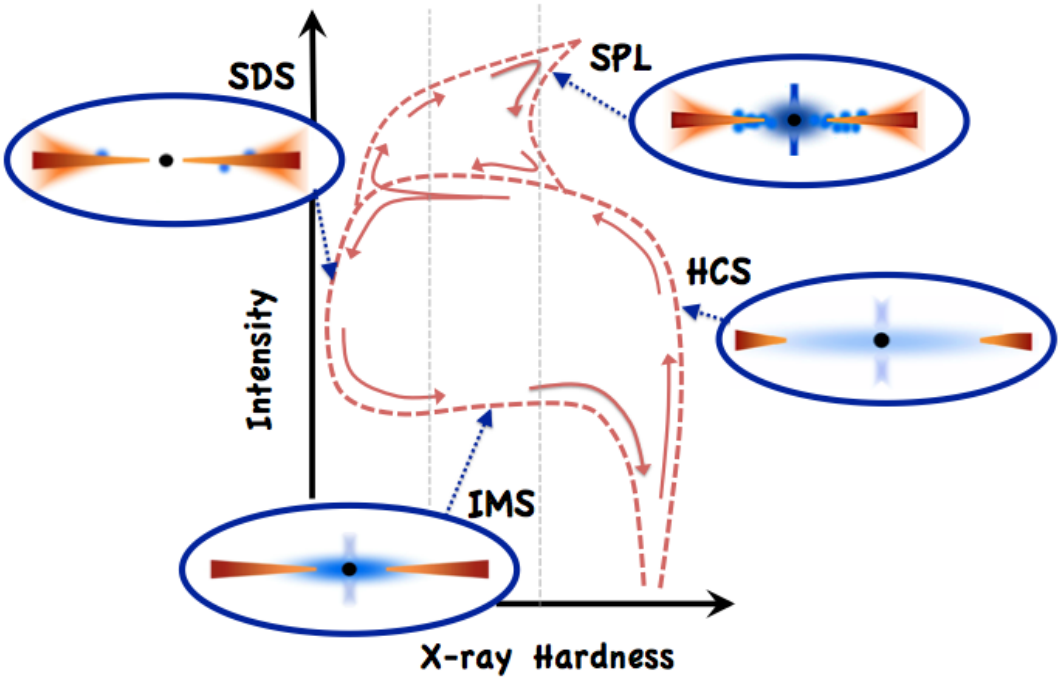

Figure 1.8: The turtlehead (or Hardness-Intensity) diagram, indicating the source geometry in each state of a BHXRB outburst. Schematic source geometries taken from Done (2010).

address the issue of terminology. While the nomenclature adopted over the years may vary a great deal and be at times confusing, its complexity reflects just how far we have come in understanding the complicated evolution of X-Ray accretion states (Done et al., 2007). To avoid confusion, for the purpose of this work, we adopt a four-state nomenclature for active accretion, which abandons the outdated jargon involving luminosity ("low", "high","very high") as a major criterion for defining states, instead focussing on the degree to which the two contributions to emission from accretion flows vary. The accretion state definitions used in this work, and their relation to previously used jargon, are presented in Table 1.1.

Table 1.1: Accretion State Nomenclature

State Name	Alternate Name	Characteristics
Hard Comptonized State (HCS)	Low/Hard State (LHS)	dominant comptonized emission: $\Gamma \sim 1.5 - 1.7$ high energy cutoff ~ 100 keV $\dot{M} \rightarrow$ low to high outflow in the form of a relativistic jet
Soft Disc-Dominated State (SDS)	High/Soft State (HSS)	dominant thermal emission: $T_{dbb} \sim 1$keV no detectable high energy cutoff $\dot{M} \rightarrow$ high to low outflow in the form of accretion disc winds
Steep Power-Law (SPL) State	Very High State (VHS)	mix of thermal and comptonized emission steeper PL: $\Gamma \sim 2.0 - 2.5$ occurring at $L > 0.2L_{edd}$
Intermediate State (IMS)	-	mix of thermal and comptonized emission steeper PL: $\Gamma \sim 2.0 - 2.5$ occurring at $L < L_{\rm SPL}$ outflow in the form of discrete relativistic jet ejections

1.3.1 Hard Comptonized State (HCS)

Generally, in the early (and late) phases of an outburst, a source is thought to be in the HCS, corresponding to the right-most vertical branch on the HID (Belloni, 2009). Spectrally this state is characterized by a dominant power-law (comptonized) component with a hard photon index of $\Gamma \sim 1.5 - 1.7$ and a high energy cutoff at $\sim$100 keV, and sometimes supplemented by a weak thermal component (see Figure 1.9).

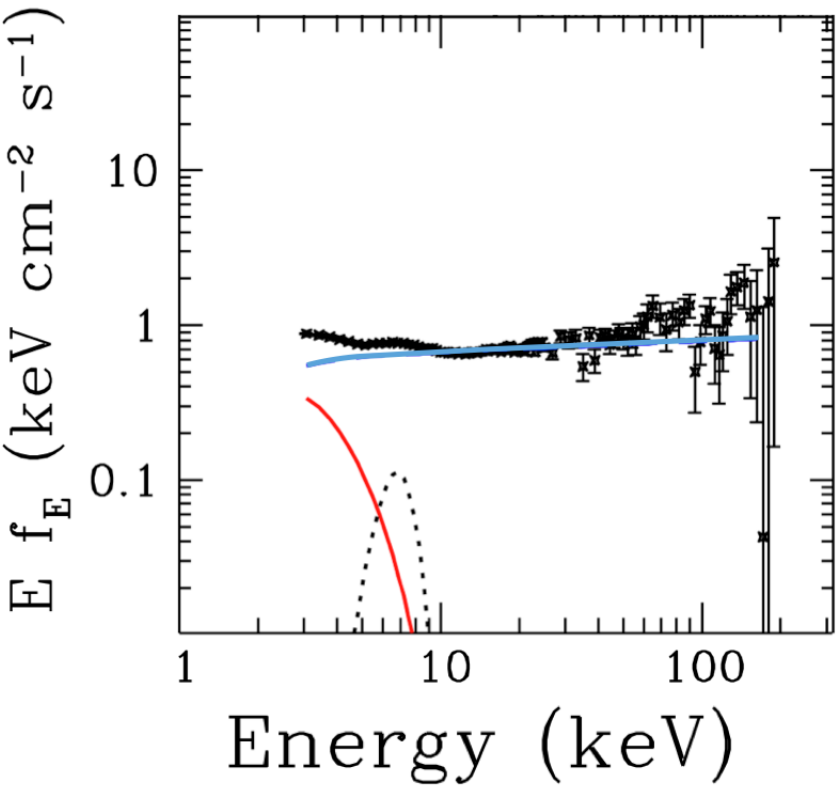

Figure 1.9: Example HCS spectra taken during the 1996/1997 outburst of GRO J1655−40. The spectrum is fit with a power-law of $\Gamma = 1.93$ (blue) and disc black body component with $T_{dbb} = 0.77$ keV (red). Figure from Remillard and McClintock (2006).

The mechanism for the dominant emission in this state is a hot, geometrically thick, optically thin flow. As discussed in Section 1.2.2, the structure of this flow is most commonly associated with ADAFs. However, because the flow is thought to be more complex, other physical processes such as convection, winds, magnetic fields

and jets should be taken into account (Done, 2010).

Observationally, this state is associated with low mass accretion rates and is typically seen only at low fractions of Eddington. At these low mass accretion rates, as a consequence of the cool disc being in thermal contact with the hot flow, the disc will (likely) evaporate into the hot inner flow via the evaporation instability described in Section 1.2.2, giving rise to a disc truncated far from the BH (Liu et al., 1999; Rozanaska and Czerny, 2000; Mayer and Pringle, 2007). If present, the weak thermal component in the spectrum is a result of the un-scattered photons from this truncated disc structure (Done, 2010).

Another defining observational characteristic of this state is a flat to slightly inverted radio spectrum thought to be associated with the presence of a compact, steady jet (Fender et al., 2004; Fender, 2009; Russell et al., 2012).

In addition to the above described spectral features, it is also common for systems in this state to exhibit two additional features. The first, a reflection component, seen as a bump between ∼10–30 keV, caused by disc photons which bounce back into the line of sight after scattering off an electron from the inner flow (Done et al., 2007). The second, a broad iron line at ∼6.4 keV. The iron line emission feature, in most cases, is thought to originate from the inner accretion disc as a result of the cold (weakly ionized) disc being irradiated by the comptonizing corona (McClintock and Remillard, 2006). Its appearance in the hard state (Miller et al., 2006a,b), which is thought to be associated with a truncated accretion disc, remains a topic of debate. For a review of relativistic iron lines from BHXRBs see Miller (2006) and for a discussion on the origins of both these features in the hard state see Done et al. (2007).

1.3.2 Soft Disc-Dominated State (SDS)

Contrary to the HCS, the spectra in the SDS, corresponding to the left most vertical of the HID (Belloni, 2009), is characterized by a dominant disc component peaking at ~ 1 keV accompanied by a weak power-law tail with $\Gamma \sim 2$, often extending past ~ 500 keV and carrying only a small portion of the power (see Figure 1.10) (Done et al., 2007).

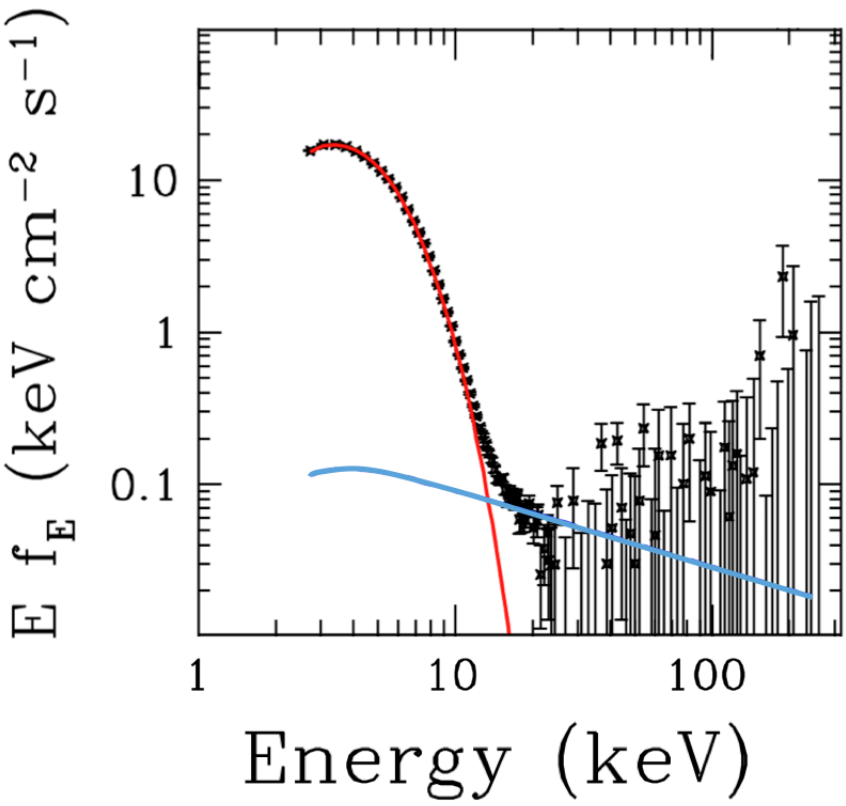

Figure 1.10: Example SDS spectra taken during the 1996/1997 outburst of GRO J1655−40. The spectrum is fit with a power-law of $\Gamma = 2.85$ (blue) and disc black body component with $T_{dbb} = 1.16$ keV (red). Figure from Remillard and McClintock (2006).

Observationally, this state is associated with high mass accretion rates, is typically seen only at high fractions of Eddington and lacks any radio emission (thought to be a result of the quenching of the radio jet in this state) (Remillard and McClintock, 2006). At these high mass accretion rates, as a consequence of the cool disc being in thermal contact with the hot flow, the hot flow will condense onto the cool disc, resulting in the optically thin flow collapsing into the Shakura-Sunyaev disc, and thus becoming optically thick. In fact, the mark of the source making the transition to the soft state is the dramatic increase in disc flux caused by the presence of an inner disc.

The mechanism for the dominant emission in this state is the geometrically thin, optically thick accretion disc extending down to the last stable orbit (ISCO). This

dominant emission from the seed photons in the disc is clearly distinct from the emission creating the high energy tail (see Figure 1.10). Such an observation allows for two possible scenarios regarding the cause of the high energy emission in this state. Either the optical depth of the inner region is very low or the region producing the high energy emission is in the form of localized active regions over and around the disc (in order to not intercept many of the seed photons).

If this tail was due to thermal Comptonization, then electron temperatures $\Theta \gtrsim 1$. Thus, to produce the proper photon index, the optical depth $\tau << 1$. The resulting spectrum would look bumpy rather than smooth due to the different Compton orders being significantly separated (see Figure 1.6b). As this type of "bumpy" spectrum is not observed, the high energy tail cannot be produced via thermal Compton Scattering and therefore must be produced via non-thermal Comptonization (see Section 1.1.3) (Done, 2010).

Finally, the most recent addition to the accretion state picture came with the discovery of another type of outflow, in the form of accretion disc winds, observed in high resolution spectra of galactic BHXRBs (Lee et al., 2002; Miller et al., 2004, 2006d,c). In contrast to the hard state strong quasi-steady relativistic jet outflows, these accretion disc winds appear to only be present in the soft state (Neilsen and Lee, 2009; Ponti et al., 2012). These winds from the outer disc have been observed to have the ability to carry away large amounts of mass (sometimes on the order of or larger then the accretion rate onto the BH, $\dot{M}_{\rm BH}$) and energy. So much so that it has been suggested that they could be the mechanism behind the quenching of the radio jet in the soft state regimes (Ponti et al., 2012).

While it has been suggested that the two outflow regimes of the hard and soft states are most likely not connected by a simple rebalancing of the same outflow power, with the wind carrying more mass but less kinetic power then that of the jet, detailed calculations of quantities such as kinetic energy, mass and momentum flux in these two types of outflows have not yet been carried out (Fender and Gallo, 2014) and as a result the physical interaction between the winds, accretion flows and jets in these systems remains not fully understood. This being said, given the observationally suggested mass flux and power of these winds and there ubiquitous appearance only

in the soft state, it stands to reason that they are perhaps a fundamental component of the accretion phenomenon (Ponti et al., 2012).

1.3.3 Intermediate State (IMS) & Steep Power-Law (SPL) State

The situation becomes far more complex during transitions between the hard and soft states. This transitional stage is often collectively referred to as the IMS.

As the source transitions from the HCS into the IMS, the X-ray luminosity increases, and the spectrum begins to change, becoming softer. The softening of the spectrum is due to two effects which happen simultaneously; the appearance of a significant thermal disc component and steepening of the hard power-law component to a photon index of $\Gamma \sim 2.0 - 2.5$ (see Figure 1.11).

Observationally, the IMS is associated with high mass accretion rates. In addition, contrary to the HCS and SDS, the spectral behaviour discussed above has been observed at both low and high fractions of Eddington. This lack of one-to-one correspondence between luminosity and state is referred to as hysteresis. However, distinguishing between these two situations is not at all trivial.

Firstly, the forward transition from the HCS to the SDS through the HIMS and SIMS need not always occur at $L_X > 0.2L_{\rm edd}$ or strictly within the SPL structure (i.e., the "dragon horn" in the top region of the HID). This transition has also been observed at $L_X < 0.2L_{\rm edd}$ in the form of a near horizontal branch in the HID (i.e., the "hornless dragon"). Secondly, while the reverse transition from the SDS to HCS always occurs at a lower luminosity then that of the forward transition, therefore allowing for clear distinction between the two, this transition also may or may not be associated with the SPL state type behaviour (see Figure 1.8).

Regardless of the above presented complicated behaviour, collectively these states usually take place on relatively short time scales (hours to days).

Much of the physics occurring during this transitional stage is largely unknown. The prevalent model (see Done (2010)), stipulates that to transition between the HCS and SDS, the mass accretion rate must increase, causing the disc to move inwards.

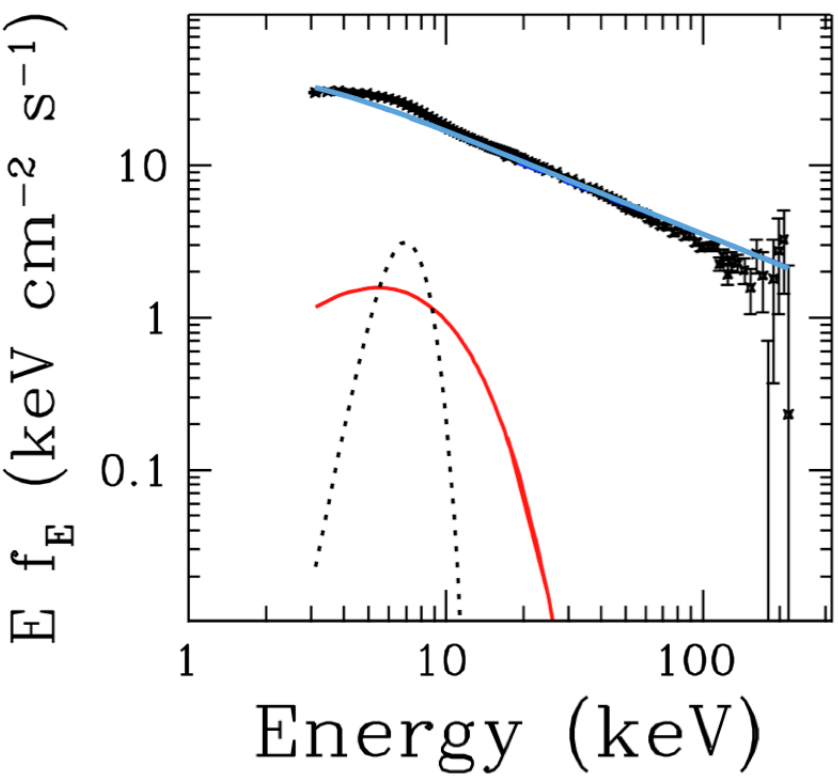

Figure 1.11: Example IMS/SPL spectra taken during the 1996/1997 outburst of GRO J1655−40. The spectrum is fit with a power-law of $\Gamma = 2.65$ (blue) and disc black body component with $T_{dbb} = 2.22$ keV (red). Figures from Remillard and McClintock (2006).

Few seed photons are intercepted by the hot inner flow when the disc is truncated the farthest from the BH, leading to a hard spectral component. As the disc moves inwards further underneath the hot flow, more disc seed photons are intercepted yielding a softer spectrum, as a result of cooler electron temperatures and a hotter disc component.

The mechanism for the high energy tail in this case proves to be much more complicated then the HCS or SDS . Spectrally, during the transition the disc is seen to merge smoothly into the high energy tail, suggesting that the hot inner region must, at some point, completely cover the disc and be optically thick. However, this high energy tail both extends past ~ 1 MeV (therefore must be due to non-thermal Comptonization) and is softer, implying a lower electron energy.

This lower electron energy, combined with an optically thick electron region suggests a situation similar to thermal Comptonization (see Section 1.1.3), where multiple scattering orders form the spectrum, only with a non-thermal distribution of electrons. Here the energy boost is small and therefore the spectrum should exhibit a rollover at the electron energy $m_e c^2 = 511$ keV (see Figure 1.12). However, this does not happen in observed spectra (see Figure 1.11), pointing to the conclusion that the high energy tail is actually produced by a combination of non-thermal and thermal Comptonization.

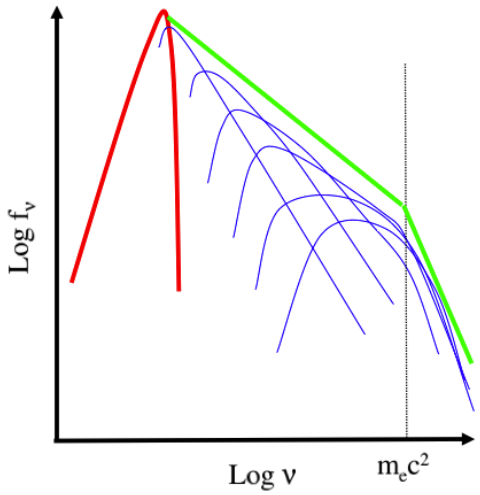

Figure 1.12: Schematic of the spectrum that would result from a non-thermal, optically thick distribution of electrons. The steep power-law spectrum (green), corresponding to a low mean electron energy, is the result of multiple inverse Compton scatterings (blue), similar to thermal Comptonization in the HCS. This type of spectrum exhibits a break at the electron energy $m_e c^2 = 511$ keV (black dotted line). Figure from Done (2010).

The fact that both non-thermal and thermal electrons are required suggests two possible geometries for the electron region. The first, a single acceleration region initially with a non-thermal distribution and as a result of scattering, a hybrid distribution caused by low energy electrons cooling through Coulomb collisions (electrons scattering off electrons) and high energy electrons cooling via Comptonization (Done et al., 2007). The second, two separate acceleration regions, one the remnant of the

hot inner flow (containing thermal electrons) and the other, magnetic reconnection regions above the disc or jet containing non-thermal electrons (Done, 2010).

Due to the optically thick electron region covering the disc in this state, it is very difficult to reconstruct the intrinsic disc spectrum, and thus model the disc component. As a result the geometry of the disc in this case remains uncertain (Done et al., 2004; Done and Kubota, 2006; Done et al., 2007).

1.4 Temporal Evolution of BHXRBs

While we have discussed in great depth the behaviour exhibited by BHXRBs during the two major stages of their life cycle, quiescence and outburst, we have not yet addressed how these two stages are connected. The transition to outburst (from quiescence) occurs as a consequence of instabilities, both thermal and viscous in nature, developing in the accretion disc causing more rapid mass transfer onto the BH, and leading to bright X-ray emission (McClintock and Remillard, 2006).

The accretion flow, at any radius of the disc, is dependent on the heating and cooling mechanisms present. A flow can be thermally unstable if small increases in temperature cause the temperature to rise further and viscously unstable, if small increases in mass accretion rate ($\dot{M}$) lead to larger increases in $\dot{M}$, causing the disc to be eaten away (Done et al., 2007).

Thermal and viscous instabilities in the disc grow on timescales of $t_{th} \sim \alpha^{-1} t_{dyn}$ and $t_{visc} \sim \alpha^{-1}(H/R)^{-2} t_{dyn}$, respectively. Hence, for a thin disc ($H/R \ll 1$), the thermal timescale is far larger than the viscous timescale allowing the thermal instability to take place without there being time to change the amount of material at a particular radius in the disc (Done et al., 2007).

1.4.1 Instabilities occurring at low $\dot{M}$

At low luminosities (and therefore low $\dot{M}$), when the material has low temperature, low opacity and is mostly neutral, the Shakura-Sunyaev disc is unstable both thermally and viscously. This unstable nature is due to the mass transfer rate onto the BH, $\dot{M}_{BH}$, being less than the mass transfer rate from the companion, $\dot{M}_{acc}$.

At temperatures correlated with the ionization of hydrogen ($10^4 - 10^5$K), small increases in temperature cause large increases in opacity as the highest energy photons on the Wien's tail of the thermal distribution ionize hydrogen in the disc. As a consequence of this process the photons are absorbed by the disc, depositing their energy in the disc and thus increasing the temperature. As the temperature increases further, more photons have the ability to ionize hydrogen.

This increase in temperature exhibited causes an increase in mass accretion rate through a particular annulus leading to the disc being eaten away at that radius and triggering the viscous instability. In fact, the ionization of hydrogen within the disc directly gives rise to this viscous instability by tying the ions to the magnetic field and therefore allowing the magnetic field lines to be dragged along with the ions movement (see Figure 1.13).

The known mechanism for the viscous instability is the MRI (Done et al., 2007). To explain how the MRI works, we present the simple analogy originally used by Balbus and Hawley (1991). Imagine that two radially neighbouring fluid elements in a differentially rotating disc located in an axial magnetic field, which has no effect on the disc equilibrium, behave like masses connected by a weak massless spring (see Figure 1.13). The inner element will rotate more rapidly than the outer element causing the spring to stretch. As spring tension is analogous to magnetic force, only a weak magnetic field is needed to begin with.

The spring will force the inner element to slow down, therefore decreasing its angular momentum and thereby moving the element to a lower orbit. Consequently, the spring will force the outer element to speed up, increasing its angular momentum, hence moving the element to a higher orbit. As the elements move further apart, the spring tension subsequently increases. This cycle will then begin again, only with the two fluid elements initially at a larger displacement (Balbus, 2003). Overall, weak magnetic fields can cause inward mass flow and outward angular momentum transport in a differentially rotating disc substantially altering the stability of the disc as a whole (Balbus and Hawley, 1991).

Eventually the temperature decreases to a point where hydrogen is allowed to recombine, triggering the thermal instability once again, only in reverse. The annulus

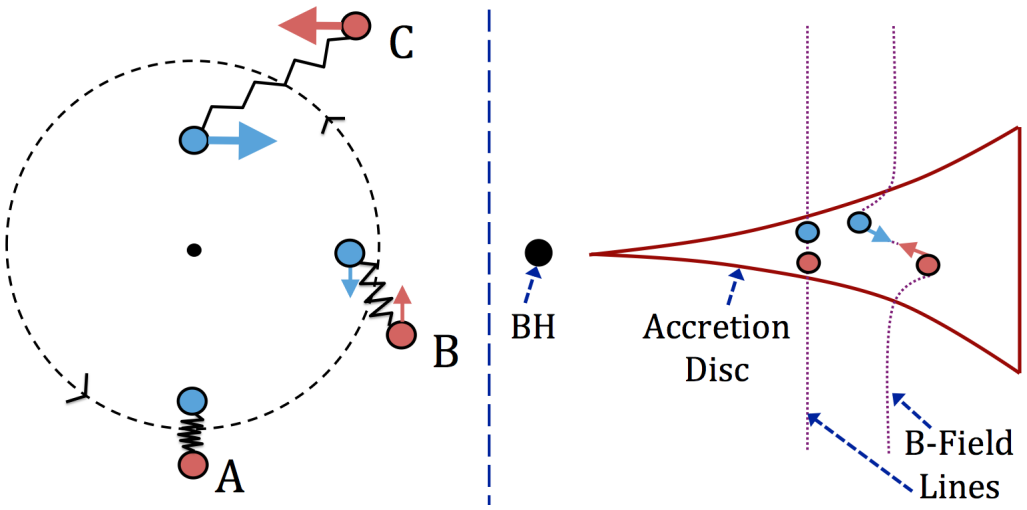

Figure 1.13: The left panel shows a mechanical representation of the Magneto-Rotational Instability (MRI), with two neighbouring fluid elements connected by a spring analogous to magnetic force in a differentially rotating disk. The inner element (blue) rotates faster than the outer element (red), the resulting force dependent only on the fluid element separation. The right panel shows the motion of the fluid elements (red and blue circles) in the accretion disc as they carry the magnetic field lines (purple line) along with them resulting in magnetic forces (red and blue arrows) from tension in the field lines. Figure adapted from Goodman (2011).

cools and subsequently the mass accretion rate, $\dot{M}_{BH}$, decreases. Eventually the material becomes completely neutral below $\sim 10^4$K. At these temperatures $\dot{M}_{BH} < \dot{M}_{acc}$, thus the disc begins to build up once more.

It is important to note that while the thermal instability is a purely local instability, discontinuous jumps in temperature and $\dot{M}_{BH}$ have the ability to effect the next annulus in the disc, therefore having a global affect on the disc as a whole (Done et al., 2007).

1.4.2 Instabilities occurring at high $\dot{M}$

The Shakura-Sunyaev disc can exhibit instabilities at high mass accretion rates as well. The radiation pressure instability occurs when the disc switches from being dominated by gas pressure, $P_{gas} \propto T$, to dominated by radiation pressure, $P_{rad} \propto T^4$, causing a rapid increase in temperature (Done et al., 2007).

Similar to the role of opacity in the hydrogen ionization instability, energy being carried with the flow to the next annulus, and lost through radiation, acts as a cooling mechanism to balance the increase in temperature (Abramowicz et al., 1988) allowing for the same thermal-viscous cycle described within the hydrogen ionization instability to occur. However, unlike the hydrogen ionization instability, this local instability only propagates in the inner, radiation pressure dominated part of the disc (Done et al., 2007).

1.4.3 The Disc Instability Model

Now that we have all the required tools at our disposal, we can finish our discussion of BHXRBs by summarizing the observed outburst mechanism via the disc instability model (DIM) (Lasota, 2001).

A quiescent disc is built up due to steady mass transfer from the companion, either as a result of RLO in LMXBs or winds in the case of HMXBs. Eventually the disc temperature will rise high enough to trigger the hydrogen ionization instability at a certain radius. The increased temperature, and hence increased $\dot{M}_{BH}$, increases $\dot{M}_{BH}$ in the next disc radius. The result is a heating wave that propagates inwards and/or outwards through the disc (Lasota, 2001; Done et al., 2007).

Irradiation from the inner disc may initially be strong enough to keep even the outer parts of the disc hot, despite the high mass accretion rate eating away at the disc ($\dot{M}_{BH} > \dot{M}_{acc}$) (van Paradijs, 1996). As the disc is eaten away, the temperature and mass accretion rate through the disc are pulled down, weakening the X-Ray irradiation. The outer disc is now able to drop below the hydrogen ionization temperature triggering a cooling wave that propagates through the disc.

If the whole disc is irradiated, the characteristic exponential decay will be observed (creating the classic Fast Rise Exponential Decay (FRED) type light curve). Eventually the irradiation weakens enough for the outer part of the disc to drop below the hydrogen ionization temperature, bringing it back to quiescence. On the other hand, linear decays are also possible when only part of the disc is irradiated. In this case, the cooling front cannot move inward on a viscous timescale as the farthest it can move inward is set by the radius of the irradiated region (King and Ritter,

1998; Lasota, 2001; Done et al., 2007).

While the DIM provides a comprehensive picture explaining the processes behind the transition from quiescence to outburst and vis versa, and the established theoretical stable accretion flow models supply us with a mechanism for the emission we see, the physical parameter(s) which actually drive the critical instability that dictates state transitions remain largely unknown.

1.5 Goals of Thesis

Enumerating the frequency at which outbursts occur and quantitatively classifying the wide range of behaviour exhibited during outburst is critical to furthering our understanding of the physical mechanisms driving mass-transfer in BHXRBs and a key step toward filling in the many gaps in our knowledge of how BHXRBs form, accrete and evolve.

Currently, a major portion of the behaviour observed during outburst in Galactic BHXRBs does not fit into the widely accepted theoretical framework. Contrary to the existing canonical picture (Fender et al., 2004, 2009; Fender and Gallo, 2014), a number of transient systems have either remained in the HCS (Harmon et al., 1994b; Hynes et al., 2000b; Belloni et al., 2002a; Brocksopp et al., 2001, 2004; Aref'ev et al., 2004; Sturner and Shrader, 2005; Brocksopp et al., 2010b; Sidoli et al., 2011; Curran and Chaty, 2013) or only transitioned as far as the IMS (Wijnands and Miller, 2002; in't Zand et al., 2002b; Capitanio et al., 2009a; Ferrigno et al., 2011; Reis et al., 2012; Soleri et al., 2012; Zhou et al., 2013; Curran et al., 2014) during outburst, never fully reaching the softer states.

Interestingly enough, this particular class of behaviour has also been exhibited by a fair number of persistently accreting systems as well. In their case, either spending long continuous periods of time in the HCS (Churazov et al., 1993; Main et al., 1999; del Santo et al., 2004; Pottschmidt et al., 2006; Soleri et al., 2012; Shaw et al., 2013; Froning et al., 2014) or periodically undergoing "failed" state transitions (Pottschmidt et al., 2003; Soleri et al., 2012), in which an attempt to reach the soft states is never fully accomplished.

When a source (whether transient or persistent) fails to transition, it does not reach the higher luminosities and larger $\dot{M}$ which characterize the softer states. As a result these so called "failed" outbursts tend to be far less luminous compared to canonical outbursts (Curran and Chaty, 2013) and therefore should have a significant effect on the mass-transfer history of the Galactic BHXRB population.

Using today's more sensitive X-ray instruments, which have given us the ability to probe the transient X-ray Universe in greater depth than ever before, we have set out to establish a comprehensive database of BH and Black Hole Candidate (BHC) outburst activity over the last 18 years, combining measurements by the all-sky monitors (ASMs) of Swift Burst Alert Telescope (BAT), Monitor of All-Sky Image (MAXI) and Rossi X-ray Timing Explorer (RXTE) as well as the X-ray scanning surveys of RXTE Proportional Counter Array (PCA) and INTErnational Gamma-Ray Observatory (INTEGRAL), thus allowing us to probe both a wide X-ray energy range and large area of the sky.

The following All-Sky Observational study includes:

- a catalog of the BH and BHC sources existing in the Galaxy;
- accumulated background of binary system properties (past and currently accepted);
- archive of detections across radio, optical, IR and X-ray wavelengths;
- complete outburst history of the population, including temporal evolution, recurrence rates, duty cycles, state transitions and empirical classification via X-ray hardness and disc fraction; and
- complete mass transfer history of the population, including a comprehensive study of outburst luminosities, X-ray Luminosity Functions (XLFs), evolution of $\dot{M}$ over the last 18 years and an empirical inquiry into the relationship existing between $\dot{M}$ and the orbital parameters of the system.

With this accumulated database we have the opportunity to not only quantify and classify both canonical and anomalous outburst behaviour exhibited by BHXRBs,

but also study the impact it has on the physical observables of individual systems alone and thus the universal properties of the Galactic population as a whole.

Chapter 2

A Census of Galactic Black Holes & Black Hole Candidates

2.1 Selection Criteria

To date, there exist numerous catalogues of XRBs (see Bradt and McClintock 1983; van Paradijs and McClintock 1995; Liu et al. 2000, 2001, 2006; Liu and van den Heuvel 2007). With the advent of more sensitive all sky and scanning survey X-ray instruments allowing the transient X-ray universe to be probed in greater depth, we are detecting a larger number of sources than ever before, culminating in the currently published catalogues quickly becoming antiquated. As an example, the Swift/BAT transient monitor alone has detected over 245 sources over the last 8 years, 17 of which were previously unknown and discovered by the transient monitor itself (Krimm et al., 2013b).

In addition to these catalogues, there also exists a copious amount of comprehensive reviews on BHXRBs and X-Ray Novae (XRN) in the literature (see Tanaka and Lewin (1995); Tanaka and Shibazaki (1996); McClintock and Remillard (2006)). For recent global X-ray spectral studies of BHXRBs see Gierlinski and Newton (2006); Remillard and McClintock (2006); Dunn et al. (2009); Fender (2009); Belloni (2009); Gilfanov (2009). However, the majority of these studies contain outdated jargon, and offer only a sampling of the sources exhibiting the well defined canonical behaviour

as observed by one telescope, often focussing on finding examples to illustrate the theory.

As a result, while invaluable references, the aforementioned compilations are incomplete and out of date. As such we have set out to build a much needed update to the current picture in the form of a fully functioning modern BHXRB database, accumulating the history of Galactic BH and BHC sources over the past 18 years.

To begin, we have compiled a sample of 76 XRB sources existing in the Galaxy. This sample has been built from the:

- McClintock & Remillard Reviews (McClintock and Remillard, 2006; Remillard and McClintock, 2006);
- Most recent versions of the Low-Mass (LMXBCAT; Liu and van den Heuvel (2007)) and High-Mass (HMXBCAT; Liu et al. (2006)) X-ray Binary Catalogues;
- Jet Acceleration and Collimation Probe of Transient X-ray Binaries[1] (JACPOT XRB) project monitoring list;
- Swift/BAT Transient Monitor[2] BH Source List; and
- Sources listed in the Astronomers Telegram[3] (ATel) with a BH keyword, which have not been shown to be a pulsar or Active Galactic Nuclei (AGN).

2.2 The Galactic Population

Of the 76 sources included in our sample, 66 are classified as transient, while the remaining 10, which have been observed to remain perpetually bright for periods of > 2 years in length, are classified as persistent. In the following Section, in ascending order of right ascension (J2000) of each source, we provide:

- a brief summary on X-ray discovery;

[1] http://www.astro.virginia.edu/xrb_jets/index.html
[2] http://swift.gsfc.nasa.gov/results/transients/
[3] http://www.astronomerstelegram.org/

- an outline of optical/IR, radio and X-ray detection;
- an overview of the outburst history/long-term behaviour;
- a summary of spectral and timing characteristics exhibited during outburst;
- a discussion on the past estimates and currently accepted orbital parameters found through dynamical studies of the system; and
- a justification of BH or BHC status.

Our sample contains 20 dynamically confirmed BH sources, 17 of which are LMXBs and 3 which are HMXBs. In this case, either the value of the mass function $f(M)$ far exceeds $\sim 3M_{\odot}$, the widely agreed upon limit for the maximum stable mass of a neutron star (NS) in General Relativity (Kalogera and Baym, 1996), or dynamical studies have allowed for the measurement of a complete set of orbital parameters, namely $f(M)$, q, and i, and therefore a definitive estimate of black hole mass $M_{\rm BH}$.

The remaining 56 sources are classified as BHCs, including 37 LMXBs, 8 HMXBs, and 12 undetermined systems. These sources either lack radial velocity data, have no known optical counterpart or, in some cases, have not been well studied at any wavelength. Nevertheless, we can still hypothesize the nature of the primary in these systems based on X-ray spectral and timing behaviour in tandem with radio characteristics (McClintock and Remillard, 2006).

At this point we must caution the reader. While compiling our sample and for the sake of completeness, we have taken a very liberal approach in determining source membership in the BHC class, contrary to many previous compilations. As such, there are sources that are far more likely to contain a BH primary than others. Nevertheless, we believe the few discrepancies we may have are justified in the interest of providing a complete sample of the BH and BHC systems in the Galaxy.

Given our liberal identification of BHCs, we have divided our sample into three separate classes,

- Class A (BHs): dynamically confirmed BHs,

- Class B (BHCs): very likely BHs, and
- Class C (BHCs): less likely BHs.

Class A contains the 20 known dynamically confirmed BH sources. Class B contains those sources that clearly have BH-like spectra (e.g., an ultra-soft spectrum; not just an observed soft-hard transition as this behaviour is exhibited in NSs as well; Muñoz-Darias et al. (2014)) and Quasi-Periodic Oscillation[4] (QPO; timing) properties, and/or radio/X-ray behaviour typical of BHs (i.e., micro-quasar/relativistic jet behaviour). While Class C includes those sources that have been shown to most likely be Galactic XRBs but only have weak supporting evidence for a BH primary.

For a summary of primary source information, orbital parameters and binary system information see Tables A.1 and A.2.

2.2.1 XTE J0421+560

The X-ray transient XTE J0421+560 was discovered by the All-Sky Monitor (ASM) aboard RXTE, when it underwent its first and only outburst in 1998 (Smith et al., 1998a). The outburst peaked first in X-rays followed by optical and radio wavelengths, a behaviour commonly associated with XRN. In addition several soft X-ray flares were observed after the initial flare (Frontera et al., 1998). The optical counterpart, CI Cam, has been classified as a B0-2 supergiant B[e] star (Robinson et al., 2002), therefore establishing the system as a HMXB.

Unfortunately there have been significant obstacles in determining the nature and behaviour of this system, mainly due to the uncertainty in distance, with distance estimates ranging from 1–17 kpc (Bartlett et al., 2013). As a result the X-ray luminosity is poorly constrained. If the distance is >2 kpc, the resulting X-ray lumi-

[4]Timing studies involve tracking variability existing within the accretion disc. The tool commonly used for probing this fast variability is called the power-density spectrum (i.e., the Fourier power spectrum of the X-ray flux time series). The narrow (finite width) peaks within this power-density spectrum (usually described with a Lorentzian $P_\nu \propto \lambda/[(\nu-\nu_0)^2+(\lambda/2)^2]$ of centroid frequency ν_0 and full width half maximum λ), referred to as QPOs, have been linked to major behavioural changes occurring during state transitions in BHXRBs (McClintock and Remillard, 2006). For a detailed discussion on X-ray timing analysis and QPOs, see van der Klis (2006) and Belloni et al. (2002b).

nosity would indicate the presence of a compact object (Neutron Star (NS) or BH) (Belloni et al., 1999a). While a closer distance would point toward a white dwarf accretor (Orlandini et al., 2000; Ishida et al., 2004). Despite the uncertainty in its nature we include this system in our BHC sample because its X-ray properties are similar to known BHXRBs.

2.2.2 GRO J0422+32

GROJ0422+32 is an LMXB discovered in 1992 by BATSE on board the Compton Gamma-ray Observatory (CGRO) when it underwent a FRED type outburst (Paciesas et al., 1992). The spectrum of this outburst was well described with a hard power-law (Sunyaev et al., 1994) and timing analysis revealed properties commonly associated with the HCS (van der Hooft et al., 1999b), ultimately pointing to the conclusion that this was in fact a "failed" outburst. The source has since undergone two additional unusual mini-outbursts in 1993, which were not detected in the hard X-rays (Shrader et al., 1997; Callanan et al., 1995).

This system has been shown, through rigorous determination of binary parameters, to contain a BH primary (Filippenko et al., 1995; Casares et al., 1995b) and an $M2^{+2}_{-1}V$ optical counterpart (Harlaftis et al., 1999; Webb et al., 2000). The detection of a radio counterpart and evolution of its spectrum is discussed by Shrader et al. (1994). The distance to this source is relatively well constrained. We adopt the distance derived by Gelino and Harrison (2003).

There has been numerous discussions on the inclination of GRO J0422+32. Orosz and Bailyn (1995); Gelino and Harrison (2003); Reynolds et al. (2007); Filippenko et al. (1995) all estimate $i > 45^{\circ}$. However, (i) the light curve of Orosz and Bailyn (1995) exhibits shape changes between two different nights and a difference in mean I magnitude of 0.05 suggesting it is probably in the active state, (ii) Gelino and Harrison (2003) and Reynolds et al. (2007) find similar mean magnitudes in the H and K light curves, but because there is evidence for IR disc contamination in the former and no detection of ellipsoidal variability in the light curves of the latter, the conflicting results suggest both authors light curves are in the active state and, (iii) while Filippenko et al. (1995) find an $i = 48 \pm 3^{\circ}$, which is consistent with the above

three results, they assume a normal mass M2V secondary.

As discussed in Kreidberg et al. (2012), having active state light curves or normal mass secondary stars are two situations that can only give us lower limits on inclination. In contrast there are also several authors who find an $i < 45^\circ$ including Casares et al. (1995a); Callanan et al. (1996); Beekman et al. (1997). However, all three make use of binned light curves. Given the significant variability exhibited by this source, the act of binning light curves may flatten their shape, therefore implying a lower inclination. Given the above arguments, we adopt the value of inclination calculated by Kreidberg et al. (2012) by adjusting the $i = 45^\circ$ value assuming the source is active. We adopt a $M_{\rm BH}$ calculated using this corrected inclination.

2.2.3 4U 0538−641

Commonly known as LMC X−3, this system was discovered by the UHURU satellite in 1971 (Leong et al., 1971). LMC X−3 is one of three known persistently accreting BHs (McClintock and Remillard, 2006). Given the large mass function, the absence of X-ray eclipses[5] and an estimated mass of the established B3V optical counterpart, Cowley et al. (1983) (and later Kuiper et al. (1988)) was able to calculate a lower limit on the mass, thereby confirming the presence of a BH (Orosz et al., 2014).

LMC X−3 is a very unusual system. While it almost continuously maintains itself in a bright state much like the persistent HMXB wind-fed systems, the BH is actually fed by RLO, resulting in a highly variable X-ray intensity similar to transient systems (Steiner et al., 2014). The X-ray spectrum is nearly constantly thermal and disc-dominated as the system has been observed to spend most of its time in the SDS (Treves et al., 1988; Ebisawa et al., 1993; Nowak et al., 2001) with the occasional transition to the HCS (Wilms et al., 2001; Smale and Boyd, 2012). Due to its membership in the Large Magellanic Cloud (LMC) (Cowley et al., 1983), the distance is well constrained.

Recently, Orosz et al. (2014) established a new dynamical model for the sys-

[5]X-ray eclipses occur when the compact object is periodically eclipsed by the companion star, thus causing X-rays to be cut off from the point of view of the observer (White et al., 1995).

tem. More high quality radial velocity data (yielding improved determination of K-velocity) and an accurate measurement of the projected rotational velocity for the companion star, along with a much larger array of ellipsoidal light curve data to analyze, has yielded a more precise $M_{\rm BH}, q$ and i than previous studies. We therefore adopt the dynamical model parameters from Orosz et al. (2014) in this study.

2.2.4 4U 0540−697

Commonly known as LMC X−1, this HMXB system was the first X-ray source to be discovered in the Magellanic Clouds (Mark et al., 1969). LMC X−1 is among the three known persistently accreting BHs (McClintock and Remillard, 2006). Spectroscopic studies of the optical counterpart (Hutchings et al., 1983, 1987) revealed a probable mass for the system, establishing it as a firm BHC. However, the presence of a BH in this system was not confirmed until an accurate measurement of the mass function was made (Haardt et al., 2001) following accurate identification of its X-ray location (by ROSAT observations) and, subsequently, optical counterpart (an O7 giant) (Cowley et al., 1995).

Similar to LMC X−3, LMC X−1 has been observed to spend most of its time in the SDS (Ebisawa et al., 1993; Nowak et al., 2001). Given its membership in the LMC (Cowley et al., 1983), the distance to the system is well determined (Freedman et al., 2001).

More recently Orosz et al. (2009) have improved upon the basic dynamical model and principal conclusions presented by Hutchings et al. (1987). High and medium resolution spectra has reduced the uncertainty in radial velocity amplitude K by a factor of 6 and allows for a secure value of rotational line broadening to be obtained. Additionally they present the first optical light curves and infrared magnitudes and colours of LMC X−1, allowing them to put a strong constraint on inclination of the system. This inclination, along with improved measurements of the orbital period as well as temperature and radius of the companion star, has allowed for an improved dynamical model of the system. We therefore adopt the dynamical model parameters from Orosz et al. (2009) in this study.

2.2.5 IGR J06074+2205

IGR J06074+2205 is a transient X-ray source discovered by JEM-X aboard INTEGRAL when it underwent a short flare between February 15 and 16 of 2003 (Chenevez et al., 2004). Halpern and Tyagi (2005) first suggested that the optical counterpart was a Be star. Tomsick et al. (2006) were able to localize the X-ray source with Chandra, and spectrally confirm that IGR J06074+2205 was a BeXB, in turn suggesting its HMXB nature. Using optical photometry and spectroscopy, Reig et al. (2010) are able to determine the spectral type of the optical counterpart to be a B0.5Ve star.

They derive a colour excess and estimate a distance of ∼4.5 kpc. However, they caution that this distance should only be taken as a lower limit because the photometric magnitudes were obtained when the source was displaying a high value of EW[6](Hα). In the absence of the disc, the colour (B−V) is expected to be smaller (or bluer), resulting in a lower colour excess and a longer distance. Due to this uncertainty in the distance estimate we instead choose to use our standard assumption of 3–8kpc[7].

Little else is known about the physical parameters of this system, including the nature of the compact object. While the majority of known BeXBs contain neutron stars, Casares et al. (2014) recently found the first BeXB containing a BH. Casares et al. (2014) estimates the luminosities of these types of systems to be $\sim 1.6 \times 10^{-7}$ $L_{\rm edd}$, therefore making such systems difficult to detect via conventional X-ray surveys and providing a reason as to why we may have not detected more of these types of systems. In addition, the source is included on the Swift/ BAT Transient Monitor BH source list, as ATels list the source with the BH keyword, and it has been shown

[6]The Equivalent Width (EW) measures the total strength of an absorption line and is defined as $W_\nu = \frac{\int_{\rm line}(F_c - F_\nu)d\nu}{F_c}$, where F_ν is the flux of the line at a wavelength ν and F_c is the flux of the continuum. As the line only covers a small range of wavelengths, F_c is considered constant, resulting in W_ν being the width of the absorption line if the line profile was a rectangle. For a discussion of EW in both the optically thin and thick cases, see Kwok (2007).

[7]When a sufficiently accurate distance estimate can not be found in the literature we implement a standard estimate of 3–8 kpc instead. This range was chosen as most Galactic BH/BHC with adequate distance estimates lie in this range.

to not be a pulsar nor AGN. For the aforementioned reasons we include this source as a possible Galactic BHC in our sample.

2.2.6 1A 0620−00

The X-ray transient 1A 0620−00 was discovered by the Ariel V Satellite during an outburst in 1975 (Elvis et al., 1975). A radio counterpart was detected almost two weeks after the beginning of the outburst, remaining visible for approximately one week (Owen et al., 1976). Kuulkers et al. (1999) collected all available data from the 1975 outburst and subsequently found multiple (jet) ejections with expansion velocities in excess of 0.5c, a type of behaviour now commonly associated with BHXRB systems (McClintock and Remillard, 2006). After the source returned to quiescence in 1976, a second outburst, occurring in 1917, was discovered on photographic plates at the Harvard College Observatory (Eachus et al., 1976).

Oke (1977) identified the optical counterpart as a K5 dwarf. Both the brightness and mass of the optical counterpart motivated a radial velocity study, leading to the measurement of the mass function and solidifying 1A 0620−00 as a strong BHC (McClintock and Remillard, 1986).

As we have discussed in Section 1.1.2, a precise determination of the mass of the BH primary is highly dependent on an accurate estimation of the inclination of the system (Cantrell et al., 2010). Many attempts have been made to measure inclination of the system; Haswell et al. (1993) found $i > 62°$, Shahbaz et al. (1994a) found $i = 36.7°$, Marsh et al. (1994) found $i = 37°$, Gelino et al. (2001b) found $i = 40.8°$ and Froning and Robinson (2001) found a wide range of inclinations ($38° < i < 75°$) corresponding to different epochs of data. Overall inclination estimates remained inconsistent at best. The reasons for this inconsistency stem from highly asymmetric ellipsoidal variations in the light curve (Leibowitz et al., 1998) and contamination of the K-star flux by light from the accretion disc (Neilsen et al., 2008).

Cantrell et al. (2010) rectify these issues, making use of an extensive data set spanning a decade from the SMARTS consortium. They restrict their sample to light curves which are in the passive state (i.e., minimal aperiodic variability) and those where the NSL fraction and magnitude calibration are well constrained, and

require each light curve to maintain the same shape over its duration. As a result of fitting an 11 parameter model to the 8 remaining light curves, they estimate a weighted average of $i = 51° \pm 0.9°$. We assume this value to be unbiased by systematic error (Kreidberg et al., 2012), and use this inclination along with $M_{\rm BH}$ inferred from it in our calculations. We also adopt the distance estimated by Cantrell et al. (2010), using their dynamical model, in our analysis.

2.2.7 GRS 1009−45

GRS 1009−45 was discovered simultaneously by the WATCH ASM aboard the GRANAT satellite (Lapshov et al., 1993) and BATSE aboard CGRO (Harmon et al., 1993b). The source was shown to have a ultra-soft spectrum typical of BHXRB systems (Kaniovsky et al., 1993). Soon after the outburst, della Valle and Benetti (1993) discovered a blue optical counterpart, which would later be shown to have a spectral type of G5-K7 (della Valle et al., 1997; Filippenko et al., 1999). Further optical photometry conducted approximately 6 months after the primary outburst revealed a secondary outburst, followed by a series of "mini-outbursts", reminiscent of the behaviour exhibited by BH XRN systems like GRO J0422+32 (Bailyn and Orosz, 1995).

While Filippenko et al. (1999) are able to obtain a mass function and mass ratio, their estimation of inclination is based on the assumption that the secondary is a K7–K8 star that is not under massive. The only analysis of ellipsoidal variability is found in Shahbaz et al. (1996b). However, because the light curve shows clear evidence of a significant non-stellar contribution and the star-only model fit yields a large χ^2, the light curve is likely active.

While it is important to note that this result conflicts with Filippenko et al. (1999) there is still some ambiguity regarding the spectral type of the secondary. Assuming the secondary is in fact a G5V star, as suggested by della Valle et al. (1998), Kreidberg et al. (2012) find a lower limit on inclination consistent with their corrected estimate. We therefore adopt this inclination in our calculation of $M_{\rm BH}$.

While there exists a number of distance estimates for this source, Hynes (2005) discusses why the estimate by Gelino (2002) is believed to be the most thorough and

reflective of the most up to date parameter estimates for the system. We therefore adopt this estimate in our calculations.

2.2.8 XTE J1118+480

XTE J1118+480 was discovered by the ASM aboard RXTE in 2000 as a weak, slowly rising X-ray source (Remillard et al., 2000). Within a few days of discovery, both optical (Uemura et al., 2000b,a) and radio (Pooley and Waldram, 2000) counterparts were found. Strong low-frequency variability and a spectra dominated by a hard power-law component extending past 100 keV (Revnivtsev et al., 2000a), accompanied by a radio spectrum, which was persistently inverted (Hynes et al., 2000b), were characteristics indicative of a BHC in the HCS (Fender et al., 2001).

This outburst lasted ∼7 months and exhibited some complex behaviour. After the first peak in January of 2000 (Remillard et al., 2000; Wren and McKay, 2000), the source decayed only to re-brighten to a plateau state (of similar brightness to the first peak (Uemura et al., 2000a)) for ∼ 5 months (Brocksopp et al., 2010b). XTE J1118+480 remained in the HCS for the duration of the outburst, placing it in the class of "failed" outburst sources (Brocksopp et al., 2004; Zurita et al., 2006).

The second outburst of this source was discovered in the optical (Zurita et al., 2005) and later confirmed by X-ray and radio observations (Remillard et al., 2005; Pooley, 2005) in 2005. Observations with RXTE would confirm, that much like the 2000 outburst, the source once again remained in the HCS for the duration of the outburst (Swank and Markwardt, 2005; Zurita et al., 2006). However, unlike the 2000 outburst, the 2005 event exhibited behaviour more typical of a soft X-ray transient, with short lived jet ejections, a more dominant disc component to the spectrum and a FRED type light curve (Brocksopp et al., 2010b).

Dynamical measurements establishing a very large mass function ($> 6M_{\odot}$), confirmed a BH primary in this system (McClintock et al., 2001a; Wagner et al., 2001). Numerous observations of the system in quiescence has allowed for refinement of system parameters (Gelino et al., 2006; Gonzalez Hernandez et al., 2008), however, estimates of inclination have proven more challenging. While the consensus in the literature is that XTE J1118+480 has a high inclination, being able to make an accu-

rate measurement is challenging due to strong super hump modulation[8] in addition to ellipsoidal variability (Zurita et al., 2002), and a large and variable NSL fraction (Wagner et al., 2001). The inclination measurements made by Wagner et al. (2001), McClintock et al. (2001b), Zurita et al. (2002) and Gelino et al. (2006) all lie in the range $68^\circ < i < 82^\circ$. While all of these estimates are consistent with each, other none are free of significant systematic errors (Kreidberg et al., 2012). Therefore, we adopt the full range of inclinations in our calculation of $M_{\rm BH}$. We adopt the distance derived by Gelino et al. (2006) using their established dynamical model.

2.2.9 GS 1124−684

The X-ray nova GS 1124−684 was simultaneously discovered by the ASM aboard the GINGA satellite (Makino and the Ginga Team, 5161) and the WATCH ASM aboard GRANAT (Lundt and Brandt, 1991) in 1991. Following discovery, GS 1124−64 was observed extensively across broadband frequencies from radio to hard X-rays (Kitamoto et al., 1992). The fact that this source displayed X-ray spectra and decay timescales similar to 1A 0620−00 (della Valle et al., 1991; Kitamoto et al., 1992), a known BH (McClintock and Remillard, 1986), coupled with the determination of orbital period and radial velocity curve of the secondary by Remillard et al. (1992), effectively established the primary as a dynamical BHC . Orosz et al. (1996), with an additional 3 years of observation in quiescence, further refined system parameters allowing for a determination of the mass function, spectral type of the secondary and inclination.

While this estimation of inclination is both higher and less precise than the estimate in Gelino et al. (2001a), there is clear evidence for non-stellar flux in the IR (Gelino et al., 2010) when the source was active. Even though the source may have been passive during the time of the Gelino et al. (2001a) observations in February 2001, this does not guarantee a negligible NSL fraction. The Orosz et al. (1996)

[8] "Superhumps" are variations in the optical light curve at a period close to that of the orbital period of the system, effectively distorting its shape. They are caused by the precession, within the binary, of an eccentric accretion disc, resulting in intrinsic variations in light observed from the disc (Charles and Coe, 2006). For discussion of superhumps in LMXBs, see Haswell et al. (2001).

estimate is also higher than that of Shahbaz et al. (1994a). However, their best fit inclination has a large χ^2 suggested to be the result of incorrect sky subtraction. For these reasons, following Kreidberg et al. (2012), we adopt the inclination range given in Orosz et al. (1996) in our calculation of $M_{\rm BH}$.

Using infrared photometry, corrected for reddening, Gelino et al. (2001a) find a distance of $\sim$ 5.1 kpc. While they do not quote uncertainty, this measurement has since been refined by Gelino (2001) with simulations. Hynes (2005) discuss why this estimate is believed to be the most thorough and reflective of the most up to date parameter estimates for the system. We therefore adopt this distance in our calculations.

2.2.10 IGR J11321−5311

The transient hard X-ray source IGR J11321−5311 was discovered by ISGRI aboard INTEGRAL in 2005 during a short flare lasting $\sim$ 3.5 hours (Krivonos et al., 2005). During this time the source exhibited a very hard spectrum with no evidence for a break up to 300 keV (Sguera et al., 2007). Krivonos et al. (2005) suggest that the spectrum is reminiscent of a BHXRB. Therefore, we include this source in our sample as a possible BHC. Little else is known about this system and no other detections at other wavelengths are available.

2.2.11 MAXI J1305−704

The X-ray transient MAXI J1305−704 was discovered by the Gas Split Camera (GSC) aboard MAXI in 2012 (Sato et al., 2012). This source was proposed to be a BHXRB based on X-ray and optical spectra as well as light curve and hardness variations over time (Greiner et al., 2012; Kennea et al., 2012b; Suwa et al., 2012; Morihana et al., 2013). Kennea et al. (2012a,d) observed dip like features and Miller et al. (2012a,b) observed possible absorption line features. These dips and absorption profiles provide a strong indication that this source has a large inclination (Shidatsu et al., 2013).

Shidatsu et al. (2013) are able to identify a 9.74 hr orbital period from the recurrence interval between absorption dips and infer an inclination between $60^\circ < i < 75^\circ$, with the most likely value being $\sim 75^\circ$ as the source shows dips but no eclipses. A precise value of inclination has not yet been determined and little else is known about the system parameters.

2.2.12 Swift J1357.2−0933

Swift J1357.2−0933, a new galactic BHC (Casares et al., 2011), was discovered by the Swift BAT in January of 2011 when it went into outburst (Krimm et al., 2011a). The source remained in the HCS for the duration of the outburst, classifying it as a "failed" outburst source (Armas Padilla et al., 2013a). Both the X-ray spectrum (Krimm et al., 2011c) and the magnitude difference (between quiescence and outburst) of the detected optical counterpart (Rau et al., 2011b) pointed to a LMXB nature.

Based on photometry from the Archival Sloan Digital Sky Survey (SDSS) it was suggested that this source contained an M4 counterpart (Rau et al., 2011b; Shahbaz et al., 2013). The distance is debatable. While Corral-Santana et al. (2013) suggest 1.5 kpc, Shahbaz et al. (2013) estimate the magnitude of the companion (which was not detected) and combine it with the expected magnitude of an M4.5V star to infer a possible distance range from 0.5−6 kpc.

Armas Padilla et al. (2013a) calculate the peak luminosity for the outburst (assuming a distance of 1.5 kpc) to be $L_{\rm X} = 1.1 \times 10^{35}$ergs s^{-1}, making it the only confirmed BH Very Faint X-ray Transient[9] (VFXT) (Armas Padilla et al., 2013a; Corral-Santana et al., 2013). Armas Padilla et al. (2013a) also note that even if the source was at a distance of 8 kpc, which is unlikely due to its high galactic latitude, the peak $L_{\rm X}$ would be on the order of a few times 10^{36}ergs s^{-1}, which is still in the faint regime.

Corral-Santana et al. (2013) establishment of $M_{\rm BH} > 3.6{\rm M}_\odot$ combined with the

[9]VFXTs are classified as systems with a peak (2−10 keV) $L_X \sim 10^{34} - 10^{36}$ergs^{-1} (Wijnands et al., 2006).

slow observed evolution in the hard spectral state, evidence for QPOs at frequencies ranging from ∼1–9 Hz and continuum power between ∼ 10 and 25 %, strongly suggests a BH accretor (Krimm et al., 2013b). Corral-Santana et al. (2013) also find an orbital period of 2.8 hours and presented an observation of intense dips in the optical light curve, which they explained as toroidal structure in the inner region of the disc, seen at high inclinations ($i \geq 70^{\circ}$), moving outward as the outburst progressed, implying we may be observing the system close to edge on. In addition, Shahbaz et al. (2013) find evidence for quiescent optically thin synchrotron emission, which they discuss could possibly arise from a jet in the system.

2.2.13 GS 1354−64

In 1987 the ASM aboard the GINGA Satellite discovered GS 1354−64 in outburst (Makino, 1987). The X-ray spectra was well fit with soft disc black body and hard power-law components (Kitamoto et al., 1990b) typical of X-ray transient outbursts and suggestive of a BH nature (Brocksopp et al., 2001). The position of GS 1354−64 is consistent with two other transient sources, Cen X−2 (Francey, 1971) and MX 1353−64 (Markert et al., 1979), which have been observed in outburst in 1967 and 1972, respectively. Both sources show different X-ray spectral properties than the 1987 outburst of GS 1354−64. If all three were in fact the same source, then GS 1354−64 must show at least four different spectral states (Kitamoto et al., 1990b). Brocksopp et al. (2001) argue that this is not unfeasible as sources such as GX 339−4 routinely show this multiple state behaviour during outburst (McClintock and Remillard, 2006). We therefore assume all three are in fact the same source.

GS 1354−64 was again observed in outburst in 1997 (Revnivtsev et al., 2000c; Brocksopp et al., 2001). During this time, optical (Castro-Tirado et al., 1997), infrared (Soria et al., 1997) and radio (Fender et al., 1997c) counterparts were detected. The radio source was unfortunately too faint to detect extended structure. However, analysis of the radio spectra showed a weak flat synchrotron spectrum, which suggested possible mass ejections in the form of a jet (Brocksopp et al., 2001).

While the first and third outbursts of GS 1354−64 show very soft X-ray spectra (Brocksopp et al., 2001, 2004), the second and fourth events display spectra domi-

nated by a hard power-law, typical of XRBs in the hard state, indicating the source "failed" to reach the softer states in these cases (Revnivtsev et al., 2000c; Brocksopp et al., 2001).

Casares et al. (2004) obtain the first radial velocity curve of the optical counterpart, BW Cir, identify its spectral type, mass ratio, period and in turn a mass function of $f(M) = 5.75 \pm 0.30 M_{\odot}$, confirming a BH primary. Casares et al. (2009) infer a lower limit on the distance of 25 kpc (from the companion's luminosity) and estimate an upper limit of 61 kpc (assuming a 10 $M_{\odot}$ BH) from calculations by Kitamoto et al. (1990b). We take the distance to be a uniform distribution between 25 and 61 kpc for the purpose of our analysis.

While Casares et al. (2009) have multi-wavelength photometry and spectroscopy between 1995 and 2003 of the source, the data is characterized by strong aperiodic variability and no discernible ellipsoidal modulation and therefore, no lower limit on inclination can be found. From the spectral type and eclipse limits Kreidberg et al. (2012) find $27.2^{\circ} < i < 80.8^{\circ}$. We take 80.8° as the upper limit on the inclination of GS 1354−64 in order to calculate a lower limit on the mass of the system.

2.2.14 1A 1524−617

The X-ray transient 1A 1524−617 was discovered by the Sky Survey Instrument (SSI) aboard the Ariel V Satellite (Pounds, 1974) and has been observed in outburst twice. This source was considered as a BHC on the basis of its ultra-soft spectrum, bi-model spectral behaviour and absence of type I X-ray bursts[10].

The 1990 outburst was observed in both the hard (Barret et al., 1992) and soft (ROSAT All-Sky Survey) X-rays. The soft X-ray spectrum could be fit equally well by a cool black body or a power-law. The presence of an ultra-soft component to the spectrum could not be ruled out (Barret et al., 1995). However, the outburst was insufficient to trigger the soft X-ray ASMs (WATCH and Ginga) and Ginga

[10]X-ray bursts occur when the accreting material is guided onto localized regions of a neutron star surface by the strong magnetic field. These "hot spots" come in and out of view as the star rotates, giving rise to pulses of X-ray emission. The key point here being that these bursts occur as a consequence of a neutron star having a surface, which is something a BH does not have (Bradt, 2008).

provided an upper limit consistent with the ROSAT detection (Barret et al., 1995; Brocksopp et al., 2004). For these reasons we include this outburst as a possible "failed" outburst (Brocksopp et al., 2004).

Murdin et al. (1977) identify a possible optical counterpart. The distance to this star is difficult to discern as no colour or reddening information is available. Based on similarities with 1A 0620−00, Murdin et al. (1977) estimate a distance of > 3 kpc. While van Paradijs and Verbunt (1984) propose a distance of 4.4 kpc assuming $M_v = 1.0$ and E(B−V)=0.7. Little else is known about the physical parameters of this system.

2.2.15 Swift J1539.2−6227

The new Galactic transient Swift J1539.2−6227 was discovered by Swift BAT in 2008 (Krimm et al., 2008a). Krimm et al. (2011b) present a complete evolution of spectral and timing properties during the outburst, including rise of the disc component in the SDS and power density spectra signatures of transitions between the HCS and SDS. These features coupled with a lack of observed pulsations establishes the source as a possible BHC (Krimm et al., 2013b). Torres et al. (2009a) performed optical spectroscopy on the source and found an optical counterpart. Other than a blue continuum, no Balmer lines, He II 4686 $\AA$ or Bowen blend emission were detected. Krimm et al. (2011b) suggest that the lack of emission features in the outburst spectrum paired with the faintness of the source in quiescence points to a low mass main sequence or degenerate donor star companion to the compact accretor.

2.2.16 MAXI J1543−564

MAXI J1543−564 was discovered by the GSC aboard MAXI in 2011 when it went into outburst (Negoro et al., 2011a). The detection of type-C QPOs, an observed decrease in fractional rms[11], hardness ratios and steepening of the photon index

[11]The integrated power $P = \int P_\nu d\nu$ of a signal's contribution to the power spectrum is proportional to its strength. This strength is usually quoted in terms of the fractional root mean squared (rms) amplitude $r \propto P^{1/2}$ (in percent %), which is a measure of the signal amplitude as a fraction of source flux (van der Klis, 2006).

during the outburst led Munoz-Darias et al. (2011) to classify the source as a BHC. Stiele et al. (2012) present a full spectral and timing analysis for the outburst, further establishing this fact.

Miller-Jones et al. (2011c) detect a radio counterpart with an optically thin spectrum and suggest this is likely caused by variable, quenched radio emission that is usually observed prior to a radio flare (Fender et al., 2004), rather than emission from a steady, compact jet.

A few possible optical counterparts have been suggested, none show detectable variability in their optical emission (Russell et al., 2011a; Rau et al., 2011a; Rojas et al., 2011). Therefore, a true detection of an optical counterpart still remains questionable at best (Stiele et al., 2012).

2.2.17 4U 1543−475

4U 1543−475 is a recurrent X-ray transient discovered in 1971 when it went into outburst (Matilsky et al., 1972). This source has been observed in outburst three additional times in 1983 (Kitamoto et al., 1984), 1992 (Harmon et al., 1992) and 2002 (Park et al., 2004; Kalemci et al., 2005). 4U 1543−475 displayed classical Soft X-ray Transient[12](SXT) behaviour during the first, second and fourth outbursts (Matilsky et al., 1972; Kitamoto et al., 1984; Park et al., 2004). However, hard X-ray observations during the third event reveal a power-law spectrum (Harmon et al., 1992). Unfortunately there are no soft X-ray observations of this source during the 1992 outburst. Therefore we cannot confirm whether there was a soft component present. Regardless, following Brocksopp et al. (2004) we include this outburst as a possible "failed" outburst. Overall the observation of the wide array of spectral features make 4U 1543−475 a strong BHC (Orosz et al., 1998b).

4U 1543−475 is one of the few sources that has close to simultaneous photometry and spectroscopy (Kreidberg et al., 2012). The optical counterpart, IL Lupi, was discovered by Pederson (1983) and later classified as star of spectral type A2V

[12]SXTs (also referred to as XRN) are transient LMXB systems which undergo recurrent outbursts (lasting weeks to months) during which the system cycles through a multitude of different accretion states. See Section 1.3 for a full description of their X-ray properties.

(Chevalier and Ilovaisky, 1992). A radio counterpart was detected by Hunstead and Webb (2002).

4U 1543−475 has been subject to many detailed dynamical studies (Orosz et al., 1998b; Orosz et al.; Orosz, 2003), resulting in the derivation of $P_{\rm orb}$, $f(M)$, q, i, and distance, therefore providing a confirmation of a BH primary. However, when estimating inclination, Orosz et al. (1998b) include the mass ratio as a free parameter, which results in a large source of error (Kreidberg et al., 2012).

While they quote an inclination between $24^\circ < i < 36^\circ$ at the 3σ level, they also make note of the possibility of additional systematic effects. There is a more precise measurement of inclination found in the conference proceedings of Orosz et al., however, there is no formal published record of the light curve. For this reason, we follow Kreidberg et al. (2012) in taking the inclination estimate from Orosz et al. (1998b) as the boundaries for a uniform distribution. A more precise measurement of distance is found in Ozel et al. (2010). We make use of this value in our calculations.

2.2.18 XTE J1550−564

The galactic microquasar XTE J1550−564 was discovered as a bright X-ray transient by the ASM aboard RXTE (Smith, 1998). Shortly after discovery, optical (Orosz et al., 1998a) and radio (Campbell-Wilson et al., 1998) counterparts were detected along with a superluminal ejection observed in the radio (Hannikainen et al., 2001). The source would quickly become a promising BHC based on observations of rapid X-ray variability, hard spectrum and the absence of X-ray bursts or pulsations (Cui et al., 1999).

Later, Orosz et al. (2002) would provide dynamical evidence confirming the BH nature of the primary. To date the source has been observed in outburst five times, 1998/1999 (Sobczak et al., 2000; Remillard et al., 2002; Kubota and Makishima, 2004), 2000 (Rodriguez et al., 2004; Kalemci et al., 2001; Miller et al., 2001b; Tomsick et al., 2001b), 2001 (Tomsick et al., 2001a), 2001/2002 (Belloni et al., 2002a) and 2003 (Sturner and Shrader, 2005; Aref'ev et al., 2004). Radio observations during the 2001/2002 outburst by Corbel et al. (2002) would confirm the presence of a hard state jet spectrum.

The first two outbursts showed the canonical BHC states. Complete spectral and timing analysis for the 1998/1999 and 2000 outbursts can be found in Sobczak et al. (2000); Homan et al. (2001); Cui et al. (1999); Remillard et al. (1999a) and Tomsick et al. (2001b); Miller et al. (2001b); Kalemci et al. (2001); Belloni et al. (2002a), respectively. The last three have been shown to be under-luminous "failed" outbursts (Tomsick et al., 2001a; Swank et al., 2002; Belloni et al., 2002a; Corbel et al., 2002; Sturner and Shrader, 2005).

Orosz et al. (2011b) provide an improved dynamical model including $P_{\rm orb}$, $f(M)$, q and i. They have determined an inclination using photometry and spectroscopy over 7 years of data. However, they use NSL fractions determined at a different time then the measurements which can produce unreliable inclination measurements (Kreidberg et al., 2012). Nevertheless, Orosz et al. (2011b) acknowledge the uncertainty and fit a model, which includes a disk and four free parameters, using eight different combinations of light curves and NSL fractions. They find a reasonably narrow possible range in inclination of $57.7^\circ < i < 77.1^\circ$. Following Kreidberg et al. (2012), we adopt an isotropic distribution over this range for our inclination, a mass ratio uniformly distributed over the range given in Orosz et al. (2011b) and use these values to calculate a $M_{\rm BH}$.

2.2.19 4U 1630−472

The recurrent X-ray transient 4U 1630−472 was discovered by the VELA 5B and UHURU satellites when it began to exhibit "transient" behaviour (Priedhorsky, 1986; Jones et al., 1976). Over the last 45 years, 4U1630−472 has undergone a total of 22 outbursts occurring quasi-regularly ($\sim$ 600–700 days (Kuulkers et al., 1997a)) and exhibiting a wide range of complex outburst behaviour (see Table A.4 for a complete list of references for each outburst).

Highly polarized radio emission was observed for the first time during the outburst in 1998, confirming the presence of jets in the system (Hjellming et al., 1999b). The most recent studies of the radio jets in 4U 1630−472 discuss possible baryonic matter content within the jets (Díaz Trigo et al., 2013; Neilsen et al., 2014). An additional outflow, in the form of an accretion disc wind, has also been detected in

this source (Ponti et al., 2012).

No optical counterpart is known, most likely due to its high reddening and crowded field (Parmar et al., 1986) resulting in difficulty performing optical and infrared studies. While no compact object mass is known, McClintock and Remillard (2006) classify it as a very likely class "A" BHC. In addition, the system is suspected to contain a BH based on spectral properties (Parmar et al., 1986) and fast timing behaviour (Kuulkers et al., 1997b).

2.2.20 XTE J1637−498

The X-ray transient XTE J1637−498 was discovered by PCA aboard RXTE during a regular scan of the galactic bulge and ridge regions in 2008 (Markwardt et al., 2008c). Wijnands et al. (2008) obtained an X-ray spectrum described by an absorbed power-law with a photon index of ∼1.5, which is consistent with the source being a LMXB, but due to the large errors on the spectral parameters they stress that other types of systems cannot be excluded.

Little else is known about the system parameters. Nevertheless, this source is a part of the Swift BAT transient monitor BH source list due to the fact that it is listed in ATel's with the BH keyword and has been shown not to be a pulsar or AGN. For this reason, we include XTE J1637−498 in our sample as a possible BHC.

2.2.21 XTE J1650−500

XTE J1650−500 is a soft X-ray transient which was discovered by the ASM aboard RXTE in 2001 (Remillard, 2001). The X-ray spectrum (Markwardt et al., 2001), power density spectra (Revnivtsev and Sunyaev, 2001; Wijnands et al., 2001), evolution through the canonical accretion states (Rossi et al., 2004; Tomsick et al., 2004) and observation of QPOs (Homan and Wijnands, 2003; Kalemci et al., 2003) during the outburst confirmed the source to be a BHC.

The optical counterpart was discovered by Castro-Tirado et al. (2001), confirmed by Groot et al. (2001); Augusteijn et al. (2001) and later classified as a star of spectral type G5–K4III (Orosz et al., 2004). The radio counterpart was discovered by Groot

et al. (2001). Corbel et al. (2004) observed the source at radio frequencies for the duration of the outburst, finding evidence for the existence of a steady compact jet. An additional outflow, in the form of an accretion disc wind, has also been detected in this source (Miller et al., 2004; Ponti et al., 2012).

Further optical observations of the source revealed the $f(M)$, $P_{\rm orb}$ and i for the system (Orosz et al., 2004). While Orosz et al. (2004) are able to determine a lower limit on the inclination of $i > 50^{\circ}$, by fitting a star only model with photometry obtained between May and August of 2003, Kreidberg et al. (2012) suggests that the source was active during the time, as there was more scatter in the light curve than one would expect from photometric errors alone, and as such, use this lower limit to calculate their own corrected inclination. We adopt this value for our calculation of $M_{\rm BH}$.

2.2.22 XTE J1652−453

The transient source XTE J1652−453 was discovered in 2009 during PCA monitoring of the galactic region (Markwardt et al., 2009c). Further observations showed a quickly rising flux and an X-ray spectrum which evolved from a soft disc blackbody (Markwardt and Swank, 2009; Markwardt and Beardmore, 2009) to a hard power-law (Coriat and Rodriguez, 2009), which suggested a BHC (Han et al., 1999). For complete spectral and timing analysis of the outburst, see Han et al. (1999) and Hiemstra et al. (2011).

While near IR observations of the field provided a possible counterpart for XTE J1652−453 (Reynolds et al., 2009), it was later shown that the candidate counterpart showed no significant variability suggesting the detection was probably an unrelated interloper star (Torres et al., 2009c).

A radio counterpart was detected by Calvelo et al. (2009), whose observations indicated emission from the decay of an optically thin synchrotron event associated with the activation of XTE J1652−453. No other information is known about the orbital parameters of the system.

2.2.23 GRO J1655−40

GRO J1655−40 was discovered in 1994 by BATSE aboard CGRO when it went into outburst (Harmon et al., 1995). During this outburst, the existence of radio jets travelling with apparent superluminal motion was discovered (Tingay et al., 1995; Hjellming and Rupen, 1995), making GRO J1655−40 only the second source with jet velocity $\geq 0.9c$, the other being GRS 1915+105 (Mirabel and Rodríguez, 1994; Fender and Belloni, 2004). These radio observations in turn allowed for a precise measurement of distance to the source (Hjellming and Rupen, 1995).

GRO J1655−40 has since undergone two additional outbursts in 1996/1997, which exhibited complex multi-peak behaviour (Zhang et al., 1997; Sobczak et al., 1999; Remillard et al., 1999b) and 2005 (Saito et al., 2006; Shaposhnikov et al., 2007; Brocksopp et al., 2006), in which once again a variable radio source, associated with the jet, was detected (Rupen et al., 2005c,e,d; Brocksopp et al., 2006).

An additional outflow, in the form of an accretion disc wind, has also been detected in this source (Miller et al., 2006c, 2008). In fact, the magnetically driven wind present in GRO J1655−40 (Kallman et al., 2009) has the largest known mass loss rate of all the BH sources in which this wind has been detected (Ponti et al., 2012).

Optical studies by Bailyn et al. (1995a) brought the discovery of the optical counterpart, with fluxes and orbital parameters which were comparable to other BHCs (Brocksopp et al., 2006). Further detailed studies of the orbital parameters in full quiescence published by Orosz and Bailyn (1997), Greene et al. (2001) and Beer and Podsiadlowski (2002), all of which are consistent with each other, have led to measurement of $P_{\rm orb}$ and $M_{\rm BH}$ for this system, in turn confirming the BH nature of the primary.

However, it is suggested in Kreidberg et al. (2012) that the distance obtained by Beer and Podsiadlowski (2002) is more accurate than that of Greene et al. (2001). For this reason we adopt the inclination and other orbital parameters given in Beer and Podsiadlowski (2002), assuming the source was passive during their observation.

2.2.24 MAXI J1659−152

MAXI J1659−152 was first reported when it was detected by Swift BAT in 2010 (Mangano et al., 2010b) and later classified as a new X-ray transient following a detection with MAXI (Negoro et al., 2010).

Optical spectroscopy would prove both the galactic origin of the source and the X-ray binary classification (de Ugarte Postigo et al., 2010; Kaur et al., 2012). The source has been established as a BHC through the fast timing behaviour observed, similar to that seen in BH transients (Kalamkar et al., 2011; Kennea et al., 2011b; Muñoz-Darias et al., 2011; Yamaoka et al., 2012). Its binary nature has been further confirmed through numerous spectral and temporal studies, including those which find an orbital period of ~ 2.4 hours (Kuulkers et al., 2010; Kennea et al., 2011b; Kuulkers et al., 2013), making MAXI J1659−152 the shortest period BHXRB source known (Kennea et al., 2010).

In addition, Kuulkers et al. (2013) constrain inclination between $65^\circ < i < 80^\circ$ due to the fact that there is material in the line of sight that obscures about 90% of the total emission on cyclical timescales, as well as the absence of eclipses. Mass estimates range from 2.2–20 $M_\odot$ (Kennea et al., 2011b; Yamaoka et al., 2012; Shaposhnikov et al., 2012), although some of the discrepancy can be resolved by taking into account BH spin (Kennea et al., 2011b; Yamaoka et al., 2012).

Distance estimates range from 1.6–4.2 kpc (Miller-Jones et al., 2011a) and 8.6 kpc (Yamaoka et al., 2012). As the distance is far from constrained we assume the standard uniform distribution between 3.0–8.0 kpc. Little else is known about the system parameters except for a possible optical counterpart, reported by Kong et al. (2010a); Kong (2012), with a spectral type suggested to be between M2 and M5 (Miller-Jones et al., 2011a; Kong, 2012; Kuulkers et al., 2013).

2.2.25 GX 339−4

The galactic X-ray binary GX 339−4, discovered in 1972 by the MIT X-ray detector aboard the Orbiting Solar Observatory (OSO) 7 satellite (Markert et al., 1973), is the most extensively studied galactic BHXRB system (Zdziarski et al., 2004). Over

the past 42 years, GX 339−4 has undergone 21 outbursts in which the entire array of spectral accretion states have been observed (Belloni et al., 1999b). In fact, GX 339−4 has been observed to undergo numerous hard state outbursts, solidifying its classification as a "failed" outburst source (Rubin et al., 1998; Kong et al., 2002; Buxton et al., 2012; Belloni et al., 2013). For a complete list of references for each outburst see Table A.4.

The secondary star is not clearly detected during quiescence, with most of the observed optical emission originating from the accretion disc. Its LMXB nature has been inferred from the upper limits on the luminosity of this companion star (Shahbaz et al., 2001). On the basis of its observed spectral and temporal characteristics, the system was classified as a BHC (Zdziarski et al., 1998; Sunyaev and Revnivtsev, 2000). Fluorescence spectroscopy of NIII and He II emission lines during outburst, formed on the donor star surface due to X-ray irradiation, allowed Hynes et al. (2003) to measure $P_{\rm orb}$ and put an upper limit on q and a lower limit on the mass function of $> 2M_{\odot}$.

The radio source associated with GX 339−4 was discovered by Sood and Cambell-Wilson (1994) in 1994 and Wilms et al. (1999) was the first to argue, that as the radio emission appeared to arise from a region larger than the binary separation, its origin could come from a compact self-absorbed jet. In fact, the ideas that the radio jet only existed in the hard states and was quenched in the soft states (Fender et al., 1999a, 2004) and disc-jet coupling implied from observed X-ray-Radio correlations (Hannikainen et al., 1998; Corbel et al., 2000, 2003; Markoff et al., 2003; Homan et al., 2005; Corbel et al., 2013) arose from numerous observations of GX 339−4.

An additional outflow, in the form of an accretion disc wind, has also been detected in this source (Miller et al., 2004; Ponti et al., 2012).

The true distance to GX 339−4 remains a topic of debate (Hynes et al., 2004). While Hynes et al. (2004) (based on optical spectra) argue that GX 339−4 is located beyond the tangent point (implying a lower limit of ≥ 6 kpc) and favour a $d \geq 15$ kpc, Zdziarski et al. (2004) prefer the location of GX 339−4 to be in the galactic bulge and use optical/IR data to estimate a favoured distance of 8 kpc, a result which is still consistent with the lower limit given by Hynes et al. (2004). For this reason

we adopt the Zdziarski et al. (2004) estimate for our analysis.

2.2.26 H 1705−250

H 1705−250 is a bright transient which was discovered by the ASM aboard the Ariel V (Griffiths et al., 1978) and HEAO 1 satellites (Kaluzienski and Holt, 1977). Shortly thereafter the optical counterpart was discovered on plates taken at the Anglo-Australian Telescope and UK Schmidt Telescope (Longmore et al., 1977; Griffiths et al., 1978) and would later be classified as a star of spectral type K5±2V (Harlaftis et al., 1997).

The light curve behaviour and observed soft (Griffiths et al., 1978) and hard (Wilson and Rothschild, 1983) components to the spectrum resembled that of other SXTs (Martin et al., 1995). This evidence, along with a dynamical mass function measurement of $f(M) = 4.86 \pm 0.13 M_{\odot}$ (Filippenko et al., 1997) led to the conformation of a BH primary.

Martin et al. (1995) made the first inclination measurement of H 1705−250 to be $48^{\circ} < i < 51^{\circ}$. Remillard and Orosz (1996) obtained a conflicting result of $i > 60^{\circ}$. However, the former only show folded light curves and the latter analyze a light curve which exhibits uneven maxima. Due to the uncertainty as to whether the source was active or passive during these observations, we agree with Kreidberg et al. (2012) and adopt the Martin et al. (1995) $i = 48^{\circ}$ as a lower limit on the inclination, yielding an upper limit on $M_{\rm BH}$. The lower limit on $M_{\rm BH}$ is given by taking $i = 90^{\circ}$. The distance to the source is quoted in Barret et al. (1996b).

2.2.27 IGR J17091−3624

IGR J17091−3624 was discovered by INTEGRAL during observations of the galactic centre in 2003 (Kuulkers et al., 2003). Spectral analysis of the outburst revealed hysteretic behaviour, where the X-ray emission softened as the outburst progressed (Lutovinov and Revnivtsev, 2003; Capitanio et al., 2006b). On the basis of spectral behaviour, IGR J17091−3624 has been classified as a probable BHC (Lutovinov and Revnivtsev, 2003).

Following discovery, an archival search of TTM-KVANT and BeppoSAX Wide Field Camera (WFC) revealed three previous outbursts in 1994, 1996 and 2001 (Revnivtsev et al., 2003; in't Zand et al., 2003; Capitanio et al., 2006b). In addition, re-analysis of archival radio observations occurring 9 days after discovery would reveal the detection of a radio counterpart, which showed a flux increase over two weeks and an inverted spectrum, characteristic of a compact jet (Capitanio et al., 2009b).

Two more outbursts have since been reported in this source in 2007, which showed spectral behaviour typical of a BHC in outburst (Capitanio et al., 2009b), and 2011–2013 (Capitanio et al., 2012). The most recent outburst has been well studied across the X-ray regime (Krimm and Kennea, 2011; Rodriguez et al., 2011b; Del Santo et al., 2011; Capitanio et al., 2011, 2012). In addition, follow up radio observations once again revealed evidence for a self-absorbed compact jet (Torres et al., 2011; Corbel et al., 2011; Rodriguez et al., 2011a) as well as discrete jet ejections (Rodriguez et al., 2011a). This outburst is unlike the others, showing peculiar pseudo periodic flare-like events ("heartbeats") (Altamirano et al., 2011c) closely resembling those observed in GRS 1915+105 (Altamirano et al., 2011a,b; Belloni et al., 2000). Little is known about the orbital parameters of this system.

2.2.28 IGR J17098−3628

The transient source IGR J17098−3628 was discovered by INTEGRAL in 2005 during observations of the galactic centre (Grebenev et al., 2005b). The source remained detectable until 2007, during which time it has been observed to evolve in both brightness and spectral shape (Grebenev et al., 2005a; Capitanio et al., 2009b), forming a basis for its probable BHC classification (Grebenev et al., 2007). Both probable radio (Rupen et al., 2005b) and optical (Steeghs et al., 2005a) counterparts have been detected for this source but little is known about the other orbital parameters of the system.

2.2.29 SAX J1711.6−3808

The transient source SAX J1711.6−3808 was discovered by the WFC aboard BeppoSAX in 2001 (in 't Zand et al., 2001). The galactic latitude, flux, spectral and timing properties confirmed the XRB nature of SAX J1711.6−3808 and the lack of observation of type I X-ray bursts and coherent oscillations along with the appearance of a broad Fe-K emission feature[13] suggested that the primary could be a BH (in't Zand et al., 2002b; Wijnands and Miller, 2002). In addition, McClintock and Remillard (2006) classify the system with a grade "B" likelihood of harbouring a BH.

The spectrum, which was dominated by a comptonized continuum, and timing properties of SAX J1711.6−3808 indicate that it never left the HCS during outburst, making it one of the "failed" outburst sources (in't Zand et al., 2002b).

The search for an optical counterpart has proven difficult due to the large extinction (in't Zand et al., 2002b) and little else is known about the system parameters.

2.2.30 Swift J1713.4−4219

The transient source Swift J1713.4−4219 was discovered by Swift/BAT in 2009 (Krimm et al., 2009b). A few days after discovery RXTE/PCA detected the source. Unfortunately, due to sun constraints the source could not be observed by Swift/XRT or UVOT and was only visible with PCA for 3 days. The PCA spectrum was well fit with a power-law of photon index $\Gamma = 1.68$ and timing analysis revealed strong, aperiodic variability in the power spectrum. Both of which point to a possible BH transient in the HCS (Krimm et al., 2013b). This source is a part of the Swift BAT transient monitor BH source list due to the fact that it is listed in ATel's with the BH keyword and has been shown not to be a pulsar or AGN. For this reason, we include Swift J1713.4−4219 in our sample as a possible BHC.

[13]The iron line emission feature originates from the inner accretion disc as a result of the cold (weakly ionized) disc being irradiated by the comptonizing corona. In some cases, it is indicative of a disc extending down to the ISCO (McClintock and Remillard, 2006).

2.2.31 XMMSL1 J171900.4−353217

The hard X-ray transient XMMSL1 J171900.4-353217 was discovered in an XMM-Newton slew from 10th March 2010 (Read et al., 2010a). Following discovery, Markwardt et al. (2010) established a likely association to a another source designated XTE J1719−356, a faint transient discovered in March 2010 by PCA aboard RXTE (Markwardt et al., 2010). Both decreases in flux (Armas Padilla et al., 2010a) and re-brightening events (Armas Padilla et al., 2010b) were observed in the source over the course of a few months, further indicating its transient nature.

This source is a part of the Swift BAT transient monitor BH source list due to the fact that it is listed in ATel's with the BH keyword and has been shown not to be a pulsar or AGN. For this reason, we include XMMSL1 J171900.4−353217 in our sample as a possible BHC.

2.2.32 XTE J1719−291

XTE J1719−291 was discovered by the RXTE/PCA bulge scans in 2008 (Markwardt and Swank, 2008). Over the course of $\sim$ 46 days, the source was observed to show both flux decreases and rebrightening events (Markwardt and Swank, 2008; Degenaar et al., 2008a,b). Later, Degenaar and Wijnands (2008) (with Swift/XRT observations) confirmed XTE J1719−291 to indeed be a transient X-ray source, observing large X-ray variability during an outburst that lasted almost two months.

Greiner et al. (2008) found a possible optical counterpart, deriving a spectral type K0V or later. Armas-Padilla et al. (2011) derive an orbital period of $P_{\rm orb} \sim 0.08$ hours and long-term mass transfer rate of $\sim 3.7 \times 10^{-13} M_{\odot} {\rm yr}^{-1}$ for the case that the compact object in this system is in fact a BH.

Assuming a distance of 8 kpc, Armas-Padilla et al. (2011) estimate that XTE J1719−291 would have had a 2–10 keV peak luminosity of $7 \times 10^{35} {\rm ergs}^{-1}$ during its 2008 outburst, therefore classifying the system as a very faint X-ray transient (VFXT).

Although no conclusive evidence is available about the nature of the accretor, this source is in the Swift BAT transient monitor BH source list due to the fact that

it is listed in ATel's with the BH keyword and has been shown not to be a pulsar or AGN. For this reason we include XTE J1719−291 in our sample as a possible BHC.

2.2.33 GRS 1716−249 (GRO J1719−24)

X-ray Nova Ophiuchi (GRS 1716−249) was discovered in 1993 by SIGMA aboard the GRANAT satellite (Ballet et al., 1993) and BATSE aboard CGRO (Harmon et al., 1993a) when it went into outburst. Follow up observations led to the discovery of the optical and radio counterparts, a derivation of distance and the suggestion that GRS 1716−249 was a LMXB system (della Valle et al., 1994).

During outburst, the X-ray spectrum was found to be comparable to Cyg X−1 in the hard state (Revnivtsev et al., 1998b) and the power spectra showed the existence of a QPO which varied in frequency (van der Hooft et al., 1996), confirming that GRS 1716−249 never left the HCS during the 1993 outburst and in turn solidifying it as a "failed" outburst source (Brocksopp et al., 2004).

In early 1995, Mir/Kvant detected renewed activity in the source in the form of five slow-rise, fast decay hard X-ray flares. These "mini-outbursts" resembled those of other SXTs, GRS 1009−45 and GRO J0422+32 (Masetti et al., 1996). Hjellming et al. (1996a) analyzed radio data occurring during these X-ray flares and found the relation between high energy X-ray and radio emission was very similar[14] to that observed in GRO J1655−40 and GRS 1915+105 (Foster et al., 1996), implying the presence of a jet which is linked to state changes in the accretion disc.

Masetti et al. (1996) estimate a period of ~ 14.7 hours and a lower limit on the mass of the primary from the super hump period[15] to be $> 4.9 M_{\odot}$. Little else is known about the system parameters.

[14] i.e., radio emission follows the peak or onset of decay in X-ray flares seen between 20–200 keV.

[15] There are two methods which exist to estimate a lower limit on compact object mass (in close binary systems) when superhump behaviour is present. If only the superhump period $P_{\rm sh}$ is known, $(M_{\rm BH}/M_{\odot}) > 0.33 P_{\rm sh}$ hr. If both $P_{\rm sh}$ and $P_{\rm orb}$ are known, $(M_{\rm BH}/M_{\odot}) \gtrsim 0.01(P_{\rm orb}/\Delta P)$ where $\Delta P \equiv (P_{\rm sh} - P_{\rm orb})/P_{\rm orb}$. For detailed analysis and application of both methods, see Mineshige et al. (1992).

2.2.34 XTE J1720−318

XTE J1720−318 was discovered by the ASM aboard RXTE as a transient source undergoing an X-ray nova like outburst in 2003 (Remillard et al., 2003). Follow up observations taken with PCA revealed an X-ray spectrum made up of a 0.6 keV thermal component and a hard tail. Both the spectral characteristics and source luminosity were typical of a BH in the soft state (Markwardt, 2003b). Cadolle Bel et al. (2004) perform a detailed spectral analysis of the outburst and conclude that XTE J1720−318 is in fact a BHC.

The radio counterpart was discovered by Rupen et al. (2003a); O'Brien et al. (2003). Brocksopp et al. (2005) analyze radio data in the context of the X-ray outburst and the broadband spectrum. They observe an unresolved radio source during the rise phase of the outburst which reached a peak approximately coincident with the X-ray light curve. Through study of the spectral indices they conclude that at least two ejection events occurred, similar to behaviour observed in XTE J1859+226. Following a period in which the radio source was not detected, the source once again switched on as XTE J1720−318 transitioned back into the hard state. Nothing is known about the orbital parameters of the system.

2.2.35 XTE J1727−476

The X-ray transient XTE J1727−476 was discovered by RXTE (Levine et al., 2005a) and INTEGRAL (Turler et al., 2005a) in 2005. Observations yield a soft spectrum, reminiscent of a BHXRB in outburst (Levine et al., 2005a; Kennea et al., 2005). We therefore include XTE J1727−476 in our sample as a possible BHC. Other than the optical counterpart, discovered by Maitra et al. (2005), little else is known about the system parameters.

2.2.36 IGR J17285−2922

IGR J17285−2922 is a X-ray transient which was discovered with INTEGRAL in 2004 (Walter et al., 2004). Based on the characteristic evolution of the spectrum from soft (Markwardt and Swank, 2010) to hard (Barlow et al., 2005) observed during the

$\sim$ 2 week outburst and the location in the galactic bulge, IGR J17285−2922 was suggested to be a LMXB undergoing transient activity (Barlow et al., 2005). Given the lack of type I X-ray bursts and the relative hardness of the spectrum, Barlow et al. (2005) tentatively suggested the system may be harbouring a BH.

Assuming a distance of 8 kpc, the peak luminosity of this outburst was $\sim 8 \times 10^{35}$ergs^{-1}, classifying it as a VFXT (Sidoli et al., 2011).

Renewed activity in the transient previously name XTE J1728−295 was observed in 2010 (Markwardt and Swank, 2010). Turler et al. (2010) confirmed that IGR J17285−2922 and XTE J1728−295 were in fact the same source. Using XMM and INTEGRAL, Sidoli et al. (2011) were able to obtain the first broadband spectrum for this source, which was dominated by a power-law with a slope consistent with the canonical range for BHXRBs in the HCS ($\Gamma \sim 1.5-1.7$) (Belloni, 2009). In fact, IGR J17285−2922 remained in the HCS for the duration of the 2010 outburst, making it a "failed" outburst source and further suggesting a BH nature (Sidoli et al., 2011).

Besides a likely optical counterpart (Russell et al., 2010; Torres et al., 2010; Kong et al., 2010b), little else is known about the system parameters.

2.2.37 GRS 1730−312

The X-ray source GRS 1730−312 was discovered in the galactic centre region by SIGMA aboard GRANAT (Churazov et al., 1994) and the TTM telescope aboard the Mir-Kvant Observatory (Borozdin et al., 1994) in 1994. Both Borozdin et al. (1995) and Vargas et al. (1996) observed that the source peak luminosity and spectral characteristics[16] during outburst resemble that of other BH sources GS 1124−684 (Ebisawa et al., 1994) and 1A 0620−00 (Ricketts et al., 1975) and therefore classified the source as a BHC. Little else is known about the system parameters.

[16]The contribution of the hard and soft components and observation of a hard to soft state transition.

2.2.38 IGR J17354−3255

IGR J17354−3255 is a hard X-ray transient discovered by INTEGRAL in 2006 (Kuulkers et al., 2006b, 2007). Sguera et al. (2011) conclude that IGR J17354−3255 is a weak persistent hard X-ray source spending a major portion of time in an out-of-outburst state with an average 18–60 keV flux of $\sim 1.4 \times 10^{-11}$ergs^{-1}. They observe the source undergoing short flaring activity between 2003–2008 (16 flares between $\sim$ 0.5h–3.5d) and 2009 ($\sim$ 6 days). Their findings in both the soft and hard X-rays strongly resemble that of Super Giant Fast X-ray Transients[17] (SFXTs).

Other than the orbital period, calculated by Sguera et al. (2011) to be $P_{\rm orb} \sim 8.4$ days, no other information is known about the system parameters.

The nature of the compact object (NS or BH) is unknown. Regardless, as this source is included in the Swift BAT transient monitor BH source list, due to the fact that it is listed in ATel's with the BH keyword and has been shown not to be a pulsar or AGN, we include the system in our sample as a possible BHC.

2.2.39 GRO J1735−27

GRO J1735−27 was discovered by the GINGA satellite during scanning observations and was first designated GS 1734−275 (Makino, 1988). As the flux level was above the detection limit of previous X-ray surveys, the source was considered to be transient. The spectrum was fit well with a black body model similar to those of BHXRBs (Yamauchi and Koyama, 1990).

Shortly thereafter, the source position was redetermined and GRO J1735−27 was subsequently shown to be in agreement with KS 1732−273 (van Paradijs and McClintock, 1995; Liu et al., 2001; Yamauchi and Nakamura, 2004), discovered by the Mir-Kvant Observatory in 1989 (in 't Zand et al., 1991) and 1RXS J173602.0-272541, discovered with the ROSAT all-sky survey in 1990 (Voges et al., 1999). With the revised position, Yamauchi and Nakamura (2004) re-analyzed the data and find it is fit well with an ultra-soft spectrum, usually found in BHXRBs in the soft states.

[17]SFXTs are a subclass of SGXBs characterized by short, bright X-ray flares on top of longer, fainter periods of persistent X-ray emission (Sguera et al., 2005, 2006).

Given the ultra-soft spectrum and transient behaviour as evidence, Yamauchi and Nakamura (2004) classify the source as a BHC. Little else is known about the system parameters.

2.2.40 IGR J17379−3747

IGR J17379−3747, originally designated XTE J1737−376, was discovered by RXTE/PCA during scans of the galactic bulge region in 2004. The outburst lasted ∼9 days. Although not reported publicly, it did appear on the PCA bulge scan webpage[18].

Later it was realized that the source position coincided with IGR J17379−3747, a weak hard X-ray source reported in the 3rd INTEGRAL catalog (Bird et al., 2007). Given positional accuracy, Markwardt et al. (2008b) concluded that XTE J1737−376 and IGR J17379−3747 were most likely the same source.

This source was again detected at significant levels by PCA, INTEGRAL and BAT in 2008 (Markwardt et al., 2008b). Further Swift/XRT observations revealed a hard spectrum with photon index $\Gamma \sim 1.78$, which was consistent with the RXTE/PCA spectrum taken (Krimm et al., 2008d).

Nothing is known about the system parameters. However, given the spectrum and the fact that the source is included in the Swift BAT transient monitor BH source list due to the fact that it is listed in ATel's with the BH keyword and has been shown not to be a pulsar or AGN, we include the system in our sample as a possible BHC.

2.2.41 GRS 1737−31

GRS 1737−31 was discovered by SIGMA aboard GRANAT during monitoring of the Galactic centre in March of 1997 (Sunyaev et al., 1997). Shortly thereafter the source was also found in RXTE and BeppoSAX data (Marshall and Smith, 1997; Cui et al., 1997b; Heise, 1997). Both the hard spectrum of the source (Sunyaev et al., 1997) and the observed chaotic variability (Cui et al., 1997a) were similar to properties observed by XRN and BH source Cyg X−1 (Sunyaev and Truemper, 1979; Sunyaev

[18]http://asd.gsfc.nasa.gov/Craig.Markwardt//galscan/main.html

et al., 1992; Vikhlinin et al., 1994; Trudolyubov et al., 1999).

Observations from Trudolyubov et al. (1999) and Cui et al. (1997a) revealed the presence of a hard power-law spectrum. Further observations using BeppoSAX and ASCA (Heise, 1997; Ueda et al., 1997) confirmed this hard spectrum was still present $\sim$2 weeks after the initial detection. Based on spectral and temporal properties, it was suggested that GRS 1737−31 was a distant XRN and BHC in the HCS (Sunyaev et al., 1997; Cui et al., 1997a; Trudolyubov et al., 1999).

In fact, GRS 1737−31 appears to have never left the hard state for the duration of the 1997 outburst, making it a "failed" outburst source (Brocksopp et al., 2004).

No optical or radio observations have ever been taken (Brocksopp et al., 2004) and little else is known about the orbital parameters of the system.

2.2.42 GRS 1739−278

The X-ray source GRS 1739−278 was discovered in the galactic center, by SIGMA aboard GRANAT during outburst in 1996 (Paul et al., 1996). The outburst was observed in the X-ray by the Mir-Kvant Observatory (Borozdin et al., 1996), ROSAT (Greiner et al., 1997), GRANAT (Vargas et al., 1997) and RXTE (Takeshima et al., 1996).

A radio counterpart was discovered with Very Large Array (VLA) data (Durouchoux et al., 1996; Hjellming et al., 1996b) and an optical counterpart was discovered by Marti et al. (1997) to be either a luminous early/middle B type main sequence star or a middle G/early K giant star.

Borozdin et al. (1998) and Vargas et al. (1997) find the light curve behaviour, optical and radio observations, evolution of the spectrum and spectral characteristics correspond to the SDS and SPL states of BHCs, and Borozdin and Trudolyubov (2000) observe QPOs, present when the source was in the SPL and SDS, allowing GRS 1739−278 to reliably be classified as a BHC and soft XRN.

In March of 2014, GRS 1739−278 was once again detected in outburst by both Swift (Krimm et al., 2014) and INTEGRAL (Filippova et al., 2014) where, much like the 1996 discovery outburst, it completed the canonical BHXRB pattern through the spectral states. Little else is known about the orbital parameters of the system.

2.2.43 1E 1740.7−2942

The micro-quasar 1E 1740.7−2942 located near the galactic centre was discovered by the Einstein Observatory in 1984 (Hertz and Grindlay, 1984). Its hard X-ray emitting nature was first reported by Skinner et al. (1987). Given the spectral shape of its soft γ-ray emission and the similarities to Cyg X−1, Sunyaev et al. (1991b) classified it as a BHC and reported it to be the strongest persistent source in the Galactic centre region. Its micro-quasar classification came with the discovery of a double-sided radio emitting jet (Mirabel et al., 1992). Its radio emission has been found to be variable and correlated with the X-ray flux (Paul et al., 1991).

1E 1740.7−2942 has been suggested as a possible source of electron-positron annihilation due to an observed high energy spectral feature with GRANAT (Bouchet et al., 1991; Sunyaev et al., 1991a), hence the common name "The Great Annihilator". However, near simultaneous observations by CGRO (Jung et al., 1995) and BATSE (Smith et al., 1996) and high energy observations by INTEGRAL (Bouchet et al., 2009) could never confirm this feature.

1E 1740.7−2942 is one of only three BHCs which not only remain persistently near their maximum luminosity but also spend most of their time in the HCS (Churazov et al., 1993; Main et al., 1999; del Santo et al., 2004), with an X-ray spectrum usually described by an absorbed power-law with photon index $\Gamma \sim 1.4 - 1.5$ (Gallo and Fender, 2002) and high energy cutoff (Sidoli et al., 1999; Natalucci et al., 2014). Occasionally the source has been observed to make the transition to the softer states (Sunyaev et al., 1991a; del Santo et al., 2004).

Unfortunately, due to a source environment characterized by a high concentration of dust and high column density ($\sim 10^{23}\mathrm{cm}^{-2}$), optical identification is difficult (Gallo and Fender, 2002) and its nature as a HMXB or LMXB, inclination and distance remain unknown. However, the high amount of absorption, position near the galactic centre and presence of bipolar jets, all favour a distance ∼8.5 kpc and disfavour a face on geometry (Natalucci et al., 2014).

Periodic modulation has been detected and interpreted as an $P_{\mathrm{orb}} \sim 12.7$ days, suggesting the object could be a red giant companion (Smith et al., 2002a). Although, contrary to this result Marti et al. (2010) have reported a candidate for an

IR counterpart which would seem to exclude the red giant companion possibility. A much longer periodicity has also been reported by Ogilvie and Dubus (2001), thought to be related to cyclic transitions between a flat and warped disc, similar to what is observed in Cyg X−1 and LMC X−3.

2.2.44 Swift J174510.8−262411 (Swift J1745-26)

The transient Swift J174510.8−262411 (or Swift J1745−26) was discovered by BAT aboard the Swift satellite in 2012 when it went into outburst (Cummings et al., 2012). While UVOT began observing the source after detection, no optical counterpart was detected (Curran et al., 2014). However an IR counterpart was identified on the basis of variability compared with archival images (Rau et al., 2012b).

The suggestion was made that Swift J1745−26 was a LMXB BH system on the basis of spectral and timing observations (by Swift and INTEGRAL). Observations which were also used to show that the source never left the hard states for the duration for the outburst (Belloni et al., 2012; Grebenev and Sunyaev, 2012; Tomsick et al., 2012; Vovk et al., 2012; Sbarufatti et al., 2013; Krimm et al., 2013b), therefore suggesting Swift J1745−26 was a "failed" outburst source (Curran et al., 2014). In addition, the observation of $H\alpha$ emission line in optical observations would further support the idea of a BH accretor being present in the system (Muñoz-Darias et al., 2013).

A radio counterpart was detected by Miller-Jones and Sivakoff (2012) and both Corbel et al. (2012) and Coriat et al. (2013a) find a spectral index suggestive of optically-thick synchrotron emission from a partially self-absorbed compact jet. See Curran et al. (2014) for complete analysis of the evolution of the jet throughout the outburst.

Muñoz-Darias et al. (2013) have carried out optical observations of the source and argue a $P_{\rm orb} \leq 21$ hours and a spectral type of the counterpart as A0 or later. Little else is known about the orbital parameters of the system at this time.

2.2.45 1A 1742−289

The transient source 1A 1742−289 was discovered by the Ariel V satellite when it went into outburst in 1975 (Eyles et al., 1975). Branduardi et al. (2001) observe similarity in spectral behaviour and timescales with transient BH source 4U 1543−475. They interpret these findings as an indication that 1A 1742−289 is a binary system containing a compact object[19] with variable mass transfer from a low mass companion of spectral type M–K.

Maeda et al. (1996) give an estimate of $P_{\rm orb} \sim 8.4$ hours. However, it has been suggested that the quiescent source observed by Maeda et al. (1996) may not actually be associated with 1A 1742−289 (Kennea and Skinner, 1996). Davies et al. (1976) find a radio counterpart and observe changes in intensity at radio and X-ray wavelengths in 1A 1742−289 similar to behaviour observed in Cyg X−1 and 1A 0620−00 (Elvis et al., 1975; Owen et al., 1976). Little else is known about the orbital parameters of the system.

While the nature of the compact object is not known, the source is included in the BHC list of McClintock and Remillard (2006) and therefore so to is included in our sample.

2.2.46 H 1743−322

H 1743−322 was discovered during a bright outburst by the Ariel V (Kaluzienski and Holt, 1977) and HEAO–1 (Doxsey et al., 1977) satellites in 1977. The source would later be classified as a BHC based on its very soft spectrum (White and Marshall, 1984).

Following the 1977 outburst, H 1743−322 would be detected twice more, once in 1984 with EXOSAT (Reynolds et al., 1999) and again in 1996 with Mir-Kvant (Emelyanov et al., 2000) only to be rediscovered in outburst once again in 2003 by INTEGRAL (Revnivtsev, 2003) and RXTE (Markwardt and Swank, 2003). During this outburst QPOs of typical BHC frequencies were observed (Homan et al., 2003b) and the system followed the canonical pattern, transitioning through hard and soft

[19]NS or BH based on high X-Ray luminosity.

accretion states (Capitanio et al., 2005; McClintock et al., 2009).

Detections of the radio (Rupen et al., 2003c) and optical (Steeghs et al., 2003) counterparts followed quickly thereafter. In fact, H1743−322 is classified as a micro-quasar as jets have been detected at both radio and soft X-ray wavelengths (Rupen et al., 2004; Corbel et al., 2005). There exists numerous studies of this source at radio wavelengths (Kalemci et al., 2006; Jonker et al., 2010; Coriat et al., 2011; Miller-Jones et al., 2012). An additional outflow, in the form of an accretion disc wind, has also been detected in this source (Miller et al., 2006c; Ponti et al., 2012).

Since 2003, H 1743−322 has been observed in outburst on 11 separate occasions, 3 of which[20] where the source never reached the softer states, therefore labelling H 1743−322 as a "failed" outburst source. For a complete list of references for each outburst, involving all available spectral and timing studies, see Table A.4.

Despite being one of the most well studied BHXRBs in the galaxy, no dynamical confirmation has ever been made on the system (Motta et al., 2010). We adopt the distance estimated by Corbel et al. (2005) from the proper motion of the jet, 10.4 ± 2.9 kpc, for the purpose of our analysis.

2.2.47 XTE J1748−288

XTE J1748−288 was discovered in 1998 by the ASM aboard RXTE (Smith et al., 1998b) and BATSE aboard CGRO (Harmon et al., 1998). General spectral and timing properties and their evolution during the outburst were very typical of BH XRN (Revnivtsev et al., 2000b). Based on X-ray spectral and timing analysis and comparison with GS 1124−684, both Revnivtsev et al. (2000b) and Brocksopp et al. (2007) suggest that the outburst began in the SPL state (even though there was an unusually dominant power-law component present). As the outburst continued, the source then passed through the SDS and made the transition back to the HCS. This behaviour was supported by the detection of QPOs associated with these states (Fox and Lewin, 1998). In addition, an iron emission line was detected during the outburst by Kotani et al. (2000) and Miller et al. (2001a).

[20] 2008 (Capitanio et al., 2009a; Motta et al., 2010), 2011/2012 and 2012.

The optically thin radio counterpart was discovered soon after by Hjellming et al. (1998c), confirmed to be associated with XTE J1748−288 (Hjellming et al., 1998b; Fender et al., 1998) and resolved by the VLA (Rupen et al., 1998). Follow-up work would reveal a jet with a velocity $> 0.93c$ (Hjellming et al., 1998e), making XTE J1748−288 only the third known galactic source which displayed superluminal motion (Brocksopp et al., 2007). No information is available on the orbital parameters of the system.

2.2.48 IGR J17497−2821

IGR J17497−2821 was discovered with ISGRI onboard INTEGRAL in 2006 when it went into outburst (Soldi et al., 2006). Assuming a distance of 8 kpc, Kuulkers et al. (2006a) estimated a peak 2–200 keV luminosity of $\sim 10^{37}\mathrm{ergs}^{-1}$. The observed position of the source[21] and this luminosity strongly suggested that IGR J17497−2821 was an XRB (Rodriguez et al., 2007).

Spectral analysis and the FRED type light curve observed further implied that the source was a BHC in the HCS (Kuulkers et al., 2006b; Walter et al., 2007). In fact complete spectral analysis of the outburst confirmed that the source never left the HCS, classifying it as a "failed" outburst source (Rodriguez et al., 2007; Walter et al., 2007; Paizis et al., 2009).

Given a refined Chandra position, Paizis et al. (2007) identified the optical/IR counterpart, suggesting the companion to be either a main sequence B-type star or a K-type red giant, therefore classifying the system as a LMXB. No radio counterpart was found (Rodriguez et al., 2007) and little else is known about the system parameters.

2.2.49 SLX 1746−331

SLX 1746−331 was discovered by the SpaceLab 2 X-ray Telescope in 1985 (Skinner et al., 1990) and again detected by the ROSAT all-sky survey in 1990 (Motch et al., 1998). Both Skinner et al. (1990) and White and van Paradijs (1996) speculated

[21] The line of sight passes close to the galactic center.

that SLX 1746−331 may harbour a BH based on both its transient nature and its soft spectrum. Further evidence was added to this claim when the source was once again detected in 2003 by the RXTE/PCA bulge scan, finding a very soft spectrum modelled by black body emission at $\sim$ 1.3 keV (Markwardt, 2003a; Remillard and Levine, 2003) and by INTEGRAL/ISGRI who in addition to the soft component also found a hard component to the spectrum which only contributed at most $\sim$ 10 % of the flux (Lutovinov et al., 2003a). Eventually, through spectral and timing analysis it was shown that the source had made the transition from the soft back to the hard states, commonly associated with BHCs (Homan and Wijnands, 2003).

SLX 1746−331 has since been detected twice more, once in 2007/2008 by both RXTE/PCA (Markwardt and Swank, 2007) and INTEGRAL/JEM-X (Kuulkers et al., 2008) and once in late 2010 by MAXI (Ozawa et al., 2011). Both outbursts showed the typical very soft spectrum, commonly associated with BHCs in the soft state.

A possible optical counterpart was detected by (Motch et al., 1998) and thought to be a G–K type star. Although, considering the expected low mass of the companion star and high interstellar absorption on the line of sight, the optical identification is likely to be difficult outside X-ray outbursts (Motch et al., 1998). Little else is known about the system parameters of SLX 1746−331.

2.2.50 XTE J1752−223

The X-ray transient XTE J1752−223 was discovered by the ASM aboard RXTE in 2009 (Markwardt et al., 2009b). Continuous monitoring at X-ray wavelengths by RXTE, MAXI and Swift would suggest that the source was a BHC as variability was indicative of an imminent state transition (Nakahira et al., 2009; Markwardt et al., 2009a; Remillard and at MIT, 2009; Shaposhnikov et al., 2009; Shaposhnikov, 2010; Shaposhnikov et al., 2010). More in depth analysis would later confirm the likelihood of the system harbouring a BH (Munoz-Darias et al., 2010; Stiele et al., 2011; Reis et al., 2011; Nakahira et al., 2012a).

Shortly after discovery the optical and near-IR counterparts were found (Torres et al., 2009b,d). Brocksopp et al. (2009) discovered the radio counterpart and found

a flat spectrum consistent with a compact jet in the hard spectral state. The source appeared to stay in the hard state for an extended period of time and finally made the transition to the softer states in mid-January 2010 (Homan, 2010; Curran et al., 2010; Nakahira et al., 2010; Shaposhnikov, 2010; Shaposhnikov et al., 2010; Chun et al., 2013). In addition, follow-up radio observations of ejection events, often associated with state changes, supported this result (Brocksopp et al., 2010a; Yang et al., 2010a, 2011). There has also been evidence to suggest that not only could XTE J1752−223 be a new superluminal source but it may also contain X-ray jets (Yang et al., 2011). For in-depth radio analysis see Brocksopp et al. (2013).

Using correlations between spectral and variability properties with GRO J1655−40 and XTEJ1550−564, Shaposhnikov et al. (2010) are able to estimate a distance and a BH mass, which we adopt for the purpose of our analysis.

2.2.51 Swift J1753.5−0127

Swift J1753.5−0127 is an X-ray transient discovered in outburst by Swift BAT in 2005 (Palmer et al., 2005). Soon after, the source was detected in UV, optical, near IR and radio bands (Still et al., 2005b; Halpern, 2005; Torres et al., 2005; Fender et al., 2005). Radio observation by Fender et al. (2005) indicated likely compact jet activity.

Despite the fact that no dynamical measurements have been made, the shape of the hard X-ray spectrum, specifically the high energy tail detected up to $\sim$ 600 keV[22], and the detection of QPOs (Morgan et al., 2005), provides a strong hint that the system harbours a BH (Cadolle Bel et al., 2007).

The system has not yet returned to quiescence since 2005, remaining active in the X-ray and optical/IR wavelength and is usually seen in the HCS, making it one of the "failed" outburst sources (Soleri et al., 2012; Shaw et al., 2013; Froning et al., 2014). It is important to note that due to the fact that it has remained active since discovery in 2005, we treat Swift J1753.5−0127 as a persistent source in our analysis. However, it has been observed to make occasional transitions to the intermediate states before

[22]No NS system has been detected past $\sim$ 200 keV (Cadolle Bel et al., 2007).

returning back to the hard state, similar to the "failed" state transitions of Cyg X−1 (Soleri et al., 2012).

Swift J1753.5−0127 is an interesting source as it follows the lower track in the X-ray/radio luminosity plane (Cadolle Bel et al., 2007), along with an increasing number of BH sources (Coriat et al., 2011; Corbel et al., 2013), and it could be the BH with the second shortest orbital period of ∼3.2 hours[23], according to Zurita et al. (2008).

For complete multi-wavelength analysis, see Froning et al. (2014); Cadolle Bel et al. (2007) and for spectral and timing analysis, see Miller et al. (2006a); Soleri et al. (2012); Mostafa et al. (2013).

2.2.52 XTE J1755−324

XTE J1755−324 was discovered by the ASM aboard RXTE when it went into outburst in 1997 (Remillard et al., 1997). The observed spectrum was fit with a multi-colour disc black body at ∼0.7 keV and a hard power-law tail extending to ∼20 keV (Remillard et al., 1997). Given the spectrum, the FRED type light curve behaviour (Revnivtsev et al., 1998a), typical of XRN (Tanaka and Shibazaki, 1996), and the fact that no type I X-ray bursts or pulsations were observed throughout the course of the outburst (Goldoni et al., 1999), the source was suggested as a good BHC (Goldoni et al., 1999). For complete X-ray spectral analysis, see Revnivtsev et al. (1998a) and Goldoni et al. (1999).

No optical (Goldoni et al., 1999) or radio (Ogley et al., 1997) counterparts have been found and little else is known about the parameters of the system.

2.2.53 IGR J17586−2129

IGR J17586−2129 was first reported in the Third INTEGRAL catalog (Bird et al., 2006). No further information was known about the source until it went into outburst in 2009 (Krimm et al., 2009a). With Swift/XRT, Krimm et al. (2009a) find the

[23]The BHC MAXI J1659−152 has the shortest known orbital period of any BH system with an $P_{\rm orb} \sim 2.4$ hrs (Kuulkers et al., 2013).

spectrum can be fit with a power-law of photon index $\Gamma \sim 1.2$. They also propose a possible optical counterpart and suggest that the brightness of the optical source implies that this system is a HMXB. Tomsick et al. (2009) agree with the suggestion that the source is an obscured HMXB.

With INTEGRAL/ISGRI, Sanchez-Fernandez et al. (2009) find the spectrum during outburst is well fit with a cutoff power-law of photon index $\Gamma \sim 1.5$ and a cutoff energy of ~ 20 keV in the 18–150 keV range. Given the spectrum and the fact that the source is included in the Swift BAT transient monitor BH source list due to the fact that it is listed in ATel's with the BH keyword and has been shown not to be a pulsar or AGN, we include the system in our sample as a possible BHC.

2.2.54 H 1755−338

H 1755−338 was discovered by the UHURU satellite when it was active in 1970 (Jones, 1977). Later, it was found to have an unusually soft spectrum (White and Marshall, 1984; White et al., 1984) and a hard X-ray tail (Pan et al., 1995), which was suggestive of a BHC (Kaaret et al., 2006). In addition, H 1755−338 shows X-ray dips[24] which indicates that the system has a high inclination and a $P_{\rm orb} \sim 4.4$ days (White et al., 1984; Mason et al., 1985).

The source was observed to still be active in 1993 (Church and Balucinska-Church, 1997) and subsequently found to be in quiescence in 1996 (Roberts et al., 1996). Therefore the source remained active for at least 23 years (if not more). As a result, we classify this source as persistent (Kaaret et al., 2006).

The distance to the source is not well constrained. However, it is likely > 4 kpc, as the optical counterpart, which was identified during outburst by McClintock et al. (1978), was not detected in quiescence (Wachter and Smale, 1998) and < 9 kpc, suggested by the low level of visual extinction (Mason et al., 1985).

In addition, Angelini and White (2003) found a linear structure in the X-ray,

[24]X-ray dips are periodic dips (which repeat with $P_{\rm orb}$) in X-ray intensity caused by the X-ray emitting region being obscured by a structure in the outer disc. This structure is believed to be the region of impact of the accretion flow from the companion star (White and Swank, 1982).

roughly symmetric, about the position of the source and extending outwards by $\sim 3'$, suggesting the presence of X-ray jets. For detailed analysis of the possible X-ray jets in this source, see Park et al. (2005) and Kaaret et al. (2006). Little else is known about the system parameters.

2.2.55 GRS 1758−258

The hard X-ray source GRS 1758−258 was discovered during observations of the galactic center with GRANAT in 1990 (Mandrou, 1990; Sunyaev et al., 1991b). The majority of the time, GRS 1758−258 displays a hard power-law spectrum with photon indices between $\Gamma \sim 1.4 - 1.9$ and a high energy cutoff above ∼100 keV (Kuznetsov et al., 1999; Main et al., 1999; Lin et al., 2000) and strong short term variability on frequencies up to 10 Hz (Smith et al., 1997; Lin et al., 2000), making it one of only three BHCs which not only remain persistently near their maximum luminosity, with the exception of a few dim states which can last up to several months (Pottschmidt et al., 2006), but also spend most of their time in the HCS. Sometimes a weak soft excess is seen in the spectrum, observed in conjunction with a slightly reduced X-ray flux, thought to be characteristic of the source transitioning into the intermediate states (Mereghetti et al., 1994, 1997; Lin et al., 2000; Heindl and Smith, 2002).

Based on both the X-ray properties and the radio detection, discovered as a point source and double sided jet structure (Rodriguez et al., 1992), GRS 1758−258 is classified as a micro-quasar (Pottschmidt et al., 2006). An additional outflow, in the form of an accretion disc wind, has also been detected in this source (Ponti et al., 2012).

Three possible counterparts have been identified, the brightest being K0 III giant, and the others main sequence A stars (Marti et al., 1998; Eikenberry et al., 2001; Rothstein et al., 2002). The former has been suggested as the most likely counterpart given the $P_{\rm orb} \sim 18.5$ days (Smith et al., 2002a).

Numerous observational campaigns on this persistent source, in both the soft (Mereghetti et al., 1994, 1997; Smith et al., 1997; Main et al., 1999; Smith et al., 2001, 2002a,b; Pottschmidt et al., 2006) and hard (Gilfanov et al., 1993; Kuznetsov et al., 1999; Pottschmidt et al., 2006) X-rays have been led over the years, as well as

a multi-wavelength study by Lin et al. (2000). Little else is known about the orbital parameters of the system.

2.2.56 XTE J1812−182

The X-ray transient XTE J1812−182 (or XMMU J181227.8-181234) was discovered by XMM-Newton in outburst in 2003. After reprocessing of data, this source was found in the RXTE/ASM data as well. No optical counterpart has been identified, most likely due to the large absorption in the direction of the source.

The spectrum of the source is fit equally well with an absorbed power-law or a multi-colour disc blackbody and no pulsations were detected in the timing analysis. A colour-colour diagram[25], along with the high absorption found in the direction of the source suggests a HMXB system. However, the power-law spectral index is more typical of a LMXB (Cackett et al., 2006).

The source was again detected in outburst in 2008 with RXTE/PCA, and was originally thought to be a new source (then named XTE J1812−182) until it was confirmed to be the same source as XMMU J181227.8−181234 (Markwardt et al., 2008d; Torres et al., 2008b). The spectrum was again consistent with a highly absorbed power-law. Markwardt et al. (2008d) argue that while Cackett et al. (2006) speculated that the source was a HMXB, one might also interpret the spectrum and variability behaviour as being a BHC in a soft state. Little else is known about this system. Regardless, following the suggestion of Markwardt et al. (2008d), we include XTE J1812−182 in our sample as a possible BHC.

2.2.57 IGR J18175−1530

The hard X-ray transient IGR J18175−1530 was discovered during observation of the galactic centre by INTEGRAL in 2007 (Paizis et al., 1248). At the time, this

[25]Similar to an HID, one can observe the evolution of a source throughout outburst by plotting hard colour vs. soft colour (van der Klis, 2006). Here hard and soft colour refer to different hardness ratios. Often three energy bands are used where hard colour is defined as the the ratio of the hard over medium band and soft colour is the ratio of the medium band over the soft band.

source was also detected during RXTE/PCA scans of the region and designated XTE J1817−155 (Markwardt et al., 2007). Cheung (2007) discuss the detection of a radio source which may be associated with IGR J18175−1530.

While very little is known about the nature of the system, it is included in the Swift BAT transient monitor BH source list as a possible BHC. Following their suggestion, we also include it in our sample as a possible BHC.

2.2.58 XTE J1817−330

XTE J1817−330 was discovered by RXTE in 2006 (Remillard et al., 2006) and shown to have a very soft spectrum, dominated by the accretion disc component, typical of transient BHCs in the soft state (Sala et al., 2007).

Shortly after the discovery, both the radio (Rupin et al., 2006a) and optical (Torres et al., 2006) counterparts were identified. Sala et al. (2007) suggest a spectral type of K–M for the optical counterpart. An outflow, in the form of an accretion disc wind, has also been detected in this source (Ponti et al., 2012).

In depth spectral analysis, providing further evidence for the BH nature of the source, shows that at the peak of the outburst, the source was in the SDS and then later transitioned back to the HCS as the source intensity gradually decreased (Gierlinski et al., 2008; Roy et al., 2011). In addition, QPOs associated with the intermediate states have also been detected in this source (Homan et al., 2006a; Roy et al., 2011). For complete analysis of QPOs present during the outburst of XTE J1817−330, see Sriram et al. (2013a). Little else is known about the system parameters.

2.2.59 XTE J1818−245

XTE J1818−245 was discovered by the ASM aboard RXTE in 2005. The hardness ratio indicated a very soft spectrum, typical of BHCs (Levine et al., 2005b) and no pulsations were detected (Markwardt et al., 2005). Soon thereafter, the optical (Steeghs et al., 2005b) and radio (Rupen et al., 2005a) counterparts were discovered. The spectral type of the optical counterpart could not be identified as the optical

emission was found to be dominated by the accretion disc (Zurita Heras et al., 2011).

Spectral parameters showed behaviour typical of the SDS and intermediate states seen in BHXRBs, including the usual decrease in disc temperature, increase in inner disc radius and decrease in disc flux as the high-energy flux became stronger, and radio flares associated with discrete ejecta (Cadolle Bel et al., 2009).

Based on the above mentioned analysis and the observed light curve behaviour, Cadolle Bel et al. (2009) concluded that XTE J1818−245 is most likely a LMXB and BHC. Cadolle Bel et al. (2009) estimate a distance range between 2.8 and 4.3 kpc. We assume a uniform distribution between this range for the purposes of our analysis. No other information is available on the orbital parameters of the system.

2.2.60 SAX J1819.3−2525

In 1999 the transient SAX J1819.3−2525 was discovered by BeppoSAX (in 't Zand et al., 1999) and RXTE (Markwardt et al., 1999b) with a position consistent with variable star V4641 Sgr. Its optical (Stubbings, 1999) and X-ray (Smith et al., 1999a,b) flux increased rapidly and then began to decline within two hours. Emission lines found in both optical and infrared spectra, during this bright X-ray flare (Ayani and Peiris, 1999; Liller, 1999; Djorgovski et al., 1999; Charles et al., 1999), were reminiscent of accretion onto a compact object, further proving that V4641 Sgr was in fact the optical counterpart of SAX J1819.3−2525.

Shortly thereafter, the radio counterpart was discovered by Hjellming et al. (1999c). Follow-up radio observations showed that the flux was declining on timescales of hours to days (Hjellming et al., 1999c,d) and the presence of ejecta (Hjellming et al., 1999a). Hjellming et al. (1999a) attributed the inferred superluminal proper motions of the radio structure to relativistic motion of a radio jet, which led to SAX J1819.3−2525 being classified as a possible micro-quasar. For a discussion of the rapid X-ray variability occurring at super-Eddington luminosities during this flare, see Wijnands and van der Klis (2000) and Revnivtsev et al. (2002).

SAX J1819.3−2525 has been observed to have undergone numerous episodic outbursts since its discovery in 1999. In addition to the discovery outburst, major outbursts have been observed in 2000 (Hjellming, 2000), 2002 (Uemura et al., 2004),

2003 (Buxton et al., 2003; Maitra and Bailyn, 2006) and 2004 (Swank, 2004). In each case the entire span of the outburst cycles was much shorter than typical compact transient systems (Maitra and Bailyn, 2006). Weaker flare-like activity has been reported in 2000 (Hjellming, 2000; Uemura et al., 2004), 2007 (Cackett and Miller, 2007), 2008/2009 (Yamaoka et al., 2008), 2010/2011 (Yamaoka and Nakahira, 2010; Yamaoka et al., 2010b,a) and 2014 (Tachibana et al., 2014).

Optical spectroscopy and photometry during quiescence allowed Orosz et al. (2001) to measure a $f(M) = 2.74 \pm 0.12 M_{\odot}$ and $P_{\rm orb}$ ∼2.8 days , estimate a distance between 7.4 and 12.3 kpc and mass between $\sim 8.7 - 11.7 M_{\odot}$, and classify V4641 Sgr as a B9III star, in turn making SAX J1819.3−2525 a firm BHC (Revnivtsev et al., 2002).

Its optical companion, with a mass estimated at $\sim 5.5 - 8.1 M_{\odot}$ (Orosz et al., 2001), is the most massive, brightest and bluest of all the galactic LMXB companion stars (MacDonald et al., 2011), which has led to the system being classified as a HMXB by some (Revnivtsev et al., 2002; Chaty et al., 2003; Pandey et al., 2007). However, MacDonald et al. (2011) argue the maintenance of the LMXB label for two reasons. The first, mass transfer occurs via RLO in the system. The second, the optical counterpart, is not more massive than the probable black hole in the system.

MacDonald et al. (2011) have compiled and subsequently separated 10 years of data on this source into passive and active states. While there is no evidence for a non-stellar contribution in the passive data, the amplitude of ellipsoidal variability requires the extreme value of $i \sim 90°$. As the X-ray data is sparse enough that we can not rule out an eclipse geometry, we follow Kreidberg et al. (2012) in adopting a range $80° < i < 90°$ and subsequently use this inclination to calculate a $M_{\rm BH}$.

2.2.61 MAXI J1836−194

MAXI J1836−194 was discovered in August of 2011 simultaneously by MAXI (Negoro et al., 2011b) and Swift/BAT (Ferrigno et al., 2011) when it went into outburst. Follow-up observations would lead to the discovery of the optical (Kennea et al., 2011a) and radio (Miller-Jones et al., 2011b) counterparts. The relatively strong radio and IR emission observed was further associated with the presence of a jet

(Miller-Jones et al., 2011b; Trushkin et al., 2011).

Strohmayer and Smith (2011) were the first to classify the source as a BHC when they observed a spectrum consistent with a power-law of photon index $\Gamma \sim 1.8$, the presence of an iron line and a transition from the HCS to the HIMS with RXTE/PCA. Through spectral and timing analysis during the outburst, Ferrigno et al. (2011) found that the source never made the transition from the HCS to the SDS, thereby classifying MAXI J1836−194 as a "failed" outburst source (also see Reis et al. (2012)). For full multi-wavelength analysis of the spectral evolution of the outburst and the evolving compact jet in the system see Russell et al. (2013) and Russell et al. (2014a).

Russell et al. (2014b), using optical spectra, infer a plausible inclination range for the system between 4° and 15° and place an upper limit on the period of < 4.9 hours based on an inferred companion mass and radius. Little else is known about the system parameters.

2.2.62 Swift J1842.5−1124

Swift J1842.5−1124 was discovered with Swift/BAT in 2008 (Krimm et al., 2008c). A series of follow-up observations were triggered to observe the entire outburst (Racusin et al., 2008; Krimm et al., 2008b,e). The spectrum of the source was fit well with a combined black body (~ 0.9 keV) and power-law model ($\Gamma \sim 1.5$), where the black body component only contributed ~ 6 % of the total 2–40 keV flux. Strong QPOs near ~ 0.8 Hz were also observed (Markwardt et al., 2008a). Further investigations also showed a weak QPO at 8 Hz and a hardness which suggested that the source was transitioning from the HCS to the SDS (Krimm et al., 2013b).

The above mentioned spectral and timing behaviours combined with the observation of the hard X-ray peak preceding the soft X-ray peak by ~ 10 days in the light curve, a behaviour also seen in BH sources Swift J1539.2−6227 (Krimm et al., 2011b) and GRO J1655−40 (Brocksopp et al., 2006), suggested the system was a BHC (Krimm et al., 2013b). It is important to note that in addition to the discovery outburst, Swift J1842.5−1124 also underwent a later, very weak outburst in February of 2010.

Besides an identified optical counterpart (Torres et al., 2008a), little else is known about the system parameters.

2.2.63 EXO 1846−031

The X-ray source EXO 1846−031 was discovered by EXOSAT when it went into outburst in 1985 (Parmar and White, 1985). Parmar et al. (1993) observe an X-ray spectrum to be well fit with a combination multi-colour disc blackbody and power-law component extending to ∼25 keV as well as significant variability in this hard component, suggesting that EXO 1846−031 is a BHC. In addition, McClintock and Remillard (2006) include this source in their list of BHCs. We therefore follow their suggestion. No optical counterpart was found (Parmar et al., 1993) and little else is known about the orbital parameters of the system.

2.2.64 IGR J18539+0727

The hard X-ray transient IGR J18539+0727 was discovered by INTEGRAL during scans of the galactic plane in 2003 (Lutovinov et al., 2003b). Lutovinov and Revnivtsev (2003) observe an X-ray spectrum that can be fit well with a power-law and a fluorescent line present at ∼6.4 keV, often observed in XRBs in the HCS (Gilfanov et al., 1999). In addition, IGR J18539+0727 also demonstrates strong flux variability on timescales of tenths to tens of seconds and a break frequency in the power spectrum at < 0.1 Hz[26].

Given the spectrum and observed properties in the power spectra of the source, Lutovinov and Revnivtsev (2003) suggest IGR J18539+0727 is a BHC. We follow their suggestion and include this source in our sample as a possible BHC. Nothing is known of the system parameters.

[26]Many NS systems don't demonstrate a break with this low of a frequency (Wijnands and van der Klis, 1999). However, Linares et al. (2007) have observed an accreting millisecond pulsar exhibiting BH-like X-ray variability, including a break frequency below 0.1Hz. As such, these power spectra properties should not be taken as strong evidence for a BH primary.

2.2.65 XTE J1856+053

XTE J1856+053 was discovered by RXTE/PCA during scans of the galactic ridge in 1996 (Marshall et al., 1996). The RXTE/ASM light curve showed two peaks corresponding to two separate outbursts, separated by $\sim$ 4.5 months. The first in April displayed a symmetric shape, and the second in September displayed a FRED pattern (Remillard, 1999). Remillard (1999) give mean hardness ratios (using the RXTE/ASM) for 1996a and 1996b of $\sim$0.4. Applying our hardness criterion for this instrument (see Chapter 3), both outbursts are classified as successful. This classification is confirmed by the HIDs presented in Sala et al. (2008).

In 2007, XTE J1856+053 was once again detected by RXTE (Levine and Remillard, 2007). Much like the 1996 outburst, two peaks were observed. However, this time they were separated by only a few weeks, and therefore are counted as only one outburst (Sala et al., 2008). Sala et al. (2008) observed that the X-ray spectrum of the 2007 outburst to be dominated by emission from the accretion disc and found no evidence for a power-law component, consistent with a BHC in the soft state (McClintock and Remillard, 2006).

They further classify XTE J1856+053 as a LMXB based on the non-detection at IR wavelengths, therefore ruling out a massive companion, and suggest a BH primary based on the low temperature of the accretion disc and their rough estimate of a mass range between $1.3 - 4.2 M_{\odot}$. Remillard (1999) also classify this source as a BHC. No other information is available on the parameters of this system.

2.2.66 XTE J1859+226

XTE J1859+226 was discovered by the ASM aboard RXTE in 1999 (Wood et al., 1999). Follow-up RXTE/PCA observations exhibited a hard power-law spectrum and the existence of QPOs of frequency 0.45 Hz (Markwardt et al., 1999a). BATSE observations would confirm the hard spectrum extending up to $\sim$200 keV and reveal that the hard X-ray flux peaked while the soft X-ray flux was still rising (McCollough and Wilson, 1999). Eventually the hard flux began to decline and the source was observed to enter into a series of soft flares (Focke et al., 2000). During these flares,

QPOs were again detected, this time at 6–7 Hz and 82–187 Hz (Cui et al., 2000). For further in-depth spectral and timing analysis of the outburst, see Farinelli et al. (2013) and Casella et al. (2004), respectively. The above mentioned X-ray and timing properties suggested a likely BH primary in the system (Brocksopp et al., 2002).

Shortly thereafter, both the radio (Pooley and Fender, 1997) and optical (Garnavich et al., 1999) counterparts were discovered. Brocksopp et al. (2002) observed the outburst in the radio and found a series of ejections occurred simultaneously with spectral hardening of the source, suggesting a disc/jet connection. Following the decay of the outburst, Garnavich and Quinn (2000) searched the optical photometry finding a potential $P_{\rm orb} \sim 9.2$ hours, which was later confirmed by Sanchez-Fernandez et al. (2000). Filippenko and Chornock (2001) were the first to determine a mass function for XTE J1859+226, thereby confirming the BH nature of the primary.

More recently, Corral-Santana et al. (2011) perform optical photometry and spectroscopy of XTE J1859+226 and find an $P_{\rm orb} \sim 6.6$ hours, a companion spectral type of K5–7V, and a $f(M) = 4.5 \pm 0.6 M_{\odot}$ which, while significantly lower than the original estimate, is still consistent with the presence of a BH primary in the system. Corral-Santana et al. (2011) fit a star-only model to find an $i = 60°$. Their data is consistent with the passive state (Kreidberg et al., 2012), therefore we adopt this value for the inclination and use it to calculate a $M_{\rm BH}$.

The distance to XTE J1859+226 remains problematic. Zurita et al. (2002) estimate 11 kpc based on the brightness of the outburst and the optical counterpart. While Hynes (2005), using the same method as Zurita et al. (2002) and the orbital parameters originally estimated for the system by Filippenko and Chornock (2001), estimate a distance of $\sim$ 21 kpc. In contrast, Markwardt (2001) use a combination of spectral and timing information to estimate $\sim$5–13 kpc and Hynes et al. (2000a), using fits to optical-UV spectral energy distribution, find an estimate of $\sim$4.6–8.0 kpc.

Due to the uncertainty that still exists in the system parameters, we agree with Hynes (2005) in believing that the outburst estimates are more reliable and adopt their estimate of 8 ± 3 kpc for the purposes of our analysis.

2.2.67 XTE J1901+014

XTE J1901+014 was discovered by the ASM aboard RXTE in 2002 (Remillard and Smith, 2002). This outburst lasted between 2 minutes and 3 hours. No conclusions could be made about the nature of the source at the time. Later, when reanalyzing RXTE/ASM data, Remillard and Smith (2002) found a previous outburst of the source occurring in 1997, lasting between 6 minutes and 8 hours.

Karasev et al. (2007) performed spectral and timing analysis on the 1997 and 2002 outbursts and suggest that these outbursts are in fact not type I X-ray bursts. Next, they fit the broadband spectrum with a power-law of photon index $\Gamma \sim 2.3$, finding no cutoffs at energies between 20–30 keV[27], or any emission lines in the spectrum. They conclude that such a non-thermal spectrum, with no evidence of cutoff, might indirectly indicate that the primary is in fact a BH.

Karasev et al. (2007) also suggest that the intense outbursts detected in XTE J1901+014 are similar in spectral and timing properties to those observed in galactic BH source SAX J1819.3−2525 (Stubbings and Pearce, 1999) and to a lesser degree, the outbursts of fast transients like SAX J1818.9-1703 (Grebenev and Sunyaev, 2005), concluding that XTE J1901+014 may belong to a class of fast X-ray transients containing a BH.

XTE J1901+014 once again became active in 2006. Karasev et al. (2008) performed spectral and timing analysis on this outburst, finding a power spectrum consistent with accreting XRBs. They also attempted (and failed) to find the optical counterpart. While they were unsuccessful, they still speculate on the nature of the companion and distance to the source. Overall they conclude, in agreement with Karasev et al. (2007), that XTE J1901+014 is probably the first fast X-ray transient in a LMXB.

In 2010, Swift/BAT detected XTE J1901+014 in outburst for the fourth time. This outburst lasted at least 2.5 minutes, at which point the spacecraft was moved due to a pre-planned slew. The time-averaged spectrum was consistent with the other three outbursts (Krimm et al., 2010). No other information is available on the

[27] A behaviour which is characteristic of pulsars (Filippova et al., 2005).

system parameters, and the nature of the compact object still remains uncertain. Nevertheless, for the reasons presented above we include this source in our sample as a possible BHC.

2.2.68 XTE J1908+094

XTE J1908+094 was discovered serendipitously in observations of SGR 1900+14 with RXTE/PCA in 2002. The spectrum was consistent with an absorbed power-law of photon index $\Gamma \sim 1.6$ and no pulsations were detected in the power spectrum suggesting that XTE J1908+094 was an XRB containing a BH primary (Woods et al., 2002). Subsequent BeppoSAX observations (in't Zand et al., 2002a) confirmed the hard spectrum, extending up to $\sim$ 250 keV, and the high galactic absorption. Detailed spectral and timing analysis by in't Zand et al. (2002c) and Gogus et al. (2004), which confirmed that the source passed through both the HCS and SDS during outburst, agreed with the conclusion drawn by Woods et al. (2002) that XTE J1908+094 is in fact a BHC.

The radio counterpart was discovered by Rupen et al. (2002). Jonker et al. (2004) analyzed simultaneous X-ray and radio observations during the outburst decay and discuss the X-ray/radio correlation. Chaty et al. (2006) discuss two possible candidates for the optical counterpart of XTE J1908+094. The companion star could be either (i) an intermediate/late type main-sequence star of spectral type A–K, located between 3–10 kpc; or (ii) a late-type main-sequence star of spectral type K or later, located between 1–3 kpc. They favour the former due to an independently determined lower limit on distance of 3 kpc derived by in't Zand et al. (2002c) from the peak bolometric flux.

XTE J1908+094 was again detected in outburst by Swift/BAT in October of 2013 (Krimm et al., 2013a). The spectrum was consistent with a power-law of photon index $\Gamma \sim 1.6$, suggesting the source was in the HCS (Krimm et al., 2013c). Following detection in the X-ray, subsequent radio observations were triggered. Miller-Jones et al. (2013) find a flat radio spectrum, often associated with compact jets known to exist in the hard spectral state of a BHXRBs. Further radio observations revealed a significant increase of the radio flux density suggesting the ejection of optically

thin radio-emitting plasma, confirming the source had started to make the hard-to-soft state transition (Coriat et al., 2013b). No other information is available on the orbital parameters of the system.

2.2.69 Swift J1910.2−0546

Swift J1910.2−0546 was simultaneously discovered by Swift/BAT (Krimm et al., 2012) and MAXI (Usui et al., 2012) (who gave it the alternate name MAXI J1910−057) in 2012. Thereafter, Rau et al. (2012a) detected the optical/near IR counterpart. Lloyd et al. (2012) and Casares et al. (2012) report possible periodic variations in the optical light curve, which could be attributed to orbital variations, of ~ 2.2 hours, and ~ 4 hours, respectively.

The complex light curve (Krimm et al., 2013b) of the source, as well as spectral analysis from MAXI (Kimura et al., 2012; Nakahira et al., 2012b) and INTEGRAL (King et al., 2012), show behaviour usually associated with BHCs, most notably the progression through state transitions throughout the outburst and the mirrored behaviour of the hard and soft X-ray flux. For this reason Krimm et al. (2013b) tentatively suggest that Swift J1910.2−0546 is a BHC. We agree with their rational and include this source in our sample as a possible BHC. No other information is available about the orbital parameters of the system.

2.2.70 SS 433

The galactic micro-quasar SS 433 was discovered in 1978 by the UHURU satellite (Margon, 1978). In the X-ray, where there are very few existing observations, SS 433 is a weak source, generally not observable past ∼30 keV (Nandi et al., 2005).

Even after more than 35 years, despite the enormous observational effort, the nature of the compact object and companion remain uncertain. In fact, the mass function and orbital period are among the few orbital parameters known (Fabrika and Bychkova, 1990). The main reason for this being the highly erratic spectral and temporal behaviour of the system combined with the internal complexity of the system (Brinkmann et al., 1989).

The basic picture that has emerged over the years involves an evolved binary being observed during extensive mass-transfer. The secondary feeds an enlarged accretion disc around a compact object (NS or BH) (Blundell et al., 2001). Some of this mass is directed through the disc toward the oppositely facing relativistic jets. As a result we observe red and blue shifted optical lines, indicating this material is being accelerated by the jets (Fabian and Rees, 1979; Milgrom, 1979; Gies et al., 2002).

Margon (1984) successfully fit a precessing jet model to these lines, finding that the jets moved near constant velocity of $\sim 0.26c$ and had a precession periodicity of 162.15 days. This model would later be confirmed by subsequent radio imaging of the source, showing twin jets with structure on scales ranging from milliarcseconds to arcseconds (Hjellming and Johnson, 1981; Vermeulen et al., 1987, 1993; Fejes et al., 1988). In addition, X-ray emission lines, which mimicked the behaviour of the "moving" optical lines, were also discovered allowing for the calculation of an an $P_{\rm orb} = 13.1$ days (Kotani et al., 1994; Marshall et al., 2002; Margon, 1984).

Given the above observations and other photometric data (Kemp et al., 1986), SS 433 is believed to be a binary system consisting of a compact object and an O or B type star (Margon, 1984). Extensive arguments for the nature of the compact object being a BH (Zwitter and Calvani, 1989; Fabrika and Bychkova, 1990) and a NS (Filippenko et al., 1988; D'Odorico et al., 1991) have been made.

Possible distance estimates range from 3.1 kpc (Dubner et al., 1998) to 5.5 kpc (Hjellming and Johnson, 1981). Blundell and Bowler (2004) calculate a distance of 5.5 ± 0.2 kpc, which is consistent with Hjellming and Johnson (1981), but substantially greater than the estimate by Dubner et al. (1998). Dubner et al. (1998) suggested that a gas cloud, seen in HI (neutral Hydrogen) emission, was interacting with the W50 nebula, and used the inferred velocity of the cloud to estimate distance (provided the rotational model of the galaxy was correct). However, the rotational model for the galaxy assumed pure circular motion and did not take into account other complicated behaviours, such as the effect the presence of a bar in the Galaxy has on gas motion near SS 433 (Binney et al., 1991). For this reason, we adopt the distance estimate from Blundell and Bowler (2004) for the purpose of our analysis.

2.2.71 GRS 1915+105

GRS 1915+105 was discovered in 1992 by the WATCH ASM aboard GRANAT (Castro-Tirado et al., 1992) and has remained active ever since (Belloni and Altamirano, 2013). The system exhibits very peculiar behaviour, in the form of complex structured variability, such as QPOs ranging in frequency from 10^{-3} Hz to 67 Hz and patterns of dips and rapid transitions between high and low intensity in the light curve (Greiner et al., 1996; Morgan et al., 1997; Belloni et al., 2000; Klein-Wolt et al., 2002; Fender and Belloni, 2004; Hannikainen et al., 2005). In fact, modelling of this X-ray variability has led to major insights into the connection between the accretion disc and relativistic jets in XRBs (Belloni et al., 1997; Klein-Wolt et al., 2002).

The probable optical counterpart was discovered by Boer et al. (1996) and the radio counterpart was found with the VLA (Mirabel et al., 1993). Further radio monitoring would reveal structures travelling at superluminal speed (Mirabel and Rodríguez, 1994), making GRS 1915+105 the first superluminal source in the Galaxy. In fact, GRS 1915+105 was originally suggested to harbour a BH based on its similarity with GRO J1655−40, the second galactic source to exhibit superluminal motion for which the dynamical mass estimate implied the presence of a BH (Bailyn et al., 1995b). In addition, according to spectral and timing analysis, the source has been observed in all four BH spectral states (Morgan et al., 1997) and its luminosity is estimated to be near Eddington (Belloni and Altamirano, 2013).

GRS 1915+105 also exhibits a second type of outflow, other then the radio jet, in the form of an accretion disc wind (Ponti et al., 2012). In fact it is the first BH source in which this type of outflow has been detected (Lee et al., 2002). Additionally, studies of the accretion disc wind in GRS 1915+105 have led to the suggestion that these winds could possibly act as the jet suppression mechanism in the soft states (Neilsen and Lee, 2009).

The binary system parameters for GRS 1915+105 remained elusive for quite some time, despite extensive observational effort (Castro-Tirado et al., 1996; Eikenberry et al., 1998; Mirabel et al., 1997; Marti et al., 2000b; Harlaftis et al., 2001; Greiner et al., 2001b). That was until Greiner et al. (2001a) was able to obtain a radial velocity curve, $P_{\rm orb}$ and therefore $f(M)$. Unfortunately, an estimate of inclination

was problematic as studies of ellipsoidal variability for this source have not been possible because of substantial disc and jet flux variation (Kreidberg et al., 2012).

Instead, inclination has been estimated based on the orientation of the jets ($i = 70^\circ \pm 2^\circ$ (Mirabel and Rodríguez, 1994) or $i = 66^\circ \pm 2^\circ$ (Fender et al., 1999b)). These parameters, along with the mass ratio estimated by Harlaftis and Greiner (2004), allowed for a dynamical mass estimate confirming the nature of the BH accretor in the system. For the purpose of our analysis, following Greiner et al. (2001a) and Kreidberg et al. (2012), we adopt the inclination and distance estimated originally by Mirabel and Rodríguez (1994) and the improved mass ratio from Harlaftis and Greiner (2004) to calculate a $M_{\rm BH}$.

2.2.72 4U 1956+350

Cygnus X−1, one of the brightest X-ray sources in the sky, was discovered in the X-rays by the UHURU satellite in 1971 (Tananbaum et al., 1972). In Cyg X−1, focussed wind from the companion star drives the source of X-ray radiation (Gies and Bolton, 1986). The X-ray emission has been shown to exhibit strong variability on timescale from millliseconds to months (Priedhorsky et al., 1983; Miyamoto and Kitamoto, 1989).

Numerous spectral and timing studies over the years (Holt et al., 1979; Ling et al., 1983; Belloni and Hasinger, 1990; Kitamoto et al., 1990a; Barr and van der Woerd, 1990; Ubertini et al., 1991a; Miyamoto et al., 1992; Gierlinski et al., 1997; Zdziarski et al., 2002; Pottschmidt et al., 2003; Wilms et al., 2006; Gierlinski et al., 2010; Grinberg et al., 2013) have shown Cyg X−1 to spend most of its time in the HCS, resulting in its X-ray spectrum never fully being disc dominated (Grinberg et al., 2013). Cyg X−1 often undergoes "failed" state transitions, never fully transitioning to the softer states (Pottschmidt et al., 2003). This extended hard state of Cygnus X−1 shows weak and persistent radio emission, which has been resolved to be a steady jet (Stirling et al., 2001). In fact, the "failed" transitions exhibited by this source are thought to be connected to the radio jet, as jet activity is thought to be quenched in the soft accretion states (Fender et al., 2004, 2006; Wilms et al., 2007). For a complete list of X-ray studies see Table A.4. For studies of Cyg X−1 at radio

wavelengths, see Hjellming and Wade (1971); Hjellming (1973); Tananbaum et al. (1972); Stirling et al. (2001); Gleissner et al. (2004); Fender et al. (2004, 2006).

This system is known to contain a O9.7Iab type supergiant companion (Gies and Bolton, 1986), which orbits around a compact object with a period of ~ 5.6 days (Holt et al., 1979). Over the past 42 years, many estimates on the mass of the compact object have been made (Orosz et al., 2011a). While there exists several low-mass models (Trimble et al., 1973; Bolton, 1975), all conventional models, which assume an O-type supergiant companion (Paczynski, 1974; Gies and Bolton, 1986; Ninkov et al., 1987; Caballero-Nieves et al., 2009), find a large (and uncertain) mass of the compact object exceeding $\sim 3M_{\odot}$, therefore confirming a BH primary. (Kalogera and Baym, 1996).

The large range of these mass estimates is mainly due to the large uncertainty in distance to the source (Reid et al., 2011). With the more recent trigonometric parallax distance measurement calculated by Reid et al. (2011), Orosz et al. (2011a) was able to build a complete improved dynamical model for Cyg X−1, including $M_{\rm BH}$, q and i. We make use of this dynamical model for the purposes of our analysis.

2.2.73 4U 1957+115

4U 1957+115 was discovered by UHURU in 1973 (Giacconi et al., 1974). Despite having an X-ray brightness which is comparable to (and occasionally larger) than the well-studied persistent BH sources LMC X−1 and LMC X−3, little is known about the nature of the system (Nowak et al., 2008).

Optical spectra reveal a power-law continuum with Hα, Hβ and He II 4686 $\mathring{A}$ emission lines (Cowley et al., 1988; Shahbaz et al., 1996a), typical of systems dominated by an accretion disc (Thorstensen, 1987). Long-term variations in the optical light curve have revealed modulations[28] with a 9.33 hour period, generally believed to be the orbital period of the system (Thorstensen, 1987).

The short orbital period, indicative of a late-type main sequence star as a com-

[28]The modulations are interpreted as evidence for an accretion disc with a large outer rim (possibly due to a warp) that is seen close to edge on (Hakala et al., 1999).

panion, and the absence of X-ray eclipses, has allowed for an upper limit estimate of inclination between 70° and 75°, which is consistent with the model of optical variability (Hakala et al., 1999). Little else is known about the orbital parameters of the system.

4U 1957+115 was first classified as a possible BHC in 1984 when EXOSAT observations revealed a very soft spectrum (Ricci et al., 1995). Observations by Nowak et al. (2008), who have analyzed the complete set of available data from RXTE, and more recently, Nowak et al. (2012), reveal that the X-ray spectrum is a pure disc spectrum ∼85% of the time, with the remaining ∼15% involving some non-thermal component.

This dominant soft spectrum, coupled with the observed low fractional variability (Nowak and Wilms, 1999; Wijnands et al., 2002; Nowak et al., 2008), both characteristic of the soft state, make 4U 1957+115 one of only three BHCs which not only remain persistently in outburst but also spend most of their time in the soft disc-dominated accretion state (Nowak et al., 2008). Further evidence for this behaviour is implied from the recent radio non-detection (Russell et al., 2011b), as jet production is believed to be quenched in the soft state. While 4U 1957+115 may not show evidence for a relativistic jet, this source has been observed to exhibit an outflow in the form of an accretion disc wind (Ponti et al., 2012).

As there exists no dynamical mass or distance measurements for the system, X-ray and optical observations, analyzed at different times, have been used to argue whether the compact object is a BH (Wijnands et al., 2002; Nowak et al., 2008, 2012; Maitra et al., 2013) or NS (Yaqoob et al., 1993; Ricci et al., 1995; Robinson et al., 2012). Regardless of the uncertainty, we include this system in our sample as a possible BHC.

2.2.74 GS 2000+251

GS 2000+251 was discovered by the ASM aboard GINGA in 1988 (Tsunemi et al., 1989). The source has been observed to exhibit spectral and temporal characteristics similar to other X-ray nova systems believed to contain BH primaries (van Paradijs and McClintock, 1995; Tanaka and Lewin, 1995).

Hjellming et al. (1988) found a transient radio source associated with GS 2000+25 exhibiting a spectrum that was fit well with a synchrotron model, similar to the radio emission observed in 1A 0620−00 (Owen et al., 1976), suggesting the possibility of a radio jet in the system. Optical photometry after this outburst revealed that the system had a ∼8.3 hour orbital period (Chevalier and Ilovaisky, 1993). Dynamical measurements first obtained by Filippenko et al. (1995) and later improved upon by Casares et al. (1995a) and Harlaftis et al. (1996) revealed a $f(M) = 5.01 \pm 0.12$, subsequently confirming the BH nature of the primary. The distance to this source is estimated by Barret et al. (1996b).

Ioannou et al. (2004) has performed the most extensive study of ellipsoidal variability. They measure an inclination of $54^\circ < i < 60^\circ$ which is consistent with estimates by Callanan et al. (1996) and Beekman et al. (1996). However, while Kreidberg et al. (2012) conclude that the source was passive during their observations, they suggest their inclination measurement is depressed due to the binning of the light curves, which can slightly decrease the amplitude of ellipsoidal variations. Therefore, following the suggestion by Kreidberg et al. (2012), we adopt the inclination from Callanan et al. (1996) of $55^\circ < i < 65^\circ$, and assume a uniform distribution across this range to calculate a $M_{\rm BH}$.

2.2.75 XTE J2012+381

The transient X-ray source XTE J2012+381 was discovered with the ASM aboard RXTE in 1998 during outburst (Remillard et al., 1998). The light curve exhibited FRED like behaviour (Chen et al., 1997) and the X-ray spectrum was well described by a combination multicolour disc black body ($T \sim 0.76$ keV) and power-law with photon index $\Gamma \sim 2.9$ (White et al., 1998), characteristic of BHXRBs (McClintock and Remillard, 2006). In addition, extensive spectral and timing analysis of this outburst reveal the source exhibited the typical canonical evolution seen in BHXRBs, transitioning between the hard and soft states (Vasiliev et al., 2000; Campana et al., 2001).

The radio counterpart was discovered by Hjellming et al. (1998d), while Hynes et al. (1999) identified the optical counterpart with a faint red star heavily blended

with a brighter foreground star. Given the light curve behaviour, spectral and timing characteristics, XTE J2012+381 is considered a BHC. No other information is available on the system parameters.

2.2.76 GS 2023+338

GS 2023+338 (V404 Cyg) was discovered with the GINGA satellite in 1989 during outburst (Makino, 1989). V404 Cyg is one of the most well-known transient X-ray sources due to both its high X-ray luminosity and levels of variability at many different wavelengths in outburst and quiescence (Tanaka and Lewin, 1995; Hynes et al., 2002). The many X-ray observations (Kitamoto et al., 1989; in 't Zand et al., 1992; Miyamoto et al., 1992, 1993) that exist show that, despite its high X-ray luminosity, there is no soft component in the spectrum (Oosterbroek et al., 1997), suggesting that V404 Cyg is a "failed" outburst source (Brocksopp et al., 2004). While this fact has been disputed by Zycki et al. (1999), who claim that the source spent a short period of time in the soft state, we consider the 1989 event as a possible "failed" outburst.

The source has also been detected at radio (Hjellming and Han, 1989) wavelengths. The persistent radio emission displays a flat spectrum, which is indicative of a self-absorbed synchrotron jet (Gallo et al., 2005; Miller-Jones et al., 2008).

The optical counterpart was discovered by Wagner et al. (1989) as Nova Cygni 1938. Further optical observations led to a calculation of the mass function by Casares et al. (1992), which was later refined by Casares and Charles (1994) to be $f(M) = 6.08 \pm 0.06 M_{\odot}$, confirming the BH nature of the primary. Shahbaz et al. (1994b) modelled ellipsoidal variations of the source obtaining a ~ 6.5 day orbital period.

More recently, Miller-Jones et al. (2009) obtained a distance to V404 Cyg of $d = 2.39 \pm 0.14$ kpc using trigonometric parallax, making this the first accurate parallax distance measurement to a BH system. We make use of this distance, which is significantly lower than the previously excepted values, for the purposes of our analysis.

The light curve of GS 2023+338 exhibits strong aperiodic variability making it

difficult to obtain precise inclination measurements for the system. Wagner et al. (1992) and Shahbaz et al. (1994a) have been able to constrain the inclination to $50^\circ < i < 80^\circ$ and $45^\circ < i < 83^\circ$, respectively. Wagner et al. (1992) obtained their lower limit from observations of Balmer spectral lines and the upper limit based on the lack of eclipses. While Shahbaz et al. (1994a) obtain their range by fitting a star only model, which provided a poor fit due incorrect colour correction. In addition, while Sanwal et al. (1996) fit a star only model to the IR data, the author's note hour time scale variability in the light curve, suggesting the source is most likely in the active state. We therefore adopt the inclination calculated by Kreidberg et al. (2012), which makes use of the inclination estimate from Sanwal et al. (1996) of $i > 62^\circ$ to obtain a corrected inclination estimate in order to calculate a $M_{\rm BH}$.

Chapter 3

Data Selection & Analysis

3.1 X-ray Telescopes

To construct the database we have incorporated data from the All-Sky Monitors (ASMs) and Galactic Bulge Scan Surveys available since 1996, making it possible to study nearly two decades of behaviour exhibited by the Galactic BHXRB population.

3.1.1 The All-Sky Monitors

ASMs provide near real-time coverage of large portions of the X-ray sky across both hard and soft X-ray energies. They usually operate on short timescales, on the order of $\sim$ 1 day or less, allowing them to track short term changes in behaviour in known sources as well as discover new sources, making them indispensable in the study of XRBs, which often exhibit large and rapid variations. In addition, these X-ray monitors accumulate vast databases of activity, which can be used to track outbursts, study evolution and state transitions and overall derive a long term history for numerous sources (e.g., McClintock and Remillard (2006); Krimm et al. (2013b)).

The Rossi X-ray Timing Explorer[1] *(RXTE)* (Swank, 1997) was perhaps the most important vehicle for the study of transient phenomena in the last decade due to its wide-sky coverage, relatively high sensitivity and fast response time (McClintock and

[1] http://heasarc.nasa.gov

Remillard, 2006). The ASM aboard RXTE, made up of three wide-field proportional counters[2], operated in the 1.5–12 keV band from 1996–2012. The ASM (Levine et al., 1996) had the ability to cover $\sim 90\%$ of the sky every orbit, which took about 90 minutes, with a sensitivity between $\sim$10–20 mCrab (integrating all orbits over a full day)(McClintock and Remillard, 2006).

The Swift Burst Alert Telescope[3] *(BAT)* (Krimm et al., 2013b) has provided near real time, wide-field (2 steradians) coverage of the X-ray sky in the 15–50 keV energy range since 2005. The BAT X-ray Monitor has the ability to observe 88% of the sky every day with a sensitivity of 5.3 mCrab (integrating scans over 1 day) and arcminute positional accuracy. One of its key characteristics is the ability to "swiftly" ($\lesssim 90$ s) and autonomously repoint itself after detection by BAT to bring the source within the field of view of the sensitive narrow-field X-ray and UV/optical instruments that are also on board the observatory.

The Monitor of All-Sky Image[4] *(MAXI) Telescope* (Matsuoka et al., 2009), mounted on the International Space Station (ISS) has the ability to scan 90–98% of the sky every 96 minutes (one orbit/rotation period of the ISS) with its wide field of view providing near real-time coverage with a positional accuracy of < 6 arcminutes and a daily sensitivity of 15 mCrab. The ASM aboard MAXI is a Gas Slit Camera (GSC) (Mihara et al., 2011) detector containing a proportional counter which covers the 2–20 keV energy band with its large detection area (5000 cm^2).

3.1.2 The Scanning Surveys

Scanning Surveys typically observe the Galactic Bulge, a region rich in bright variable high-energy X-ray sources, regularly during all visible periods, ultimately providing high sensitivity long-term light curves of numerous X-ray sources.

[2]Proportional counters contain a windowed gas cell subdivided into regions of low and high electric fields using electrodes. The signal induced on these electrodes, via photoionization of the gas by X-rays, contains information on arrival times, energies and interaction position of the photons transmitted by the window. For a detailed description of Proportional Counters see Fraser (2009).

[3]http://swift.gsfc.nasa.gov/results/transients/

[4]http://maxi.riken.jp/top/

The Proportional Counter Array[5] *(PCA)* (Jahoda et al., 1996; Swank and Markwardt, 2001) aboard RXTE has provided periodic scans of the galactic bulge region, in the 2.5–10 keV energy band, from 1999–2011. The PCA consists of an array of five proportional counters, with a total collecting area of 6500cm^2 and a daily sensitivity of 0.1 mCrab.

The INTErnational Gamma-Ray Astrophysics Laboratory[6] *(INTEGRAL)* (Winkler et al., 2003; Kuulkers et al., 2007) has provided periodic scans of the Galactic Bulge since 2005. Data is taken approximately every 3 days (the length of one orbit) and is provided in the form of single observations lasting ∼1.8 ksec. There are two Joint European X-Ray Monitor (JEM-X) X-ray detectors aboard INTEGRAL, and one imager, the Integral Soft Gamma-Ray Imager (ISGRI), which collectively cover a total energy range of 3–100 keV. The JEM-X field of view is more limited than that of ISGRI, covering only ∼10% of the area of sky visible by ISGRI.

3.1.3 The Transmission & Absorption of X-rays in the Interstellar Medium (ISM)

As we are studying sources within the Galaxy across a wide energy range, X-ray absorption by the ISM becomes important, especially in the soft X-ray regime. The degree to which X-rays are transmitted through the ISM is dependent on two factors (Seward, 2000):

- Column Density: Denoted as N_H and expressed in terms of number of hydrogen atoms per cm^2; and
- Elemental composition: commonly used models today include *phabs*[7] or *tbabs*[8], which take a variety of elemental abundances (e.g., Wilms et al. (2000)) and cross-sections (e.g., Verner et al. (1996)).

[5]http://asd.gsfc.nasa.gov/Craig.Markwardt//galscan/main.html

[6]http://integral.esac.esa.int/BULGE/

[7]A model in XSPEC used to calculate photoelectric absorption by the ISM given cross-sections and abundances.

[8]tbabs refers to the Tuebingen-Boulder ISM absorption model in XSPEC which calculates the cross section for X-ray absorption by the ISM using the sum of the cross sections due to the gas-phase, the grain-phase, and the molecules in the ISM.

At low photon energies, $\epsilon \ll m_e c^2$, the dominant process governing a photon's interaction with matter is photoelectric (bound-free) absorption. In the photoelectric absorption process, an incident X-ray photon transfers all of its energy to an electron, which is subsequently ejected from the atom. For the process to occur, the energy of the incident photon ϵ must be greater than or equal to the binding energy of the electron (E_1) it is ejecting.

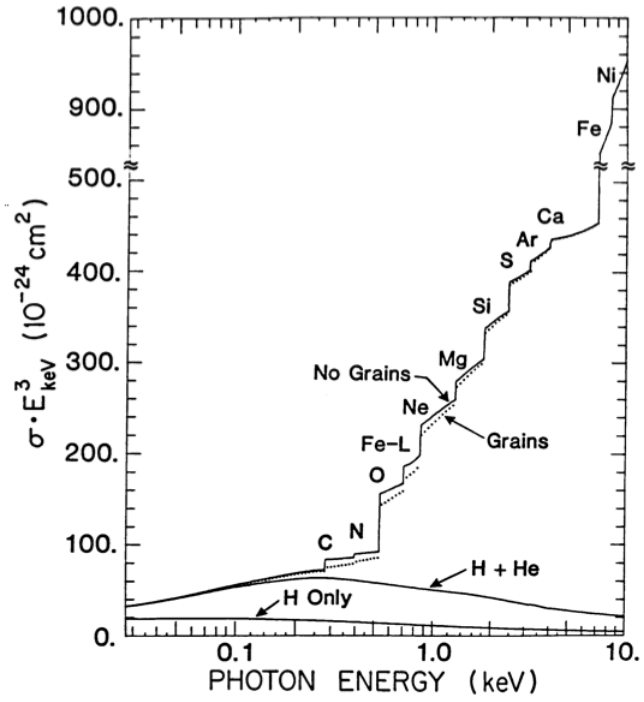

Figure 3.1: X-ray absorption coefficient σ as a function of energy for the ISM. The vertical (or upward sloping) jumps are due to the absorption edges of each element occurring when the incident photon energy is equal to the electron binding energy. The two most prominent absorption edges are that of oxygen (O) at 0.53 keV and iron (Fe) at 7.1 keV. Figure from Seward (2000).

The photon energy $\epsilon = E_1$ corresponds to a discontinuity in the spectrum of radiation, referred to as an absorption edge. They occur because it is impossible for photons of $\epsilon < E_1$ to eject an electron. The cross-section of photons (with $\epsilon > E_1$) goes as $\sigma \propto \epsilon^{-3}$ (Longair, 2011).

In the case of the ISM, rather surprising, most of the absorption of X-rays is not a result of hydrogen as the "H" in the column density suggests, rather it is in

oxygen (O) and iron (Fe). The relative importance of these elements in this process can physically be seen in the vertical jumps in absorption cross section (caused by the absorption edges) of these elements at specific photon energies (see Figure 3.1) (Seward, 2000).

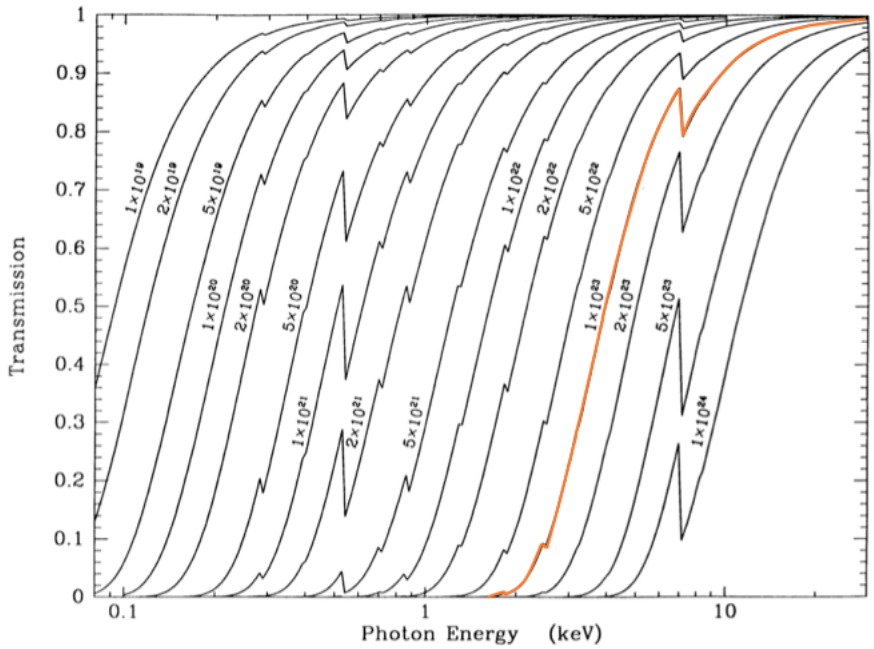

Figure 3.2: X-ray transmission fraction as a function of energy for a wide range of column densities in the ISM. For a typical column density observed in the Galactic Center region, $N_H \sim 10^{23}$ atoms cm^{-2} (orange line), the transmission fraction is effectively zero for all soft X-rays < 2 keV. Thus, we expect the spectrum of Galactic X-ray sources to exhibit a turn-over at ~ 2 keV due to the effects of interstellar photoelectric absorption. Figure from Seward (2000).

Overall, we can observe the dominant effect the photoelectric absorption process has on the X-ray spectrum at soft (low) energies over a large range of column densities from Figure 3.2. If we adopt a typical column density observed in the Galactic Center region, $N_H \sim 1 \times 10^{23}$atoms cm^{-2} (private communication with C.O. Heinke), we can conclude that, for the given N_H, the spectrum of most Galactic X-ray sources will turn over at $\sim$2 keV due to interstellar photoelectric absorption[9] (Longair, 2011).

[9]Actually for a typical LMXB in the Galaxy, $N_H \sim 1 \times 10^{22} - 2 \times 10^{22}$ is more common (making the cutoff between 1 and 1.5 keV). Nevertheless, including data below 2 keV requires explicit modelling of N_H, so our argument is still valid.

It is for this reason that we omit from our analysis bands which involve energies below 2 keV, specifically RXTE A (1.5–3 keV), as using this band would require us to introduce more modelling of the effect of absorption when dealing with a sample across a range of Galactic N_H.

3.1.4 The Crab Nebula as a standard candle in the X-ray regime

While the use of multiple telescopes brings with it the advantage of being able to probe the X-ray sky over a wide energy range and long consecutive time periods, it forces us to address the non-trivial issue of how to effectively compare emission from multiple telescopes/instruments in a logical way.

We have chosen to solve this problem by using the Crab Nebula as a comparison tool. The Crab Nebula is often used an an X-ray calibration source due to the fact that it has been observed to be a bright, approximately steady X-ray source producing a constant spectrum. We make use of the now accepted "canonical" simple power-law spectrum, originally estimated by Toor and Seward (1974), of the form,

$$I(E) = (9.7 \pm 1.0)E^{(-1.10\pm0.03)}\mathrm{keV\,cm^{-2}\,s^{-1}\,keV^{-1}} \tag{3.1}$$

valid in the 2–50 keV range. Note, in this form, the index on the power-law is quoted as $\alpha = \Gamma - 1$. See Kirsch et al. (2005) for a review of past estimates of this spectrum.

Using crabs as a baseline unit of flux not only allows us to calculate approximate count rate equivalences in each energy band, therefore giving us the ability to directly compare data from a particular source across telescopes and instruments (i.e., light curves, hardness ratios etc.), but also gives us a straightforward method for converting between count rate and flux in a given energy band (via integration of the known spectrum over the given band).

That being said, our analysis clearly relies heavily on the assumption that the Crab is a steady X-ray source in any given band (specifically the count rate over the instrumental area (or flux density in counts $\mathrm{cm^{-2}s^{-1}}$) is constant). This assumption brings with it three separate issues. The first being that the Crab is variable, more so

at higher energies then lower energies (Wilson-Hodge et al., 2010), which will subtly effect Swift/BAT and INTEGRAL data. However, as this would be very hard to correct for and should not have a large impact on our results, we consider the effect negligible (Private Communication with C.O. Heinke).

The second, MAXI has serious problems with its calibration. These problems are most obvious in the MAXI soft (2–4 keV) band, where the Crab light curve displays uncharacteristic oscillatory behaviour (see Figure 3.3). Including this band would thus lead to a large systematic uncertainty. In addition, we omit the MAXI hard (10–20 keV) band based on its relatively poor signal-to-noise ratio.

Lastly, assuming that the spectrum is Crab-like obviously induces errors in the flux computations. However, within each (fairly narrow) classification band these are relatively small, so we can justify our approach.

Table 3.1 presents specific details on the telescopes, instruments, and energy bands used in this study. Data for this work has been acquired from the BAT Transient Monitor, the MAXI Database, the NASA RXTE/ASM source catalog, Craig Markwardt's (RXTE/PCA) Galactic Bulge Survey Webpage, and the INTEGRAL Galactic Bulge Monitoring Program.

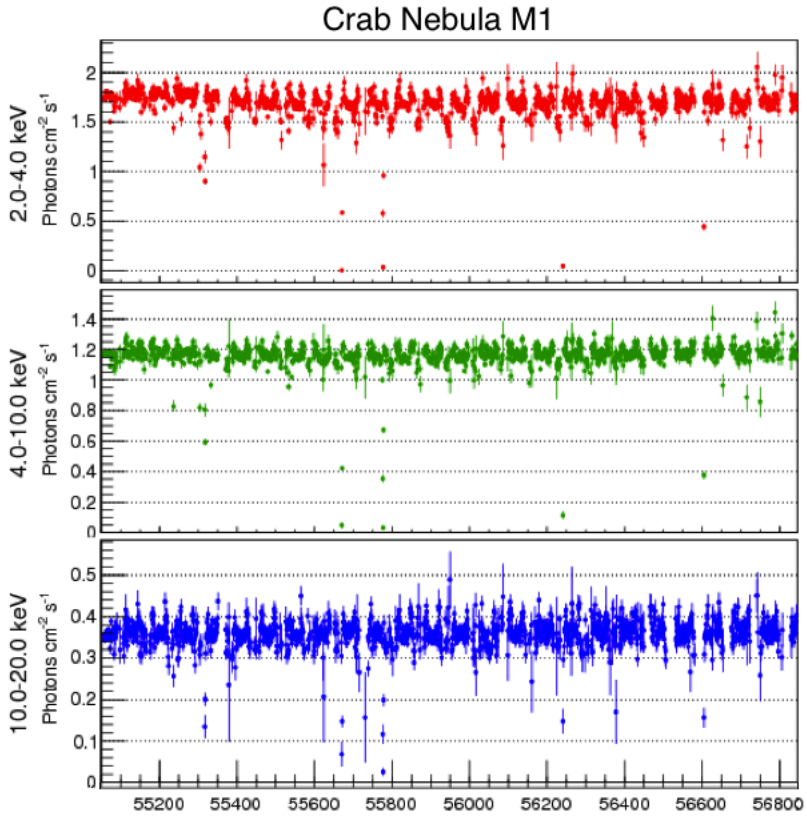

Figure 3.3: Light curves of the Crab Nebula in the three separate MAXI bands, 2–4 keV (red), 4–10 keV (green) and 10–20 keV (blue). Note both the oscillatory behaviour seen most notably in the 2–4 keV and and to a much lesser degree in the 4–10 keV band and the intervals of poor data quality (i.e., 55600–55800), which have lead to drastic drops in the count rate in the 10–20 keV band. Image taken from the MAXI Database: http://maxi.riken.jp/top/.

Table 3.1: Telescope/Instrument Technical Details

Telescope	Instruments	Type[c]	t_{active}[d] (MJD)	Energy Band (keV)	Reported Units	Data[d] Type	Crab Conversion[e] (crabs)	Flux Conversion[g] (erg cm^{-2} s^{-1})	Band[h] Usage
RXTE	ASM	all-sky	50088–55924	$3-5$	ct s^{-1}	orbital	23.3	6.93×10^{-9}	D,C
				$5-12$			25.4	1.10906×10^{-8}	D,C
				$3-12$[b]			-	1.80248×10^{-8}	D,C
	PCA	scan	51214–55869	$2.5-10$[i]	ct s^{-1}5 PCU^{-1}	daily	13930	1.84×10^{-8}	D,C
INTEGRAL	JEM-X	scan	53419–	$3-10$	ct s^{-1}	orbital	235/249[f]	1.58×10^{-8}	D,C
				$10-25$			74/70[g]	1.08086×10^{-8}	D
	ISGRI	scan	53419–	$18-40$	ct s^{-1}	orbital	210	8.93×10^{-9}	D,C
				$40-100$			104	9.40945×10^{-9}	D
Swift	BAT	all-sky	53414–	$15-50$	ct cm^{-2}s^{-1}	daily	0.22	1.34×10^{-8}	D,C
MAXI	GSC	all-sky	55058.5–	$4-10$	ph cm^{-2}s^{-1}	daily	1.24	1.18×10^{-8}	D,C
				$4-20$[b]			-	2.01127×10^{-8}	D

Note. –

[a] Indicates whether the instrument functions as an all-sky monitor or a scanning survey .

[b] Energy bands manufactured (after crab conversion per band) via an addition process.

[c] Data type collected from the original source. All orbital data was converted to daily averaged data by calculating a weighted mean count rate per day.

[d] The time period the instrument has been active.

[e] The average photon flux for the Crab Nebula in a given energy band.

[f] Their are two JEM-X units, each with a separate crab conversion. The column format given is J1/J2.

[g] Equivalent of 1 crab in flux units (erg cm^{-2}s^{-1}) assuming the Crab Nebula has a spectrum $I(E) = 9.7(\pm1)^{-1.10(\pm.03)}\text{keVcm}^{-2}\text{s}^{-1}\text{keV}^{-1}$. See section 3.1.4 for detailed discussion.

[h] Indicates whether the energy band in question is used for outburst detection (D), quantitative outburst classification (C) or both.

[i] The RXTE Bulge Scan energy range was roughly 2.5–10 keV with slow 5% changes as the detector gain varied over the mission (Cartwright et al., 2013).

3.2 The Algorithm: Outburst Discovery, Tracking and Classification

Data from the six instruments listed in Table 3.1 are run through a custom pipeline composed of a comprehensive algorithm built to discover, track, and quantitatively classify outbursts. The products produced via this algorithm can then be used to analyze the details of behaviour occurring during outburst, including luminosity functions, state transitions and mass transfer rates of Galactic BHXRB systems. This algorithm consists of a 7 stage process; precursory analysis, detection, sensitivity selection, X-ray hardness computation, bolometric luminosity and disc fraction estimation, X-ray Luminosity Function (XLF) creation and mass-transfer rate estimation, and empirical classification.

3.2.1 Precursory Analysis

The purpose of precursory analysis is two-fold. As we have found the background subtraction performed by the surveys to be inadequate and the quoted errors to be underestimated across all four telescopes[10], it becomes necessary to perform a further background subtraction on the data and include an additional factor in the treatment of the errors.

Daily & Orbital Data: The following analysis is performed on data averaged over one day. If the data is collected in the form of orbital data, it is first converted to daily average data by calculating the weighted mean count rate (and uncertainty) over each day of data available. The weighted mean of a sample is defined as (Bevington and Robinson, 2003),

$$\mu_w = \frac{\Sigma\left(x_i/\sigma_i^2\right)}{\Sigma\left(1/\sigma_i^2\right)}, \tag{3.2}$$

where each data point x_i is weighted by the inverse of its own variance σ_i^2.

The uncertainty in this weighted mean can be calculated to be (Bevington and

[10]While the aforementioned problems are most prominently seen in MAXI, they do propagate throughout data from RXTE, Swift and INTEGRAL to a lesser degree as well.

Robinson, 2003),

$$\sigma_{\mu_w} = \left[\frac{1}{\Sigma\left(1/\sigma_i^2\right)}\right]^{1/2}. \tag{3.3}$$

Background Subtraction: For each energy range, instrument, and source combination, the background rate R_{bg} is calculated by iteratively calculating a bi-weight location and scale, using (3)σ-clipping. To perform this task we make use of the *astLib.astStats*[11] python module. This module uses methods described in Beers et al. (1990) to provide robust estimations of location (mean) and scale (standard deviation).

The one-step bi-weight location estimator, a member of the family of "M" estimators, originally suggested by Tukey (Andrews et al., 1972) to deal with cases involving non-gaussian or contaminated normal distributions, is defined as follows,

$$C_{BI} = M + \frac{\Sigma_{|u_i|<1}(x_i - M)(1-u_i^2)^2}{\Sigma_{|u_i|<1}(1-u_i^2)^2}, \tag{3.4}$$

where u_i is,

$$u_i = \frac{(x_i - M)}{c\,\mathrm{MAD}}, \tag{3.5}$$

M is the sample median, MAD is the median absolute deviation from the sample median $MAD = \mathrm{median}(|x_i - M|)$, and c is the tuning constant specifically chosen to give C_{BI} high efficiency for an extensive range of distributions[12].

The one-step bi-weight scale estimator is defined as,

$$S_{BI} = n^{1/2}\frac{\left[\Sigma_{|u_i|<1}(x_i - M)^2(1-u_i^2)^4\right]^{1/2}}{|\Sigma_{|u_i|<1}(1-u_i^2)(1-5u_i^2)|}, \tag{3.6}$$

where u_i is defined in Equation 3.5, n is the sample size, and c is set to a value of 9.0. Note that S_{BI} is essentially the standard deviation of the sample. We are after the standard error (or the uncertainty in the determination of the location (mean)) referred to as the standard deviation of the mean and calculated as $\sigma_\mu = (S_{BI}/n^{1/2})$

[11]Created by Matt Hilton and Steven Boada and available on SourceForge:http://astlib.sourceforge.net.

[12]The best value of c has been found to be $c = 6.0$. This value allows for the inclusion of data up to four standard deviations away from the central mean (Mostellar and Tukey, 1977).

(Bevington and Robinson, 2003).

This one-step method, for both location and scale, can be improved by using the processes of iteration and σ-clipping. In this case we take M as the initial guess, calculate u_i, $C_{\rm BI}$ and $S_{\rm BI}$. We then check whether each data point p in our sample lies in the interval $C_{BI} - \sigma_\mu \sigma_{cut} < p < C_{BI} + \sigma_\mu \sigma_{cut}$, thereby creating a new sample. This new sample replaces the initial sample and the process is repeated until convergence. Note that we have chosen to use a $\sigma_{cut} = 3$ in our analysis.

It is important to note that while the above analysis is adequate for the transient sources, the persistent sources must be handled differently. Here we calculate an average background rate for all the transient sources (via the bi-weight method described above), per energy band, and use this as the background rate for each persistent source.

This being said, it would make sense to use error estimates for persistent sources reflective of the local source density (e.g., Galactic Center persistent sources will likely have larger errors than a source in the SMC). One could use, instead of transient BHs, nearby sources that are not expected to show variations (e.g., supernova remnants or other sources at the limit of detectability) near each source, to estimate the rms (Private Communication C.O. Heinke). Checking the impact of such changes is beyond the scope of this work but is certainly a possibility for future work.

Error Estimation: Generally, if the quoted errors σ_{quo} are correct, you would expect the quiescent data ($< 3\sigma$ above the background rate, R_{bg}) to follow a Gaussian distribution (Bevington and Robinson, 2003). Unfortunately this is not what is observed in the case of our data, which becomes a serious problem when we begin to split our data into quiescent and outburst states (see Section 3.2.2).

In order to remedy this problem we employ an *adhoc* method, defining a correction factor C_σ as the standard deviation of a Gaussian distribution fit to the quiescent data. C_σ then acts as a multiplicative factor, scaling up the quoted errors appropriately to be $\sigma_{corr} = C_\sigma \sigma_{quo}$.

Again, while the above analysis is adequate for the transient sources, the persistent sources must be handed differently. Similar to the procedure adopted for background subtraction, we calculate an average error correction for all the transient

sources (via the bi-weight method described above), per energy band, and use this as the error correction for each persistent source.

3.2.2 Detection

The detection stage begins by first performing a second background subtraction (via the method outlined in Section 3.3.1) on the now error corrected data, followed by differentiating the data into two separate states,

- *outburst detection:* in which the count rate $R_c \geq R_{bg} + 3\sigma_{corr}$; and
- *quiescent non-detection:* in which $R_c < R_{bg} + 3\sigma_{corr}$.

Note that negative count rates, which happen on occasion due to over background subtraction are included in the quiescent non-detections.

From here lists of individual outbursts detected, in every given energy band (see Table A.3), are produced based on the minimum criteria that there must be at least 2 detections occurring every 8 days to be counted as an outburst. Lists of outbursts detected per energy band are then combined, creating outburst lists per instrument, telescope and lastly into one final outburst list for each individual source, taking into account detections from all four telescopes in our data sample.

The detection stage is equipped to deal with:

- situations in which there exists large gaps in the data: For instance these may be due to Sun constraints, lack of continuous daily coverage (i.e., survey instruments) and known down time (i.e., Space Shuttle docked at the International Space Station (ISS) effecting MAXI coverage); and
- complicated non-trivial behaviour exhibited during outburst: Examples include double (or multiple) peak features (i.e., XTE J1550−564; Kubota and Makishima (2004)), extended flare-like activity (i.e., 4U 1630−472; Tomsick et al. (2005)) and prolonged outburst periods (i.e., GX 339−4; Zdziarski et al. (2004)).

The second item is accomplished by repeating the precursory analysis (Section 3.2.1) and detection (this Section) stages on both weekly (8-day averaged) and

monthly (24-day averaged) data with the minimum criteria for an outburst being at least 2 detections occurring every 24 days and at least 2 detections occurring every 72 days, respectively. This is followed by combining the produced results (1-day average, 8-day average and 24-day average) into one final list of outbursts detected in an individual source.

3.2.3 Sensitivity Selection

Given the variable data quality at times, to ensure that our algorithm is catching "real" features rather than artificial flare-like/dip-like profiles, which can be the product of unexpected background increases/decreases (i.e., sun glints) or instrumental errors, we implement a sensitivity limit on our outburst detector (Section 3.2.2).

During the sensitivity selection stage, a weighted mean method (see Section 3.2.1 under Daily & Orbital Data) is used to calculate the mean count rate per outburst, R_{μ_w}. This calculation is followed by the application of a σ-clip, whereby only outbursts with a $R_{\mu_w} > 10\sigma_{\mu_w}$ are considered "real" features.

3.2.4 X-Ray Hardness Computation

In the hardness computation stage we calculate X-ray hardness ratios using six different combinations of energy bands, each of which are listed in Table 3.2. The form of the hardness ratio H_X is simply defined as the hard band flux density (in crab units) divided by the soft band flux density (in crab units).

To calculate the ratio, we make use of a Markov Chain Monte-Carlo (MCMC) method via the *emcee* python module (Foreman-Mackey et al., 2012).

Table 3.2: Empirical Outburst Classification Criteria

Telescope[a] ID	Hard Band (keV)	Soft Band keV	C_{hard}[b]	C_{soft}[b]
SM	15–50	4–10	0.2996	0.3902
SR	15–50	3–12	0.1658	0.2732

Continued on Next Page...

Table 3.2 – Continued

Telescope[a] ID	Hard Band (keV)	Soft Band keV	Critical[b]	Critical[b]
SRp	15–50	2.5–10	0.5646	0.8649
SI	15–50	3–10	0.5070	0.5932
RR	5–12	3–5	0.3821	0.4279
II	18–40	3–10	0.5098	0.5544

Note. –

[a]S=Swift, M=MAXI, R=RXTE/ASM, Rp=RXTE/PCA and I=INTEGRAL

[b]The hardness ratio boundaries defining the HCS and SDS.

Markov Chain Monte-Carlo via *emcee*: *emcee* generates a random walk in the parameter space, making use of the Metropolis-Hastings Algorithm[13] in determining which steps to take. The idea behind the the Metropolis-Hastings Algorithm (Mackay, 2003) is as follows. For a given probability distribution $P(\mathbf{x})$,

1. a "walker" is placed in parameter space at some initial position $\mathbf{x}_0$ and the distribution is evaluated at this position yielding $P(\mathbf{x}_0)$;

2. a possible next step is drawn by the random walk, $\mathbf{x}_1$, and once again the distribution is evaluated at this position yielding $P(\mathbf{x}_1)$;

3. if $P(\mathbf{x}_1) > P(\mathbf{x}_0)$, the step is accepted, the "walker" moves to the new position $\mathbf{x}_1$, and $\mathbf{x}_1$ is added to the sequence of steps;

4. if $P(\mathbf{x}_1) < P(\mathbf{x}_0)$, the step is declined, the "walker" stays in the current position $\mathbf{x}_0$, and $\mathbf{x}_0$ is added to the sequence of steps; and

5. steps 2–4 are repeated.

[13]Actually the *emcee* module makes use of two other methods for step decisions in addition to Metropolis-Hastings, "the stretch move" and "parallel stretch move". These methods involve advancing a group of K "walkers" $S = \{X_k\}$ simultaneously, whereby the proposal distribution for one walker k is based only on the current positions of the $K-1$ walkers in the group. While the details of these methods are beyond the scope of this work, we direct the reader to the the paper describing the *emcee* package for step-by-step descriptions of the algorithms, Foreman-Mackey et al. (2012), as well as the original publication proposing the algorithm, Goodman and Weare (2010), for more detail.

The sequence of steps generated by this algorithm is referred to as a Markov Chain because each successive step $\mathbf{x}_{n+1}$ is only dependent on the step directly before it $\mathbf{x}_n$. Eventually, given time, and a multitude of "walkers" parsing the parameter space, the Markov Chain generated will become a representative sample of the probability distribution $P(\mathbf{x})$ (Mackay, 2003).

The key to MCMC is the initial position, if not set accurately enough your "walkers" may get lost in the woods (i.e., stuck in low probability modes present in a multi-modal probability landscape). There exists many different methods to handle this initialization. For example, one may start the "walkers" spread out over a reasonable range in the parameter space or, in contrast, start the "walkers" in a very compact sphere in parameter space around the point which is expected to be close to the maximum probability point.

In our case, we make use of the first suggestion in combination with the implementation of what is referred to as a "burn in" phase, whereby your "walkers" are permitted to explore the parameter space with a given number of steps. After "burn in" the final position of the "walkers" then becomes the initial position to which they start, and the algorithm is repeated (Foreman-Mackey et al., 2012).

The Generative Model: Now that we have laid out the basics of the MCMC process, the question that remains is, how do we represent $P(\mathbf{x})$? The answer lies in making a generative model for the data. A generative model is defined as a parameterized, quantitative explanation of a statistical procedure that could reasonably have generated the data you have obtained.

Following the procedure outlined in Hog et al. (2010), we consider the case of a known functional form $f(\mathbf{x})$ to fit to the data. In order to illustrate the concept we first present a basic example, a linear line of the form $f(x) = y = mx + b$ with Gaussian uncertainties σ_y in one dimension. To create the generative model one can imagine a situation where all our data in fact comes from the functional form $f(x)$, with deviations occurring only as a result of small changes, drawn from a Gaussian distribution with a mean and variance of $\mu = 0$ and σ_y^2, in the y-direction.

In this case, the frequency distribution[14] for y_i can be written as,

$$p(y_i|x_i, \sigma_{y_i}, m, b) = -\frac{1}{\sqrt{2\pi\sigma_{y_i}^2}} \exp\left(-\frac{(y_i - mx_i - b)^2}{\sigma_{y_i}^2} \right), \tag{3.7}$$

where m is our slope and b is our intercept. What we are looking for are the specific parameters m and b (i.e., the straight line) which maximize the probability of the observed data given the model (i.e., maximize the likelihood of the parameters). This likelihood $\mathcal{L}$ is the product of conditional probabilities (as our data points are independently drawn) such that,

$$\mathcal{L} = \prod_{i=1}^{N} p(y_i|x_i, \sigma_{y_i}, m, b). \tag{3.8}$$

If we take the logarithm of Equation 3.8,

$$\ln \mathcal{L} = K - \sum_{i=1}^{N} \frac{(y_i - mx_i - b)^2}{\sigma_{y_i}^2}, \tag{3.9}$$

where K is a constant, we can see that the process of maximizing the likelihood is the same as minimizing chi-squared, χ^2 (the method used in least-square algorithms). The reason for this stems from the fact that the first factor in Equation 3.9 is constant (not dependent on m or b), therefore maximizing $p(y_i|x_i, \sigma_{y_i}, m, b)$ is equivalent to minimizing the term in the exponential, referred to as the chi-squared[15] (Bevington and Robinson, 2003).

Parametrizing $\mathbf{H_X}$: The process presented so far has assumed that the uncertainties in the x-direction were negligible. Unfortunately, this is not a valid assumption for our particular problem due to the fact that we have two-dimensional uncertainties (i.e., errors in both hard band flux density and soft band flux density). Hog et al.

[14]The expected frequency, as a result of a hypothetical set of repeated experiments, of drawing a y_i in the (infinitesimal) range $[y_i, y_i + dy]$ per unit dy.

[15]In a least-squares fitting algorithm, the optimum fit to the data is determined by finding the values of m and b which minimize the weighted sum of the squares of the deviations, χ^2. The difference here is that least-squares only provides estimates for the parameters, while MCMC will provide probability density functions (PDFs) for each parameter (Bevington and Robinson, 2003).

(2010) discusses that, because the m parameter has a lot of real estate in parameter space, particularly near the y-axis (i.e., very large values of m), the standard formulation ($y = mx + b$) is ill-suited.

Instead, Hog et al. (2010) propose an alternative model, which we make use of, involving parameterizing the slope m in terms of the angle that the generative locus (line) makes with x-axis. Adapting this technique, we can parametrize our hardness ratio H_X (slope) in terms of hard band flux density (y-variable) and soft band flux density (x-variable) such that,

$$H_X = \tan\theta = \frac{f_{hard}}{f_{soft}}. \tag{3.10}$$

This parametrization distributes the slope uniformly in the angle θ. In this case, our log liklihood ($\ln\mathcal{L}$) can be shown to be (Hog et al., 2010),

$$\ln\mathcal{L} = K - \sum_{i=1}^{N} \frac{(f_{hard}\cos\theta - f_{soft}\sin\theta)^2}{\sigma_{soft}^2\sin^2\theta + \sigma_{hard}^2\cos^2\theta}. \tag{3.11}$$

Making use of Equation 3.11 we can perform the likelihood maximization (as outlined above) on θ. To set the initialization of our "walkers" we make use of the prescription $x_0 = (\pi/4) + (0.1)r$, where r is a random number[16] in the range $(0, 1]$ (Private Communication with E. Rosolowsky) in combination with "burn in" described above.

From here, we can end up with a PDF of H_X by simply taking the tangent of the PDF for θ found via the MCMC algorithm. We take the median of the distribution to be the value of H_X at the particular time t, and define the 1σ confidence interval as the upper and lower limits on H_X.

Detections & Non-Detections: Within our data sets we must deal with three separate situations. On any given day t_d we may have,

1. detection in both hard and soft bands;

2. detection in the hard band and non-detection in the soft band or;

3. detection in the soft band and non-detection in the hard band.

[16]The pseudo-random number generator *numpy.random.rand* is used here.

In case 1, both upper and lower limits on H_X are tabulated. However, in cases 2 and 3 the situation is more complex. Here we must be particularly cautious as there is a possibility for large errors on the non-detection data. We disregard the data with large errors by applying a σ-cut. Here we only consider non-detection data points in which the errors are within $2\sigma_{\text{mean}}$ of the mean error value for the given band[17]. Note that this σ-cut is not applied to detection data (i.e., times in which we have detections in both the hard and soft bands).

In a case 2 situation, where there is only a hard detection, only lower limits on H_X are tabulated. This indicates the source is most likely in the HCS, assuming similar sensitivity in hard and soft bands. Similarly, in a case 3 situation, where there is only a soft detection, only upper limits on H_X are tabulated. This indicates the source is most likely in the SDS.

The last part of the hardness computation stage involves a calculation of a total hardness range for each outburst, followed by the placement of a "classification flag" on each outburst indicating whether or not it meets what we refer to as the "minimum data requirement". This requirement indicates whether or not we have enough data for the outburst to later be confidently classified (via procedure outlined in Section 3.2.6). In order to receive a "classification flag" the outburst must consist of at least 5 data points in which H_X has been computed.

Note that in addition to not having enough data, an outburst will also fail to receive a "classification flag" in a situation where data is only available in one energy band (making the calculation of a H_X impossible).

3.2.5 Bolometric Luminosity and Disc Fraction Estimation

By modelling each day's flux of a BHXRB as a combination of a:

- disc black body spectral component; and
- comptonized spectral component;

[17]This mean and error on this mean are calculated via the bi-weight method outlined in Section 3.2.1.

assuming a Crab-like spectrum in each given energy band and a known distance (from the literature), it is possible to obtain bolometric X-ray luminosity $L_{\rm bol}$ for a source on a given day t_d, deconvolve this luminosity into two separate components, $L_{\rm disc}$ and $L_{\rm comp}$ and finally, obtain a disc fraction d_f.

We model the disc black body component via *diskbb* in XSPEC. *diskbb* is a representation of a multi-colour disc black body (Mitsuda et al., 1984; Makishima et al., 1986) given two input parameters: T_{in} corresponding to the temperature at inner disk radius in keV and a normalization factor $n = [(R_{in}/\mathrm{km})/(\mathrm{d}/\mathrm{kpc})]^2 \cos\theta$ (Kubota et al., 1998), corresponding to a correction factor between the apparent inner disk radius and the realistic radius, where R_{in} is the apparent inner disc radius, d is the distance to the source and θ is the angle of the disc (i.e., $\theta = 0$ is face on). We have chosen $T_{in} = 1$ keV, a typical peak temperature for the disc component of BHXRBs in SDS (McClintock and Remillard, 2006).

The comptonized component is modelled via *compTT* in XSPEC. *compTT* is an analytic model describing up-scattering of soft photons in a hot plasma, including relativistic effects (Titarchuk, 1994; Titarchuk and Lyubarskij, 1995; Hua et al., 1995). The comptonized spectrum is determined by the plasma temperature T_e (the electron temperature in the hot inner coronal flow), plasma optical depth τ and input soft photon temperature T_{in} in keV. We have again chosen $T_{in} = 1$ keV, and $T_e = 50$ keV. The optical depth τ can be calculated via Equation 1.18 given a photon index Γ and an electron energy $\Theta = kT_e/m_ec^2$. Substituting $\Gamma = 1.7$, typical of a BHXRB in the HCS (McClintock and Remillard, 2006) and the $T_e = 50$ keV yields a $\tau = 1.26$.

Each day's flux in a given energy band for any given source can now be modelled as,

$$f_X = am_1 + bm_2, \tag{3.12}$$

where m_1 and m_2 are the flux of the *diskbb* and *compTT* models in the given energy band, respectively. If we have a minimum of one available energy band which can act as a hard band, one available energy band which can act as a soft band, and at least one of these bands exhibits a detection of the source on this particular day, we can use the MCMC method (outlined in Section 3.2.4) to fit for our normalization

parameters a and b. For a list of the m_1 and m_2 constants corresponding to each energy band see Table 3.3.

In this case, our log likelihood ($\ln \mathcal{L}$), which follows from Equation 3.7–3.9, is,

$$\ln \mathcal{L} = K - \sum_{i=1}^{N} \frac{(y_i - am_1 - bm_2)^2}{\sigma_{y_i}^2}. \tag{3.13}$$

Making use of Equation 3.13 we can perform the likelihood maximization (as outlined in Section 3.2.4) on our normalization parameters a and b. To set the initialization of our "walkers" we make use of the idea of starting the "walkers" in a very compact grid in parameter space around the point which is expected to be close to the maximum probability point in combination with the implementation of a "burn in" phase (as described in Section 3.2.4).

In order to compute where this "compact grid" is located in a particular case we fit for a and b from Equation 3.12 using a bounded least-squares fitting algorithm (*leastsqbound*) created by Jonathan J. Helmus[18], as bounds are necessary (both a and b must be greater than zero) in order to obtain a "physical" flux (i.e., non-negative).

leastsqbound is a modified version of the *scipy.optimize.leastsq* module which allows input of bounds on each fit parameter. Constraints are enforced by using an unconstrained internal parameter list, which is transformed into a constrained parameter list, using non-linear functions.

Once a and b are obtained from *leastsqbound*, we need to determine a suitable range for each parameter (i.e obtain the "compact grid"). To do so we perform a simple grid search, splitting the parameter space from $0 \rightarrow a$ and $0 \rightarrow b$ into four equal fractional sections (i.e., 1/8, 3/8, 5/8, and 7/8 multiples of the parameter). The section with the minimum $\Delta\chi^2 = \chi^2_{new} - \chi^2_{fit}$ is applied as a symmetric error, thereby creating the "compact grid" for each parameter.

From here, we calculate the PDFs of a and b via the MCMC algorithm. Once again, we take the median of the distributions to be our values of a and b on a particular day t_d, and define the 1σ confidence intervals as the upper and lower

[18]The source code is available via GitHub:https://github.com/jjhelmus/leastsqbound-scipy/.

limits on a and b.

Table 3.3: Spectral Fitting Constants

Energy Band (keV)	*diskbb* flux (ergs^{-1})	*compTT* flux (ergs^{-1})
15–50	4.99×10^{-16}	3.23×10^{-7}
18–40	4.24×10^{-17}	2.12×10^{-7}
40–100	7.29×10^{-26}	7.06×10^{-8}
3–10	5.55×10^{-12}	1.60×10^{-7}
10-25	2.95×10^{-14}	2.00×10^{-7}
2–4	6.91×10^{-12}	4.42×10^{-8}
4–10	2.92×10^{-12}	1.36×10^{-7}
2.5–10	9.83×10^{-12}	1.80×10^{-7}
3–5	4.08×10^{-12}	5.08×10^{-8}
5–12	1.49×10^{-12}	1.43×10^{-7}
3–12	5.57×10^{-12}	1.94×10^{-7}

Knowing the values of a and b on any given day, we now have the ability to obtain the flux in the 2–50 keV band. This band limited flux is then converted to bolometric flux (in the ? range) by multiplying each component (disc and comptonized) by a derived bolometric correction from the XSPEC models. Following this procedure the disc and comptonized flux components are obtained via,

$$f_{\rm bol} = am_{1,\rm bol} + bm_{2,\rm bol} = f_{\rm disc} + f_{\rm comp}. \tag{3.14}$$

Equipped with the fluxes from Equation 3.14 and distances (d) obtained from the literature (see Chapter 2 and Table A.2), we are able to simply calculate luminosities ($L_{\rm bol}, L_{\rm disc}, L_{\rm comp}$) as,

$$L = f(4\pi d^2) \tag{3.15}$$

and in turn obtain a disc fraction $d_f = L_{\rm disc}/L_{\rm bol}$.

The last part of the bolometric luminosity and disc fraction estimation stage involves an estimate of total energy released during an outburst (or "fluence"). This

"fluence" is defined as the $L_{\rm bol}$ integrated over the duration of an outburst and is calculated by first finding the weighted mean of $L_{\rm bol}$ during outburst then multiplying it by the total duration (number of days) in the outburst. However, the situation is not as simple as was presented in Section 3.2.1 due to the presence of asymmetric errors on $L_{\rm bol}$.

In order to calculate the weighted mean we must do so iteratively. The basic idea involves starting with the mean bolometric luminosity $\mu_{L_{\rm bol}} = \Sigma_i L_{\rm bol,i}/N$, parsing through the data and checking whether $L_{\rm bol}$ is greater than or less then this mean value. If $L_{\rm bol} \geq \mu_{L_{\rm bol}}$ then the lower limit is used in the calculation of weights, while if $L_{\rm bol} < \mu_{L_{\rm bol}}$, the upper limit is used in the weight calculation. From here a new $\mu_{L_{\rm bol}}$ is calculated and the process will continue until convergence.

3.2.6 X-ray Luminosity Function (XLF) creation and mass-transfer rate estimation

Now that we have outlined a method to obtain bolometric X-ray luminosity $L_{\rm bol}$ for a source on any given day t_d, we can now obtain the XLF for each transient BHXRB, obtain a time-averaged bolometric luminosity (over the last 18 years) for the given source and derive a mass-transfer history for the source.

Transient Systems: For transient systems, we set $L_{\rm bol} = 0$ during quiescent periods and use the days in which data was available (and thus those days we have an estimate of $L_{\rm bol}$ via Section 3.2.5) during outburst to interpolate a $L_{\rm bol}$ for the missing days in between, ultimately obtaining an estimate for $L_{\rm bol}$ for every day a source was in outburst and therefore a complete transient XLF.

In order to accomplish this task, our algorithm will parse through an outburst, by individual day, checking if a $L_{\rm bol}$ estimate exists. If no estimate exists, the algorithm takes the nearest days bracketing the missing day on either side (call them t_1 and t_2), which do have estimates and performs a linear interpolation (fit for m and b) using the MCMC method outlined in Section 3.2.4. In this case, our log likelihood

($\ln \mathcal{L}$), is simply Equation 3.9,

$$\ln \mathcal{L} = K - \sum_{i=1}^{N} \frac{(y_i - mx_i - b)^2}{\sigma_{y_i}^2}. \tag{3.16}$$

Making use of Equation 3.16 we can perform the likelihood maximization (as outlined in Section 3.2.4) on our parameters m and b. However, while our $\ln \mathcal{L}$ takes the same form as the simple linear fit example presented in Section 3.2.4, the situation is more complex due to the fact that our flux values (y_i's) have asymmetric errors. To deal with this situation we must add a conditional statement into our $\ln \mathcal{L}$ function. If the fit (the flux calculated from fitted parameters m and b) obtains a flux value greater than that of the input data point (i.e., the fit is above the data), the upper error bar is used in $\ln \mathcal{L}$. In contrast, if the fit obtains a flux value less than that of the input data point (i.e., the fit is below the data), the lower error bar is used in $\ln \mathcal{L}$ (Private Communication with E. Rosolowsky).

This more complex asymmetric error situation in turn also complicates our initialization procedure. To set the initialization of our "walkers" we again make use of the idea of starting the "walkers" in a very compact grid in parameter space around the point which is expected to be close to the maximum probability point in combination with the implementation of a "burn in" phase (as described in Section 3.2.4).

However, in order to compute the "compact grid", we must modify the procedure presented in Section 3.2.5, which makes use of the bounded least squares algorithm by performing a simple Monte-Carlo sampling for each data point (flux f_X) in the range created by the asymmetric error bars $(f_X - \sigma_i^-) < f_X < (\sigma_i^+ - f_X)$. The modified procedure involves drawing 1000 random samples r_i from a normal distribution. For each sample:

- <u>if $r_i > 0$:</u>
  $f_{X,1} = f_{X,1} + r_i \sigma_1^+$
  $f_{X,2} = f_{X,2} + r_i \sigma_2^+$

- <u>elif $r_i < 0$:</u>

$$f_{X,1} = f_{X,1} - r_i\sigma_1^-$$
$$f_{X,2} = f_{X,2} - r_i\sigma_2^-$$

- a bounded least squares fit is performed on $f_{X,1}$ and $f_{X,2}$ using *leastsqbound*
- fit parameters m and b are recorded in separate arrays

As a result of this procedure we are able to define a suitable range for each parameter, via the 1σ confidence intervals of each distribution and therefore create the "compact grid".

From here, the MCMC algorithm provides us with the optimal values of m and b in the form of PDFs, giving us the final values of our parameters using the median of the distributions as the values and the 1σ confidence intervals as the upper and lower limits on each parameter. Knowing the values of m and b across the time interval $t_1 \rightarrow t_2$, we now have the ability to interpolate $f_{\rm bol}$ (and in turn calculate $L_{\rm bol}$) for the days missing estimates in this time interval and as such calculate a time-averaged bolometric luminosity,

$$L_{\rm bol,avg} = \frac{\sum_{i=1}^{N} L_{\rm bol,i}}{t_{\rm tot}}. \tag{3.17}$$

Note that $L_{\rm bol,avg}$ is calculated via the procedure outlined above for persistent systems as well. However, XLFs are only created for transient systems.

Mass-Transfer Rate: The last piece of the puzzle involves using our $L_{\rm bol,avg}$ to calculate an average mass-transfer rate. We begin with the fact that energy is generated through mass accretion. Matter of mass m falling towards a BH from infinity (i.e., into a potential well) releases energy,

$$E = \frac{GMm}{R}. \tag{3.18}$$

This matter passes through the accretion disc before falling onto the BH. According to the virial theorem, it will give up half its potential energy to radiation, and retain the other half as increased kinetic energy, as it descends to any given radius. Therefore, material at radius R should have a kinetic energy of

$$K = -\frac{1}{2}U = \frac{GMm}{2R}. \tag{3.19}$$

If the rate at which mass is accreted onto the BH is $\dot{M} = dm/dt$, the rate at which the kinetic energy is dissipated at some radius R, and hence the accretion luminosity can be written as,

$$L_{\rm acc} = \frac{GM\dot{M}}{2R}. \tag{3.20}$$

The radius of the ISCO (i.e., the last orbit where material can have stable orbits around the BH) sets how efficiently the rest mass energy of the accreted material is converted into radiation, referred to as the accretion efficiency ϵ. Thus, the resulting accretion luminosity generated by a mass accretion rate, $\dot{M}$, through the disc can be rewritten as (Carroll and Ostlie, 2007),

$$L_{acc} = \epsilon \dot{M} c^2. \tag{3.21}$$

Using Equation 3.21, we can now calculate an average mass-transfer rate as,

$$\dot{M}_{\rm avg} = \frac{L_{\rm bol,avg}}{c^2 \epsilon}. \tag{3.22}$$

In order to provide an accurate estimate of $\dot{M}_{\rm avg}$, we must take into account the uncertainties which come into the calculation in the form of errors in distance (d), spectral modelling (fit parameters a and b) and accretion efficiency (ϵ). Similar to the procedure presented above, in order to accomplish this we use a simple Monte-Carlo procedure involving drawing 1000 random samples r_i from a normal distribution. For each sample:

- <u>if $r_i > 0$:</u>
  $f_{\rm bol,avg} = f_{\rm bol,avg} + r_i \sigma_{\rm f}^{+}$
  $d = d + r_i \sigma_d^{+}$
  $\epsilon = \epsilon + r_i \sigma_\epsilon^{+}$

- <u>elif $r_i < 0$:</u>
  $f_{\rm bol,avg} = f_{\rm bol,avg} - r_i \sigma_{\rm f}^{-}$
  $d = d - r_i \sigma_d^{-}$
  $\epsilon = \epsilon - r_i \sigma_\epsilon^{-}$

- calculate $L_{\rm bol,avg} = f_{\rm bol,avg}(4\pi d^2)$
- calculate $\dot{M}_{\rm avg} = L_{\rm bol,avg}/(c^2\epsilon)$
- record $\dot{M}_{\rm avg}$ in an array

As the radius of the ISCO ranges from 3 to 0.5 Schwarzschild radii[19], for non-rotating (Schwarzschild) to maximally spinning (Kerr) BHs, resulting in an accretion efficiencies between 5.72% and 42.3% (Hobson et al., 2006), we take ϵ to range from 0.06–0.40 with a favoured value of 0.10 (Frank et al., 2002). As a result of this procedure we can end up with a PDF of $\dot{M}_{\rm avg}$. Once again, we take the median of the distribution to be our value and define the 1σ confidence intervals as the upper and lower limits.

3.2.7 Empirical Classification & Analysis

In the final stage, the algorithm makes use of two separate empirical parameters, the hardness ratio H_X and the disc fraction d_f, to categorize outburst behaviour into one of four classes: "successful", "indeterminate", "failed" or "undefined".

The classification procedure, begins by differentiating data for each outburst into hard, soft and intermediate states based on a critical hard $C_{\rm hard}$ and critical soft $C_{\rm soft}$ hardness values. As these critical values will differ depending on the telescopes involved in H_X, we make use of 10 calibration sources (found in Table 3.4) to set these baseline critical values. These sources have been chosen based on the criteria that they have exhibited (proven via spectral and/or timing analysis) either "failed" outbursts, or a combination of "successful" and "failed" outbursts over the last 18 years. The literature classification is then used to find the baseline critical values for each of the six H_X combinations.

The criteria for an outburst to be "successful" involves <u>at least one</u> upper limit on H_X, $\sigma_{\rm H,high} < C_{\rm soft}$. In turn for an outburst to be "failed", <u>all</u> lower limits on H_X, $\sigma_{\rm H,low} > C_{\rm hard}$. Those outbursts which do not fall into either category are referred to as indeterminate.

[19]The Schwarzschild radius is defined as $R_{\rm g} = 2GM/c^2$, where M is the mass of the BH and c is the speed of light.

$C_{\rm hard}$ is found by taking the minimum $\sigma_{\rm H,low}$ for each "failed" calibration outburst, followed by finding the absolute minimum of these values across all calibration sources, yielding the softest a source can be while still remaining in the hard state. $C_{\rm soft}$ is found by taking the minimum $\sigma_{\rm H,high}$ for each "successful" calibration outburst (thus fullfilling the minimum requirement for a "successful" outburst that at least one $\sigma_{\rm H,high} < C_{\rm soft}$), followed by finding the absolute maximum of these values across all calibration sources, yielding the hardest a source can be while still being in the soft state.

As we are dealing with multiple telescope pairs (between 1–6 separate pairs) contributing separate ranges in H_X, and therefore different classifications for each outburst, we must take into account all possible combinations of "successful", "failed" and "indeterminate" labels. To accomplish this, we use the following algorithm,

1. Check for a "classification flag", if no flag exists the outburst will have a final classification of "undetermined";

2. If a "classification flag" exists, check for at least one "successful" designation;

3. if found, the outburst will have a final classification of "successful"[20];

4. If no "successful" designations exist, check for at least one indeterminate designation;

5. if found, the outburst will have a final classification of "indeterminate"; and

6. If no "successful" or "indeterminate" designations are found (i.e., all designations are "failed"), the outburst will have a final classification of "failed".

In addition to classification via H_X, we have also classified each outburst, using the same procedure above, via d_f. Again we begin by differentiating data for each outburst into hard, soft and intermediate states based on a critical soft $C_{\rm soft}$ and critical hard $C_{\rm hard}$ disc fraction values. Similar to the above, the criteria for an outburst to be "successful" involves <u>at least one</u> lower limit on d_f, $\sigma_{\rm df,low} > C_{\rm soft}$.

[20]This is because we have chosen to set the absolute default label as "successful".

In-turn for an outburst to be "failed" all upper limits on d_f, $\sigma_{\mathrm{df,high}} < C_{\mathrm{hard}}$. Those outbursts which do not fall into either category are referred to as "indeterminate".

In this case C_{hard} is found by taking the maximum $\sigma_{\mathrm{df,high}}$ for each "failed" calibration outburst, followed by finding the absolute maximum of these values across all calibration sources, yielding the largest a disc fraction can be in a source while still remaining in the hard state. C_{soft} is found by taking the maximum $\sigma_{\mathrm{df,low}}$ for each "successful" calibration outburst (thus full-filling the minimum requirement for a "successful" outburst that at least one $\sigma_{\mathrm{df,low}} > C_{\mathrm{soft}}$), followed by finding the absolute minimum of these values across all calibration sources, yielding the the smallest a disc fraction can be in a source while still being in the soft state. The critical values have been computed to be $C_{\mathrm{soft}} = 0.4695$ and $C_{\mathrm{hard}} = 0.4230$.

The last part of the classification stage involves using the above criteria defining hard, soft and intermediate states in order to track the state a source is in throughout outburst, as well as information obtained in Sections 3.2.1–3.2.6 to yield a full record of source behaviour per outburst, including:

- outburst classification (via H_X and d_f),
- outburst duration,
- peak bolometric luminosity of outburst,
- total energy released ($\int L dt$) during outburst,
- differentiation between rise and decline phases of outburst,
- state transitions and the approximate times they have occurred,
- total time spent in the hard, soft and intermediate states, and
- peak bolometric luminosity in the hard and soft states.

Table 3.4: Calibration Source Details

Source Name	Outburst ID	Calibration[a] Type	References[b]
GX 339−4	1997–1999	S	1,2
	2002/2003	S	3
	2004/2005	S	4
	2006	F	5
	2006/2007	S	5,6
	2009/2011	S	7
H 1743−322	2003	S	3,8–11
	2004	S	12
	2005	S	12
	2007/2008	S	13,14
	2008	F	15,16
	2010	S	14,17,18
MAXI J1836−194	2011/2012	F	19–21
XTE J1118+480	1999/2000	F	22–26
GS 1354−64	1997/1998	F	27–29
IGR J17497−2821	2006	F	30–32
XTE J1550−564	1998/1999	S	33–35
	2001	F	36
	2001/2002	F	37
	2003	F	38,39
SAX J1711.6−3808	2001	F	40
IGR J17285−2922	2010	F	41
Swift J174510.8−262411	2012/2013	F	42,43

[a] States whether the outburst was used to calibrate the hardness limits for a successful (S) or failed (F) outburst.

[b] [1] Zdziarski et al. (2004),[2] Belloni et al. (1999b), [3] Homan et al. (2005), [4] Belloni et al. (2006), [5] Buxton et al. (2012), [6] Motta et al. (2009), [7] Debnath et al. (2013b), [8] Capitanio et al. (2005), [9] Miller et al. (2006d), [10] Kalemci et al. (2006), [11] McClintock et al. (2009), [12] Capitanio et al. (2006a), [13] Capitanio et al. (2010), [14] Zhou et al. (2013), [15] Capitanio et al. (2009a), [16] Motta et al. (2010), [17] Corral-Santana et al. (2011), [18] Debnath et al. (2013a), [19] Ferrigno et al. (2011), [20] Reis et al. (2012), [21] Russell et al. (2014a), [22] Hynes et al. (2000b), [23] McClintock et al. (2001b), [24] Brocksopp et al. (2010b),[25] Frontera et al. (2001), [26] Revnivtsev et al. (2000a), [27] Brocksopp et al. (2001), [28] Brocksopp et al. (2004), [29] Revnivtsev et al. (2000c), [30] Rodriguez et al. (2007), [31] Walter et al. (2007), [32] Paizis et al. (2009), [33] Sobczak et al. (2000), [34] Remillard et al. (2002), [35] Kubota and Makishima (2004), [36] Tomsick et al. (2001a),[37] Belloni et al. (2002a),[38] Sturner and Shrader (2005), [39] Aref'ev et al. (2004), [40] in't Zand et al. (2002b), [41] Sidoli et al. (2011), [42] Krimm et al. (2013b), [43] Curran et al. (2014)

Chapter 4

Results & Discussion

4.1 Outburst History & Behavioural Analysis

This section is presented in two separate segments. The first segment will give an overview of the major results of the algorithm from a population standpoint, while the second will present the detailed data products, created via the algorithm, on a source by source basis.

4.1.1 Population Analysis

Using a combination of today's more sensitive all-sky X-ray instruments, which have made an in-depth exploration of the transient X-ray Universe possible, and our custom pipeline, composed of a comprehensive algorithm built to discover, track, and quantitatively analyze both transient outbursts and long-term persistent behaviour, we have detected over 90 outbursts occurring in 43 transient BHXRBs and have tracked the long-term behaviour of 9 persistent BHXRBs over the last 18 years. Table 4.1 below provides a summary of the transient activity, including categorized outbursts, recurrence times, duty cycles, states achieved and, a comparison of time spent in quiescence vs. outburst. Take note of the range in duty cycles exhibited by the transient population (0.7–61%).

Table 4.1: Activity of the Transient Galactic BHXRB Population from 1996-2014

Source Name (s)	Successful[a] Outbursts	Indeterminate[a] Outbursts	Failed[a] Outbursts	Total Outbursts	$t_{\rm quies}$[b] (days)	$t_{\rm out}$[c] (days)	$< t_{\rm recur} >$[d] (days)	Duty Cycle[e] (%)	States[f] Achieved
XTEJ0421+560	0	0	1	1	6633	49	>5885	0.73	HCS
GROJ0422+32	-	-	-	-	-	-	-	-	-
1A0620−00	-	-	-	-	-	-	-	-	-
IGRJ06074+2205	-	-	-	-	-	-	-	-	-
GRS1009−45	-	-	-	-	-	-	-	-	-
XTEJ1118+480	0	0	1	1	6431	251	>5232	3.76	HCS
GS1124−684	-	-	-	-	-	-	-	-	-
IGRJ11321−5311	-	-	-	-	-	-	-	-	-
MAXIJ1305−704	1	0	0	1	6502	181	>761	2.71	HCS,SDS,IMS
SWIFTJ1357.2−0933	0	0	1	1	5845	837	>1494	12.53	HCS
GS1354−64	0	0	1	1	6526	156	>6056	2.33	HCS
1A1524−617	-	-	-	-	-	-	-	-	-
SWIFTJ1539.2−6227	1	0	0	1	6508	174	>1978	2.60	HCS,SDS,IMS
MAXIJ1543−564	1	0	0	1	6521	161	>1089	2.41	HCS,SDS,IMS
4U1543−475	1	0	0	1	6629	53	>4335	0.79	HCS,SDS,IMS

Continued on Next Page. . .

Table 4.1 – Continued

Source Name (s)	Successful[a] Outbursts	Indeterminate[a] Outbursts	Failed[a] Outbursts	Total Outbursts	t_{quies}[b] (days)	t_{out}[c] (days)	$< t_{recur} >$[d] (days)	Duty Cycle[e] (%)	States[f] Achieved
XTEJ1550−564	1	1	3	5	6173	509	416	7.62	HCS,SDS,IMS
4U1630−472	4	3	2	9	3690	2993	722	44.79	HCS,SDS,IMS
XTEJ1637−498	-	-	-	-	-	-	-	-	-
XTEJ1650−500	1	0	0	1	6325	357	>4621	5.34	HCS,SDS,IMS
XTEJ1652−453	1	0	0	1	6514	168	>1780	2.51	HCS,SDS,IMS
GROJ1655−40	2	0	0	2	5896	786	3214	11.76	HCS,SDS,IMS
MAXIJ1659−152	1	0	0	1	6465	217	>1312	3.25	HCS,SDS,IMS
GX339−4	6	0	4	10	3626	3056	694	45.73	HCS,SDS,IMS
H1705−250	-	-	-	-	-	-	-	-	-
IGRJ17091−3624	1	0	0	1	5735	947	>1181	14.17	HCS,SDS,IMS
IGRJ17098−3628	-	-	-	-	-	-	-	-	-
SAXJ1711.6−3808	0	0	1	1	6553	129	>4843	1.93	HCS
Swift J1713.4−4219	-	-	-	-	-	-	-	-	-
XMMSL1J171900.4−353217	0	0	4	4	4626	2056	301	30.77	HCS
XTEJ1719−291	-	-	-	-	-	-	-	-	-

Continued on Next Page. . .

Table 4.1 – Continued

Source Name (s)	Successful[a] Outbursts	Indeterminate[a] Outbursts	Failed[a] Outbursts	Total Outbursts	t_{quies}[b] (days)	t_{out}[c] (days)	$< t_{recur} >$[d] (days)	Duty Cycle[e] (%)	States[f] Achieved
GRS1716−249	-	-	-	-	-	-	-	-	-
XTEJ1720−318	1	0	0	1	6453	229	>4126	3.43	HCS,SDS,IMS
XTEJ1727−476	1	0	0	1	6604	78	>3131	1.17	HCS,SDS,IMS
IGRJ17285−2922	0	0	1	1	6491	191	>1344	2.86	HCS
GRS1730−312	-	-	-	-	-	-	-	-	-
IGRJ17354−3255	-	-	-	-	-	-	-	-	-
GROJ1735−27	-	-	-	-	-	-	-	-	-
IGRJ17379−3747	0	0	1	1	6555	127	>2069	1.90	HCS
GRS1737−31	0	0	1	1	6582	100	>6273	1.50	HCS
GRS1739−278	2	0	0	2	6372	310	6589	4.64	HCS,SDS,IMS
SWIFTJ174510.8−262411	0	0	1	1	6397	285	>592	4.27	HCS
H1743−322	7	2	3	12	5340	1342	343	20.08	HCS,SDS,IMS
XTEJ1748−288	0	0	1	1	6605	77	>5809	1.15	HCS
IGRJ17497−2821	0	0	1	1	6584	98	>2807	1.47	HCS
SLX1746−331	1	1	1	3	5456	1226	1338	18.35	HCS,SDS,IMS

Continued on Next Page. . .

Table 4.1 – Continued

Source Name (s)	Successful[a] Outbursts	Indeterminate[a] Outbursts	Failed[a] Outbursts	Total Outbursts	t_{quies}[b] (days)	t_{out}[c] (days)	$< t_{recur} >$[d] (days)	Duty Cycle[e] (%)	States[f] Achieved
XTEJ1752−223	1	0	0	1	5958	725	>1687	10.85	HCS,SDS,IMS
XTEJ1755−324	1	0	0	1	6558	124	>6133	1.86	HCS,SDS,IMS
IGRJ17586−2129	0	0	1	1	6469	213	>1773	3.19	HCS
H1755−338	-	-	-	-	-	-	-	-	-
XTEJ1812−182	1	0	1	2	6548	134	2039	2.01	HCS,SDS,IMS
IGRJ18175−1530	-	-	-	-	-	-	-	-	-
XTEJ1817−330	1	0	0	1	6427	255	>3026	3.82	HCS,SDS,IMS
XTEJ1818−245	1	0	0	1	6560	122	>3195	1.83	HCS,SDS,IMS
SAXJ1819.3−2525	0	1	6	7	2628	4055	274	60.68	HCS,IMS
MAXIJ1836−194	0	0	1	1	6393	289	>973	4.33	HCS
SWIFTJ1842.5−1124	1	0	0	1	6455	227	>2140	3.40	HCS,SDS,IMS
EXO1846−031	-	-	-	-	-	-	-	-	-
IGRJ18539+0727	-	-	-	-	-	-	-	-	-
XTEJ1856+053	3	1	0	4	6301	381	1579	5.70	HCS,SDS,IMS
XTEJ1859+226	1	0	0	1	6458	224	>5333	3.35	HCS,SDS,IMS

Continued on Next Page. . .

Table 4.1 – Continued

Source Name (s)	Successful[a] Outbursts	Indeterminate[a] Outbursts	Failed[a] Outbursts	Total Outbursts	$t_{\rm quies}$[b] (days)	$t_{\rm out}$[c] (days)	$< t_{\rm recur} >$[d] (days)	Duty Cycle[e] (%)	States[f] Achieved
XTEJ1901+014	-	-	-	-	-	-	-	-	-
XTEJ1908+094	1	1	0	2	6031	651	4254	9.74	HCS,SDS,IMS
SWIFTJ1910.2−0546	1	0	0	1	6425	257	>711	3.85	HCS,SDS,IMS
GS2000+251	-	-	-	-	-	-	-	-	-
XTEJ2012+381	1	0	0	1	6481	201	>5830	3.01	HCS,SDS,IMS
GS2023+338	-	-	-	-	-	-	-	-	-

Note. –

[a]The number of successful, indeterminate and failed outbursts (occurring in the last 18 years) detected and classified by the algorithm.

[b]Days spent in quiescence over the last 18 years.

[c]Days spent in Outburst over the last 18 years.

[d]Outburst recurrence time calculated over the last 18 years. A lower limit (indicated by >) is given when only one outburst has been detected.

[e]Duty cycle calculated over the last 18 years.

[f]States achieved by each source during outbursts occurring in the last 18 years.

Prevalence of "Failed" Outbursts: Perhaps our most noteworthy result comes in our discovery that, despite the prevailing literature on "canonical" BHXRB behaviour (Fender et al., 2004, 2009; Fender and Gallo, 2014), the outbursts undergone by BHXRBs that do not complete the canonical pattern, failing to transition from the HCS to the SDS, the so-called "failed" outbursts, make up $\sim 50\%$ (i.e., $0.446^{+0.058}_{-0.056}$) of all outbursts occurring in Galactic transient BHXRBs in the past 18 years. Table 4.2 presents the "failed ratio", quoted with 1σ binomial Gehrels errors (Gehrels, 1986), computed for each of the six separate hardness ratios used in the algorithm. In contrast, using the disc fraction rather than hardness ratio we are able to classify 84 outbursts (54 successful and 27 failed) yielding a "failed ratio" of $0.329^{+0.060}_{-0.055}$.

Table 4.2: Failed Outburst Ratios as Revealed by X-ray Hardness

Telescope[a] ID	Hard Band (keV)	Soft Band (keV)	Number of Successful Detected	Number of Failed Detected	Failed[b] Ratio
SM	15–50	4–10	9	6	$0.400^{+0.161}_{-0.145}$
SR	15–50	3–12	39	27	$0.409^{+0.069}_{-0.066}$
SRp	15–50	2.5–10	14	16	$0.533^{+0.104}_{-0.107}$
SI	15–50	3–10	2	4	$0.667^{+0.212}_{-0.282}$
RR	5–12	3–5	29	17	$0.370^{+0.084}_{-0.078}$
II	18–40	3–10	3	5	$0.625^{+0.196}_{-0.235}$

Note. –

[a]S=Swift, M=MAXI, R=RXTE, Rp=RXTE/PCA and I=INTEGRAL.

[b]ratio of failed to successful plus failed outbursts detected with 1σ binomial Gehrels errors.

Such a high fraction of "failed" outbursts challenges the standard paradigm for accretion behaviour in transient BHXRBs (Fender et al., 2004, 2009; Fender and Gallo, 2014). This brings into question the validity of using the canonical model to describe the general behaviour of BHXRBs. We note that the canonical model has been largely based after numerous "successful" outbursts of GX339−4, even though its "successful" to "failed" outburst ratio over the last 18 years is nearly 1-to-1.

This "failed" behaviour is neither a rare nor recent phenomena. In fact, through an extensive literature search (as presented in Table A.3), we find a near constant

appearance of these "failed" outbursts over the last ~ 50 years.

In addition, by splitting the 18 year period into logical segments, defined by the addition/loss of each instrument, we detect no evolution of the failed ratio over time. This is in conflict with what you might expect given the advent of more sensitive hard X-ray instruments (see Table 4.3).

Table 4.3: Detected Failed Outburst Ratio over Time

Time Segment	Time Period (MJD)	Total Successful	Total Failed	Failed Outburst[a] Ratio
A: RXTE/ASM ON–RXTE/PCA ON	50088–51214	8	6	$0.429^{+0.167}_{-0.155}$
B: RXTE/PCA ON–Swift/BAT & INTEGRAL ON	51214–53414	12	7	$0.368^{+0.141}_{-0.125}$
C: Swift/BAT & INTEGRAL ON–MAXI ON	53414–55058.0	17	15	$0.469^{+0.103}_{-0.101}$
D: MAXI ON–RXTE/ASM OFF	55058.0–55924	9	8	$0.470^{+0.147}_{-0.143}$
E: RXTE/ASM OFF–Present	55924–Present	5	5	$0.500^{+0.195}_{-0.195}$

Note. –

[a]ratio of failed to successful plus failed outbursts detected with 1σ binomial Gehrels errors.

This finding paired with the appearance of these "failed" outbursts over the last ~ 50 years may suggest that this prevalence of observed "failed" behaviour is actually a phenomena driven by some physical parameter or process occurring within the system rather than a product of the increase in sensitivity of X-ray instruments over the years. Such a physical process would likely involve decreases in mass-transfer rates, resulting in a failure to transverse through the softer states and finally an untimely trip back into quiescence (i.e., the disc instability is completed before the still unknown critical instability that dictates a successful state transition).

This being said, additional factors need to be addressed before such a strong claim against selection biases are made. Examples include (i) the effect distance could have on the outburst behaviours we are able to observe, as an increase in sensitivity could largely increase the distance range within which we could observe the same outburst behaviours, and (ii) the significance of individual instrument performance on outburst detection rates over time (e.g., RXTE detected significantly less outbursts towards the end of its life in 2011–2012 (when compared to previous years).

Interestingly enough, we find, through our ability to track the accretion state of a source throughout an outburst via the algorithm (as presented in Table A.4), that this particular class of behaviour is not limited to the transient systems, but is also exhibited by a number of persistently accreting systems in the form of long continuous periods spent in the HCS (in the case of 1E 1740.7−2942, GRS 1758−258, and SS 433) or periodic "failed" state transitions (in the case of Cyg X−1, Swift J1753.5−0127, and 4U 1957+115).

Elevated Outburst Detection Rates: The other result comes with the discovery that with the current suite of more sensitive instruments in space (i.e., BAT, GSC, ISGRI, and JEM-X) we are detecting a greater number of sources than in the RXTE era. Our findings suggest that $\sim$ 6–12 transient BHXRB outbursts are observable every year, more than a factor of two larger than with RXTE alone.

Table 4.4 presents the outburst rate with quoted 1σ Gehrels errors for each individual instrument calculated using only the time in which data was being taken by the instrument ($f_{\rm collect} * t_{\rm active}$), rather than the total time the instrument was active ($t_{\rm active}$).

The reason for this choice of time resides in the fact that, while the ASMs are assumed to have taken data daily for the time period they have been active (i.e., $f_{\rm collect} = 1.0$), the scanning surveys only take data in short consecutive intervals resulting in $f_{\rm collect} \ll 1.0$. From a statistical standpoint, as there was no possibility of outburst detection during the times in which the scanning surveys were not observing, such times should not be counted in the analysis.

It is also important to note that, while both JEM-X and ISGRI have been active and taken data for similar periods of time, JEM-X only covers $\sim$ 10% of the sky that ISGRI does, resulting in a vast difference in the number of outbursts detected between the two instruments.

Table 4.4: Outburst Rate per Instrument

Telescope	Instrument	Type	$t_{\rm active}$[a] (yrs)	$f_{\rm collect}$[b]	Outbursts Detected	Rate[c] ($\rm yr^{-1}$)
Swift	BAT	all-sky	9.19	1.0	61	$6.91^{+1.00}_{-0.88}$
MAXI	GSC	all-sky	4.69	1.0	22	$6.99^{+1.51}_{-1.26}$
RXTE	ASM	all-sky	15.98	1.0	54	$3.38^{+0.53}_{-0.46}$
	PCA	scan	12.74	0.75	29	$4.67^{+0.81}_{-0.70}$
INTEGRAL	JEM-X	scan	9.17	0.20	8	$5.10^{+2.41}_{-1.71}$
	ISGRI	scan	9.17	0.27	22	$9.65^{+2.44}_{-1.99}$

Note. –

[a] Amount of time the instrument has been active.

[b] fraction of time the instrument was taking data over the total time the instrument was active.

[c] Corrected outburst detection rate of the instrument over the last 18 years, quoted with 1σ Gehrels errors.

Complete Outburst History: Combining the outburst detector and, tracker, and empirical classification tools of the algorithm with an exhaustive literature review we have been able to compose a relatively complete outburst history for the Galactic (transient and persistent) BHXRB population encompassing over 50 years of activity (presented in Table A.3). Note that any discrepancies between the literature classification and algorithm classification will be discussed on a source by source basis in the following section. Below we present an excerpt from the outburst history table. The full table can be found in Appendix A.

Table 4.5: Excerpt from Galactic BHXRB Outburst History

Source Name	$t_{\rm beg}$ [a]	$t_{\rm end}$ [a]	Outburst ID	Literature [b] Class	Algorithm Class [b] H_X	d_f	Instrument [c] Detection	References [d]
SwiftJ1357.2−0933	55563.5	55687.5	2011	F	F	F	**BAT**,EPIC,**MAXI**,PCA,RGS,XRT	122,126,127
GS1354−64	-	-	1967	S	-	-	Skylark	74,75,242,257
	-	-	1972	F	-	-	MIT	74,75,242,258
	-	-	1987	S	-	-	GINGA/ASM,LAC	74,75,242
	50714.0	50870.0	1997/1998	F	F	F	**ASM**,BATSE,GINGA/ASM	28,242,259
				S			HEXTE,PCA	
1A 1524−617	-	-	1974	S	-	-	Ariel V/ASM,SSI	242,278
	-	-	1990	F	-	-	SIGMA	242,279,280
SwiftJ1539.2−6227	54792.0	54966.0	2008/2009	S	S	S	**ASM,BAT**,HEXTE,PCA,XRT	121,122
MAXIJ1543−564	55681.0	55833.5	2011	S	S	S	**BAT,MAXI**,PCA,XRT	86
4U1543−475	-	-	1971	S	-	-	UHURU	1,242
	-	-	1983/1984	S	-	-	Tenma	2,242
	-	-	1992	F	-	-	BATSE	3,242
	52435.0	52488.0	2002	S	S	S	**ASM**,EPIC,HEXTE,PCA	4,242
XTEJ1550−564	51062.0	51316.0	1998/1999	S	S	S	**ASM**,BATSE,HEXTE,PCA	150–152,385–387
	51597.0	51703.0	2000	I	I	S	**ASM**,Chandra,HEXTE,PCA	153–156
	51934.0	51983.0	2001	F	F	-	**ASM**,Chandra	157
	52261.0	52312.0	2001/2002	F	F	-	**ASM**,HEXTE,PCA	158,388
	52726.0	52775.0	2003	F	F	F	**ASM**,ISGRI,JEM-X,PCA	159,160

State Transitions: In addition to classification, our algorithm makes use of the X-ray hardness ratio to track a source as it transitions through varying combinations of the four accretion states, during outburst and/or periods of continuous activity on a day-by-day basis. In Table A.4 we present the results of tracking the 43 transient and 9 persistent sources. Each outburst (or period of long-term activity) is first differentiated into three separate stages:

- rise → times preceding the outburst peak (in luminosity);
- decline → times following the outburst peak (in luminosity); and
- transition → time periods in which the source makes (or attempts to make) the hard-to-soft or soft-to-hard transitions.

In addition to stage differentiation, an outburst (or period of long-term activity) is also separated into 3 possible accretion states: HCS, SDS, or IMS. Unfortunately, due to a lack of spectral information, while we observe the SPL state occurring in a number of sources over the last 18 years (see Section 4.1.2 for further discussion), we do not have the ability to empirically differentiate it from the other three accretion states using hardness ratio alone.

In addition to single states represented, we present transitions of two different forms,

- (state name one) → (state name two); and
- (state name one) → IMS → (state name two).

The first depicts the canonical full transitions between hard and soft states, while the second describes the attempted transitions (or erratic "jumps") between one of the two principal states and the IMS. It is important to note that as we only have daily time resolution, HCS to SDS transitions taking less than 1 day to complete are not shown here.

Lastly, we also include the - symbol in the table. This symbol represents times when we do not have adequate information to define the state of the system. This symbol is indicative of either having only one energy band available at the time,

which is adequate for outburst detection but not for classification via H_X, or having no data available on this particular time period.

Below we present an excerpt from the state transitions table (Table A.4) of one transient outburst (GX 339−4) and one period of long term persistently bright behaviour (1E 1740.7−2942). The full table can be found in Appendix A.

Table 4.6: Excerpt from State Transitions occurring in Galactic BHXRBs Between 1996-2014

Source Name	Outburst ID	Stage	State(s)	$t_{\rm beg}$[a] (MJD)	$t_{\rm end}$[a] (MJD)	$t_{\rm dur}$[b] (days)
GX 339−4	1997-1999	rise	-	50456	50469	13
		rise	HDS	50469	50818	349
		transition	HDS → SDS	50818	50827	9
		rise	SDS	50827	50885	58
		decline	SDS	50885	51053	168
		transition	SDS → IMS → SDS	51053	-	1
		decline	SDS	51054	51157	103
		transition	SDS → HDS	51157	51189	32
		decline	HDS	51189	51215	26
		decline	-	51215	51296	81
1E1740.7−2942	2008-2014	rise	-	54504	54511	7
		rise	HDS	54511	54526	15
		transition	HDS → SDS	54526	54528	2
		rise	SDS	54528	54530	2
		transition	SDS → HDS	54530	-	1
		rise	HDS	54531	54599	68
		transition	HDS → IMS → HDS	54599	-	1
		rise	HDS	54600	54659	59
		transition	HDS → IMS → HDS	54659	54661	2
		rise	HDS	54661	55309	648
		transition	HDS → IMS → HDS	55309	55328	19
		rise	HDS	55328	55457	129
		transition	HDS → SDS	55457	55720	263
		rise	SDS	55720	55735	15
		decline	SDS	55735	55735	0
		decline	HDS	55735	56363	628

Continued on Next Page...

Table 4.6 – Continued

Source Name	Outburst ID	Stage	State(s)	$t_{\rm beg}$ [a] (MJD)	$t_{\rm end}$ [a] (MJD)	$t_{\rm dur}$ [b] (days)
		transition	HDS → IMS → HDS	56363	56372	9
		decline	HDS	56372	56543	171
		transition	HDS → IMS → HDS	56543	56545	2
		decline	HDS	56545	56761	216
		decline	-	56761	56769	8

Note. –

[a] The start and end times of a particular stage in an outburst, given in MJD.

[b] Duration of the particular outburst stage in days.

4.1.2 Individual Source Investigation

In Appendix B we present the detailed data products, created via the algorithm, on a source by source basis. These data products come in two separate forms: long-term light curves, available for the 43 transient and 9 persistent sources, depicting the structure of the outbursts undergone in each available energy band and an analysis package available for each detected transient outburst or period of long-term persistent activity.

In addition, this section also offers, where necessary, a discussion of any discrepancies between the literature and the findings of our algorithm in each given source (located after the example data products below).

The long-term light curves have been colour coded by instrument. Here data from RXTE/ASM is displayed in blue, RXTE/PCA in purple, INTEGRAL/ISGRI in dark green, INTEGRAL/JEM-X in light green, Swift/BAT in red and MAXI/GSC in yellow.

The outburst analysis package presented includes the following:

- individual hard and soft band light curves for the outburst;
- the evolution of H_X over the duration of the outburst;

- the complete HID of the outburst; and
- the evolution of disc fraction d_f throughout the outburst.

Firstly, note that in creating our HIDs we have taken the "intensity" on any particular day to be the maximum of the hard and soft bands. Secondly, within the products in the analysis package you will find each data point colour coded with respect to the state the system was in on that particular day (using H_X as a basis for state classification). Here blue represents the HCS, red represents the SDS, and yellow represents the IMS.

Once again we stress that, due to a lack of more detailed spectral information, we do not have the ability to empirically differentiate the SPL state from the other three accretion states. However, we do observe the signature of the SPL state, namely the "dragon horn" in numerous HIDs. This "dragon horn", in most cases, appears to either curl backwards (i.e., a significant increase in hardness, followed by a softening of the source) or stand close to straight up (i.e., a near constant hardness during the time period). Interestingly enough we observe this type of behaviour spanning hardness ratios associated with all three accretion states, resulting in the appearance of unusually high or low disc fractions paired with H_X's associated with the HCS and SDS, respectively.

While further study of this phenomena is beyond the scope of this work, we make note of its appearance where possible, which will hopefully lead to a future avenue of investigation.

Below we present an example data product for one transient source and one persistent source. The complete package of data products for the population can be found in Appendix B.

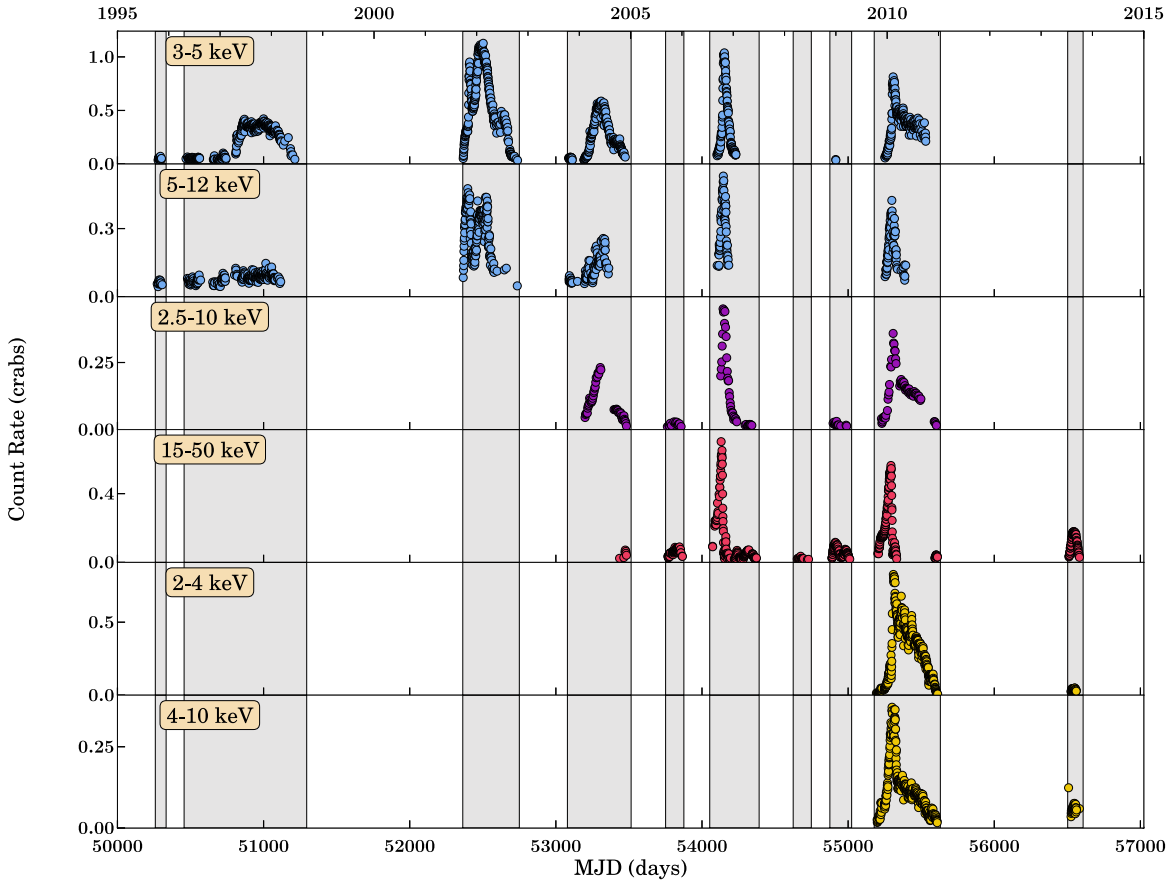

(a) Long-term Light Curve

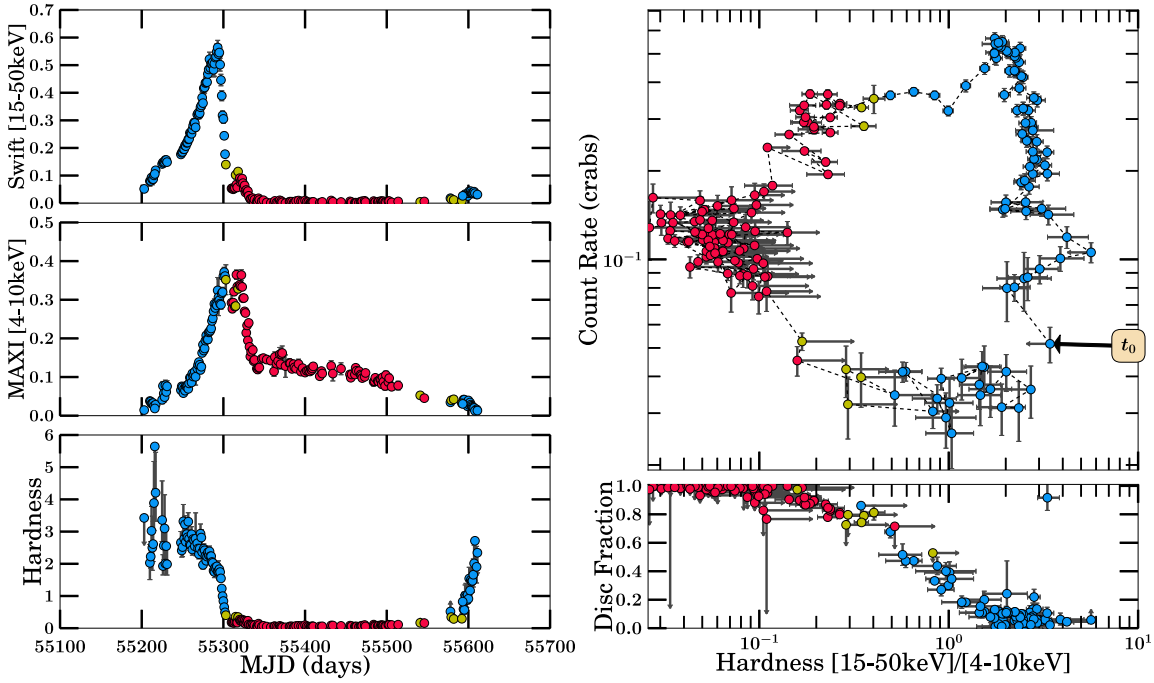

(b) 2009-2011 Outburst Analysis

Figure 4.1: Example data product: GX 339−4

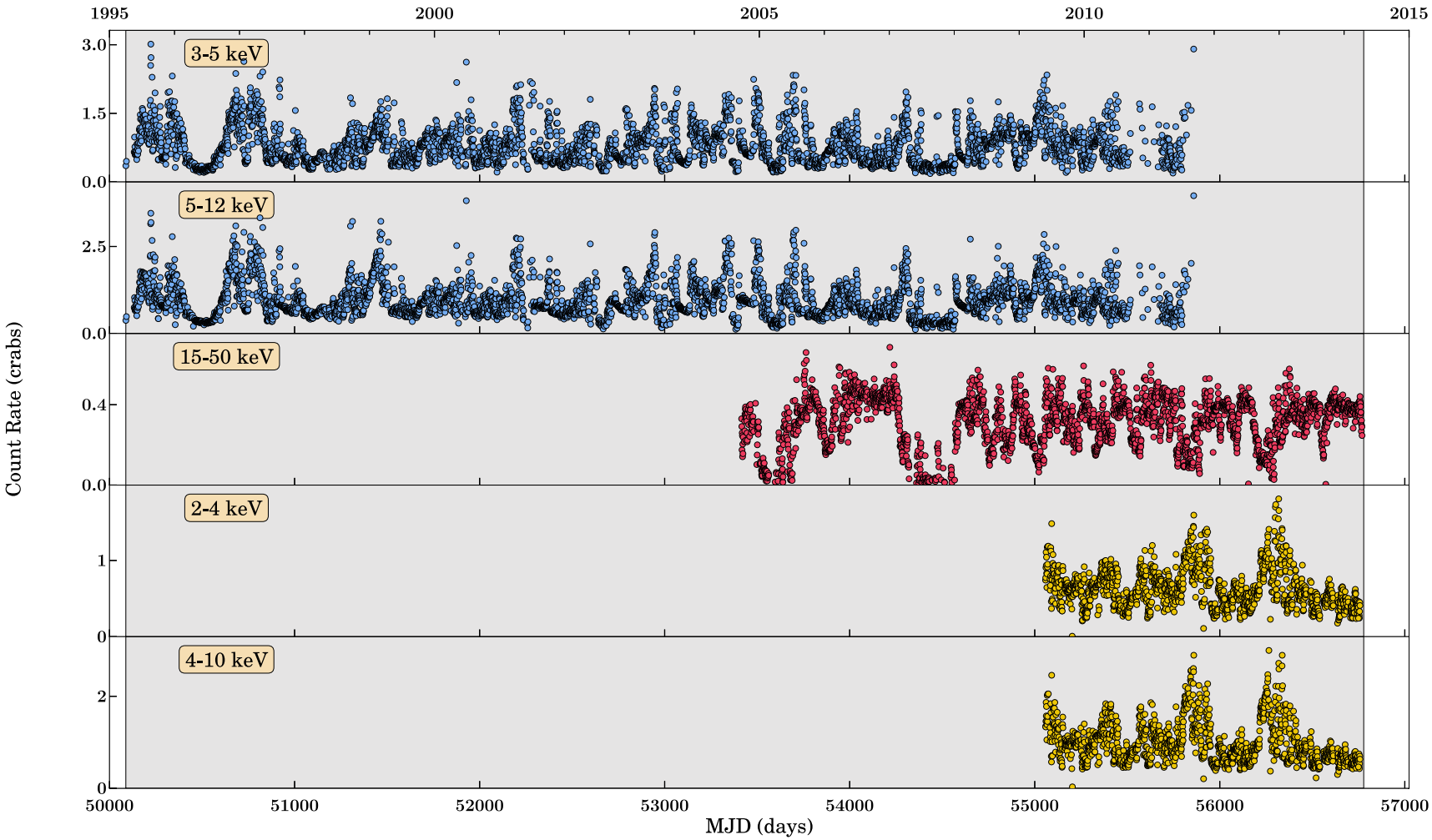

Figure 4.2: Example data product: GRS 1915+105 Part 1

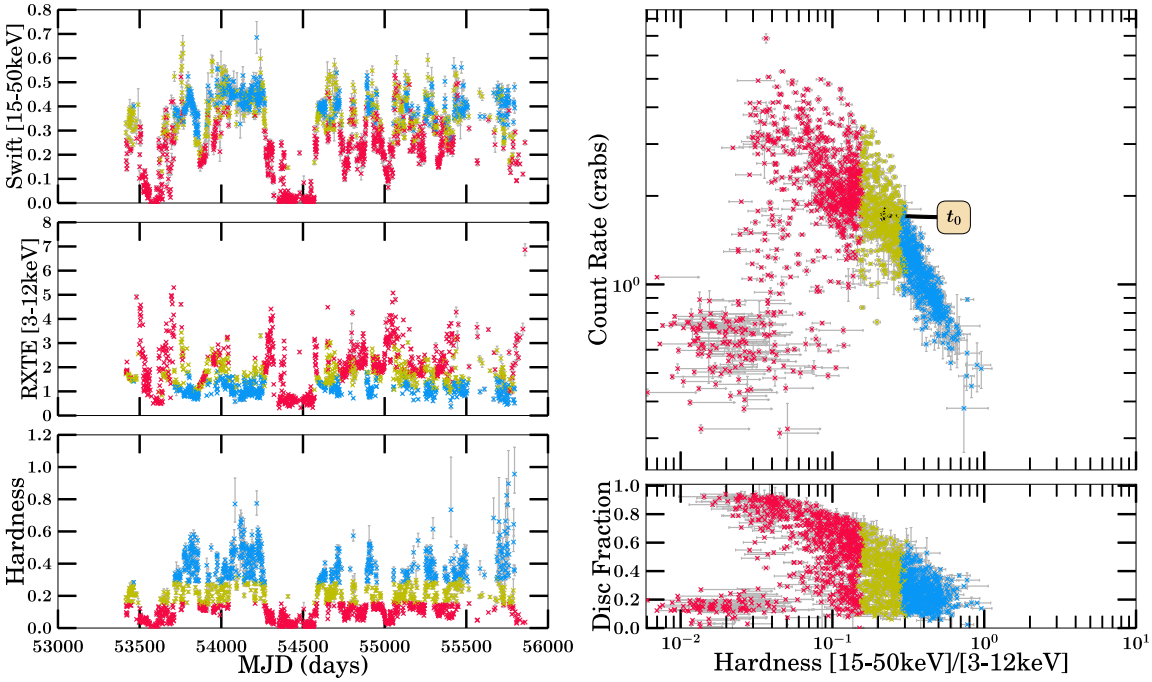

(a) 1996–2014 Outburst Analysis

Figure 4.3: Example data product: GRS 1915+105 Part 2

Discontinuities and Exceptions:

XTE J1637−498: While our algorithm detects the 2008 outburst, the detection is below our minimum data requirement, cannot be classified, and therefore is not included in our analysis.

MAXI J1543−564: Our algorithm also detects this source in 2013 both above the detection threshold and minimum data requirement. However, the fact that we only detect it with MAXI and it is not found in the literature points to the conclusion that this is most likely an artificial feature and therefore the 2013 outburst is not included in our analysis.

IGR J11321−5311: Due to the short variability exhibited by this source (see Chapter 2 for detail) our algorithm was unable to catch the 2005 outburst.

XTE J1650−500: It is important to note that in addition to the outburst in 2001, our algorithm has also caught two flare-like events in the softer MAXI bands during of period stretching from 55310–55608. These features are due to contamination by the close by source GX 339−4, which was bright during this period, and therefore are ignored. For details see the MAXI website.

IGR J17091−3624: Data from the INTEGRAL bulge scan has only been available as of February of 2005 and as a result our algorithm has only caught the 2007 and 2011 outbursts of this source. The 2003 outburst could not be classified as only BAT data is available.

IGR J17098−3628: While our algorithm detects activity in this source in 2005 with BAT, PCA and ISGRI, the detections did not meet our minimum data requirement and therefore are not included in our analysis.

Swift J1713.4−4219: Due to the lack of quality data available for this source (see Chapter 2 for detail) our algorithm was unable to catch the 2009 outburst.

XMMSL1J171900.4−353217: In addition to the activity listed in Table A.4, our algorithm is able to classify 2 other outbursts (2007,2008/2009) and detects this source on 13 other occasions (mostly in archival RXTE/PCA data). While we believe these outbursts to be real features, because they have only been detected by RXTE/PCA, we are unable to classify them.

XTEJ1719−291: Armas-Padilla et al. (2011) estimate that XTE J1719−291 would

have had a 2–10 keV peak luminosity of 7×10^{35}ergs^{-1} during its 2008 outburst, therefore classifying the system as a very faint X-ray transient (VFXT), solidifying the reason why our algorithm did not detect this outburst.

IGR J17354−3255: Due to the short variability exhibited by this source (see Chapter 2 for detail) our algorithm was unable to detect any of the activity occurring between 2003–2009.

IGR J17379−3747: While our algorithm was able to detect the 2004 outburst of this source, it was unable to classify the outburst as the only data available at that time was from the PCA.

SLX1746−331: In addition to the 5 outbursts discussed in Table A.4, our algorithm detects an additional 3 periods of activity in 2009/2010, 2011/2012, and 2012/2013. While each are above our detection threshold and minimum data requirement, they are only significantly detected with MAXI, which not only makes classification impossible but also brings into question the validity of the detections. For these reasons these three are not included in our analysis.

XTEJ1752−223: In addition to the outburst in 2009/2010, our algorithm has caught 3 flare-like events with MAXI between 2011 and 2012. While all 3 are above our detection threshold and minimum data requirement, they are only detected with our algorithm in MAXI data, and are not mentioned at all in the literature. Therefore they are are assumed to be artificial features.

IGRJ17586−2129: Our algorithm also detects the source in 2010 with RXTE/PCA. While this outburst is above our detection threshold and minimum data requirement, their is only sufficient data with RXTE/PCA making classification impossible.

IGRJ18175−1530: While our algorithm detects this source in 2007, there is only a significant amount of data in RXTE/PCA and therefore the outburst could not be classified.

SAX J1819.3−2525: Our algorithm detects an additional 13 separate flare-like events (mainly using RXTE/PCA), each of which are above our detection threshold and minimum data requirement. Given the high sensitivity of RXTE/PCA (when compared with the 5 other instruments we make use of), all 13 are treated as real features and included in our analysis. We note that source activity has also been reported

by MAXI in 2014. However, because the detection was below the minimum data requirement, this activity is not included in our analysis.

Swift J1842.5−1124: In addition to the discovery outburst, this source also underwent a later, very weak outburst in February of 2010. This activity was not detected by our algorithm.

IGR J18539+0727: Our algorithm was unable to detect IGR J18539+0727 in 2003 as there is no data available for this source in the INTEGRAL Bulge Scan.

XTE J1856+053: In addition to the outbursts in 1996 and 2006/2007, our algorithm has also caught an additional outburst in 2009 with RXTE/PCA. While this outburst is above our detection threshold and minimum data requirement, it has only been significantly detected by RXTE/PCA and we are unable to classify it.

XTEJ1901+014: Due to its fast variability (see Chapter 2), our algorithm was unable to detect any of the previously mentioned activity in this source.

4.2 Mass Accretion History of the Population

We have seen that when a source (whether transient or persistent) fails to transition, it does not reach the higher luminosities and larger $\dot{M}$ that characterize the softer states, resulting in under luminous "failed" outbursts or extended periods spent in the HCS.

The questions that remains are: what kind of ramifications does this prominent "failed" behaviour have on the mass-accretion history of the Galactic BHXRB population and what observational parameters can be used to probe the degree to which this behaviour impacts the population as a whole?

The answer, which we will present in this section, lies in the investigation of two empirically measurable parameters, luminosity and mass-transfer rate.

4.2.1 Luminosity

By modelling the daily flux of a source as a combination of a:

- disc black body spectral component and a

- comptonized spectral component,

assuming a Crab-like spectrum in each given energy band and a known distance (from the literature), we have been able to measure the bolometric X-ray luminosity $L_{\rm bol}$ for a source on a given day t_d.

Outburst Luminosity Analysis: From here we can analyze luminosity data for individual transient outbursts or long-term activity in the case of persistent sources. Table A.5 presents peak luminosities in the HCS, SDS, and for the outburst as a whole, a deconvolution of the outburst into total time spent in the HCS, SDS, and in transition, and an estimate of total energy released during outburst (or "fluence").

Firstly, note the clear demonstration of the under-luminous nature of a "failed" outburst (or long-term period spent in the HCS), perpetuated by the sub-Eddington peak luminosities, when compared to the canonical outbursts (or long-term persistently canonical behaviour).

Secondly, note the state in which the peak luminosity of an outburst occurs. While typically, according to the canonical theory (Fender et al., 2004, 2009; Fender and Gallo, 2014), you would expect the peak luminosity to occur in the soft state due to the larger $\dot{M}$ associated with this state resulting in the movement of the initially truncated disc inward toward the ISCO, a fair number of sources exhibit the opposite behaviour in which the peak occurs in the hard state. This fact, coupled with the peak occurring at larger fractions of Eddington (i.e $> 0.2L_{\rm edd}$) and the occasional appearance of the "dragon horn" feature in the HID during the time period, is perhaps of SPL/anomalous high L_X behaviour.

Thirdly, take note of the fraction of time over the last 18 years that a source spends in each state, particularly in the case of the persistent sources. Doing so, in combination with analysis of the state transitions occurring (see Table A.4), has allowed us to separate the 9 persistent sources into three separate classes based on long term behavioural characteristics as follows,

- mainly HCS behaviour $\rightarrow$ the source spends, on average, $\gtrsim 85\%$ of the time it has been "on" (i.e., in an X-ray bright state) in the HCS.

- mixed behaviour $\rightarrow$ while the source has been observed to make occasional

transitions to the SDS, it spends a significant amount of time undergoing "failed" state transitions (i.e., attempted hard-soft transitions in which the source only reaches as soft as the IMS).

- anomalous SPL/high L_X behaviour $\rightarrow$ while the source appears to spend the majority of its time in the HCS, it peaks at high fractions of Eddington, suggesting presence in a high luminosity state such as an SPL state or perhaps a more complicated situation (e.g., "heartbeat" states of GRS 1915+105; Neilsen et al. 2011).

Lastly, we caution the reader to pay attention to the degree that we know the bolometric luminosity (i.e., the errors), which is highly dependent on how well we know the distance to the particular source (see Table A.2), and as a result can vary in size by large factors from source to source (e.g., GS 1354−64).

Below we present an excerpt from the luminosity data table (Table A.5). The full table can be found in Appendix A.

Table 4.7: Excerpt from Luminosity data for Galactic BHs & BHCs Between 1996-2014

Source Name	Outburst ID	$t_{\rm dur}$ [a] (days)	$\int L dt$ [b] ($\times 10^{38}$ erg)	$L_{\rm peak,tot}$ [c] ($\times 10^{38}$ erg)	$L_{\rm edd}$ [c] ($L_{\rm peak,tot}/L_{\rm edd}$)	$L_{\rm peak,HCS}$ [d] ($\times 10^{38}$ erg)	$L_{\rm peak,SDS}$ [e] ($\times 10^{38}$ erg)	$t_{\rm HCS}$ [f] (days)	$t_{\rm SDS}$ [g] (days)	$t_{\rm IMS}$ [h] (days)	$t_{\rm und}$ [i] (days)
XTEJ0421+560	1998	50	0.69 ± 0.44	3.8 ± 3.4	0.29 ± 0.30	3.8 ± 3.4	-	5	0	0	45
4U0538−641	1996-2003	2905	604.8 ± 5.5	$28.2^{+8.1}_{-8.3}$	$3.12^{+0.91}_{-0.93}$	$28.2^{+8.1}_{-8.3}$	9.3 ± 2.2	1915	56	920	14
	2004-2014	3695	1615.3 ± 9.2	$23^{+7.1}_{-10}$	$2.6^{+0.8}_{-1.1}$	$23.1^{+4.8}_{-4.9}$	$21.4^{+3.7}_{-3.8}$	851	1160	1548	136
4U0540−697	1996-2014	6663	14186 ± 50	$28^{+9.9}_{-11}$	$1.99^{+0.74}_{-0.84}$	$27^{+8.8}_{-10}$	$28^{+9.9}_{-11}$	2863	1367	2281	152
XTEJ1118+480	1999/2000	203	0.0559 ± 0.0037	0.0257 ± 0.0047	$0.00271^{+0.00056}_{-0.00057}$	0.0257 ± 0.0047	-	183	0	0	20
MAXIJ1305−704	2012	182	7.90 ± 0.80	0.17 ± 0.16	0.013 ± 0.014	0.17 ± 0.16	-	54	0	41	87
SWIFTJ1357.2−0933	2010-2012	836	4.14 ± 0.30	$0.032^{+0.057}_{-0.056}$	0.0025 ± 0.0045	0.029 ± 0.049	-	20	0	0	816
GS1354−64	1997/1998	157	879 ± 93	27 ± 25	$1.9^{+1.9}_{-1.8}$	27 ± 25	-	109	0	0	48
SWIFTJ1539.2−6227	2008/2009	175	12.5 ± 1.7	0.88 ± 0.82	$0.068^{+0.071}_{-0.072}$	0.42 ± 0.38	0.19 ± 0.19	77	1	45	52

Continued on Next Page...

Table 4.7 – Continued

Source Name	Outburst ID	$t_{\rm dur}$[a] (days)	$\int Ldt$[b] ($\times 10^{38}$ erg)	$L_{\rm peak,tot}$[c] ($\times 10^{38}$ erg)	$L_{\rm edd}$[c] ($L_{\rm peak,tot}/L_{\rm edd}$)	$L_{\rm peak,HCS}$[d] ($\times 10^{38}$ erg)	$L_{\rm peak,SDS}$[e] ($\times 10^{38}$ erg)	$t_{\rm HCS}$[f] (days)	$t_{\rm SDS}$[g] (days)	$t_{\rm IMS}$[h] (days)	$t_{\rm und}$[i] (days)
MAXIJ1543−564	2011	153	4.02 ± 0.41	0.18 ± 0.16	0.014 ± 0.014	0.18 ± 0.16	0.11 ± 0.10	40	3	22	88
4U1543−475	2002	54	23.8 ± 1.0	20.5 ± 2.7	1.70 ± 0.43	13.2 ± 1.8	20.5 ± 2.7	12	20	15	7

Note. –

$L_{\rm peak,HCS}$ ="-" and $t > 0$ or $L_{\rm peak,SDS}$ ="-" and $t > 0$, indicate the minimum requirement of two different bands (one hard and one soft) for the spectral modelling process has not been met.

[a]Indicates the duration of the outburst in days.

[b]Indicates the total amount of energy released during outburst ("fluence").

[c]Indicates the peak (bolometric) luminosity reached during outburst.

[d]Indicates the peak (bolometric) luminosity reached when the source was in the (HCS).

[e]Indicates the peak (bolometric) luminosity reached when the source was in the (SDS).

[f]Indicates the total time the source spends in the HCS measured in days.

[g]Indicates the total time the source spends in the SDS measured in days.

[h]Indicates the total time the source spends in transition between the HCS and the SDS measured in days.

[i]Indicates the total amount of time we do not have sufficient data for the source.

Bolometric XLFs: Using the methods described in Section 3.2.6, and given bolometric X-ray luminosity $L_{\rm bol}$ for a source on any given day t_d, we have obtained the following empirical XLFs for the 43 transient sources.

Here luminosity data (purple) have been arranged into 31 bins between 0 and $10^{40}\,{\rm erg\,s^{-1}}$, where any values below $10^{34}\,{\rm erg\,s^{-1}}$ are placed in the lowest bin. The errors on each bin (blue) are quoted as 1σ Gehrels errors. As described in Section 3.2.6, these transient XLFs are comprised of only "good detections" (purple), corresponding to times when the source was in outburst.

Take note of the steady appearance of a double peaked feature, indicative of the presence of the source (over the last 18 years) in two distinct "states", associated with different luminosity regimes. In the case of those sources that have been observed to undergo canonical (or a mix of canonical and failed) behaviour, the peak contribution located at the lower luminosity ($\sim 10^{35} - 10^{36}{\rm ergs^{-1}}$) corresponds to the HCS, while the peak contribution located at the higher luminosity ($\sim 10^{37} - 10^{38}{\rm ergs^{-1}}$) represents the SDS.

In contrast, you will notice most of the exclusively "failed" outburst source XLFs only exhibit one peak located at lower luminosities as expected (with the exception of XTE J1118+480, SAX J1711.6−3808, and GRS 1737−31), seemingly associated with the HCS, to which the source has been observed to remain in for the duration of outburst periods.

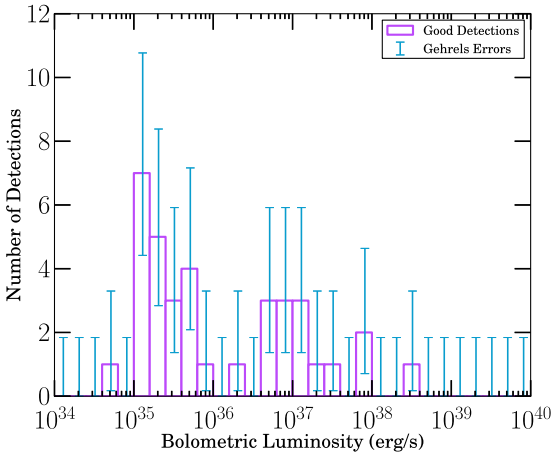

(a) XTE J0421+560

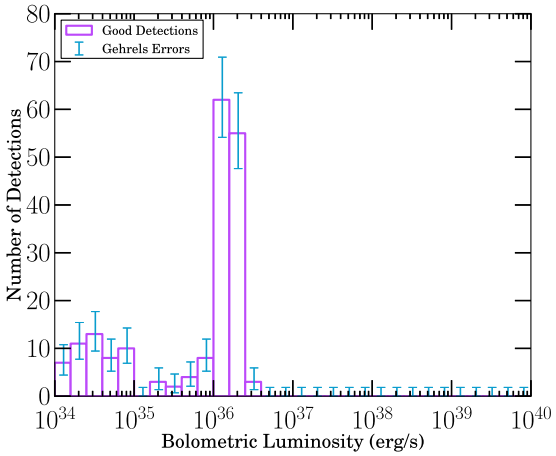

(b) XTE J1118+480

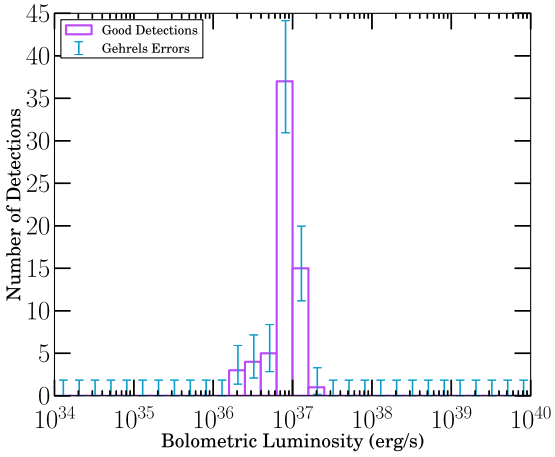

(c) MAXI J1305−704

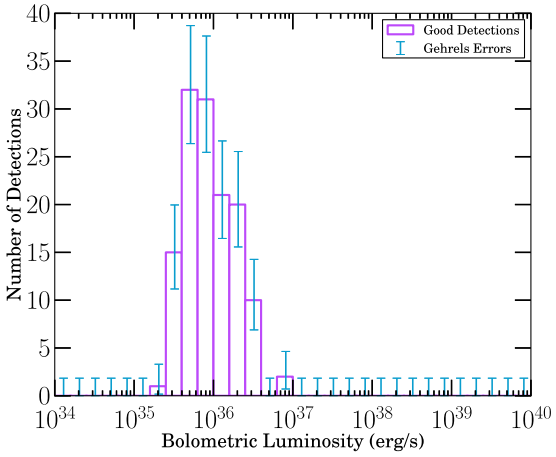

(d) Swift J1357.2−0933

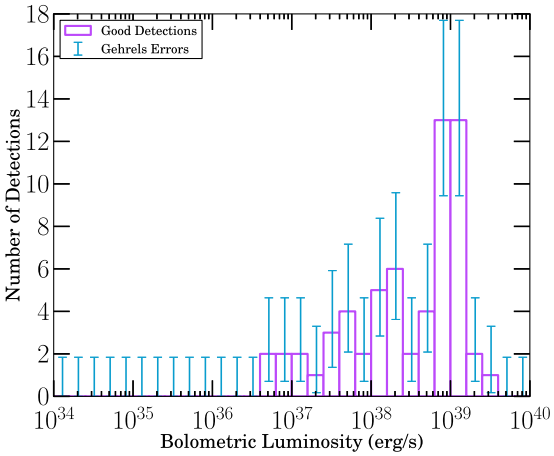

(e) GS 1354−64

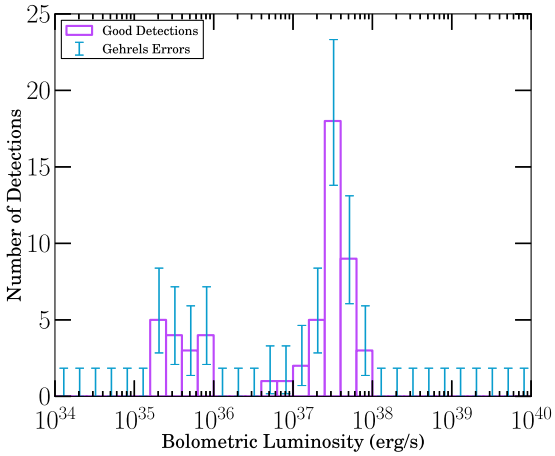

(f) Swift J1539.2−6227

Figure 4.4: Transient XLFs: Part 1

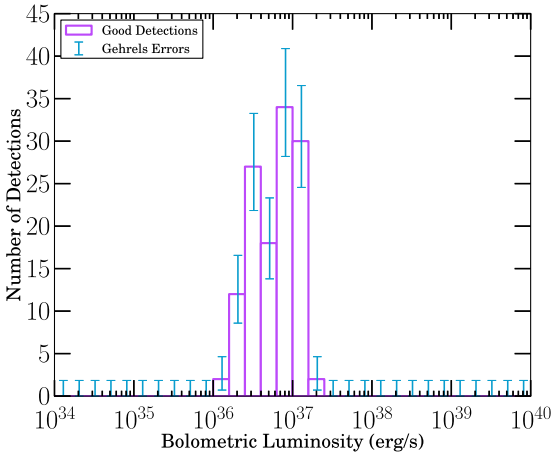

(a) MAXI J1543−564

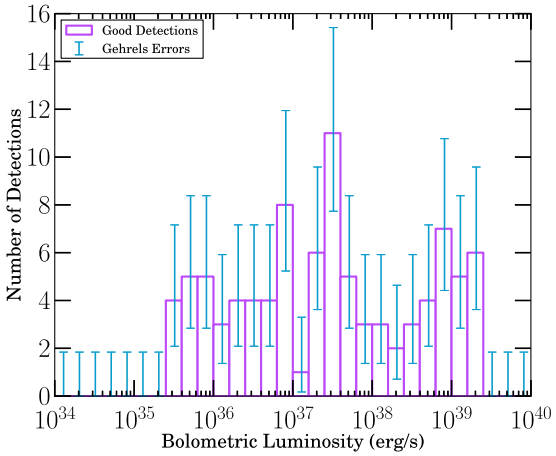

(b) 4U 1543−475

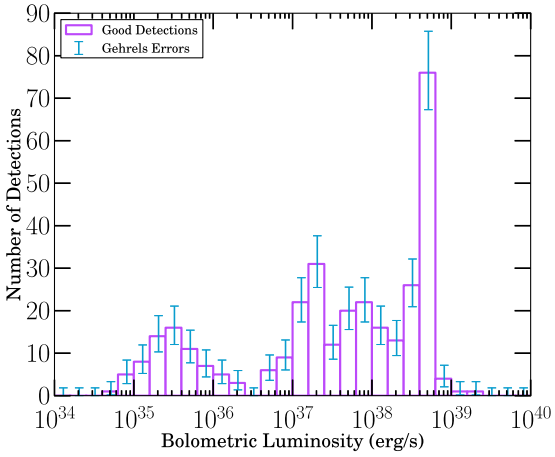

(c) XTE J1550−564

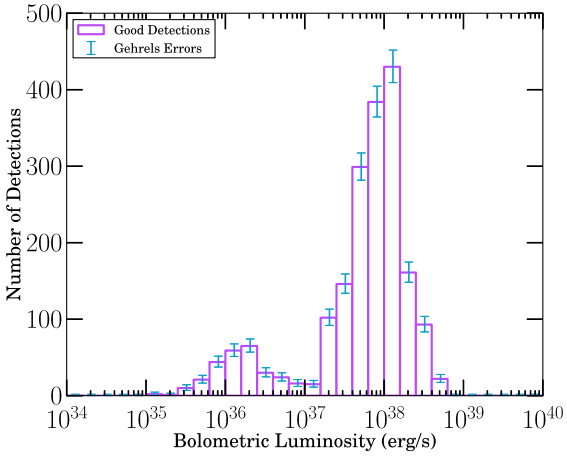

(d) 4U 1630−472

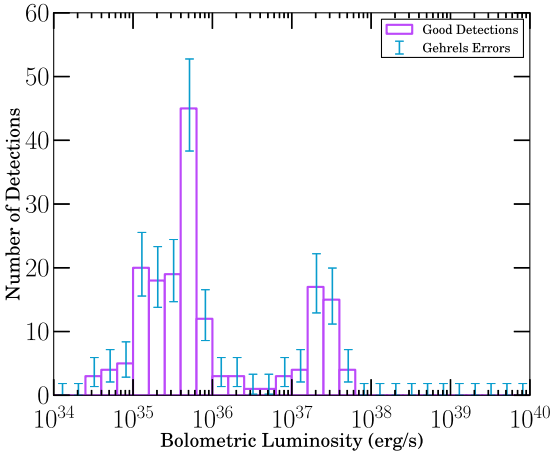

(e) XTE J1650−500

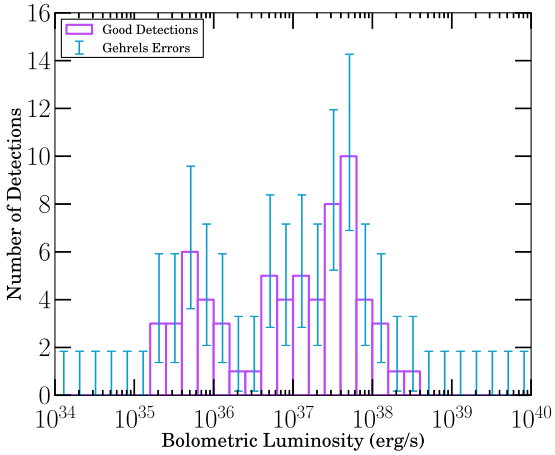

(f) XTE J1652−453

Figure 4.5: Transient XLFs: Part 2

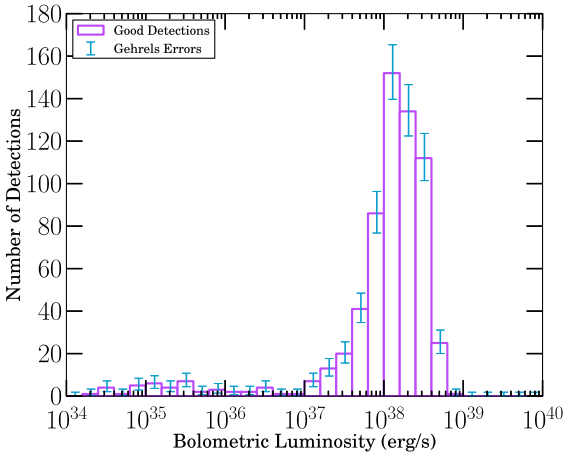

(a) GRO J1655−40

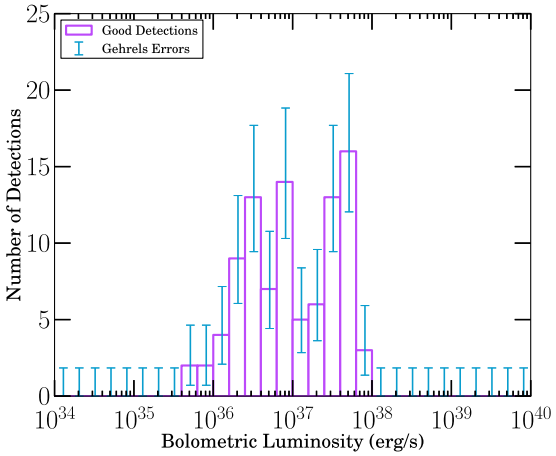

(b) MAXI J1659−152

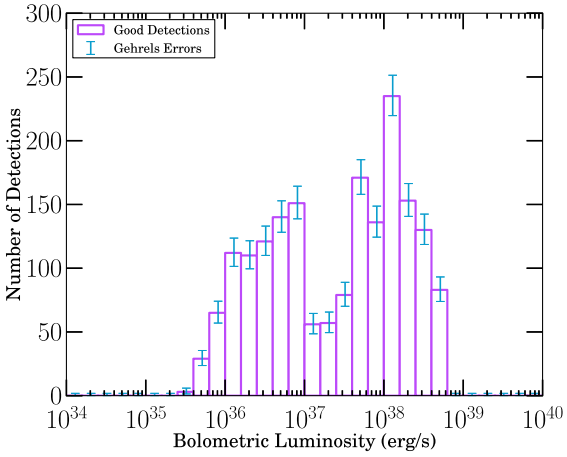

(c) GX 339−4

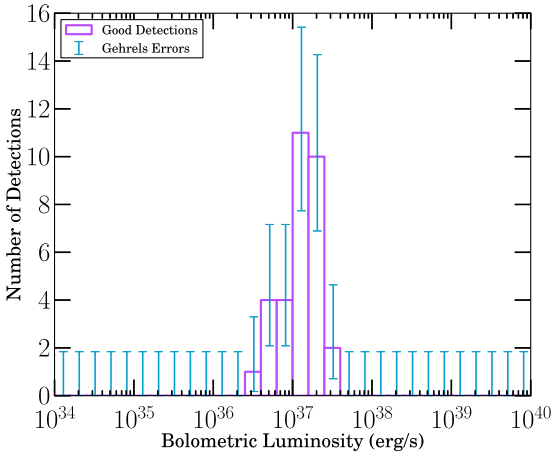

(d) IGR J17091−3624

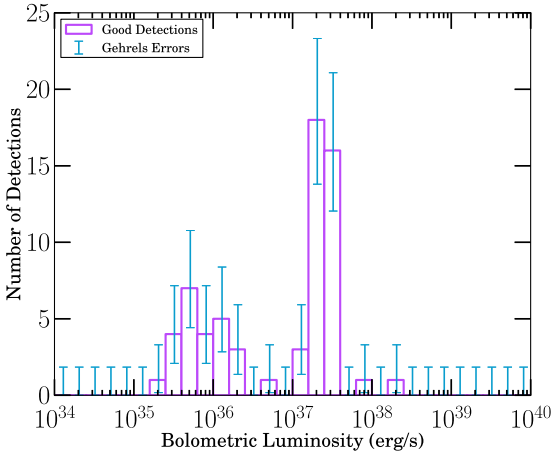

(e) SAX J1711.6−3808

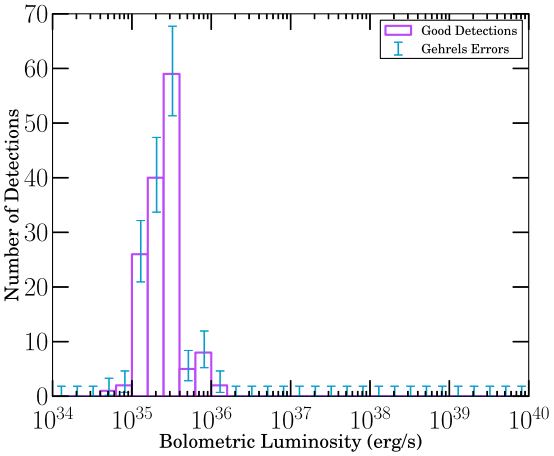

(f) XMMSL1 J171900.4−353217

Figure 4.6: Transient XLFs: Part 3

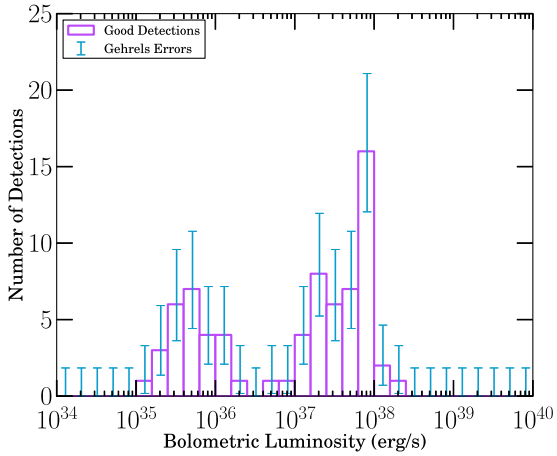

(a) XTE J1720−318

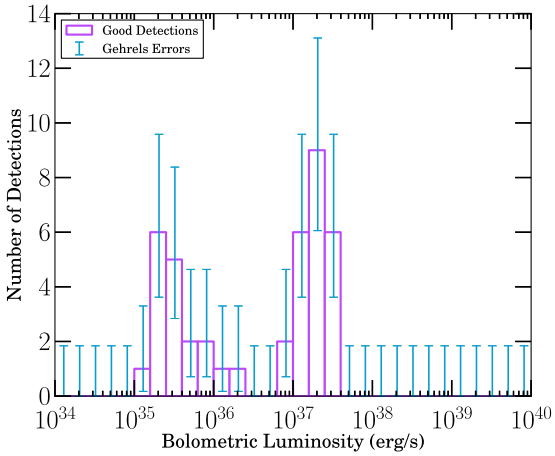

(b) XTE J1727−476

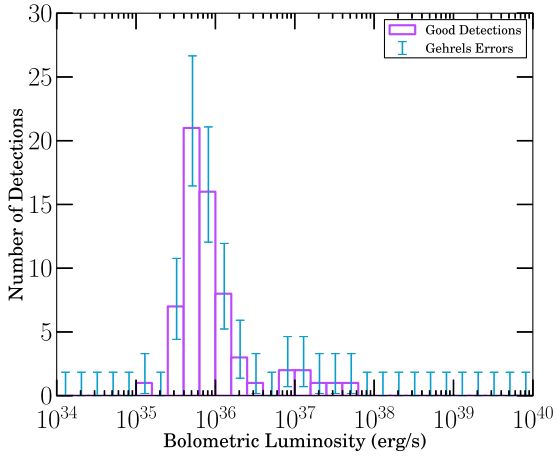

(c) IGR J17285−2922

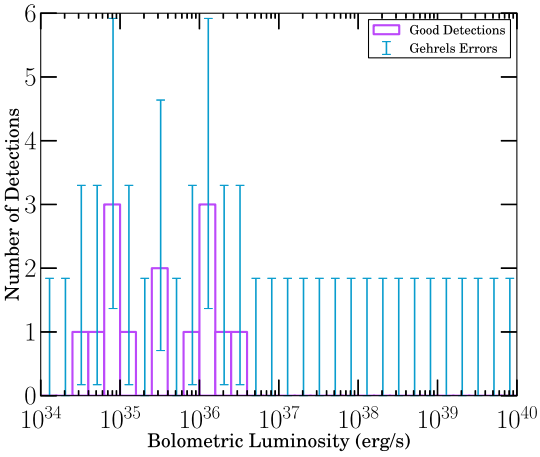

(d) IGRJ17379−3747

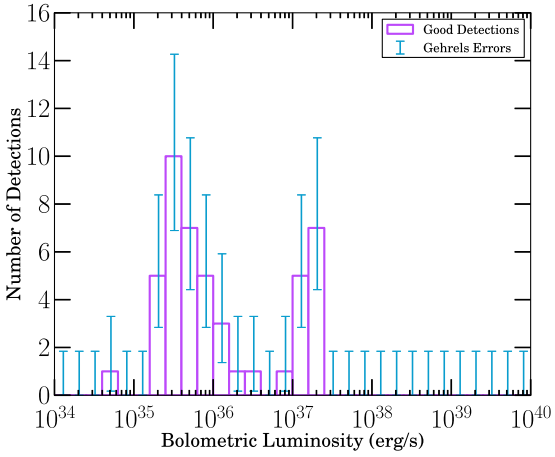

(e) GRS 1737−31

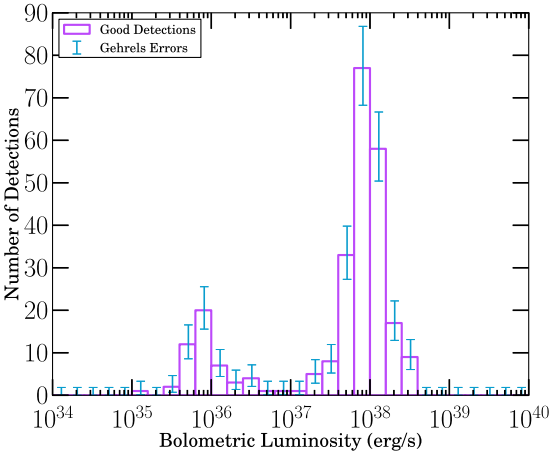

(f) GRS 1739−278

Figure 4.7: Transient XLFs: Part 4

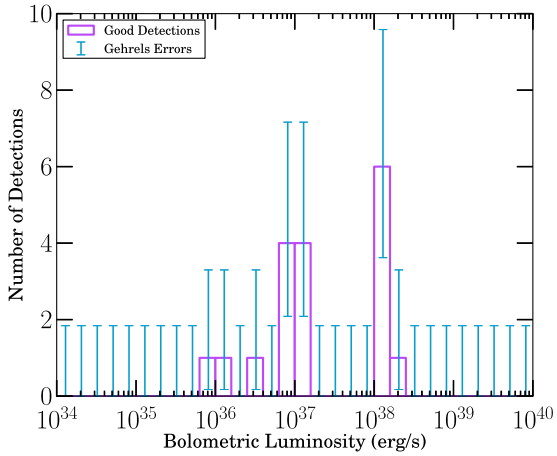

(a) SWIFT J174510.8−262411

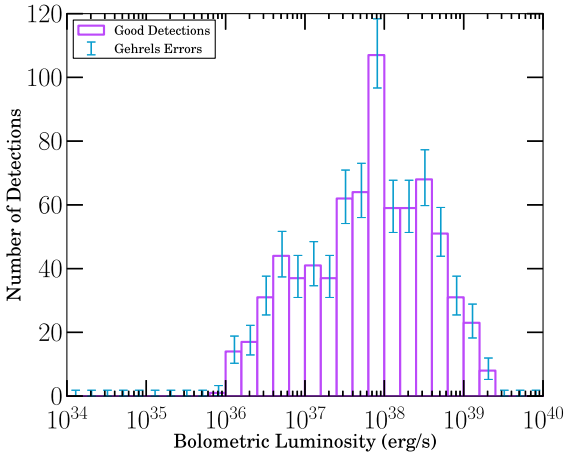

(b) H 1743−322

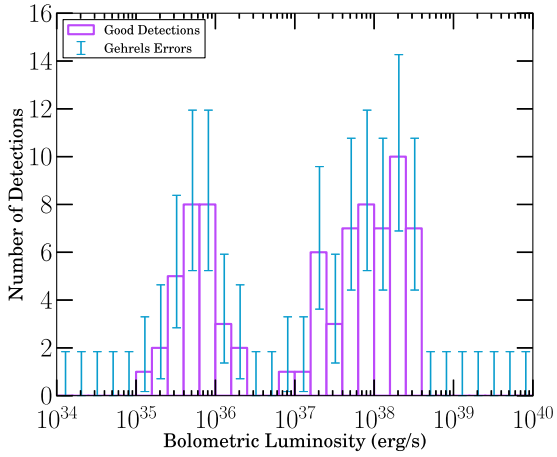

(c) XTE J1748−288

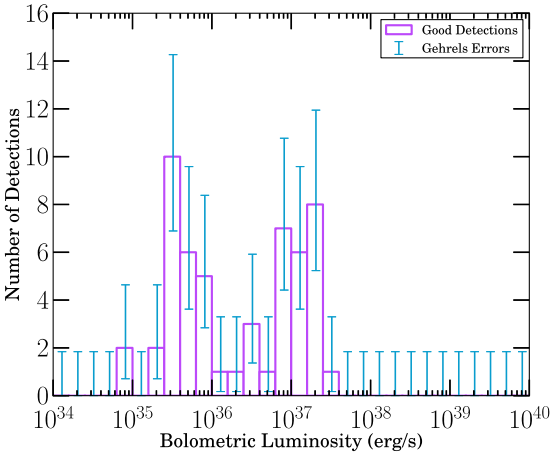

(d) IGRJ17497−2821

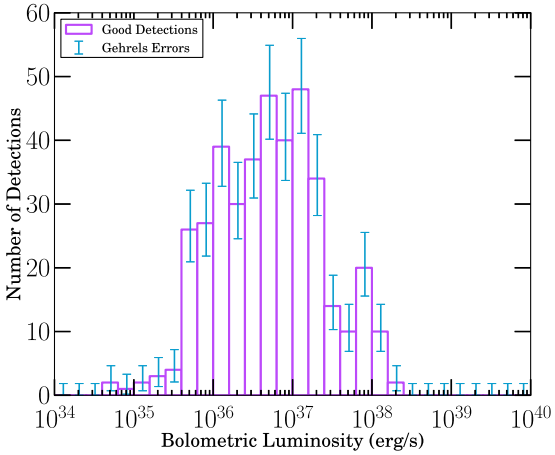

(e) SLX J1746−331

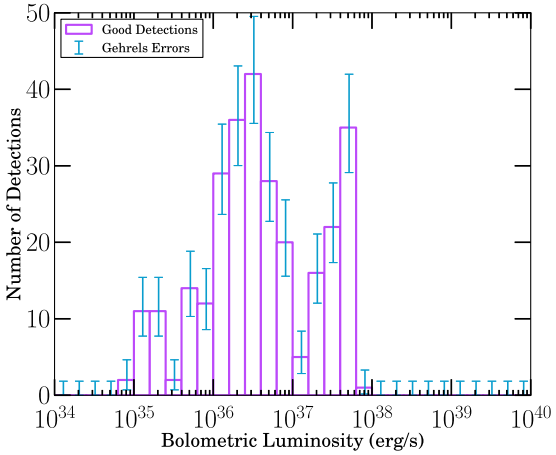

(f) XTE J1752−223

Figure 4.8: Transient XLFs: Part 5

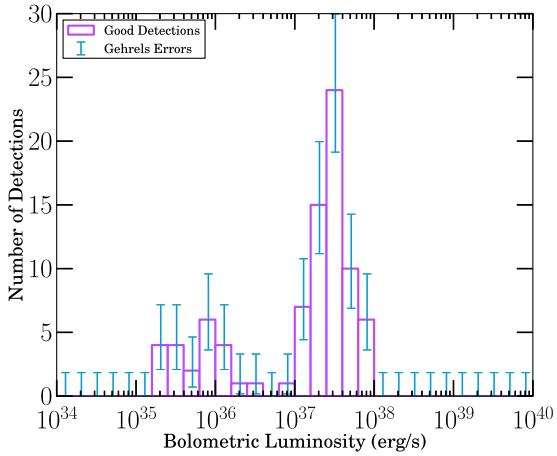

(a) XTE J1755−324

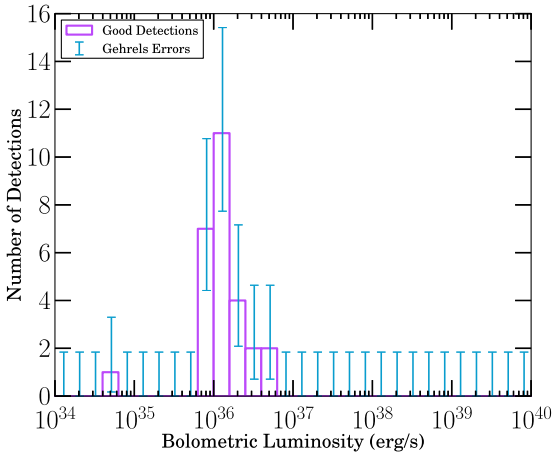

(b) IGR J17586−2129

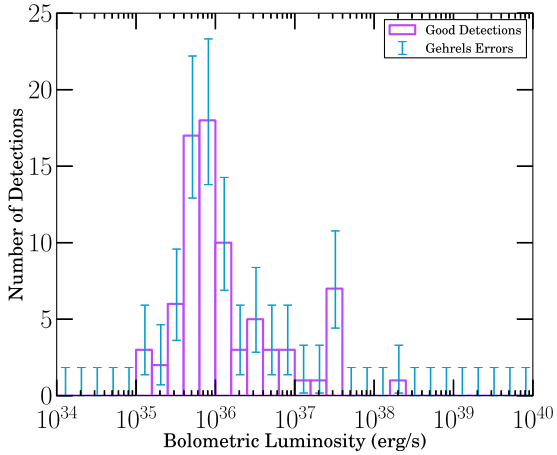

(c) XTE J1812−182

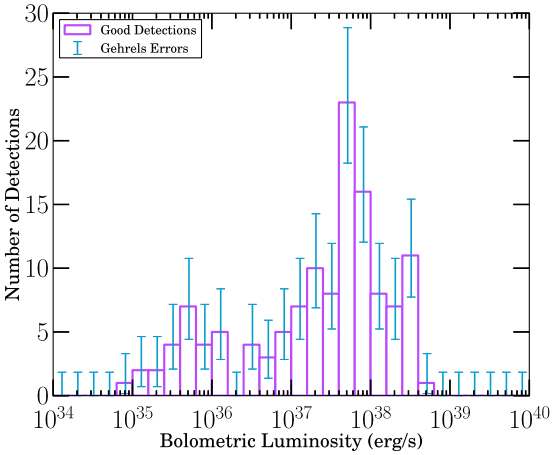

(d) XTE J1817−330

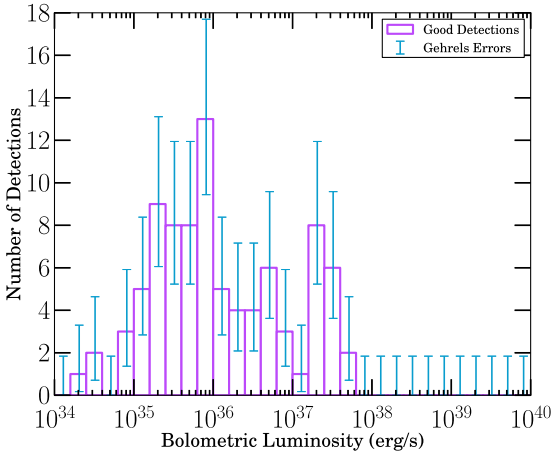

(e) XTE J1818−245

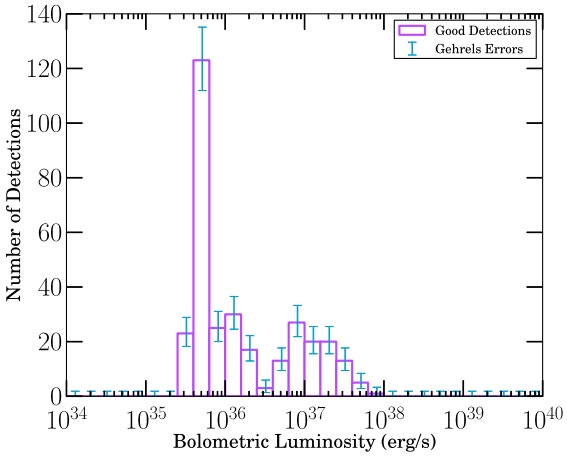

(f) SAX J1819.2−2525

Figure 4.9: Transient XLFs: Part 6

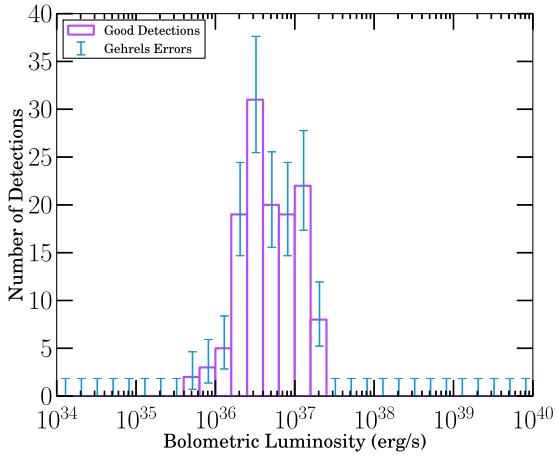

(a) MAXI J1836−194

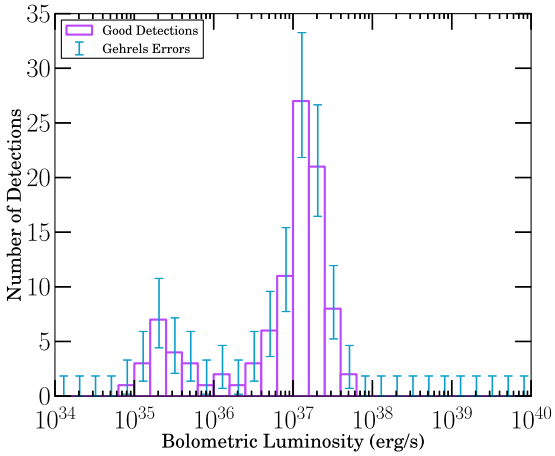

(b) Swift J1842.5−1124

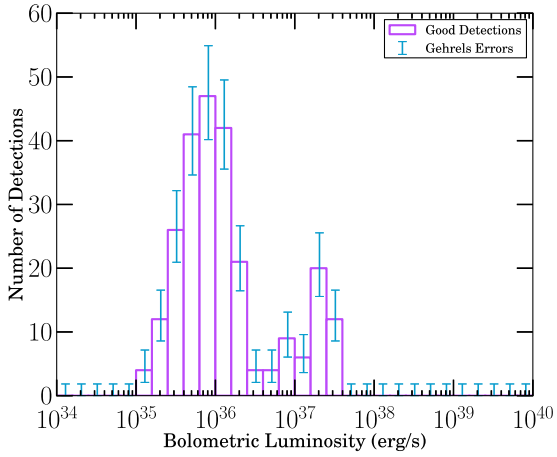

(c) XTE J1856+053

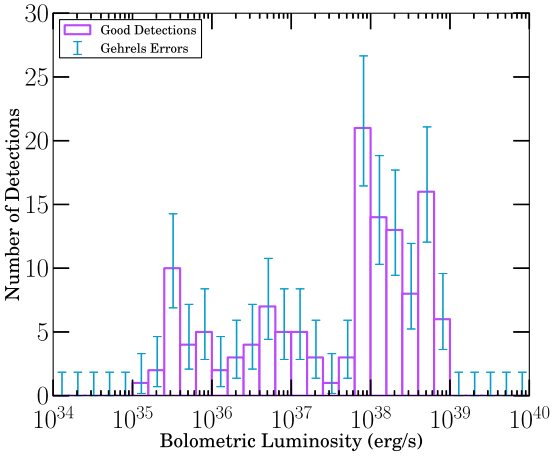

(d) XTE J1859+226

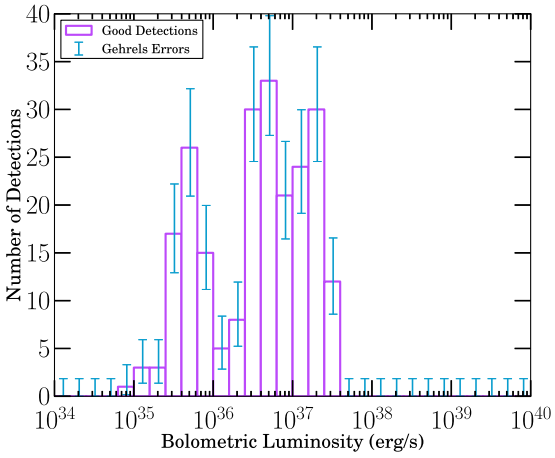

(e) XTE J1908+094

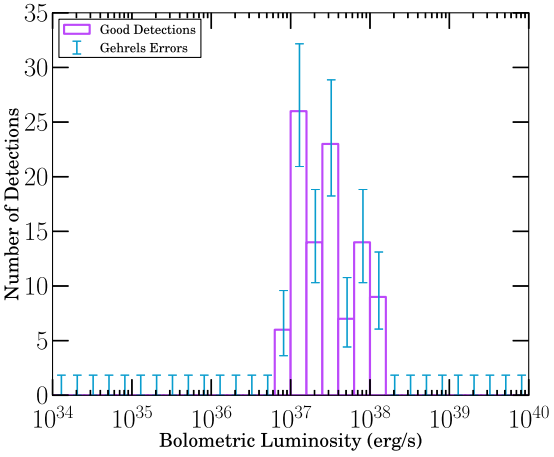

(f) Swift J1910.2−0546

Figure 4.10: Transient XLFs: Part 7

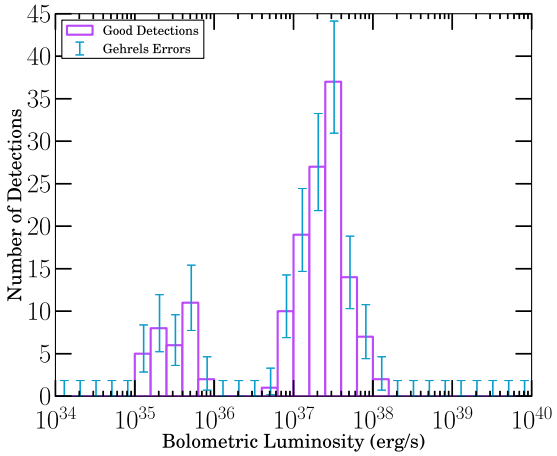

(a) XTE J2012+381

Figure 4.11: Transient XLFs: Part 8

From here, a combined XLF over time for the Galactic transient BHXRB population can be derived by randomly selecting 500 observations from each individual transient source XLF (see Figure 4.12). Each luminosity bin in the population XLF has been colour coded by state, where blue, red, and yellow represent the HCS, SDS, and IMS, respectively. Note that we only include those sources that belong to BH classes A or B (i.e., securely classified BHs or BHCs) and have available distance estimates.

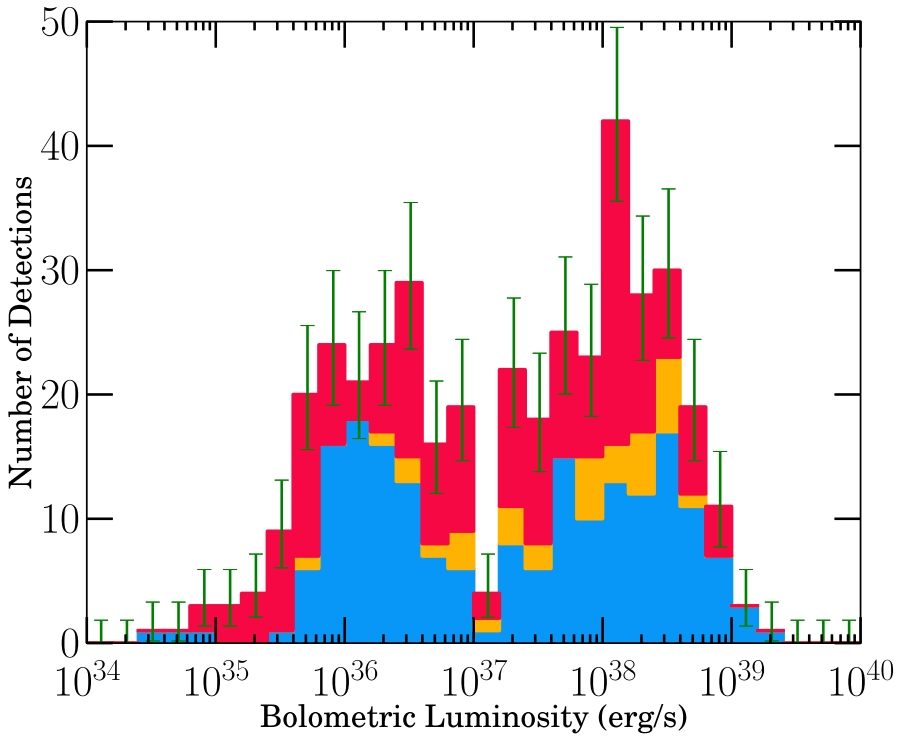

Figure 4.12: A combined XLF over time for the Galactic transient BHXRB population. Each bin is colour coded by state, where blue, red, and yellow represent the HCS, SDS, and IMS respectively. The 1σ Gehrels errors (green) are shown for each bin. Note that only those sources that belong to BH classes A or B and have distance estimates are included here.

We begin by first noting the appearance of a double peaked profile, a complete deviation from the power-law type distribution found for the entire XRB population of the galaxy in previous studies (Grimm et al., 2002). This is perhaps suggestive of transient sources spending significant amounts of time in distinct luminosity regimes

(i.e., separate accretion states over time).

Secondly, take note of the significant hard state contribution at low luminosities. This is perhaps indicative of the prominent failed outburst behaviour, associated with sub-eddington peak luminosities, resulting in transient sources spending significantly more time in the low-luminosity hard state regime than generally expected.

To definitively prove that the large contribution at low-luminosities is in fact due to the "failed" outbursts, rather then as a result of just a prolonged hard state as a part of a classic canonical outburst, we exclude "failed" outburst detections from our sampling scheme. To accomplish this, if a "failed" outburst detection is selected, the detection is thrown out and a new sample is chosen. The result of this re-sampling process is shown in Figure 1.13. Take note of the clear reduction in hard state detections in the low-luminosity contribution of the XLF, indicating that this large low-luminosity hard state contribution, evident in Figure 1.12, is in fact mainly due to the prominent transient "failed" behaviour.

Third, we also observe a hard state contribution at high luminosities ($10^{38} - 10^{39}$), usually a regime associated with the radiatively efficient accretion flows of the soft state. There are two separate possibilities for this observation. Either it is indicative of the rising hard state (i.e., just before transition to the soft state) or of the SPL/anomalous high L_X state, whose horn like structure is present in a significant portion of our samples HIDs.

Fourth, take note of detections in all states being dispersed across a wide range of luminosities, indicative of the lack of one to one correspondence between luminosity and state (referred to as hysteresis), which is exhibited in BH systems.

Lastly, we note that we may possibly be dealing with incompleteness at lower luminosities due to the limited sensitivity of the all-sky and scanning instruments. In analyzing the XLFs for the individual transient sources it becomes clear that the limiting luminosity at which the number of detections for a given source begin to fall off is highly dependent on distance. In the case of close by sources (e.g., XTE J1118+480 at $\sim$1.7 kpc) we have a significant amount of detections at luminosities as low as a few times $10^{34}\,\mathrm{erg\,s^{-1}}$. While detections in Galactic Center sources (e.g., GX 339−4 at $\sim$8 kpc) appear to fall off at luminosities between $\sim 5\times10^{35} - 10^{36}\,\mathrm{erg\,s^{-1}}$.

Despite this possible bias, the existence of at least two distinct "states" in the XLF, as opposed to a single power-law distribution, is robust.

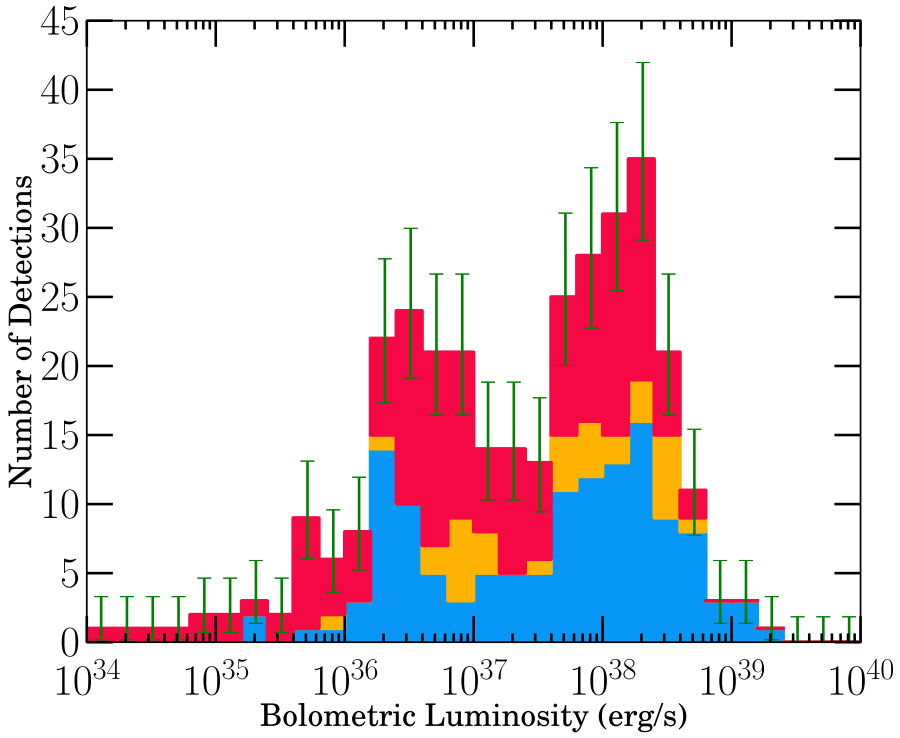

Figure 4.13: A re-sampled combined XLF over time for the Galactic transient BHXRB population excluding "failed" outburst detections. Each bin is colour coded by state where blue, red and yellow represent the HCS, SDS and IMS, respectively. The 1σ Gehrels errors (green) are shown for each bin. Note that only those sources that belong to BH classes A or B and have distance estimates are included here.

4.2.2 Mass-Transfer Rate $\dot{M}$

We have derived the time averaged bolometric luminosity and long-term mass transfer rates making use of the method described in Section 3.2.6 for the 43 transient and 9 persistent sources. The resulting values, coupled with a summary of the prominent outburst behaviour, are presented in Table 4.7.

In the case of the transient sources, the outburst behaviour column indicates whether the source has undergone only "successful", only "failed" or a combination

of "successful" and "failed" outbursts over the last 18 years. While in the case of persistent sources, it indicates one of the three long-term behavioural characteristics discussed above.

Note that if a transient source has only undergone one outburst, the $\dot{M}$ in Table 4.7 should only be considered an upper limit (indicated by a "<").

Table 4.8: Mass Transfer History of the Galactic BHXRB Population from 1996-2014

Source Name	Source[a] Type	$< L_{\rm Bol} >_{\rm t}$ [b] ($\times 10^{36}$ ergs/s)	$< \dot{\rm M} >_{\rm t}$ [c] ($\times 10^{-9} M_{\odot}$/yr)	Outburst[d] Behaviour
XTEJ0421+560	T	$0.161^{+0.118}_{-0.054}$	$< 0.0157^{+0.0131}_{-0.0073}$	failed only
4U0538−641	P	$241^{+17.7}_{-10}$	$28^{+8.0}_{-18}$	anomalous high L_X
4U0540−697	P	$473^{+35.0}_{-22}$	55^{+16}_{-35}	anomalous high L_X
XTEJ1118+480	T	$0.0349^{+0.0035}_{-0.0021}$	$< 0.0042^{+0.0010}_{-0.0026}$	failed only
MAXIJ1305−704	T	$0.222^{+0.145}_{-0.071}$	$< 0.022^{+0.013}_{-0.010}$	successful only
SWIFTJ1357.2−0933	T	$0.26^{+0.27}_{-0.12}$	$< 0.0198^{+0.0275}_{-0.0047}$	failed only
GS1354−64	T	$30.2^{+18.6}_{-9.4}$	$< 3.1^{+1.7}_{-1.5}$	failed only
SWIFTJ1539.2−6227	T	$0.58^{+0.37}_{-0.18}$	$< 0.056^{+0.036}_{-0.024}$	successful only
MAXIJ1543−564	T	$0.257^{+0.162}_{-0.082}$	$< 0.026^{+0.015}_{-0.012}$	successful only
4U1543−475	T	$4.50^{+0.48}_{-0.28}$	$< 0.54^{+0.13}_{-0.33}$	successful only
XTEJ1550−564	T	$13.5^{+2.4}_{-1.4}$	$1.8^{+0.2}_{-1.1}$	combined
4U1630−472	T	57^{+37}_{-17}	$6.0^{+3.2}_{-2.8}$	combined
XTEJ1650−500	T	$0.278^{+0.107}_{-0.060}$	$< 0.035^{+0.006}_{-0.021}$	successful only
XTEJ1652−453	T	$0.73^{+0.50}_{-0.24}$	$< 0.074^{+0.044}_{-0.033}$	successful only
GROJ1655−40	T	$20.8^{+4.8}_{-2.7}$	$2.9^{+0.1}_{-1.9}$	successful only
MAXIJ1659−152	T	$0.54^{+0.33}_{-0.17}$	$< 0.055^{+0.031}_{-0.026}$	successful only
GX339−4	T	$38.5^{+13.9}_{-7.7}$	$5.0^{+0.6}_{-3.0}$	combined
IGRJ17091−3624	T	$1.01^{+0.64}_{-0.32}$	$< 0.102^{+0.060}_{-0.046}$	successful only
SAXJ1711.6−3808	T	$0.44^{+0.29}_{-0.14}$	$< 0.043^{+0.028}_{-0.018}$	failed only
XMMSL1J171900.4−353217	T	$0.135^{+0.084}_{-0.043}$	$0.0135^{+0.0078}_{-0.0061}$	failed only
XTEJ1720−318	T	$1.66^{+1.07}_{-0.53}$	$< 0.160^{+0.104}_{-0.067}$	successful only
XTEJ1727−476	T	$0.120^{+0.082}_{-0.040}$	$< 0.0114^{+0.0080}_{-0.0047}$	successful only

Continued on Next Page...

Table 4.8 – Continued

Source Name	Source[a] Type	$< L_{\rm Bol} >_{\rm t}$[b] ($\times 10^{36}$ ergs/s)	$< \dot{\rm M} >_{\rm t}$[c] ($\times 10^{-9} M_{\odot}$/yr)	Outburst[d] Behaviour
IGRJ17285−2922	T	$0.0273^{+0.0182}_{-0.0088}$	$< 0.0027^{+0.0017}_{-0.0012}$	failed only
IGRJ17379−3747	T	$0.0068^{+0.0047}_{-0.0023}$	$< 0.00065^{+0.00046}_{-0.00027}$	failed only
GRS1737−31	T	$0.172^{+0.122}_{-0.057}$	$< 0.0162^{+0.0116}_{-0.0063}$	failed only
GRS1739−278	T	$6.7^{+4.1}_{-2.1}$	$0.69^{+0.37}_{-0.32}$	successful only
1E1740.7−2942	P	$2.13^{+1.31}_{-0.67}$	$0.22^{+0.12}_{-0.10}$	mainly HCS
SWIFTJ174510.8−262411	T	$3.5^{+2.1}_{-1.1}$	$< 0.36^{+0.20}_{-0.17}$	failed only
H1743−322	T	$36.7^{+14.5}_{-8.0}$	$4.6^{+0.8}_{-2.7}$	combined
XTEJ1748−288	T	$1.64^{+1.03}_{-0.51}$	$< 0.167^{+0.093}_{-0.077}$	failed only
IGRJ17497−2821	T	$0.114^{+0.074}_{-0.036}$	$< 0.0117^{+0.0067}_{-0.0053}$	failed only
SLX1746−331	T	$3.2^{+2.0}_{-1.0}$	$0.32^{+0.19}_{-0.14}$	combined
XTEJ1752−223	T	$0.899^{+0.161}_{-0.093}$	$< 0.116^{+0.013}_{-0.075}$	successful only
SWIFTJ1753.5−0127	P	$8.7^{+5.1}_{-2.7}$	$0.90^{+0.47}_{-0.42}$	mixed
XTEJ1755−324	T	$0.79^{+0.50}_{-0.26}$	$< 0.080^{+0.047}_{-0.037}$	successful only
IGRJ17586−2129	T	$0.051^{+0.033}_{-0.016}$	$< 0.0048^{+0.0034}_{-0.0019}$	failed only
GRS1758−258	P	$3.8^{+2.3}_{-1.2}$	$0.38^{+0.22}_{-0.18}$	mainly HCS
XTEJ1812−182	T	$0.181^{+0.117}_{-0.059}$	$0.0174^{+0.0117}_{-0.0072}$	combined
XTEJ1817−330	T	$3.12^{+1.94}_{-0.98}$	$< 0.32^{+0.17}_{-0.15}$	successful only
XTEJ1818−245	T	$0.095^{+0.030}_{-0.017}$	$< 0.0120^{+0.0016}_{-0.0073}$	successful only
SAXJ1819.3−2525	T	$1.48^{+0.54}_{-0.29}$	$0.19^{+0.02}_{-0.12}$	failed only
MAXIJ1836−194	T	$0.298^{+0.185}_{-0.095}$	$< 0.030^{+0.018}_{-0.013}$	failed only
SWIFTJ1842.5−1124	T	$0.38^{+0.24}_{-0.12}$	$< 0.038^{+0.022}_{-0.017}$	successful only
XTEJ1856+053	T	$0.31^{+0.20}_{-0.10}$	$0.031^{+0.019}_{-0.013}$	successful only
XTEJ1859+226	T	$6.1^{+3.1}_{-1.7}$	$< 0.65^{+0.28}_{-0.33}$	successful only
XTEJ1908+094	T	$0.64^{+0.41}_{-0.20}$	$0.064^{+0.038}_{-0.029}$	combined
SWIFTJ1910.2−0546	T	$1.57^{+0.98}_{-0.49}$	$< 0.162^{+0.088}_{-0.076}$	successful only
SS433	P	$1.280^{+0.075}_{-0.048}$	$0.149^{+0.044}_{-0.092}$	mainly HCS
GRS1915+105	P	1730^{+306}_{-190}	220^{+25}_{-140}	anomalous high L_X
4U1956+350	P	$19.1^{+1.9}_{-1.2}$	$2.3^{+0.5}_{-1.4}$	mixed

Continued on Next Page...

Table 4.8 – Continued

Source Name	Source[a] Type	$< L_{\rm Bol} >_{\rm t}$[b] ($\times 10^{36}$ ergs/s)	$< \dot{\rm M} >_{\rm t}$[c] ($\times 10^{-9} M_{\odot}$/yr)	Outburst[d] Behaviour
4U1957+115	P	$18.3^{+11.2}_{-5.7}$	$1.86^{+1.03}_{-0.87}$	mixed
XTEJ2012+381	T	$1.07^{+0.67}_{-0.34}$	$< 0.111^{+0.062}_{-0.052}$	successful only

Note. –

[a] Indicates transient (T) or persistent (P).

[b] The time averaged (over the last 18 years) bolometric luminosity.

[c] The average mass-transfer rate (over the last 18 years).

The effects the transient "failed" or long-term hard state behaviours have on the mass-accretion history of the population can be further investigated by plotting in the $\dot{M} - P_{\rm orb}$ plane (see Figure 4.14). Here we plot the calculated $\dot{M}$ for the 14 transient and 9 persistent sources from our sample for which the orbital period is known (see Chapter 2 or Table A.2 for references).

Transient sources (filled circles) are colour coded with respect to the following three behaviours exhibited during outburst; exclusively "failed" (red), exclusively "successful" (green), or a combination of the two (yellow). In contrast, the persistent sources (filled triangles) are colour coded with regards to one of the following three long-term characteristics; exhibiting mainly HCS behaviour ($\gtrsim$ 85% of the X-ray bright periods over the last 18 years; orange), significant periods of SPL/anomalous high luminosity behaviour (i.e., $L_X > 0.2 L_{\rm edd}$; purple), or exhibiting occasional soft state transitions but spending significant periods of time undergoing "failed" state transitions (i.e., attempted hard-soft transitions in which the source only reaches the IMS before transitioning back to the hard state; pink).

Generally, you would expect a typical 1-to-1 relation as a larger $P_{\rm orb}$ should correspond to a larger $\dot{M}$ (Podsiadlowski et al., 2002). However, we observe the appearance of numerous outliers and a great deal of scatter, amounting to up to two orders of magnitude difference between our observed $\dot{M}_{\rm BH}$ and the value which is theoretically expected. There exists several possibilities to explain this observation.

First, the scatter could imply a change in efficiency between the two regimes (e.g., more advection of energy during the hard state). As such, considerable thought has been put into the effect that differences in accretion efficiency (ϵ) between the hard and soft states may have on the scatter observed. Namely, the possibility that this scatter could diminish if the hard spectral states have systematically lower accretion efficiencies, which some models suggest (see the discussion of radiatively inefficient accretion flows in Section 1.2.2).

That being said, given the observed absence of a clear luminosity change during spectral transitions in these types of systems (Maccarone, 2005), the difference in accretion efficiencies between the hard and soft states (at the transition luminosity) is most likely minimal. However, we note that this does not rule out by any means the possibility that low-luminosity hard states (suggested to be associated with "failed" outbursts), well below the transition luminosity, could have significantly lower efficiency as a result of the dominant radiatively inefficient accretion flows associated with this regime (Knevitt et al., 2014).

Along these lines, it has also been postulated that the low peak outburst luminosities associated with short period BH LMXBs[1] could potentially cause them to remain in this low luminosity hard state (as peak outburst luminosity drops near the limit for radiatively inefficient accretion), rather than entering the high luminosity soft state expected for radiatively efficient accretion. This points to the idea that short period systems may be more prone to "failed" outbursts then the longer period systems (Meyer-Hofmeister, 2004; Knevitt et al., 2014).

Second, if we assume that the mass transfer rate from the companion is similar in all Galactic BH systems then, specifically in the case of "failed" outbursts, the question becomes just where is all the accreted material going, if it is not contributing to the accretion luminosity (i.e., falling through the disc toward the BH). In this case, we must consider the possibility that the hard state leads to a substantial outflow not seen in the soft state (e.g., a relativistic plasma jet).

[1]The relationship between $P_{\rm orb}$ and peak outburst luminosity for LMXBs is well established. See Shahbaz et al. (1998) and Portegies Zwart et al. (2004). Also see Wu et al. (2010) for a comprehensive study of outburst luminosities for a sample of transient LMXBs observed with RXTE.

Along similar lines, because we also observe outliers that correspond to sources that routinely spend significant periods of time in the soft state, we must also consider the opposite, namely significant outflows that exist in the soft state but are not observed in the hard state. Originally predicted by the early works on accretion disc theory (Shakura and Sunyaev, 1972), the presence of winds from the outer accretion disc have been observed in many galactic BH systems (Lee et al., 2002; Miller et al., 2004, 2006d,c), indicating that these systems can drive outflows in forms other then jets (Diaz Trigo et al., 2011).

Recent work has actually indicated that these winds appear only in the soft accretion state where the jet is not present (Neilsen and Lee, 2009; Ponti et al., 2012). Further, Ponti et al. (2012) estimate the wind outflow rate, $\dot{M}_{\rm wind}$, in the majority of the sources in which a wind has been detected, to be at least twice the $\dot{M}_{\rm BH}$. Given the ability of this wind to remove a significant portion of material from the system and its proven existence only in the outer accretion disc region, it is certainly possible that it could remove a large portion of accreted material from the system before it has the chance to contribute to the $L_{\rm acc}$ and therefore $\dot{M}_{\rm BH}$ (as the material lost via this wind would not have travelled through enough of the accretion disc to reach a temperature at which it would emit in the X-ray regime and therefore contribute to $L_{\rm acc}$).

Third, we certainly can not ignore the fact that the reverse causation may hold; that some BHXRBs may have lower mass transfer rates from their companions than others at a similar $P_{\rm orb}$, and as a result these systems may consequently tend to have more "failed" outbursts.

Lastly, we must also consider the possibility that a systematic difference between the inferred $\dot{M}_{\rm BH}$ of systems that are largely in the hard states as opposed to soft states, might imply a problem with our bolometric corrections.

Overall, to make any claims as to the mechanisms driving this observed deviation from the theoretically expected 1-to-1 relation in the $\dot{M} - P_{\rm orb}$ plane, further investigation is needed.

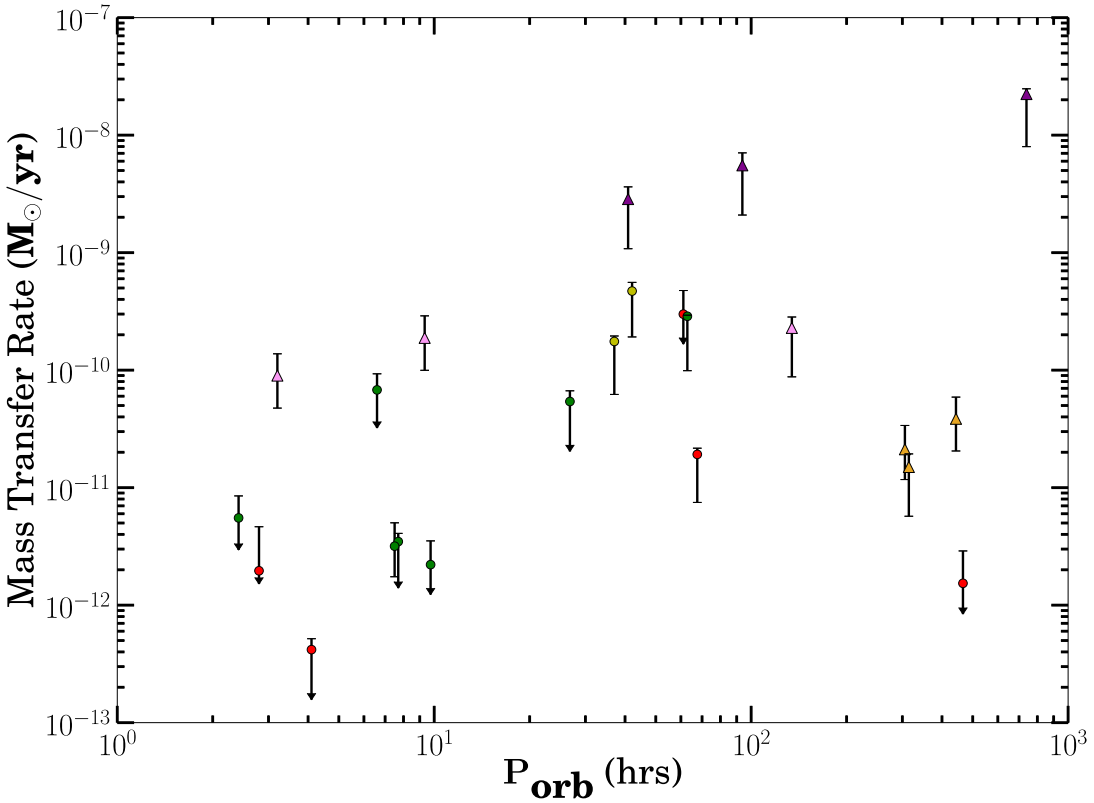

Figure 4.14: Long term mass-transfer rates vs. orbital period for Galactic BH/BHC systems. Filled circles represent transient systems and filled triangles represent persistent systems. Colour denotes behaviour: exclusively "failed" (red), exclusively "successful" (green), combination "successful"/"failed" (yellow), exhibiting mainly HCS behaviour ($\gtrsim$ 85% of the X-ray bright periods over the last 18 years; orange), significant periods of SPL/anomalous high luminosity behaviour (purple) and exhibiting occasional soft state transitions but spending significant periods of time undergoing "failed" state transitions (i.e., attempted hard-soft transitions in which the source only reaches the IMS before transitioning back to the hard state; pink). Note that if a transient source has only undergone one outburst, the $\dot{M}$ is denoted as an upper limit. Errors are quoted to the 1σ confidence level.

Chapter 5

Conclusion & Future Work

5.1 Summary

Stellar mass BHs existing in binary systems provide us with unique insight into how binary systems evolve and how mass is transferred via accretion. Although in recent years a canonical picture of the outburst behaviour in BHXRBs has emerged (Fender et al., 2004, 2009; Fender and Gallo, 2014), these systems have been shown to exhibit a wide range of unorthodox behaviour as well. Using today's more sensitive all-sky and scanning X-ray instruments, which have made an in-depth exploration of the transient X-ray Universe possible, we have established a comprehensive database of BH (and BHC) XRB activity over the last 18 years, as revealed by the instruments on board Swift, MAXI, RXTE, and INTEGRAL. This database has allowed us to quantitatively classify the range of different behaviours exhibited by these accreting black holes.

Our database, which makes use of six different instruments, has been assembled from a custom pipeline composed of a comprehensive algorithm built to discover, track, and quantitatively classify outbursts. To date, this algorithm, making use of the empirical parameter of X-ray hardness, has detected and classified 90 outbursts occurring in 43 transient BHXRBs and has tracked the long-term behaviour of 9 persistent BHXRBs over the last 18 years. In addition, the products produced by means of this algorithm have allowed for further analysis of behaviour occurring

during outburst, including temporal evolution via HIDs, outburst recurrence rates, duty cycles, luminosity profiles for individual sources and the population as a whole, state transitions, and mass-transfer rates.

In addition, this analysis has helped us to identify the elusive SPL and high luminosity states occurring over a range of X-ray hardness associated with the SDS and HCS in both transient and persistent sources. In the case of the transient sources, we observe the signature of the SPL state in two separate observational markers. The first, in the form of a "dragon horn" in numerous HIDs (e.g., GX 339−4, H 1743−322, 4U 1630−472). This "dragon horn", in most cases, appears to either curl backwards (i.e., a significant increase in hardness, followed by a softening of the source) or stand close to straight up (i.e., a near constant hardness during the time period).

The second, within the luminosity data. While typically, according to the canonical theory (Fender et al., 2004, 2009; Fender and Gallo, 2014), you would expect the peak luminosity to occur in the soft state due to the larger $\dot{M}$ resulting in the movement of the initially truncated disc inward toward the ISCO, a fair number of sources exhibit the opposite behaviour in which the peak is either occurring in the hard state or during transition (IMS), which is suggestive of SPL state behaviour.

In the case of the persistently accreting sources, namely LMC X−1, LMC X−3, and GRS 1915+105, the signature of these high luminosity states manifests themselves in a combination of X-ray hardness that seems to indicate a long term presence in the hard state and peak luminosities at high fractions of Eddington.

Perhaps most significantly, we have found that not only are our current suite of more sensitive X-ray instruments in space detecting a greater number of sources, an estimated $\sim 6 - 12$ transient outbursts per year, but $\sim 50\%$ of the detected outbursts do not complete the canonical pattern, failing to transition from the HCS to the SDS. Interestingly enough, we have also been able to observe this "failed" behaviour in a fair number of persistently accreting systems as well in the form of long continuous periods spent in the HCS or periodic "failed" state transitions (attempted hard-soft state transitions in which the source only reached as far as the IMS before transitioning back to the hard state).

This "failed" behaviour is neither a rare nor recent phenomena. In fact, through

an extensive literature search (as presented in Table A.3), we find a near constant appearance of these "failed" outbursts over the last ~ 50 years. This finding, paired with the surprising result that the number of "failed" outbursts has not increased even with the advent of more sensitive hard X-ray instruments (as you might expect), could indicate that this observed "failed" behaviour is not likely a product of the increase in sensitivity of X-ray instruments over the years. Rather it is a result of the disk instability being completed before the (unknown) critical instability that dictates a successful state transition occours, resulting in premature decreases in the mass-transfer rates and an untimely trip back into quiescence.

The observed high fraction of "failed" outbursts (and persistently hard behaviour) challenges the standard paradigm (Fender et al., 2004, 2009; Fender and Gallo, 2014) for accretion behaviour in both transient and persistent BHXRBs. This brings into question the validity of using the canonical model to describe the general behaviour of BHXRBs. We note that the canonical model has been largely based after numerous "successful" outbursts of GX339−4, even though its "successful" to "failed" outburst ratio over the last 18 years is nearly 1-to-1.

This prevalent anomalous behaviour has led us to consider the ramifications the larger number of these so-called "failed" outbursts, and the BHXRB outbursts in general, have on the mass-accretion history of the Galactic BHXRB population. Through the investigation of two empirically measurable parameters, luminosity and mass-transfer rate, we have been able to demonstrate by means of empirical XLFs, investigation of peak outburst luminosities, and calculation of 18 year averaged $\dot{M}$'s, the long lasting effects that the under luminous (usually sub-Eddington) nature of this "failed" behaviour has on both individual sources and the entire population.

Firstly, within both the long-term luminosity profiles for each individual transient source we see the replacement of the expected double-peaked, two-state luminosity profile (indicative of the canonical cyclic patterns of temporal evolution in BHXRBs) with a low-luminosity ($\sim 10^{35} - 10^{36}$ergs^{-1}), single peak contribution.

Secondly, we observe that the profile for the entire population also exhibits a double peaked profile, a complete deviation from the power-law type distribution found for the entire XRB population of the Galaxy in previous studies (Grimm

et al., 2002). Within this profile there is a significant hard state contribution at both low luminosities, which we prove to be mainly a consequence of the anomalous low luminosity feature exhibited on the individual source level (i.e., contributions from the transient "failed" outbursts), and high luminosities, which we postulate is indicative of either the rising hard state (i.e., just before transition) or of the SPL/anomalous high L_X states, whose horn like structure is present in a significant portion of our samples HIDs. In addition, we find the population XLF displays the hysteretic behaviour (i.e., lack of 1-to-1 correlation between luminosity and state) common in BHXRB systems.

Lastly, we have observed lower then theoretically expected long-term mass accretion rates both numerically in the two orders of magnitude differences between the observed $\dot{M}$'s of some individual sources and the theoretically expected value for the system at a particular $P_{\rm orb}$, and graphically in the $\dot{M} - P_{\rm orb}$ plane, where we can distinguish numerous outliers from the theoretically expected 1-to-1 relation.

This deviation from the theory could be indicative of (a) the dominance of radiatively inefficient accretion flows in the lower-luminosity hard state, as recent work seems to suggest (Knevitt et al., 2014), (b) further indirect observational evidence signifying the importance of outflows, exclusively existing in either the hard or soft states, which have the ability to remove significant amounts of mass from these systems (Neilsen and Lee, 2009; Ponti et al., 2012), or (c) perhaps a varying mass transfer rate, $M_{\rm acc}$, from the companion star across Galactic BH systems.

Lastly we note that these results to point to the possibility of certain system geometries (i.e., short orbital periods, Knevitt et al. 2014, or lower then standard $M_{\rm acc}$) having a pre-disposition toward exhibiting "failed" outbursts.

Overall, this thesis has presented the detailed findings of our database, making use of the observationally measurable parameters of X-ray hardness, luminosity, disc fraction, and mass-transfer rate to probe both canonical and anomalous outburst behaviour exhibited by BHXRBs, its impact on the physical observables of individual systems alone, and thus the universal properties of the Galactic population as a whole. In turn, this demonstrates that enumerating the frequency at which outbursts occur and quantitatively classifying the wide range of behaviour exhibited

during outburst is critical to furthering our understanding of the physical mechanisms driving mass-accretion in BHXRBs and a key step toward filling in the many gaps in our knowledge of how BHXRBs form, accrete and evolve.

5.2 Future Work

First and foremost, our goal is to make this database available to the public via an online interface, including an interactive mode that can create custom data products.

Second, the next step will be to advance the structure of our database, through the use of more sensitive pointed observations. Not only will these pointed observations give us access to more detailed spectral information, thereby giving us an avenue to confirm our outburst classifications, state definitions and luminosity profiles, but they will also allow us to add the additional dimension of timing analysis to our spectral survey. Timing, involving the tracking of variability existing within the accretion disc, has been linked to major behavioural changes occurring during state transitions, and therefore provides us with the opportunity to investigate the physical mechanisms and/or parameters that cause and drive these transitions in BHXRBs in detail.

Third, spectral and timing information will also afford us the opportunity to further investigate specific misunderstood outburst behaviour on a source by source basis, most notably the elusive SPL state and its "dragon horn" shaped profile currently found in numerous source HIDs.

Lastly, given the lack of data and information on a large number of BHCs in our sample (especially in BH class C) we hope to perform quiescent (optical/IR) studies on these systems to put constraints on the orbital parameters and ultimately be able to strengthen their BHC status.

Appendices

Appendix A

Tables

Table A.1: Galactic BH/BHC Primary Source Information

Source Name[a]	Optical Counterpart/[a] Alternate Name(s)	Class[b]	Type[c]	RA (J2000)[d]	DEC (J2000)[d]	Discovery[e] Year	Telescope	Outbursts[f] Undergone	References[g]
XTE J0421+560	CI Cam	C	BHC,T,R	04 19 42.141 (0.0566″)	+55 59 57.70 (0.0678″)	1998	Rx	1	5,185–189,276–278,367
GRO J0422+32	V518 Per Nova Per 1992	A	BH,T,R	04 21 42.79 (0.2″)	+32 54 27.1 (0.2″)	1992	CG	3	1,36–38,279
4U 0538−641	LMC X−3	A	BH,P	05 38 56.299 (0.15″)	−64 05 03.00 (0.15″)	1971	U	-	1,11,12
4U 0540−697	LMC X−1	A	BH,P	05 39 38.839 (0.0015″)	−69 44 35.66 (0.0015″)	1971	U	-	1,12,13
IGR J06074+2205	2MASSJ06072661+2205477	C	BHC,T	06 07 26.61 (0.035″)	+22 05 47.8 (0.030″)	2003	I	1	5,13,80–83
1A 0620−00	V616 Mon Nova Mon 1975 Mon X−1	A	BH,T,R,J	06 22 44.503 (0.18″)	−00 20 44.72 (0.10″)	1975	Ar	2	1,5,6,280–284,365
GRS 1009−45	MM Vel Nova Vel 1993	A	BH,T	10 13 36.377 (0.16″)	−45 04 31.95 (0.15″)	1993	G,CG	1	1,13,26,274,386
XTE J1118+480	KV UMa	A	BH,T,R,J	11 18 10.80 (0.11″)	+48 02 12.6 (0.04″)	2000	Rx	2	1,13,190–195,285,286
GS 1124−684	GU Mus Nova Muscae 1991	A	BH,T,R	11 26 26.7 (0.60″)	−68 40 32.6 (0.17″)	1991	G,GS	1	1,45,46,287,385
IGR J11321−5311	-	C	BHC,T	11 32.1 (2.0′)	−53 11 (2.0′)	2005	I	1	5,84,85
MAXI J1305−704	-	B	BHC,T	13 06 56.440 (5.0 ″)	−70 27 04.91 (5.0″)	2012	Mx	1	123–127
SWIFT J1357.2−0933	SWIFT J13572−093313	B	BHC,T,R,J?	13 57 16.818 (0.255″)	−09 19 12.00 (0.164″)	2011	Sw	1	164,175–179
GS 1354−64	BW Cir	A	BH,T,R,J?	13 58 09.74 (0.5″)	−64 44 05.2 (0.5″)	1987	GS	4	1,45,47,48,288,384
1A 1524−617	KY TrA TrA X−1	B	BHC,T	15 28 17.2 (3.0″)	−61 52 58 (3.0″)	1974	Ar	2	1,7–9,275,382
Swift J1539.2−6227	-	B	BHC,T	15 39 11.963 (0.5 ″)	−62 28 02.30 (0.5″)	2008	Sw	1	162–164
MAXI J1543−564	-	B	BHC,T,R,J?	15 43 17.336 (0.6″)	−56 24 48.35 (0.6″)	2011	Mx	1	128–132,289

Continued on Next Page...

Table A.1 – Continued

Source Name[a]	Optical Counterpart/[a] Alternate Name(s)	Class[b]	Type[c]	RA (J2000)[d]	DEC (J2000)[d]	Discovery[e] Year	Telescope	Outbursts[f] Undergone	References[g]
4U 1543−475	IL Lupi	A	BH,T,R	15 47 08.6 (30.0″)	−47 40 10 (30.0″)	1971	U	4	1,7,14, 268–271,290
XTE J1550−564	V381 Nor	A	BH,T,R,J	15 50 58.78 (2.0″)	−56 28 35.0 (2.0″)	1998	Rx,CG	5	1,5,196–202,291–294,368
4U 1630−472	Nor X−1	B	BHC,T,R,J,W	16 34 01.61 (0.30″)	−47 23 34.8 (0.30″)	1970	U,V	22	1,5,15–21,295,323,388
XTE J1637−498	-	C	BHC,T	16 37 02.67 (1.8″)	−49 51 40.6 (1.8″)	2008	Rx	1	203,204
XTE J1650−500	-	A	BH,T,R,J?,W	16 50 00.98 (0.6″)	−49 57 43.6 (0.6″)	2001	Rx	1	1,5,205–208,388,391
XTE J1652−453	-	B	BHC,T,R	16 52 20.33 (2.5″)	−45 20 39.6 (2.5″)	2009	Rx	1	209–212,296
GRO J1655−40	V1033 Sco Nova Sco 1994	A	BH,T,R,J,W	16 54 00.137 (0.23″)	−39 50 44.90 (0.20″)	1994	CG	3	1,5,39–41,297–300,369 388–390,395
MAXI J1659−152	CXOU J165902.6−151518	B	BHC,T,R	16 59 01.71 (0.7″)	−15 15 28.5 (0.7″)	2010	Sw	1	133–137,301
GX 339−4	V821 Ara 3A 1659−487	A	BH,T,R,J,W	17 02 49.36 (0.05″)	−48 47 22.8 (0.05″)	1972	O7	21	1,13,53–61,302–305 388,391
H 1705−250	V2107 Oph Nova Oph 1977	A	BH,T	17 08 14.6 (3.0″)	−25 05 29 (2.0″)	1977	Ar,H	1	1,7,62–65
IGR J17091−3624	SAX J1709.1−3624	B	BHC,T,R,J	17 09 08 (24.0″)	−36 24.4 (24.0″)	2003	I	6	5,86–93,306,307
IGR J17098−3628	2MASSJ17094612−3627573	B	BHC,T,R	17 09 46.124 (0.03″)	−36 27 57.31 (0.03″)	2005	I	1	5,13,94–97,308
SAX J1711.6−3808	-	C	BHC,T	17 11 37.1 (3.2″)	−38 07 06 (3.2″)	2001	Be	1	1,5,142–144
Swift J1713.4−4219	-	C	BHC,T	17 13 26.60 (3.0′)	−42 19 37.2 (3.0′)	2009	Sw	1	164,387
XMMSL1J171900.4−353217	XTE J1719−356	C	BHC,T	17 19 00.4 (8.0″)	−35 32 17 (8.0″)	2010	X	15	183,184
XTE J1719−291	Swift J171916.9−290410	C	BHC,T	17 19 16.970 (3.8″)	−29 04 10.35 (3.8″)	2008	Rx	1	213–215
GRS 1716−249	V2293 Oph GRO J1719−24 Nova Oph 1993	B	BHC,T,R,J?	17 19 36.93 (0.5″)	−25 01 03.4 (0.5″)	1993	G,CG	2	1,7,27,28,310,311

Continued on Next Page...

Table A.1 – Continued

Source Name[a]	Optical Counterpart/[a] Alternate Name(s)	Class[b]	Type[c]	RA (J2000)[d]	DEC (J2000)[d]	Discovery[e] Year	Discovery[e] Telescope	Outbursts[f] Undergone	References[g]
XTE J1720−318	V1228 Sco Nova Sco 2003	B	BHC,T,R,J?	17 19 58.994 (0.25″)	−31 45 01.25 (0.25″)	2003	Rx	1	5,216–218,309
XTE J1727−476	IGR J17269−4737	C	BHC,T	17 26 49.28 (0.3″)	−47 38 24.9 (0.3″)	2005	Rx,I	1	5,219,220,370
IGR J17285−2922	XTE J1728−295	C	BHC,T	17 28 38.97 (3.5″)	−29 21 44.9 (3.5″)	2004	I	2	5,99,101–102
GRS 1730−312	KS 1730−312 AX J1733.9−3112	C	BHC,T	17 33 52.3 (2′)	−31 12 25 (2′)	1994	G,M	1	1,5,29,30
IGR J17354−3255	SWIFT J1735.6−3255 2MASS J17352760−3255544	C	BHC,T	17 35 25 (1.4′)	−32 56.3 (1.4′)	2006	I	17	93,103–105
GRO J1735−27	GS 1734−275 KS 1732−273	B	BHC,T	17 36 02.0 (7.0″)	−27 25 41 (7.0″)	1988	GS	1	5,42–44,371
IGR J17379−3747	XTE J1737−376	C	BHC,T	17 37 58.81 (5.3′)	−37 46 19.6 (5.3′)	2004	Rx	2	106–109
GRS 1737−31	AX J1740.1−3102	C	BHC,T	17 40 09 (30″)	−31 02.4 (30″)	1997	G	1	1,5,31,32,372
GRS 1739−278	XTE J1739−278 V2606 Oph	B	BHC,T,R	17 42 40.03 (0.4″)	−27 44 52.7 (0.4″)	1996	G	2	1,5,33,272,313
1E 1740.7−2942	Great Annihilator Swift J1743.9−2944	B	BHC,P,R,J	17 43 54.83 (0.1″)	−29 44 42.6 (0.1″)	1984	E	-	1–4,314–317
Swift J174510.8−262411	Swift J1745.1−2624	B	BHC,T,R,J	17 45 10.849 (0.01″)	−26 24 12.60 (0.01″)	2012	Sw	1	164–166,318–320
1A 1742−289	-	B	BHC,T,R	17 45 37.0 (3.0″)	−29 01 07 (3.0″)	1975	Ar	1	1,7,10,312,373
H 1743−322	IGR J17464−3213 XTE J17464−3213	B	BHC,T,R,J,W	17 46 15.608 (0.17″)	−32 14 00.60 (0.5″)	1977	Ar,H	15	1,68–79,321,366 388,392
XTE J1748−288	AX J1748.0−2829	B	BHC,T	17 48 05.06 (0.6″)	−28 28 25.8 (0.6″)	1998	Rx,CG	1	5,221–224
IGR J17497−2821	SWIFT J1749.6−2820	C	BHC,T	17 49 38.037 (0.6″)	−28 21 17.37 (0.6″)	2006	I	1	5,110–114
SLX 1746−331	1RXS J174948.4−331215	B	BHC,T	17 49 48.50 (18.4″)	−33 12 18.3 (18.4″)	1990	S2	7	1,23,155–160,374

Continued on Next Page...

Table A.1 – Continued

Source Name[a]	Optical Counterpart/[a] Alternate Name(s)	Class[b]	Type[c]	RA (J2000)[d]	DEC (J2000)[d]	Discovery[e] Year	Telescope	Outbursts[f] Undergone	References[g]
XTE J1752−223	SWIFT J1752.1−2220	B	BHC,T,R,J	17 52 15.0950 (0.3″)	−22 20 32.782 (0.3″)	2009	Rx	1	225–230,322
Swift J1753.5−0127	SwiftJ175328.5−012704	B	BHC,P,R,J	17 53 28.29 (0.05″)	−01 27 06.2 (0.05″)	2005	Sw	1	5,164,167–172,324
XTE J1755−324	-	C	BHC,T	17 55 28.6 (1.0′)	−32 28 39 (1.0′)	1997	Rx	1	1,5,7,231–233
IGR J17586−2129	CXOU J175834.5−212321 SWIFT J175834.6−212331	C	BHC,T	17 58 34.559 (0.03″)	−21 23 21.53 (0.03″)	2006	I	2	13,115–118
H 1755−338	V4134 Sgr	B	BHC,P	17 58 40.0 (20.0″)	−33 48 27 (20.0″)	1971		-	1,7,66,67,267,373
GRS 1758−258	SWIFT J1801.2−2544	B	BHC,P,R,J,W	18 01 12.40 (0.15″)	−25 44 36.1 (0.20″)	1990	G	-	1,3,5,34,325,326,388
XTE J1812−182	XMMUJ181227.8−181234	C	BHC,T	18 12 27.8 (2.0″)	−18 12 34 (2.0″)	2003	X	2	5,234,235
IGR J18175−1530	XTE J1817−155	C	BHC,T	18 17 34.3 (2.5′)	−15 30 41 (2.5′)	2007	I	1	119–121
XTE J1817−330	SWIFT J1817.6−3300	B	BHC,T,R,W	18 17 43.54 (30.0″)	−33 01 07.8 (30.0″)	2006	Rx	1	5,236–241,327,388
XTE J1818−245	-	B	BHC,T,R	18 18 24.8 (7.0″)	−24 32 15 (7.0″)	2005	Rx	1	5,242–245,328
SAX J1819.3−2525	V4641 Sgr XTE J1819−254	A	BH,T,R,J	18 19 21.63 (0.7″)	−25 24 25.8 (0.7″)	1999	Be,Rx	20	1,13,145–154,329,375
MAXI J1836−194	-	B	BHC,T,R,J	18 35 43.43 (1.8″)	−19 19 12.1 (1.8″)	2011	Mx	1	138–141,330,331
Swift J1842.5−1124	-	C	BHC,T	18 42 17.45 (0.6″)	−11 25 03.9 (0.6″)	2008	Sw	2	164,173,174
EXO 1846−031	-	C	BHC,T	18 49 17.1 (11.0″)	−03 03 44 (11.0″)	1985	EX	1	1,7, 25
IGR J18539+0727	-	C	BHC,T	18 53.9 (3.0′)	+07 27 (3.0′)	2003	I	1	5,87,122
XTE J1856+053	-	C	BHC,T	18 56 39 (1.8′)	+05 19.8 (1.8′)	1996	Rx	4	5,246–248
XTE J1859+226	V406 Vul	A	BH,T,R,J	18 58 41.58 (0.5″)	+22 39 29.4 (0.5″)	1999	Rx	1	1,5,249–251,273,332,376
XTE J1901+014	SWIFT J1901.6+0127 1RXSJ190141.0+012618	C	BHC,T	19 01 41.00 (12.0″)	+01 26 18.5 (12.0″)	2002	Rx	4	83,253–257

Continued on Next Page...

Table A.1 – Continued

Source Name[a]	Optical Counterpart/[a] Alternate Name(s)	Class[b]	Type[c]	RA (J2000)[d]	DEC (J2000)[d]	Discovery[e] Year	Telescope	Outbursts[f] Undergone	References[g]
XTE J1908+094	-	B	BHC,T,R,J	19 08 53.077 (0.1″)	+09 23 04.90 (0.1″)	2002	Rx	2	1,5,258–262,333
SWIFT J1910.2−0546	MAXI J1910−057	C	BHC,T,R	19 10 22.8 (3.5″)	−05 47 58 (3.5″)	2012	Sw,Mx	1	164,180–182,334,377
SS 433	V1343 Aql 3A 1909+048	C	BHC,P,R,J	19 11 49.57 (0.15″)	+04 58 57.9 (0.10″)	1978	U	-	13,83,161,338-343,381
GRS 1915+105	V1487 Aql	A	BH,P,R,J,W	19 15 11.55 (0.001″)	+10 56 44.8 (0.001″)	1992	G	1	1,5,35,344-357,378 388,393,394
4U 1956+350	V1357 Cyg Cyg X−1	A	BH,P,R,J	19 58 21.675 (0.003″)	+35 12 05.778 (0.003″)	1971	U	-	1,22,358-364
4U 1957+115	V1408 Aql	C	BHC,P,W	19 59 24.21 (1.0″)	+11 42 32.4 (1.0″)	1973	U	-	1,23,24,383,388
GS 2000+251	QZ Vul Nova Vul 1988	A	BH,T,R,J?	20 02 49.58 (0.60″)	+25 14 11.3 (0.70″)	1988	GS	1	1,5,49,335,379
XTE J2012+381	-	C	BHC,T,R	20 12 37.67 (0.40″)	+38 11 01.2 (0.40″)	1998	Rx	1	1,5,263–266,336
GS 2023+338	V404 Cyg	A	BH,T,R	20 24 03.83 (8.33×10^{-9} ″)	+33 52 02.2 (0.00005″)	1989	GS	3	1,13,50–52,337,380

[a] The first column states the name exclusively used in this work. The second column states name(s) recognized by the SIMBAD Database or the Astrophysics Data System (ADS).

[b] System class identified by A, B or C as defined in Chapter 2.

[c] Confirmed Black Hole (BH) or Black Hole Candidate (BHC), system type: T - transient or P - persistent, radio detection (R), confirmed jet (J), possible jet (J?) or accretion disc wind (W).

[d] Right Ascension (RA) and Declination (DEC) in J2000 coordinates with errors in parentheses stated in arc seconds (″) or arc minutes (′). If the original reference is quoted as (i) an error radius (r_X), then errors in RA and DEC are quoted as this radius, or (ii) an error ellipse, an equal side error box, calculated from the projection of the semi-major axis onto the xy plane, is quoted.

[e] Telescope: Ar - Ariel V, Be - BeppoSAX, CG - CGRO, E - Einstein Observatory, EX - EXOSAT, G - GRANAT, GS - GINGA, H - HEAO 1, I - INTEGRAL, Mx - MAXI, M - MIR Space Station, O7 - OSO 7, Rx - RXTE, Ro - ROSAT, S2 - Spacelab 2 Telescope, Sw - Swift, U - UHURU, V - VELA 5B, X - XMM-Newton.

[f] Total number of outbursts detected in each source, including those referenced in the literature and the results of our algorithm.

[g] [1] McClintock and Remillard (2006) and references therein, [2] Marti et al. (2000a), [3] Sunyaev et al. (1991b), [4] Hertz and Grindlay (1984), [5] Liu and van den Heuvel (2007) and references therein ,[6] Elvis et al. (1975), [7] Ebisawa et al. (2003), [8] Kaluzienski et al. (1975), [9] Pounds (1974), [10] Eyles et al. (1975), [11] Bonanos et al. (2009), [12] Leong et al. (1971), [13] Cutri et al. (2003), [14] Matilsky et al. (1972), [15] Jones et al. (1976), [16] Tomsick et al. (2005) and references therein, [17] Priedhorsky (1986), [18] Tomsick (2005), [19] Kalemci et al. (2008), [20] Tomida et al. (2009), [21] Nakahira et al. (2011),[22] van Leeuwen (2007), [23] Fuhrmeister and Schmitt (2003), [24] Giacconi et al. (1974), [25] Parmar et al. (1993), [26] Filippenko et al. (1999), [27] Ballet et al. (1993), [28] Harmon et al. (1993b), [29] Borozdin et al. (1995), [30] Vargas et al. (1996), [31] Trudolyubov et al. (1999), [32] Sunyaev et al. (1997), [33] Paul et al. (1996), [34] Mandrou (1990), [35] Castro-Tirado et al. (1992), [36] McCrosky (1992), [37] Paciesas et al. (1992), [38] Shrader et al. (1997), [39] Zhang et al. (1994), [40] Brocksopp et al. (2006), [41] Sobczak et al. (1999),

[42] Yamauchi and Koyama (1990), [43] Makino (1988), [44] Yamauchi and Nakamura (2004), [45] Downes et al. (2001), [46] Kitamoto et al. (1992) and references therein, [47] Makino (1987), [48] Casares et al. (2004), [49] Tsunemi et al. (1989), [50] Richer (1987), [51] Kitamoto et al. (1989), [52] Zycki et al. (1999), [53] Markert et al. (1973), [54] Motch et al. (1985), [55] Zdziarski et al. (2004) and references therein, [56] Rubin et al. (1998), [57] Motta et al. (2009), [58] Buxton et al. (2012) and references therein, [59] Belloni (2009) and references therein, [60] Corbel et al. (2013) and references therein, [61] Buxton et al. (2013), [62] Griffiths et al. (1977), [63] Griffiths et al. (1978), [64] Kaluzienski and Holt (1977), [65] Watson et al. (1978), [66] White et al. (1988), [67] Pan et al. (1995), [68] Steeghs et al. (2003), [69] Doxsey et al. (1977), [70] Kaluzienski et al. (1977), [71] Reynolds et al. (1999), [72] Emelyanov et al. (2000), [73] Zhou et al. (2013) and references therein, [74] Corbel et al. (2005) and references therein, [75] Capitanio et al. (2010) and references therein, [76] Nakahira et al. (2013), [77] Shidatsu et al. (2012), [78] Negoro et al. (2012a), [79] Debnath et al. (2013a), [80] Chenevez et al. (2004), [81] Halpern and Tyagi (2005), [82] Reig et al. (2010), [83] Liu et al. (2006) and references therein, [84] Krivonos et al. (2005), [85] Sguera et al. (2007), [86] Kuulkers et al. (2003), [87] Lutovinov and Revnivtsev (2003), [88] Capitanio et al. (2006b), [89] Revnivtsev et al. (2003), [90] in't Zand et al. (2003), [91] Capitanio et al. (2012) and references therein, [92] Altamirano et al. (2011b), [93] Bird et al. (2010), [94] Grebenev et al. (2005b), [95] Grebenev et al. (2005a), [96] Grebenev et al. (2007), [97] Capitanio et al. (2009b), [99] Yang et al. (2010b), [100] Barlow et al. (2005), [101] Walter et al. (2004), [102] Sidoli et al. (2011), [103] Kuulkers et al. (2006b), [104] Kuulkers et al. (2007), [105] Sguera et al. (2011), [106] Bird et al. (2007), [107] Markwardt et al. (2008b), [108] Shaw et al. (2008), [109] Krimm et al. (2008d), [110] Soldi et al. (2006), [111] Rodriguez et al. (2007), [112] Walter et al. (2007), [113] Paizis et al. (2007), [114] Paizis et al. (2009), [115] Bird et al. (2006), [116] Tomsick et al. (2009), [117] Krimm et al. (2009a), [118] Sanchez-Fernandez et al. (2009), [119] Paizis et al. (1248), [120] Markwardt et al. (2007), [121] Cheung (2007), [122] Lutovinov et al. (2003b), [123] Greiner et al. (2012), [124] Sato et al. (2012), [125] Suwa et al. (2012), [126] Morihana et al. (2013), [127] Shidatsu et al. (2013), [128] Chakrabarty et al. (2011), [129] Negoro et al. (2011a), [130] Munoz-Darias et al. (2011), [131] Stiele et al. (2012), [132] Negoro et al. (2012b), [133] Kennea et al. (2011b), [134] Negoro et al. (2010), [135] Mangano et al. (2010a), [136] Kuulkers et al. (2013), [137] Yamaoka et al. (2012), [138] Ferrigno et al. (2011), [139] Negoro et al. (2011b), [140] Remillard et al. (2002), [141] Russell et al. (2014a), [142] in 't Zand et al. (2001), [143] in't Zand et al. (2002b), [144] Wijnands and Miller (2002), [145] in 't Zand et al. (1999), [146] Markwardt et al. (1999b), [147] Wijnands and van der Klis (2000), [148] Orosz et al. (2001), [149] Maitra and Bailyn (2006) and references therein, [150] in't Zand et al. (2000), [151] Tachibana et al. (2014), [152] Yamaoka et al. (2008); Yamaoka and Nakahira (2010); Yamaoka et al. (2010a), [153] Cackett and Miller (2007), [154] Revnivtsev et al. (2002), [155] White and van Paradijs (1996), [156] Skinner et al. (1990), [157] Markwardt (2003a), [158] Markwardt and Swank (2007), [159] Kuulkers et al. (2008), [160] Ozawa et al. (2011), [161] Margon (1978), [162] Krimm et al. (2008a), [163] Krimm et al. (2011b), [164] Krimm et al. (2013b) and references therein, [165] Cummings et al. (2012), [166] Curran et al. (2014), [167] Palmer et al. (2005), [168] Soleri et al. (2012), [169] Cadolle Bel et al. (2007), [170] Shaw et al. (2013), [171] Froning et al. (2014), [172] Mostafa et al. (2013), [173] Markwardt et al. (2008a), [174] Krimm et al. (2008c), [175] Sivakoff et al. (2011), [176] Krimm et al. (2011a), [177] Armas Padilla et al. (2013a), [178] Armas Padilla et al. (2013b), [179] Shahbaz et al. (2013), [180] Krimm et al. (2012), [181] Usui et al. (2012), [182] Reis et al. (2013), [183] Read et al. (2010a), [184] Markwardt et al. (2010), [185] Hog et al. (2000a), [186] Robinson et al. (2002), [187] Belloni et al. (1999a), [188] Smith et al. (1998a), [189] Bartlett et al. (2013), [190] Remillard et al. (2000), [191] Hynes et al. (2000b), [192] McClintock et al. (2001b), [193] Remillard et al. (2005), [194] Zurita et al. (2006), [195] Brocksopp et al. (2010b), [196] Smith (1998), [197] Sobczak et al. (2000), [198] Sturner and Shrader (2005), [199] Rodriguez et al. (2004), [200] Belloni et al. (2002a), [201] Tomsick et al. (2001a), [202] Curran and Chaty (2013), [203] Starling et al. (2008), [204] Markwardt et al. (2008c), [205] Remillard (2001), [206] Corbel et al. (2004), [207] Rossi et al. (2004), [208] Tomsick et al. (2004), [209] Ozel et al. (2010), [210] Hiemstra et al. (2011), [211] Markwardt et al. (2009c), [212] Han et al. (2011), [213] Degenaar et al. (2008a), [214] Markwardt and Swank (2008), [215] Armas-Padilla et al. (2011), [216] Remillard et al. (2003), [217] Cadolle Bel et al. (2004), [218] Brocksopp et al. (2005), [219] Levine et al. (2005a), [220] Turler et al. (2005a), [221] Hjellming et al. (1998c), [222] Smith et al. (1998b), [223] Brocksopp et al. (2007), [224] Revnivtsev et al. (2000b), [225] Brocksopp et al. (2009), [226] Markwardt et al. (2009b), [227] Munoz-Darias et al. (2010), [228] Stiele et al. (2011), [299] Curran et al. (2011), [230] Chun et al. (2013), [231] Revnivtsev et al. (1998a), [232] Goldoni et al. (1999), [233] Remillard et al. (1997), [234] Cackett et al. (2006), [235] Markwardt et al. (2008d), [236] Rupin et al. (2006a), [237] Remillard et al. (2006), [238] Sriram et al. (2013a), [239] Roy et al. (2011), [240] Gierlinski et al. (2009), [241] Sala et al. (2007), [242] Still et al. (2005a), [243] **?**, [244] Cadolle Bel et al. (2009), [245] Zurita Heras et al. (2011), [246] Barret et al. (1996a), [247] Marshall et al. (1996), [248] Sala et al. (2008), [249] Wood et al. (1999), [250] Farinelli et al. (2013), [251] Casella et al. (2004), [252] Sriram et al. (2013b), [253] Stephen et al. (2005), [254] Remillard and Smith (2002), [255] Karasev et al. (2007), [256] Karasev et al. (2008), [257] Krimm et al. (2010), [258] Woods et al. (2002), [259] in't Zand et al. (2002c), [260] Gogus et al. (2004), [261] Jonker et al. (2004), [262] Krimm et al. (2013a), [263] Hynes et al. (1999), [264] Remillard et al. (1998), [265] Campana et al. (2002), [266] Vasiliev et al. (2000), [267] Remillard and McClintock (2006), [268] Kitamoto et al. (1984), [269] Harmon et al. (1992), [270] Park et al. (2004), [271] Kalemci et al. (2005), [272] Krimm et al. (2014), [273] Cui et al. (2000), [274] Lapshov et al. (1993), [275] Barret et al. (1992), [276] Hjellming et al. (1998a), [277] Clark et al. (2000), [278]Mioduszewski and Rupen (2004), [279] Shrader et al. (1994), [280] Davis et al. (1975), [281] Duldig et al. (1979), [282] Geldzahler (1983), [283] Gallo et al. (2006), [284] Owen et al. (1976), [285] Uemura et al. (2000b), [286] Fender et al. (2001), [287] Ball et al. (1995), [288] Brocksopp et al. (2001), [289] Miller-Jones et al. (2011c),[290] Hunstead and Webb (2002), [291] Hannikainen et al. (2001), [292] Corbel et al. (2002), [293] Tomsick et al. (2003), [294] Kaaret et al. (2003), [295] Hjellming et al. (1999b), [296] Calvelo et al. (2009), [297] Tavani et al. (1996), [298] Harmon et al. (1995), [299] Hjellming and Rupen (1995), [300] Tingay et al. (1995), [301] van der Horst et al. (2010), [302] Corbel et al. (2000), [303] Fender et al. (1997b), [304] Fender et al. (1999a), [305] Hannikainen et al. (1998), [306] Rupen et al. (2003e), [307] Pandey et al. (2005), [308] Rupen et al. (2005b), [309] Rupen et al. (2003a), [310] della Valle et al. (1994), [311] Hjellming et al. (1996a), [312] Davies et al. (1976), [313] Hjellming et al. (1996b), [314] Anantharamaiah et al. (1993), [315] Reich and Schlickeiser (1992), [316] Heindl et al. (1994), [317] Mirabel et al. (1992), [318] Miller-Jones and Sivakoff (2012), [319] Corbel et al. (2012), [320] Coriat et al. (2013a), [321] Rupen et al. (2003b), [322] Brocksopp et al. (2013), [323] Díaz Trigo et al. (2013),[324] Fender et al. (2005), [325] Martí et al. (2002), [326] Rodriguez et al. (1992), [327] Rupin et al. (2006b), [328] Rupen et al. (2005a), [329] Hjellming et al. (2000), [330] Reis et al. (2012), [331] Russell et al. (2014b), [332] Brocksopp et al. (2002), [333] Rupen et al. (2002), [334]King et al. (2012),[335] Hjellming et al. (1988), [336] Hjellming et al. (1998d), [337] Han and Hjellming (1992), [338] Abell and Margon (1979), [339] Blundell et al. (2001), [340] Fender et al. (2000a), [341] Chakrabarti et al. (2003), [342] Chakrabarti et al. (2005), [343] Gies et al. (2002), [344] Eikenberry et al. (1998), [345] Harmon et al. (1997), [346] Atoyan and Aharonian (1997), [347] Fender et al. (2002), [348] Fender et al. (1997a), [349] Fender and Pooley (1998), [350] Pooley and Fender (1997), [351] Rodríguez and Mirabel (1997), [352] Rodriguez and Mirabel (1998), [353] Rodriguez et al. (1995), [354] Mirabel and Rodríguez (1994), [355] Miller-Jones et al. (2005), [356] Foster et al. (1996), [357] Chaty et al. (1996), [358] Braes and Miley (1971), [359] Braes and Miley (1976), [360] Hjellming (1973), [361] Hjellming and Wade (1971), [362] Tigelaar et al. (2004), [363] Stirling et al. (2001), [364] Fender et al. (2000b), [365] Kuulkers et al. (1999), [366] Miller-Jones et al. (2012), [367]Hog et al. (2000b), [368] Jain et al. (1999), [369] Bailyn et al. (1995a), [370] Maitra et al. (2005), [371] Voges et al. (1999), [372] Ueda et al. (1997), [373] Bradt and McClintock (1983), [374] Motch et al. (1998), [375] Samus et al. (1999), [376] Garnavich et al. (1999), [377] Kennea et al. (2012c), [378] Dhawan et al. (2000), [379] Okamura and Noguchi (1988), [380] Miller-Jones et al. (2009), [381] Kaplin et al. (1980), [382] Bradt et al. (1979), [383] Margon et al. (1978), [384] Kitamoto et al. (1990b), [385] della Valle et al. (1991), [386] Bailyn and Orosz (1995), [387] Krimm et al. (2009b), [388] Ponti et al. (2012), [389] Miller et al. (2006c), [390] Miller et al. (2008), [391] Miller et al. (2004), [392] Miller et al. (2006d), [393] Lee et al. (2002), [394] Neilsen and Lee (2009), [395] Kallman et al. (2009)

Table A.2: Galactic BH/BHC Binary Source Information

Source Name	Distance[b] (kpc)	$M_{\rm BH}$ ($M_\odot$)	$f(M)$ ($M_\odot$)	i (deg)	q ($(M_2/M_{\rm BH})$)	Spectral Type	$P_{\rm orb}$ (hr)	References[c]
XTE J0421+560	[3.0–8.0]	[5.0–15.0]	-	-	-	B0–2	465.84	92–94
GRO J0422+32	2.49±0.3	3.69±0.41[a]	1.19±0.02	63.7±5.2	0.116±0.08	M2(+2/-1)V	5.1	1,4,17–20,107
4U 0538−641	48.1±2.2	6.95±0.33	2.3±0.3	69.65±0.56	0.532±0.096	B3V	40.9	8–10,57
4U 0540−697	50±2.3	10.91±1.41	0.866±0.037	36.38±1.92	0.343±0.220	O7III	93.8	2,7,9–11,55
IGR J06074+2205	[3.0–8.0]	[5.0–15.0]	-	-	-	B0.5Ve	-	86,89
1A 0620−00	1.06±0.12	6.60±0.25	3.1±0.04	51±0.9	0.060±0.004	K5V	7.8	1,3,4
GRS 1009−45	3.82±0.27	5.95±0.89[a]	3.17±0.12	62.0±5.1	0.137±0.015	G5–K7V	6.8	1,4,17,25,26
XTE J1118+480	1.72±0.1	7.30±0.73[a]	6.27±0.04	68.0–82.0	0.024±0.009	K5V	4.1	1,4,52,58
GS 1124−684	5.89±0.26	5.99±1.14[a]	3.01±0.15	54.0–65.0	0.128±0.040	K3–4V	10.4	1,4,17,35,36
IGR J11321−5311	[3.0–8.0]	[5.0–15.0]	-	-	-	-	-	76
MAXI J1305−704	[3.0–8.0]	[5.0–15.0]	-	60.0–75.0	-	-	9.74	77
Swift J1357.2−0933	1.5–6.3	[5.0–15.0]	-	-	-	M4.5V	2.8	74,106
GS 1354−64	25.0–61.0	7.47[a]	5.73±0.29	27.2–80.8	0.12±0.04	G0–5III	61.1	1,4,37,38
1A 1524−617	4.4	[5.0–15.0]	-	-	-	-	-	4,5
Swift J1539.2−6227	[3.0–8.0]	[5.0–15.0]	-	-	-	-	-	-
MAXI J1543−564	[3.0–8.0]	[5.0–15.0]	-	-	-	-	-	78
4U 1543−475	7.5±0.5	9.4±2.0	0.25±0.01	24.0–36.0	0.25–0.31	A2V	26.8	2,4,12,13,24
XTE J1550−564	4.4±0.5	10.39±2.26[a]	7.65±0.38	57.7–77.1	0.031–0.037	K3±1III	37.0	1,4,53,108
4U 1630−472	[3.0–8.0]	[5.0–15.0]	-	-	-	-	-	4
XTE J1637−498	[3.0–8.0]	[5.0–15.0]	-	-	-	-	-	100
XTE J1650−500	2.6±0.7	4.72±2.16[a]	2.73±0.56	75.2±5.9	0.0–0.5	G5–K4III	7.7	1,4,54,59
XTE J1652−453	[3.0–8.0]	[5.0–15.0]	-	-	-	-	-	-
GRO J1655−40	3.2±0.5	5.4±0.3	2.73±0.09	69.0±3.0	0.38±0.05	F6III	62.9	1,4,21–23
MAXI J1659−152	[3.0–8.0]	[5.0–15.0]	-	65.0–80.0	-	M2–5V	2.414	73,109,110

Continued on Next Page. . .

Table A.2 – Continued

Source Name	Distance[b] (kpc)	$M_{\rm BH}$ ($M_\odot$)	$f(M)$ ($M_\odot$)	i (deg)	q ($(M_2/M_{\rm BH})$)	Spectral Type	$P_{\rm orb}$ (hr)	References[c]
GX 339−4	8.0±2.0	[5.0–15.0]	5.8±0.5	-	<0.08	-	42.1	4,45,46,111,112
H 1705−250	8.6±2.1	4.99–12.48[a]	4.86±0.13	>48.0	0.0–0.053	K5±2V	12.5	4,39,44,47–49
IGR J17091−3624	[3.0–8.0]	[5.0–15.0]	-	-	-	-	-	88
IGR J17098−3628	[3.0–8.0]	[5.0–15.0]	-	-	-	-	-	87
SAX J1711.6−3808	[3.0–8.0]	[5.0–15.0]	-	-	-	-	-	4
Swift J1713.4−4219	[3.0–8.0]	[5.0–15.0]	-	-	-	-	-	80,114
XMMSL1J171900.4−353217	[3.0–8.0]	[5.0–15.0]	-	-	-	-	-	-
XTE J1719−291	[3.0–8.0]	[5.0–15.0]	-	-	-	K0V or later	-	101,102
GRS 1716−249	2.4±0.4	[5.0–15.0]	-	-	-	K (or later)	14.7	4,27,28,55
XTE J1720−318	[3.0–8.0]	[5.0–15.0]	-	-	-	-	-	4,98
XTE J1727−476	[3.0–8.0]	[5.0–15.0]	-	-	-	-	-	4,99
IGR J17285−2922	[3.0–8.0]	[5.0–15.0]	-	-	-	-	-	85
GRS 1730−312	[3.0–8.0]	[5.0–15.0]	-	-	-	-	-	4,7
IGR J17354−3255	[3.0–8.0]	[5.0–15.0]	-	-	-	-	201.6	90
GRO J1735−27	[3.0–8.0]	[5.0–15.0]	-	-	-	-	-	4
IGR J17379−3747	[3.0–8.0]	[5.0–15.0]	-	-	-	-	-	-
GRS 1737−31	[3.0–8.0]	[5.0–15.0]	-	-	-	-	-	4,7
GRS 1739−278	[3.0–8.0]	[5.0–15.0]	-	-	-	B,G or K	-	4,7,29
1E 1740.7−2942	[3.0–8.0]	[5.0–15.0]	-	-	-	-	305.52	4,6,70
Swift J174510.8−262411	[3.0–8.0]	[5.0–15.0]	-	-	-	A0 or later	≤ 21	80,82
1A 1742−289	[3.0–8.0]	[5.0–15.0]	-	-	-	-	-	4,62
H 1743−322	10.4 ± 2.9	[5.0–15.0]	-	-	-	-	-	72
XTE J1748−288	[3.0–8.0]	[5.0–15.0]	-	-	-	-	-	4
IGR J17497−2821	[3.0–8.0]	[5.0–15.0]	-	-	-	B or K	-	84

Continued on Next Page. . .

Table A.2 – Continued

Source Name	Distance[b] (kpc)	$M_{\rm BH}$ ($M_\odot$)	$f(M)$ ($M_\odot$)	i (deg)	q ($(M_2/M_{\rm BH})$)	Spectral Type	$P_{\rm orb}$ (hr)	References[c]
SLX 1746−331	[3.0–8.0]	[5.0–15.0]	-	-	-	G–K	-	83
XTE J1752−223	3.5±0.4	9.6±0.9	-	-	-	-	-	71
Swift J1753.5−0127	[3.0–8.0]	[5.0–15.0]	-	-	-	-	3.2	81
XTE J1755−324	[3.0–8.0]	[5.0–15.0]	-	-	-	-	-	4
IGR J17586−2129	[3.0–8.0]	[5.0–15.0]	-	-	-	-	-	91
H 1755−338	[3.0–8.0]	[5.0–15.0]	-	-	-	-	4.4	50,63
GRS 1758−258	[3.0–8.0]	[5.0–15.0]	-	-	-	K0III	442.8	4,30–32,70
XTE J1812−182	[3.0–8.0]	[5.0–15.0]	-	-	-	-	-	4,103
IGR J18175−1530	[3.0–8.0]	[5.0–15.0]	-	-	-	-	-	-
XTE J1817−330	[3.0–8.0]	[5.0–15.0]	-	-	-	-	-	4,105
XTE J1818−245	2.8–4.3	[5.0–15.0]	-	-	-	-	-	4,75
SAX J1819.3−2525	7.4–12.3	7.73±0.53[a]	2.74±0.12	80.0–90.0	0.67±0.04	B9III	67.6	1,51,113
MAXI J1836−194	[3.0–8.0]	[5.0–15.0]	-	4.0–15.0	-	-	<4.9	79
Swift J1842.5−1124	[3.0–8.0]	[5.0–15.0]	-	-	-	-	-	80
EXO 1846−031	[3.0–8.0]	[5.0–15.0]	-	-	-	-	-	4,7
IGR J18539+0727	[3.0–8.0]	[5.0–15.0]	-	-	-	-	-	-
XTE J1856+053	[3.0–8.0]	[5.0–15.0]	-	-	-	-	-	4,104
XTE J1859+226	8±3	10.83±4.67[a]	4.5±0.6	60±3	0.0–0.5	K5–7V	6.6	1,4,17,60,61
XTE J1901+014	[3.0–8.0]	[5.0–15.0]	-	-	-	-	-	96
XTE J1908+094	[3.0–8.0]	[5.0–15.0]	-	-	-	A–K	-	97
Swift J1910.2−0546	[3.0–8.0]	[5.0–15.0]	-	-	-	-	-	80
SS 433	5.5±0.2	[5.0–15.0]	$7.7^{+3.0}_{-2.4}$	-	-	-	314.4	65,66–69
GRS 1915+105	12.5±1.5	12.82±4.15[a]	9.5±3.0	70.0±2.0	0.058±0.033	K0–7III	739	1,4,33,34,50
4U 1956+350	1.86±0.12	14.81±0.98	0.251±0.007	27.06±0.76	1.294±0.154	O9.7Iab	134.4	2,4,14–16,56

Continued on Next Page. . .

Table A.2 – Continued

Source Name	Distance[b] (kpc)	$M_{\rm BH}$ ($M_\odot$)	$f(M)$ ($M_\odot$)	i (deg)	q ($(M_2/M_{\rm BH})$)	Spectral Type	$P_{\rm orb}$ (hr)	References[c]
4U 1957+115	[3.0–8.0]	[5.0–15.0]	-	-	-	-	9.33	4,7,55,64
GS 2000+251	2.7±0.7	8.37±1.30[a]	5.01±0.12	55.0–65.0	0.042±0.012	K3–6V	8.3	1,4,39–41
XTE J2012+381	[3.0–8.0]	[5.0–15.0]	-	-	-	-	-	95
GS 2023+338	2.39±0.14	7.15±0.35[a]	6.08±0.06	80.1±5.1	0.060±0.005	K0IV	155.3	1,4,42–44

Note. – All error quantities are quoted to the 1σ confidence level.

[a] Indicates the $M_{\rm BH}$ has been recalculated based on improved measurements of the orbital parameters of the system. For details per source see the individual source sections.

[b] The distances and masses quoted in [ ] are the assumed ranges when no acceptable estimates for these quantities are available.

[c] [1] Kreidberg et al. (2012), [2] Ozel et al. (2010), [3] Cantrell et al. (2010), [4] Liu and van den Heuvel (2007), [5] van Paradijs and Verbunt (1984), [6] Marti et al. (2010), [7] McClintock and Remillard (2006), [8] Orosz et al. (2014), [9] Cowley (1992), [10] Orosz et al. (2009), [11] Barret et al. (1996b), [12] Orosz (2003), [13] Orosz et al. (1998b), [14] Orosz et al. (2011a), [15] Reid et al. (2011), [16] Caballero-Nieves et al. (2009), [17] Hynes (2005), [18] Filippenko et al. (1995), [19] Harlaftis et al. (1999), [20] Webb et al. (2000), [21] Beer and Podsiadlowski (2002), [22] Hjellming and Rupen (1995), [23] Shahbaz et al. (1999), [24] Orosz et al., [25] Filippenko et al. (1999), [26] Shahbaz et al. (1996b), [27] della Valle et al. (1994), [28] Masetti et al. (1996), [29] Marti et al. (1997), [30] Marti et al. (1998), [31] Eikenberry et al. (2001), [32] Rothstein et al. (2002), [33] Greiner et al. (2001a), [34] Harlaftis and Greiner (2004), [35] Orosz et al. (1996), [36] Casares et al. (1997), [37] Casares et al. (2009), [38] Casares et al. (2004), [39] Barret et al. (1996b), [40] Harlaftis et al. (1996), [41] Casares et al. (1995a), [42] Miller-Jones et al. (2009), [43] Casares and Charles (1994), [44] Charles and Coe (2006), [45] Hynes et al. (2003), [46] Shaposhnikov and Titarchuk (2009), [47] Martin et al. (1995), [48] Filippenko et al. (1997), [49] Harlaftis et al. (1997),[50] Neil et al. (2007), [51] Orosz et al. (2001), [52] Gelino et al. (2006), [53] Orosz et al. (2011b), [54] Homan et al. (2006b), [55] Remillard and McClintock (2006), [56] Gies and Bolton (1982), [57] Cowley et al. (1983), [58] Gonzalez Hernandez et al. (2008), [59] Orosz et al. (2004), [60] Corral-Santana et al. (2011), [61] Jonker et al. (2004), [62] Maeda et al. (1996), [63] Mason et al. (1985), [64] Thorstensen (1987), [65] Crampton and Hutchings (1987), [66] Blundell and Bowler (2004), [67] Margon and Anderson (1989), [68] Fabrika and Bychkova (1990), [69] Gies et al. (2002), [70] Smith et al. (2002a), [71] Shaposhnikov et al. (2010), [72] Shaposhnikov and Titarchuk (2009), [73] Kuulkers et al. (2013), [74] Corral-Santana et al. (2013), [75] Cadolle Bel et al. (2009), [76] Sguera et al. (2007), [77] Shidatsu et al. (2013), [78] Stiele et al. (2012), [79] Russell et al. (2014b), [80] Krimm et al. (2013b), [81] Zurita et al. (2008), [82] Muñoz-Darias et al. (2013), [83] Motch et al. (1998), [84]Paizis et al. (2007), [85] Sidoli et al. (2011), [86] Halpern and Tyagi (2005), [87] Steeghs et al. (2005a), [88] Liu et al. (2006), [89] Reig et al. (2010), [90] Sguera et al. (2011), [91] Tomsick et al. (2009), [92] Barsukova et al. (2005), [93] Robinson et al. (2002), [94] Bartlett et al. (2013), [95] Hynes et al. (1999), [96] Karasev et al. (2007), [97] Chaty et al. (2006), [98] Brocksopp et al. (2005), [99] Maitra et al. (2005), [100] Starling et al. (2008), [101] Armas-Padilla et al. (2011), [102] Greiner et al. (2008), [103] Cackett et al. (2006), [104] Sala et al. (2008), [105] Torres et al. (2006), [106] Shahbaz et al. (2013), [107] Gelino and Harrison (2003), [108] Orosz et al. (2002), [109] Miller-Jones et al. (2011a), [110] Kong (2012), [111] Hynes et al. (2004), [112] Zdziarski et al. (2004), [113] MacDonald et al. (2011), [114] (Krimm et al., 2009b)

Table A.3: Galactic BHXRB Outburst History

Source Name	t_{beg} [a]	t_{end} [a]	Outburst ID	Literature Class [b]	Algorithm Class [b] H_X	d_f	Instrument [c] Detection	References [d]
XTEJ0421+560	50885.0	50934.0	1998	-	F	F	**ASM**,BATSE,EPIC,NFI,PCA	140–143
GROJ0422+32	-	-	1992	F	-	-	BATSE	242,271–274
	-	-	1993a	-	-	-	GIS,PSPC,SIS	270,272
	-	-	1993b	-	-	-	GIS,PSPC,SIS	270,272
4U0538−641	-	-	1971–2014	-	-	-	A-2,**ASM,BAT**,LAC,**MAXI**,ME,NFI SSS,UHURU,PCA	296–303,344,345
4U0540−697	-	-	1971–2014	-	-	-	A-2,**ASM,BAT**,LAC,**MAXI**,ME,NFI SSS,UHURU,PCA	296–303, 344,345
IGR J06074+2205	-	-	2003	-	-	-	Chandra,JEM-X	228–230
1A 0620−00	-	-	1917	-	-	-	HCO	281
	-	-	1975	S	-	-	SSI	282,395
GRS 1009−45	-	-	1993	-	-	-	BATSE,HEXE,TTM,WATCH	265-267
XTEJ1118+480	51538.0	51740.0	1999/2000	F	F	F	**ASM**,Chandra, HEXTE,NFI,PCA	144–147,260,382-384
	53364.0	53413.0	2004/2005	F	-	-	**ASM**,BAT,HEXTE,PCA	148,149
GS 1124−684	-	-	1992	S	-	-	GINGA/ASM,WATCH	244,396
IGR J11321−5311	-	-	2005	-	-	-	ISGRI	231,232
MAXIJ1305−704	56009.5	56190.0	2012	S	S	S	**BAT**,HXD,**MAXI**,XIS,XRT	84,85
SwiftJ1357.2−0933	55563.5	55687.5	2011	F	F	F	**BAT**,EPIC,**MAXI**,PCA,RGS,XRT	122,126,127
GS1354−64	-	-	1967	S	-	-	Skylark	74,75,242,257
	-	-	1972	F	-	-	MIT	74,75,242,258
	-	-	1987	S	-	-	GINGA/ASM,LAC	74,75,242
	50714.0	50870.0	1997/1998	F	F	F	**ASM**,BATSE,GINGA/ASM	28,242,259
				S			HEXTE,PCA	
1A 1524−617	-	-	1974	S	-	-	Ariel V/ASM,SSI	242,278

Continued on Next Page...

Table A.3 – Continued

Source Name	t_{beg} [a]	t_{end} [a]	Outburst ID	Literature[b] Class	Algorithm Class[b] H_X	d_f	Instrument [c] Detection	References[d]
	-	-	1990	F	-	-	SIGMA	242,279,280
SwiftJ1539.2−6227	54792.0	54966.0	2008/2009	S	S	S	**ASM,BAT**,HEXTE,PCA,XRT	121,122
MAXIJ1543−564	55681.0	55833.5	2011	S	S	S	**BAT,MAXI**,PCA,XRT	86
4U1543−475	-	-	1971	S	-	-	UHURU	1,242
	-	-	1983/1984	S	-	-	Tenma	2,242
	-	-	1992	F	-	-	BATSE	3,242
	52435.0	52488.0	2002	S	S	S	**ASM**,EPIC,HEXTE,PCA	4,242
XTEJ1550−564	51062.0	51316.0	1998/1999	S	S	S	**ASM**,BATSE,HEXTE,PCA	150–152,385–387
	51597.0	51703.0	2000	I	I	S	**ASM**,Chandra,HEXTE,PCA	153–156
	51934.0	51983.0	2001	F	F	-	**ASM**,Chandra	157
	52261.0	52312.0	2001/2002	F	F	-	**ASM**,HEXTE,PCA	158,388
	52726.0	52775.0	2003	F	F	F	**ASM**,ISGRI,JEM-X,PCA	159,160
4U1630−472	-	-	1969	-	-	-	XC	5
	-	-	1970/1971	-	-	-	SSI,UHURU,XC	5,6
	-	-	1972	-	-	-	SSI,UHURU,XC	5,6
	-	-	1974	-	-	-	SSI,UHURU,XC	5,6
	-	-	1976	-	-	-	SSI,UHURU,XC	5,6
	-	-	1977	-	-	-	A-2,LASS,SSI	7
	-	-	1978	-	-	-	LASS	7
	-	-	1979	-	-	-	GIS,HRI,LAC,PSPC,SSS	8,10
	-	-	1984	S	-	-	ME,Tenma	9
	-	-	1987	-	-	-	GINGA/ASM,LAC	7
	-	-	1988	-	-	-	GINGA/ASM,GIS,HRI,LAC	7,8
	-	-	1992	-	-	-	PSPC,SSS	10
	-	-	1994	-	-	-	GIS,HRI,LAC	8
	50134.0	50333.0	1996	-	I	F	**ASM**,PCA	7,338
	50840.0	51079.0	1998	-	F	F	**ASM**,BATSE,HEXTE,NFI,PCA,PSPC	11–13,38,337
	51221.0	51396.0	1999	-	F	F	**ASM**,HEXTE,PCA	11
	51842.0	52075.0	2000/2001	-	F	F	**ASM**,HEXTE,PCA	19

Continued on Next Page...

Table A.3 – Continued

Source Name	t_{beg}[a]	t_{end}[a]	Outburst ID	Literature[b] Class	Algorithm Class[b] H_X	d_f	Instrument[c] Detection	References[d]
	52514.0	53334.0	2002-2004	S	I	F	**ASM**,HEXTE,ISGRI,,**PCA**	14
	53700.0	53883.0	2005/2006	S	S	S	**ASM,BAT,PCA**	15
	54453.0	54652.0	2007/2008	-	S	S	**ASM,BAT,PCA**	16
	55178.0	55429.0	2009/2010	S	S	S	**ASM,BAT,MAXI,PCA**	17
	55881.5	56600.5	2011–2013	S	S	S	**BAT**,Chandra,EPIC,**MAXI**	18,20,354
XTEJ1637−498	-	-	2008	-	-	-	PCA,XRT	203,204
XTEJ1650−500	52149.0	52256.0	2001	S	S	S	**ASM**,Chandra,HEXTE,PCA	161–165
XTEJ1652−453	54990.0	55158.0	2009	S	S	S	**ASM,BAT,ASM**,EPIC,**PCA**,XRT	166,167
GROJ1655−40	-	-	1994	S	-	-	BATSE,GIS,OSSE,WATCH	21
	50184.0	50690.0	1996/1997	S	S	S	**ASM**,HEXTE,PCA	23,391,393
	53398.0	53678.0	2005	S	S	S	**BAT,ASM,PCA,ISGRI**,XRT	22,389,390,392
MAXIJ1659−152	55458.5	55592.0	2010/2011	S	S	S	**ASM,BAT**,EPIC,**ISGRI,MAXI** PCA,RGS,XRT	87,88,89
GX339−4	-	-	1973	S	-	-	MIT,VELA5B	29,35
	-	-	1981	S	-	-	HAKUCHO,ME	30
	-	-	1988	S	-	-	GINGA/ASM,LAC	31,35
	-	-	1990	S	-	-	GINGA/ASM,SIGMA	33,35
	-	-	1991	S	-	-	BATSE,GINGA/ASM,OSSE,SIGMA,WATCH	32–35
	-	-	1992	S	-	-	BATSE,SIGMA	32–34
	-	-	1993/1994	S	-	-	BATSE	33,34
	-	-	1994	F	-	-	BATSE,SIGMA	34,35
	-	-	1995a	F	-	-	BATSE	34,35
	-	-	1995b	F	-	-	BATSE	34,35
	50134.0	50160.0	1996a	F	-	-	**ASM**,BATSE,PCA	34,35
	50259.0	50333.0	1996b	F	F	F	**ASM**,BATSE,PCA	34,35
	50456.0	51295.0	1997–1999	S	S	S	**ASM**,BATSE,HEXTE,PCA	36,37
	52363.0	52750.0	2002/2003	S	S	S	**ASM**,HEXTE,PCA	50
	53079.0	53515.0	2004/2005	S	S	S	**ASM,BAT**,HEXTE,ISGRI,**PCA**	39

Continued on Next Page...

Table A.3 – Continued

Source Name	t_{beg} [a]	t_{end} [a]	Outburst ID	Literature [b] Class	Algorithm Class [b] H_X	d_f	Instrument [c] Detection	References [d]
	53751.0	53876.0	2006	F	F	F	**ASM,BAT,PCA**	40
	54053.0	54391.0	2006/2007	S	S	S	**ASM,BAT,PCA**	40,41
	54624.0	54748.0	2008	F	F	-	**ASM,BAT,PCA**	40
	54875.0	55024.0	2009	F	F	F	**ASM,BAT,PCA**	40
	55178.5	55631.0	2009–2011	S	S	S	**ASM,BAT,MAXI,PCA**	42
	56502.5	56608.0	2013	F	F	F	**BAT,MAXI**,XRT	43
H 1705−250	-	-	1977	-	-	-	A-3, Ariel V/ASM,SSI	233–236
IGRJ17091−3624	-	-	1994	-	-	-	TTM	65
	-	-	1996	-	-	-	ISGRI,WFC	66
	-	-	2001	-	-	-	ISGRI,WFC	66
	-	-	2003	S	-	-	HEXTE,ISGRI,JEM-X,PCA	67,68
	54267.0	54391.0	2007	S	-	-	**BAT**,ISGRI,JEM-X,XRT	73
	55589.0	56412.0	2011–2013	S	S	S	**ASM,BAT,ISGRI**, JEM-X,**PCA**,XRT	69,70
IGRJ17098−3628	-	-	2005–2007	S	-	-	**BAT**,EPIC,**ISGRI,PCA**,RGS,XRT	226,227
SAXJ1711.6−3808	51927.0	52056.0	2001	F	F	F	**ASM**,EPIC,NFI,PCA,RGS,WFC	93
Swift J1713.4−4219	-	-	2009	-	-	-	**ASM,BAT,PCA,ISGRI**	122,398
XMMSL1J171900.4−353217	53150.0	53291.0	2004	-	-	-	**PCA**	-
	53463.0	53580.0	2005	-	-	-	**PCA**	-
	53643.0	53779.0	2005/2006	-	-	-	**PCA**	-
	53853.0	54013.0	2006	-	-	-	**PCA**	-
	54025.0	54144.0	2006/2007	-	-	-	**BAT,PCA**	-
	54157.0	54285.0	2007a	-	F	-	**BAT,PCA**	-
	54312.0	54349.0	2007b	-	-	-	**PCA**	-
	54363.0	54642.0	2007/2008	-	F	S	**PCA**	-
	54651.0	54714.0	2008	-	-	-	**PCA,ISGRI**	-
	54728.0	54969.0	2008/2009	-	F	S	**BAT,PCA**	-
	54990.0	55037.0	2009	-	-	-	**PCA**	-
	55059.0	55463.0	2009/2010	-	F	S	**BAT**,EPIC,**ISGRI,PCA**,XRT	132–136,346

Continued on Next Page...

Table A.3 – Continued

Source Name	t_{beg}[a]	t_{end}[a]	Outburst ID	Literature[b] Class	Algorithm Class[b] H_X	d_f	Instrument[c] Detection	References[d]
	55628.0	55699.0	2011a	-	-	-	**PCA**	-
	555718.0	55789.0	2011b	-	-	-	**PCA**	-
XTEJ1719−291	-	-	2008	-	-	-	Chandra,EPIC,PCA,XRT	205–209
GRS 1716−249	-	-	1993	F	-	-	BATSE,SIGMA,TTM	242,263,264
	-	-	1995	F	-	-	BATSE,TTM	394
XTEJ1720−318	52644.0	52873.0	2003	S	S	S	**ASM**,EPIC,ISGRI,JEM-X,**PCA**	168,169
XTEJ1727−476	53639.0	53717.0	2005	S	S	S	**ASM**,ISGRI,JEM-X,XRT	170–173
IGRJ17285−2922	52849.0	52951.0	2003	-	-	-	**PCA**,ISGRI,JEM-X	71
	55426.0	55515.0	2010	F	F	-	**ASM,BAT**,EPIC,**PCA,ISGRI**	72
GRS 1730−312	-	-	1994	S	-	-	SIGMA,TTM	261,262
IGRJ17354−3255	-	-	2003–2008	-	-	-	BAT,ISGRI,JEM-X,XRT	225
	-	-	2009	-	-	-	BAT,ISGRI,JEM-X,XRT	225
GROJ1735−27	-	-	1988	S	-	-	LAC	268,269
IGRJ17379−3747	53042.0	53094.0	2004	-	-	-	ISGRI,**PCA**	76
	54701.0	54776.0	2008	-	F	S	**BAT**,ISGRI,**PCA**,XRT	76,77,78
GRS1737−31	50497.0	50597.0	1997	F	F	-	**ASM**,GIS,HEXTE,PCA,SIGMA,WFC	24,242,256,347–349
GRS1739−278	50136.0	50387.0	1996	S	S	S	**ASM**,HEXTE,ROSAT/HRI,PCA,SIGMA,TTM	25,26,350
	56702.0	56777.0	2014	-	S	S	**BAT,JEM-X,ISGRI**	27
1E1740.7−2942	-	-	1984–2014	-	-	-	ART-P,**ASM,BAT**,HEXE,HEXTE,IPC **ISGRI,JEM-X**,NuSTAR,OSSE,**PCA**,PSPC SIGMA,TTM	284–295
SwiftJ174510.8−262411	56178.0	56463.0	2012/2013	F	F	-	**BAT,JEM-X,ISGRI**,XRT	122,123
1A 1742−289	-	-	1975	-	-	-	ANS,MSSL,RMC,PCS	276,277
H1743−322	-	-	1977	-	-	-	A-4	58,59

Continued on Next Page...

Table A.3 – Continued

Source Name	t_{beg} [a]	t_{end} [a]	Outburst ID	Literature [b] Class	Algorithm Class [b] H_X	d_f	Instrument [c] Detection	References [d]
	-	-	1984	-	-	-	ME	44
	-	-	1996	-	-	-	TTM	45
	52713.0	52953.0	2003	S	S	S	**ASM**,Chandra,HEXTE,ISGRI,JEM-X,**PCA**	46–50
	53182.0	53315.0	2004	S	S	S	**ASM**.Chandra,ISGRI,JEM-X,**PCA**	51
	53575.0	53655.0	2005	S	S	S	**ASM,BAT**,Chandra,**ISGRI,JEM-X,PCA**	51
	54446.0	54513.0	2007/2008	S	S	-	**ASM,BAT**,Chandra,**ISGRI,JEM-X,PCA**,XRT	55,56,351
	54714.0	54813.0	2008	F	F	F	**ASM,BAT**,HEXTE,**ISGRI,JEM-X,PCA**,XRT	52,53
	54953.0	55053.0	2009	S	S	S	**ASM,BAT**,HEXTE,**ISGRI,JEM-X,PCA**	53,54,57
	55186.5	55286.5	2009/2010	S	I	F	**ASM,BAT,ISGRI,JEM-X,MAXI,PCA**	56
	55387.5	55488.0	2010	S	S	S	**ASM,BAT**,HEXTE,**ISGRI,JEM-X,MAXI,PCA**	56,60,61
	55536.5	55730.0	2010/2011	S	I	F	**ASM,BAT,ISGRI,JEM-X,MAXI,PCA**	56,61
	55897.5	55988.0	2011/2012	-	F	F	**BAT,ISGRI,JEM-X,MAXI**	62
	56185.0	56249.5	2012	-	F	F	**BAT,ISGRI,JEM-X,MAXI**	63
	56489.0	56563.0	2013	-	S	S	**BAT,ISGRI,JEM-X,MAXI**	64
XTEJ1748−288	50961.0	51038.0	1998	S	F	F	**ASM**,BATSE,HEXTE,PCA	137,283,352
IGRJ17497−2821	53963.0	54061.0	2006	F	F	F	**ASM,BAT**,Chandra,HEXTE,HXD,**ISGRI JEM-X,PCA**,XIS,XRT	79–81
SLX1746−331	-	-	1985	-	-	-	ROSAT/XRT	397
	-	-	1990	-	-	-	SpaceLab2	112
	52713.0	52967.0	2003	S	I	S	**ASM**,ISGRI,JEM-X,**PCA**,PSPC	113–116
	54359.0	54612.0	2007/2008	S	S	S	**ASM,BAT**,ISGRI,**JEM-X,PCA**,XRT	117–119
	55387.5	55713.5	2010/2011	S	F	S	**ASM,BAT,ISGRI,JEM-X,MAXI**	120
XTEJ1752−223	55083.5	55423.0	2009/2010	S	S	S	**ASM,BAT**,EPIC,HEXTE,**ISGRI,PCA MAXI**,RGS,XIS	174–177,353
SwiftJ1753.5−0127	53529.0	56678.0	2005-2014	-	-	-	**ASM,BAT**,EPIC,HEXTE,ISGRI,JEM-X **MAXI**,PCA,RGS,XRT	213–219
XTEJ1755−324	50637.0	50761.0	1997	S	S	S	**ASM**,HEXTE,PCA,SIGMA	138,139
IGRJ17586−2129	54997.0	55158.0	2009	-	F	S	**BAT,ISGRI,PCA**,XRT	82,83

Continued on Next Page...

Table A.3 – Continued

Source Name	t_{beg} [a]	t_{end} [a]	Outburst ID	Literature [b] Class	Algorithm Class [b] H_X	d_f	Instrument [c] Detection	References [d]
	55316.0	55368.0	2010	-	-	-	**BAT,PCA**	-
H 1755−338	-	-	1970–1993	-	-	-	CMA,EPIC,GSPC,ME,TTM	333–336
GRS1758−258	-	-	1990–2014	-	-	-	**ASM,BAT**,Chandra,GIS,**ISGRI,JEM-X** PCA,PSPC,SIGMA	285,293,327–332
XTEJ1812−182	52656.0	52710.0	2003	-	F	F	**ASM**,EPIC	178
	54695.0	54775.0	2008	-	S	S	**ASM,BAT,PCA**,XRT	179,180
IGRJ18175−1530	54309.0	54385.0	2007	-	-	-	**ASM,BAT**,ISGRI,**PCA**	222–224
XTEJ1817−330	53744.0	53999.0	2006	S	S	S	**ASM,BAT**,EPIC,HEXTE,ISGRI,JEM-X,PCA RGS,XRT	181–184
XTEJ1818−245	53575.0	53690.0	2005	S	S	S	**ASM,BAT**,HEXTE,**ISGRI**,JEM-X **PCA**,XRT	185,186
SAXJ1819.3−2525	51214.0	51605.0	1999/2000	F	-	-	ASM,HEXTE,NFI,**PCA**,WFC	94–97,104,105
	51615.0	51636.0	2000a	-	-	-	**PCA**	-
	51645.0	51697.0	2000b	-	-	-	**PCA**	-
	51743.0	52560.0	2000-2002	-	-	-	**PCA**	98,99
	52680.0	52761.0	2003	-	-	-	**PCA**	-
	52776.0	53147.0	2003/2004	F	-	-	HEXTE,**PCA**	100–102
	53189.0	53207.0	2004	-	-	-	**PCA**	103
	53218.0	53589.0	2004/2005	-	-	-	**BAT,PCA**	-
	53652.0	53864.0	2005/2006	-	F	-	**BAT,PCA**	-
	53878.0	54222.0	2006/2007	-	F	F	**BAT,PCA**	-
	54232.0	54347.0	2007	F	F	F	**BAT,PCA**,XRT	106
	54518.0	54584.0	2008a	-	F	-	**BAT,PCA**	-
	54598.0	54682.0	2008b	-	-	-	**PCA**	-
	54691.0	54942.0	2008/2009	-	F	-	**BAT,PCA**,XRT	107
	54951.0	55166.0	2009	-	F	F	**BAT,MAXI,PCA**	-
	55235.5	55279.0	2010	-	-	-	**MAXI,PCA**	-
	55293.0	55587.0	2010/2011	-	I	S	**BAT,MAXI,PCA**,XRT	108–111

Continued on Next Page...

Table A.3 – Continued

Source Name	t_{beg} [a]	t_{end} [a]	Outburst ID	Literature [b] Class	Algorithm Class [b] H_X	d_f	Instrument [c] Detection	References [d]
	55603.0	55719.0	2011a	-	-	-	**MAXI,PCA**	-
	55754.0	55769.0	2011b	-	-	-	**MAXI,PCA**	-
	55783.0	55846.0	2011c	-	-	-	**MAXI,PCA**	-
MAXIJ1836−194	55797.5	56085.5	2011/2012	F	F	F	**BAT**,HXD,**ISGRI**,JEM-X,**MAXI**,PCA XIS,XRT	90–92
SwiftJ1842.5−1124	54630.0	54857.0	2008/2009	S	S	S	**ASM,BAT,PCA**,XRT	122,124,125
	-	-	2010	-	-	-	ASM,BAT	122
EXO 1846−031	-	-	1985	S	-	-	CMA,GSPC,ME	275
IGRJ18539+0727	-	-	2003	F	-	-	HEXTE,ISGRI,PCA	220,221
XTEJ1856+053	50190.0	50216.0	1996a	S	S	S	**ASM**,PCA	187,188
	50311.0	50410.0	1996b	S	S	S	**ASM**,BATSE,PCA	187–190
	54088.0	54312.0	2006/2007	S	S	S	**ASM,BAT**,EPIC,PCA,RGS,XRT	188
	54912.0	54961.0	2009	-	I	S	**ASM,PCA**	-
XTEJ1859+226	51437.0	51661.0	1999/2000	S	S	S	**ASM**,BATSE,Chandra,NFI,PCA	191–193,355
XTEJ1901+014	-	-	1997	-	-	-	ASM,ISGRI,PCA,PSPC	210,211
	-	-	2002	-	-	-	ASM,ISGRI,PCA,PSPC	210,211
	-	-	2006	-	-	-	BAT,EPIC	211,212
	-	-	2010	-	-	-	BAT	212
XTEJ1908+094	52327.0	52750.0	2002/2003	S	S	S	**ASM**,Chandra, NFI,PCA	194–196
	56581.0	56705.0	2013/2014	I	I	S	**BAT,MAXI**,XRT	197–200
SwiftJ1910.2−0546	56059.5	56316.5	2012/2013	S	S	S	**BAT**,EPIC,ISGRI,**MAXI**,XRT	122,128–131
SS433	-	-	1978-2014	-	-	-	A-2,**ASM**,ArielVI,**BAT**,Chandra,CMA GSPC,LAC,**MAXI**,ME,MPC,**PCA**,SIS SSI,SSS,Tenma,UHURU	339–343 356–364
GRS 1915+105	-	-	1992–2014	-	-	-	**ASM,BAT**,BATSE,Chandra,IXAE,**MAXI** PCA,PSPC,SIGMA,WATCH	245–255 365,366

Continued on Next Page...

Table A.3 – Continued

Source Name	$t_{\rm beg}$ [a]	$t_{\rm end}$ [a]	Outburst ID	Literature [b] Class	Algorithm Class [b] H_X	d_f	Instrument [c] Detection	References [d]
4U1956+350	-	-	1971–2014	-	-	-	A-2,A-4,Ariel V/ASM,**ASM,BAT**,BATSE BBXRT,CMA,GBM,GCXSE,GIS,GPSC,HEXE HEXTE,HRGRS,HSEM,LAC,LE,**MAXI** ME,OSSE,PCA,SIS,Tenma,UHURU,VELA5B	310–326 369–379
4U1957+115	-	-	1973–2014	-	-	-	A-2,**ASM,BAT**,Chandra,CMA,EPIC,GIS GSPC,HEXTE,LAC,LE,**MAXI**,ME,PCA,PSPC RGS,SIS,UHURU,XRT	304–309 367,368
GS 2000+251	-	-	1988	-	-	-	GINGA/ASM	243
XTEJ2012+381	50940.0	51141.0	1998	S	S	S	**ASM**,HEXTE,NFI,PCA	201,202
GS 2023+338	-	-	1938	-	-	-	SO	237
	-	-	1956	-	-	-	SO	237
	-	-	1989	F	-	-	GINGA/ASM,LAC	237–242

[a] The begin and end times of each outburst in MJD as calculated via the algorithm.

[b] Outburst classification via the algorithm (both using hardness (H_X) and disc fraction (d_f)) or spectral and/or timing analysis found in the literature (where available). S - Successful/Canonical, F - Failed, I - In determined.

[c] List of instruments which have detected the outburst. Bold indicates instrument(s) which have contributed to it's classification via the algorithm. A-2-Cosmic X-ray Experiment (CXE) involving six separate proportional counters aboard the High Energy Astronomy Observatory (HEAO) 1, A-3 - Modulation Colliamtor (MC) aboard HEAO 1, A-4 - Hard X-Ray/Low Energy Gamma Ray Experiment aboard HEAO 1, ANS - medium energy detector aboard the Astronomical Netherlands Satellite (ANS), ART-P - ART-P telescope aboard GRANAT, ASM - All-Sky Monitor aboard Rossi X-Ray Timing Explorer (RXTE), Ariel V/ASM - ASM aboard Ariel V Satellite, ArielVI - two Proportional Counters aboard the Ariel VI Satellite, BAT-Burst Alert Telescope aboard Swift X-Ray Observatory, BATSE - Burst And Transient Source Experiment aboard Compton Gamma-Ray Observatory (CGRO), BBXRT - Broad-Band X-ray Telescope, Chandra - Chandra X-Ray Observatory, CMA - Channel Electron Multiplier detector aboard European X-Ray Observatory Satellite (EXOSAT), EPIC - European Photon Imaging Camera aboard XMM-Newton, GBM - Gamma-Ray Burst Monitor aboard the Fermi Gamma-Ray Space Telescope, GCXSE - Cosmic X-Ray Spectroscopy Experiment aboard Orbiting Solar Observatory (OSO) 8, GINGA/ASM - ASM aboard GINGA satellite, GIS-Gas Imaging Spectrometer aboard Advanced Satellite for Cosmology and Astrophysics (ASCA), GSPC- Gas Scintillation Proportional Counter aboard EXOSAT, HAKUCHO - X-Ray detectors aboard the HAKUCHO (CORSA-5b) Satellite, HCO - Photographic Plates Collection at the Harvard College Observatory,HEXE - High Energy X-Ray Experiment aboard the MIr-Kvant Observatory, HEXTE - High Energy X-Ray Timing Experiment aboard RXTE, HRI - High Resolution Imager aboard the Einstein Observatory, HSEM - High Speed Event Monitor aboard the Small Astronomy Satellite (SAS) 3, HRGRS - High Resolution Gamma-Ray Spectrometer aboard HEAO 3, HXD - Hard X-Ray Detector aboard Suzaku, IPC - Image Proportional Counter aboard the Einstein Observatory, ISGRI - Integral Soft Gamma-Ray Imager aboard International Gamma-Ray Astrophysical Observatory (INTEGRAL), IXAE - 3 Proportional Counter's and 1 Sky Monintor (XSM) aboard the Indian X-ray Astronomy Experiment (IXAE), JEM-X - Two units aboard INTEGRAL, LAC - Large Area Proportional Counter aboard GINGA Satellite, LASS - Large Area Sky Survey Experiment (A-2) aboard HEAO 1, LE - Low Energy Instruments aboard EXOSAT, MAXI - Gas-Slit Camera aboard Monitor of All-Sky Image (MAXI) telescope, ME - Medium Energy Proportional Counter aboard (EXOSAT), MIT - MIT Cosmic X-Ray Experiment aboard Orbiting Solar Observatory 7 (OSO 7), MPC - Monitor Proportional Counter aboard the Einstein Observatory, MSSL - Mullard Space Science Laboratory X-ray detector aboard the Copernicus Satellite, NFI - Narrow field Instruments aboard BeppoSAX, NuSTAR - Nuclear Spectroscopic Telescope Array, OSSE- Oriented Scintillation Spectrometer Experiment aboard CGRO, PCA - Proportional counter array aboard RXTE, PCS - High resolution proportional counter array aboard the Ariel V Satellite, PSPC - Position Sensitive Proportional Counter aboard ROentgen SATellite (ROSAT), RGS - Reflection Grating Spectrometer abaod XMM-Newton, ROSAT HRI - The high Resolution IMages aboard ROSAT, SIS - Solid-state Imaging Spectrometer aboard ASCA, ROSAT/XRT - X-ray Telescope aboard ROSAT, SIGMA - hard X-ray and low-energy gamma-ray telescope aboard GRANAT, SO - Photographic platesat the Sonnenberg Observatory,SpaceLab2 - XRT aboard Space Lab 2 Satellite, RMC - Rotation Modulation Collimator aboard the Ariel V Satellite, Skylark - X-Ray detectors aboard the Skylark rockets, SSI - Sky Survey Instrument aboard Ariel V Satellite, SSS - Solid State Spectrometer aboard the Einstein Observatory, Tenma - Proportional Counters aboard the Tenma (ASTRO B) Satellite, TTM - a coded mask imaging spectrometer / wide-angle camera aboard the MIr-Kvant Observatory UHURU - two proportional counters aboard UHURU Satellite, VELA5B - ASM aboard VELA 5B Satellite, WATCH - ASM aboard GRANAT Satellite, WFC - Wide Field Camera aboard BeppoSAX, XC - Scintillation X-ray Detector aboard Vela 5B Satellite, XIS - X-ray Imaging Spectrometer aboard Suzaku, XRT - X-Ray telescope aboard Swift

[d] [1] Matilsky et al. (1972), [2] Kitamoto et al. (1984), [3] Harmon et al. (1992), [4] Park et al. (2004), [5] Priedhorsky (1986), [6] Jones et al. (1976), [7] Kuulkers et al. (1997a), [8] Parmar et al. (1997), [9] Parmar et al. (1986), [10] Parmar et al. (1995), [11] Trudolyubov et al. (2001), [12] Tomsick and Kaaret (2000), [13] Oosterbroek et al. (1998), [14] Tomsick et al. (2005), [15] Tomsick (2005), [16] Kalemci et al. (2008), [17] Tomida et al. (2009), [18] Nakahira et al. (2011), [19] Abe et al. (2005), [20] Neilsen et al. (2014), [21] Zhang et al. (1997), [22] Brocksopp et al. (2006), [23] Sobczak et al. (1999), [24] Cui et al. (1997a), [25] Borozdin et al. (1998), [26] Borozdin and Trudolyubov (2000), [27] Krimm et al. (2014), [28] Brocksopp et al. (2001), [29] Markert et al. (1973), [30] Motch et al. (1985), [31] Miyamoto et al. (1991), [32] Harmon et al. (1994b), [33] Trudolyubov et al. (1998), [34] Rubin et al. (1998), [35] Kong et al. (2002),[36] Belloni et al. (1999b), [37] Zdziarski et al. (2004), [38] Dieters et al. (2000), [39] Belloni et al. (2006), [40] Buxton et al. (2012), [41] Motta et al. (2009), [42] Debnath et al. (2013b),[43] Belloni et al. (2013), [44] Reynolds et al. (1999), [45] Emelyanov et al. (2000), [46] Capitanio et al. (2005), [47] Miller et al. (2006d), [48] Kalemci et al. (2006), [49] McClintock et al. (2009), [50] Homan et al. (2005), [51] Capitanio et al. (2006a), [52] Capitanio et al. (2009a), [53] Motta et al. (2010), [54] Chen et al. (2010), [55] Capitanio et al. (2010), [56] Zhou et al. (2013), [57] Miller-Jones et al. (2012), [58] Doxsey et al. (1977), [59] Cooke et al. (1984), [60] Coriat et al. (2011), [61] Debnath et al. (2013a), [62] Negoro et al. (2012a), [63] Shidatsu et al. (2012), [64] Nakahira et al. (2013), [65] Revnivtsev et al. (2003), [66] in't Zand et al. (2003), [67] Lutovinov and Revnivtsev (2003), [68] Capitanio et al. (2006b), [69] Capitanio et al. (2012), [70] Altamirano et al. (2011b), [71] Barlow et al. (2005), [72] Sidoli et al. (2011), [73] Capitanio et al. (2009b), [74] Kitamoto et al. (1990b), [75] Makino (1987), [76] Markwardt et al. (2008b), [77] Shaw et al. (2008), [78] Krimm et al. (2008d), [79] Rodriguez et al. (2007), [80] Walter et al. (2007), [81] Paizis et al. (2009), [82] Krimm et al. (2009a), [83] Sanchez-Fernandez et al. (2009), [84] Morihana et al. (2013), [85] Shidatsu et al. (2013), [86] Stiele et al. (2012), [87] Yamaoka et al. (2012), [88] Kennea et al. (2011b), [89] Kuulkers et al. (2013), [90] Ferrigno et al. (2011), [91] Reis et al. (2012), [92] Russell et al. (2014a), [93] in't Zand et al. (2002b), [94] in 't Zand et al. (1999), [95] Markwardt et al. (1999b), [96] Wijnands and van der Klis (2000), [97] Hjellming et al. (2000), [98] Hjellming (2000), [99] Uemura et al. (2004), [100] Bailyn et al. (2003), [101] Rupen et al. (2003d), [102] Maitra and Bailyn (2006), [103] Swank (2004), [104] in't Zand et al. (2000), [105] Revnivtsev et al. (2002), [106] Cackett and Miller (2007), [107] Yamaoka et al. (2008), [108] Yamaoka and Nakahira (2010), [109] Yamaoka et al. (2010b), [110] Yamaoka et al. (2010a), [111] Tachibana et al. (2014), [112] Skinner et al. (1990), [113] Markwardt (2003a), [114] Remillard and Levine (2003), [115] Lutovinov et al. (2003a), [116] Homan and Wijnands (2003), [117] Markwardt and Swank (2007), [118] Kennea et al. (2007), [119] Kuulkers et al. (2008), [120] Ozawa et al. (2011), [121] Krimm et al. (2011b), [122] Krimm et al. (2013b), [123] Curran et al. (2014), [124] Markwardt et al. (2008a), [125] Krimm et al. (2008c), [126] Armas Padilla et al. (2013a), [127] Armas Padilla et al. (2013b), [128] Kimura et al. (2012), [129] Nakahira et al. (2012b), [130] Bodaghee et al. (2012), [131] Reis et al. (2013), [132] Read et al. (2010a), [133] Markwardt et al. (2010), [134] Read et al. (2010b), [135] Armas Padilla et al. (2010a), [136] Armas Padilla et al. (2010b), [137] Revnivtsev et al. (2000b), [138] Revnivtsev et al. (1998a), [139] Goldoni et al. (1999), [140] Belloni et al. (1999b), [141] Bartlett et al. (2013), [142] Frontera et al. (1998), [143] Simon et al. (2006), [144] Hynes et al. (2000b), [145] McClintock et al. (2001b), [146] Brocksopp et al. (2010b),[147] Frontera et al. (2001), [148] Brocksopp et al. (2010b), [149] Zurita et al. (2006), [150] Sobczak et al. (2000), [151] Remillard et al. (2002), [152] Kubota and Makishima (2004), [153] Rodriguez et al. (2004), [154] Kalemci et al. (2001), [155] Miller et al. (2001b) [156] Tomsick et al. (2001b), [157] Tomsick et al. (2001a),[158] Belloni et al. (2002a),[159] Sturner and Shrader (2005), [160] Aref'ev et al. (2004), [161] Corbel et al. (2004), [162] Rossi et al. (2004), [163] Tomsick et al. (2004), [164] Homan et al. (2003a), [165] Kalemci et al. (2003), [166] Han et al. (2011), [167] Hiemstra et al. (2011), [168] Cadolle Bel et al. (2004), [169] Brocksopp et al. (2005), [170] Turler et al. (2005a), [171] Turler et al. (2005b), [172] Kong (2005), [173] Kennea et al. (2005), [174]

Munoz-Darias et al. (2010), [175] Stiele et al. (2011), [176] Curran et al. (2011), [177] Chun et al. (2013), [178] Cackett et al. (2006), [179] Markwardt et al. (2008d), [180] Torres et al. (2008b), [181] Sala et al. (2007), [182] Sriram et al. (2013a), [183] Roy et al. (2011), [184] Gierlinski et al. (2009), [185] Cadolle Bel et al. (2009), [186] Zurita Heras et al. (2011),[187] Remillard (1999), [188] Sala et al. (2008), [189] Marshall et al. (1996), [190] Barret et al. (1996a), [191] Casella et al. (2004), [192] Farinelli et al. (2013), [193] Cui et al. (2000), [194] in't Zand et al. (2002c), [195] Gogus et al. (2004), [196] Jonker et al. (2004), [197] Krimm et al. (2013a), [198] Krimm et al. (2013c), [199] Miller-Jones et al. (2013), [200] Coriat et al. (2013b), [201] Vasiliev et al. (2000), [202] Campana et al. (2002), [203] Markwardt et al. (2008c), [204] Wijnands et al. (2008), [205] Armas-Padilla et al. (2011), [206] Degenaar et al. (2008a), [207] Markwardt and Swank (2008), [208] Degenaar et al. (2008b), [209] Degenaar and Wijnands (2008), [210] Karasev et al. (2007), [211] Karasev et al. (2008), [212] Krimm et al. (2010), [213] Cadolle Bel et al. (2007), [214] Soleri et al. (2012), [215] Shaw et al. (2013), [216] Mostafa et al. (2013), [217] Froning et al. (2014), [218] Zurita et al. (2008), [219] Miller et al. (2006a), [220] Lutovinov et al. (2003b), [221] Lutovinov and Revnivtsev (2003), [222] Paizis et al. (1248). [223] Markwardt et al. (2007), [224] Cheung (2007), [225] Sguera et al. (2011), [226] Grebenev et al. (2007), [227] Capitanio et al. (2009b), [228] Chenevez et al. (2004), [229] Halpern and Tyagi (2005), [230] Reig et al. (2010), [231] Krivonos et al. (2005), [232] Sguera et al. (2007), [233] Griffiths et al. (1978), [234] Watson et al. (1978), [235] Griffiths et al. (1977), [236] Kaluzienski and Holt (1977), [237] Richer (1987), [238] Zycki et al. (1999), [239] Kitamoto et al. (1989), [240] Han and Hjellming (1992), [241] Oosterbroek et al. (1997), [242] Brocksopp et al. (2004), [243] Tsunemi et al. (1989), [244] Kitamoto et al. (1992), [245] Greiner et al. (1996), [246] Castro-Tirado et al. (1994), [247] Paul et al. (1997), [248] Paul et al. (1998), [249] Harmon et al. (1994a), [250] Foster et al. (1996), [251] Belloni et al. (1997), [252] Fender et al. (1999b), [253] Mirabel and Rodríguez (1994), [254] Belloni and Altamirano (2013), [255] Neilsen et al. (2011), [256] Ueda et al. (1997), [257] Francey (1971), [258] Markert et al. (1979), [259] Revnivtsev et al. (2000c), [260] Revnivtsev et al. (2000a), [261] Borozdin et al. (1995), [262] Vargas et al. (1996), [263] Revnivtsev et al. (1998b), [264] van der Hooft et al. (1999a), [265] Lapshov et al. (1993), [266] Kaniovsky et al. (1993), [267] Filippenko et al. (1999), [268] Yamauchi and Koyama (1990), [269] Yamauchi and Nakamura (2004), [270] Shrader et al. (1997), [271] Sunyaev et al. (1994), [272] Callanan et al. (1995), [273] Shrader et al. (1994), [274] van der Hooft et al. (1999b), [275] Parmar et al. (1993), [276] Branduardi et al. (2001), [277] Eyles et al. (1975), [278] Kaluzienski et al. (1975), [279] Barret et al. (1992), [280] Barret et al. (1995), [281] Eachus et al. (1976), [282] Elvis et al. (1975), [283] Brocksopp et al. (2007), [284] Sunyaev et al. (1991b), [285] Sunyaev et al. (1991c), [286] Skinner et al. (1991), [287] Bazzano et al. (1992), [288] Cordier et al. (1993), [289] Churazov et al. (1993), [290] Cordier et al. (1994), [291] Jung et al. (1995), [292] Smith et al. (1997), [293] Main et al. (1999), [294] del Santo et al. (2004), [295] Natalucci et al. (2014), [296] Haardt et al. (2001), [297] Yao et al. (2005), [298] Wilms et al. (2001), [299] Smale and Boyd (2012), [300] **?**, [301] White and Marshall (1984), [302] Steiner et al. (2014), [303] Nowak et al. (2001), [304] Nowak and Wilms (1999), [305] Maitra et al. (2013), [306] Yaqoob et al. (1993), [307] Wijnands et al. (2002), [308] Ricci et al. (1995), [309] Nowak et al. (2008), [310] Grinberg et al. (2013), [311] Grinberg et al. (2014), [312] Gierlinski et al. (2010), [313] Gierlinski et al. (1997), [314] Belloni and Hasinger (1990), [315] Tananbaum et al. (1972), [316] Gleissner et al. (2004), [317] Holt et al. (1979), [318] Ubertini et al. (1991a), [319] Ubertini et al. (1991b), [320] Wilms et al. (2006), [321] Miyamoto et al. (1992), [322] Zdziarski et al. (2002), [323] Pottschmidt et al. (2003), [324] Ling et al. (1983), [325] Barr and van der Woerd (1990), [326] Kitamoto et al. (1990a), [327] Smith et al. (2001), [328] Pottschmidt et al. (2006), [329] Mereghetti et al. (1997), [330] Smith et al. (1997), [331] Mereghetti et al. (1994), [332] Gilfanov et al. (1993), [333] White et al. (1988), [334] Kaaret et al. (2006), [335] Pan et al. (1995), [336] White et al. (1984), [337] Hjellming et al. (1999b), [338] Cui et al. (2000), [339] Nandi et al. (2005), [340] Brinkmann et al. (1989), [341] Brinkmann et al. (1991), [342] Grindlay et al. (1984), [343] Band (1989), [344] Treves et al. (1988), [345] Ebisawa et al. (1993), [346] Ishibashi et al. (2010), [347] Sunyaev et al. (1997), [348] Heise (1997), [349] Trudolyubov et al. (1997), [350] Greiner et al. (1997), [351] Jonker et al. (2010), [352] Harmon et al. (1998),[353] Reis et al. (2011), [354] Díaz Trigo et al. (2013), [355] Brocksopp et al. (2002), [356] Watson et al. (1986), [357] Marshall et al. (1979), [358] Ricketts et al. (1981), [359] Yuan et al. (1995), [360] **?**, [361] Kotani et al. (1994), [362] Marshall et al. (2002), [363] Namiki et al. (2003), [364] Seward et al. (1986), [365] Greiner and Reid (1993), [366] Greiner et al. (1994), [367] Giacconi et al. (1974), [368] Singh et al. (1994), [369] Marshall et al. (1993), [370] **?**, [371] Priedhorsky et al. (1983), [373] Nolan and Matteson (1983), [374] Nolan et al. (1983), [375] Dolan et al. (1979), [376] Doebereiner et al. (1989), [377] Ubertini et al. (1991b), [378] Miyamoto and Kitamoto (1989), [379] Ling et al. (1987), [380] Bailyn and Orosz (1995), [382] Remillard et al. (2000), [383] Wren and McKay (2000), [384] Uemura et al. (2000a), [385] Homan et al. (2001), [386] Cui et al. (1999), [387] Remillard et al. (1999a), [388] Swank et al. (2002), [389] Saito et al. (2006), [390] Shaposhnikov et al. (2007), [391] Remillard et al. (1999b), [392] Motta et al. (2012), [393] Tomsick et al. (1999), [394] Hjellming et al. (1996a), [395] Ricketts et al. (1975), [396] Ebisawa et al. (1994), [397] Motch et al. (1998), [398] (Krimm et al., 2009b)

Table A.4: State Transitions occurring in Galactic BHXRBs Between 1996-2014

Source Name	Outburst ID	Stage	State(s)	$t_{\rm beg}$ [a] (MJD)	$t_{\rm end}$ [a] (MJD)	$t_{\rm dur}$ [b] (days)
XTEJ0421+560	1998	rise	-	50885	50903	18
		rise	HDS	50903	50905	2
		decline	HDS	50905	50908	3
		decline	-	50908	50935	27
4U0538−641	1996-2003	rise	-	50087	50092	5
		transition	- → HDS	50092	50125	33
		rise	HDS	50125	50166	41
		transition	HDS → IMS → HDS	50166	-	1
		rise	HDS	50167	50184	17
		transition	HDS → IMS → HDS	50184	50186	2
		rise	HDS	50186	50188	2
		transition	HDS → IMS → HDS	50188	50193	5
		rise	HDS	50193	50195	2
		transition	HDS → IMS → HDS	50195	50202	7
		rise	HDS	50202	50205	3
		transition	HDS → IMS → HDS	50205	-	1
		rise	HDS	50206	50210	4
		transition	HDS → IMS → HDS	50210	-	1
		rise	HDS	50211	50213	2
		transition	HDS → IMS → HDS	50213	50215	2
		rise	HDS	50215	50224	9
		transition	HDS → IMS → HDS	50224	-	1
		rise	HDS	50225	50230	5
		transition	HDS → IMS → HDS	50230	50238	8
		rise	HDS	50238	50240	2
		transition	HDS → IMS → HDS	50240	-	1
		rise	HDS	50241	50282	41
		transition	HDS → IMS → HDS	50282	-	1
		rise	HDS	50283	50308	25
		transition	HDS → IMS → HDS	50308	-	1
		rise	HDS	50309	50312	3
		rise	SDS	50312	-	1
		transition	SDS → HDS	50313	50318	5
		rise	HDS	50318	50360	42
		rise	SDS	50360	-	1
		transition	SDS → HDS	50361	50364	3

Continued on Next Page...

Table A.4 – Continued

Source Name	Outburst ID	Stage	State(s)	$t_{\rm beg}$[a] (MJD)	$t_{\rm end}$[a] (MJD)	$t_{\rm dur}$[b] (days)
		rise	HDS	50364	50372	8
		transition	HDS → IMS → HDS	50372	50379	7
		rise	HDS	50379	50389	10
		transition	HDS → IMS → HDS	50389	-	1
		rise	HDS	50390	50404	14
		transition	HDS → IMS → HDS	50404	50406	2
		rise	HDS	50406	50424	18
		transition	HDS → IMS → HDS	50424	50426	2
		rise	HDS	50426	50431	5
		transition	HDS → IMS → HDS	50431	-	1
		rise	HDS	50432	50435	3
		transition	HDS → IMS → HDS	50435	50441	6
		rise	HDS	50441	50454	13
		transition	HDS → IMS → HDS	50454	50487	33
		rise	HDS	50487	50492	5
		transition	HDS → SDS	50492	50496	4
		rise	SDS	50496	50499	3
		rise	HDS	50499	50502	3
		transition	HDS → IMS → HDS	50502	-	1
		rise	HDS	50503	50506	3
		transition	HDS → IMS → HDS	50506	50509	3
		rise	HDS	50509	50513	4
		transition	HDS → IMS → HDS	50513	-	1
		rise	HDS	50514	50524	10
		transition	HDS → IMS → HDS	50524	-	1
		rise	HDS	50525	50534	9
		transition	HDS → IMS → HDS	50534	50537	3
		rise	HDS	50537	50557	20
		transition	HDS → IMS → HDS	50557	50559	2
		rise	HDS	50559	50575	16
		rise	SDS	50575	-	1
		transition	SDS → HDS	50576	50578	2
		rise	HDS	50578	50580	2
		transition	HDS → IMS → HDS	50580	50582	2
		rise	HDS	50582	50593	11
		transition	HDS → IMS → HDS	50593	50618	25
		rise	HDS	50618	50626	8

Continued on Next Page...

Table A.4 – Continued

Source Name	Outburst ID	Stage	State(s)	$t_{\rm beg}$[a] (MJD)	$t_{\rm end}$[a] (MJD)	$t_{\rm dur}$[b] (days)
		transition	HDS → IMS → HDS	50626	50631	5
		rise	HDS	50631	50643	12
		transition	HDS → IMS → HDS	50643	-	1
		rise	HDS	50644	50658	14
		transition	HDS → IMS → HDS	50658	50696	38
		rise	HDS	50696	50707	11
		transition	HDS → IMS → HDS	50707	50709	2
		rise	HDS	50709	50712	3
		transition	HDS → IMS → HDS	50712	50714	2
		rise	HDS	50714	50718	4
		transition	HDS → IMS → HDS	50718	50731	13
		rise	HDS	50731	50738	7
		transition	HDS → IMS → HDS	50738	50747	9
		rise	HDS	50747	50761	14
		transition	HDS → IMS → HDS	50761	50765	4
		rise	HDS	50765	50778	13
		transition	HDS → IMS → HDS	50778	-	1
		rise	HDS	50779	50784	5
		transition	HDS → IMS → HDS	50784	50804	20
		rise	HDS	50804	50815	11
		decline	HDS	50815	50817	2
		transition	HDS → IMS → HDS	50817	50819	2
		decline	HDS	50819	50823	4
		transition	HDS → IMS → HDS	50823	50827	4
		decline	HDS	50827	50866	39
		transition	HDS → IMS → HDS	50866	-	1
		decline	HDS	50867	50872	5
		transition	HDS → SDS	50872	50874	2
		decline	SDS	50874	50876	2
		decline	HDS	50876	50878	2
		transition	HDS → IMS → HDS	50878	50881	3
		decline	HDS	50881	50884	3
		transition	HDS → IMS → HDS	50884	50887	3
		decline	HDS	50887	50890	3
		decline	SDS	50890	-	1
		decline	HDS	50891	50920	29
		transition	HDS → IMS → HDS	50920	-	1

Continued on Next Page...

Table A.4 – Continued

Source Name	Outburst ID	Stage	State(s)	$t_{\rm beg}$[a] (MJD)	$t_{\rm end}$[a] (MJD)	$t_{\rm dur}$[b] (days)
		decline	HDS	50921	50929	8
		transition	HDS → IMS → HDS	50929	-	1
		decline	HDS	50930	50933	3
		transition	HDS → IMS → HDS	50933	50936	3
		decline	HDS	50936	50969	33
		transition	HDS → IMS → HDS	50969	50986	17
		decline	HDS	50986	51021	35
		transition	HDS → IMS → HDS	51021	-	1
		decline	HDS	51022	51036	14
		transition	HDS → IMS → HDS	51036	51041	5
		decline	HDS	51041	51045	4
		transition	HDS → IMS → HDS	51045	51047	2
		decline	HDS	51047	51115	68
		transition	HDS → IMS → HDS	51115	51135	20
		decline	HDS	51135	51143	8
		transition	HDS → IMS → HDS	51143	51147	4
		decline	HDS	51147	51149	2
		decline	SDS	51149	-	1
		transition	SDS → HDS	51150	51156	6
		decline	HDS	51156	51181	25
		transition	HDS → IMS → HDS	51181	51195	14
		decline	HDS	51195	51197	2
		decline	SDS	51197	51201	4
		decline	HDS	51201	51210	9
		transition	HDS → IMS → HDS	51210	-	1
		decline	HDS	51211	51287	76
		transition	HDS → IMS → HDS	51287	51289	2
		decline	HDS	51289	51300	11
		transition	HDS → SDS	51300	51302	2
		decline	SDS	51302	51304	2
		transition	SDS → HDS	51304	51306	2
		decline	HDS	51306	51308	2
		transition	HDS → IMS → HDS	51308	51310	2
		decline	HDS	51310	51323	13
		transition	HDS → IMS → HDS	51323	-	1
		decline	HDS	51324	51331	7
		transition	HDS → IMS → HDS	51331	-	1

Continued on Next Page...

Table A.4 – Continued

Source Name	Outburst ID	Stage	State(s)	$t_{\rm beg}$[a] (MJD)	$t_{\rm end}$[a] (MJD)	$t_{\rm dur}$[b] (days)
		decline	HDS	51332	51337	5
		transition	HDS → IMS → HDS	51337	51339	2
		decline	HDS	51339	51351	12
		transition	HDS → IMS → HDS	51351	-	1
		decline	HDS	51352	51380	28
		transition	HDS → IMS → HDS	51380	51386	6
		decline	HDS	51386	51405	19
		transition	HDS → IMS → HDS	51405	-	1
		decline	HDS	51406	51409	3
		transition	HDS → IMS → HDS	51409	-	1
		decline	HDS	51410	51428	18
		decline	SDS	51428	-	1
		decline	HDS	51429	51460	31
		transition	HDS → IMS → HDS	51460	-	1
		decline	HDS	51461	51472	11
		transition	HDS → IMS → HDS	51472	51474	2
		decline	HDS	51474	51485	11
		transition	HDS → IMS → HDS	51485	51487	2
		decline	HDS	51487	51499	12
		transition	HDS → IMS → HDS	51499	51501	2
		decline	HDS	51501	51512	11
		transition	HDS → IMS → HDS	51512	-	1
		decline	HDS	51513	51523	10
		transition	HDS → IMS → HDS	51523	51530	7
		decline	HDS	51530	51532	2
		transition	HDS → IMS → HDS	51532	51534	2
		decline	HDS	51534	51536	2
		decline	SDS	51536	51539	3
		decline	HDS	51539	51559	20
		transition	HDS → IMS → HDS	51559	51561	2
		decline	HDS	51561	51565	4
		transition	HDS → IMS → HDS	51565	-	1
		decline	HDS	51566	51568	2
		transition	HDS → IMS → HDS	51568	-	1
		decline	HDS	51569	51572	3
		transition	HDS → IMS → HDS	51572	51576	4
		decline	HDS	51576	51580	4

Continued on Next Page...

Table A.4 – Continued

Source Name	Outburst ID	Stage	State(s)	$t_{\rm beg}$[a] (MJD)	$t_{\rm end}$[a] (MJD)	$t_{\rm dur}$[b] (days)
		transition	HDS → IMS → HDS	51580	-	1
		decline	HDS	51581	51617	36
		transition	HDS → IMS → HDS	51617	51686	69
		decline	HDS	51686	51702	16
		transition	HDS → IMS → HDS	51702	51717	15
		decline	HDS	51717	51720	3
		decline	SDS	51720	51722	2
		transition	SDS → HDS	51722	-	1
		decline	HDS	51723	51753	30
		transition	HDS → IMS → HDS	51753	51763	10
		decline	HDS	51763	51778	15
		transition	HDS → IMS → HDS	51778	51785	7
		decline	HDS	51785	51788	3
		decline	SDS	51788	-	1
		decline	HDS	51789	51791	2
		transition	HDS → SDS	51791	51813	22
		decline	SDS	51813	51815	2
		decline	HDS	51815	51821	6
		transition	HDS → IMS → HDS	51821	51827	6
		decline	HDS	51827	51829	2
		transition	HDS → IMS → HDS	51829	51831	2
		decline	HDS	51831	51835	4
		transition	HDS → IMS → HDS	51835	-	1
		decline	HDS	51836	51839	3
		transition	HDS → IMS → HDS	51839	-	1
		decline	HDS	51840	51863	23
		transition	HDS → IMS → HDS	51863	51866	3
		decline	HDS	51866	51883	17
		transition	HDS → IMS → HDS	51883	-	1
		decline	HDS	51884	51890	6
		transition	HDS → IMS → HDS	51890	51892	2
		decline	HDS	51892	51908	16
		transition	HDS → IMS → HDS	51908	51930	22
		decline	HDS	51930	51933	3
		transition	HDS → IMS → HDS	51933	-	1
		decline	HDS	51934	51941	7
		transition	HDS → IMS → HDS	51941	-	1

Continued on Next Page...

Table A.4 – Continued

Source Name	Outburst ID	Stage	State(s)	$t_{\rm beg}$[a] (MJD)	$t_{\rm end}$[a] (MJD)	$t_{\rm dur}$[b] (days)
		decline	HDS	51942	51962	20
		transition	HDS → IMS → HDS	51962	51965	3
		decline	HDS	51965	51968	3
		transition	HDS → IMS → HDS	51968	-	1
		decline	HDS	51969	51973	4
		transition	HDS → IMS → HDS	51973	51977	4
		decline	HDS	51977	51985	8
		transition	HDS → IMS → HDS	51985	51987	2
		decline	HDS	51987	51994	7
		transition	HDS → IMS → HDS	51994	51997	3
		decline	HDS	51997	52000	3
		transition	HDS → IMS → HDS	52000	52007	7
		decline	HDS	52007	52025	18
		transition	HDS → IMS → HDS	52025	-	1
		decline	HDS	52026	52039	13
		transition	HDS → IMS → HDS	52039	52042	3
		decline	HDS	52042	52048	6
		transition	HDS → IMS → HDS	52048	-	1
		decline	HDS	52049	52055	6
		transition	HDS → IMS → HDS	52055	52057	2
		decline	HDS	52057	52102	45
		transition	HDS → IMS → HDS	52102	52104	2
		decline	HDS	52104	52111	7
		transition	HDS → IMS → HDS	52111	52124	13
		decline	HDS	52124	52128	4
		transition	HDS → IMS → HDS	52128	-	1
		decline	HDS	52129	52137	8
		transition	HDS → IMS → HDS	52137	52146	9
		decline	HDS	52146	52149	3
		transition	HDS → IMS → HDS	52149	52152	3
		decline	HDS	52152	52154	2
		transition	HDS → IMS → HDS	52154	52162	8
		decline	HDS	52162	52165	3
		transition	HDS → SDS	52165	52183	18
		decline	SDS	52183	52190	7
		transition	SDS → HDS	52190	52194	4
		decline	HDS	52194	52196	2

Continued on Next Page...

Table A.4 – Continued

Source Name	Outburst ID	Stage	State(s)	$t_{\rm beg}$[a] (MJD)	$t_{\rm end}$[a] (MJD)	$t_{\rm dur}$[b] (days)
		transition	HDS → IMS → HDS	52196	-	1
		decline	HDS	52197	52200	3
		transition	HDS → IMS → HDS	52200	52202	2
		decline	HDS	52202	52207	5
		decline	SDS	52207	52213	6
		transition	SDS → HDS	52213	52217	4
		decline	HDS	52217	52222	5
		transition	HDS → IMS → HDS	52222	52226	4
		decline	HDS	52226	52253	27
		transition	HDS → IMS → HDS	52253	52257	4
		decline	HDS	52257	52276	19
		transition	HDS → IMS → HDS	52276	52280	4
		decline	HDS	52280	52287	7
		transition	HDS → IMS → HDS	52287	52291	4
		decline	HDS	52291	52293	2
		transition	HDS → IMS → HDS	52293	52296	3
		decline	HDS	52296	52299	3
		transition	HDS → IMS → HDS	52299	-	1
		decline	HDS	52300	52302	2
		transition	HDS → IMS → HDS	52302	52304	2
		decline	HDS	52304	52311	7
		transition	HDS → SDS	52311	-	1
		decline	SDS	52312	52314	2
		decline	HDS	52314	52323	9
		transition	HDS → IMS → HDS	52323	52332	9
		decline	HDS	52332	52334	2
		transition	HDS → IMS → HDS	52334	-	1
		decline	HDS	52335	52338	3
		decline	SDS	52338	52340	2
		decline	HDS	52340	52349	9
		decline	SDS	52349	52352	3
		transition	SDS → HDS	52352	52358	6
		decline	HDS	52358	52360	2
		transition	HDS → SDS	52360	-	1
		decline	SDS	52361	52364	3
		decline	HDS	52364	52382	18
		transition	HDS → IMS → HDS	52382	52397	15

Continued on Next Page...

Table A.4 – Continued

Source Name	Outburst ID	Stage	State(s)	$t_{\rm beg}$ [a] (MJD)	$t_{\rm end}$ [a] (MJD)	$t_{\rm dur}$ [b] (days)
		decline	HDS	52397	52414	17
		transition	HDS → IMS → HDS	52414	52424	10
		decline	HDS	52424	52444	20
		transition	HDS → IMS → HDS	52444	52448	4
		decline	HDS	52448	52453	5
		transition	HDS → IMS → HDS	52453	52460	7
		decline	HDS	52460	52463	3
		transition	HDS → IMS → HDS	52463	52466	3
		decline	HDS	52466	52471	5
		transition	HDS → IMS → HDS	52471	52473	2
		decline	HDS	52473	52485	12
		transition	HDS → IMS → HDS	52485	52491	6
		decline	HDS	52491	52493	2
		transition	HDS → IMS → HDS	52493	52497	4
		decline	HDS	52497	52520	23
		transition	HDS → IMS → HDS	52520	-	1
		decline	HDS	52521	52537	16
		transition	HDS → IMS → HDS	52537	-	1
		decline	HDS	52538	52546	8
		transition	HDS → IMS → HDS	52546	52549	3
		decline	HDS	52549	52555	6
		transition	HDS → SDS	52555	52558	3
		decline	SDS	52558	-	1
		decline	HDS	52559	52561	2
		transition	HDS → IMS → HDS	52561	-	1
		decline	HDS	52562	52564	2
		transition	HDS → IMS → HDS	52564	52577	13
		decline	HDS	52577	52600	23
		decline	SDS	52600	-	1
		decline	HDS	52601	52612	11
		transition	HDS → IMS → HDS	52612	52644	32
		decline	HDS	52644	52649	5
		decline	SDS	52649	-	1
		decline	HDS	52650	52668	18
		transition	HDS → IMS → HDS	52668	52671	3
		decline	HDS	52671	52676	5
		transition	HDS → IMS → HDS	52676	52729	53

Continued on Next Page...

Table A.4 – Continued

Source Name	Outburst ID	Stage	State(s)	$t_{\rm beg}$[a] (MJD)	$t_{\rm end}$[a] (MJD)	$t_{\rm dur}$[b] (days)
		decline	HDS	52729	52743	14
		transition	HDS → IMS → HDS	52743	52747	4
		decline	HDS	52747	52751	4
		transition	HDS → IMS → HDS	52751	52754	3
		decline	HDS	52754	52763	9
		decline	SDS	52763	-	1
		decline	HDS	52764	52772	8
		transition	HDS → IMS → HDS	52772	52775	3
		decline	HDS	52775	52777	2
		decline	SDS	52777	52779	2
		decline	HDS	52779	52807	28
		transition	HDS → IMS → HDS	52807	52809	2
		decline	HDS	52809	52816	7
		transition	HDS → IMS → HDS	52816	52825	9
		decline	HDS	52825	52827	2
		decline	SDS	52827	52829	2
		decline	HDS	52829	52841	12
		transition	HDS → IMS → HDS	52841	52847	6
		decline	HDS	52847	52855	8
		transition	HDS → IMS → HDS	52855	52858	3
		decline	HDS	52858	52861	3
		transition	HDS → IMS → HDS	52861	52865	4
		decline	HDS	52865	52871	6
		transition	HDS → IMS → HDS	52871	52875	4
		decline	HDS	52875	52893	18
		transition	HDS → IMS → HDS	52893	52908	15
		decline	HDS	52908	52922	14
		transition	HDS → IMS → HDS	52922	52926	4
		decline	HDS	52926	52961	35
		transition	HDS → IMS → HDS	52961	52966	5
		decline	HDS	52966	52982	16
		transition	HDS → -	52982	-	1
		decline	-	52983	52992	9
	2004-2014	rise	-	53089	53095	6
		rise	HDS	53095	53101	6
		transition	HDS → IMS → HDS	53101	-	1
		rise	HDS	53102	53119	17

Continued on Next Page...

Table A.4 – Continued

Source Name	Outburst ID	Stage	State(s)	$t_{\rm beg}$[a] (MJD)	$t_{\rm end}$[a] (MJD)	$t_{\rm dur}$[b] (days)
		transition	HDS → IMS → HDS	53119	53125	6
		rise	HDS	53125	53127	2
		transition	HDS → IMS → HDS	53127	-	1
		rise	HDS	53128	53130	2
		rise	SDS	53130	-	1
		transition	SDS → HDS	53131	53134	3
		rise	HDS	53134	53136	2
		transition	HDS → IMS → HDS	53136	53140	4
		rise	HDS	53140	53165	25
		transition	HDS → IMS → HDS	53165	53170	5
		rise	HDS	53170	53176	6
		rise	SDS	53176	-	1
		rise	HDS	53177	53204	27
		transition	HDS → IMS → HDS	53204	53206	2
		rise	HDS	53206	53220	14
		transition	HDS → IMS → HDS	53220	-	1
		rise	HDS	53221	53234	13
		transition	HDS → IMS → HDS	53234	53236	2
		rise	HDS	53236	53253	17
		transition	HDS → IMS → HDS	53253	-	1
		rise	HDS	53254	53260	6
		transition	HDS → IMS → HDS	53260	53265	5
		rise	HDS	53265	53270	5
		transition	HDS → IMS → HDS	53270	53280	10
		rise	HDS	53280	53283	3
		transition	HDS → IMS → HDS	53283	53288	5
		rise	HDS	53288	53337	49
		transition	HDS → IMS → HDS	53337	53360	23
		rise	HDS	53360	53368	8
		transition	HDS → IMS → HDS	53368	53370	2
		rise	HDS	53370	53373	3
		transition	HDS → IMS → HDS	53373	53377	4
		rise	HDS	53377	53385	8
		transition	HDS → IMS → HDS	53385	-	1
		rise	HDS	53386	53400	14
		transition	HDS → IMS → HDS	53400	53402	2
		rise	HDS	53402	53409	7

Continued on Next Page...

Table A.4 – Continued

Source Name	Outburst ID	Stage	State(s)	$t_{\rm beg}$[a] (MJD)	$t_{\rm end}$[a] (MJD)	$t_{\rm dur}$[b] (days)
		rise	SDS	53409	-	1
		rise	HDS	53410	53415	5
		transition	HDS → IMS → HDS	53415	-	1
		rise	HDS	53416	53420	4
		transition	HDS → SDS	53420	-	1
		rise	SDS	53421	53483	62
		rise	HDS	53483	53487	4
		transition	HDS → SDS	53487	53509	22
		rise	SDS	53509	53605	96
		transition	SDS → HDS	53605	53617	12
		rise	HDS	53617	53620	3
		transition	HDS → IMS → HDS	53620	53629	9
		rise	HDS	53629	53637	8
		transition	HDS → IMS → HDS	53637	53639	2
		rise	HDS	53639	53652	13
		transition	HDS → SDS	53652	-	1
		rise	SDS	53653	53658	5
		transition	SDS → IMS → SDS	53658	53689	31
		rise	SDS	53689	-	1
		transition	SDS → IMS → SDS	53690	53738	48
		rise	SDS	53738	53759	21
		transition	SDS → IMS → SDS	53759	53850	91
		rise	SDS	53850	53882	32
		transition	SDS → IMS → SDS	53882	53911	29
		rise	SDS	53911	53964	53
		transition	SDS → IMS → SDS	53964	53967	3
		rise	SDS	53967	53970	3
		transition	SDS → IMS → SDS	53970	53974	4
		rise	SDS	53974	54001	27
		transition	SDS → IMS → SDS	54001	-	1
		rise	SDS	54002	54010	8
		transition	SDS → IMS → SDS	54010	-	1
		rise	SDS	54011	54030	19
		transition	SDS → IMS → SDS	54030	-	1
		rise	SDS	54031	54034	3
		transition	SDS → HDS	54034	54055	21
		rise	HDS	54055	54071	16

Continued on Next Page...

Table A.4 – Continued

Source Name	Outburst ID	Stage	State(s)	$t_{\rm beg}$[a] (MJD)	$t_{\rm end}$[a] (MJD)	$t_{\rm dur}$[b] (days)
		transition	HDS → SDS	54071	54078	7
		rise	SDS	54078	54080	2
		transition	SDS → IMS → SDS	54080	54112	32
		rise	SDS	54112	54117	5
		transition	SDS → IMS → SDS	54117	54127	10
		rise	SDS	54127	54148	21
		transition	SDS → HDS	54148	54150	2
		rise	HDS	54150	54167	17
		transition	HDS → SDS	54167	54187	20
		rise	SDS	54187	54213	26
		transition	SDS → IMS → SDS	54213	54222	9
		rise	SDS	54222	54229	7
		transition	SDS → IMS → SDS	54229	54279	50
		rise	SDS	54279	54339	60
		transition	SDS → IMS → SDS	54339	54355	16
		rise	SDS	54355	54417	62
		transition	SDS → IMS → SDS	54417	-	1
		rise	SDS	54418	54432	14
		transition	SDS → IMS → SDS	54432	54461	29
		rise	SDS	54461	54571	110
		transition	SDS → IMS → SDS	54571	54576	5
		rise	SDS	54576	54591	15
		transition	SDS → IMS → SDS	54591	54625	34
		rise	SDS	54625	54665	40
		transition	SDS → IMS → SDS	54665	54759	94
		rise	SDS	54759	54785	26
		rise	HDS	54785	54793	8
		transition	HDS → IMS → HDS	54793	54799	6
		rise	HDS	54799	54810	11
		transition	HDS → IMS → HDS	54810	54948	138
		rise	HDS	54948	54987	39
		transition	HDS → SDS	54987	55057	70
		rise	SDS	55057	55088	31
		transition	SDS → IMS → SDS	55088	55091	3
		rise	SDS	55091	55114	23
		transition	SDS → IMS → SDS	55114	55117	3
		rise	SDS	55117	-	1

Continued on Next Page...

Table A.4 – Continued

Source Name	Outburst ID	Stage	State(s)	$t_{\rm beg}$[a] (MJD)	$t_{\rm end}$[a] (MJD)	$t_{\rm dur}$[b] (days)
		transition	SDS → IMS → SDS	55118	55120	2
		rise	SDS	55120	55124	4
		transition	SDS → IMS → SDS	55124	55153	29
		rise	SDS	55153	55224	71
		transition	SDS → IMS → SDS	55224	55258	34
		rise	SDS	55258	55262	4
		transition	SDS → IMS → SDS	55262	55270	8
		rise	SDS	55270	55294	24
		transition	SDS → IMS → SDS	55294	55304	10
		rise	SDS	55304	55420	116
		transition	SDS → IMS → SDS	55420	55472	52
		rise	SDS	55472	55476	4
		transition	SDS → IMS → SDS	55476	55486	10
		rise	SDS	55486	55495	9
		transition	SDS → IMS → SDS	55495	55498	3
		rise	SDS	55498	-	1
		transition	SDS → IMS → SDS	55499	55592	93
		rise	SDS	55592	55603	11
		transition	SDS → HDS	55603	55639	36
		rise	HDS	55639	55655	16
		transition	HDS → IMS → HDS	55655	55736	81
		decline	HDS	55736	55749	13
		transition	HDS → IMS → HDS	55749	55761	12
		decline	HDS	55761	55788	27
		transition	HDS → IMS → HDS	55788	-	1
		decline	HDS	55789	55809	20
		transition	HDS → IMS → HDS	55809	-	1
		decline	HDS	55810	55814	4
		transition	HDS → IMS → HDS	55814	55835	21
		decline	HDS	55835	55868	33
		transition	HDS → IMS → HDS	55868	55870	2
		decline	HDS	55870	55885	15
		transition	HDS → IMS → HDS	55885	55889	4
		decline	HDS	55889	55955	66
		transition	HDS → IMS → HDS	55955	55964	9
		decline	HDS	55964	55983	19
		decline	SDS	55983	55992	9

Continued on Next Page...

Table A.4 – Continued

Source Name	Outburst ID	Stage	State(s)	$t_{\rm beg}$[a] (MJD)	$t_{\rm end}$[a] (MJD)	$t_{\rm dur}$[b] (days)
		transition	SDS → IMS → SDS	55992	55996	4
		decline	SDS	55996	55998	2
		transition	SDS → IMS → SDS	55998	-	1
		decline	SDS	55999	56003	4
		transition	SDS → HDS	56003	-	1
		decline	HDS	56004	56006	2
		transition	HDS → IMS → HDS	56006	56016	10
		decline	HDS	56016	56043	27
		transition	HDS → IMS → HDS	56043	56045	2
		decline	HDS	56045	56050	5
		transition	HDS → SDS	56050	56057	7
		decline	SDS	56057	56131	74
		transition	SDS → IMS → SDS	56131	56138	7
		decline	SDS	56138	56150	12
		transition	SDS → HDS	56150	56163	13
		decline	HDS	56163	56165	2
		transition	HDS → IMS → HDS	56165	56186	21
		decline	HDS	56186	56201	15
		transition	HDS → IMS → HDS	56201	-	1
		decline	HDS	56202	56207	5
		transition	HDS → IMS → HDS	56207	56209	2
		decline	HDS	56209	56214	5
		transition	HDS → IMS → HDS	56214	56216	2
		decline	HDS	56216	56231	15
		transition	HDS → IMS → HDS	56231	56233	2
		decline	HDS	56233	56241	8
		transition	HDS → IMS → HDS	56241	56245	4
		decline	HDS	56245	56249	4
		decline	SDS	56249	56254	5
		transition	SDS → HDS	56254	56257	3
		decline	HDS	56257	56264	7
		transition	HDS → IMS → HDS	56264	-	1
		decline	HDS	56265	56279	14
		transition	HDS → SDS	56279	56291	12
		decline	SDS	56291	56300	9
		transition	SDS → IMS → SDS	56300	56309	9
		decline	SDS	56309	56312	3

Continued on Next Page...

Table A.4 – Continued

Source Name	Outburst ID	Stage	State(s)	$t_{\rm beg}$[a] (MJD)	$t_{\rm end}$[a] (MJD)	$t_{\rm dur}$[b] (days)
		transition	SDS → IMS → SDS	56312	-	1
		decline	SDS	56313	56319	6
		transition	SDS → IMS → SDS	56319	56325	6
		decline	SDS	56325	56328	3
		transition	SDS → IMS → SDS	56328	56330	2
		decline	SDS	56330	56332	2
		decline	HDS	56332	56341	9
		transition	HDS → IMS → HDS	56341	56350	9
		decline	HDS	56350	56371	21
		transition	HDS → IMS → HDS	56371	56381	10
		decline	HDS	56381	56396	15
		decline	SDS	56396	56405	9
		transition	SDS → HDS	56405	56455	50
		decline	HDS	56455	56459	4
		transition	HDS → IMS → HDS	56459	56467	8
		decline	HDS	56467	56491	24
		transition	HDS → IMS → HDS	56491	56498	7
		decline	HDS	56498	56505	7
		transition	HDS → IMS → HDS	56505	56508	3
		decline	HDS	56508	56528	20
		transition	HDS → IMS → HDS	56528	56537	9
		decline	HDS	56537	56570	33
		transition	HDS → IMS → HDS	56570	56580	10
		decline	HDS	56580	56593	13
		transition	HDS → IMS → HDS	56593	56600	7
		decline	HDS	56600	56603	3
		decline	SDS	56603	-	1
		transition	SDS → HDS	56604	56615	11
		decline	HDS	56615	56624	9
		transition	HDS → IMS → HDS	56624	56627	3
		decline	HDS	56627	56629	2
		transition	HDS → IMS → HDS	56629	56635	6
		decline	HDS	56635	56642	7
		transition	HDS → SDS	56642	56653	11
		decline	SDS	56653	-	1
		decline	-	56654	56784	130

Continued on Next Page...

Table A.4 – Continued

Source Name	Outburst ID	Stage	State(s)	$t_{\rm beg}$[a] (MJD)	$t_{\rm end}$[a] (MJD)	$t_{\rm dur}$[b] (days)
4U0540−697	1996-2014	rise	-	50087	50144	57
		transition	- → HDS	50144	50151	7
		rise	HDS	50151	50167	16
		rise	SDS	50167	-	1
		rise	HDS	50168	50177	9
		rise	SDS	50177	50185	8
		rise	HDS	50185	50200	15
		rise	SDS	50200	-	1
		rise	HDS	50201	50204	3
		rise	SDS	50204	-	1
		rise	HDS	50205	50210	5
		rise	SDS	50210	50218	8
		rise	HDS	50218	50242	24
		rise	SDS	50242	-	1
		rise	HDS	50243	50248	5
		transition	HDS → SDS	50248	-	1
		rise	SDS	50249	50252	3
		rise	HDS	50252	50273	21
		rise	SDS	50273	50278	5
		rise	HDS	50278	50290	12
		transition	HDS → IMS → HDS	50290	-	1
		rise	HDS	50291	50303	12
		transition	HDS → SDS	50303	50306	3
		rise	SDS	50306	50309	3
		rise	HDS	50309	50315	6
		rise	SDS	50315	50319	4
		rise	HDS	50319	50323	4
		rise	SDS	50323	50326	3
		rise	HDS	50326	50360	34
		rise	SDS	50360	50364	4
		rise	HDS	50364	50367	3
		rise	SDS	50367	50372	5
		rise	HDS	50372	50382	10
		rise	SDS	50382	50384	2
		rise	HDS	50384	50393	9
		transition	HDS → IMS → HDS	50393	50395	2
		rise	HDS	50395	50407	12

Continued on Next Page...

Table A.4 – Continued

Source Name	Outburst ID	Stage	State(s)	$t_{\rm beg}$[a] (MJD)	$t_{\rm end}$[a] (MJD)	$t_{\rm dur}$[b] (days)
		transition	HDS → IMS → HDS	50407	50414	7
		rise	HDS	50414	50429	15
		transition	HDS → SDS	50429	-	1
		rise	SDS	50430	-	1
		rise	HDS	50431	50471	40
		rise	SDS	50471	-	1
		rise	HDS	50472	50488	16
		rise	SDS	50488	50494	6
		rise	HDS	50494	50503	9
		transition	HDS → IMS → HDS	50503	50507	4
		rise	HDS	50507	50520	13
		rise	SDS	50520	50523	3
		rise	HDS	50523	50529	6
		transition	HDS → IMS → HDS	50529	50551	22
		rise	HDS	50551	50557	6
		transition	HDS → IMS → HDS	50557	50569	12
		rise	HDS	50569	50576	7
		transition	HDS → IMS → HDS	50576	50578	2
		rise	HDS	50578	50628	50
		transition	HDS → IMS → HDS	50628	50632	4
		rise	HDS	50632	50647	15
		rise	SDS	50647	50652	5
		rise	HDS	50652	50658	6
		rise	SDS	50658	50661	3
		transition	SDS → HDS	50661	-	1
		rise	HDS	50662	50685	23
		transition	HDS → IMS → HDS	50685	50692	7
		rise	HDS	50692	50698	6
		transition	HDS → SDS	50698	-	1
		rise	SDS	50699	50701	2
		rise	HDS	50701	50713	12
		transition	HDS → IMS → HDS	50713	50722	9
		rise	HDS	50722	50734	12
		transition	HDS → IMS → HDS	50734	50752	18
		rise	HDS	50752	50769	17
		transition	HDS → IMS → HDS	50769	50772	3
		rise	HDS	50772	50774	2

Continued on Next Page...

Table A.4 – Continued

Source Name	Outburst ID	Stage	State(s)	$t_{\rm beg}$[a] (MJD)	$t_{\rm end}$[a] (MJD)	$t_{\rm dur}$[b] (days)
		transition	HDS → IMS → HDS	50774	50777	3
		rise	HDS	50777	50781	4
		transition	HDS → IMS → HDS	50781	50783	2
		rise	HDS	50783	50787	4
		transition	HDS → IMS → HDS	50787	50803	16
		rise	HDS	50803	50822	19
		transition	HDS → IMS → HDS	50822	50824	2
		rise	HDS	50824	50844	20
		transition	HDS → SDS	50844	50869	25
		rise	SDS	50869	-	1
		rise	HDS	50870	50873	3
		transition	HDS → IMS → HDS	50873	50875	2
		rise	HDS	50875	50888	13
		rise	SDS	50888	50892	4
		rise	HDS	50892	50914	22
		rise	SDS	50914	50923	9
		rise	HDS	50923	50933	10
		transition	HDS → IMS → HDS	50933	50936	3
		rise	HDS	50936	50943	7
		transition	HDS → IMS → HDS	50943	-	1
		rise	HDS	50944	50948	4
		transition	HDS → IMS → HDS	50948	50954	6
		rise	HDS	50954	50963	9
		transition	HDS → SDS	50963	50968	5
		rise	SDS	50968	50972	4
		rise	HDS	50972	50986	14
		rise	SDS	50986	-	1
		rise	HDS	50987	50993	6
		rise	SDS	50993	-	1
		rise	HDS	50994	51001	7
		rise	SDS	51001	51018	17
		rise	HDS	51018	51023	5
		transition	HDS → IMS → HDS	51023	51046	23
		rise	HDS	51046	51080	34
		transition	HDS → IMS → HDS	51080	51082	2
		rise	HDS	51082	51086	4
		transition	HDS → IMS → HDS	51086	51095	9

Continued on Next Page...

Table A.4 – Continued

Source Name	Outburst ID	Stage	State(s)	$t_{\rm beg}$[a] (MJD)	$t_{\rm end}$[a] (MJD)	$t_{\rm dur}$[b] (days)
		rise	HDS	51095	51139	44
		transition	HDS → IMS → HDS	51139	51148	9
		rise	HDS	51148	51150	2
		transition	HDS → IMS → HDS	51150	51163	13
		rise	HDS	51163	51169	6
		rise	SDS	51169	51191	22
		rise	HDS	51191	51206	15
		rise	SDS	51206	51212	6
		rise	HDS	51212	51233	21
		rise	SDS	51233	-	1
		rise	HDS	51234	51250	16
		rise	SDS	51250	51277	27
		rise	HDS	51277	51288	11
		rise	SDS	51288	-	1
		rise	HDS	51289	51292	3
		transition	HDS → IMS → HDS	51292	51294	2
		rise	HDS	51294	51300	6
		rise	SDS	51300	51308	8
		transition	SDS → HDS	51308	-	1
		rise	HDS	51309	51312	3
		transition	HDS → IMS → HDS	51312	51320	8
		rise	HDS	51320	51325	5
		transition	HDS → IMS → HDS	51325	51339	14
		rise	HDS	51339	51364	25
		transition	HDS → IMS → HDS	51364	51366	2
		rise	HDS	51366	51375	9
		rise	SDS	51375	51402	27
		rise	HDS	51402	51414	12
		rise	SDS	51414	51419	5
		rise	HDS	51419	51422	3
		rise	SDS	51422	51434	12
		rise	HDS	51434	51443	9
		rise	SDS	51443	51445	2
		rise	HDS	51445	51448	3
		rise	SDS	51448	51453	5
		transition	SDS → IMS → SDS	51453	51458	5
		rise	SDS	51458	-	1

Continued on Next Page...

Table A.4 – Continued

Source Name	Outburst ID	Stage	State(s)	$t_{\rm beg}$[a] (MJD)	$t_{\rm end}$[a] (MJD)	$t_{\rm dur}$[b] (days)
		rise	HDS	51459	51462	3
		rise	SDS	51462	-	1
		rise	HDS	51463	51466	3
		rise	SDS	51466	-	1
		rise	HDS	51467	51469	2
		rise	SDS	51469	51472	3
		rise	HDS	51472	51485	13
		rise	SDS	51485	51488	3
		rise	HDS	51488	51501	13
		rise	SDS	51501	51506	5
		rise	HDS	51506	51509	3
		rise	SDS	51509	-	1
		rise	HDS	51510	51513	3
		rise	SDS	51513	51518	5
		rise	HDS	51518	51521	3
		rise	SDS	51521	51523	2
		rise	HDS	51523	51542	19
		rise	SDS	51542	51551	9
		rise	HDS	51551	51558	7
		rise	SDS	51558	51560	2
		transition	SDS → IMS → SDS	51560	-	1
		rise	SDS	51561	51563	2
		rise	HDS	51563	51567	4
		rise	SDS	51567	-	1
		rise	HDS	51568	51602	34
		transition	HDS → IMS → HDS	51602	51604	2
		rise	HDS	51604	51606	2
		rise	SDS	51606	51629	23
		rise	HDS	51629	51655	26
		transition	HDS → IMS → HDS	51655	51664	9
		rise	HDS	51664	51672	8
		transition	HDS → IMS → HDS	51672	51676	4
		rise	HDS	51676	51680	4
		transition	HDS → IMS → HDS	51680	51683	3
		rise	HDS	51683	51722	39
		transition	HDS → IMS → HDS	51722	51724	2
		rise	HDS	51724	51728	4

Continued on Next Page...

Table A.4 – Continued

Source Name	Outburst ID	Stage	State(s)	$t_{\rm beg}$[a] (MJD)	$t_{\rm end}$[a] (MJD)	$t_{\rm dur}$[b] (days)
		transition	HDS → IMS → HDS	51728	51735	7
		rise	HDS	51735	51748	13
		transition	HDS → IMS → HDS	51748	51759	11
		rise	HDS	51759	51783	24
		rise	SDS	51783	-	1
		rise	HDS	51784	51793	9
		transition	HDS → IMS → HDS	51793	51801	8
		rise	HDS	51801	51814	13
		transition	HDS → IMS → HDS	51814	-	1
		rise	HDS	51815	51836	21
		transition	HDS → IMS → HDS	51836	51874	38
		rise	HDS	51874	51878	4
		rise	SDS	51878	51885	7
		rise	HDS	51885	51888	3
		rise	SDS	51888	51890	2
		rise	HDS	51890	51892	2
		transition	HDS → IMS → HDS	51892	51898	6
		rise	HDS	51898	51901	3
		rise	SDS	51901	-	1
		rise	HDS	51902	51929	27
		rise	SDS	51929	-	1
		rise	HDS	51930	51934	4
		rise	SDS	51934	-	1
		rise	HDS	51935	51966	31
		rise	SDS	51966	51970	4
		rise	HDS	51970	51987	17
		rise	SDS	51987	51995	8
		rise	HDS	51995	51997	2
		transition	HDS → IMS → HDS	51997	52004	7
		rise	HDS	52004	52017	13
		transition	HDS → IMS → HDS	52017	52019	2
		rise	HDS	52019	52034	15
		transition	HDS → SDS	52034	-	1
		rise	SDS	52035	52037	2
		rise	HDS	52037	52044	7
		transition	HDS → IMS → HDS	52044	52046	2
		rise	HDS	52046	52050	4

Continued on Next Page...

Table A.4 – Continued

Source Name	Outburst ID	Stage	State(s)	$t_{\rm beg}$[a] (MJD)	$t_{\rm end}$[a] (MJD)	$t_{\rm dur}$[b] (days)
		rise	SDS	52050	-	1
		rise	HDS	52051	52053	2
		rise	SDS	52053	-	1
		rise	HDS	52054	52059	5
		transition	HDS → IMS → HDS	52059	52072	13
		rise	HDS	52072	52083	11
		rise	SDS	52083	52085	2
		rise	HDS	52085	52088	3
		rise	SDS	52088	-	1
		rise	HDS	52089	52100	11
		rise	SDS	52100	52105	5
		rise	HDS	52105	52109	4
		rise	SDS	52109	52118	9
		decline	SDS	52118	52148	30
		decline	HDS	52148	52150	2
		decline	SDS	52150	52152	2
		decline	HDS	52152	52154	2
		decline	SDS	52154	52157	3
		decline	HDS	52157	52160	3
		decline	SDS	52160	52163	3
		decline	HDS	52163	52166	3
		decline	SDS	52166	52169	3
		decline	HDS	52169	52172	3
		transition	HDS → IMS → HDS	52172	52193	21
		decline	HDS	52193	52197	4
		transition	HDS → IMS → HDS	52197	52200	3
		decline	HDS	52200	52203	3
		decline	SDS	52203	52206	3
		transition	SDS → HDS	52206	52212	6
		decline	HDS	52212	52246	34
		transition	HDS → IMS → HDS	52246	-	1
		decline	HDS	52247	52257	10
		transition	HDS → IMS → HDS	52257	52259	2
		decline	HDS	52259	52263	4
		transition	HDS → IMS → HDS	52263	-	1
		decline	HDS	52264	52275	11
		decline	SDS	52275	52292	17

Continued on Next Page...

Table A.4 – Continued

Source Name	Outburst ID	Stage	State(s)	$t_{\rm beg}$[a] (MJD)	$t_{\rm end}$[a] (MJD)	$t_{\rm dur}$[b] (days)
		decline	HDS	52292	52306	14
		decline	SDS	52306	-	1
		decline	HDS	52307	52315	8
		decline	SDS	52315	52333	18
		decline	HDS	52333	52336	3
		decline	SDS	52336	52338	2
		decline	HDS	52338	52348	10
		transition	HDS → IMS → HDS	52348	52353	5
		decline	HDS	52353	52357	4
		transition	HDS → IMS → HDS	52357	52359	2
		decline	HDS	52359	52362	3
		transition	HDS → SDS	52362	52372	10
		decline	SDS	52372	52386	14
		decline	HDS	52386	52391	5
		decline	SDS	52391	52396	5
		decline	HDS	52396	52403	7
		decline	SDS	52403	-	1
		decline	HDS	52404	52407	3
		decline	SDS	52407	-	1
		decline	HDS	52408	52414	6
		decline	SDS	52414	52438	24
		decline	HDS	52438	52440	2
		decline	SDS	52440	-	1
		decline	HDS	52441	52446	5
		decline	SDS	52446	52448	2
		decline	HDS	52448	52455	7
		transition	HDS → IMS → HDS	52455	-	1
		decline	HDS	52456	52458	2
		transition	HDS → IMS → HDS	52458	-	1
		decline	HDS	52459	52464	5
		transition	HDS → IMS → HDS	52464	-	1
		decline	HDS	52465	52467	2
		transition	HDS → IMS → HDS	52467	52483	16
		decline	HDS	52483	52489	6
		transition	HDS → IMS → HDS	52489	52497	8
		decline	HDS	52497	52503	6
		transition	HDS → IMS → HDS	52503	52515	12

Continued on Next Page...

Table A.4 – Continued

Source Name	Outburst ID	Stage	State(s)	$t_{\rm beg}$[a] (MJD)	$t_{\rm end}$[a] (MJD)	$t_{\rm dur}$[b] (days)
		decline	HDS	52515	52517	2
		transition	HDS → IMS → HDS	52517	52530	13
		decline	HDS	52530	52546	16
		transition	HDS → IMS → HDS	52546	52553	7
		decline	HDS	52553	52556	3
		transition	HDS → IMS → HDS	52556	52560	4
		decline	HDS	52560	52563	3
		transition	HDS → IMS → HDS	52563	52600	37
		decline	HDS	52600	52602	2
		transition	HDS → IMS → HDS	52602	52605	3
		decline	HDS	52605	52612	7
		decline	SDS	52612	52616	4
		decline	HDS	52616	52635	19
		decline	SDS	52635	52645	10
		decline	HDS	52645	52654	9
		decline	SDS	52654	-	1
		decline	HDS	52655	52658	3
		decline	SDS	52658	-	1
		decline	HDS	52659	52675	16
		transition	HDS → IMS → HDS	52675	52692	17
		decline	HDS	52692	52697	5
		transition	HDS → IMS → HDS	52697	52716	19
		decline	HDS	52716	52718	2
		transition	HDS → IMS → HDS	52718	52731	13
		decline	HDS	52731	52741	10
		transition	HDS → IMS → HDS	52741	52743	2
		decline	HDS	52743	52746	3
		transition	HDS → IMS → HDS	52746	52750	4
		decline	HDS	52750	52753	3
		transition	HDS → IMS → HDS	52753	52760	7
		decline	HDS	52760	52765	5
		decline	SDS	52765	52767	2
		decline	HDS	52767	52771	4
		transition	HDS → IMS → HDS	52771	-	1
		decline	HDS	52772	52778	6
		transition	HDS → IMS → HDS	52778	52807	29
		decline	HDS	52807	52810	3

Continued on Next Page...

Table A.4 – Continued

Source Name	Outburst ID	Stage	State(s)	$t_{\rm beg}$[a] (MJD)	$t_{\rm end}$[a] (MJD)	$t_{\rm dur}$[b] (days)
		transition	HDS → IMS → HDS	52810	52822	12
		decline	HDS	52822	52827	5
		transition	HDS → IMS → HDS	52827	52838	11
		decline	HDS	52838	52865	27
		transition	HDS → IMS → HDS	52865	52867	2
		decline	HDS	52867	52876	9
		decline	SDS	52876	52883	7
		decline	HDS	52883	52916	33
		decline	SDS	52916	52919	3
		decline	HDS	52919	52923	4
		decline	SDS	52923	52925	2
		decline	HDS	52925	52929	4
		decline	SDS	52929	52938	9
		decline	HDS	52938	52961	23
		decline	SDS	52961	52975	14
		decline	HDS	52975	52983	8
		transition	HDS → SDS	52983	52985	2
		decline	SDS	52985	52994	9
		decline	HDS	52994	53008	14
		decline	SDS	53008	-	1
		transition	SDS → HDS	53009	53012	3
		decline	HDS	53012	53021	9
		transition	HDS → IMS → HDS	53021	53025	4
		decline	HDS	53025	53028	3
		transition	HDS → SDS	53028	53032	4
		decline	SDS	53032	53049	17
		decline	HDS	53049	53057	8
		transition	HDS → IMS → HDS	53057	53061	4
		decline	HDS	53061	53067	6
		transition	HDS → IMS → HDS	53067	53072	5
		decline	HDS	53072	53074	2
		transition	HDS → IMS → HDS	53074	-	1
		decline	HDS	53075	53109	34
		transition	HDS → IMS → HDS	53109	53116	7
		decline	HDS	53116	53120	4
		transition	HDS → IMS → HDS	53120	53122	2
		decline	HDS	53122	53130	8

Continued on Next Page...

Table A.4 – Continued

Source Name	Outburst ID	Stage	State(s)	$t_{\rm beg}$[a] (MJD)	$t_{\rm end}$[a] (MJD)	$t_{\rm dur}$[b] (days)
		transition	HDS → IMS → HDS	53130	53132	2
		decline	HDS	53132	53162	30
		transition	HDS → SDS	53162	53166	4
		decline	SDS	53166	-	1
		decline	HDS	53167	53173	6
		decline	SDS	53173	53175	2
		transition	SDS → HDS	53175	-	1
		decline	HDS	53176	53182	6
		transition	HDS → IMS → HDS	53182	53187	5
		decline	HDS	53187	53193	6
		transition	HDS → IMS → HDS	53193	53225	32
		decline	HDS	53225	53232	7
		transition	HDS → IMS → HDS	53232	53254	22
		decline	HDS	53254	53268	14
		transition	HDS → IMS → HDS	53268	53271	3
		decline	HDS	53271	53280	9
		transition	HDS → IMS → HDS	53280	-	1
		decline	HDS	53281	53283	2
		decline	SDS	53283	53316	33
		decline	HDS	53316	53318	2
		decline	SDS	53318	53321	3
		decline	HDS	53321	53326	5
		transition	HDS → IMS → HDS	53326	-	1
		decline	HDS	53327	53334	7
		decline	SDS	53334	53336	2
		decline	HDS	53336	53371	35
		transition	HDS → IMS → HDS	53371	53376	5
		decline	HDS	53376	53380	4
		transition	HDS → IMS → HDS	53380	53383	3
		decline	HDS	53383	53398	15
		transition	HDS → IMS → HDS	53398	53403	5
		decline	HDS	53403	53416	13
		decline	SDS	53416	53419	3
		transition	SDS → HDS	53419	53424	5
		decline	HDS	53424	53430	6
		decline	SDS	53430	-	1
		decline	HDS	53431	53436	5

Continued on Next Page...

Table A.4 – Continued

Source Name	Outburst ID	Stage	State(s)	$t_{\rm beg}$[a] (MJD)	$t_{\rm end}$[a] (MJD)	$t_{\rm dur}$[b] (days)
		transition	HDS → SDS	53436	53464	28
		decline	SDS	53464	53482	18
		transition	SDS → IMS → SDS	53482	53486	4
		decline	SDS	53486	53528	42
		decline	HDS	53528	53573	45
		decline	SDS	53573	53580	7
		transition	SDS → HDS	53580	53584	4
		decline	HDS	53584	53588	4
		transition	HDS → IMS → HDS	53588	-	1
		decline	HDS	53589	53608	19
		decline	SDS	53608	53620	12
		transition	SDS → HDS	53620	53626	6
		decline	HDS	53626	53634	8
		decline	SDS	53634	53664	30
		transition	SDS → IMS → SDS	53664	53669	5
		decline	SDS	53669	53703	34
		transition	SDS → HDS	53703	53717	14
		decline	HDS	53717	53726	9
		transition	HDS → SDS	53726	53733	7
		decline	SDS	53733	53743	10
		decline	HDS	53743	53775	32
		decline	SDS	53775	53787	12
		decline	HDS	53787	53791	4
		transition	HDS → IMS → HDS	53791	-	1
		decline	HDS	53792	53797	5
		transition	HDS → IMS → HDS	53797	53835	38
		decline	HDS	53835	53837	2
		transition	HDS → IMS → HDS	53837	53857	20
		decline	HDS	53857	53876	19
		decline	SDS	53876	53957	81
		transition	SDS → IMS → SDS	53957	53963	6
		decline	SDS	53963	53992	29
		transition	SDS → IMS → SDS	53992	54010	18
		decline	SDS	54010	54029	19
		transition	SDS → IMS → SDS	54029	54063	34
		decline	SDS	54063	54115	52
		transition	SDS → IMS → SDS	54115	54127	12

Continued on Next Page...

Table A.4 – Continued

Source Name	Outburst ID	Stage	State(s)	$t_{\rm beg}$[a] (MJD)	$t_{\rm end}$[a] (MJD)	$t_{\rm dur}$[b] (days)
		decline	SDS	54127	54141	14
		transition	SDS → IMS → SDS	54141	54164	23
		decline	SDS	54164	54182	18
		transition	SDS → IMS → SDS	54182	54248	66
		decline	SDS	54248	54268	20
		transition	SDS → IMS → SDS	54268	54316	48
		decline	SDS	54316	54338	22
		transition	SDS → IMS → SDS	54338	54361	23
		decline	SDS	54361	54375	14
		decline	HDS	54375	54397	22
		decline	SDS	54397	54406	9
		decline	HDS	54406	54430	24
		decline	SDS	54430	54437	7
		decline	HDS	54437	54443	6
		decline	SDS	54443	54445	2
		transition	SDS → HDS	54445	54450	5
		decline	HDS	54450	54499	49
		transition	HDS → IMS → HDS	54499	54501	2
		decline	HDS	54501	54503	2
		transition	HDS → IMS → HDS	54503	54548	45
		decline	HDS	54548	54550	2
		transition	HDS → IMS → HDS	54550	54580	30
		decline	HDS	54580	54605	25
		transition	HDS → SDS	54605	54655	50
		decline	SDS	54655	54728	73
		transition	SDS → HDS	54728	54786	58
		decline	HDS	54786	54816	30
		transition	HDS → IMS → HDS	54816	54832	16
		decline	HDS	54832	54837	5
		transition	HDS → IMS → HDS	54837	54846	9
		decline	HDS	54846	54852	6
		transition	HDS → IMS → HDS	54852	54898	46
		decline	HDS	54898	54901	3
		transition	HDS → IMS → HDS	54901	54904	3
		decline	HDS	54904	54915	11
		transition	HDS → SDS	54915	54953	38
		decline	SDS	54953	54965	12

Continued on Next Page...

Table A.4 – Continued

Source Name	Outburst ID	Stage	State(s)	$t_{\rm beg}$[a] (MJD)	$t_{\rm end}$[a] (MJD)	$t_{\rm dur}$[b] (days)
		transition	SDS → IMS → SDS	54965	55101	136
		decline	SDS	55101	55105	4
		transition	SDS → IMS → SDS	55105	-	1
		decline	SDS	55106	55126	20
		transition	SDS → IMS → SDS	55126	55142	16
		decline	SDS	55142	55149	7
		transition	SDS → IMS → SDS	55149	55155	6
		decline	SDS	55155	55186	31
		transition	SDS → IMS → SDS	55186	55192	6
		decline	SDS	55192	55196	4
		transition	SDS → IMS → SDS	55196	55199	3
		decline	SDS	55199	55203	4
		transition	SDS → IMS → SDS	55203	55487	284
		decline	SDS	55487	55512	25
		transition	SDS → IMS → SDS	55512	55515	3
		decline	SDS	55515	55519	4
		transition	SDS → IMS → SDS	55519	55524	5
		decline	SDS	55524	55552	28
		transition	SDS → HDS	55552	55583	31
		decline	HDS	55583	55590	7
		transition	HDS → IMS → HDS	55590	55600	10
		decline	HDS	55600	55603	3
		transition	HDS → IMS → HDS	55603	55608	5
		decline	HDS	55608	55614	6
		transition	HDS → IMS → HDS	55614	55618	4
		decline	HDS	55618	55636	18
		transition	HDS → IMS → HDS	55636	55644	8
		decline	HDS	55644	55654	10
		transition	HDS → IMS → HDS	55654	55724	70
		decline	HDS	55724	55745	21
		transition	HDS → IMS → HDS	55745	55780	35
		decline	HDS	55780	55795	15
		transition	HDS → IMS → HDS	55795	55798	3
		decline	HDS	55798	55811	13
		transition	HDS → IMS → HDS	55811	55814	3
		decline	HDS	55814	55825	11
		transition	HDS → IMS → HDS	55825	55831	6

Continued on Next Page...

Table A.4 – Continued

Source Name	Outburst ID	Stage	State(s)	$t_{\rm beg}$[a] (MJD)	$t_{\rm end}$[a] (MJD)	$t_{\rm dur}$[b] (days)
		decline	HDS	55831	55850	19
		transition	HDS → IMS → HDS	55850	55867	17
		decline	HDS	55867	55876	9
		decline	SDS	55876	55879	3
		decline	HDS	55879	55885	6
		decline	SDS	55885	-	1
		decline	HDS	55886	55891	5
		decline	SDS	55891	-	1
		decline	HDS	55892	55900	8
		decline	SDS	55900	-	1
		decline	HDS	55901	55906	5
		transition	HDS → IMS → HDS	55906	55908	2
		decline	HDS	55908	55917	9
		transition	HDS → IMS → HDS	55917	-	1
		decline	HDS	55918	55921	3
		transition	HDS → IMS → HDS	55921	-	1
		decline	HDS	55922	55932	10
		transition	HDS → IMS → HDS	55932	55941	9
		decline	HDS	55941	55966	25
		transition	HDS → IMS → HDS	55966	55969	3
		decline	HDS	55969	55988	19
		transition	HDS → IMS → HDS	55988	56003	15
		decline	HDS	56003	56009	6
		transition	HDS → IMS → HDS	56009	56011	2
		decline	HDS	56011	56022	11
		transition	HDS → IMS → HDS	56022	56045	23
		decline	HDS	56045	56062	17
		transition	HDS → IMS → HDS	56062	56119	57
		decline	HDS	56119	56188	69
		transition	HDS → IMS → HDS	56188	56201	13
		decline	HDS	56201	56206	5
		transition	HDS → IMS → HDS	56206	56210	4
		decline	HDS	56210	56216	6
		decline	SDS	56216	56222	6
		decline	HDS	56222	56231	9
		decline	SDS	56231	56236	5
		decline	HDS	56236	56241	5

Continued on Next Page...

Table A.4 – Continued

Source Name	Outburst ID	Stage	State(s)	$t_{\rm beg}$[a] (MJD)	$t_{\rm end}$[a] (MJD)	$t_{\rm dur}$[b] (days)
		transition	HDS → IMS → HDS	56241	56246	5
		decline	HDS	56246	56250	4
		transition	HDS → IMS → HDS	56250	56255	5
		decline	HDS	56255	56258	3
		transition	HDS → IMS → HDS	56258	56270	12
		decline	HDS	56270	56279	9
		decline	SDS	56279	56284	5
		decline	HDS	56284	56307	23
		transition	HDS → IMS → HDS	56307	56312	5
		decline	HDS	56312	56317	5
		transition	HDS → IMS → HDS	56317	56326	9
		decline	HDS	56326	56348	22
		transition	HDS → SDS	56348	56356	8
		decline	SDS	56356	56359	3
		decline	HDS	56359	56365	6
		decline	SDS	56365	56371	6
		decline	HDS	56371	56381	10
		decline	SDS	56381	-	1
		decline	HDS	56382	56448	66
		decline	SDS	56448	56494	46
		decline	HDS	56494	56561	67
		decline	SDS	56561	56567	6
		transition	SDS → IMS → SDS	56567	56572	5
		decline	SDS	56572	56575	3
		transition	SDS → IMS → SDS	56575	56579	4
		decline	SDS	56579	56582	3
		decline	HDS	56582	56600	18
		transition	HDS → SDS	56600	56602	2
		decline	SDS	56602	-	1
		decline	HDS	56603	56609	6
		decline	SDS	56609	56612	3
		transition	SDS → IMS → SDS	56612	56616	4
		decline	SDS	56616	56620	4
		transition	SDS → IMS → SDS	56620	56622	2
		decline	SDS	56622	56625	3
		transition	SDS → IMS → SDS	56625	56631	6
		decline	SDS	56631	56650	19

Continued on Next Page...

Table A.4 – Continued

Source Name	Outburst ID	Stage	State(s)	$t_{\rm beg}$[a] (MJD)	$t_{\rm end}$[a] (MJD)	$t_{\rm dur}$[b] (days)
		transition	SDS → -	56650	56655	5
		decline	-	56655	56750	95
XTEJ1118+480	1999/2000	rise	-	51538	51547	9
		rise	HDS	51547	51668	121
		decline	HDS	51668	51730	62
		decline	-	51730	51741	11
MAXIJ1305−704	2012	rise	-	56009	56022	13
		rise	HDS	56022	56028	6
		decline	HDS	56028	56039	11
		transition	HDS → IMS → HDS	56039	56046	7
		decline	HDS	56046	56051	5
		transition	HDS → IMS → HDS	56051	56054	3
		decline	HDS	56054	56084	30
		transition	HDS → IMS → HDS	56084	56095	11
		decline	HDS	56095	56097	2
		transition	HDS → -	56097	56117	20
		decline	-	56117	56191	74
SWIFTJ1357.2−0933	2010-2012	rise	-	55276	55590	314
		decline	HDS	55590	55610	20
		decline	-	55610	56112	502
GS1354−64	1997/1998	rise	-	50714	50727	13
		rise	HDS	50727	50776	49
		decline	HDS	50776	50836	60
		decline	-	50836	50871	35
SWIFTJ1539.2−6227	2008/2009	rise	-	54792	54799	7
		rise	HDS	54799	54804	5
		transition	HDS → IMS → HDS	54804	54829	25
		decline	HDS	54829	54835	6
		transition	HDS → IMS → HDS	54835	-	1
		decline	HDS	54836	54842	6
		transition	HDS → SDS	54842	54850	8

Continued on Next Page...

Table A.4 – Continued

Source Name	Outburst ID	Stage	State(s)	$t_{\rm beg}$[a] (MJD)	$t_{\rm end}$[a] (MJD)	$t_{\rm dur}$[b] (days)
		decline	SDS	54850	-	1
		transition	SDS → HDS	54851	54856	5
		decline	HDS	54856	54885	29
		transition	HDS → IMS → HDS	54885	54891	6
		decline	HDS	54891	54922	31
		decline	-	54922	54967	45
MAXIJ1543−564	2011	rise	-	55681	55687	6
		rise	HDS	55687	55699	12
		transition	HDS → IMS → HDS	55699	-	1
		rise	HDS	55700	55706	6
		decline	HDS	55706	55707	1
		transition	HDS → IMS → HDS	55707	-	1
		decline	HDS	55708	55714	6
		transition	HDS → IMS → HDS	55714	55718	4
		decline	HDS	55718	55729	11
		transition	HDS → SDS	55729	55739	10
		decline	SDS	55739	55742	3
		transition	SDS → HDS	55742	55744	2
		decline	HDS	55744	55748	4
		transition	HDS → -	55748	55752	4
		decline	-	55752	55834	82
4U1543−475	2002	rise	-	52435	52441	6
		rise	HDS	52441	52444	3
		rise	SDS	52444	52446	2
		decline	SDS	52446	52451	5
		transition	SDS → IMS → SDS	52451	-	1
		decline	SDS	52452	52465	13
		transition	SDS → HDS	52465	52478	13
		decline	HDS	52478	52481	3
		transition	HDS → IMS → HDS	52481	-	1
		decline	HDS	52482	52488	6
		decline	-	52488	-	1
XTEJ1550−564	1998/1999	rise	HDS	51062	51117	55
		transition	HDS → SDS	51117	-	1

Continued on Next Page...

Table A.4 – Continued

Source Name	Outburst ID	Stage	State(s)	$t_{\rm beg}$[a] (MJD)	$t_{\rm end}$[a] (MJD)	$t_{\rm dur}$[b] (days)
		decline	SDS	51118	51122	4
		transition	SDS → IMS → SDS	51122	51155	33
		decline	SDS	51155	51166	11
		transition	SDS → IMS → SDS	51166	-	1
		decline	SDS	51167	51169	2
		decline	HDS	51169	51176	7
		transition	HDS → IMS → HDS	51176	-	1
		decline	HDS	51177	51261	84
		transition	HDS → SDS	51261	51263	2
		decline	SDS	51263	51265	2
		transition	SDS → IMS → SDS	51265	-	1
		decline	SDS	51266	51268	2
		transition	SDS → IMS → SDS	51268	51273	5
		decline	SDS	51273	51288	15
		transition	SDS → HDS	51288	51290	2
		decline	HDS	51290	51293	3
		transition	HDS → SDS	51293	51295	2
		decline	SDS	51295	51297	2
		decline	HDS	51297	51308	11
		decline	-	51308	51317	9
	2000	rise	-	51597	51605	8
		rise	HDS	51605	51663	58
		decline	HDS	51663	51693	30
		decline	-	51693	51704	11
	2001	rise	-	51934	51940	6
		rise	HDS	51940	51960	20
		decline	HDS	51960	51973	13
		decline	-	51973	51984	11
	2001/2002	rise	-	52261	-	1
		rise	HDS	52262	52279	17
		decline	HDS	52279	52295	16
		decline	-	52295	52313	18
	2003	rise	-	52726	-	1
		rise	HDS	52727	52739	12
		decline	HDS	52739	52754	15
		decline	-	52754	52776	22

Continued on Next Page...

Table A.4 – Continued

Source Name	Outburst ID	Stage	State(s)	$t_{\rm beg}$[a] (MJD)	$t_{\rm end}$[a] (MJD)	$t_{\rm dur}$[b] (days)
4U1630−472	1996	rise	-	50134	50154	20
		transition	- → HDS	50154	50157	3
		rise	HDS	50157	50265	108
		decline	HDS	50265	50308	43
		transition	HDS → -	50308	-	1
		decline	-	50309	50334	25
	1998	rise	-	50840	50849	9
		rise	HDS	50849	50868	19
		decline	HDS	50868	50949	81
		decline	-	50949	51080	131
	1999	rise	-	51221	51300	79
		rise	HDS	51300	51360	60
		decline	HDS	51360	51389	29
		decline	-	51389	51397	8
	2000/2001	rise	-	51842	51859	17
		rise	HDS	51859	51885	26
		decline	HDS	51885	52055	170
		decline	-	52055	52076	21
	2002-2004	rise	-	52514	52526	12
		rise	HDS	52526	52628	102
		decline	HDS	52628	53308	680
		decline	-	53308	53335	27
	2005/2006	rise	-	53700	53717	17
		rise	HDS	53717	53758	41
		rise	SDS	53758	53777	19
		decline	SDS	53777	53855	78
		decline	HDS	53855	53864	9
		transition	HDS → IMS → HDS	53864	-	1
		decline	HDS	53865	53872	7
		decline	-	53872	53884	12
	2007/2008	rise	-	54453	54462	9
		rise	HDS	54462	54480	18
		rise	SDS	54480	54491	11
		decline	SDS	54491	54623	132

Continued on Next Page...

Table A.4 – Continued

Source Name	Outburst ID	Stage	State(s)	$t_{\rm beg}$[a] (MJD)	$t_{\rm end}$[a] (MJD)	$t_{\rm dur}$[b] (days)
		transition	SDS → -	54623	54630	7
		decline	-	54630	54653	23
	2009/2010	rise	-	55178	55194	16
		rise	HDS	55194	55197	3
		transition	HDS → SDS	55197	55200	3
		rise	SDS	55200	55205	5
		transition	SDS → IMS → SDS	55205	55207	2
		rise	SDS	55207	55220	13
		decline	SDS	55220	55224	4
		transition	SDS → IMS → SDS	55224	55228	4
		decline	SDS	55228	55243	15
		transition	SDS → HDS	55243	55253	10
		decline	HDS	55253	55256	3
		transition	HDS → IMS → HDS	55256	55261	5
		decline	HDS	55261	-	1
		transition	HDS → SDS	55262	55270	8
		decline	SDS	55270	55386	116
		transition	SDS → HDS	55386	55416	30
		decline	HDS	55416	55422	6
		decline	-	55422	55430	8
	2011-2013	rise	-	55907	55915	8
		rise	SDS	55915	55927	12
		decline	SDS	55927	56050	123
		decline	HDS	56050	56097	47
		transition	HDS → SDS	56097	56103	6
		decline	SDS	56103	56107	4
		transition	SDS → IMS → SDS	56107	56119	12
		decline	SDS	56119	56196	77
		transition	SDS → IMS → SDS	56196	56207	11
		decline	SDS	56207	56400	193
		transition	SDS → HDS	56400	56415	15
		decline	HDS	56415	56464	49
		transition	HDS → SDS	56464	56466	2
		decline	SDS	56466	56556	90
		decline	-	56556	56601	45

Continued on Next Page...

Table A.4 – Continued

Source Name	Outburst ID	Stage	State(s)	$t_{\rm beg}$[a] (MJD)	$t_{\rm end}$[a] (MJD)	$t_{\rm dur}$[b] (days)
XTEJ1650−500	2001	rise	-	52149	52156	7
		rise	HDS	52156	52162	6
		decline	HDS	52162	52173	11
		transition	HDS → SDS	52173	-	1
		decline	SDS	52174	52189	15
		transition	SDS → IMS → SDS	52189	-	1
		decline	SDS	52190	52227	37
		transition	SDS → HDS	52227	52234	7
		decline	HDS	52234	-	1
		decline	-	52235	52257	22
XTEJ1652−453	2009	rise	-	54990	55010	20
		rise	SDS	55010	55015	5
		decline	SDS	55015	55047	32
		transition	SDS → HDS	55047	55067	20
		decline	HDS	55067	55117	50
		transition	HDS → IMS → HDS	55117	55124	7
		decline	HDS	55124	55128	4
		decline	-	55128	55159	31
GROJ1655−40	1996/1997	rise	-	50184	50198	14
		transition	- → HDS	50198	50204	6
		rise	HDS	50204	50285	81
		decline	HDS	50285	50413	128
		transition	HDS → IMS → HDS	50413	50437	24
		decline	HDS	50437	50446	9
		transition	HDS → IMS → HDS	50446	50456	10
		decline	HDS	50456	50460	4
		transition	HDS → SDS	50460	-	1
		decline	SDS	50461	50470	9
		transition	SDS → IMS → SDS	50470	-	1
		decline	SDS	50471	50473	2
		transition	SDS → IMS → SDS	50473	50475	2
		decline	SDS	50475	50480	5
		transition	SDS → HDS	50480	50487	7
		decline	HDS	50487	50489	2
		transition	HDS → IMS → HDS	50489	50496	7

Continued on Next Page...

Table A.4 – Continued

Source Name	Outburst ID	Stage	State(s)	$t_{\rm beg}$[a] (MJD)	$t_{\rm end}$[a] (MJD)	$t_{\rm dur}$[b] (days)
		decline	HDS	50496	50498	2
		transition	HDS → IMS → HDS	50498	50500	2
		decline	HDS	50500	50520	20
		transition	HDS → IMS → HDS	50520	-	1
		decline	HDS	50521	50636	115
		transition	HDS → IMS → HDS	50636	-	1
		decline	HDS	50637	50643	6
		transition	HDS → IMS → HDS	50643	50646	3
		decline	HDS	50646	50654	8
		transition	HDS → SDS	50654	50661	7
		decline	SDS	50661	50670	9
		decline	HDS	50670	50676	6
		decline	-	50676	50691	15
	2005	rise	-	53398	53418	20
		rise	HDS	53418	53442	24
		rise	SDS	53442	53509	67
		decline	SDS	53509	53627	118
		decline	HDS	53627	53648	21
		decline	-	53648	53679	31
MAXIJ1659−152	2010/2011	rise	-	55458	55465	7
		rise	HDS	55465	55472	7
		transition	HDS → SDS	55472	55476	4
		rise	SDS	55476	-	1
		rise	HDS	55477	55478	1
		decline	HDS	55478	55479	1
		transition	HDS → SDS	55479	55482	3
		decline	SDS	55482	55484	2
		transition	SDS → IMS → SDS	55484	55486	2
		decline	SDS	55486	55491	5
		transition	SDS → HDS	55491	55525	34
		decline	HDS	55525	55545	20
		transition	HDS → SDS	55545	55576	31
		decline	SDS	55576	55586	10
		transition	SDS → IMS → SDS	55586	55591	5
		decline	SDS	55591	-	1
		decline	-	55592	-	1

Continued on Next Page...

Table A.4 – Continued

Source Name	Outburst ID	Stage	State(s)	$t_{\rm beg}$ [a] (MJD)	$t_{\rm end}$ [a] (MJD)	$t_{\rm dur}$ [b] (days)
GX339−4	1996	rise	-	50259	50272	13
		rise	HDS	50272	50285	13
		decline	HDS	50285	50307	22
		decline	-	50307	50334	27
	1997-1999	rise	-	50456	50469	13
		rise	HDS	50469	50818	349
		transition	HDS → SDS	50818	50827	9
		rise	SDS	50827	50885	58
		decline	SDS	50885	51053	168
		transition	SDS → IMS → SDS	51053	-	1
		decline	SDS	51054	51157	103
		transition	SDS → HDS	51157	51189	32
		decline	HDS	51189	51215	26
		decline	-	51215	51296	81
	2002/2003	rise	-	52363	52366	3
		rise	HDS	52366	52409	43
		transition	HDS → IMS → HDS	52409	-	1
		rise	HDS	52410	52413	3
		transition	HDS → SDS	52413	-	1
		rise	SDS	52414	52416	2
		transition	SDS → HDS	52416	-	1
		rise	HDS	52417	52419	2
		transition	HDS → SDS	52419	52422	3
		rise	SDS	52422	52430	8
		transition	SDS → IMS → SDS	52430	-	1
		rise	SDS	52431	52435	4
		transition	SDS → IMS → SDS	52435	52438	3
		rise	SDS	52438	52465	27
		transition	SDS → IMS → SDS	52465	52467	2
		rise	SDS	52467	52503	36
		transition	SDS → IMS → SDS	52503	-	1
		rise	SDS	52504	52508	4
		transition	SDS → IMS → SDS	52508	52511	3
		rise	SDS	52511	52520	9
		decline	SDS	52520	52522	2

Continued on Next Page...

Table A.4 – Continued

Source Name	Outburst ID	Stage	State(s)	$t_{\rm beg}$[a] (MJD)	$t_{\rm end}$[a] (MJD)	$t_{\rm dur}$[b] (days)
		transition	SDS → HDS	52522	52525	3
		decline	HDS	52525	52527	2
		transition	HDS → IMS → HDS	52527	52531	4
		decline	HDS	52531	52535	4
		transition	HDS → SDS	52535	52537	2
		decline	SDS	52537	52545	8
		transition	SDS → IMS → SDS	52545	52547	2
		decline	SDS	52547	52558	11
		transition	SDS → IMS → SDS	52558	-	1
		decline	SDS	52559	52656	97
		transition	SDS → IMS → SDS	52656	52670	14
		decline	SDS	52670	52693	23
		transition	SDS → IMS → SDS	52693	52695	2
		decline	SDS	52695	52697	2
		decline	HDS	52697	52702	5
		transition	HDS → IMS → HDS	52702	52706	4
		decline	HDS	52706	52711	5
		transition	HDS → IMS → HDS	52711	52714	3
		decline	HDS	52714	52739	25
		decline	-	52739	52751	12
	2004/2005	rise	-	53079	53088	9
		rise	HDS	53088	53233	145
		transition	HDS → SDS	53233	53240	7
		rise	SDS	53240	53260	20
		transition	SDS → IMS → SDS	53260	53263	3
		rise	SDS	53263	53267	4
		transition	SDS → IMS → SDS	53267	53271	4
		rise	SDS	53271	53278	7
		transition	SDS → IMS → SDS	53278	53284	6
		rise	SDS	53284	53310	26
		transition	SDS → IMS → SDS	53310	53343	33
		decline	SDS	53343	53353	10
		transition	SDS → IMS → SDS	53353	53377	24
		decline	SDS	53377	53402	25
		transition	SDS → IMS → SDS	53402	-	1
		decline	SDS	53403	53469	66
		transition	SDS → HDS	53469	-	1

Continued on Next Page...

Table A.4 – Continued

Source Name	Outburst ID	Stage	State(s)	$t_{\rm beg}$[a] (MJD)	$t_{\rm end}$[a] (MJD)	$t_{\rm dur}$[b] (days)
		decline	HDS	53470	53484	14
		decline	-	53484	53516	32
	2006	rise	-	53751	53763	12
		rise	HDS	53763	53830	67
		decline	HDS	53830	53867	37
		decline	-	53867	53877	10
	2006/2007	rise	-	54053	54102	49
		rise	HDS	54102	54144	42
		transition	HDS → SDS	54144	-	1
		rise	SDS	54145	54147	2
		decline	SDS	54147	54233	86
		transition	SDS → HDS	54233	-	1
		decline	HDS	54234	54373	139
		decline	-	54373	54392	19
	2008	rise	-	54624	54652	28
		rise	HDS	54652	54688	36
		decline	HDS	54688	54730	42
		decline	-	54730	54749	19
	2009	rise	-	54875	54891	16
		rise	HDS	54891	54899	8
		decline	HDS	54899	55012	113
		decline	-	55012	55025	13
	2009-2011	rise	-	55178	55203	25
		rise	HDS	55203	55302	99
		transition	HDS → SDS	55302	-	1
		rise	SDS	55303	55304	1
		decline	SDS	55304	55561	257
		transition	SDS → HDS	55561	55598	37
		decline	HDS	55598	55612	14
		decline	-	55612	55632	20
	2013	rise	-	56502	56509	7
		transition	- → HDS	56509	56511	2
		rise	HDS	56511	56550	39
		decline	HDS	56550	56583	33
		transition	HDS → -	56583	-	1

Continued on Next Page...

Table A.4 – Continued

Source Name	Outburst ID	Stage	State(s)	$t_{\rm beg}$ [a] (MJD)	$t_{\rm end}$ [a] (MJD)	$t_{\rm dur}$ [b] (days)
		decline	-	56584	56609	25
IGRJ17091−3624	2011-2013	rise	-	55589	55593	4
		rise	HDS	55593	55617	24
		transition	HDS → SDS	55617	55739	122
		decline	SDS	55739	55860	121
		decline	-	55860	56413	553
SAXJ1711.6−3808	2001	rise	-	51927	51952	25
		rise	HDS	51952	51953	1
		decline	HDS	51953	52017	64
		decline	-	52017	52057	40
XMMSL1J171900.4−353217	2007	rise	HDS	54157	54264	107
		decline	-	54264	54286	22
	2007/2008	rise	-	54363	54370	7
		rise	HDS	54370	54601	231
		decline	HDS	54601	54604	3
		decline	-	54604	54643	39
	2008/2009	rise	HDS	54728	54946	218
		decline	-	54946	54970	24
	2009/2010	rise	-	55059	55080	21
		rise	HDS	55080	55278	198
		decline	HDS	55278	55422	144
		decline	-	55422	55464	42
XTEJ1720−318	2003	rise	-	52644	52648	4
		rise	HDS	52648	52653	5
		rise	SDS	52653	52656	3
		transition	SDS → IMS → SDS	52656	52702	46
		decline	SDS	52702	52707	5
		transition	SDS → HDS	52707	52717	10
		decline	HDS	52717	52834	117
		decline	-	52834	52874	40

Continued on Next Page...

Table A.4 – Continued

Source Name	Outburst ID	Stage	State(s)	$t_{\rm beg}$[a] (MJD)	$t_{\rm end}$[a] (MJD)	$t_{\rm dur}$[b] (days)
XTEJ1727−476	2005	rise	-	53639	53647	8
		rise	HDS	53647	53649	2
		rise	SDS	53649	53650	1
		decline	SDS	53650	53660	10
		transition	SDS → -	53660	53663	3
		decline	-	53663	53718	55
IGRJ17285−2922	2010	rise	-	55426	55436	10
		rise	HDS	55436	55440	4
		decline	HDS	55440	55457	17
		transition	HDS → IMS → HDS	55457	55461	4
		decline	HDS	55461	55496	35
		decline	-	55496	55516	20
IGRJ17379−3747	2008	rise	-	54701	54714	13
		rise	HDS	54714	54716	2
		decline	HDS	54716	54753	37
		decline	-	54753	54777	24
GRS1737−31	1997	rise	-	50497	50500	3
		rise	HDS	50500	50506	6
		decline	HDS	50506	50538	32
		decline	-	50538	50598	60
GRS1739−278	1996	rise	HDS	50136	50180	44
		transition	HDS → IMS → HDS	50180	50183	3
		decline	HDS	50183	50202	19
		transition	HDS → IMS → HDS	50202	-	1
		decline	HDS	50203	50205	2
		transition	HDS → SDS	50205	50208	3
		decline	SDS	50208	50210	2
		transition	SDS → HDS	50210	50214	4
		decline	HDS	50214	50216	2
		transition	HDS → SDS	50216	50220	4
		decline	SDS	50220	50222	2
		transition	SDS → HDS	50222	50224	2
		decline	HDS	50224	50226	2

Continued on Next Page...

Table A.4 – Continued

Source Name	Outburst ID	Stage	State(s)	$t_{\rm beg}$[a] (MJD)	$t_{\rm end}$[a] (MJD)	$t_{\rm dur}$[b] (days)
		transition	HDS → IMS → HDS	50226	50237	11
		decline	HDS	50237	50240	3
		transition	HDS → IMS → HDS	50240	-	1
		decline	HDS	50241	50246	5
		transition	HDS → IMS → HDS	50246	50259	13
		decline	HDS	50259	50261	2
		transition	HDS → IMS → HDS	50261	50264	3
		decline	HDS	50264	50291	27
		transition	HDS → SDS	50291	50297	6
		decline	SDS	50297	50299	2
		transition	SDS → IMS → SDS	50299	50301	2
		decline	SDS	50301	50304	3
		transition	SDS → IMS → SDS	50304	50308	4
		decline	SDS	50308	50319	11
		transition	SDS → IMS → SDS	50319	50323	4
		decline	SDS	50323	50325	2
		transition	SDS → IMS → SDS	50325	-	1
		decline	SDS	50326	50328	2
		transition	SDS → HDS	50328	50334	6
		decline	HDS	50334	50336	2
		transition	HDS → IMS → HDS	50336	50342	6
		decline	HDS	50342	50344	2
		transition	HDS → IMS → HDS	50344	50347	3
		decline	HDS	50347	50351	4
		decline	SDS	50351	50355	4
		transition	SDS → HDS	50355	50364	9
		decline	HDS	50364	50366	2
		decline	SDS	50366	50368	2
		transition	SDS → HDS	50368	50370	2
		decline	HDS	50370	50375	5
		transition	HDS → IMS → HDS	50375	50378	3
		decline	HDS	50378	50388	10
	2014	rise	-	56725	-	1
		rise	HDS	56726	56752	26
		transition	HDS → SDS	56752	56754	2
		rise	SDS	56754	56761	7
		decline	SDS	56761	56768	7

Continued on Next Page...

Table A.4 – Continued

Source Name	Outburst ID	Stage	State(s)	$t_{\rm beg}$[a] (MJD)	$t_{\rm end}$[a] (MJD)	$t_{\rm dur}$[b] (days)
		transition	SDS → -	56768	56772	4
		decline	-	56772	56785	13
1E1740.7−2942	1996-2004	rise	-	50094	50166	72
		rise	HDS	50166	50198	32
		decline	HDS	50198	52106	1908
		transition	HDS → IMS → HDS	52106	52114	8
		decline	HDS	52114	52392	278
		transition	HDS → IMS → HDS	52392	52396	4
		decline	HDS	52396	53300	904
		decline	-	53300	53314	14
	2005-2007	rise	-	53412	53416	4
		rise	HDS	53416	53752	336
		transition	HDS → SDS	53752	53762	10
		rise	SDS	53762	53780	18
		rise	HDS	53780	53841	61
		transition	HDS → IMS → HDS	53841	53866	25
		rise	HDS	53866	54003	137
		transition	HDS → IMS → HDS	54003	54012	9
		rise	HDS	54012	54173	161
		decline	HDS	54173	54223	50
		decline	SDS	54223	54242	19
		transition	SDS → HDS	54242	54286	44
		decline	HDS	54286	54301	15
		transition	HDS → -	54301	54398	97
		decline	-	54398	54413	15
	2008-2014	rise	-	54504	54511	7
		rise	HDS	54511	54526	15
		transition	HDS → SDS	54526	54528	2
		rise	SDS	54528	54530	2
		transition	SDS → HDS	54530	-	1
		rise	HDS	54531	54599	68
		transition	HDS → IMS → HDS	54599	-	1
		rise	HDS	54600	54659	59
		transition	HDS → IMS → HDS	54659	54661	2
		rise	HDS	54661	55309	648
		transition	HDS → IMS → HDS	55309	55328	19

Continued on Next Page...

Table A.4 – Continued

Source Name	Outburst ID	Stage	State(s)	$t_{\rm beg}$[a] (MJD)	$t_{\rm end}$[a] (MJD)	$t_{\rm dur}$[b] (days)
		rise	HDS	55328	55457	129
		transition	HDS → SDS	55457	55720	263
		rise	SDS	55720	55735	15
		decline	SDS	55735	55735	0
		decline	HDS	55735	56363	628
		transition	HDS → IMS → HDS	56363	56372	9
		decline	HDS	56372	56543	171
		transition	HDS → IMS → HDS	56543	56545	2
		decline	HDS	56545	56761	216
		decline	-	56761	56769	8
SWIFTJ174510.8−262411	2012/2013	rise	-	56178	56187	9
		rise	HDS	56187	56207	20
		decline	HDS	56207	56392	185
		decline	-	56392	56464	72
H1743−322	2003	rise	-	52713	52726	13
		rise	HDS	52726	52754	28
		decline	HDS	52754	52825	71
		transition	HDS → IMS → HDS	52825	52828	3
		decline	HDS	52828	52830	2
		transition	HDS → IMS → HDS	52830	-	1
		decline	HDS	52831	52838	7
		transition	HDS → IMS → HDS	52838	52844	6
		decline	HDS	52844	52846	2
		transition	HDS → IMS → HDS	52846	-	1
		decline	HDS	52847	52857	10
		transition	HDS → IMS → HDS	52857	-	1
		decline	HDS	52858	52861	3
		transition	HDS → IMS → HDS	52861	52879	18
		decline	HDS	52879	52881	2
		transition	HDS → SDS	52881	52887	6
		decline	SDS	52887	52890	3
		transition	SDS → HDS	52890	-	1
		decline	HDS	52891	52894	3
		transition	HDS → SDS	52894	52897	3
		decline	SDS	52897	52901	4

Continued on Next Page...

Table A.4 – Continued

Source Name	Outburst ID	Stage	State(s)	$t_{\rm beg}$[a] (MJD)	$t_{\rm end}$[a] (MJD)	$t_{\rm dur}$[b] (days)
		transition	SDS → IMS → SDS	52901	-	1
		decline	SDS	52902	52904	2
		transition	SDS → HDS	52904	52932	28
		decline	HDS	52932	52935	3
		transition	HDS → -	52935	-	1
		decline	-	52936	52954	18
	2004	rise	-	53182	53190	8
		rise	HDS	53190	53192	2
		transition	HDS → SDS	53192	53195	3
		rise	SDS	53195	53200	5
		transition	SDS → IMS → SDS	53200	53202	2
		rise	SDS	53202	53204	2
		transition	SDS → IMS → SDS	53204	-	1
		rise	SDS	53205	53209	4
		transition	SDS → HDS	53209	53225	16
		rise	HDS	53225	53227	2
		transition	HDS → SDS	53227	53230	3
		rise	SDS	53230	53232	2
		transition	SDS → HDS	53232	53247	15
		decline	HDS	53247	53256	9
		transition	HDS → IMS → HDS	53256	-	1
		decline	HDS	53257	53259	2
		transition	HDS → IMS → HDS	53259	53271	12
		decline	HDS	53271	53290	19
		transition	HDS → IMS → HDS	53290	53292	2
		decline	HDS	53292	53296	4
		decline	-	53296	53316	20
	2005	rise	-	53575	53588	13
		transition	- → HDS	53588	53590	2
		rise	HDS	53590	53597	7
		transition	HDS → SDS	53597	53599	2
		rise	SDS	53599	53602	3
		decline	SDS	53602	53611	9
		transition	SDS → IMS → SDS	53611	53613	2
		decline	SDS	53613	53622	9
		decline	HDS	53622	53637	15

Continued on Next Page...

Table A.4 – Continued

Source Name	Outburst ID	Stage	State(s)	$t_{\rm beg}$[a] (MJD)	$t_{\rm end}$[a] (MJD)	$t_{\rm dur}$[b] (days)
		decline	-	53637	53656	19
	2007/2008	rise	-	54446	54455	9
		rise	HDS	54455	54456	1
		decline	HDS	54456	54461	5
		transition	HDS → IMS → HDS	54461	-	1
		decline	HDS	54462	54464	2
		decline	SDS	54464	54483	19
		transition	SDS → HDS	54483	54487	4
		decline	HDS	54487	54506	19
		decline	-	54506	54508	2
		decline	HDS	54508	54512	4
		decline	-	54512	54514	2
	2008	rise	-	54714	54730	16
		rise	HDS	54730	54749	19
		decline	HDS	54749	54787	38
		decline	-	54787	54814	27
	2009	rise	-	54953	54973	20
		rise	HDS	54973	54986	13
		transition	HDS → SDS	54986	54988	2
		rise	SDS	54988	54992	4
		decline	SDS	54992	54998	6
		transition	SDS → HDS	54998	55011	13
		decline	HDS	55011	55031	20
		decline	-	55031	55054	23
	2009/2010	rise	-	55186	55195	9
		rise	HDS	55195	55208	13
		decline	HDS	55208	55211	3
		transition	HDS → IMS → HDS	55211	55213	2
		decline	HDS	55213	55245	32
		decline	-	55245	55287	42
	2010	rise	-	55387	55411	24
		rise	HDS	55411	55426	15
		decline	HDS	55426	55426	0
		transition	HDS → SDS	55426	55433	7
		decline	SDS	55433	55440	7

Continued on Next Page...

Table A.4 – Continued

Source Name	Outburst ID	Stage	State(s)	$t_{\rm beg}$[a] (MJD)	$t_{\rm end}$[a] (MJD)	$t_{\rm dur}$[b] (days)
		transition	SDS → HDS	55440	55449	9
		decline	HDS	55449	-	1
		transition	HDS → IMS → HDS	55450	55453	3
		decline	HDS	55453	55469	16
		decline	-	55469	55489	20
	2010/2011	rise	-	55536	55657	121
		rise	HDS	55657	55675	18
		decline	HDS	55675	55678	3
		transition	HDS → IMS → HDS	55678	55686	8
		decline	HDS	55686	55711	25
		decline	-	55711	55731	20
	2011/2012	rise	-	55897	55924	27
		rise	HDS	55924	55928	4
		decline	HDS	55928	55960	32
		decline	-	55960	55971	11
		decline	HDS	55971	-	1
		decline	-	55972	55989	17
	2012	rise	-	56185	56192	7
		rise	HDS	56192	56207	15
		decline	HDS	56207	56228	21
		decline	-	56228	56250	22
	2013	rise	-	56489	56504	15
		rise	HDS	56504	56524	20
		decline	HDS	56524	56529	5
		transition	HDS → IMS → HDS	56529	56531	2
		decline	HDS	56531	56553	22
		decline	-	56553	56564	11
XTEJ1748−288	1998	rise	-	50961	50968	7
		rise	HDS	50968	50970	2
		decline	HDS	50970	51021	51
		decline	-	51021	51039	18
IGRJ17497−2821	2006	rise	-	53963	53996	33
		rise	HDS	53996	54015	19

Continued on Next Page...

Table A.4 – Continued

Source Name	Outburst ID	Stage	State(s)	$t_{\rm beg}$ [a] (MJD)	$t_{\rm end}$ [a] (MJD)	$t_{\rm dur}$ [b] (days)
		decline	HDS	54015	54039	24
		decline	-	54039	54062	23
SLX1746−331	2003	rise	-	52713	52732	19
		transition	- → HDS	52732	52735	3
		rise	HDS	52735	52741	6
		decline	HDS	52741	52790	49
		transition	HDS → IMS → HDS	52790	52792	2
		decline	HDS	52792	52796	4
		transition	HDS → IMS → HDS	52796	52805	9
		decline	HDS	52805	52821	16
		transition	HDS → IMS → HDS	52821	52825	4
		decline	HDS	52825	52902	77
		transition	HDS → IMS → HDS	52902	52937	35
		decline	HDS	52937	52942	5
		transition	HDS → IMS → HDS	52942	52950	8
		decline	HDS	52950	52952	2
		transition	HDS → IMS → HDS	52952	-	1
		decline	HDS	52953	52955	2
		decline	-	52955	52968	13
	2007/2008	rise	-	54359	54379	20
		rise	HDS	54379	54382	3
		rise	SDS	54382	54476	94
		decline	SDS	54476	54554	78
		transition	SDS → HDS	54554	54560	6
		decline	HDS	54560	54596	36
		decline	-	54596	54613	17
	2010/2011	rise	-	55387	55412	25
		rise	HDS	55412	55417	5
		transition	HDS → SDS	55417	55422	5
		rise	SDS	55422	55439	17
		transition	SDS → HDS	55439	55450	11
		rise	HDS	55450	55574	124
		transition	HDS → SDS	55574	55668	94
		rise	SDS	55668	55670	2
		transition	SDS → IMS → SDS	55670	55674	4

Continued on Next Page...

Table A.4 – Continued

Source Name	Outburst ID	Stage	State(s)	$t_{\rm beg}$[a] (MJD)	$t_{\rm end}$[a] (MJD)	$t_{\rm dur}$[b] (days)
		rise	SDS	55674	55675	1
		decline	SDS	55675	55679	4
		transition	SDS → IMS → SDS	55679	55682	3
		decline	SDS	55682	55687	5
		decline	HDS	55687	55690	3
		decline	-	55690	55714	24
XTEJ1752−223	2009/2010	rise	-	55083	55127	44
		rise	HDS	55127	55179	52
		decline	HDS	55179	55217	38
		transition	HDS → SDS	55217	55221	4
		decline	SDS	55221	55285	64
		transition	SDS → HDS	55285	55288	3
		decline	HDS	55288	55310	22
		transition	HDS → IMS → HDS	55310	55315	5
		decline	HDS	55315	55342	27
		transition	HDS → IMS → HDS	55342	55354	12
		decline	HDS	55354	55407	53
		transition	HDS → SDS	55407	55410	3
		decline	SDS	55410	55417	7
		decline	-	55417	55424	7
SWIFTJ1753.5−0127	2005-2014	rise	-	53529	53551	22
		rise	HDS	53551	53766	215
		transition	HDS → IMS → HDS	53766	-	1
		rise	HDS	53767	53845	78
		transition	HDS → IMS → HDS	53845	53869	24
		rise	HDS	53869	53871	2
		transition	HDS → IMS → HDS	53871	53904	33
		rise	HDS	53904	53906	2
		transition	HDS → IMS → HDS	53906	53924	18
		rise	HDS	53924	53926	2
		transition	HDS → IMS → HDS	53926	53947	21
		rise	HDS	53947	53949	2
		transition	HDS → IMS → HDS	53949	54019	70
		rise	HDS	54019	54021	2
		transition	HDS → IMS → HDS	54021	54064	43

Continued on Next Page...

Table A.4 – Continued

Source Name	Outburst ID	Stage	State(s)	$t_{\rm beg}$[a] (MJD)	$t_{\rm end}$[a] (MJD)	$t_{\rm dur}$[b] (days)
		rise	HDS	54064	54077	13
		transition	HDS → IMS → HDS	54077	54180	103
		rise	HDS	54180	54182	2
		transition	HDS → IMS → HDS	54182	54214	32
		rise	HDS	54214	54216	2
		transition	HDS → IMS → HDS	54216	54380	164
		rise	HDS	54380	54382	2
		transition	HDS → IMS → HDS	54382	54538	156
		rise	HDS	54538	54540	2
		transition	HDS → IMS → HDS	54540	55260	720
		decline	HDS	55260	55262	2
		transition	HDS → IMS → HDS	55262	55264	2
		decline	HDS	55264	55267	3
		transition	HDS → IMS → HDS	55267	55335	68
		decline	HDS	55335	55338	3
		transition	HDS → SDS	55338	55526	188
		decline	SDS	55526	55540	14
		transition	SDS → IMS → SDS	55540	55700	160
		decline	SDS	55700	55710	10
		transition	SDS → HDS	55710	55783	73
		decline	HDS	55783	56655	872
		decline	-	56655	56787	132
XTEJ1755−324	1997	rise	-	50637	50654	17
		transition	- → SDS	50654	50656	2
		rise	SDS	50656	50663	7
		decline	SDS	50663	50684	21
		transition	SDS → HDS	50684	-	1
		decline	HDS	50685	50698	13
		transition	HDS → SDS	50698	-	1
		decline	SDS	50699	50702	3
		transition	SDS → HDS	50702	-	1
		decline	HDS	50703	50708	5
		transition	HDS → IMS → HDS	50708	-	1
		decline	HDS	50709	50715	6
		transition	HDS → IMS → HDS	50715	50717	2
		decline	HDS	50717	50734	17

Continued on Next Page...

Table A.4 – Continued

Source Name	Outburst ID	Stage	State(s)	$t_{\rm beg}$[a] (MJD)	$t_{\rm end}$[a] (MJD)	$t_{\rm dur}$[b] (days)
		transition	HDS → IMS → HDS	50734	50738	4
		decline	HDS	50738	50746	8
		transition	HDS → -	50746	50753	7
		decline	-	50753	50762	9
IGRJ17586−2129	2009	rise	-	54997	55047	50
		rise	HDS	55047	55125	78
		decline	HDS	55125	55139	14
		decline	-	55139	55159	20
GRS1758−258	1996-2002	rise	-	50136	50141	5
		rise	HDS	50141	50505	364
		transition	HDS → IMS → HDS	50505	50507	2
		rise	HDS	50507	50917	410
		transition	HDS → IMS → HDS	50917	50919	2
		rise	HDS	50919	50941	22
		decline	HDS	50941	51423	482
		transition	HDS → IMS → HDS	51423	51427	4
		decline	HDS	51427	51714	287
		transition	HDS → IMS → HDS	51714	-	1
		decline	HDS	51715	51969	254
		transition	HDS → IMS → HDS	51969	52129	160
		decline	HDS	52129	52375	246
		transition	HDS → IMS → HDS	52375	52377	2
		decline	HDS	52377	52597	220
		decline	-	52597	52602	5
	2003/2004	rise	-	52677	52690	13
		rise	HDS	52690	52695	5
		transition	HDS → IMS → HDS	52695	52700	5
		rise	HDS	52700	52705	5
		decline	HDS	52705	52762	57
		transition	HDS → IMS → HDS	52762	52780	18
		decline	HDS	52780	52788	8
		transition	HDS → IMS → HDS	52788	-	1
		decline	HDS	52789	53181	392
		transition	HDS → IMS → HDS	53181	53189	8
		decline	HDS	53189	53306	117

Continued on Next Page...

Table A.4 – Continued

Source Name	Outburst ID	Stage	State(s)	$t_{\rm beg}$[a] (MJD)	$t_{\rm end}$[a] (MJD)	$t_{\rm dur}$[b] (days)
		decline	-	53306	53346	40
	2005-2014	rise	-	53391	53400	9
		rise	HDS	53400	53479	79
		transition	HDS → IMS → HDS	53479	53481	2
		rise	HDS	53481	53858	377
		transition	HDS → IMS → HDS	53858	53860	2
		rise	HDS	53860	53988	128
		transition	HDS → IMS → HDS	53988	53995	7
		rise	HDS	53995	54035	40
		rise	SDS	54035	54039	4
		transition	SDS → HDS	54039	-	1
		rise	HDS	54040	54270	230
		transition	HDS → IMS → HDS	54270	54275	5
		rise	HDS	54275	54283	8
		transition	HDS → IMS → HDS	54283	54285	2
		rise	HDS	54285	54292	7
		transition	HDS → IMS → HDS	54292	54304	12
		rise	HDS	54304	54344	40
		transition	HDS → IMS → HDS	54344	54356	12
		rise	HDS	54356	-	1
		transition	HDS → IMS → HDS	54357	-	1
		rise	HDS	54358	54361	3
		transition	HDS → SDS	54361	54374	13
		rise	SDS	54374	54377	3
		rise	HDS	54377	54394	17
		transition	HDS → IMS → HDS	54394	54397	3
		rise	HDS	54397	54408	11
		transition	HDS → IMS → HDS	54408	54413	5
		rise	HDS	54413	54526	113
		transition	HDS → IMS → HDS	54526	-	1
		rise	HDS	54527	54531	4
		transition	HDS → IMS → HDS	54531	54536	5
		rise	HDS	54536	54548	12
		transition	HDS → IMS → HDS	54548	54551	3
		rise	HDS	54551	54591	40
		transition	HDS → IMS → HDS	54591	54598	7
		rise	HDS	54598	54642	44

Continued on Next Page...

Table A.4 – Continued

Source Name	Outburst ID	Stage	State(s)	$t_{\rm beg}$[a] (MJD)	$t_{\rm end}$[a] (MJD)	$t_{\rm dur}$[b] (days)
		transition	HDS → IMS → HDS	54642	-	1
		rise	HDS	54643	55046	403
		transition	HDS → IMS → HDS	55046	55049	3
		rise	HDS	55049	55067	18
		transition	HDS → IMS → HDS	55067	-	1
		rise	HDS	55068	55134	66
		transition	HDS → IMS → HDS	55134	55137	3
		rise	HDS	55137	55205	68
		transition	HDS → SDS	55205	55208	3
		rise	SDS	55208	55344	136
		transition	SDS → IMS → SDS	55344	55356	12
		rise	SDS	55356	55385	29
		transition	SDS → IMS → SDS	55385	55405	20
		rise	SDS	55405	55452	47
		transition	SDS → IMS → SDS	55452	55659	207
		rise	SDS	55659	55730	71
		decline	SDS	55730	55809	79
		transition	SDS → HDS	55809	55832	23
		decline	HDS	55832	56223	391
		decline	SDS	56223	-	1
		decline	HDS	56224	56761	537
		decline	-	56761	56782	21
XTEJ1812−182	2003	rise	-	52656	52674	18
		rise	HDS	52674	52689	15
		decline	HDS	52689	52708	19
		decline	-	52708	52711	3
	2008	rise	-	54695	54713	18
		rise	SDS	54713	54741	28
		decline	SDS	54741	54753	12
		decline	HDS	54753	54757	4
		transition	HDS → -	54757	54759	2
		decline	-	54759	54776	17
XTEJ1817−330	2006	rise	-	53744	53760	16
		rise	SDS	53760	53763	3
		decline	SDS	53763	53867	104

Continued on Next Page...

Table A.4 – Continued

Source Name	Outburst ID	Stage	State(s)	$t_{\rm beg}$[a] (MJD)	$t_{\rm end}$[a] (MJD)	$t_{\rm dur}$[b] (days)
		transition	SDS → HDS	53867	53899	32
		decline	HDS	53899	53978	79
		decline	SDS	53978	-	1
		decline	HDS	53979	53981	2
		decline	-	53981	54000	19
XTEJ1818−245	2005	rise	-	53575	53594	19
		rise	HDS	53594	-	1
		rise	SDS	53595	53597	2
		decline	SDS	53597	53654	57
		transition	SDS → -	53654	53671	17
		decline	-	53671	53691	20
SAXJ1819.3−2525	2005/2006	rise	-	53652	53659	7
		rise	HDS	53659	53852	193
		rise	-	53852	53862	10
		decline	-	53862	53865	3
	2006/2007	rise	-	53878	53890	12
		rise	HDS	53890	53970	80
		decline	HDS	53970	54223	253
	2007	rise	-	54232	54243	11
		rise	HDS	54243	54303	60
		decline	HDS	54303	54320	17
		decline	-	54320	54348	28
	2008	rise	HDS	54518	54572	54
		decline	-	54572	54585	13
	2008/2009	rise	HDS	54691	54915	224
		decline	-	54915	54943	28
	2009	rise	-	54951	54985	34
		rise	HDS	54985	55125	140
		rise	-	55125	55167	42
		decline	-	55167	55167	0
	2010/2011	rise	HDS	55293	55469	176
		transition	HDS → IMS → HDS	55469	55490	21
		decline	HDS	55490	55496	6

Continued on Next Page...

Table A.4 – Continued

Source Name	Outburst ID	Stage	State(s)	$t_{\rm beg}$[a] (MJD)	$t_{\rm end}$[a] (MJD)	$t_{\rm dur}$[b] (days)
		decline	-	55496	55588	92
MAXIJ1836−194	2011/2012	rise	-	55797	55802	5
		rise	HDS	55802	55811	9
		decline	HDS	55811	56048	237
		decline	-	56048	56086	38
SWIFTJ1842.5−1124	2008/2009	rise	-	54630	54651	21
		rise	HDS	54651	54731	80
		transition	HDS → SDS	54731	-	1
		rise	SDS	54732	-	1
		transition	SDS → IMS → SDS	54733	54756	23
		decline	SDS	54756	-	1
		transition	SDS → HDS	54757	54765	8
		decline	HDS	54765	54768	3
		transition	HDS → -	54768	54787	19
		decline	-	54787	54858	71
XTEJ1856+053	1996	rise	-	50190	50196	6
		rise	HDS	50196	50198	2
		transition	HDS → SDS	50198	50201	3
		decline	SDS	50201	50209	8
		transition	SDS → -	50209	50216	7
		decline	-	50216	-	1
	1996	rise	-	50311	50328	17
		rise	HDS	50328	50340	12
		rise	SDS	50340	50342	2
		rise	HDS	50342	50343	1
		decline	HDS	50343	50344	1
		decline	SDS	50344	50348	4
		transition	SDS → IMS → SDS	50348	50351	3
		decline	SDS	50351	50354	3
		transition	SDS → IMS → SDS	50354	-	1
		decline	SDS	50355	50366	11
		transition	SDS → HDS	50366	-	1
		decline	HDS	50367	50371	4

Continued on Next Page...

Table A.4 – Continued

Source Name	Outburst ID	Stage	State(s)	$t_{\rm beg}$[a] (MJD)	$t_{\rm end}$[a] (MJD)	$t_{\rm dur}$[b] (days)
		transition	HDS → SDS	50371	-	1
		decline	SDS	50372	50381	9
		transition	SDS → IMS → SDS	50381	50385	4
		decline	SDS	50385	50390	5
		transition	SDS → HDS	50390	50395	5
		decline	HDS	50395	50397	2
		decline	-	50397	50411	14
	2006/2007	rise	-	54088	54150	62
		rise	HDS	54150	54160	10
		transition	HDS → SDS	54160	-	1
		rise	SDS	54161	54199	38
		transition	SDS → IMS → SDS	54199	54204	5
		rise	SDS	54204	54211	7
		transition	SDS → HDS	54211	-	1
		rise	HDS	54212	54215	3
		rise	SDS	54215	54217	2
		transition	SDS → HDS	54217	54230	13
		rise	HDS	54230	54257	27
		rise	SDS	54257	54266	9
		decline	SDS	54266	54306	40
		decline	HDS	54306	-	1
		decline	-	54307	54313	6
	2009	transition	IMS	54926	54932	6
		decline	HDS	54932	54945	13
		decline	-	54945	54959	14
XTEJ1859+226	1999/2000	rise	-	51437	51460	23
		rise	HDS	51460	51468	8
		decline	HDS	51468	51490	22
		transition	HDS → SDS	51490	51501	11
		decline	SDS	51501	51504	3
		transition	SDS → IMS → SDS	51504	51506	2
		decline	SDS	51506	51512	6
		transition	SDS → IMS → SDS	51512	51534	22
		decline	SDS	51534	51538	4
		transition	SDS → IMS → SDS	51538	51540	2

Continued on Next Page...

Table A.4 – Continued

Source Name	Outburst ID	Stage	State(s)	$t_{\rm beg}$[a] (MJD)	$t_{\rm end}$[a] (MJD)	$t_{\rm dur}$[b] (days)
		decline	SDS	51540	51543	3
		transition	SDS → HDS	51543	51548	5
		decline	HDS	51548	51564	16
		transition	HDS → IMS → HDS	51564	51574	10
		decline	HDS	51574	51612	38
		decline	-	51612	51662	50
XTEJ1908+094	2002/2003	rise	-	52327	52333	6
		rise	HDS	52333	52371	38
		decline	HDS	52371	52374	3
		transition	HDS → SDS	52374	52376	2
		decline	SDS	52376	52378	2
		decline	HDS	52378	52381	3
		decline	SDS	52381	52391	10
		transition	SDS → IMS → SDS	52391	-	1
		decline	SDS	52392	52395	3
		transition	SDS → HDS	52395	52421	26
		decline	HDS	52421	52691	270
		decline	-	52691	52751	60
	2013/2014	rise	-	56581	56591	10
		rise	HDS	56591	56595	4
		decline	HDS	56595	56608	13
		transition	HDS → -	56608	-	1
		decline	-	56609	56731	122
SWIFTJ1910.2−0546	2012/2013	rise	-	56059	56078	19
		rise	HDS	56078	56083	5
		transition	HDS → SDS	56083	-	1
		rise	SDS	56084	56100	16
		decline	SDS	56100	56100	0
		transition	SDS → IMS → SDS	56100	56104	4
		decline	SDS	56104	56107	3
		transition	SDS → HDS	56107	56120	13
		decline	HDS	56120	56292	172
		decline	-	56292	56317	25

Continued on Next Page...

Table A.4 – Continued

Source Name	Outburst ID	Stage	State(s)	$t_{\rm beg}$[a] (MJD)	$t_{\rm end}$[a] (MJD)	$t_{\rm dur}$[b] (days)
SS433	1996-2001	rise	-	50088	50090	2
		rise	HDS	50090	50317	227
		transition	HDS → IMS → HDS	50317	-	1
		rise	HDS	50318	51830	1512
		transition	HDS → IMS → HDS	51830	51891	61
		rise	HDS	51891	52087	196
		decline	HDS	52087	52211	124
		decline	-	52211	52226	15
	2002-2004	rise	-	52315	52369	54
		rise	HDS	52369	52752	383
		decline	HDS	52752	53294	542
		decline	-	53294	53302	8
	2005-2014	rise	-	53481	53485	4
		rise	HDS	53485	54021	536
		transition	HDS → IMS → HDS	54021	54029	8
		rise	HDS	54029	54147	118
		transition	HDS → IMS → HDS	54147	54190	43
		rise	HDS	54190	54246	56
		transition	HDS → IMS → HDS	54246	54267	21
		rise	HDS	54267	54553	286
		transition	HDS → IMS → HDS	54553	54557	4
		rise	HDS	54557	54647	90
		transition	HDS → IMS → HDS	54647	54673	26
		rise	HDS	54673	54830	157
		transition	HDS → IMS → HDS	54830	54889	59
		rise	HDS	54889	54929	40
		transition	HDS → IMS → HDS	54929	54989	60
		rise	HDS	54989	55083	94
		transition	HDS → IMS → HDS	55083	55092	9
		rise	HDS	55092	55118	26
		transition	HDS → IMS → HDS	55118	55128	10
		rise	HDS	55128	55133	5
		transition	HDS → IMS → HDS	55133	55139	6
		rise	HDS	55139	55167	28
		transition	HDS → IMS → HDS	55167	55169	2
		rise	HDS	55169	55179	10
		transition	HDS → SDS	55179	55191	12

Continued on Next Page...

Table A.4 – Continued

Source Name	Outburst ID	Stage	State(s)	$t_{\rm beg}$[a] (MJD)	$t_{\rm end}$[a] (MJD)	$t_{\rm dur}$[b] (days)
		rise	SDS	55191	-	1
		transition	SDS → IMS → SDS	55192	55206	14
		rise	SDS	55206	55257	51
		transition	SDS → HDS	55257	55259	2
		rise	HDS	55259	55265	6
		transition	HDS → IMS → HDS	55265	55267	2
		rise	HDS	55267	55277	10
		transition	HDS → SDS	55277	55315	38
		rise	SDS	55315	55426	111
		transition	SDS → HDS	55426	55787	361
		decline	HDS	55787	56028	241
		transition	HDS → IMS → HDS	56028	-	1
		decline	HDS	56029	56054	25
		transition	HDS → IMS → HDS	56054	56059	5
		decline	HDS	56059	56099	40
		transition	HDS → IMS → HDS	56099	56113	14
		decline	HDS	56113	56133	20
		transition	HDS → IMS → HDS	56133	56138	5
		decline	HDS	56138	56183	45
		transition	HDS → IMS → HDS	56183	56196	13
		decline	HDS	56196	56220	24
		transition	HDS → IMS → HDS	56220	56226	6
		decline	HDS	56226	56248	22
		transition	HDS → SDS	56248	56252	4
		decline	SDS	56252	56256	4
		decline	HDS	56256	56265	9
		transition	HDS → IMS → HDS	56265	56285	20
		decline	HDS	56285	56338	53
		transition	HDS → IMS → HDS	56338	56340	2
		decline	HDS	56340	56362	22
		transition	HDS → IMS → HDS	56362	-	1
		decline	HDS	56363	56379	16
		transition	HDS → IMS → HDS	56379	56426	47
		decline	HDS	56426	56469	43
		decline	SDS	56469	56474	5
		decline	HDS	56474	56534	60
		transition	HDS → IMS → HDS	56534	56552	18

Continued on Next Page...

Table A.4 – Continued

Source Name	Outburst ID	Stage	State(s)	$t_{\rm beg}$[a] (MJD)	$t_{\rm end}$[a] (MJD)	$t_{\rm dur}$[b] (days)
		decline	HDS	56552	56654	102
		transition	HDS → IMS → HDS	56654	56680	26
		decline	HDS	56680	56724	44
		transition	HDS → IMS → HDS	56724	56726	2
		decline	HDS	56726	56730	4
		transition	HDS → IMS → HDS	56730	56734	4
		decline	HDS	56734	56756	22
		decline	-	56756	56762	6
GRS1915+105	1996-2014	rise	HDS	50088	53416	3328
		transition	HDS → SDS	53416	53418	2
		decline	SDS	53418	53430	12
		transition	SDS → IMS → SDS	53430	53438	8
		decline	SDS	53438	53447	9
		transition	SDS → IMS → SDS	53447	-	1
		decline	SDS	53448	53464	16
		decline	HDS	53464	53717	253
		transition	HDS → IMS → HDS	53717	53721	4
		decline	HDS	53721	53726	5
		transition	HDS → IMS → HDS	53726	53731	5
		decline	HDS	53731	53737	6
		transition	HDS → IMS → HDS	53737	-	1
		decline	HDS	53738	53752	14
		transition	HDS → SDS	53752	-	1
		decline	SDS	53753	53759	6
		transition	SDS → IMS → SDS	53759	53762	3
		decline	SDS	53762	53770	8
		decline	HDS	53770	53789	19
		decline	SDS	53789	53792	3
		decline	HDS	53792	53799	7
		decline	SDS	53799	-	1
		decline	HDS	53800	53843	43
		decline	SDS	53843	53845	2
		decline	HDS	53845	53863	18
		decline	SDS	53863	53868	5
		transition	SDS → IMS → SDS	53868	53870	2
		decline	SDS	53870	53872	2

Continued on Next Page...

Table A.4 – Continued

Source Name	Outburst ID	Stage	State(s)	$t_{\rm beg}$[a] (MJD)	$t_{\rm end}$[a] (MJD)	$t_{\rm dur}$[b] (days)
		transition	SDS → IMS → SDS	53872	53876	4
		decline	SDS	53876	53878	2
		transition	SDS → IMS → SDS	53878	53881	3
		decline	SDS	53881	53886	5
		transition	SDS → IMS → SDS	53886	53901	15
		decline	SDS	53901	53903	2
		transition	SDS → IMS → SDS	53903	53905	2
		decline	SDS	53905	53907	2
		transition	SDS → HDS	53907	53911	4
		decline	HDS	53911	53919	8
		decline	SDS	53919	-	1
		decline	HDS	53920	53924	4
		decline	SDS	53924	53927	3
		decline	HDS	53927	53931	4
		decline	SDS	53931	53951	20
		transition	SDS → HDS	53951	53963	12
		decline	HDS	53963	53973	10
		decline	SDS	53973	53979	6
		decline	HDS	53979	53996	17
		decline	SDS	53996	-	1
		decline	HDS	53997	54003	6
		transition	HDS → IMS → HDS	54003	-	1
		decline	HDS	54004	54010	6
		transition	HDS → IMS → HDS	54010	-	1
		decline	HDS	54011	54014	3
		transition	HDS → SDS	54014	-	1
		decline	SDS	54015	54017	2
		decline	HDS	54017	54020	3
		decline	SDS	54020	54026	6
		decline	HDS	54026	54028	2
		decline	SDS	54028	-	1
		decline	HDS	54029	54031	2
		decline	SDS	54031	-	1
		decline	HDS	54032	54040	8
		decline	SDS	54040	-	1
		decline	HDS	54041	54048	7
		decline	SDS	54048	54051	3

Continued on Next Page...

Table A.4 – Continued

Source Name	Outburst ID	Stage	State(s)	$t_{\rm beg}$[a] (MJD)	$t_{\rm end}$[a] (MJD)	$t_{\rm dur}$[b] (days)
		decline	HDS	54051	54053	2
		decline	SDS	54053	54093	40
		decline	HDS	54093	54103	10
		decline	SDS	54103	54138	35
		decline	HDS	54138	54140	2
		decline	SDS	54140	-	1
		decline	HDS	54141	54166	25
		decline	SDS	54166	54182	16
		decline	HDS	54182	54184	2
		decline	SDS	54184	54200	16
		decline	HDS	54200	54202	2
		decline	SDS	54202	-	1
		decline	HDS	54203	54213	10
		transition	HDS → IMS → HDS	54213	-	1
		decline	HDS	54214	54241	27
		transition	HDS → IMS → HDS	54241	54243	2
		decline	HDS	54243	54253	10
		transition	HDS → IMS → HDS	54253	54255	2
		decline	HDS	54255	54265	10
		decline	SDS	54265	-	1
		decline	HDS	54266	54599	333
		decline	SDS	54599	-	1
		decline	HDS	54600	54603	3
		decline	SDS	54603	54607	4
		decline	HDS	54607	54609	2
		decline	SDS	54609	54624	15
		decline	HDS	54624	54627	3
		decline	SDS	54627	54640	13
		decline	HDS	54640	54673	33
		decline	SDS	54673	54680	7
		decline	HDS	54680	54695	15
		transition	HDS → IMS → HDS	54695	-	1
		decline	HDS	54696	54699	3
		transition	HDS → IMS → HDS	54699	-	1
		decline	HDS	54700	54703	3
		transition	HDS → IMS → HDS	54703	54706	3
		decline	HDS	54706	54726	20

Continued on Next Page...

Table A.4 – Continued

Source Name	Outburst ID	Stage	State(s)	$t_{\rm beg}$[a] (MJD)	$t_{\rm end}$[a] (MJD)	$t_{\rm dur}$[b] (days)
		decline	SDS	54726	54735	9
		transition	SDS → HDS	54735	54737	2
		decline	HDS	54737	54790	53
		decline	SDS	54790	54795	5
		transition	SDS → IMS → SDS	54795	54802	7
		decline	SDS	54802	54804	2
		transition	SDS → HDS	54804	54808	4
		decline	HDS	54808	54891	83
		decline	SDS	54891	54898	7
		decline	HDS	54898	54900	2
		decline	SDS	54900	54923	23
		decline	HDS	54923	54944	21
		transition	HDS → SDS	54944	54946	2
		decline	SDS	54946	-	1
		decline	HDS	54947	54950	3
		decline	SDS	54950	-	1
		decline	HDS	54951	54954	3
		transition	HDS → SDS	54954	54956	2
		decline	SDS	54956	54958	2
		transition	SDS → IMS → SDS	54958	54973	15
		decline	SDS	54973	54978	5
		transition	SDS → IMS → SDS	54978	55053	75
		decline	SDS	55053	-	1
		decline	HDS	55054	55058	4
		transition	HDS → SDS	55058	-	1
		decline	SDS	55059	55067	8
		transition	SDS → IMS → SDS	55067	-	1
		decline	SDS	55068	55071	3
		transition	SDS → IMS → SDS	55071	-	1
		decline	SDS	55072	55075	3
		transition	SDS → IMS → SDS	55075	-	1
		decline	SDS	55076	55085	9
		transition	SDS → IMS → SDS	55085	-	1
		decline	SDS	55086	55109	23
		transition	SDS → IMS → SDS	55109	-	1
		decline	SDS	55110	55112	2
		transition	SDS → IMS → SDS	55112	-	1

Continued on Next Page...

Table A.4 – Continued

Source Name	Outburst ID	Stage	State(s)	$t_{\rm beg}$[a] (MJD)	$t_{\rm end}$[a] (MJD)	$t_{\rm dur}$[b] (days)
		decline	SDS	55113	55116	3
		transition	SDS → IMS → SDS	55116	55122	6
		decline	SDS	55122	55124	2
		decline	HDS	55124	-	1
		transition	HDS → IMS → HDS	55125	55129	4
		decline	HDS	55129	-	1
		decline	SDS	55130	-	1
		decline	HDS	55131	55133	2
		decline	SDS	55133	-	1
		transition	SDS → IMS → SDS	55134	55143	9
		decline	SDS	55143	55145	2
		transition	SDS → HDS	55145	-	1
		decline	HDS	55146	55152	6
		decline	SDS	55152	55160	8
		decline	HDS	55160	55163	3
		decline	SDS	55163	55170	7
		transition	SDS → IMS → SDS	55170	-	1
		decline	SDS	55171	55180	9
		decline	HDS	55180	55194	14
		decline	SDS	55194	55199	5
		decline	HDS	55199	55202	3
		decline	SDS	55202	55205	3
		transition	SDS → HDS	55205	-	1
		decline	HDS	55206	55249	43
		decline	SDS	55249	-	1
		decline	HDS	55250	-	1
		transition	HDS → IMS → HDS	55251	-	1
		decline	HDS	55252	55254	2
		transition	HDS → IMS → HDS	55254	55267	13
		decline	HDS	55267	55270	3
		decline	SDS	55270	55295	25
		transition	SDS → HDS	55295	-	1
		decline	HDS	55296	55298	2
		transition	HDS → IMS → HDS	55298	-	1
		decline	HDS	55299	55304	5
		decline	SDS	55304	55311	7
		decline	HDS	55311	55314	3

Continued on Next Page...

Table A.4 – Continued

Source Name	Outburst ID	Stage	State(s)	$t_{\rm beg}$[a] (MJD)	$t_{\rm end}$[a] (MJD)	$t_{\rm dur}$[b] (days)
		decline	SDS	55314	55316	2
		decline	HDS	55316	55318	2
		transition	HDS → SDS	55318	55321	3
		decline	SDS	55321	55341	20
		decline	HDS	55341	55348	7
		transition	HDS → IMS → HDS	55348	55350	2
		decline	HDS	55350	55368	18
		transition	HDS → SDS	55368	55372	4
		decline	SDS	55372	55390	18
		decline	HDS	55390	-	1
		transition	HDS → SDS	55391	55393	2
		decline	SDS	55393	55404	11
		decline	HDS	55404	55408	4
		transition	HDS → SDS	55408	-	1
		decline	SDS	55409	55415	6
		decline	HDS	55415	55424	9
		decline	SDS	55424	55435	11
		decline	HDS	55435	55437	2
		decline	SDS	55437	-	1
		decline	HDS	55438	55441	3
		transition	HDS → SDS	55441	55444	3
		decline	SDS	55444	-	1
		decline	HDS	55445	55448	3
		transition	HDS → IMS → HDS	55448	-	1
		decline	HDS	55449	55451	2
		decline	SDS	55451	55453	2
		decline	HDS	55453	55455	2
		transition	HDS → SDS	55455	55458	3
		decline	SDS	55458	55464	6
		transition	SDS → IMS → SDS	55464	55469	5
		decline	SDS	55469	55472	3
		transition	SDS → IMS → SDS	55472	55474	2
		decline	SDS	55474	55481	7
		transition	SDS → IMS → SDS	55481	55483	2
		decline	SDS	55483	55512	29
		transition	SDS → HDS	55512	55519	7
		decline	HDS	55519	55551	32

Continued on Next Page...

Table A.4 – Continued

Source Name	Outburst ID	Stage	State(s)	$t_{\rm beg}$[a] (MJD)	$t_{\rm end}$[a] (MJD)	$t_{\rm dur}$[b] (days)
		transition	HDS → IMS → HDS	55551	55557	6
		decline	HDS	55557	55584	27
		decline	SDS	55584	55606	22
		decline	HDS	55606	55608	2
		decline	SDS	55608	55628	20
		decline	HDS	55628	55633	5
		transition	HDS → IMS → HDS	55633	-	1
		decline	HDS	55634	55648	14
		decline	SDS	55648	-	1
		decline	HDS	55649	-	1
		transition	HDS → SDS	55650	55654	4
		decline	SDS	55654	-	1
		transition	SDS → IMS → SDS	55655	55670	15
		decline	SDS	55670	55678	8
		transition	SDS → IMS → SDS	55678	55683	5
		decline	SDS	55683	55686	3
		decline	HDS	55686	55712	26
		transition	HDS → IMS → HDS	55712	55715	3
		decline	HDS	55715	55718	3
		transition	HDS → IMS → HDS	55718	55721	3
		decline	HDS	55721	55723	2
		transition	HDS → SDS	55723	-	1
		decline	SDS	55724	55736	12
		transition	SDS → HDS	55736	-	1
		decline	HDS	55737	55763	26
		transition	HDS → SDS	55763	-	1
		decline	SDS	55764	55790	26
		decline	HDS	55790	55797	7
		decline	SDS	55797	55860	63
		transition	SDS → IMS → SDS	55860	55867	7
		decline	SDS	55867	55869	2
		transition	SDS → IMS → SDS	55869	-	1
		decline	SDS	55870	55872	2
		transition	SDS → IMS → SDS	55872	55895	23
		decline	SDS	55895	55897	2
		transition	SDS → IMS → SDS	55897	55900	3
		decline	SDS	55900	55903	3

Continued on Next Page...

Table A.4 – Continued

Source Name	Outburst ID	Stage	State(s)	$t_{\rm beg}$[a] (MJD)	$t_{\rm end}$[a] (MJD)	$t_{\rm dur}$[b] (days)
		decline	HDS	55903	55920	17
		decline	SDS	55920	-	1
		transition	SDS → IMS → SDS	55921	-	1
		decline	SDS	55922	55925	3
		decline	HDS	55925	55929	4
		decline	SDS	55929	-	1
		transition	SDS → IMS → SDS	55930	55932	2
		decline	SDS	55932	55934	2
		transition	SDS → HDS	55934	55944	10
		decline	HDS	55944	55950	6
		transition	HDS → IMS → HDS	55950	-	1
		decline	HDS	55951	55953	2
		transition	HDS → IMS → HDS	55953	55995	42
		decline	HDS	55995	55997	2
		transition	HDS → SDS	55997	56000	3
		decline	SDS	56000	56007	7
		transition	SDS → HDS	56007	56010	3
		decline	HDS	56010	56057	47
		transition	HDS → IMS → HDS	56057	56059	2
		decline	HDS	56059	56074	15
		decline	SDS	56074	56077	3
		transition	SDS → IMS → SDS	56077	-	1
		decline	SDS	56078	56089	11
		transition	SDS → IMS → SDS	56089	56096	7
		decline	SDS	56096	56098	2
		transition	SDS → IMS → SDS	56098	56100	2
		decline	SDS	56100	-	1
		decline	HDS	56101	56104	3
		transition	HDS → IMS → HDS	56104	56106	2
		decline	HDS	56106	56120	14
		decline	SDS	56120	-	1
		decline	HDS	56121	56181	60
		transition	HDS → IMS → HDS	56181	56185	4
		decline	HDS	56185	56189	4
		transition	HDS → SDS	56189	56192	3
		decline	SDS	56192	56271	79
		decline	HDS	56271	56308	37

Continued on Next Page...

Table A.4 – Continued

Source Name	Outburst ID	Stage	State(s)	$t_{\rm beg}$[a] (MJD)	$t_{\rm end}$[a] (MJD)	$t_{\rm dur}$[b] (days)
		decline	SDS	56308	-	1
		decline	HDS	56309	56347	38
		decline	SDS	56347	56352	5
		decline	HDS	56352	56358	6
		decline	SDS	56358	-	1
		transition	SDS → IMS → SDS	56359	56361	2
		decline	SDS	56361	-	1
		decline	HDS	56362	56382	20
		decline	SDS	56382	-	1
		decline	HDS	56383	56397	14
		transition	HDS → SDS	56397	-	1
		decline	SDS	56398	56402	4
		transition	SDS → IMS → SDS	56402	56408	6
		decline	SDS	56408	56413	5
		decline	HDS	56413	56421	8
		transition	HDS → IMS → HDS	56421	-	1
		decline	HDS	56422	56427	5
		decline	SDS	56427	56429	2
		decline	HDS	56429	56442	13
		decline	SDS	56442	56445	3
		decline	HDS	56445	56449	4
		decline	SDS	56449	56455	6
		decline	HDS	56455	56462	7
		transition	HDS → IMS → HDS	56462	-	1
		decline	HDS	56463	56492	29
		transition	HDS → IMS → HDS	56492	56494	2
		decline	HDS	56494	56497	3
		transition	HDS → IMS → HDS	56497	56526	29
		decline	HDS	56526	56529	3
		transition	HDS → IMS → HDS	56529	56555	26
		decline	HDS	56555	56567	12
		transition	HDS → IMS → HDS	56567	56573	6
		decline	HDS	56573	56576	3
		decline	SDS	56576	-	1
		decline	HDS	56577	56582	5
		transition	HDS → IMS → HDS	56582	56586	4
		decline	HDS	56586	56588	2

Continued on Next Page...

Table A.4 – Continued

Source Name	Outburst ID	Stage	State(s)	$t_{\rm beg}$[a] (MJD)	$t_{\rm end}$[a] (MJD)	$t_{\rm dur}$[b] (days)
		transition	HDS → IMS → HDS	56588	56593	5
		decline	HDS	56593	56595	2
		transition	HDS → IMS → HDS	56595	56598	3
		decline	HDS	56598	56600	2
		transition	HDS → -	56600	56751	151
		decline	-	56751	56779	28
4U1956+350	1996-2014	rise	HDS	50087	52457	2370
		rise	SDS	52457	-	1
		rise	HDS	52458	52463	5
		rise	SDS	52463	-	1
		rise	HDS	52464	52472	8
		rise	SDS	52472	-	1
		rise	HDS	52473	52478	5
		rise	SDS	52478	52482	4
		rise	HDS	52482	52489	7
		transition	HDS → IMS → HDS	52489	52491	2
		rise	HDS	52491	52494	3
		rise	SDS	52494	-	1
		rise	HDS	52495	52502	7
		rise	SDS	52502	-	1
		rise	HDS	52503	52509	6
		rise	SDS	52509	52512	3
		rise	HDS	52512	52514	2
		rise	SDS	52514	-	1
		rise	HDS	52515	52518	3
		rise	SDS	52518	52527	9
		rise	HDS	52527	52529	2
		rise	SDS	52529	-	1
		rise	HDS	52530	52532	2
		rise	SDS	52532	52534	2
		rise	HDS	52534	52536	2
		rise	SDS	52536	52538	2
		rise	HDS	52538	52540	2
		rise	SDS	52540	52823	283
		decline	SDS	52823	52823	0
		decline	HDS	52823	52826	3

Continued on Next Page...

Table A.4 – Continued

Source Name	Outburst ID	Stage	State(s)	$t_{\rm beg}$[a] (MJD)	$t_{\rm end}$[a] (MJD)	$t_{\rm dur}$[b] (days)
		decline	SDS	52826	53381	555
		decline	HDS	53381	53383	2
		decline	SDS	53383	54088	705
		decline	HDS	54088	54090	2
		decline	SDS	54090	55399	1309
		decline	HDS	55399	55401	2
		decline	SDS	55401	55408	7
		transition	SDS → IMS → SDS	55408	55410	2
		decline	SDS	55410	-	1
		transition	SDS → HDS	55411	-	1
		decline	HDS	55412	-	1
		decline	SDS	55413	55468	55
		decline	HDS	55468	55470	2
		transition	HDS → SDS	55470	-	1
		decline	SDS	55471	55475	4
		transition	SDS → IMS → SDS	55475	55477	2
		decline	SDS	55477	55486	9
		transition	SDS → IMS → SDS	55486	55488	2
		decline	SDS	55488	55495	7
		decline	HDS	55495	-	1
		decline	SDS	55496	-	1
		decline	HDS	55497	55501	4
		transition	HDS → SDS	55501	-	1
		decline	SDS	55502	55519	17
		transition	SDS → IMS → SDS	55519	55527	8
		decline	SDS	55527	-	1
		decline	HDS	55528	55532	4
		transition	HDS → IMS → HDS	55532	55559	27
		decline	HDS	55559	55566	7
		transition	HDS → SDS	55566	55584	18
		decline	SDS	55584	55601	17
		transition	SDS → IMS → SDS	55601	55626	25
		decline	SDS	55626	55631	5
		transition	SDS → IMS → SDS	55631	-	1
		decline	SDS	55632	55636	4
		transition	SDS → IMS → SDS	55636	-	1
		decline	SDS	55637	55639	2

Continued on Next Page...

Table A.4 – Continued

Source Name	Outburst ID	Stage	State(s)	$t_{\rm beg}$[a] (MJD)	$t_{\rm end}$[a] (MJD)	$t_{\rm dur}$[b] (days)
		transition	SDS → IMS → SDS	55639	55644	5
		decline	SDS	55644	55646	2
		transition	SDS → IMS → SDS	55646	55650	4
		decline	SDS	55650	-	1
		transition	SDS → IMS → SDS	55651	55654	3
		decline	SDS	55654	-	1
		transition	SDS → IMS → SDS	55655	55661	6
		decline	SDS	55661	-	1
		transition	SDS → HDS	55662	55716	54
		decline	HDS	55716	55718	2
		transition	HDS → IMS → HDS	55718	55796	78
		decline	HDS	55796	55799	3
		transition	HDS → SDS	55799	55801	2
		decline	SDS	55801	55840	39
		transition	SDS → IMS → SDS	55840	55849	9
		decline	SDS	55849	-	1
		transition	SDS → IMS → SDS	55850	55860	10
		decline	SDS	55860	-	1
		transition	SDS → IMS → SDS	55861	55866	5
		decline	SDS	55866	-	1
		transition	SDS → IMS → SDS	55867	55870	3
		decline	SDS	55870	-	1
		decline	HDS	55871	55882	11
		decline	SDS	55882	55884	2
		transition	SDS → HDS	55884	-	1
		decline	HDS	55885	55892	7
		decline	SDS	55892	55947	55
		decline	HDS	55947	55949	2
		decline	SDS	55949	55951	2
		decline	HDS	55951	55953	2
		transition	HDS → IMS → HDS	55953	55956	3
		decline	HDS	55956	55958	2
		transition	HDS → IMS → HDS	55958	55991	33
		decline	HDS	55991	55993	2
		transition	HDS → IMS → HDS	55993	56003	10
		decline	HDS	56003	56005	2
		decline	SDS	56005	-	1

Continued on Next Page...

Table A.4 – Continued

Source Name	Outburst ID	Stage	State(s)	$t_{\rm beg}$[a] (MJD)	$t_{\rm end}$[a] (MJD)	$t_{\rm dur}$[b] (days)
		decline	HDS	56006	56114	108
		decline	SDS	56114	56118	4
		transition	SDS → HDS	56118	56127	9
		decline	HDS	56127	56139	12
		decline	SDS	56139	-	1
		decline	HDS	56140	56145	5
		decline	SDS	56145	-	1
		transition	SDS → HDS	56146	-	1
		decline	HDS	56147	56151	4
		transition	HDS → IMS → HDS	56151	-	1
		decline	HDS	56152	56155	3
		decline	SDS	56155	56157	2
		decline	HDS	56157	56165	8
		decline	SDS	56165	-	1
		decline	HDS	56166	56169	3
		transition	HDS → IMS → HDS	56169	-	1
		decline	HDS	56170	56174	4
		decline	SDS	56174	56202	28
		transition	SDS → HDS	56202	56204	2
		decline	HDS	56204	56208	4
		decline	SDS	56208	-	1
		decline	HDS	56209	56214	5
		decline	SDS	56214	-	1
		transition	SDS → HDS	56215	-	1
		decline	HDS	56216	56220	4
		decline	SDS	56220	-	1
		decline	HDS	56221	56232	11
		decline	SDS	56232	56234	2
		transition	SDS → HDS	56234	-	1
		decline	HDS	56235	56239	4
		decline	SDS	56239	-	1
		decline	HDS	56240	56285	45
		decline	SDS	56285	56287	2
		transition	SDS → HDS	56287	56290	3
		decline	HDS	56290	56296	6
		decline	SDS	56296	56299	3
		transition	SDS → HDS	56299	-	1

Continued on Next Page...

Table A.4 – Continued

Source Name	Outburst ID	Stage	State(s)	$t_{\rm beg}$[a] (MJD)	$t_{\rm end}$[a] (MJD)	$t_{\rm dur}$[b] (days)
		decline	HDS	56300	56303	3
		decline	SDS	56303	-	1
		decline	HDS	56304	56311	7
		transition	HDS → IMS → HDS	56311	-	1
		decline	HDS	56312	56315	3
		transition	HDS → IMS → HDS	56315	56345	30
		decline	HDS	56345	56347	2
		transition	HDS → IMS → HDS	56347	56349	2
		decline	HDS	56349	56352	3
		decline	SDS	56352	56354	2
		decline	HDS	56354	56357	3
		transition	HDS → IMS → HDS	56357	-	1
		decline	HDS	56358	56361	3
		transition	HDS → IMS → HDS	56361	-	1
		decline	HDS	56362	56365	3
		decline	SDS	56365	-	1
		decline	HDS	56366	56370	4
		decline	SDS	56370	-	1
		transition	SDS → IMS → SDS	56371	-	1
		decline	SDS	56372	56374	2
		decline	HDS	56374	56382	8
		transition	HDS → SDS	56382	56385	3
		decline	SDS	56385	-	1
		decline	HDS	56386	56389	3
		transition	HDS → IMS → HDS	56389	56420	31
		decline	HDS	56420	56432	12
		decline	SDS	56432	56435	3
		decline	HDS	56435	56438	3
		decline	SDS	56438	56443	5
		decline	HDS	56443	56460	17
		transition	HDS → IMS → HDS	56460	-	1
		decline	HDS	56461	56463	2
		transition	HDS → IMS → HDS	56463	56479	16
		decline	HDS	56479	56499	20
		decline	SDS	56499	-	1
		decline	HDS	56500	56511	11
		transition	HDS → IMS → HDS	56511	-	1

Continued on Next Page...

Table A.4 – Continued

Source Name	Outburst ID	Stage	State(s)	$t_{\rm beg}$[a] (MJD)	$t_{\rm end}$[a] (MJD)	$t_{\rm dur}$[b] (days)
		decline	HDS	56512	56514	2
		decline	SDS	56514	56517	3
		decline	HDS	56517	56519	2
		decline	SDS	56519	56525	6
		decline	HDS	56525	56529	4
		decline	SDS	56529	-	1
		decline	HDS	56530	56535	5
		transition	HDS → IMS → HDS	56535	56562	27
		decline	HDS	56562	56564	2
		transition	HDS → IMS → HDS	56564	-	1
		decline	HDS	56565	56568	3
		transition	HDS → IMS → HDS	56568	-	1
		decline	HDS	56569	56572	3
		decline	SDS	56572	56574	2
		transition	SDS → IMS → SDS	56574	-	1
		decline	SDS	56575	56578	3
		transition	SDS → IMS → SDS	56578	-	1
		decline	SDS	56579	-	1
		decline	HDS	56580	56585	5
		decline	SDS	56585	-	1
		decline	HDS	56586	56599	13
		decline	SDS	56599	56601	2
		transition	SDS → IMS → SDS	56601	56606	5
		decline	SDS	56606	56608	2
		transition	SDS → IMS → SDS	56608	56623	15
		decline	SDS	56623	56630	7
		decline	HDS	56630	56643	13
		decline	SDS	56643	56646	3
		decline	HDS	56646	56648	2
		transition	HDS → -	56648	56751	103
		decline	-	56751	56782	31
4U1957+115	1996-2014	rise	-	50136	50144	8
		rise	HDS	50144	50164	20
		transition	HDS → IMS → HDS	50164	50166	2
		rise	HDS	50166	50224	58
		transition	HDS → IMS → HDS	50224	50233	9

Continued on Next Page...

Table A.4 – Continued

Source Name	Outburst ID	Stage	State(s)	$t_{\rm beg}$[a] (MJD)	$t_{\rm end}$[a] (MJD)	$t_{\rm dur}$[b] (days)
		rise	HDS	50233	50235	2
		transition	HDS → IMS → HDS	50235	50250	15
		rise	HDS	50250	50254	4
		transition	HDS → IMS → HDS	50254	50299	45
		rise	HDS	50299	50301	2
		transition	HDS → IMS → HDS	50301	50318	17
		rise	HDS	50318	50320	2
		transition	HDS → IMS → HDS	50320	50323	3
		rise	HDS	50323	50325	2
		transition	HDS → IMS → HDS	50325	50327	2
		rise	HDS	50327	50329	2
		transition	HDS → IMS → HDS	50329	50345	16
		rise	HDS	50345	50350	5
		transition	HDS → IMS → HDS	50350	50356	6
		rise	HDS	50356	50358	2
		transition	HDS → IMS → HDS	50358	-	1
		rise	HDS	50359	50362	3
		transition	HDS → IMS → HDS	50362	50364	2
		rise	HDS	50364	50380	16
		transition	HDS → IMS → HDS	50380	50382	2
		rise	HDS	50382	50392	10
		transition	HDS → IMS → HDS	50392	50394	2
		rise	HDS	50394	50397	3
		transition	HDS → IMS → HDS	50397	-	1
		rise	HDS	50398	50402	4
		rise	SDS	50402	50424	22
		rise	HDS	50424	50439	15
		rise	SDS	50439	50442	3
		rise	HDS	50442	50490	48
		rise	SDS	50490	50495	5
		rise	HDS	50495	50514	19
		rise	SDS	50514	50516	2
		rise	HDS	50516	50537	21
		transition	HDS → IMS → HDS	50537	50540	3
		rise	HDS	50540	50583	43
		transition	HDS → IMS → HDS	50583	50591	8
		rise	HDS	50591	50593	2

Continued on Next Page...

Table A.4 – Continued

Source Name	Outburst ID	Stage	State(s)	$t_{\rm beg}$[a] (MJD)	$t_{\rm end}$[a] (MJD)	$t_{\rm dur}$[b] (days)
		rise	SDS	50593	50597	4
		rise	HDS	50597	50605	8
		rise	SDS	50605	50610	5
		rise	HDS	50610	50625	15
		rise	SDS	50625	50629	4
		rise	HDS	50629	50631	2
		rise	SDS	50631	-	1
		rise	HDS	50632	50740	108
		rise	SDS	50740	-	1
		rise	HDS	50741	50750	9
		rise	SDS	50750	-	1
		rise	HDS	50751	50765	14
		rise	SDS	50765	50779	14
		rise	HDS	50779	50786	7
		transition	HDS → IMS → HDS	50786	50791	5
		rise	HDS	50791	50795	4
		transition	HDS → IMS → HDS	50795	-	1
		rise	HDS	50796	50802	6
		transition	HDS → IMS → HDS	50802	50805	3
		rise	HDS	50805	50807	2
		transition	HDS → IMS → HDS	50807	50846	39
		rise	HDS	50846	50848	2
		transition	HDS → IMS → HDS	50848	50859	11
		rise	HDS	50859	50861	2
		transition	HDS → IMS → HDS	50861	50868	7
		rise	HDS	50868	50871	3
		transition	HDS → IMS → HDS	50871	50877	6
		rise	HDS	50877	50879	2
		transition	HDS → IMS → HDS	50879	50887	8
		rise	HDS	50887	50889	2
		transition	HDS → IMS → HDS	50889	50900	11
		rise	HDS	50900	50902	2
		transition	HDS → IMS → HDS	50902	50910	8
		rise	HDS	50910	50912	2
		transition	HDS → IMS → HDS	50912	-	1
		rise	HDS	50913	50936	23
		transition	HDS → IMS → HDS	50936	-	1

Continued on Next Page...

Table A.4 – Continued

Source Name	Outburst ID	Stage	State(s)	$t_{\rm beg}$[a] (MJD)	$t_{\rm end}$[a] (MJD)	$t_{\rm dur}$[b] (days)
		rise	HDS	50937	51080	143
		rise	SDS	51080	-	1
		rise	HDS	51081	51092	11
		rise	SDS	51092	-	1
		rise	HDS	51093	51143	50
		rise	SDS	51143	51231	88
		rise	HDS	51231	51233	2
		rise	SDS	51233	-	1
		rise	HDS	51234	51251	17
		rise	SDS	51251	51254	3
		rise	HDS	51254	51337	83
		rise	SDS	51337	-	1
		rise	HDS	51338	51351	13
		rise	SDS	51351	51362	11
		rise	HDS	51362	51388	26
		rise	SDS	51388	-	1
		rise	HDS	51389	51396	7
		rise	SDS	51396	-	1
		rise	HDS	51397	51400	3
		rise	SDS	51400	-	1
		rise	HDS	51401	51422	21
		rise	SDS	51422	-	1
		rise	HDS	51423	51438	15
		rise	SDS	51438	51440	2
		rise	HDS	51440	51442	2
		rise	SDS	51442	51445	3
		rise	HDS	51445	51447	2
		rise	SDS	51447	-	1
		rise	HDS	51448	51451	3
		rise	SDS	51451	51496	45
		rise	HDS	51496	51498	2
		rise	SDS	51498	51502	4
		rise	HDS	51502	51504	2
		rise	SDS	51504	51519	15
		rise	HDS	51519	51524	5
		rise	SDS	51524	51529	5
		rise	HDS	51529	51531	2

Continued on Next Page...

Table A.4 – Continued

Source Name	Outburst ID	Stage	State(s)	$t_{\rm beg}$[a] (MJD)	$t_{\rm end}$[a] (MJD)	$t_{\rm dur}$[b] (days)
		rise	SDS	51531	51537	6
		rise	HDS	51537	51539	2
		rise	SDS	51539	51542	3
		rise	HDS	51542	51544	2
		rise	SDS	51544	51609	65
		rise	HDS	51609	51611	2
		rise	SDS	51611	51641	30
		rise	HDS	51641	51644	3
		rise	SDS	51644	-	1
		transition	SDS → HDS	51645	-	1
		rise	HDS	51646	51651	5
		transition	HDS → IMS → HDS	51651	-	1
		rise	HDS	51652	51659	7
		transition	HDS → IMS → HDS	51659	-	1
		rise	HDS	51660	51673	13
		transition	HDS → IMS → HDS	51673	51680	7
		rise	HDS	51680	51705	25
		transition	HDS → IMS → HDS	51705	51708	3
		rise	HDS	51708	51711	3
		transition	HDS → IMS → HDS	51711	51714	3
		rise	HDS	51714	51716	2
		rise	SDS	51716	51718	2
		rise	HDS	51718	51733	15
		rise	SDS	51733	51737	4
		rise	HDS	51737	51777	40
		rise	SDS	51777	-	1
		rise	HDS	51778	51781	3
		rise	SDS	51781	51790	9
		rise	HDS	51790	51792	2
		rise	SDS	51792	51802	10
		rise	HDS	51802	51807	5
		rise	SDS	51807	51814	7
		rise	HDS	51814	51816	2
		rise	SDS	51816	51820	4
		rise	HDS	51820	51822	2
		rise	SDS	51822	51834	12
		rise	HDS	51834	51843	9

Continued on Next Page...

Table A.4 – Continued

Source Name	Outburst ID	Stage	State(s)	$t_{\rm beg}$[a] (MJD)	$t_{\rm end}$[a] (MJD)	$t_{\rm dur}$[b] (days)
		rise	SDS	51843	-	1
		rise	HDS	51844	51846	2
		rise	SDS	51846	51848	2
		rise	HDS	51848	51850	2
		rise	SDS	51850	-	1
		rise	HDS	51851	51856	5
		rise	SDS	51856	51861	5
		rise	HDS	51861	51869	8
		rise	SDS	51869	-	1
		rise	HDS	51870	51899	29
		rise	SDS	51899	51916	17
		rise	HDS	51916	51981	65
		rise	SDS	51981	-	1
		rise	HDS	51982	52057	75
		rise	SDS	52057	52063	6
		rise	HDS	52063	52065	2
		rise	SDS	52065	52067	2
		rise	HDS	52067	52069	2
		rise	SDS	52069	52071	2
		rise	HDS	52071	52083	12
		rise	SDS	52083	52099	16
		rise	HDS	52099	52108	9
		rise	SDS	52108	-	1
		rise	HDS	52109	52113	4
		rise	SDS	52113	-	1
		rise	HDS	52114	52118	4
		rise	SDS	52118	-	1
		rise	HDS	52119	52121	2
		rise	SDS	52121	52127	6
		rise	HDS	52127	52130	3
		rise	SDS	52130	52133	3
		rise	HDS	52133	52136	3
		transition	HDS → IMS → HDS	52136	52138	2
		rise	HDS	52138	52140	2
		transition	HDS → IMS → HDS	52140	52166	26
		rise	HDS	52166	52168	2
		transition	HDS → IMS → HDS	52168	52170	2

Continued on Next Page...

Table A.4 – Continued

Source Name	Outburst ID	Stage	State(s)	$t_{\rm beg}$[a] (MJD)	$t_{\rm end}$[a] (MJD)	$t_{\rm dur}$[b] (days)
		rise	HDS	52170	52173	3
		transition	HDS → IMS → HDS	52173	52184	11
		rise	HDS	52184	52186	2
		transition	HDS → IMS → HDS	52186	52188	2
		rise	HDS	52188	52190	2
		transition	HDS → IMS → HDS	52190	52200	10
		rise	HDS	52200	52203	3
		transition	HDS → IMS → HDS	52203	-	1
		rise	HDS	52204	52226	22
		transition	HDS → IMS → HDS	52226	-	1
		rise	HDS	52227	52233	6
		transition	HDS → IMS → HDS	52233	-	1
		rise	HDS	52234	52267	33
		transition	HDS → IMS → HDS	52267	52339	72
		rise	HDS	52339	52343	4
		transition	HDS → IMS → HDS	52343	52346	3
		rise	HDS	52346	52348	2
		transition	HDS → IMS → HDS	52348	52364	16
		rise	HDS	52364	52366	2
		transition	HDS → IMS → HDS	52366	52370	4
		rise	HDS	52370	52373	3
		transition	HDS → IMS → HDS	52373	52375	2
		rise	HDS	52375	52380	5
		transition	HDS → IMS → HDS	52380	52383	3
		rise	HDS	52383	52385	2
		transition	HDS → IMS → HDS	52385	-	1
		rise	HDS	52386	52399	13
		transition	HDS → IMS → HDS	52399	-	1
		rise	HDS	52400	52483	83
		transition	HDS → IMS → HDS	52483	52486	3
		rise	HDS	52486	52488	2
		transition	HDS → IMS → HDS	52488	-	1
		rise	HDS	52489	52494	5
		transition	HDS → IMS → HDS	52494	-	1
		rise	HDS	52495	52497	2
		transition	HDS → IMS → HDS	52497	-	1
		rise	HDS	52498	52511	13

Continued on Next Page...

Table A.4 – Continued

Source Name	Outburst ID	Stage	State(s)	$t_{\rm beg}$[a] (MJD)	$t_{\rm end}$[a] (MJD)	$t_{\rm dur}$[b] (days)
		transition	HDS → IMS → HDS	52511	52513	2
		rise	HDS	52513	52520	7
		transition	HDS → IMS → HDS	52520	52522	2
		rise	HDS	52522	52527	5
		transition	HDS → IMS → HDS	52527	-	1
		rise	HDS	52528	52545	17
		rise	SDS	52545	-	1
		rise	HDS	52546	52589	43
		rise	SDS	52589	52597	8
		rise	HDS	52597	52606	9
		rise	SDS	52606	52685	79
		rise	HDS	52685	52692	7
		rise	SDS	52692	52704	12
		rise	HDS	52704	52708	4
		rise	SDS	52708	-	1
		rise	HDS	52709	52743	34
		transition	HDS → IMS → HDS	52743	-	1
		rise	HDS	52744	52748	4
		transition	HDS → IMS → HDS	52748	52775	27
		rise	HDS	52775	52777	2
		transition	HDS → IMS → HDS	52777	-	1
		rise	HDS	52778	52780	2
		transition	HDS → IMS → HDS	52780	52784	4
		rise	HDS	52784	52786	2
		transition	HDS → IMS → HDS	52786	-	1
		rise	HDS	52787	52789	2
		transition	HDS → IMS → HDS	52789	52832	43
		rise	HDS	52832	52834	2
		transition	HDS → IMS → HDS	52834	52844	10
		rise	HDS	52844	52846	2
		transition	HDS → IMS → HDS	52846	52874	28
		rise	HDS	52874	52878	4
		transition	HDS → IMS → HDS	52878	52880	2
		rise	HDS	52880	52887	7
		transition	HDS → IMS → HDS	52887	52893	6
		rise	HDS	52893	52895	2
		transition	HDS → IMS → HDS	52895	52907	12

Continued on Next Page...

Table A.4 – Continued

Source Name	Outburst ID	Stage	State(s)	$t_{\rm beg}$[a] (MJD)	$t_{\rm end}$[a] (MJD)	$t_{\rm dur}$[b] (days)
		rise	HDS	52907	52917	10
		transition	HDS → IMS → HDS	52917	52927	10
		rise	HDS	52927	52930	3
		transition	HDS → IMS → HDS	52930	52935	5
		rise	HDS	52935	52938	3
		transition	HDS → IMS → HDS	52938	52940	2
		rise	HDS	52940	52945	5
		transition	HDS → IMS → HDS	52945	52967	22
		rise	HDS	52967	52975	8
		transition	HDS → IMS → HDS	52975	52979	4
		rise	HDS	52979	52981	2
		transition	HDS → IMS → HDS	52981	-	1
		rise	HDS	52982	52984	2
		transition	HDS → IMS → HDS	52984	52989	5
		rise	HDS	52989	52992	3
		transition	HDS → IMS → HDS	52992	53040	48
		rise	HDS	53040	53076	36
		transition	HDS → IMS → HDS	53076	53093	17
		rise	HDS	53093	53096	3
		rise	SDS	53096	53105	9
		rise	HDS	53105	53107	2
		rise	SDS	53107	53142	35
		rise	HDS	53142	53145	3
		rise	SDS	53145	53147	2
		rise	HDS	53147	53151	4
		rise	SDS	53151	53161	10
		rise	HDS	53161	53166	5
		transition	HDS → IMS → HDS	53166	53184	18
		rise	HDS	53184	53186	2
		transition	HDS → IMS → HDS	53186	-	1
		rise	HDS	53187	53190	3
		rise	SDS	53190	-	1
		rise	HDS	53191	53265	74
		rise	SDS	53265	53284	19
		rise	HDS	53284	53286	2
		rise	SDS	53286	53311	25
		rise	HDS	53311	53313	2

Continued on Next Page...

Table A.4 – Continued

Source Name	Outburst ID	Stage	State(s)	$t_{\rm beg}$[a] (MJD)	$t_{\rm end}$[a] (MJD)	$t_{\rm dur}$[b] (days)
		rise	SDS	53313	53329	16
		rise	HDS	53329	53331	2
		rise	SDS	53331	53335	4
		rise	HDS	53335	53337	2
		rise	SDS	53337	53341	4
		rise	HDS	53341	53354	13
		rise	SDS	53354	53412	58
		rise	HDS	53412	53417	5
		rise	SDS	53417	53430	13
		transition	SDS → HDS	53430	53442	12
		rise	HDS	53442	53454	12
		rise	SDS	53454	53467	13
		transition	SDS → IMS → SDS	53467	53485	18
		rise	SDS	53485	-	1
		transition	SDS → IMS → SDS	53486	53489	3
		rise	SDS	53489	-	1
		transition	SDS → IMS → SDS	53490	53493	3
		rise	SDS	53493	-	1
		transition	SDS → IMS → SDS	53494	53497	3
		rise	SDS	53497	53504	7
		transition	SDS → IMS → SDS	53504	53509	5
		rise	SDS	53509	53512	3
		transition	SDS → IMS → SDS	53512	53515	3
		rise	SDS	53515	53614	99
		transition	SDS → IMS → SDS	53614	53616	2
		rise	SDS	53616	53647	31
		transition	SDS → IMS → SDS	53647	-	1
		rise	SDS	53648	53665	17
		rise	HDS	53665	53844	179
		rise	SDS	53844	-	1
		rise	HDS	53845	53851	6
		rise	SDS	53851	-	1
		rise	HDS	53852	53867	15
		rise	SDS	53867	-	1
		rise	HDS	53868	53878	10
		decline	HDS	53878	53902	24
		decline	SDS	53902	-	1

Continued on Next Page...

Table A.4 – Continued

Source Name	Outburst ID	Stage	State(s)	$t_{\rm beg}$[a] (MJD)	$t_{\rm end}$[a] (MJD)	$t_{\rm dur}$[b] (days)
		decline	HDS	53903	53941	38
		transition	HDS → IMS → HDS	53941	53954	13
		decline	HDS	53954	53968	14
		transition	HDS → IMS → HDS	53968	-	1
		decline	HDS	53969	54000	31
		decline	SDS	54000	-	1
		decline	HDS	54001	54005	4
		decline	SDS	54005	54007	2
		decline	HDS	54007	54010	3
		decline	SDS	54010	54015	5
		decline	HDS	54015	54017	2
		decline	SDS	54017	54020	3
		decline	HDS	54020	54034	14
		transition	HDS → IMS → HDS	54034	54048	14
		decline	HDS	54048	54051	3
		decline	SDS	54051	54066	15
		transition	SDS → IMS → SDS	54066	54160	94
		decline	SDS	54160	54171	11
		transition	SDS → IMS → SDS	54171	54176	5
		decline	SDS	54176	54281	105
		transition	SDS → IMS → SDS	54281	54293	12
		decline	SDS	54293	54302	9
		transition	SDS → IMS → SDS	54302	54315	13
		decline	SDS	54315	54343	28
		transition	SDS → IMS → SDS	54343	54358	15
		decline	SDS	54358	54363	5
		transition	SDS → IMS → SDS	54363	54365	2
		decline	SDS	54365	54378	13
		transition	SDS → IMS → SDS	54378	54380	2
		decline	SDS	54380	54383	3
		transition	SDS → IMS → SDS	54383	54385	2
		decline	SDS	54385	54406	21
		transition	SDS → IMS → SDS	54406	54408	2
		decline	SDS	54408	54446	38
		transition	SDS → IMS → SDS	54446	54460	14
		decline	SDS	54460	54515	55
		transition	SDS → IMS → SDS	54515	54554	39

Continued on Next Page...

Table A.4 – Continued

Source Name	Outburst ID	Stage	State(s)	$t_{\rm beg}$[a] (MJD)	$t_{\rm end}$[a] (MJD)	$t_{\rm dur}$[b] (days)
		decline	SDS	54554	54557	3
		transition	SDS → IMS → SDS	54557	54564	7
		decline	SDS	54564	54574	10
		transition	SDS → IMS → SDS	54574	54580	6
		decline	SDS	54580	54630	50
		transition	SDS → IMS → SDS	54630	54669	39
		decline	SDS	54669	54672	3
		transition	SDS → IMS → SDS	54672	-	1
		decline	SDS	54673	54696	23
		transition	SDS → IMS → SDS	54696	54702	6
		decline	SDS	54702	54706	4
		transition	SDS → IMS → SDS	54706	54716	10
		decline	SDS	54716	-	1
		transition	SDS → IMS → SDS	54717	54720	3
		decline	SDS	54720	54728	8
		transition	SDS → IMS → SDS	54728	54731	3
		decline	SDS	54731	54759	28
		transition	SDS → IMS → SDS	54759	54761	2
		decline	SDS	54761	54763	2
		transition	SDS → IMS → SDS	54763	54766	3
		decline	SDS	54766	54769	3
		transition	SDS → IMS → SDS	54769	54775	6
		decline	SDS	54775	-	1
		transition	SDS → IMS → SDS	54776	54780	4
		decline	SDS	54780	54785	5
		transition	SDS → IMS → SDS	54785	54797	12
		decline	SDS	54797	54801	4
		transition	SDS → IMS → SDS	54801	54854	53
		decline	SDS	54854	54858	4
		decline	HDS	54858	54866	8
		transition	HDS → SDS	54866	54875	9
		decline	SDS	54875	54897	22
		transition	SDS → IMS → SDS	54897	54913	16
		decline	SDS	54913	54917	4
		transition	SDS → IMS → SDS	54917	54920	3
		decline	SDS	54920	54924	4
		transition	SDS → IMS → SDS	54924	54937	13

Continued on Next Page...

Table A.4 – Continued

Source Name	Outburst ID	Stage	State(s)	$t_{\rm beg}$[a] (MJD)	$t_{\rm end}$[a] (MJD)	$t_{\rm dur}$[b] (days)
		decline	SDS	54937	54949	12
		transition	SDS → IMS → SDS	54949	55019	70
		decline	SDS	55019	55055	36
		transition	SDS → IMS → SDS	55055	55060	5
		decline	SDS	55060	55151	91
		transition	SDS → HDS	55151	55275	124
		decline	HDS	55275	55278	3
		transition	HDS → IMS → HDS	55278	55286	8
		decline	HDS	55286	55299	13
		transition	HDS → IMS → HDS	55299	55305	6
		decline	HDS	55305	55311	6
		transition	HDS → IMS → HDS	55311	-	1
		decline	HDS	55312	55318	6
		decline	SDS	55318	55322	4
		transition	SDS → IMS → SDS	55322	55329	7
		decline	SDS	55329	55347	18
		transition	SDS → IMS → SDS	55347	55357	10
		decline	SDS	55357	55363	6
		transition	SDS → IMS → SDS	55363	55388	25
		decline	SDS	55388	55392	4
		transition	SDS → IMS → SDS	55392	55397	5
		decline	SDS	55397	55470	73
		transition	SDS → IMS → SDS	55470	55515	45
		decline	SDS	55515	55526	11
		transition	SDS → IMS → SDS	55526	55530	4
		decline	SDS	55530	55555	25
		transition	SDS → IMS → SDS	55555	55566	11
		decline	SDS	55566	55569	3
		decline	HDS	55569	55613	44
		decline	SDS	55613	55619	6
		transition	SDS → IMS → SDS	55619	55628	9
		decline	SDS	55628	55631	3
		transition	SDS → IMS → SDS	55631	55634	3
		decline	SDS	55634	55636	2
		decline	HDS	55636	55788	152
		transition	HDS → SDS	55788	55790	2
		decline	SDS	55790	55792	2

Continued on Next Page...

Table A.4 – Continued

Source Name	Outburst ID	Stage	State(s)	$t_{\rm beg}$[a] (MJD)	$t_{\rm end}$[a] (MJD)	$t_{\rm dur}$[b] (days)
		decline	HDS	55792	55875	83
		transition	HDS → SDS	55875	55879	4
		decline	SDS	55879	55896	17
		decline	HDS	55896	55931	35
		transition	HDS → IMS → HDS	55931	55946	15
		decline	HDS	55946	55953	7
		transition	HDS → IMS → HDS	55953	55982	29
		decline	HDS	55982	56000	18
		transition	HDS → IMS → HDS	56000	56003	3
		decline	HDS	56003	56019	16
		transition	HDS → SDS	56019	56022	3
		decline	SDS	56022	56033	11
		transition	SDS → IMS → SDS	56033	56037	4
		decline	SDS	56037	56050	13
		transition	SDS → IMS → SDS	56050	56060	10
		decline	SDS	56060	56066	6
		transition	SDS → IMS → SDS	56066	56071	5
		decline	SDS	56071	56082	11
		decline	HDS	56082	56219	137
		transition	HDS → IMS → HDS	56219	56231	12
		decline	HDS	56231	56320	89
		transition	HDS → SDS	56320	56353	33
		decline	SDS	56353	56360	7
		decline	HDS	56360	56368	8
		decline	SDS	56368	56372	4
		decline	HDS	56372	56377	5
		decline	SDS	56377	56403	26
		transition	SDS → HDS	56403	56423	20
		decline	HDS	56423	56429	6
		transition	HDS → SDS	56429	56438	9
		decline	SDS	56438	56459	21
		decline	HDS	56459	56728	269
		decline	SDS	56728	56734	6
		transition	SDS → -	56734	56756	22
		decline	-	56756	56762	6
XTEJ2012+381	1998	rise	-	50940	50956	16

Continued on Next Page...

Table A.4 – Continued

Source Name	Outburst ID	Stage	State(s)	$t_{\rm beg}$[a] (MJD)	$t_{\rm end}$[a] (MJD)	$t_{\rm dur}$[b] (days)
		rise	HDS	50956	50961	5
		transition	HDS → SDS	50961	50963	2
		rise	SDS	50963	50986	23
		decline	SDS	50986	50989	3
		transition	SDS → IMS → SDS	50989	-	1
		decline	SDS	50990	50998	8
		transition	SDS → IMS → SDS	50998	-	1
		decline	SDS	50999	51035	36
		transition	SDS → IMS → SDS	51035	51039	4
		decline	SDS	51039	51046	7
		decline	HDS	51046	51054	8
		transition	HDS → IMS → HDS	51054	51085	31
		decline	HDS	51085	51090	5
		transition	HDS → SDS	51090	51100	10
		decline	SDS	51100	51113	13
		transition	SDS → IMS → SDS	51113	51116	3
		decline	SDS	51116	51120	4
		transition	SDS → IMS → SDS	51120	51123	3
		decline	SDS	51123	51125	2
		decline	-	51125	51142	17

Note. –

[a] The start and end times of a particular stage in an outburst, given in MJD.

[b] Duration of the particular outburst stage in days.

Table A.5: Luminosity data for Galactic BHs & BHCs Between 1996-2014

Source Name	Outburst ID	$t_{\rm dur}$ [a] (days)	$\int L dt$ [b] ($\times 10^{38}$ erg)	$L_{\rm peak,tot}$ [c] ($\times 10^{38}$ erg)	$L_{\rm edd}$ [c] ($L_{\rm peak,tot}/L_{\rm edd}$)	$L_{\rm peak,HCS}$ [d] ($\times 10^{38}$ erg)	$L_{\rm peak,SDS}$ [e] ($\times 10^{38}$ erg)	$t_{\rm HCS}$ [f] (days)	$t_{\rm SDS}$ [g] (days)	$t_{\rm IMS}$ [h] (days)	$t_{\rm und}$ [i] (days)
Note. – XTEJ0421+560	1998	50	0.69 ± 0.44	3.8 ± 3.4	0.29 ± 0.30	3.8 ± 3.4	-	5	0	0	45
4U0538−641	1996-2003	2905	604.8 ± 5.5	$28.2^{+8.1}_{-8.3}$	$3.12^{+0.91}_{-0.93}$	$28.2^{+8.1}_{-8.3}$	9.3 ± 2.2	1915	56	920	14
	2004-2014	3695	1615.3 ± 9.2	$23^{+7.1}_{-10}$	$2.6^{+0.8}_{-1.1}$	$23.1^{+4.8}_{-4.9}$	$21.4^{+3.7}_{-3.8}$	851	1160	1548	136
4U0540−697	1996-2014	6663	14186 ± 50	$28^{+9.9}_{-11}$	$1.99^{+0.74}_{-0.84}$	$27^{+8.8}_{-10}$	$28^{+9.9}_{-11}$	2863	1367	2281	152
XTEJ1118+480	1999/2000	203	0.0559 ± 0.0037	0.0257 ± 0.0047	$0.00271^{+0.00056}_{-0.00057}$	0.0257 ± 0.0047	-	183	0	0	20
MAXIJ1305−704	2012	182	7.90 ± 0.80	0.17 ± 0.16	0.013 ± 0.014	0.17 ± 0.16	-	54	0	41	87
SWIFTJ1357.2−0933	2010-2012	836	4.14 ± 0.30	$0.032^{+0.057}_{-0.056}$	0.0025 ± 0.0045	0.029 ± 0.049	-	20	0	0	816
GS1354−64	1997/1998	157	879 ± 93	27 ± 25	$1.9^{+1.9}_{-1.8}$	27 ± 25	-	109	0	0	48
SWIFTJ1539.2−6227	2008/2009	175	12.5 ± 1.7	0.88 ± 0.82	$0.068^{+0.071}_{-0.072}$	0.42 ± 0.38	0.19 ± 0.19	77	1	45	52

Continued on Next Page...

Table A.5 – Continued

Source Name	Outburst ID	$t_{\rm dur}$[a] (days)	$\int Ldt$[b] ($\times10^{38}$ erg)	$L_{\rm peak,tot}$[c] ($\times10^{38}$ erg)	$L_{\rm edd}$[c] ($L_{\rm peak,tot}/L_{\rm edd}$)	$L_{\rm peak,HCS}$[d] ($\times10^{38}$ erg)	$L_{\rm peak,SDS}$[e] ($\times10^{38}$ erg)	$t_{\rm HCS}$[f] (days)	$t_{\rm SDS}$[g] (days)	$t_{\rm IMS}$[h] (days)	$t_{\rm und}$[i] (days)
MAXIJ1543−564	2011	153	4.02 ± 0.41	0.18 ± 0.16	0.014 ± 0.014	0.18 ± 0.16	0.11 ± 0.10	40	3	22	88
4U1543−475	2002	54	23.8 ± 1.0	20.5 ± 2.7	1.70 ± 0.43	13.2 ± 1.8	20.5 ± 2.7	12	20	15	7
XTEJ1550−564	1998/1999	255	0.633 ± 0.096	18.1 ± 4.1	1.34 ± 0.42	18.1 ± 4.1	3.53 ± 0.80	160	38	48	9
	2000	107	0.264 ± 0.039	2.18 ± 0.50	0.161 ± 0.051	2.18 ± 0.50	-	88	0	0	19
	2001	50	0.115 ± 0.018	$0.144^{+0.038}_{-0.042}$	$0.0106^{+0.0036}_{-0.0039}$	$0.144^{+0.038}_{-0.042}$	-	33	0	0	17
	2001/2002	52	0.242 ± 0.031	$0.33^{+0.09}_{-0.10}$	$0.0246^{+0.0086}_{-0.0093}$	$0.33^{+0.09}_{-0.10}$	-	33	0	0	19
	2003	50	0.189 ± 0.032	0.244 ± 0.057	0.0181 ± 0.0058	0.244 ± 0.057	-	27	0	0	23
4U1630−472	1996	200	0.91 ± 0.23	1.8 ± 1.6	0.14 ± 0.14	1.8 ± 1.6	-	151	0	4	45
	1998	240	0.880 ± 0.098	2.3 ± 2.1	0.18 ± 0.19	2.3 ± 2.1	-	100	0	0	140
	1999	176	0.41 ± 0.11	1.3 ± 1.2	0.10 ± 0.10	1.3 ± 1.2	-	89	0	0	87
	2000/2001	234	1.16 ± 0.22	2.9 ± 2.7	0.23 ± 0.24	2.9 ± 2.7	-	196	0	0	38
	2002-2004	821	9.9 ± 1.1	5.2 ± 4.7	0.40 ± 0.41	5.2 ± 4.7	-	782	0	0	39
	2005/2006	184	1.74 ± 0.31	1.6 ± 1.5	0.13 ± 0.13	1.6 ± 1.5	1.6 ± 1.5	57	97	1	29
	2007/2008	200	1.70 ± 0.31	1.6 ± 1.5	0.12 ± 0.13	1.5 ± 1.4	1.6 ± 1.5	18	143	7	32

Continued on Next Page...

Table A.5 – Continued

Source Name	Outburst ID	$t_{\rm dur}$[a] (days)	$\int L dt$[b] ($\times 10^{38}$ erg)	$L_{\rm peak,tot}$[c] ($\times 10^{38}$ erg)	$L_{\rm edd}$[c] ($L_{\rm peak,tot}/L_{\rm edd}$)	$L_{\rm peak,HCS}$[d] ($\times 10^{38}$ erg)	$L_{\rm peak,SDS}$[e] ($\times 10^{38}$ erg)	$t_{\rm HCS}$[f] (days)	$t_{\rm SDS}$[g] (days)	$t_{\rm IMS}$[h] (days)	$t_{\rm und}$[i] (days)
	2009/2010	252	3.33 ± 0.31	1.7 ± 1.6	0.13 ± 0.14	$0.077^{+0.073}_{-0.072}$	1.7 ± 1.6	13	153	62	24
	2011-2013	694	132.9 ± 6.4	2.5 ± 2.2	0.19 ± 0.20	2.2 ± 2.1	2.5 ± 2.2	96	499	46	53
XTEJ1650−500	2001	108	0.282 ± 0.036	0.42 ± 0.22	0.068 ± 0.048	0.42 ± 0.22	0.28 ± 0.15	18	52	9	29
XTEJ1652−453	2009	169	7.62 ± 0.87	1.3 ± 1.2	0.10 ± 0.10	0.32 ± 0.31	1.3 ± 1.2	54	37	27	51
GROJ1655−40	1996/1997	507	1.02 ± 0.22	4.6 ± 1.4	0.66 ± 0.21	4.6 ± 1.4	0.75 ± 0.24	381	25	72	29
	2005	281	0.190 ± 0.021	6.8 ± 2.1	0.97 ± 0.31	0.76 ± 0.24	6.8 ± 2.1	45	185	0	51
MAXIJ1659−152	2010/2011	135	2.95 ± 0.36	0.72 ± 0.66	0.056 ± 0.058	0.72 ± 0.66	0.60 ± 0.54	29	19	79	8
GX339−4	1996	75	0.608 ± 0.070	0.64 ± 0.33	0.049 ± 0.036	0.64 ± 0.33	-	35	0	0	40
	1997-1999	840	13.80 ± 0.50	$2.8^{+1.8}_{-1.9}$	0.21 ± 0.18	1.33 ± 0.68	$2.8^{+1.8}_{-1.9}$	375	329	42	94
	2002/2003	388	9.37 ± 0.60	5.3 ± 2.7	0.41 ± 0.29	5.3 ± 2.6	5.3 ± 2.7	89	233	51	15
	2004/2005	437	10.45 ± 0.48	3.2 ± 1.6	0.25 ± 0.18	$1.36^{+0.70}_{-0.71}$	2.8 ± 1.5	159	158	79	41
	2006	126	0.920 ± 0.075	0.27 ± 0.14	0.021 ± 0.015	0.27 ± 0.14	-	104	0	0	22
	2006/2007	339	3.32 ± 0.19	3.5 ± 1.7	0.27 ± 0.19	3.3 ± 1.7	3.5 ± 1.7	181	88	2	68

Continued on Next Page...

Table A.5 – Continued

Source Name	Outburst ID	$t_{\rm dur}$[a] (days)	$\int Ldt$[b] ($\times10^{38}$ erg)	$L_{\rm peak,tot}$[c] ($\times10^{38}$ erg)	$L_{\rm edd}$[c] ($L_{\rm peak,tot}/L_{\rm edd}$)	$L_{\rm peak,HCS}$[d] ($\times10^{38}$ erg)	$L_{\rm peak,SDS}$[e] ($\times10^{38}$ erg)	$t_{\rm HCS}$[f] (days)	$t_{\rm SDS}$[g] (days)	$t_{\rm IMS}$[h] (days)	$t_{\rm und}$[i] (days)
	2008	125	0.662 ± 0.065	0.021 ± 0.013	0.0016 ± 0.0013	0.021 ± 0.013	-	78	0	0	47
	2009	150	1.269 ± 0.088	0.081 ± 0.042	0.0062 ± 0.0045	0.081 ± 0.042	-	121	0	0	29
	2009-2011	454	25.0 ± 1.2	2.9 ± 1.5	0.22 ± 0.16	2.6 ± 1.3	2.9 ± 1.5	113	258	38	45
	2013	107	19.4 ± 1.3	0.64 ± 0.32	0.049 ± 0.035	0.64 ± 0.32	-	72	0	3	32
IGRJ17091−3624	2011-2013	824	18.7 ± 1.5	$0.29^{+0.30}_{-0.29}$	0.022 ± 0.025	0.21 ± 0.20	0.27 ± 0.27	24	121	122	557
SAXJ1711.6−3808	2001	130	13.8 ± 1.8	0.38 ± 0.36	0.030 ± 0.031	0.38 ± 0.36	-	65	0	0	65
XMMSL1J171900.4−353217	2007	129	0.228 ± 0.027	$0.0045^{+0.0048}_{-0.0049}$	0.00035 ± 0.00041	$0.0045^{+0.0048}_{-0.0049}$	-	107	0	0	22
	2007/2008	280	0.571 ± 0.041	0.0034 ± 0.0037	0.00026 ± 0.00031	0.0034 ± 0.0037	-	234	0	0	46
	2008/2009	242	0.378 ± 0.028	$0.0036^{+0.0038}_{-0.0039}$	$0.00028^{+0.00032}_{-0.00033}$	$0.0036^{+0.0038}_{-0.0039}$	-	218	0	0	24
	2009/2010	405	0.875 ± 0.055	0.012 ± 0.011	$0.00089^{+0.00094}_{-0.00095}$	0.012 ± 0.011	-	342	0	0	63
XTEJ1720−318	2003	230	28.7 ± 2.3	1.6 ± 1.5	0.12 ± 0.13	1.3 ± 1.2	1.2 ± 1.1	122	8	56	44
XTEJ1727−476	2005	79	3.76 ± 0.84	0.39 ± 0.37	0.030 ± 0.032	0.31 ± 0.29	0.39 ± 0.37	2	11	3	63

Continued on Next Page...

Table A.5 – Continued

Source Name	Outburst ID	$t_{\rm dur}$[a] (days)	$\int Ldt$[b] ($\times10^{38}$ erg)	$L_{\rm peak,tot}$[c] ($\times10^{38}$ erg)	$L_{\rm edd}$[c] ($L_{\rm peak,tot}/L_{\rm edd}$)	$L_{\rm peak,HCS}$[d] ($\times10^{38}$ erg)	$L_{\rm peak,SDS}$[e] ($\times10^{38}$ erg)	$t_{\rm HCS}$[f] (days)	$t_{\rm SDS}$[g] (days)	$t_{\rm IMS}$[h] (days)	$t_{\rm und}$[i] (days)
IGRJ17285−2922	2010	90	0.375 ± 0.055	$0.022^{+0.023}_{-0.024}$	0.0017 ± 0.0020	$0.022^{+0.023}_{-0.024}$	-	56	0	4	30
IGRJ17379−3747	2008	76	0.061 ± 0.011	0.028 ± 0.026	0.0022 ± 0.0023	0.028 ± 0.026	-	39	0	0	37
GRS1737−31	1997	101	6.1 ± 1.0	0.24 ± 0.24	0.018 ± 0.020	0.24 ± 0.24	-	38	0	0	63
GRS1739−278	1996	252	1.81 ± 0.32	3.9 ± 3.5	0.30 ± 0.31	3.9 ± 3.5	0.90 ± 0.82	131	30	91	0
	2014	60	1.41 ± 0.54	0.98 ± 0.89	0.076 ± 0.078	0.93 ± 0.85	0.98 ± 0.89	26	14	6	14
1E1740.7−2942	1996-2004	3220	12.66 ± 0.30	0.28 ± 0.26	0.021 ± 0.023	0.28 ± 0.26	-	3122	0	12	86
	2005-2007	1001	5.08 ± 0.21	0.103 ± 0.094	0.0080 ± 0.0083	0.103 ± 0.094	0.066 ± 0.063	760	37	185	19
	2008-2014	2265	9.61 ± 0.40	0.70 ± 0.65	0.054 ± 0.057	0.18 ± 0.17	0.70 ± 0.65	1934	17	299	15
SWIFTJ174510.8−262411	2012/2013	286	19.8 ± 1.9	1.9 ± 1.8	0.15 ± 0.15	1.9 ± 1.8	-	205	0	0	81
H1743−322	2003	241	13.5 ± 1.5	24 ± 14	1.9 ± 1.4	24 ± 14	3.0 ± 1.7	131	9	70	31
	2004	134	2.95 ± 0.35	4.1 ± 2.3	0.32 ± 0.24	3.9 ± 2.2	3.4 ± 1.9	38	13	55	28
	2005	81	1.94 ± 0.30	2.5 ± 1.4	0.19 ± 0.14	2.4 ± 1.3	2.5 ± 1.4	22	21	6	32

Continued on Next Page...

Table A.5 – Continued

Source Name	Outburst ID	$t_{\rm dur}$[a] (days)	$\int Ldt$[b] ($\times10^{38}$ erg)	$L_{\rm peak,tot}$[c] ($\times10^{38}$ erg)	$L_{\rm edd}$[c] ($L_{\rm peak,tot}/L_{\rm edd}$)	$L_{\rm peak,HCS}$[d] ($\times10^{38}$ erg)	$L_{\rm peak,SDS}$[e] ($\times10^{38}$ erg)	$t_{\rm HCS}$[f] (days)	$t_{\rm SDS}$[g] (days)	$t_{\rm IMS}$[h] (days)	$t_{\rm und}$[i] (days)
	2007/2008	68	1.41 ± 0.23	3.9 ± 2.3	0.30 ± 0.23	3.9 ± 2.3	$1.27^{+0.75}_{-0.76}$	31	19	5	13
	2008	100	3.26 ± 0.36	1.18 ± 0.66	0.091 ± 0.068	1.18 ± 0.66	-	57	0	0	43
	2009	101	1.89 ± 0.22	3.2 ± 1.8	0.25 ± 0.19	1.34 ± 0.76	3.2 ± 1.8	33	10	15	43
	2009/2010	101	4.08 ± 0.56	1.66 ± 0.95	0.128 ± 0.097	1.66 ± 0.95	-	48	0	2	51
	2010	102	2.84 ± 0.37	1.54 ± 0.86	0.119 ± 0.089	1.54 ± 0.86	0.76 ± 0.43	32	7	19	44
	2010/2011	195	17.0 ± 1.1	1.57 ± 0.88	0.121 ± 0.091	1.57 ± 0.88	-	46	0	8	141
	2011/2012	92	10.00 ± 0.97	0.93 ± 0.53	0.072 ± 0.054	0.93 ± 0.53	-	37	0	0	55
	2012	65	13.6 ± 1.4	1.00 ± 0.56	0.077 ± 0.058	1.00 ± 0.56	-	36	0	0	29
	2013	75	3.24 ± 0.57	1.18 ± 0.66	0.091 ± 0.068	1.18 ± 0.66	-	47	0	2	26
XTEJ1748−288	1998	78	16.1 ± 2.8	2.9 ± 2.7	0.23 ± 0.23	2.9 ± 2.7	-	53	0	0	25
IGRJ17497−2821	2006	99	3.24 ± 0.55	0.23 ± 0.21	0.018 ± 0.019	0.23 ± 0.21	-	43	0	0	56
SLX1746−331	2003	255	1.64 ± 0.16	1.6 ± 1.5	0.12 ± 0.13	1.6 ± 1.5	-	161	0	62	32
	2007/2008	254	1.77 ± 0.18	0.96 ± 0.90	0.074 ± 0.078	0.024 ± 0.022	0.96 ± 0.90	39	172	6	37
	2010/2011	327	3.68 ± 0.40	0.30 ± 0.27	0.023 ± 0.024	0.22 ± 0.21	0.30 ± 0.27	132	29	117	49

Continued on Next Page...

Table A.5 – Continued

Source Name	Outburst ID	$t_{\rm dur}$[a] (days)	$\int Ldt$[b] ($\times10^{38}$ erg)	$L_{\rm peak,tot}$[c] ($\times10^{38}$ erg)	$L_{\rm edd}$[c] ($L_{\rm peak,tot}/L_{\rm edd}$)	$L_{\rm peak,HCS}$[d] ($\times10^{38}$ erg)	$L_{\rm peak,SDS}$[e] ($\times10^{38}$ erg)	$t_{\rm HCS}$[f] (days)	$t_{\rm SDS}$[g] (days)	$t_{\rm IMS}$[h] (days)	$t_{\rm und}$[i] (days)
XTEJ1752−223	2009/2010	341	2.960 ± 0.083	0.67 ± 0.17	0.053 ± 0.015	0.67 ± 0.17	0.250 ± 0.058	192	71	27	51
SWIFTJ1753.5−0127	2005-2014	3258	221.3 ± 4.7	1.1 ± 1.1	0.087 ± 0.092	0.87 ± 0.79	0.15 ± 0.14	1204	24	1876	154
XTEJ1755−324	1997	125	21.3 ± 2.2	0.85 ± 0.80	$0.065^{+0.069}_{-0.070}$	$0.44^{+0.44}_{-0.45}$	0.85 ± 0.80	49	31	19	26
IGRJ17586−2129	2009	162	1.30 ± 0.14	0.046 ± 0.042	0.0035 ± 0.0037	0.046 ± 0.042	-	92	0	0	70
GRS1758−258	1996-2002	2466	10.08 ± 0.27	0.52 ± 0.48	0.040 ± 0.042	0.52 ± 0.48	-	2285	0	171	10
	2003/2004	669	3.67 ± 0.19	0.37 ± 0.35	0.028 ± 0.031	0.37 ± 0.35	-	584	0	32	53
	2005-2014	3391	20.46 ± 0.56	1.9 ± 1.8	0.15 ± 0.15	0.45 ± 0.42	1.9 ± 1.8	2637	370	354	30
XTEJ1812−182	2003	55	0.399 ± 0.086	0.39 ± 0.36	0.030 ± 0.032	0.39 ± 0.36	-	34	0	0	21
	2008	81	0.593 ± 0.090	$0.098^{+0.095}_{-0.097}$	$0.0075^{+0.0082}_{-0.0084}$	0.012 ± 0.011	$0.098^{+0.095}_{-0.097}$	4	40	2	35
XTEJ1817−330	2006	256	9.7 ± 1.2	4.9 ± 4.5	0.38 ± 0.39	$0.15^{+0.15}_{-0.14}$	4.9 ± 4.5	81	108	32	35

Continued on Next Page...

Table A.5 – Continued

Source Name	Outburst ID	$t_{\rm dur}$[a] (days)	$\int Ldt$[b] ($\times10^{38}$ erg)	$L_{\rm peak,tot}$[c] ($\times10^{38}$ erg)	$L_{\rm edd}$[c] ($L_{\rm peak,tot}/L_{\rm edd}$)	$L_{\rm peak,HCS}$[d] ($\times10^{38}$ erg)	$L_{\rm peak,SDS}$[e] ($\times10^{38}$ erg)	$t_{\rm HCS}$[f] (days)	$t_{\rm SDS}$[g] (days)	$t_{\rm IMS}$[h] (days)	$t_{\rm und}$[i] (days)
XTEJ1818−245	2005	116	0.247 ± 0.022	0.54 ± 0.23	0.041 ± 0.027	0.0046 ± 0.0025	0.54 ± 0.23	1	59	17	39
SAXJ1819.3−2525	2005/2006	213	0.894 ± 0.052	$0.0120^{+0.0090}_{-0.0089}$	$0.00119^{+0.00090}_{-0.00089}$	$0.0067^{+0.0050}_{-0.0049}$	-	193	0	0	20
	2006/2007	345	1.866 ± 0.088	0.016 ± 0.011	0.0015 ± 0.0011	0.016 ± 0.011	-	333	0	0	12
	2007	116	0.695 ± 0.065	0.025 ± 0.019	0.0025 ± 0.0019	0.025 ± 0.019	-	77	0	0	39
	2008	67	0.219 ± 0.026	$0.0125^{+0.0101}_{-0.0092}$	$0.00124^{+0.00101}_{-0.00092}$	$0.0125^{+0.0101}_{-0.0092}$	-	54	0	0	13
	2008/2009	252	2.15 ± 0.13	$0.025^{+0.017}_{-0.019}$	$0.0025^{+0.0017}_{-0.0019}$	$0.025^{+0.017}_{-0.019}$	-	224	0	0	28
	2009	216	1.057 ± 0.073	0.22 ± 0.11	0.022 ± 0.011	0.119 ± 0.060	-	140	0	0	76
	2010/2011	295	1.75 ± 0.13	0.34 ± 0.17	0.034 ± 0.017	0.34 ± 0.17	-	182	0	21	92
MAXIJ1836−194	2011/2012	289	5.07 ± 0.37	0.19 ± 0.17	0.014 ± 0.015	0.19 ± 0.17	-	246	0	0	43
SWIFTJ1842.5−1124	2008/2009	228	6.25 ± 0.68	$0.59^{+0.56}_{-0.58}$	$0.046^{+0.049}_{-0.050}$	0.43 ± 0.39	0.36 ± 0.33	83	2	51	92
XTEJ1856+053	1996	27	0.086 ± 0.023	0.26 ± 0.24	0.020 ± 0.021	0.22 ± 0.21	0.012 ± 0.011	2	8	10	7
	1996	100	0.242 ± 0.038	0.29 ± 0.26	0.022 ± 0.023	0.29 ± 0.26	0.20 ± 0.18	20	34	15	31
	2006/2007	225	1.22 ± 0.12	0.35 ± 0.33	0.027 ± 0.029	0.21 ± 0.20	0.35 ± 0.33	41	96	20	68
	2009	33	0.084 ± 0.020	$0.054^{+0.059}_{-0.056}$	$0.0042^{+0.0050}_{-0.0048}$	$0.039^{+0.051}_{-0.046}$	-	13	0	6	14

Continued on Next Page...

Table A.5 – Continued

Source Name	Outburst ID	$t_{\rm dur}$[a] (days)	$\int Ldt$[b] ($\times10^{38}$ erg)	$L_{\rm peak,tot}$[c] ($\times10^{38}$ erg)	$L_{\rm edd}$[c] ($L_{\rm peak,tot}/L_{\rm edd}$)	$L_{\rm peak,HCS}$[d] ($\times10^{38}$ erg)	$L_{\rm peak,SDS}$[e] ($\times10^{38}$ erg)	$t_{\rm HCS}$[f] (days)	$t_{\rm SDS}$[g] (days)	$t_{\rm IMS}$[h] (days)	$t_{\rm und}$[i] (days)
XTEJ1859+226	1999/2000	225	33.8 ± 3.6	8.4 ± 6.3	0.59 ± 0.51	8.4 ± 6.3	2.2 ± 1.7	84	16	52	73
XTEJ1908+094	2002/2003	424	1.448 ± 0.098	0.34 ± 0.31	0.026 ± 0.027	0.34 ± 0.31	0.22 ± 0.21	314	15	29	66
	2013/2014	150	6.79 ± 0.80	0.20 ± 0.18	0.015 ± 0.016	0.20 ± 0.18	-	17	0	1	132
SWIFTJ1910.2−0546	2012/2013	258	27.0 ± 1.9	1.1 ± 1.0	0.084 ± 0.088	0.43 ± 0.40	1.1 ± 1.0	177	19	18	44
SS433	1996-2001	2138	4.337 ± 0.044	0.75 ± 0.19	0.057 ± 0.032	0.75 ± 0.19	-	2059	0	62	17
	2002-2004	987	2.263 ± 0.033	$0.131^{+0.021}_{-0.017}$	$0.0101^{+0.0053}_{-0.0052}$	$0.131^{+0.021}_{-0.017}$	-	925	0	0	62
	2005-2014	3281	13.479 ± 0.093	0.43 ± 0.12	0.033 ± 0.019	$0.345^{+0.095}_{-0.093}$	$0.165^{+0.042}_{-0.044}$	2254	172	845	10
GRS1915+105	1996-2014	6691	54860 ± 200	80 ± 20	4.8 ± 2.0	80 ± 20	36.7 ± 8.8	5131	871	661	28
4U1956+350	1996-2014	6695	969.1 ± 1.7	0.647 ± 0.086	0.0336 ± 0.0050	0.525 ± 0.068	0.647 ± 0.086	2872	3213	579	31
4U1957+115	1996-2014	6626	469.2 ± 7.3	1.1 ± 1.0	0.085 ± 0.089	1.1 ± 1.0	$0.47^{+0.45}_{-0.46}$	3094	1852	1666	14

Continued on Next Page...

Table A.5 – Continued

Source Name	Outburst ID	$t_{\rm dur}$[a] (days)	$\int L dt$[b] ($\times 10^{38}$ erg)	$L_{\rm peak,tot}$[c] ($\times 10^{38}$ erg)	$L_{\rm edd}$[c] ($L_{\rm peak,tot}/L_{\rm edd}$)	$L_{\rm peak,HCS}$[d] ($\times 10^{38}$ erg)	$L_{\rm peak,SDS}$[e] ($\times 10^{38}$ erg)	$t_{\rm HCS}$[f] (days)	$t_{\rm SDS}$[g] (days)	$t_{\rm IMS}$[h] (days)	$t_{\rm und}$[i] (days)
XTEJ2012+381	1998	202	19.1 ± 1.6	$1.06^{+0.97}_{-0.98}$	0.081 ± 0.085	0.38 ± 0.35	$1.06^{+0.97}_{-0.98}$	18	96	55	33

Note. –

$L_{\rm peak,HCS}$ ="-" and $t > 0$ or $L_{\rm peak,SDS}$ ="-" and $t > 0$, indicate the minimum requirement of two different bands (one hard and one soft) for the spectral modelling process has not been met.

[a]Indicates the duration of the outburst in days.

[b]Indicates the total amount of energy released during outburst ("fluence").

[c]Indicates the peak (bolometric) luminosity reached during outburst.

[d]Indicates the peak (bolometric) luminosity reached when the source was in the (HCS).

[e]Indicates the peak (bolometric) luminosity reached when the source was in the (SDS).

[f]Indicates the total time the source spends in the HCS measured in days.

[g]Indicates the total time the source spends in the SDS measured in days.

[h]Indicates the total time the source spends in transition between the HCS and the SDS measured in days.

[i]Indicates the total amount of time we do not have sufficient data for the source.

Appendix B

Data Products

This appendix is split into two sections, transient sources and persistent sources. Each section is presented by source in ascending order of RA in J2000 coordinates.

Transient Sources

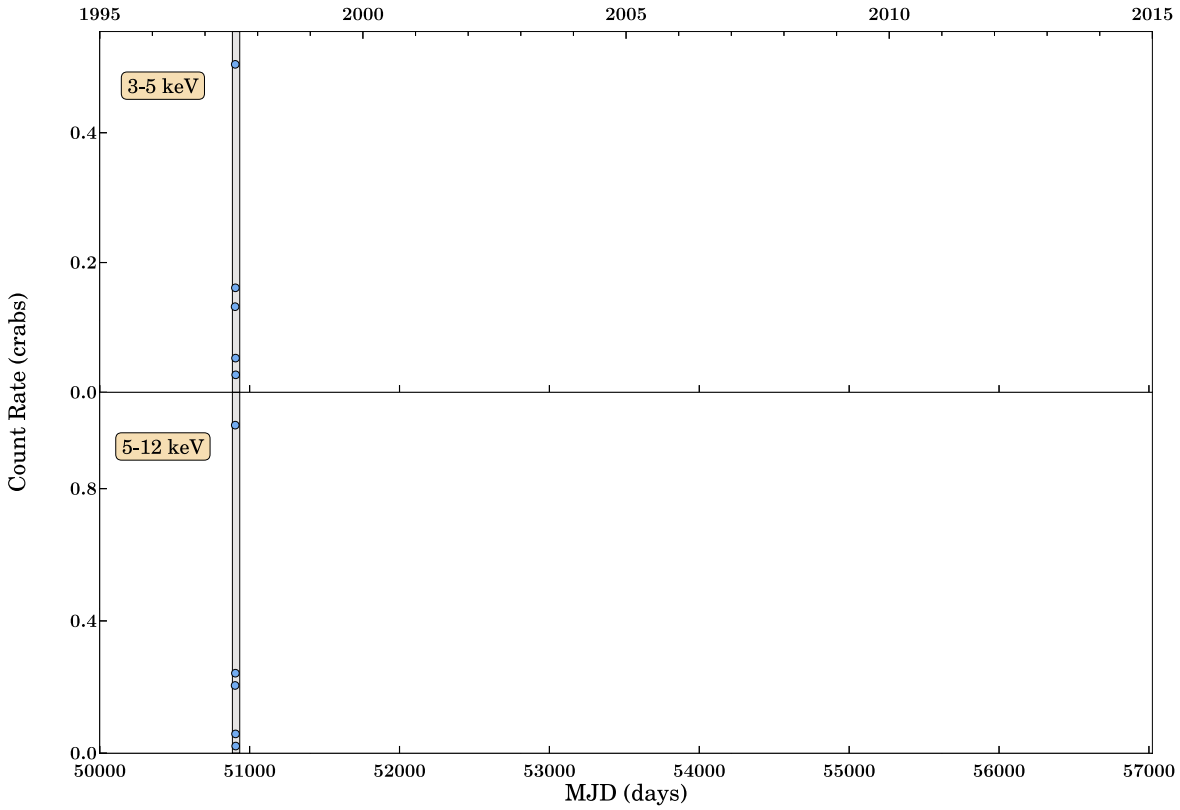

(a) Long-term Light Curve

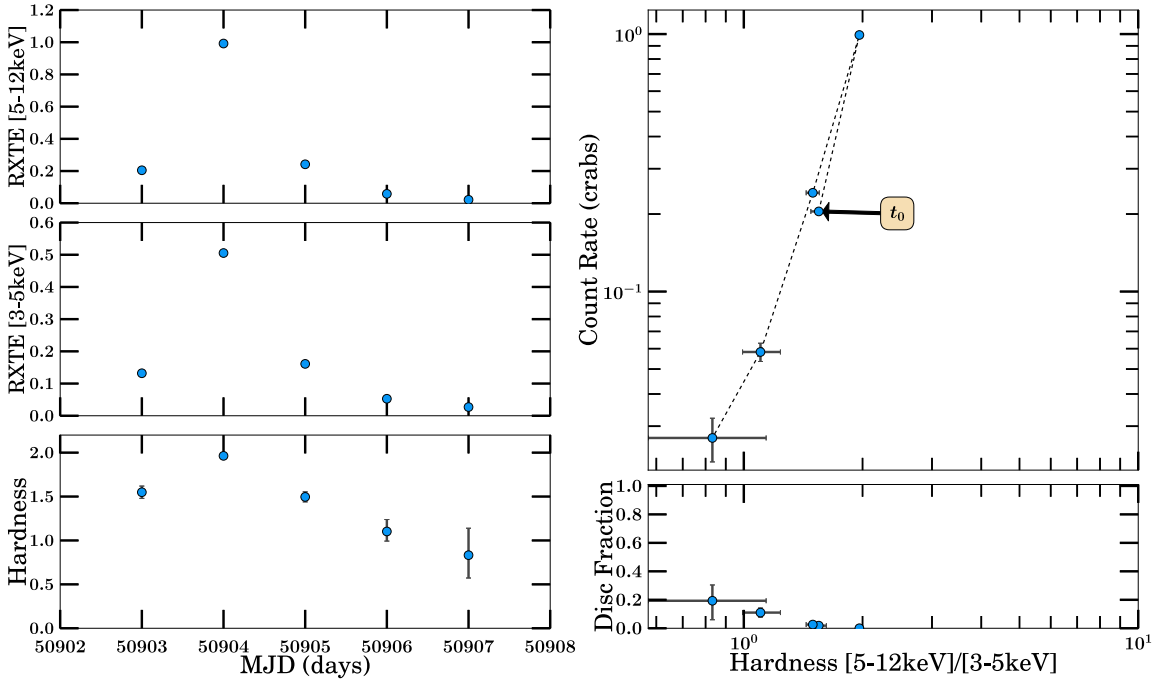

(b) 1997 Outburst Analysis

Figure B.1: XTE J0421+560

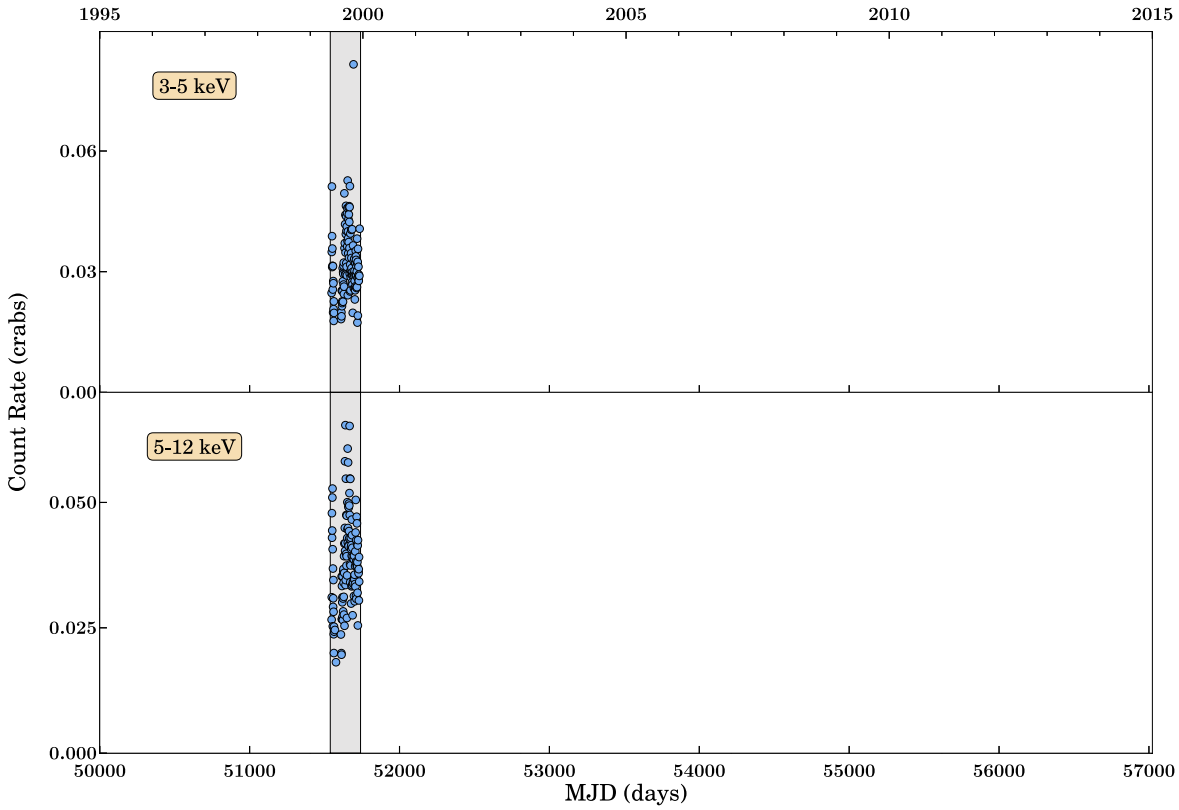

(a) Long-term Light Curve

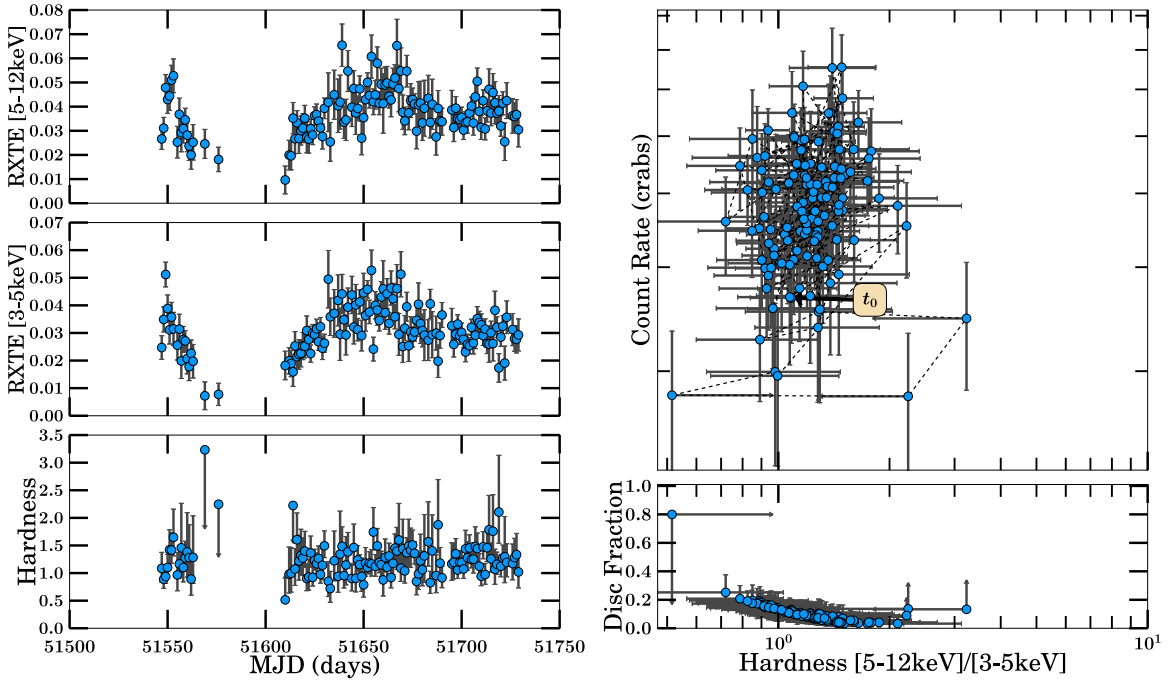

(b) 2000 Outburst Analysis

Figure B.2: XTE J1118+480

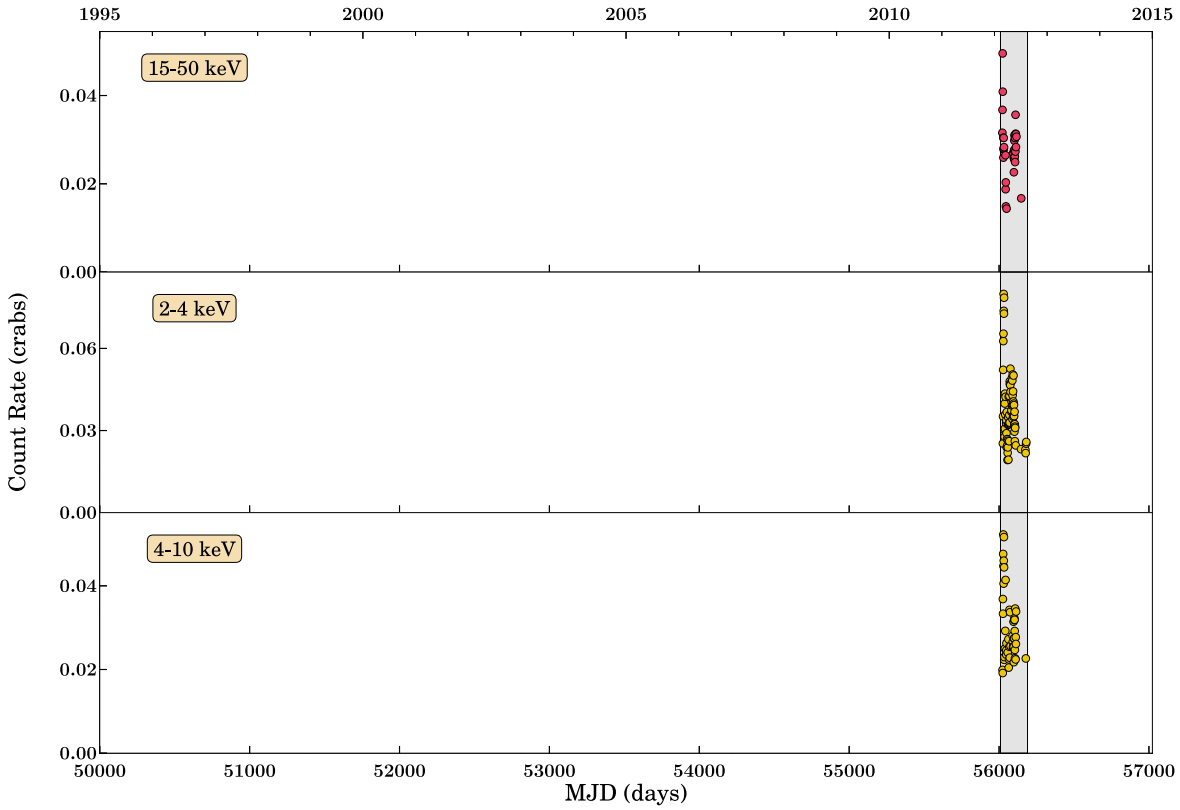

(a) Long-term Light Curve

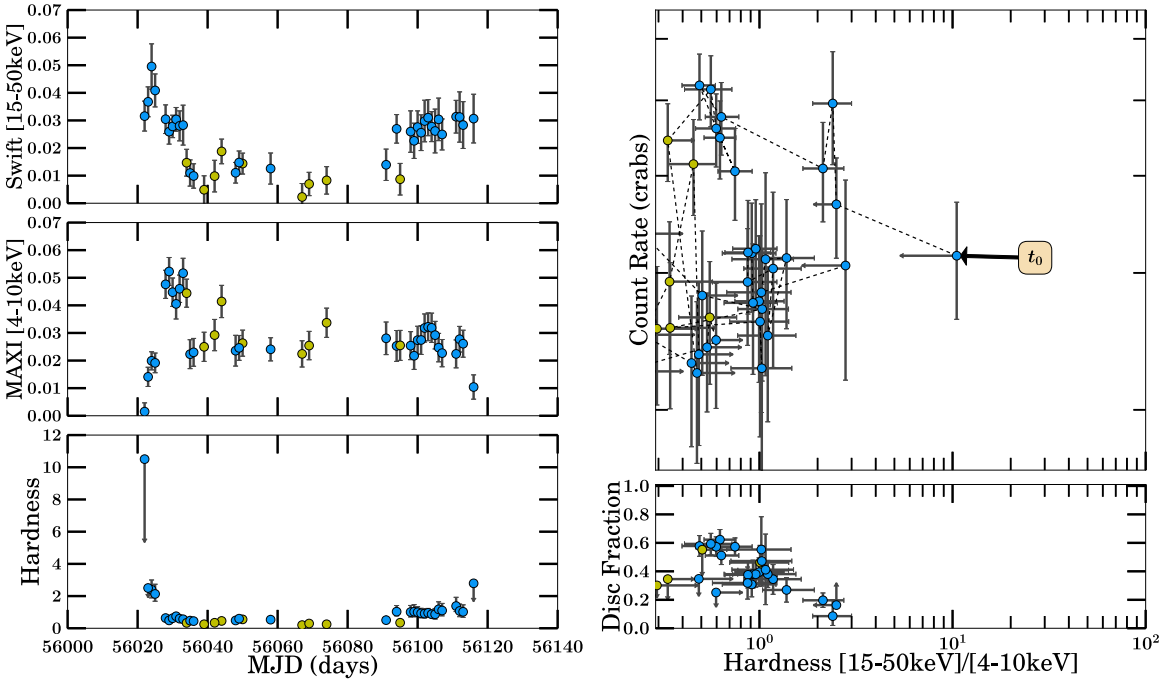

(b) 2012 Outburst Analysis

Figure B.3: MAXI J1305−704

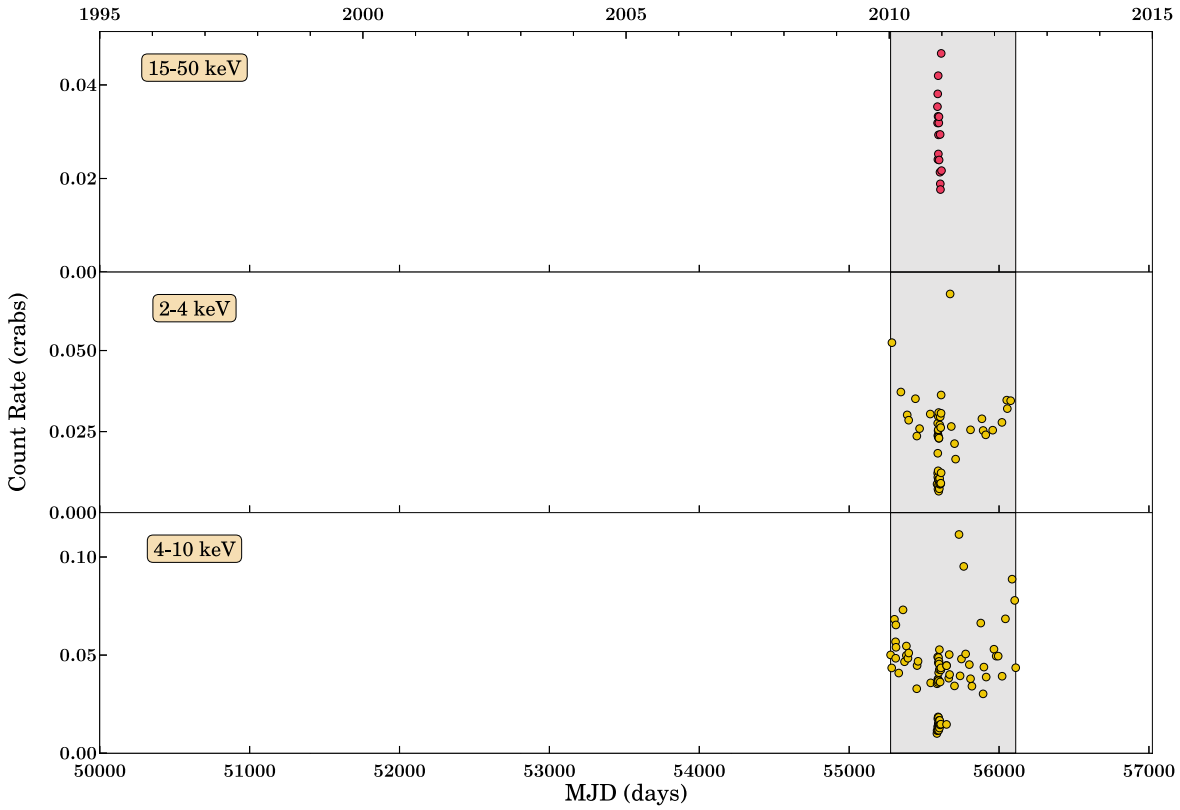

(a) Long-term Light Curve

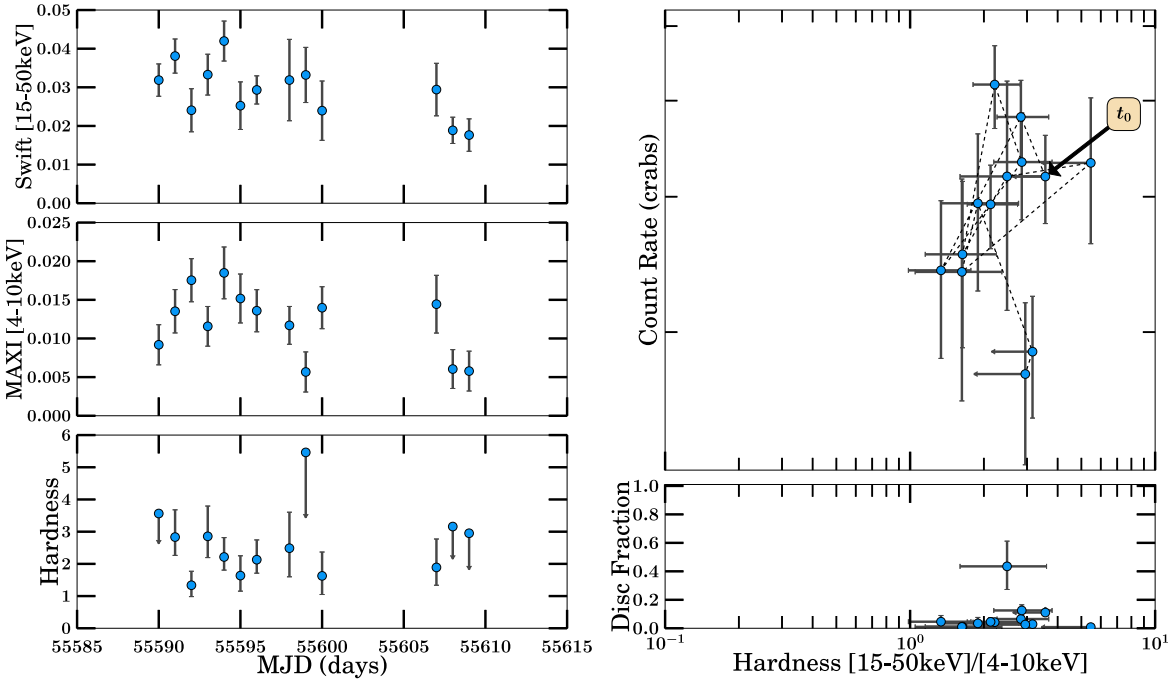

(b) 2011 Outburst Analysis

Figure B.4: SWIFT J1357.2−0933

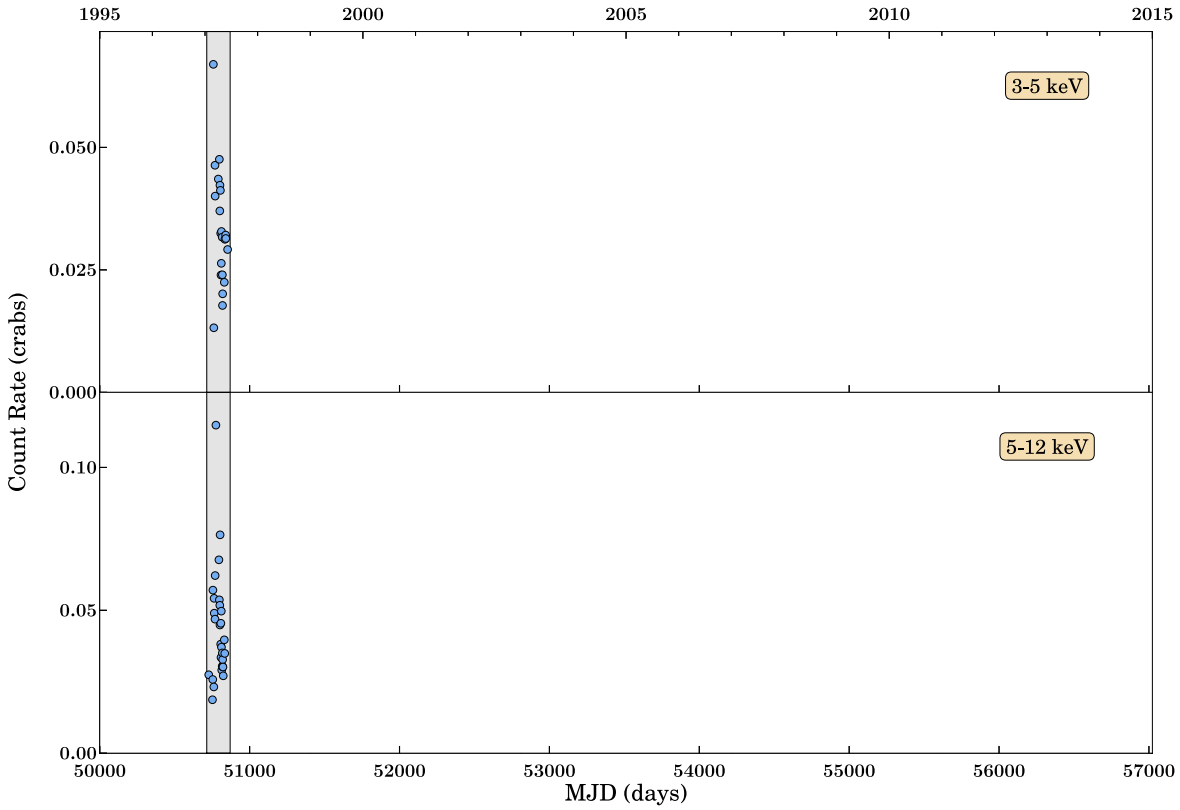

(a) Long-term Light Curve

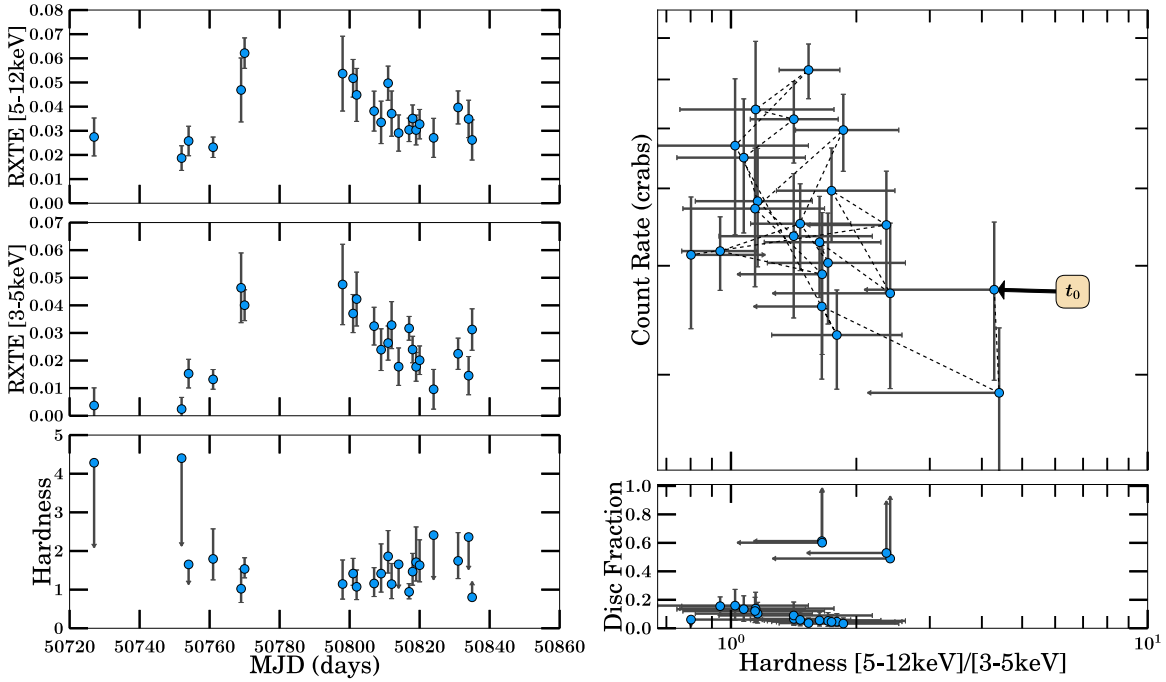

(b) 1997/1998 Outburst Analysis

Figure B.5: GS 1354−64

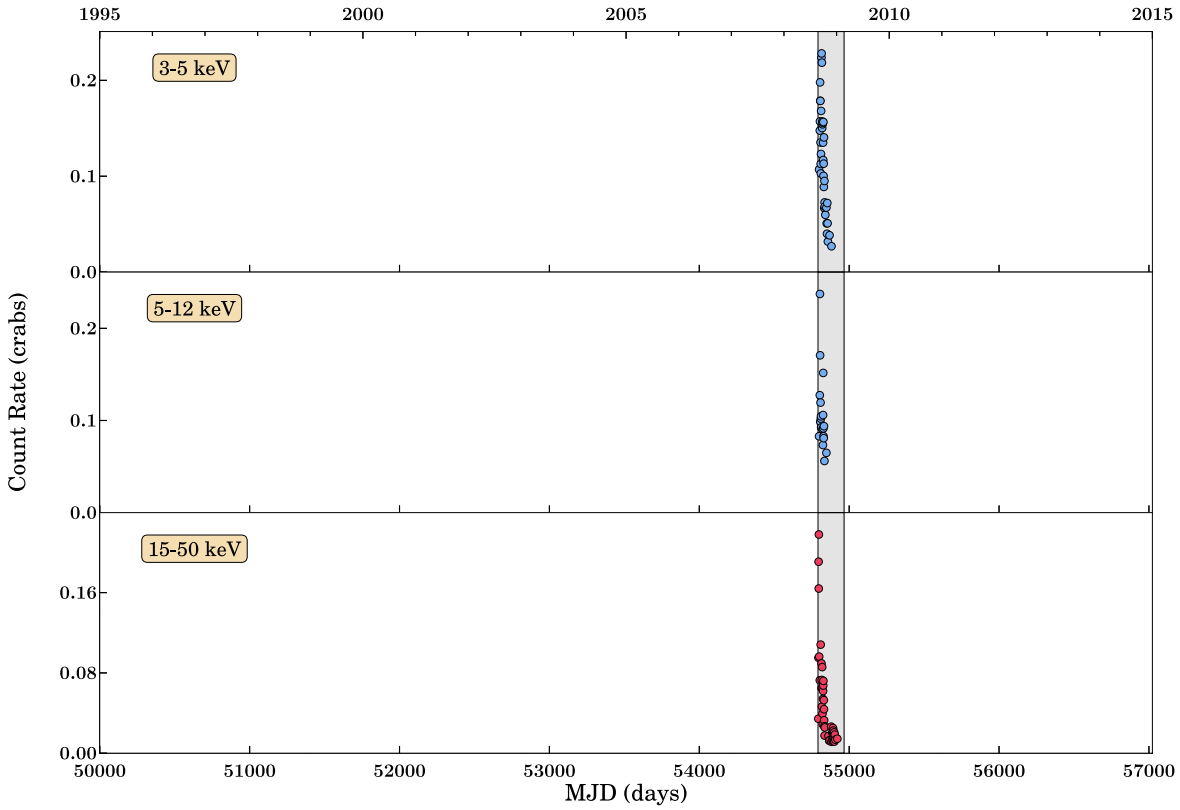

(a) Long-term Light Curve

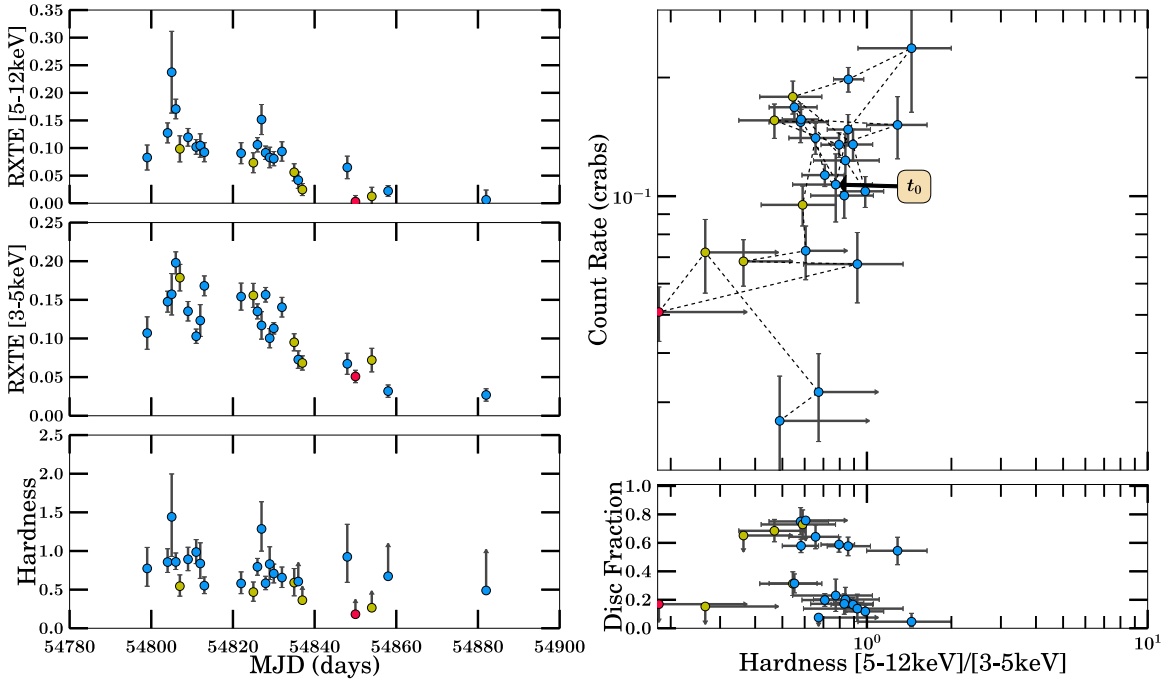

(b) 2008/2009 Outburst Analysis

Figure B.6: Swift J1539.2−6227 Part 1

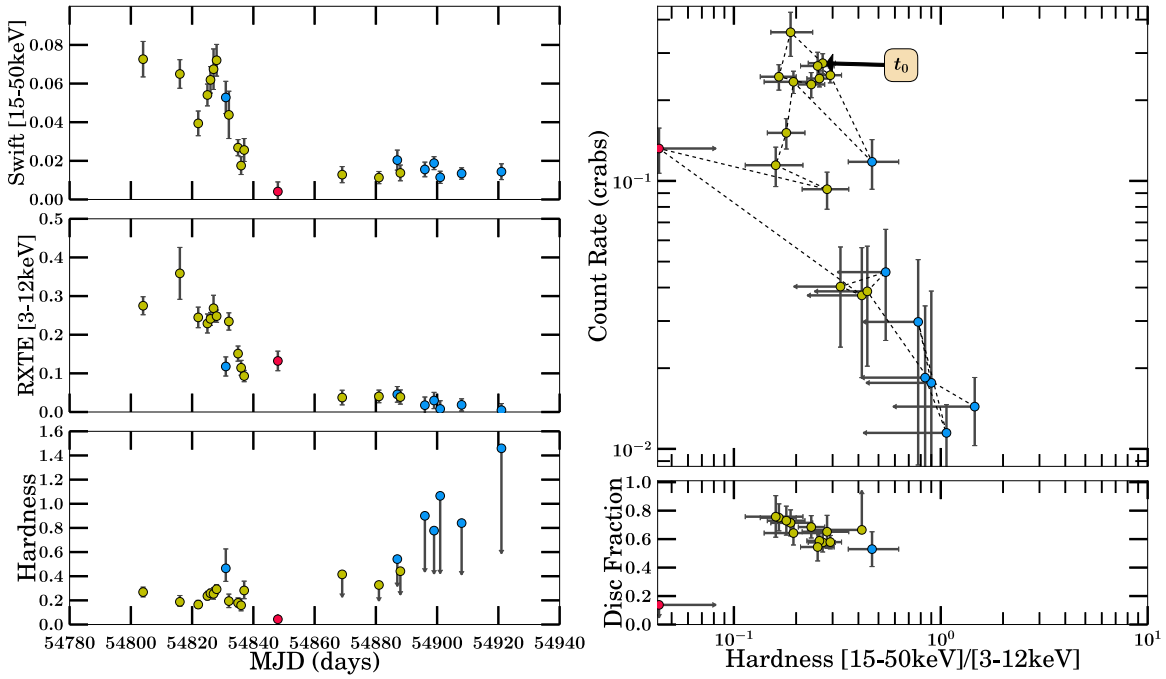

(a) 2008/2009 Outburst Analysis

Figure B.7: Swift J1539.2−6227 Part 2

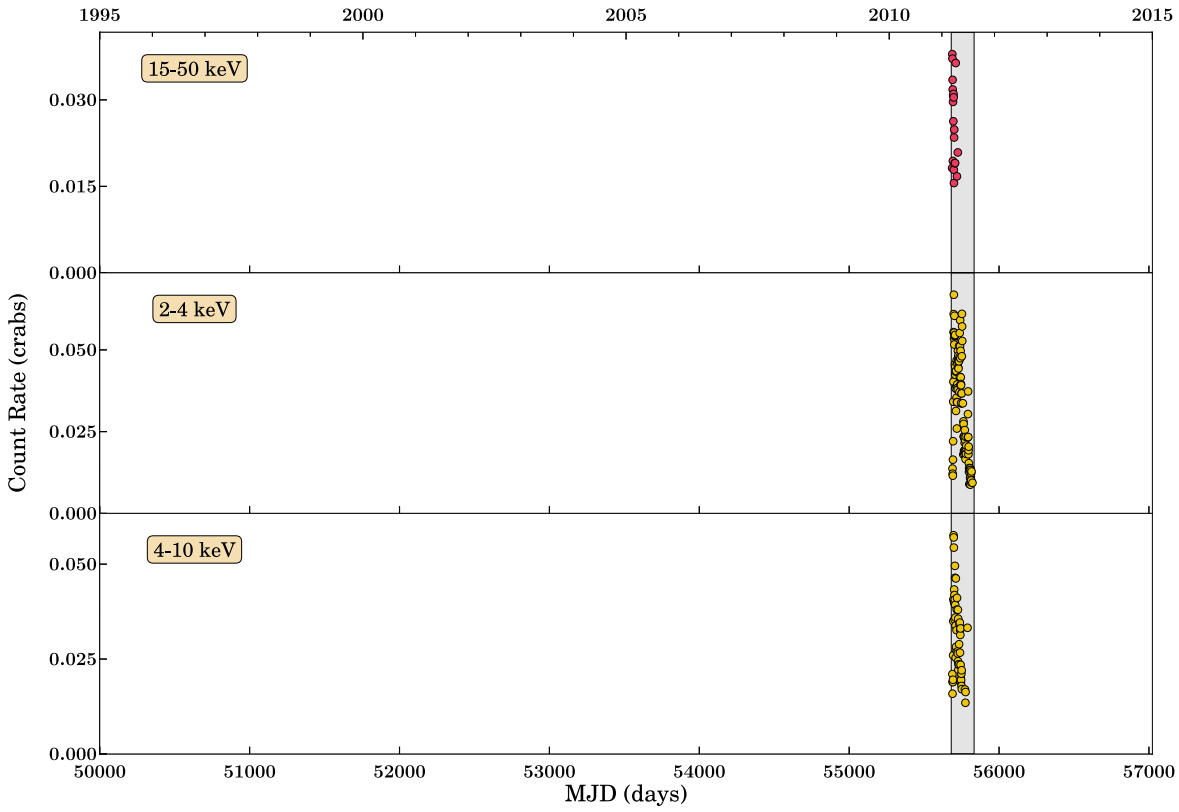

(a) Long-term Light Curve

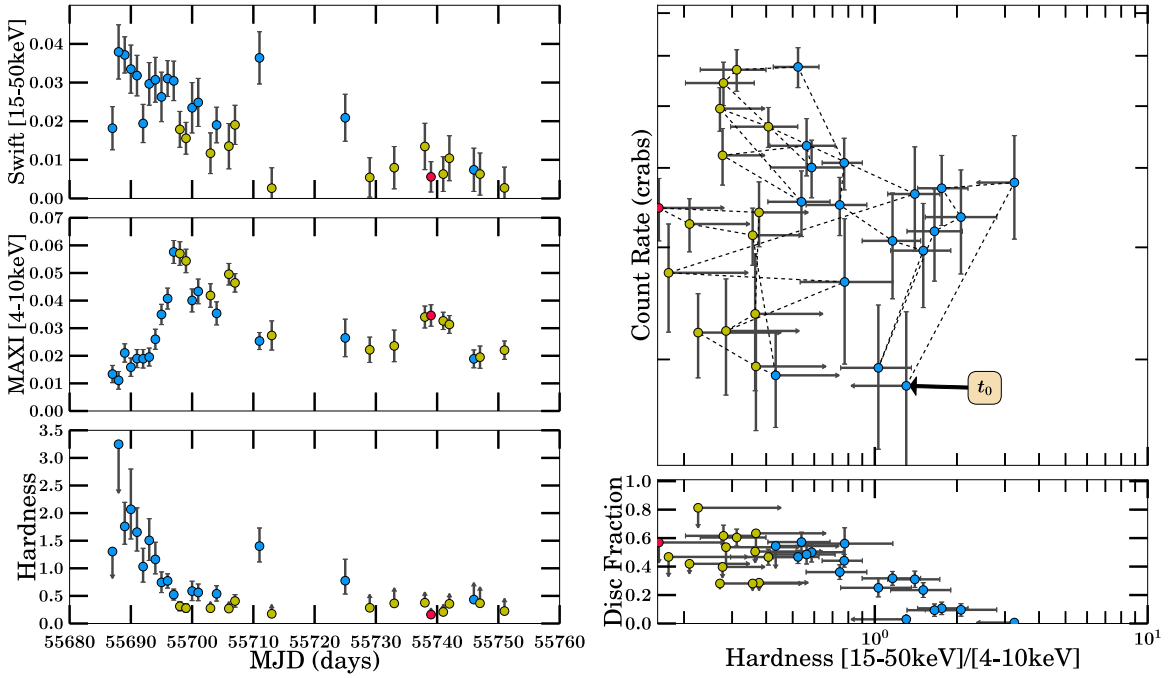

(b) 2011 Outburst Analysis

Figure B.8: MAXI J1543−564

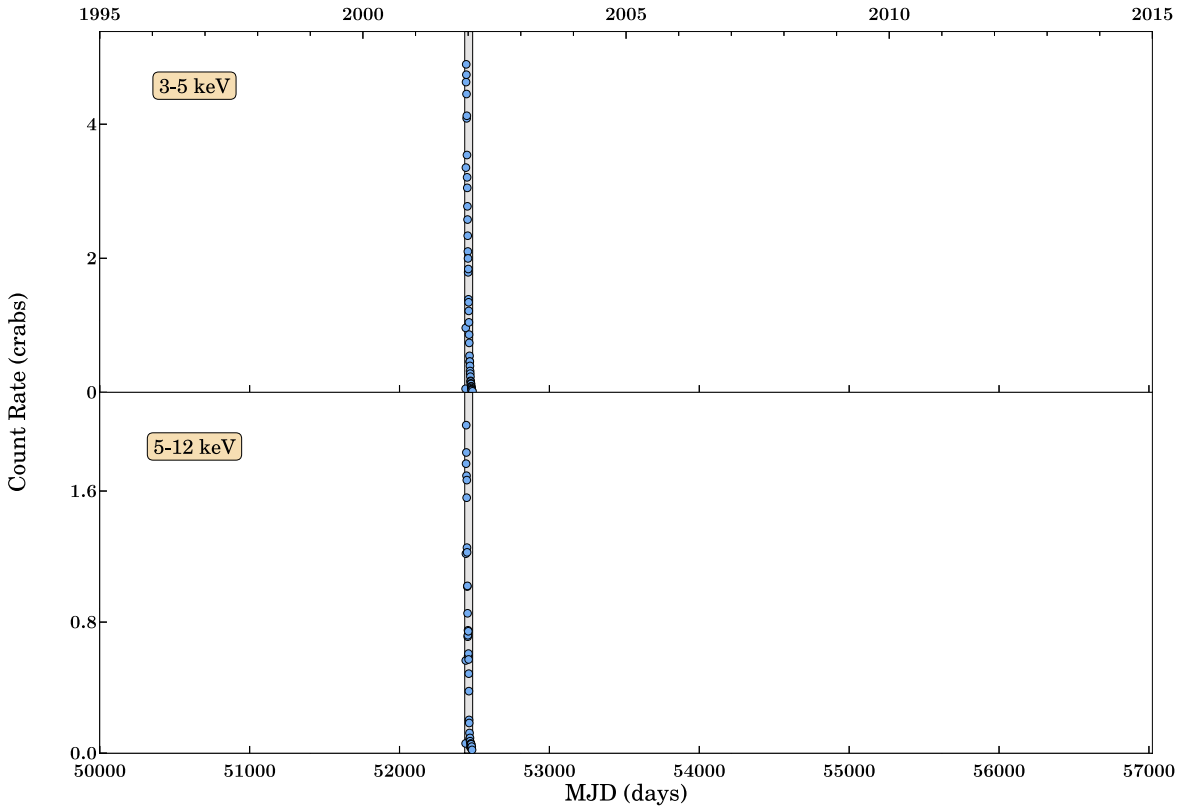

(a) Long-term Light Curve

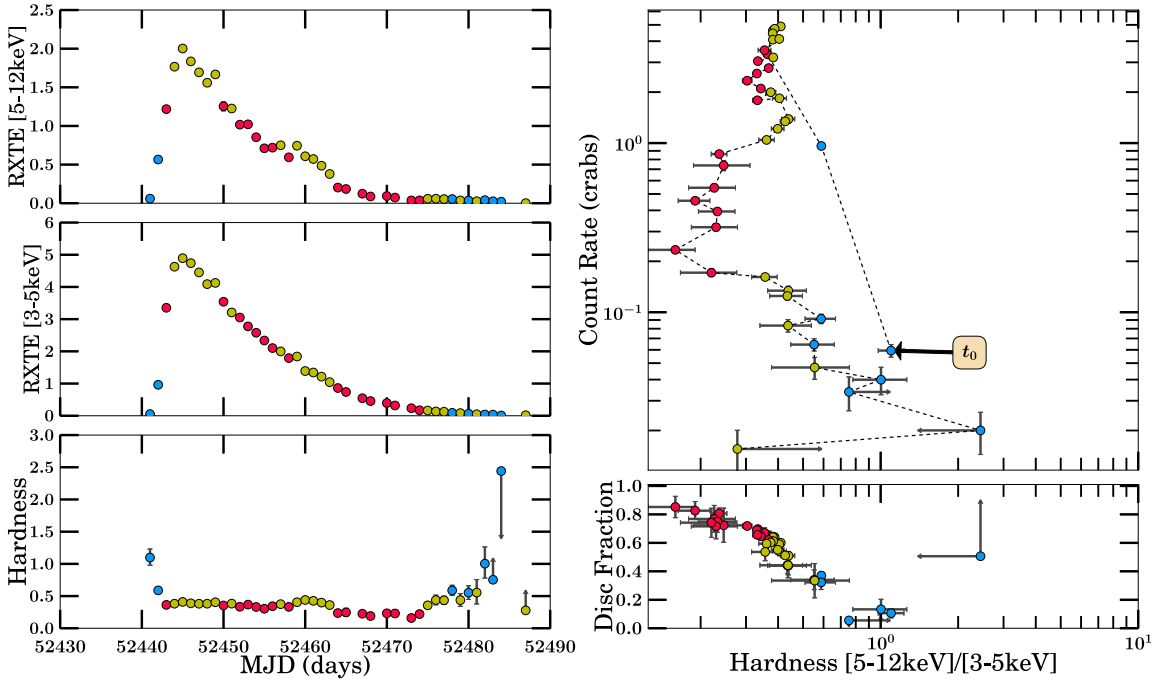

(b) 2002 Outburst Analysis

Figure B.9: 4U 1543−475

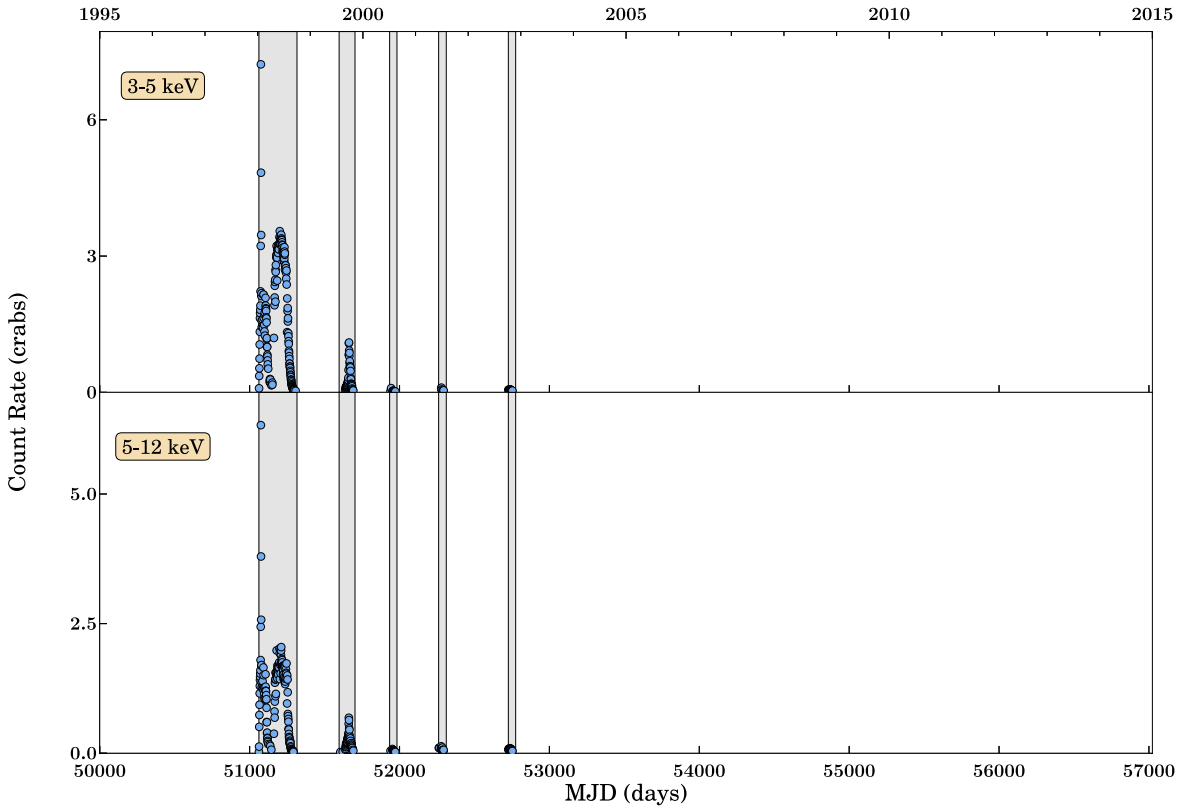

(a) Long-term Light Curve

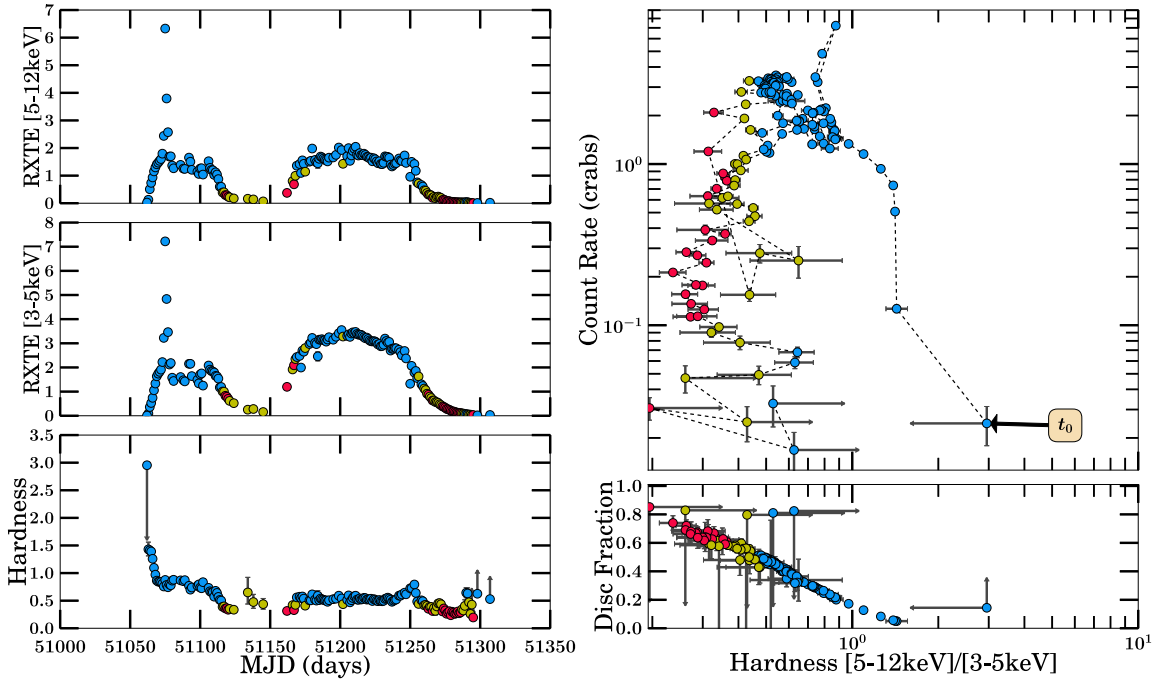

(b) 1998/1999 Outburst Analysis

Figure B.10: XTE J1550−564 Part 1

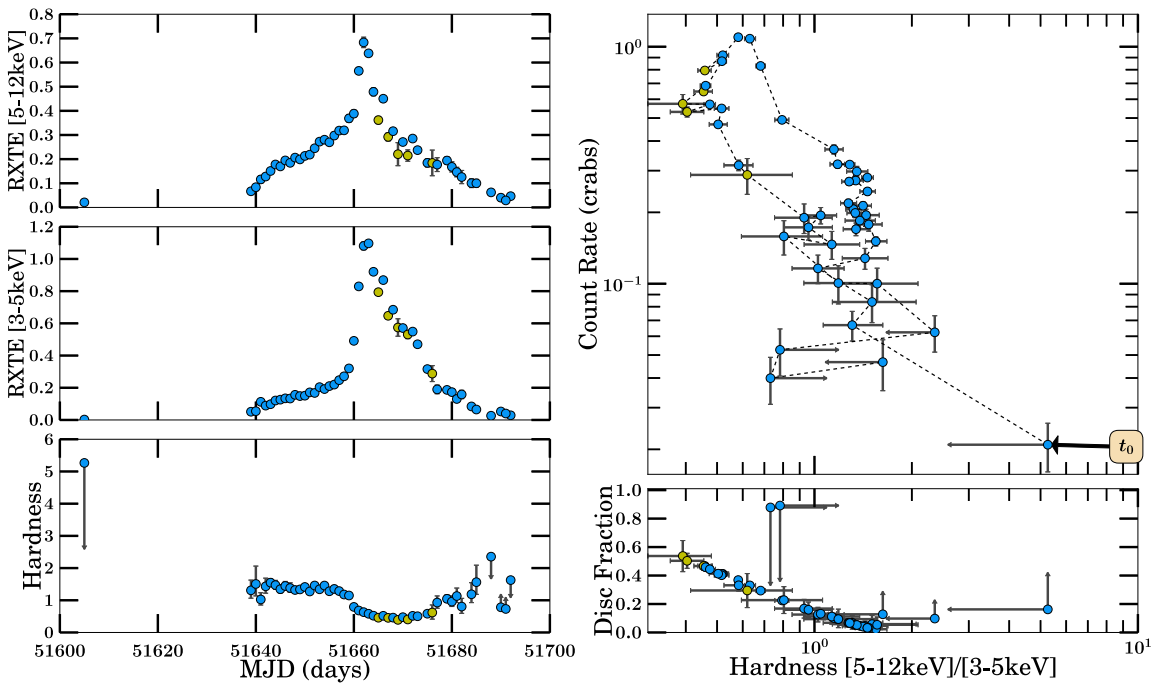

(a) 2000 Outburst Analysis

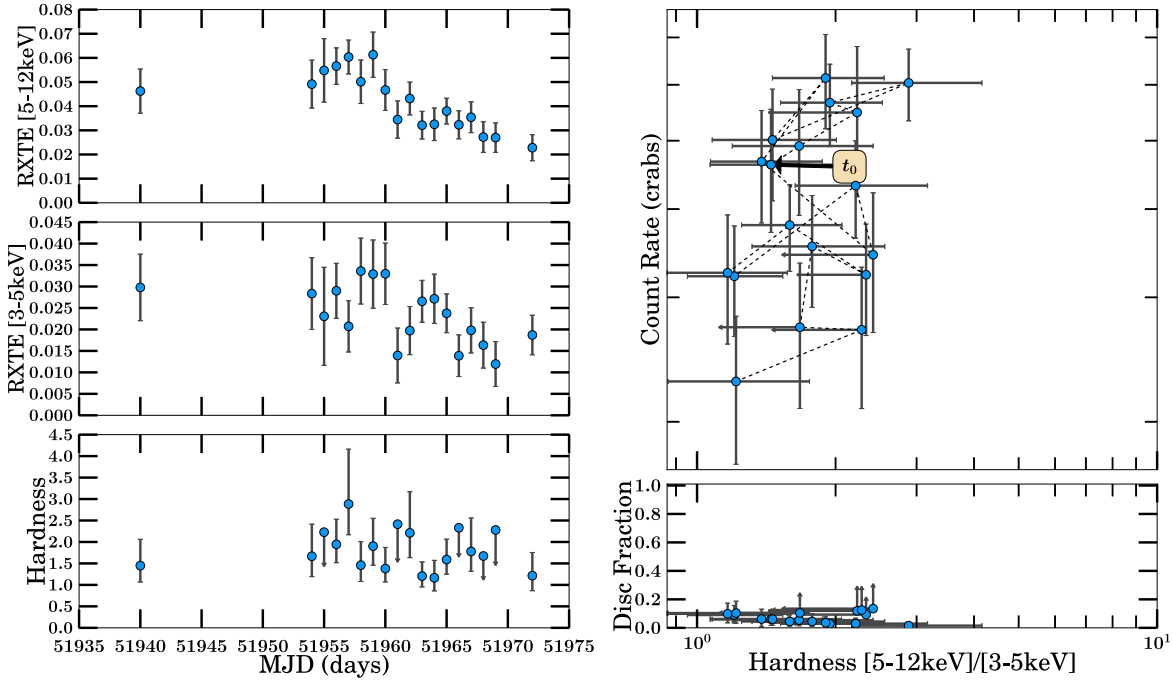

(b) 2001 Outburst Analysis

Figure B.11: XTE J1550−564 Part 2

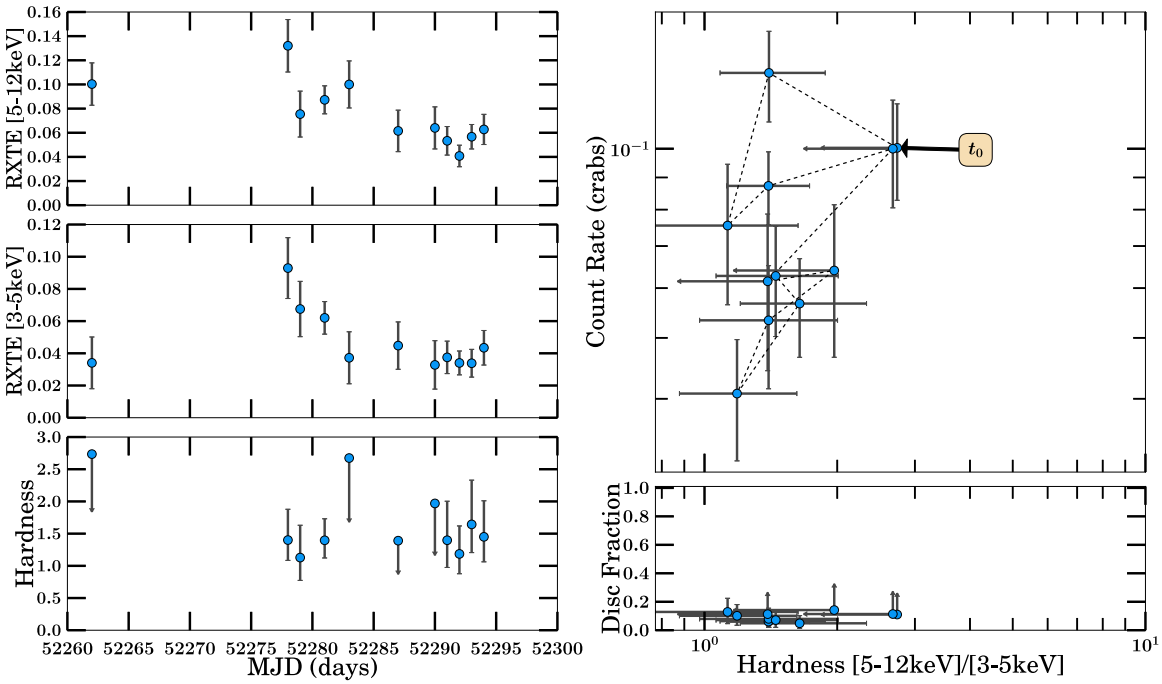

(a) 2001/2002 Outburst Analysis

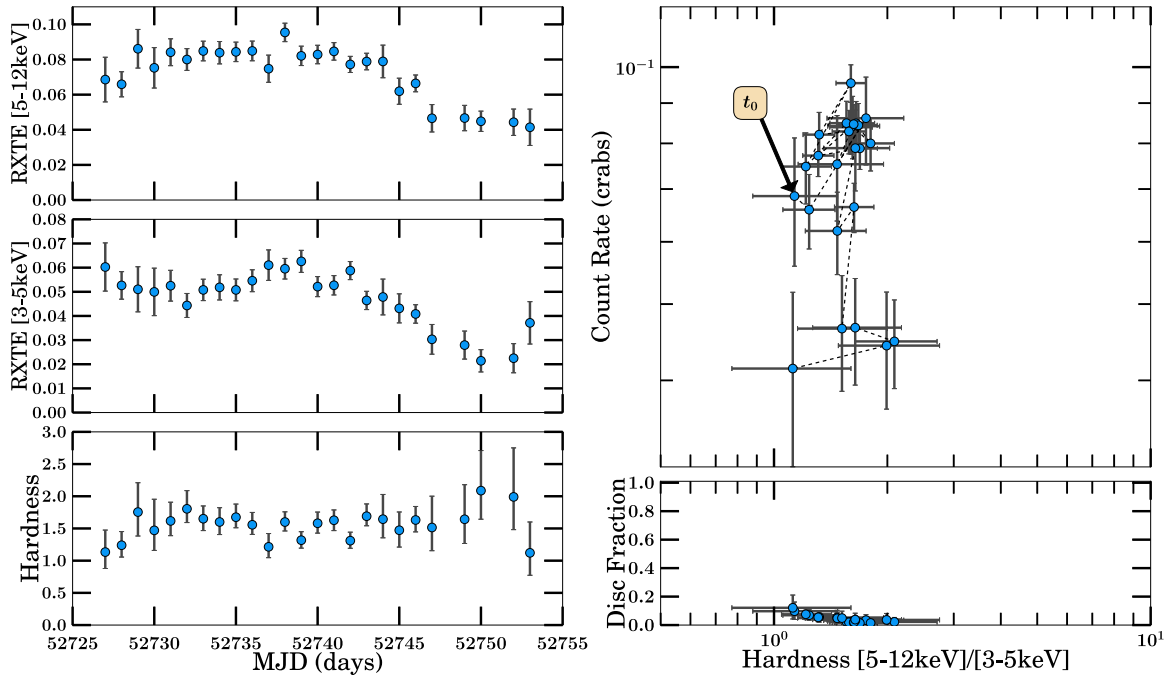

(b) 2003 Outburst Analysis

Figure B.12: XTE J1550−564 Part 3

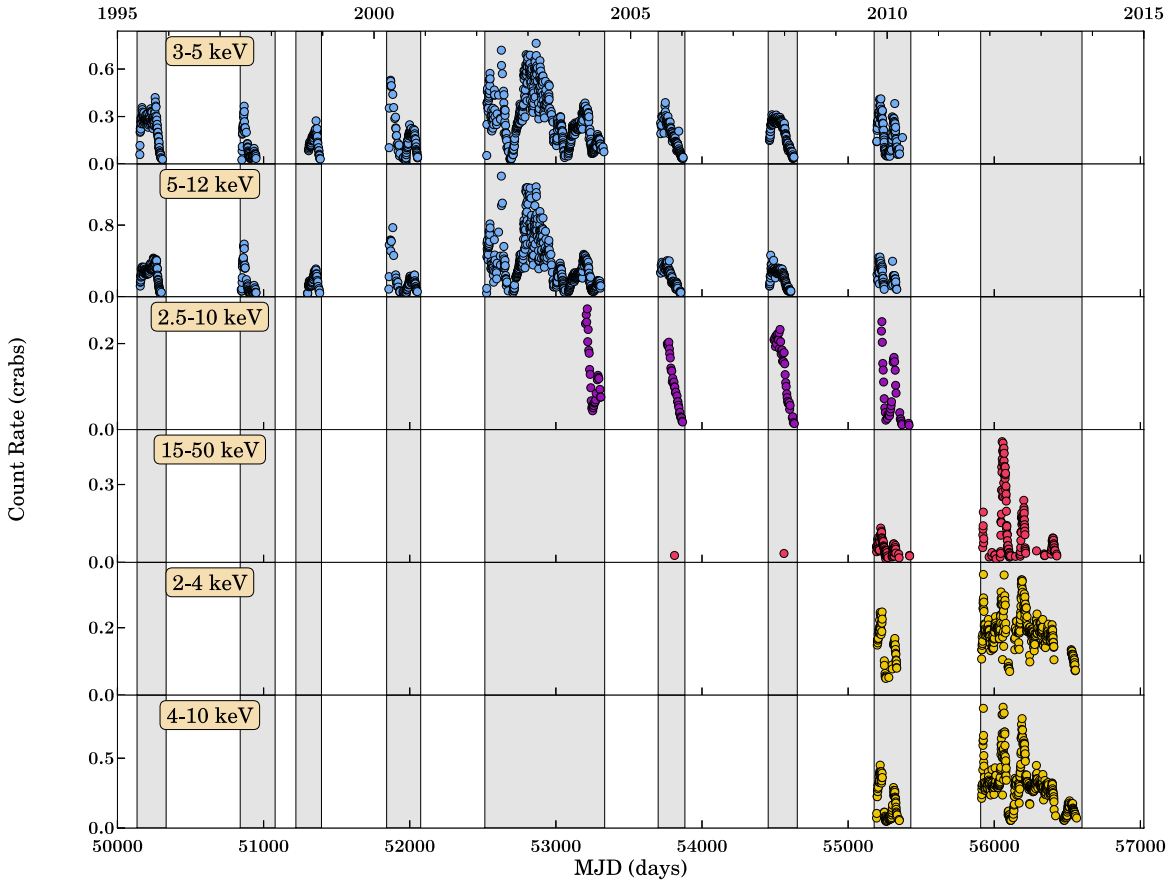

(a) Long-term Light Curve

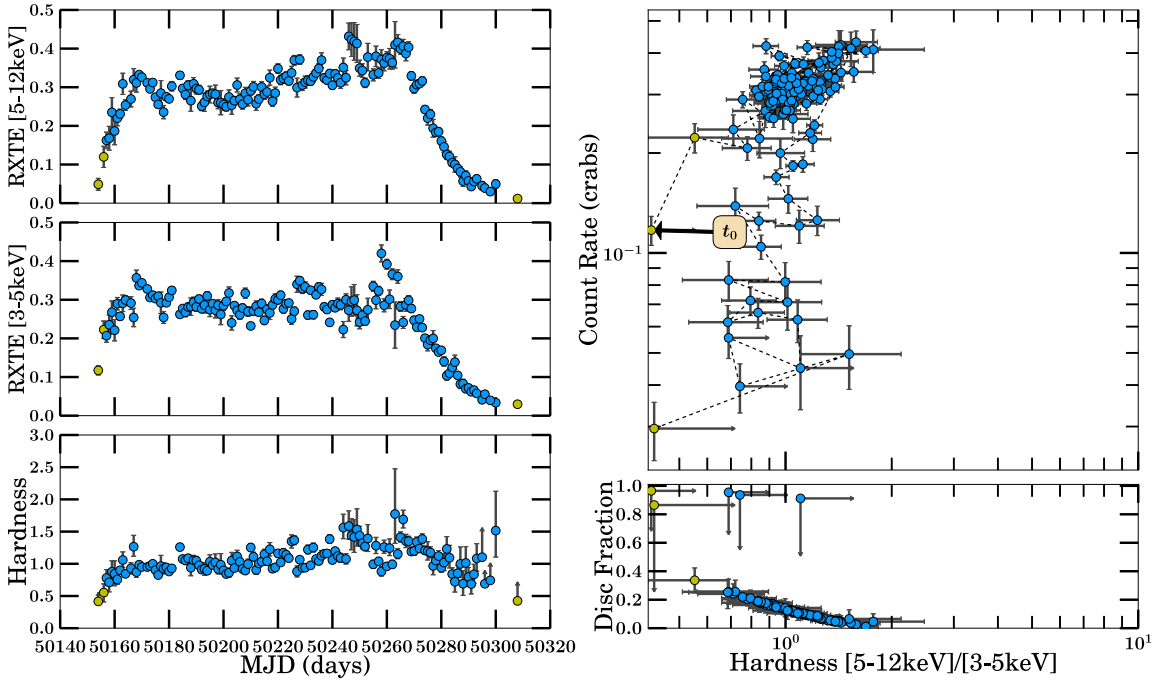

(b) 1996 Outburst Analysis

Figure B.13: 4U 1630−472 Part 1

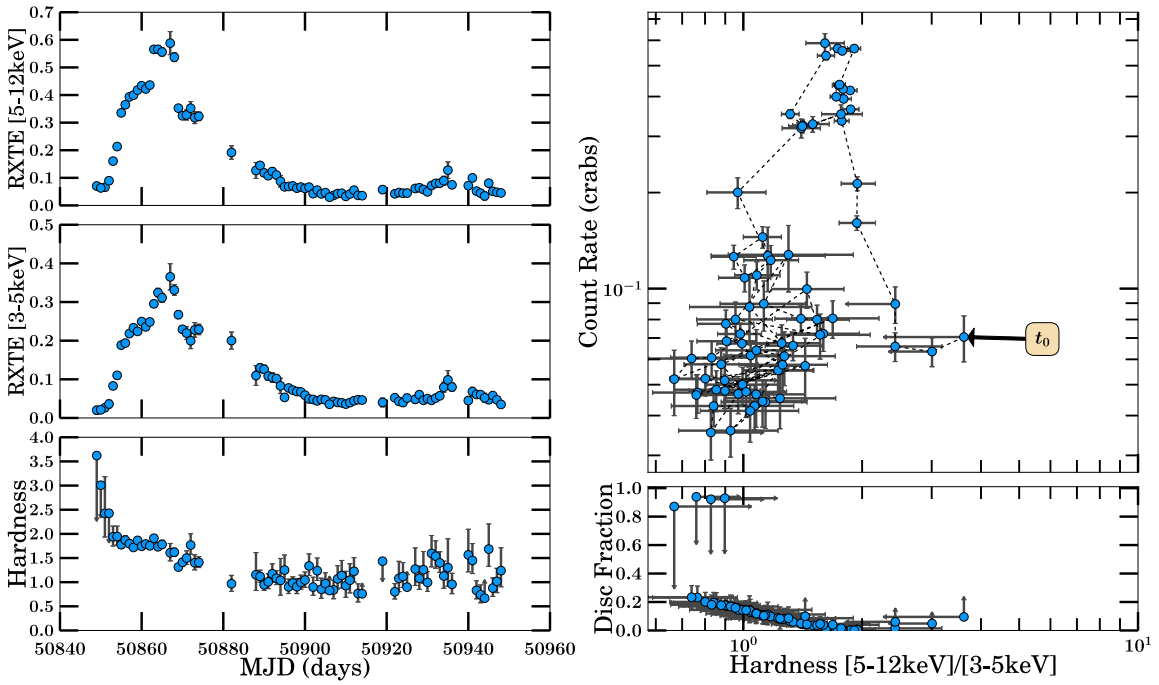

(a) 1998 Outburst Analysis

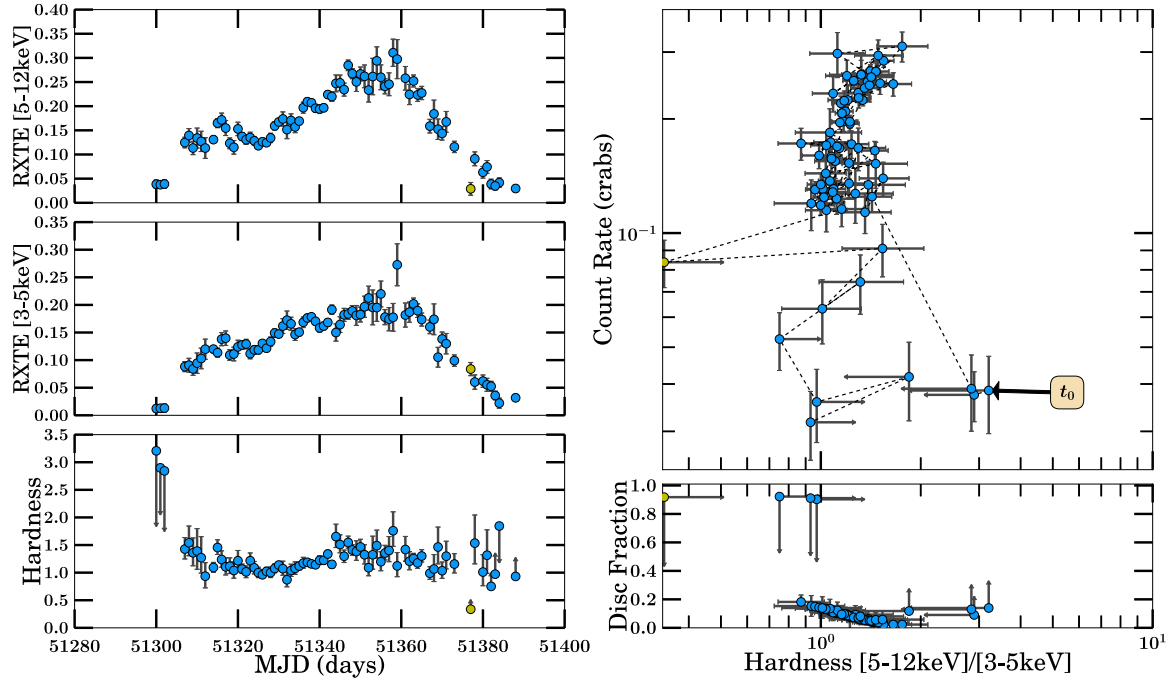

(b) 1999 Outburst Analysis

Figure B.14: 4U 1630−472 Part 2

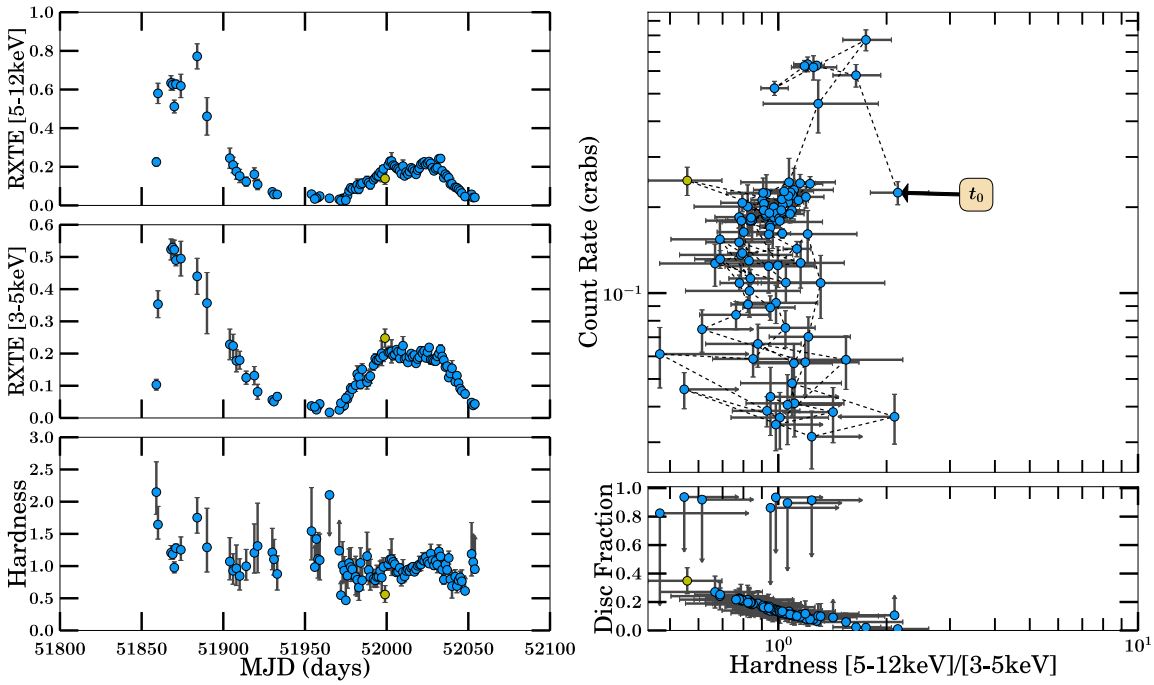

(a) 2000/2001 Outburst Analysis

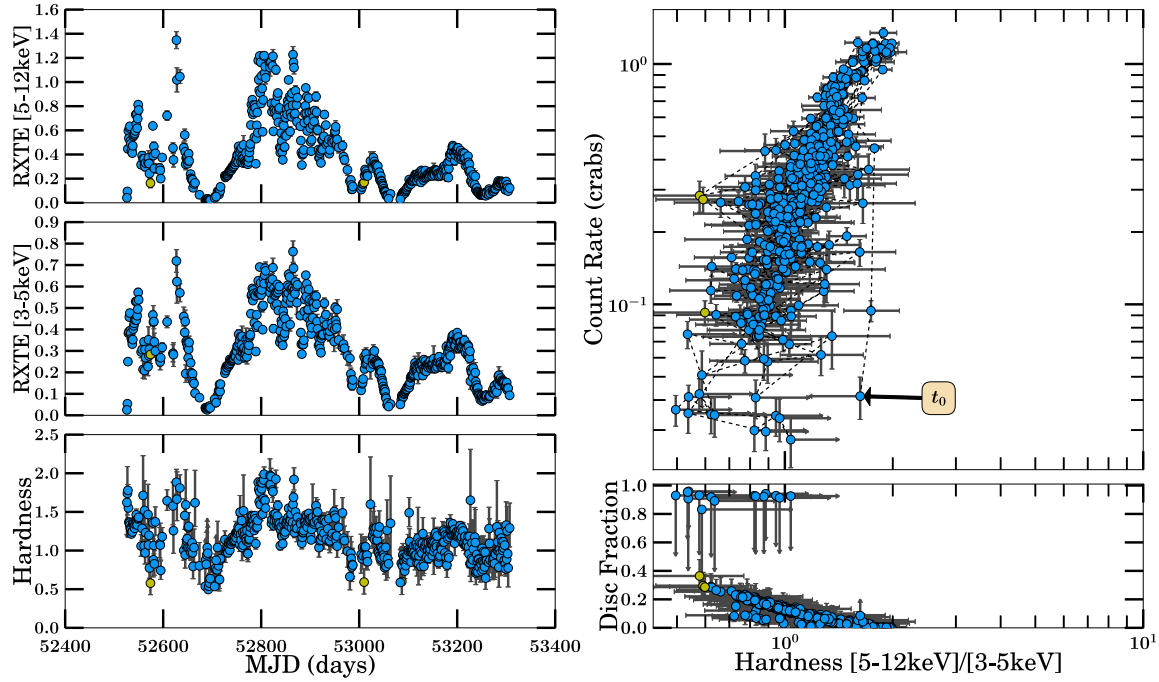

(b) 2002-2004 Outburst Analysis

Figure B.15: 4U 1630−472 Part 3

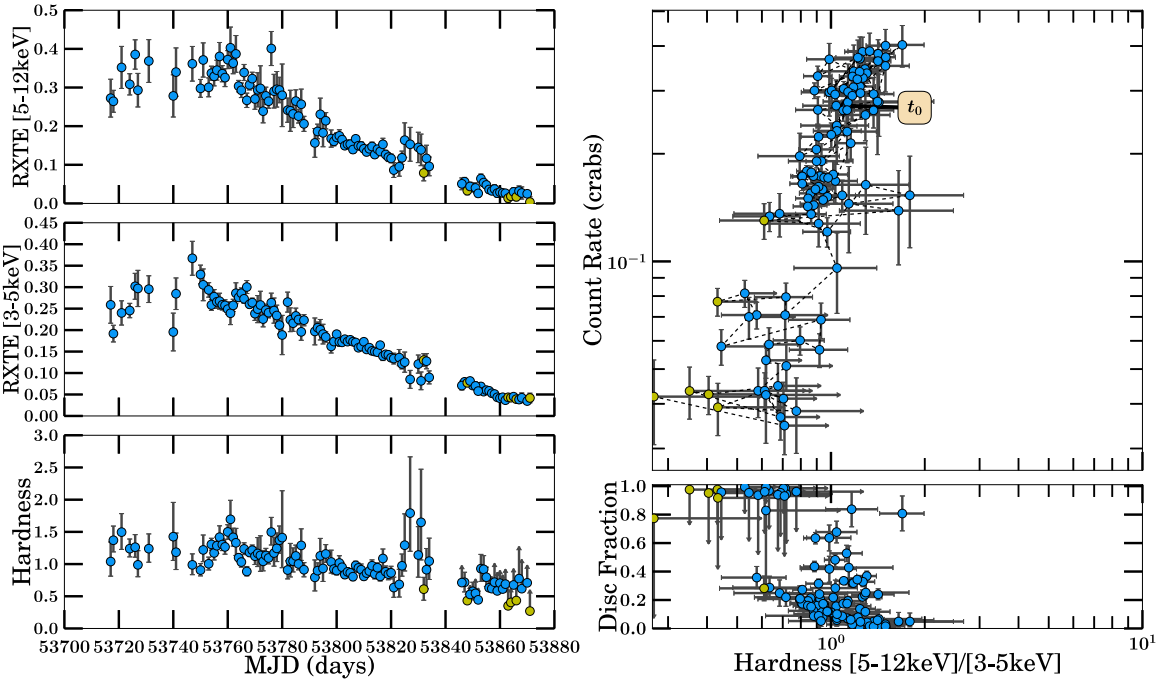

(a) 2005/2006 Outburst Analysis

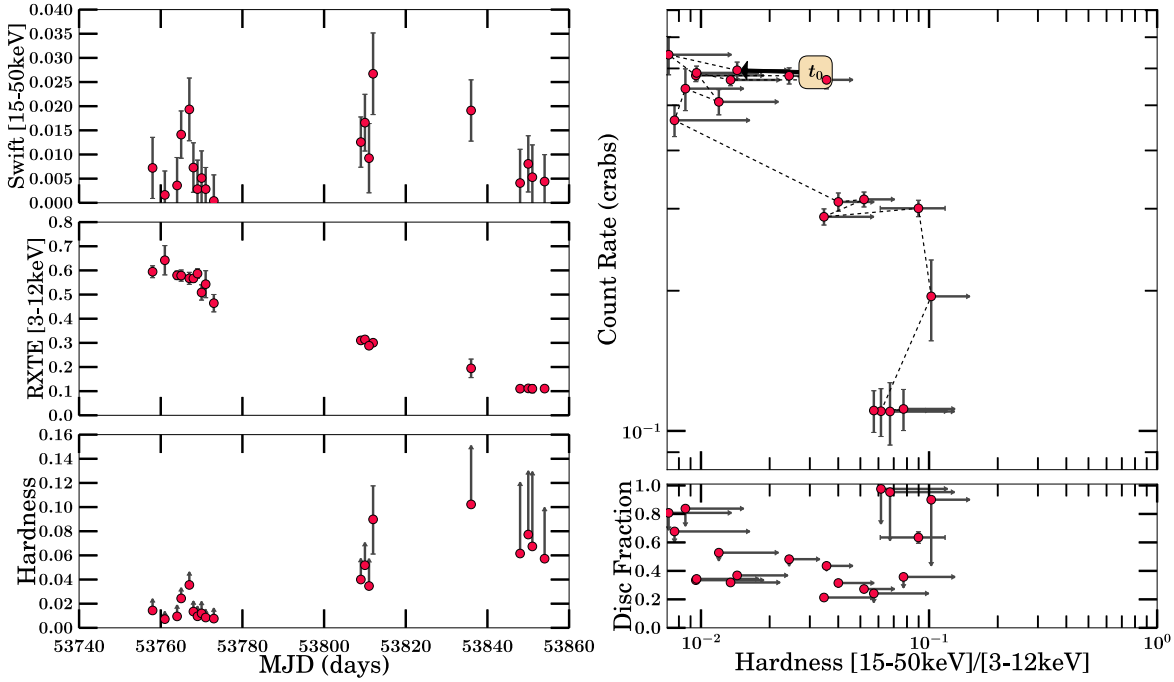

(b) 2005/2006 Outburst Analysis

Figure B.16: 4U 1630−472 Part 4

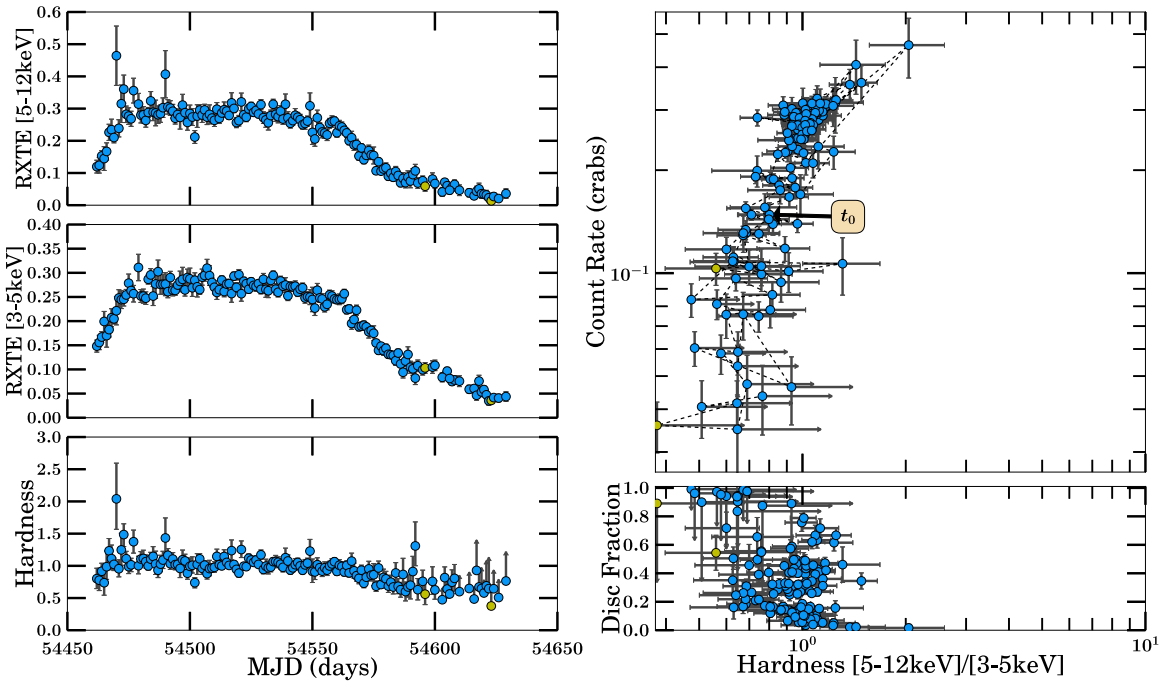

(a) 2007/2008 Outburst Analysis

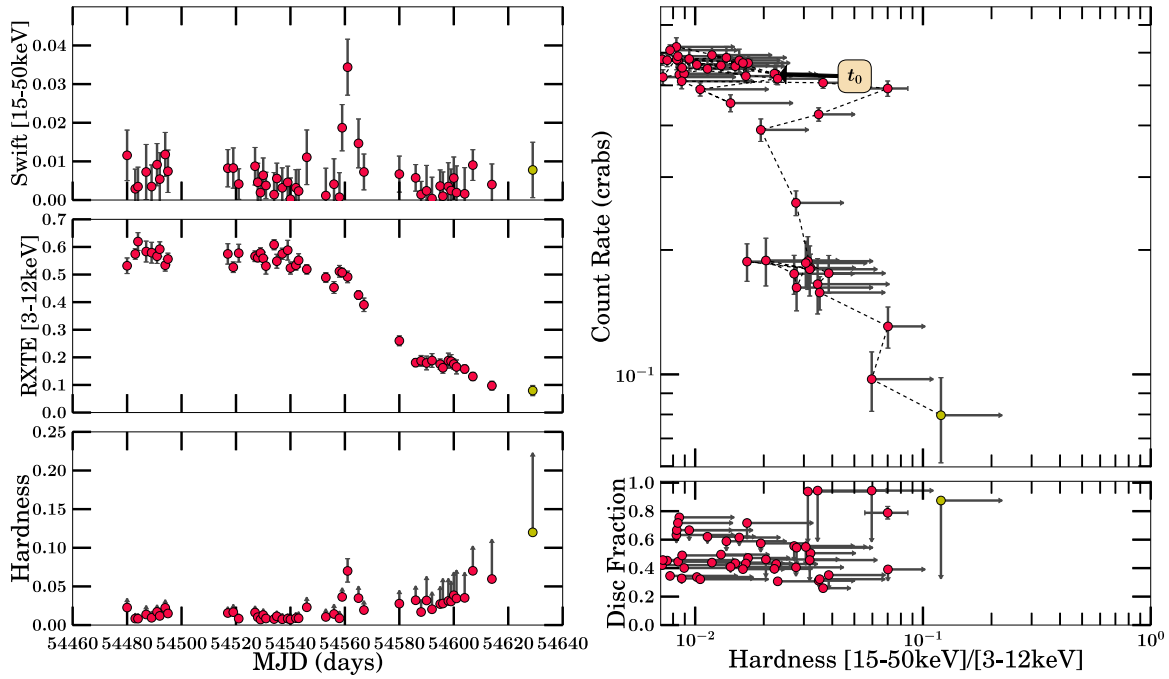

(b) 2007/2008 Outburst Analysis

Figure B.17: 4U 1630−472 Part 5

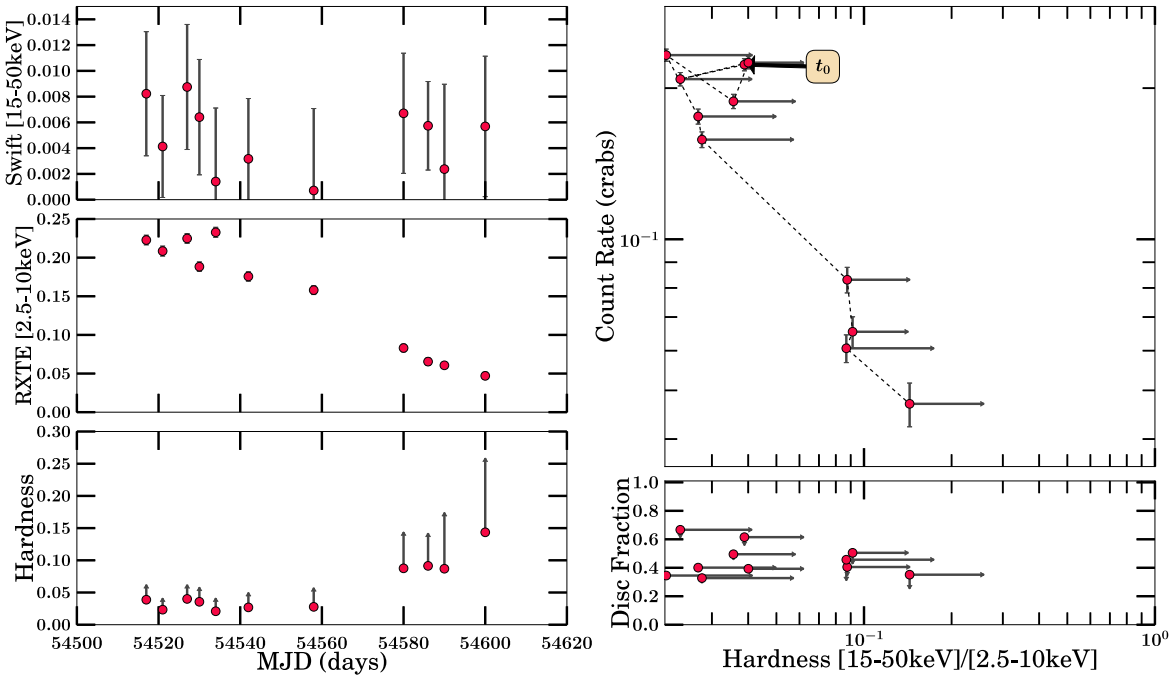

(a) 2007/2008 Outburst Analysis

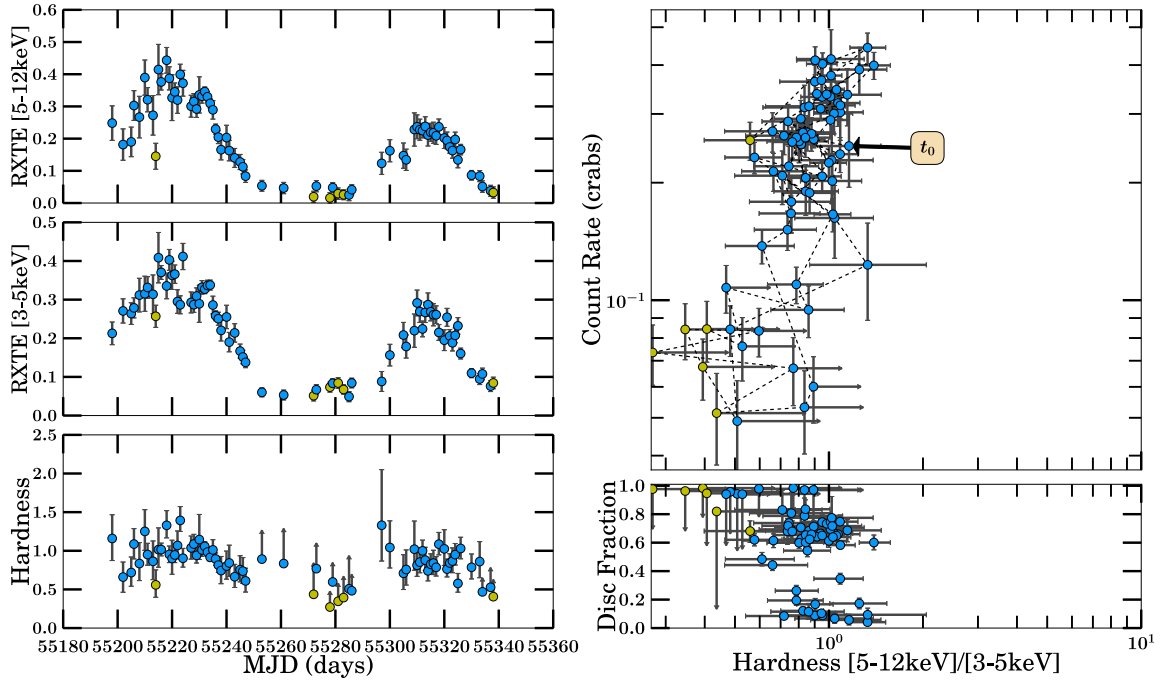

(b) 2009/2010 Outburst Analysis

Figure B.18: 4U 1630−472 Part 6

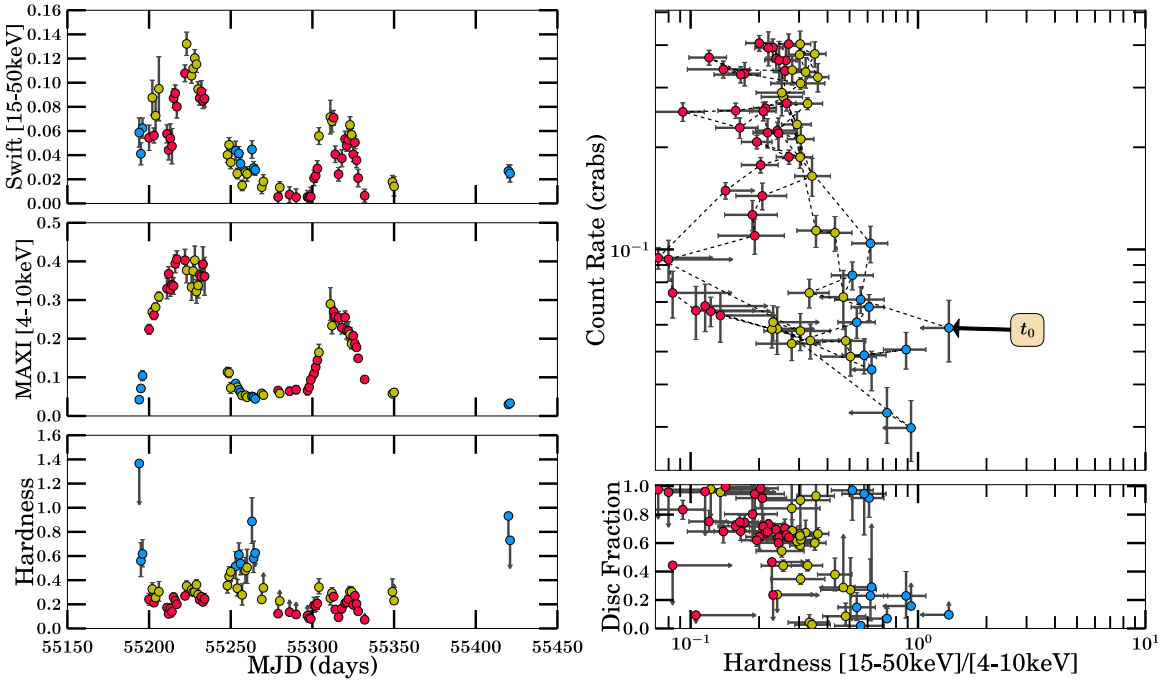

(a) 2009/2010 Outburst Analysis

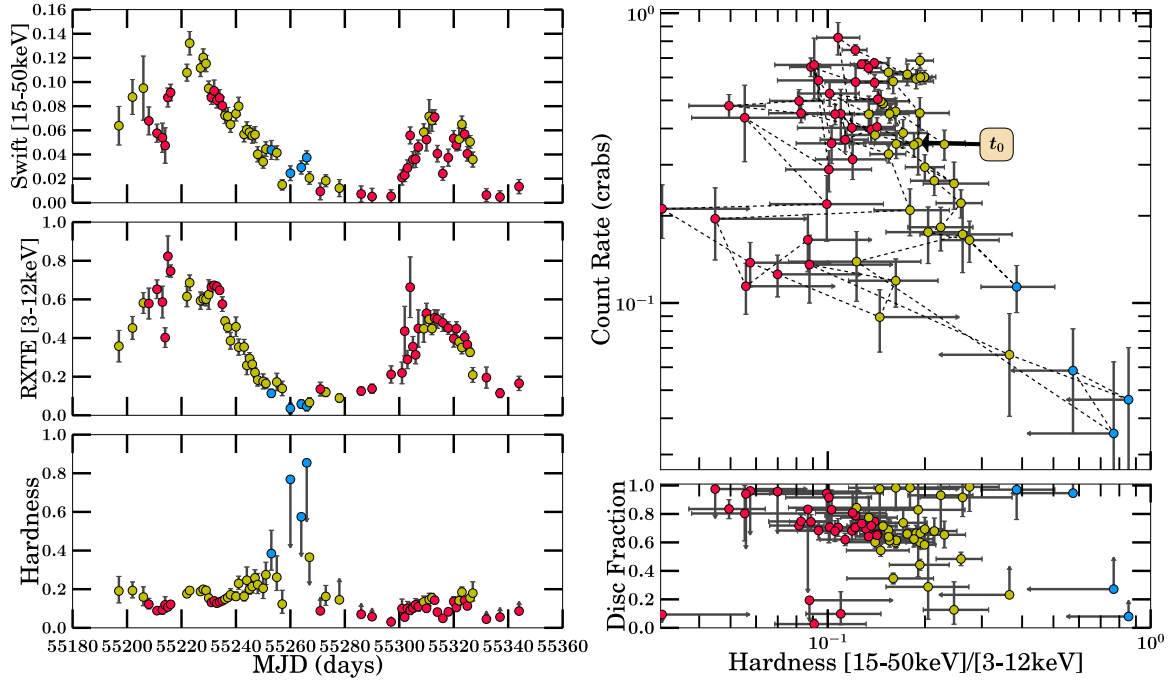

(b) 2009/2010 Outburst Analysis

Figure B.19: 4U 1630−472 Part 7

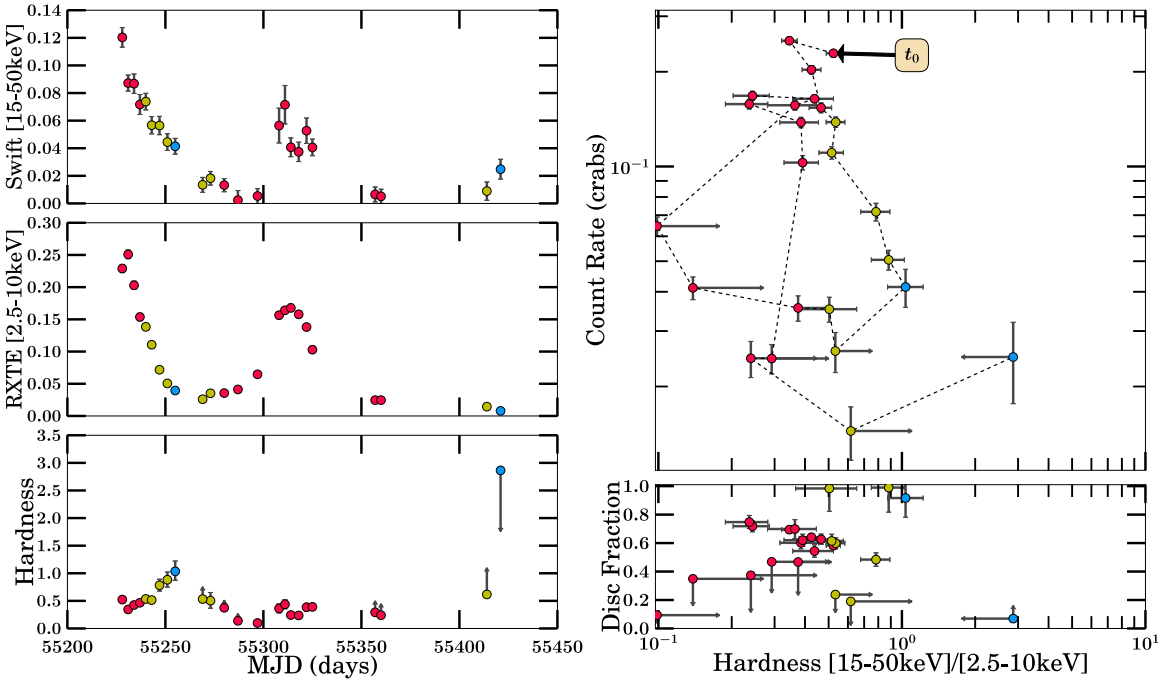

(a) 2009/2010 Outburst Analysis

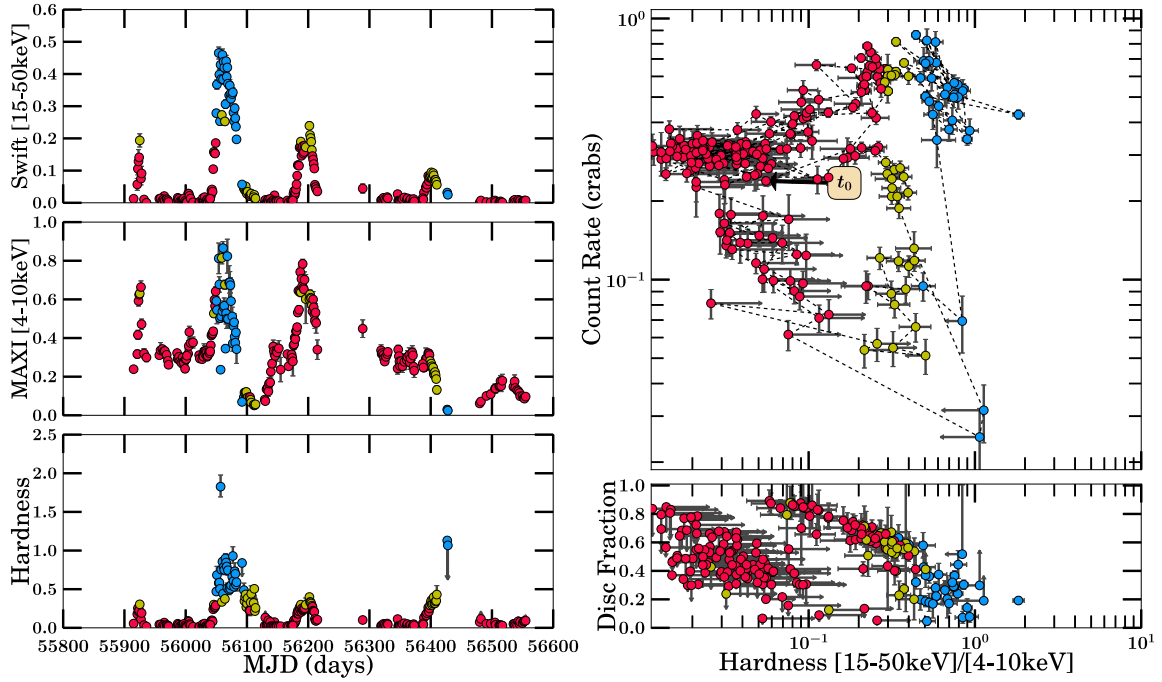

(b) 2011-2013 Outburst Analysis

Figure B.20: 4U 1630−472 Part 8

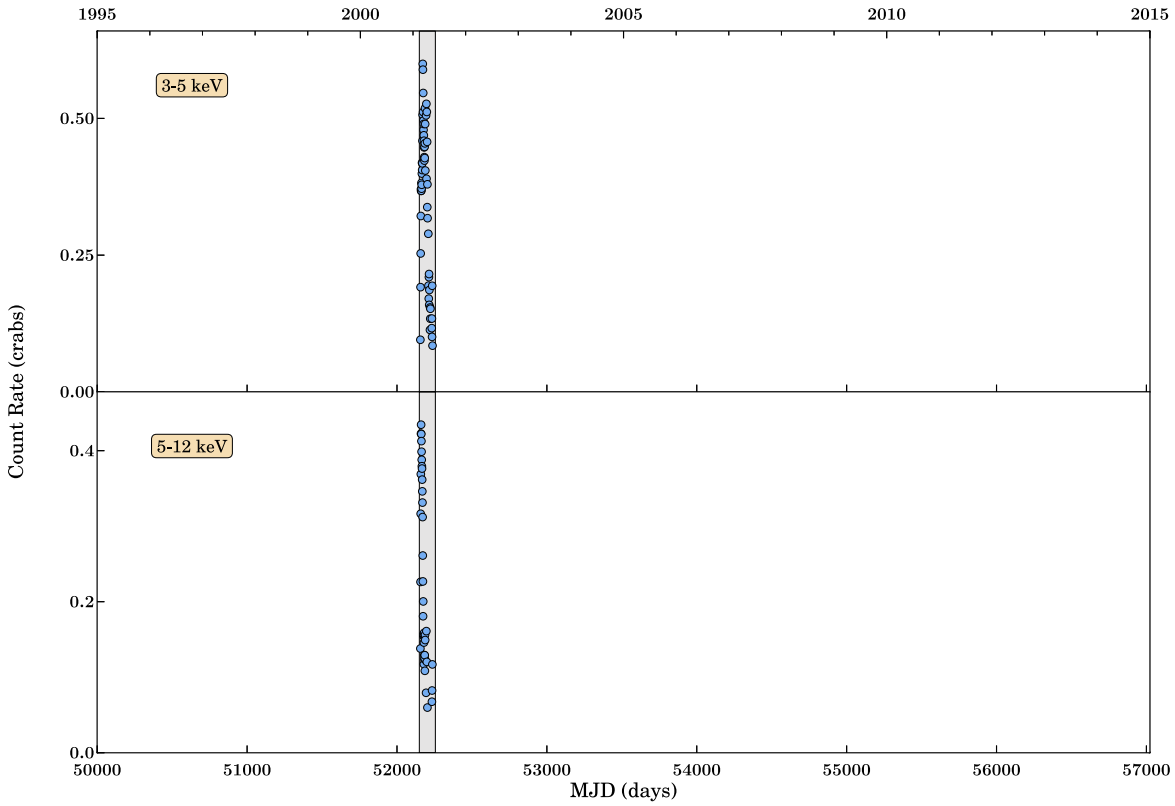

(a) Long-term Light Curve

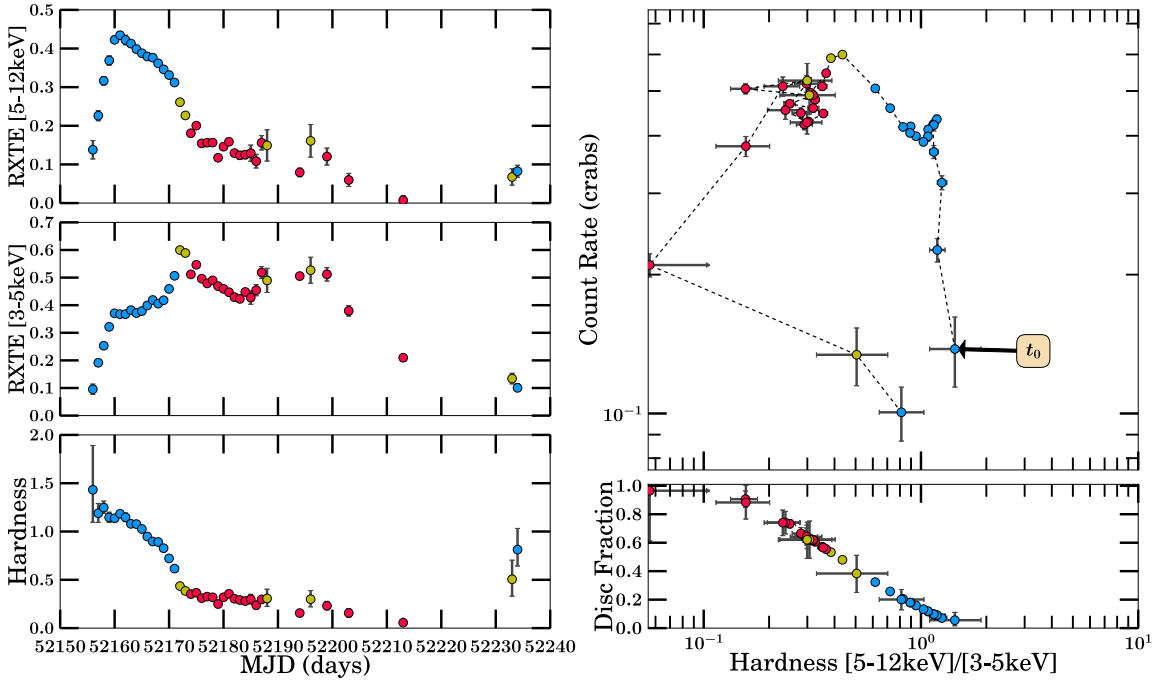

(b) 2001 Outburst Analysis

Figure B.21: XTE J1650−500

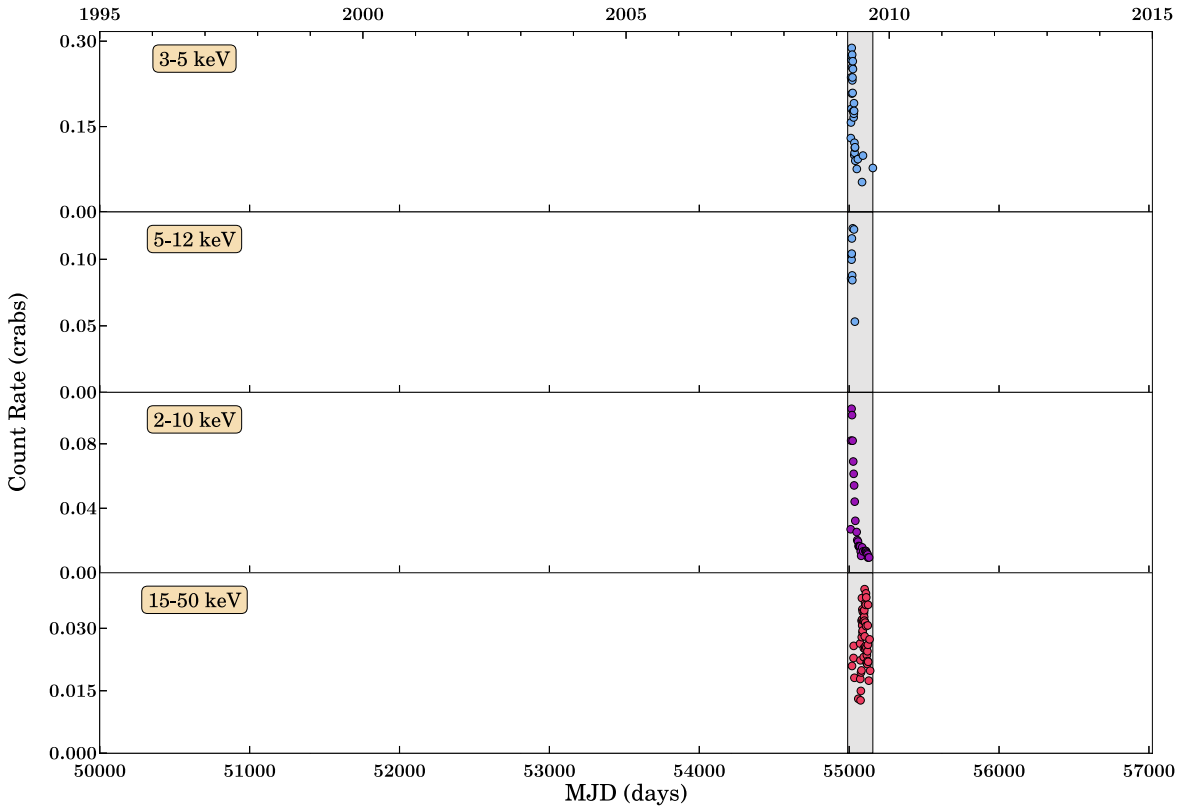

(a) Long-term Light Curve

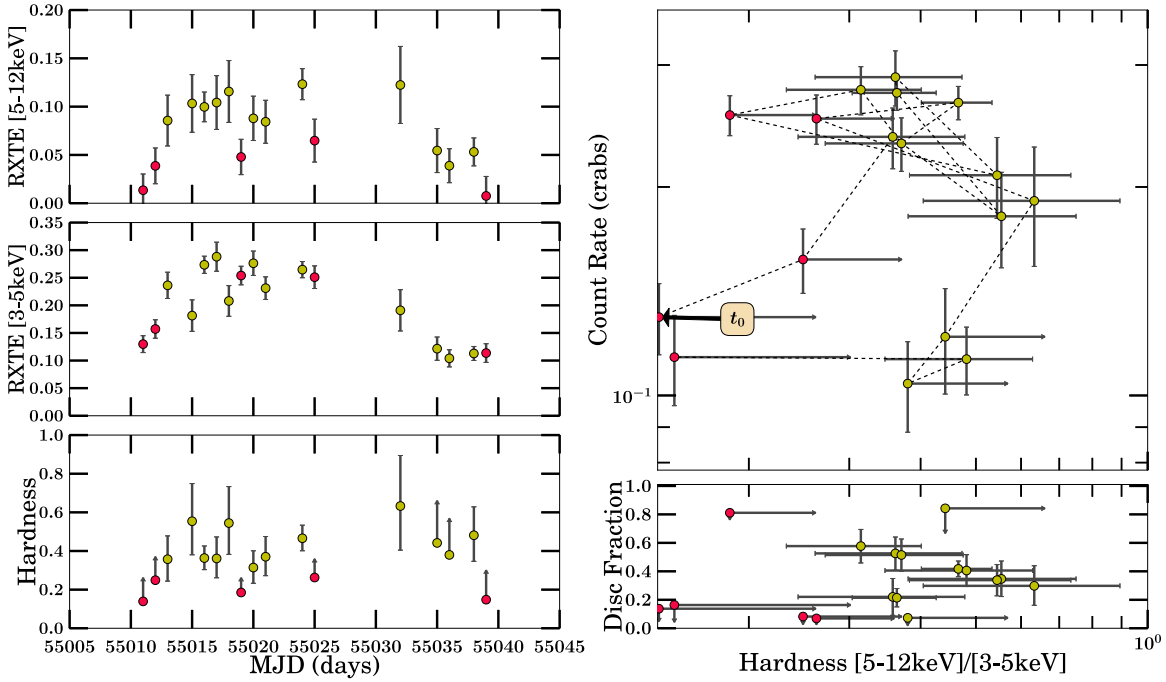

(b) 2009 Outburst Analysis

Figure B.22: XTE J1652−453 Part 1

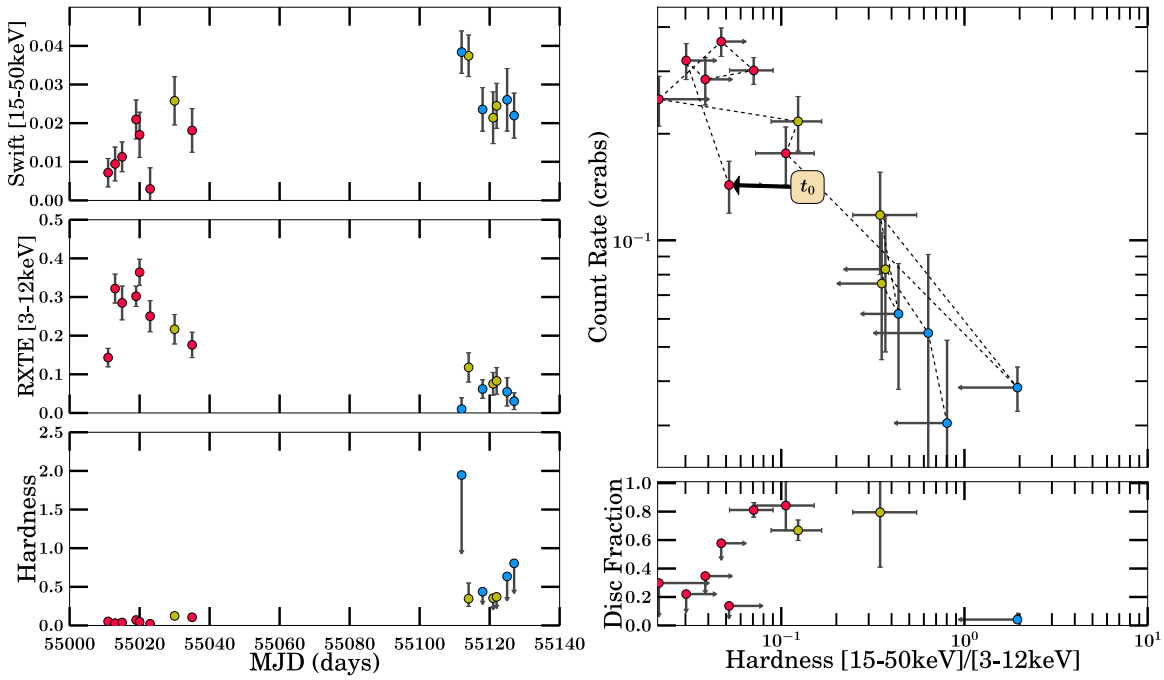

(a) 2009 Outburst Analysis

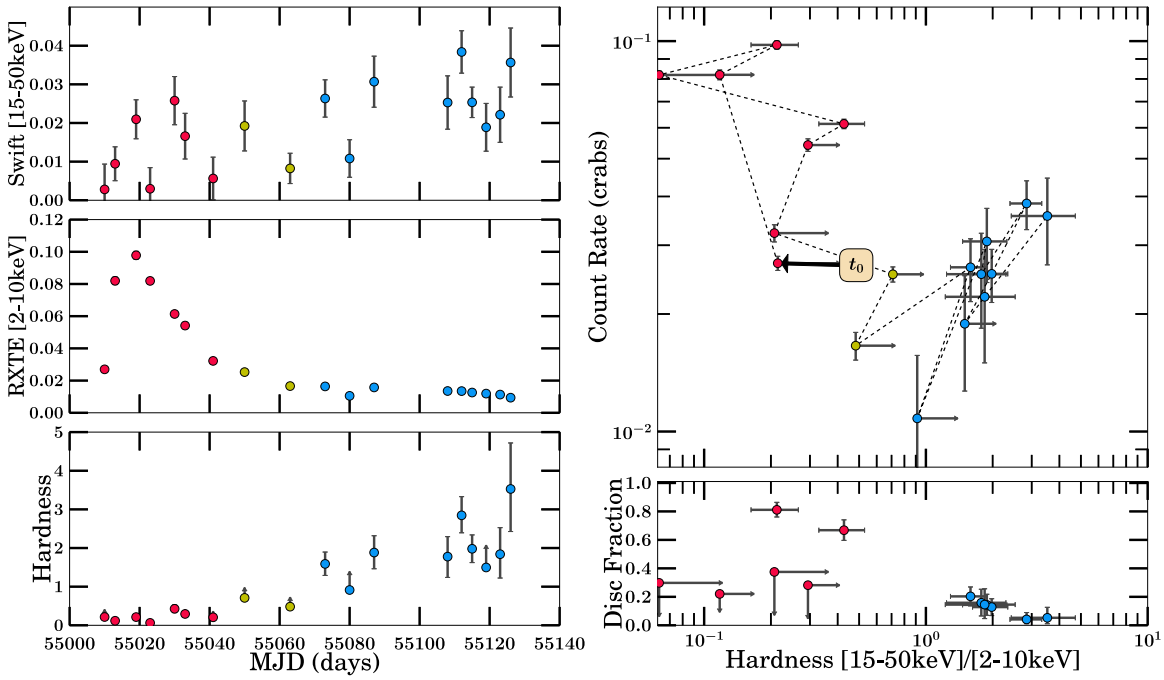

(b) 2009 Outburst Analysis

Figure B.23: XTE J1652−453 Part 2

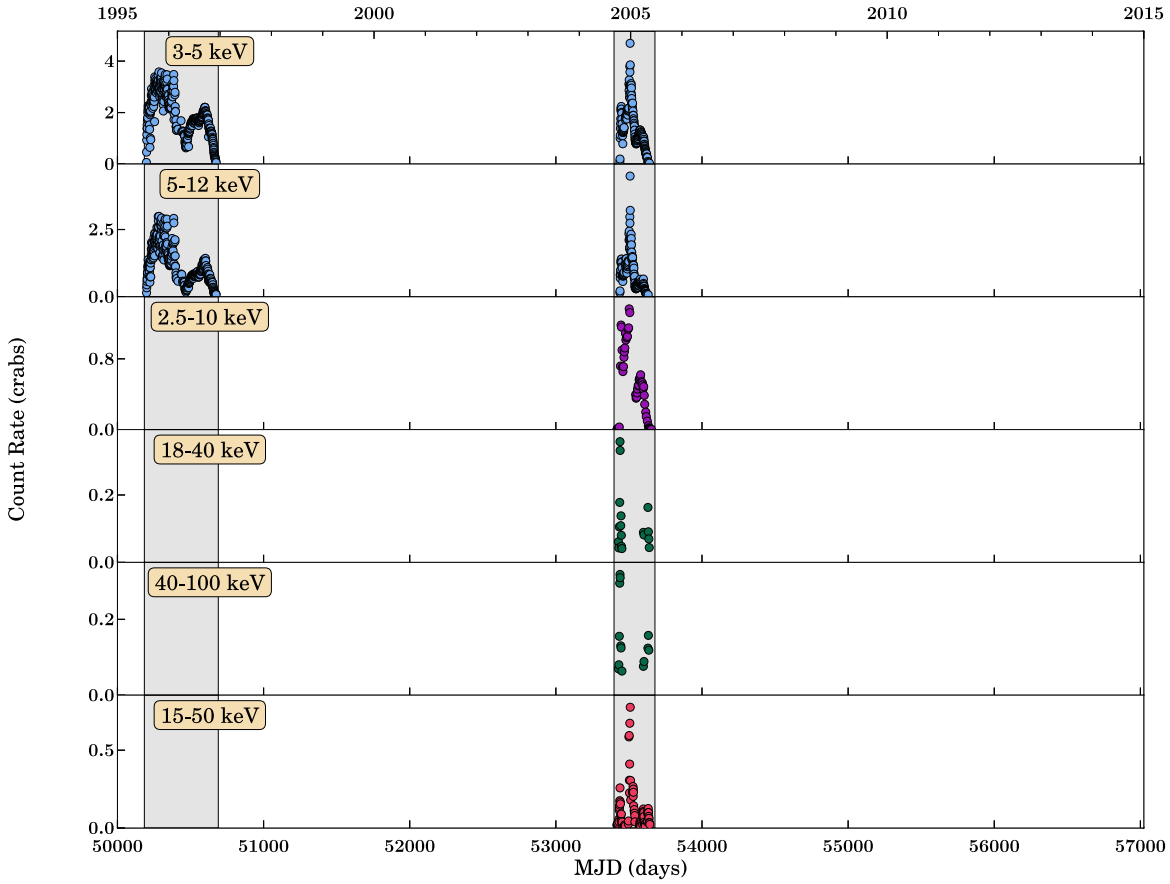

(a) Long-term Light Curve

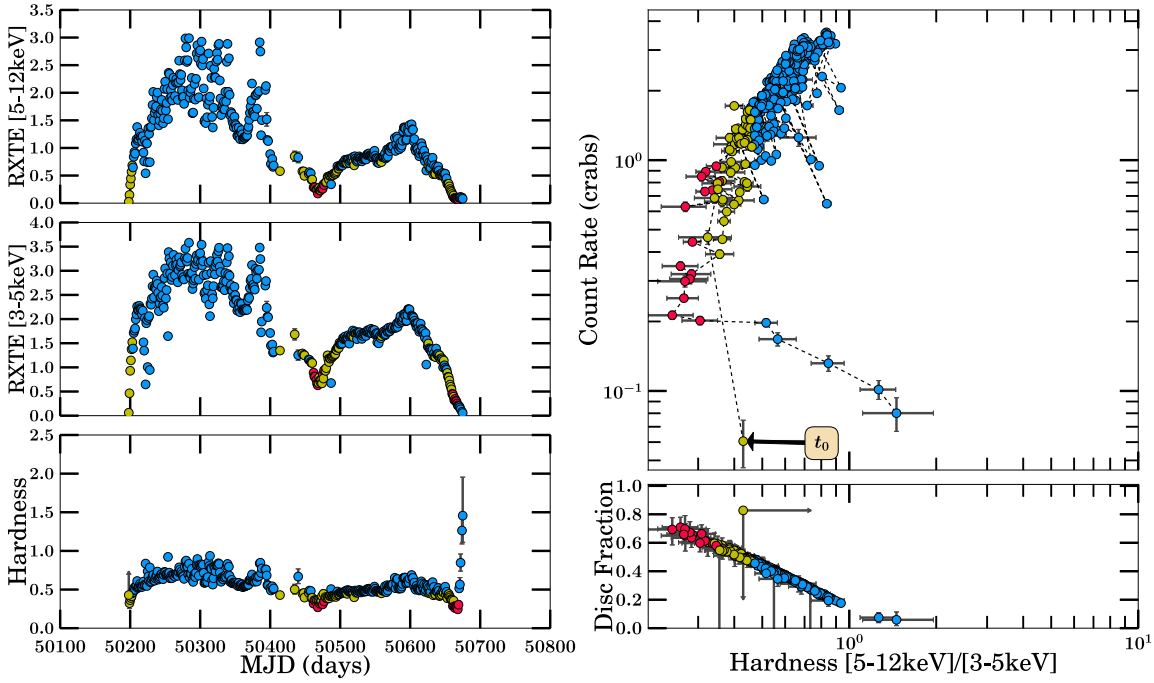

(b) 1996/1997 Outburst Analysis

Figure B.24: GRO J1655−40 Part 1

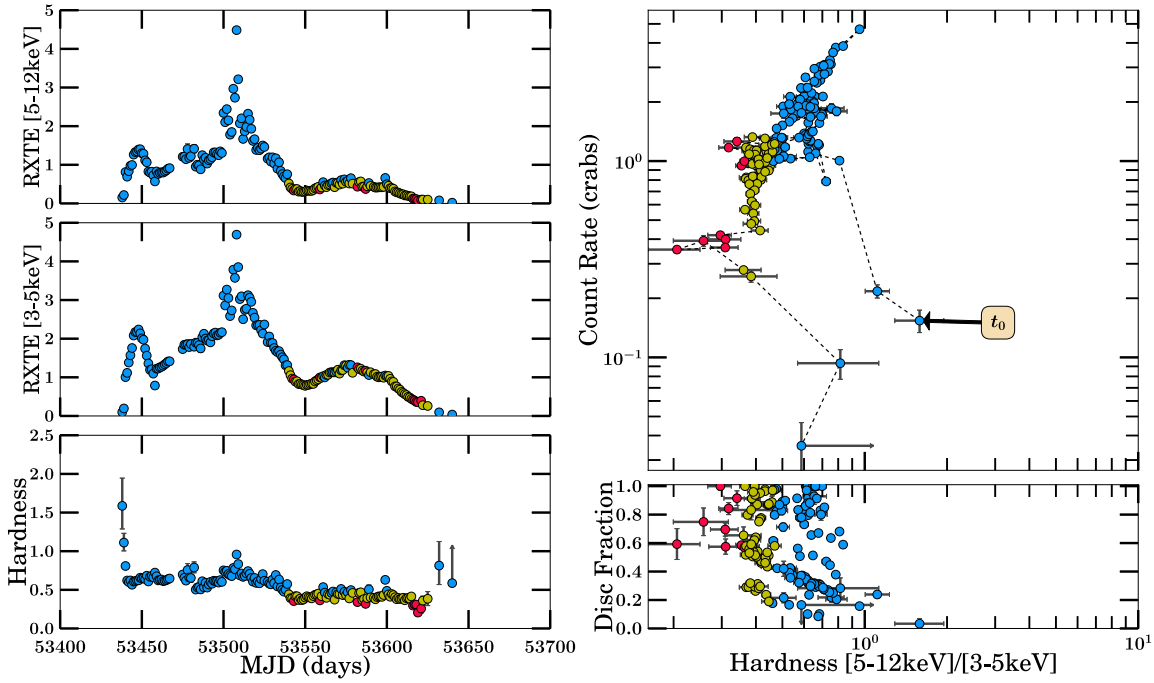

(a) 2005 Outburst Analysis

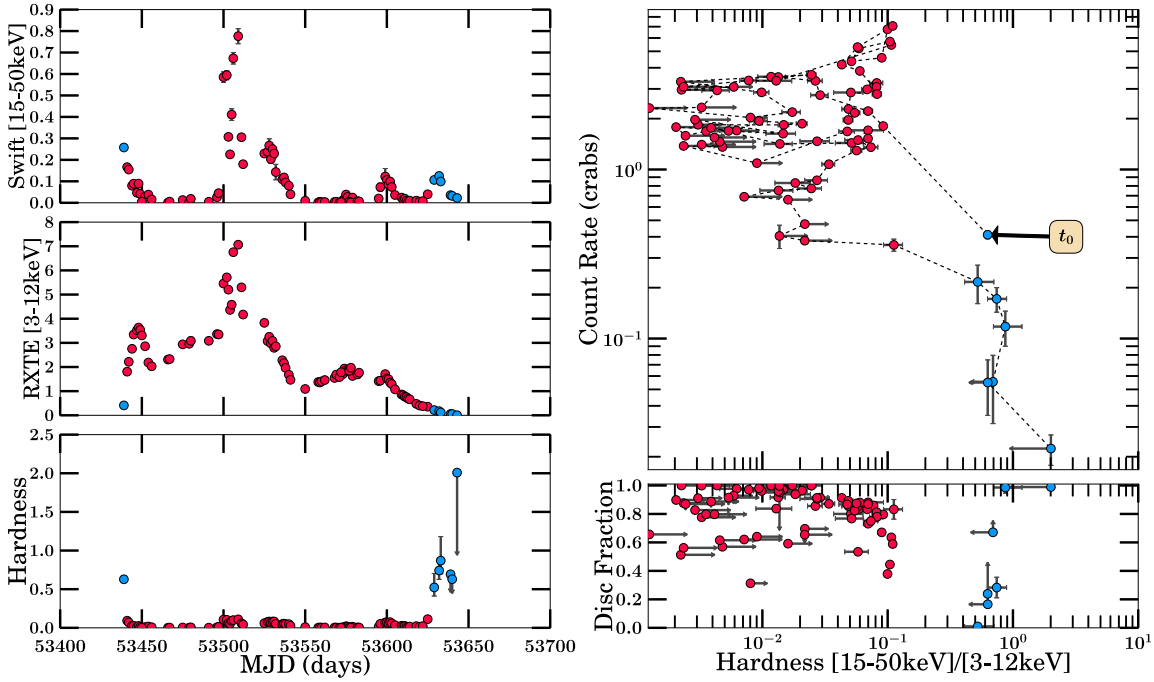

(b) 2005 Outburst Analysis

Figure B.25: GRO J1655−40 Part 2

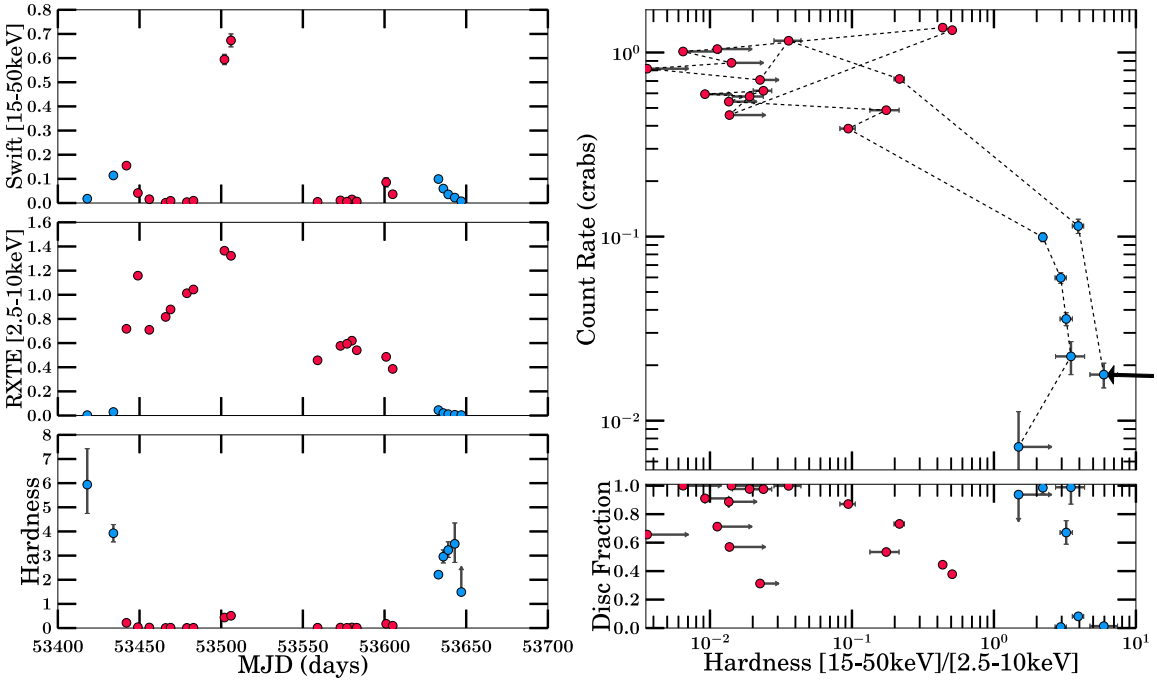

(a) 2005 Outburst Analysis

Figure B.26: GRO J1655−40 Part 3

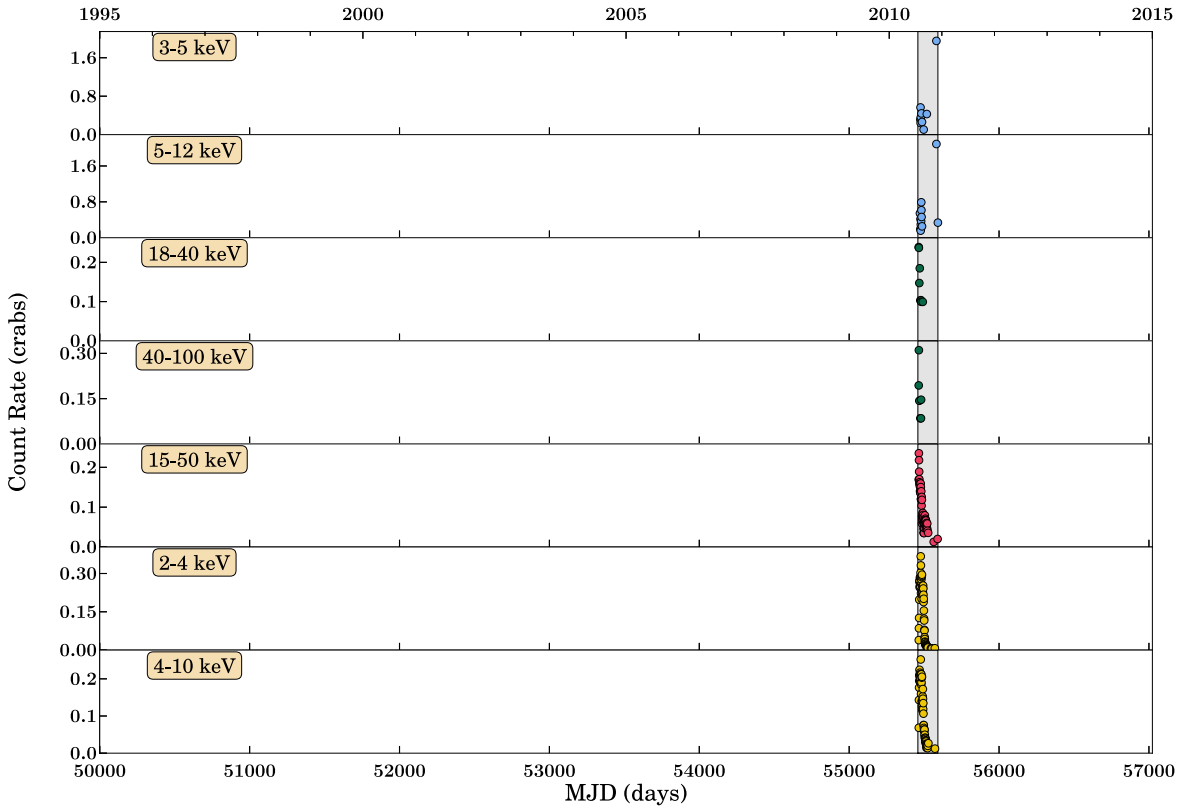

(a) Long-term Light Curve

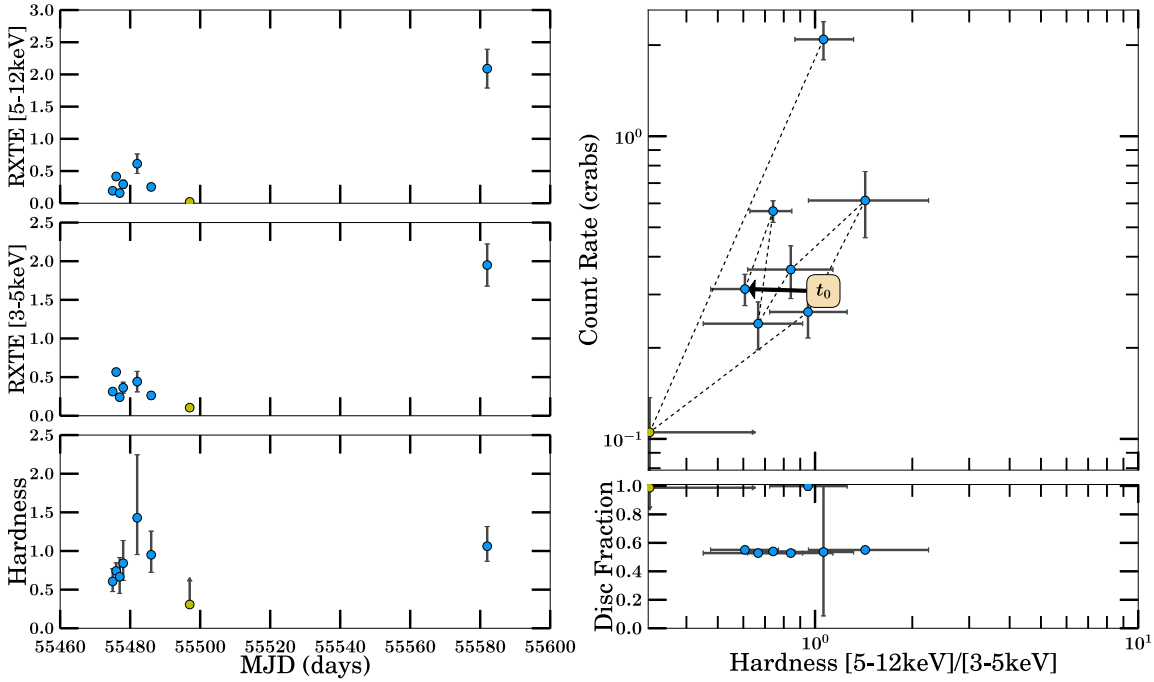

(b) 2010/2011 Outburst Analysis

Figure B.27: MAXI J1659−152 Part 1

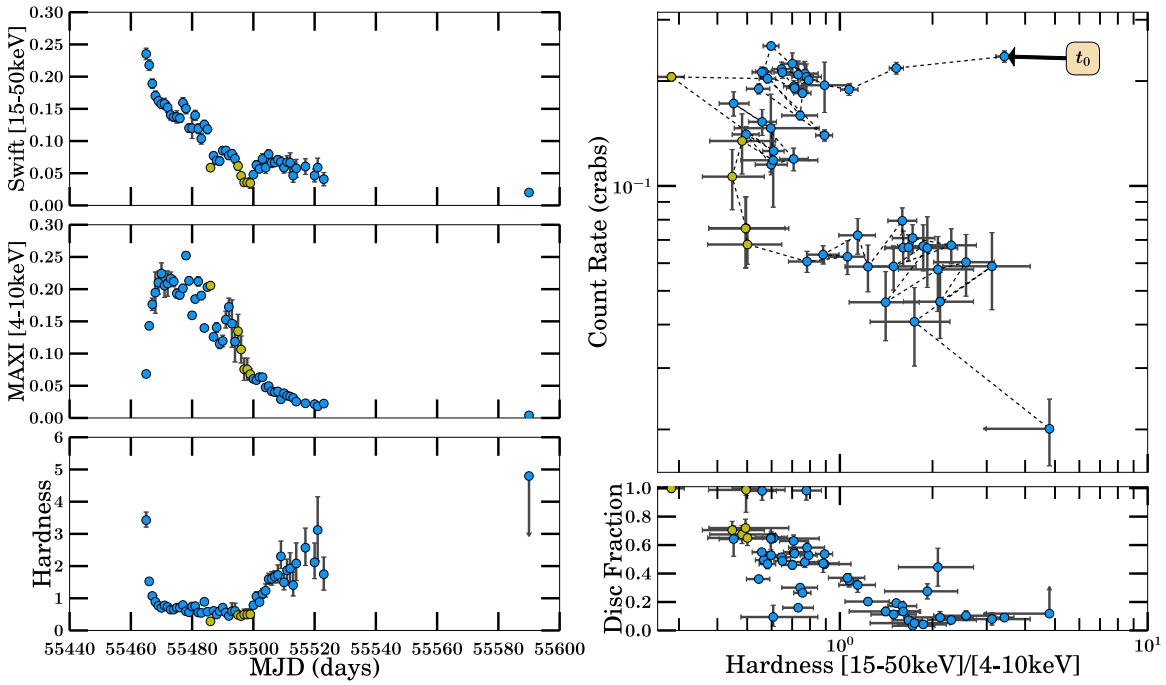

(a) 2010/2011 Outburst Analysis

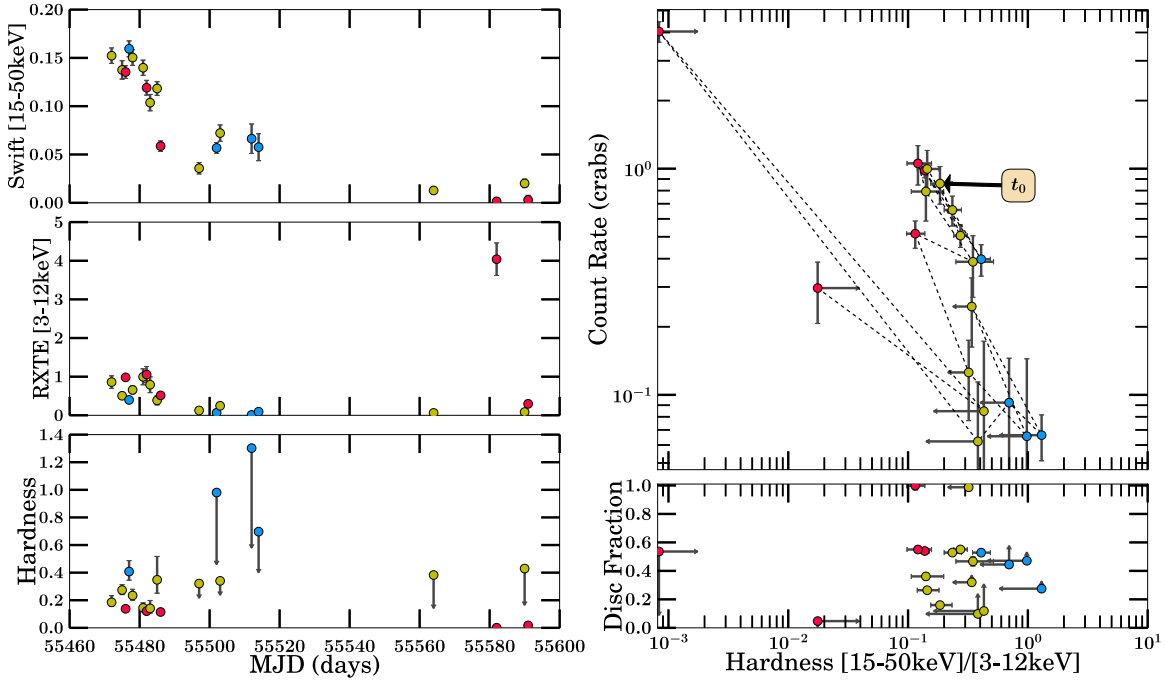

(b) 2010/2011 Outburst Analysis

Figure B.28: MAXI J1659−152 Part 2

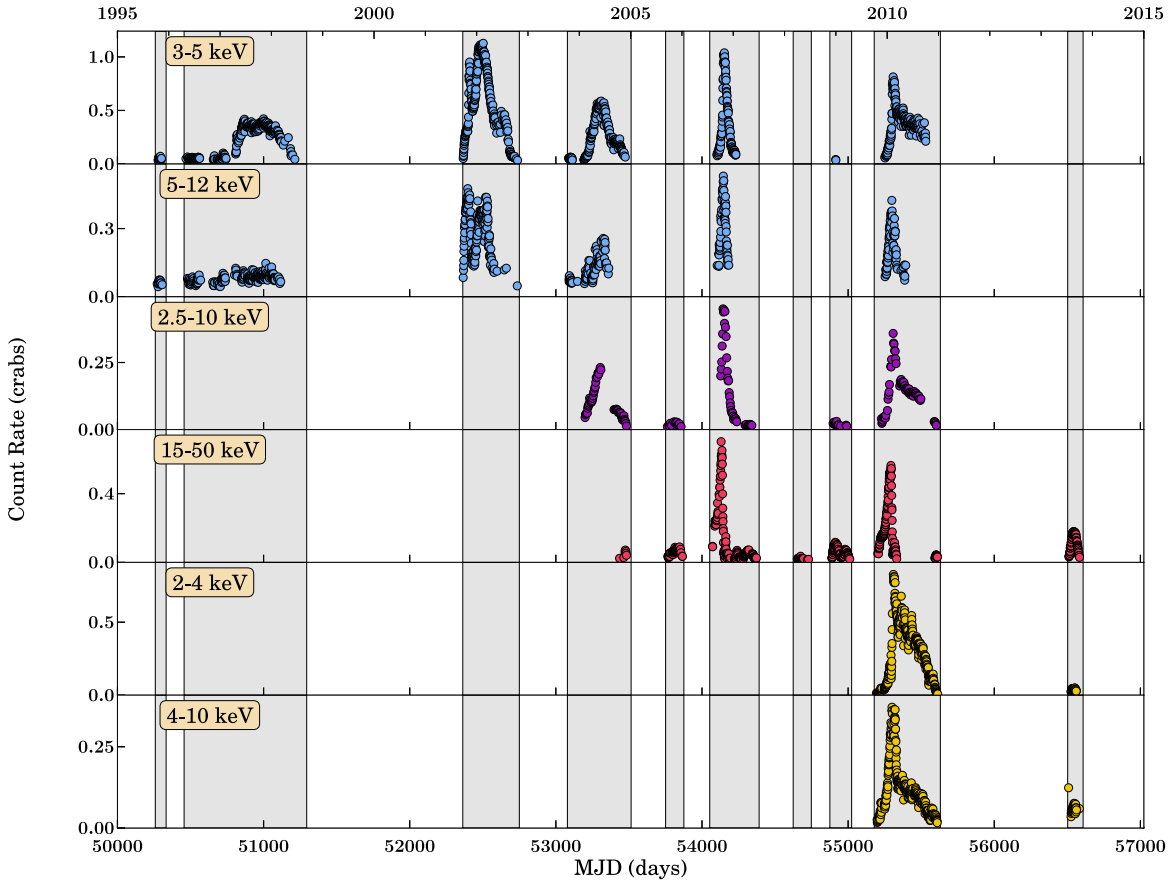

(a) Long-term Light Curve

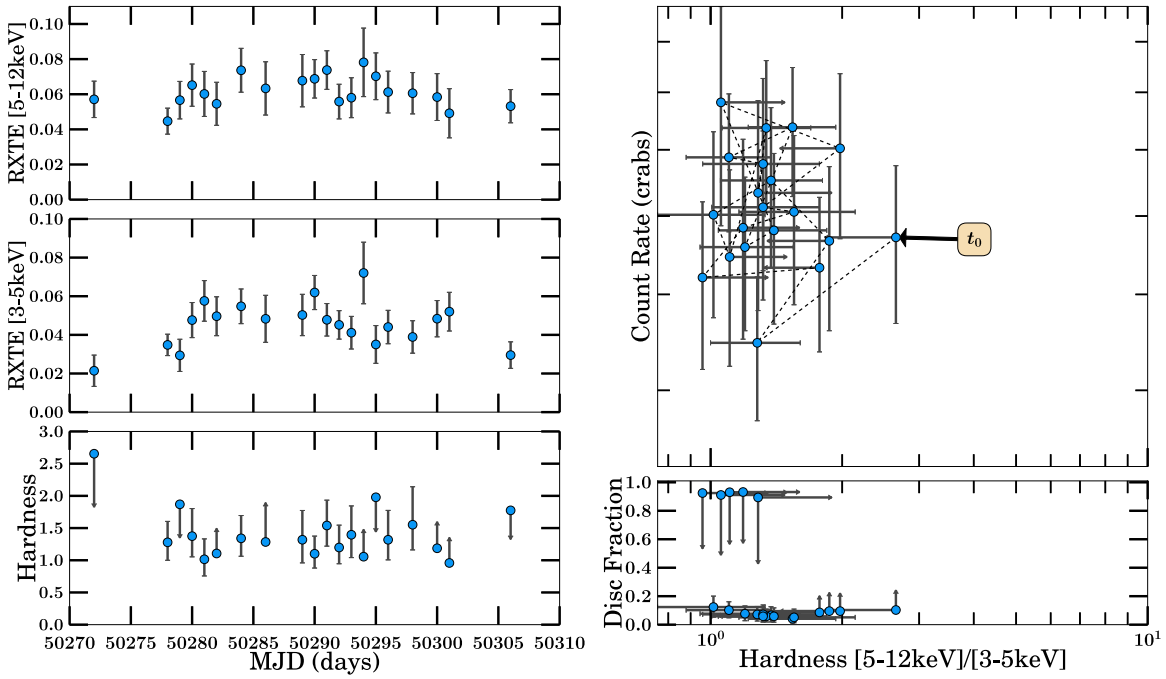

(b) 1996b Outburst Analysis

Figure B.29: GX 339−4 Part 1

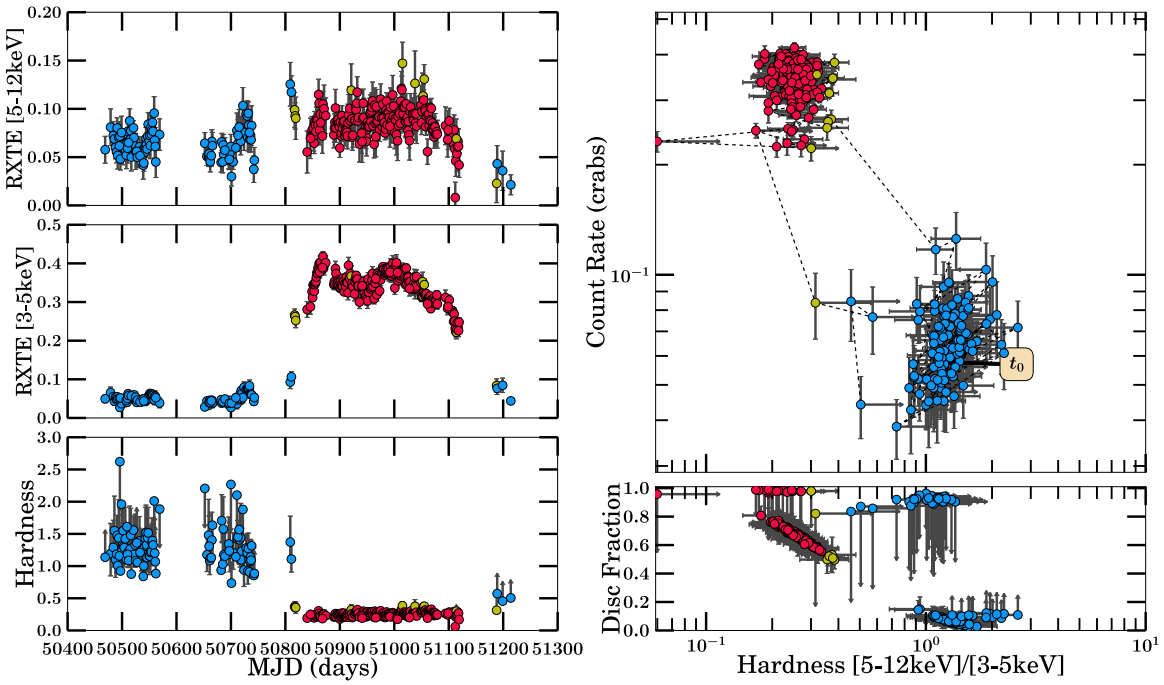

(a) 1997-1999 Outburst Analysis

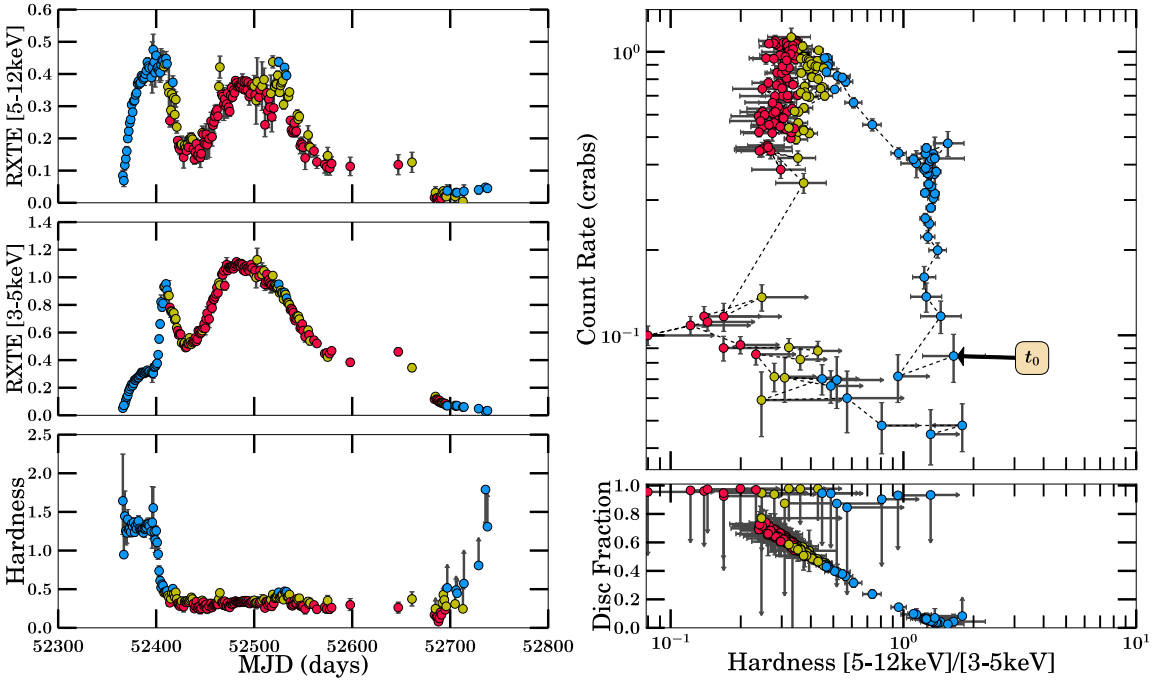

(b) 2002/2003 Outburst Analysis

Figure B.30: GX 339−4 Part 2

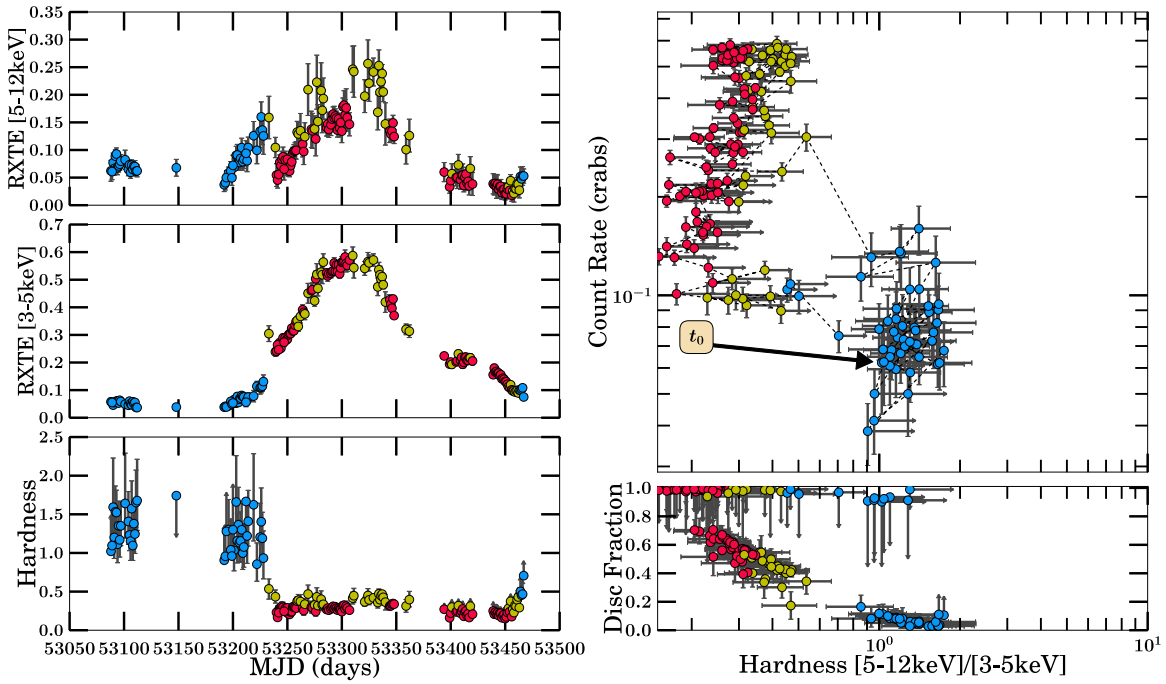

(a) 2004/2005 Outburst Analysis

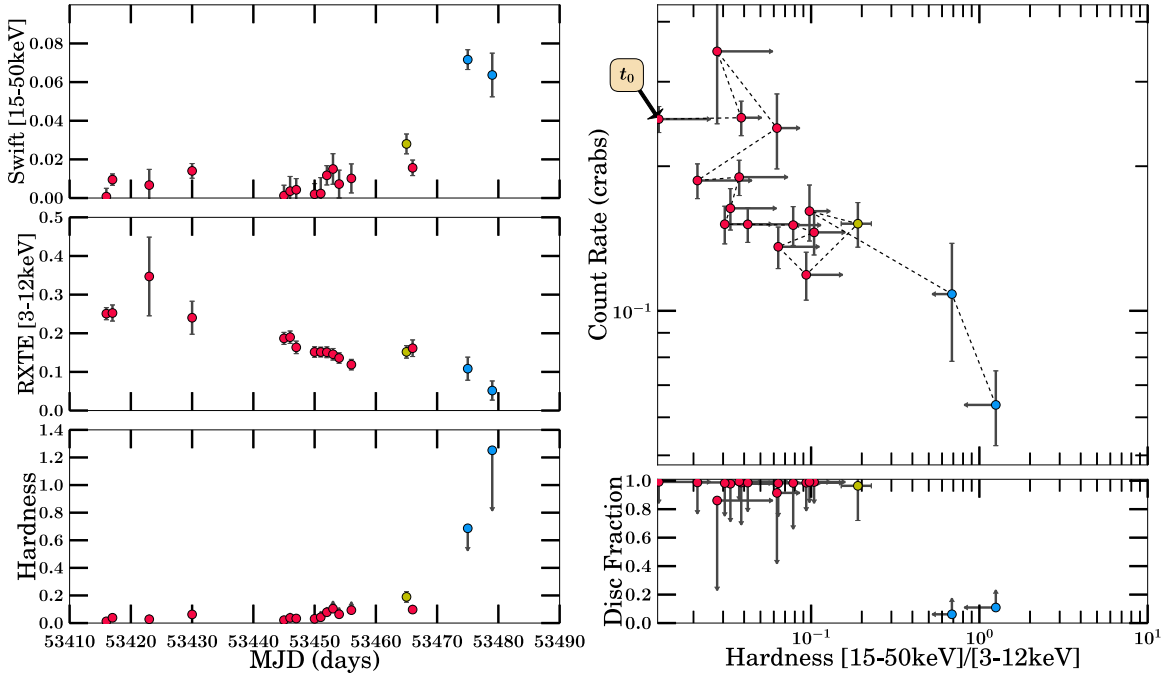

(b) 2004/2005 Outburst Analysis

Figure B.31: GX 339−4 Part 3

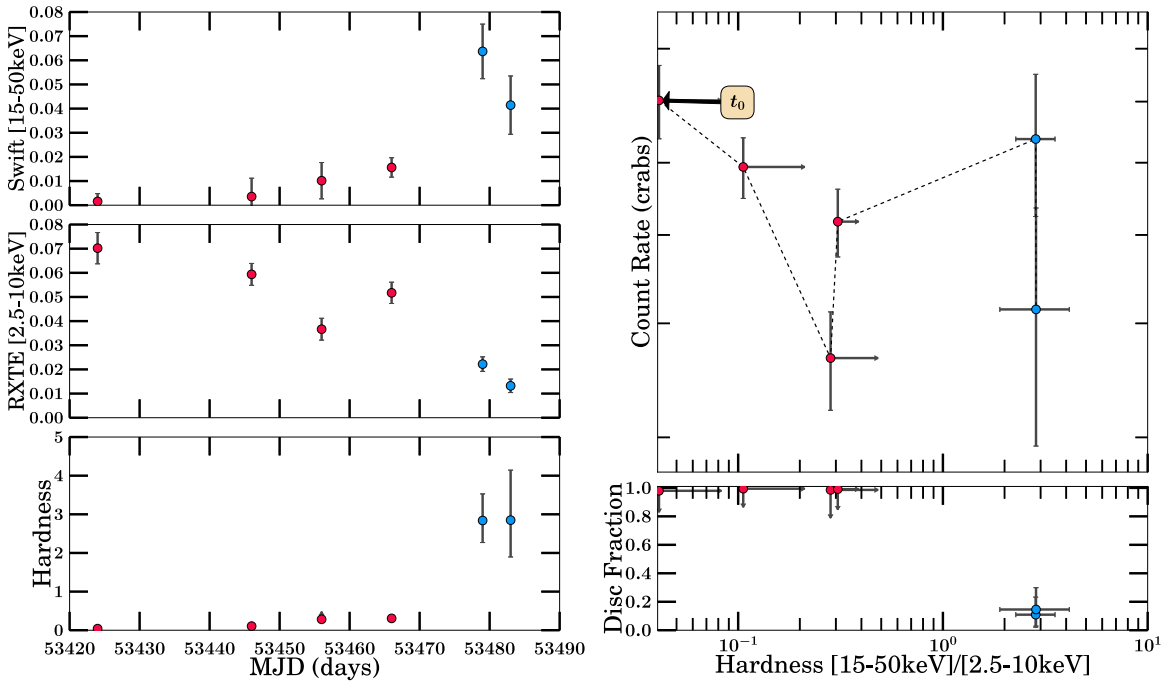

(a) 2004/2005 Outburst Analysis

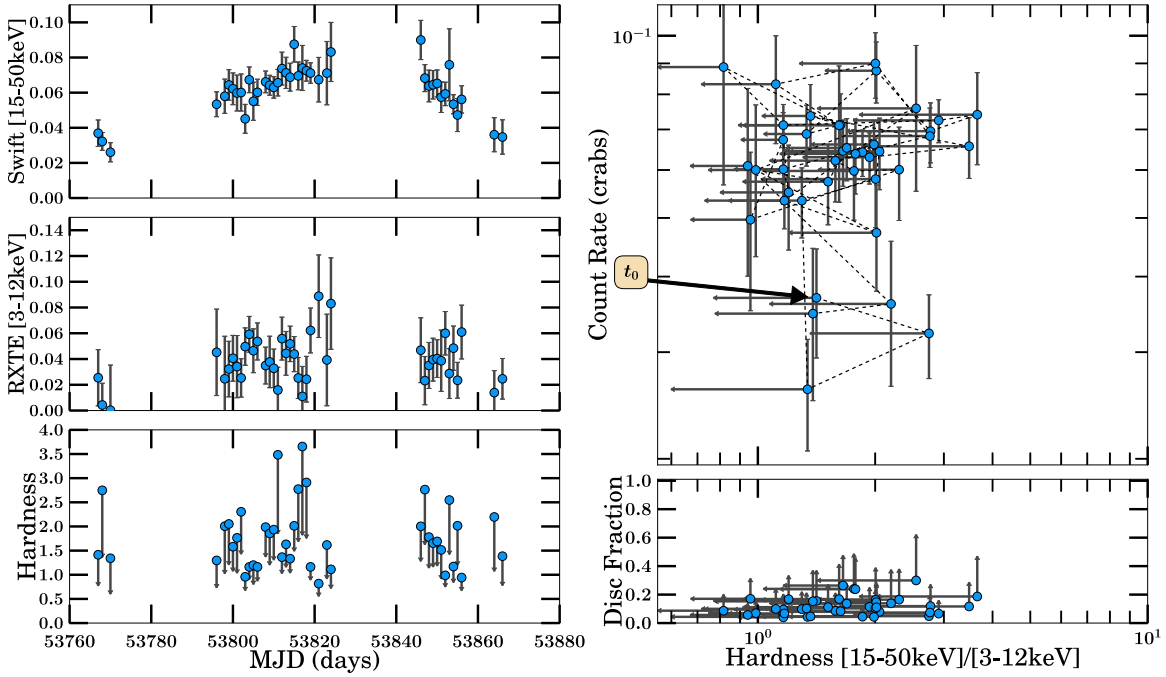

(b) 2006 Outburst Analysis

Figure B.32: GX 339−4 Part 4

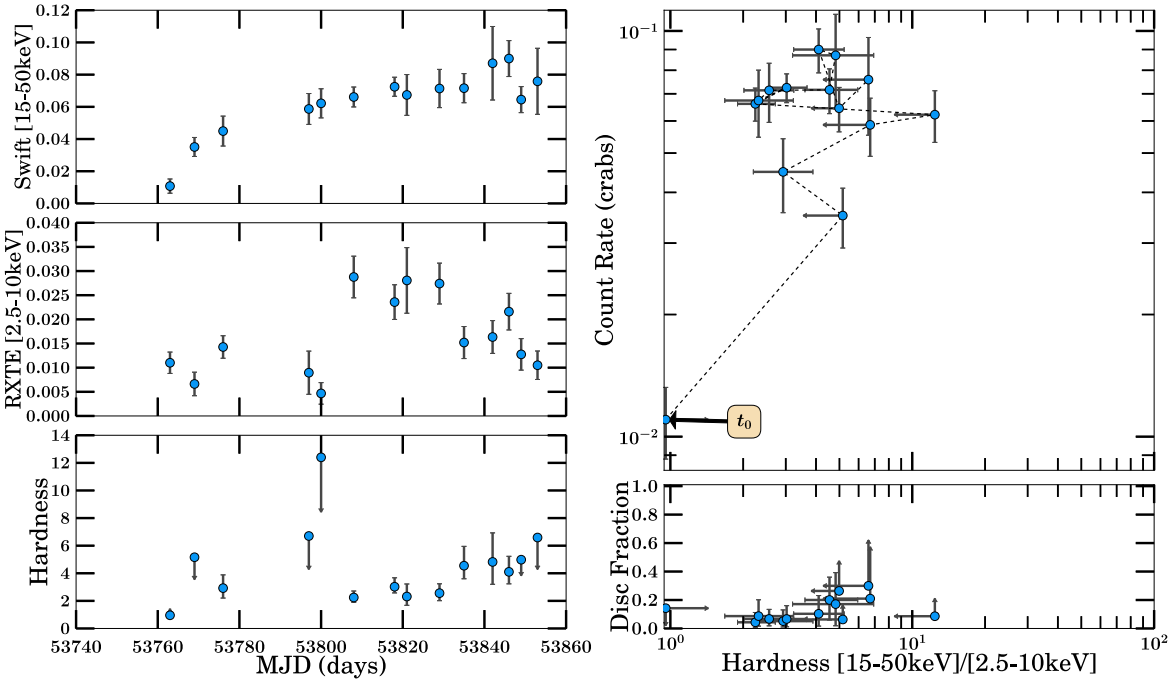

(a) 2006 Outburst Analysis

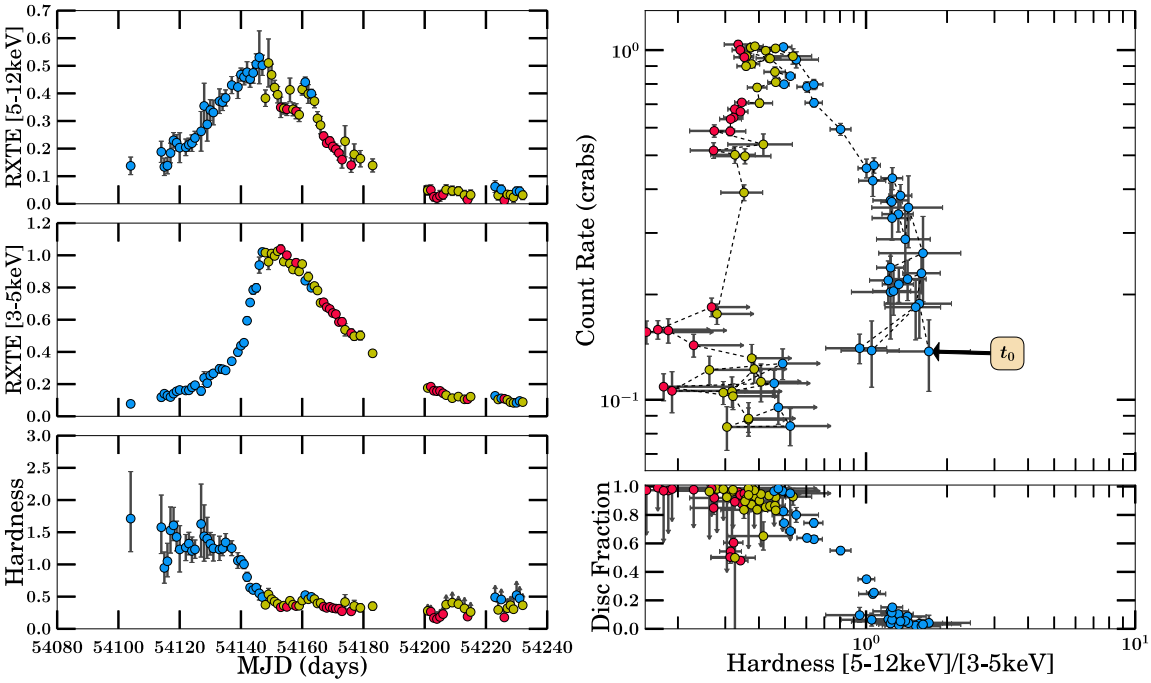

(b) 2006/2007 Outburst Analysis

Figure B.33: GX 339−4 Part 5

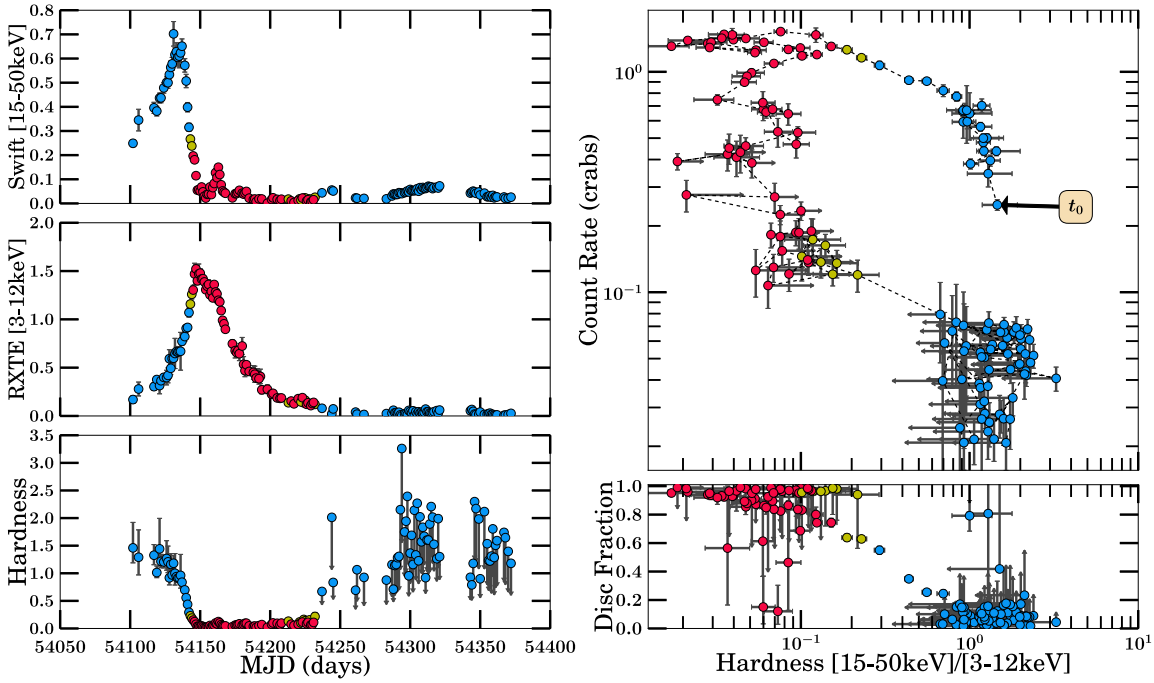

(a) 2006/2007 Outburst Analysis

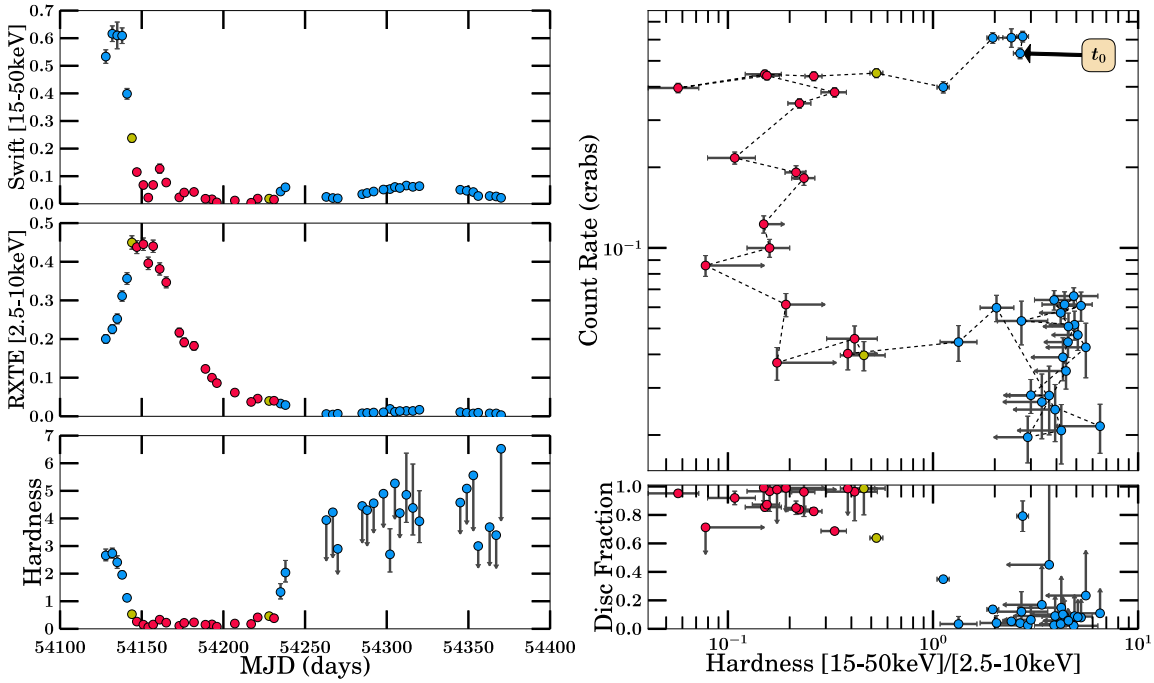

(b) 2006/2007 Outburst Analysis

Figure B.34: GX 339−4 Part 6

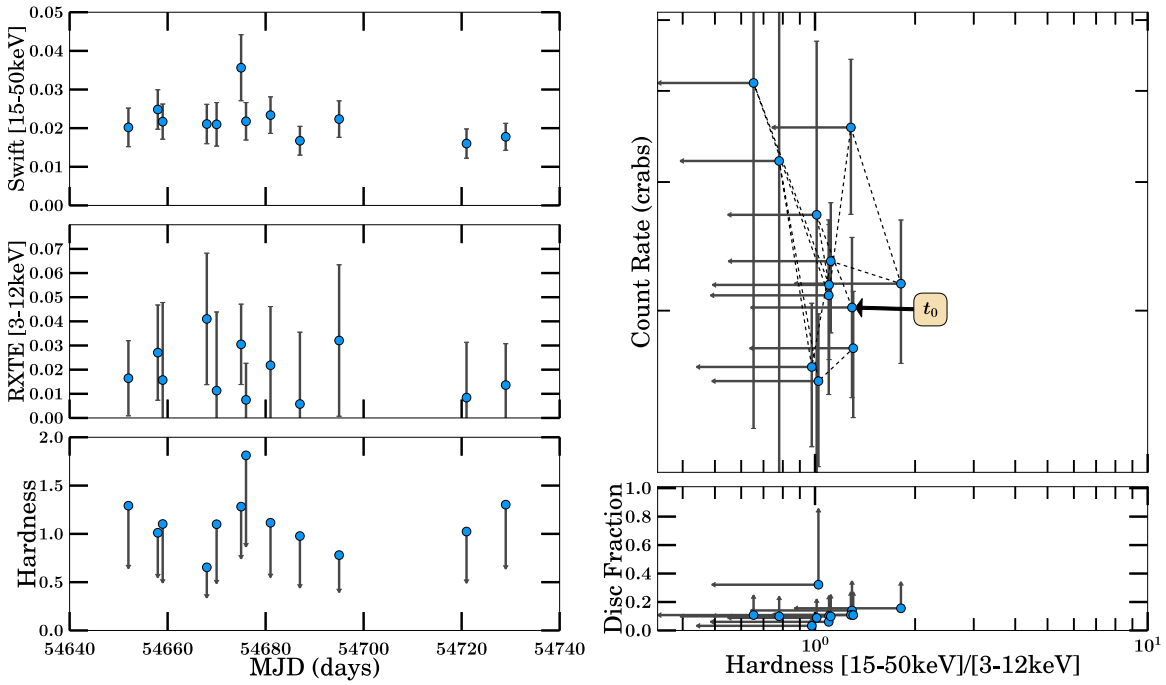

(a) 2008 Outburst Analysis

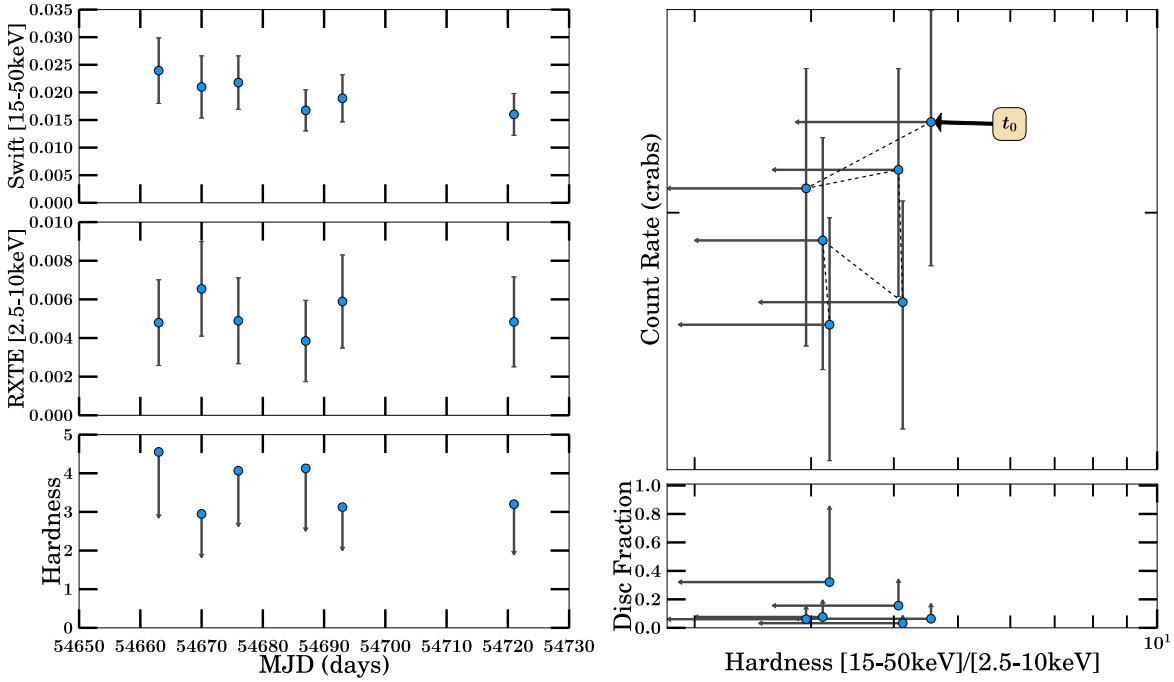

(b) 2008 Outburst Analysis

Figure B.35: GX 339−4 Part 7

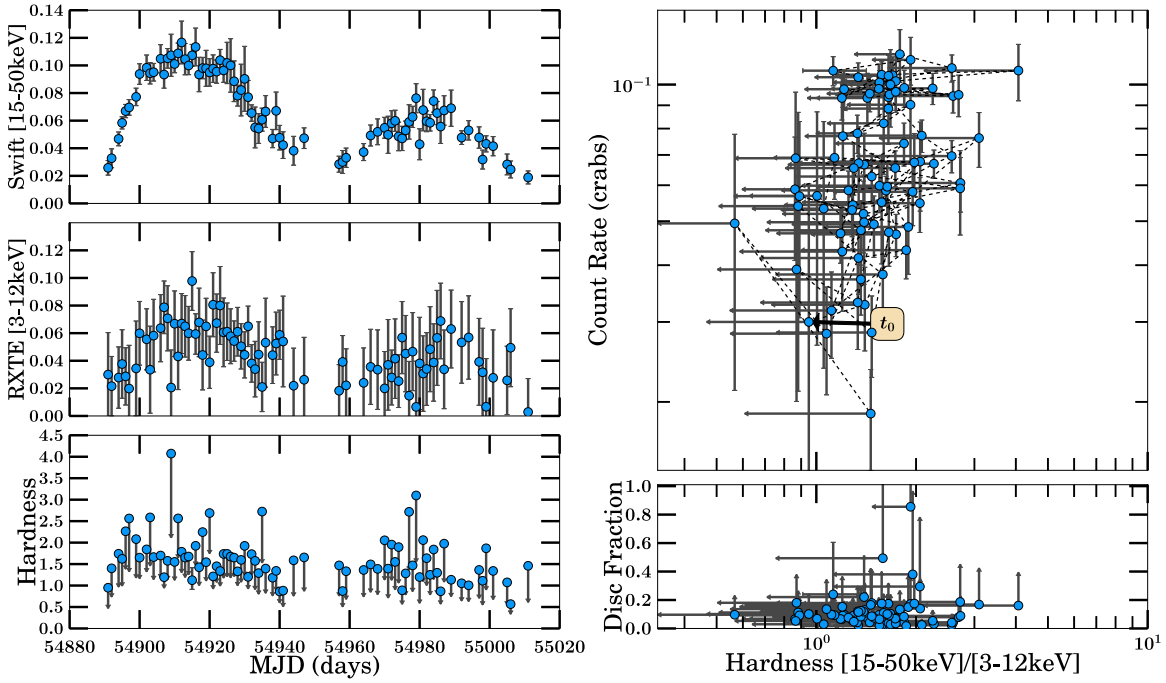

(a) 2009 Outburst Analysis

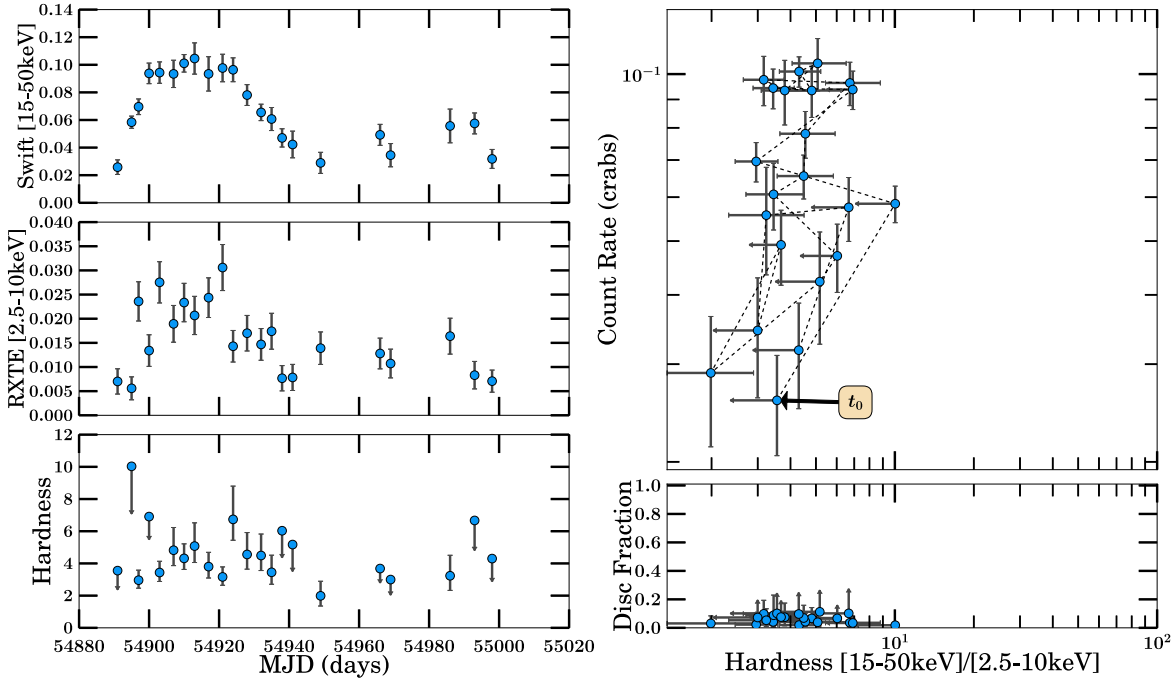

(b) 2009 Outburst Analysis

Figure B.36: GX 339−4 Part 8

Page intentionally left blank

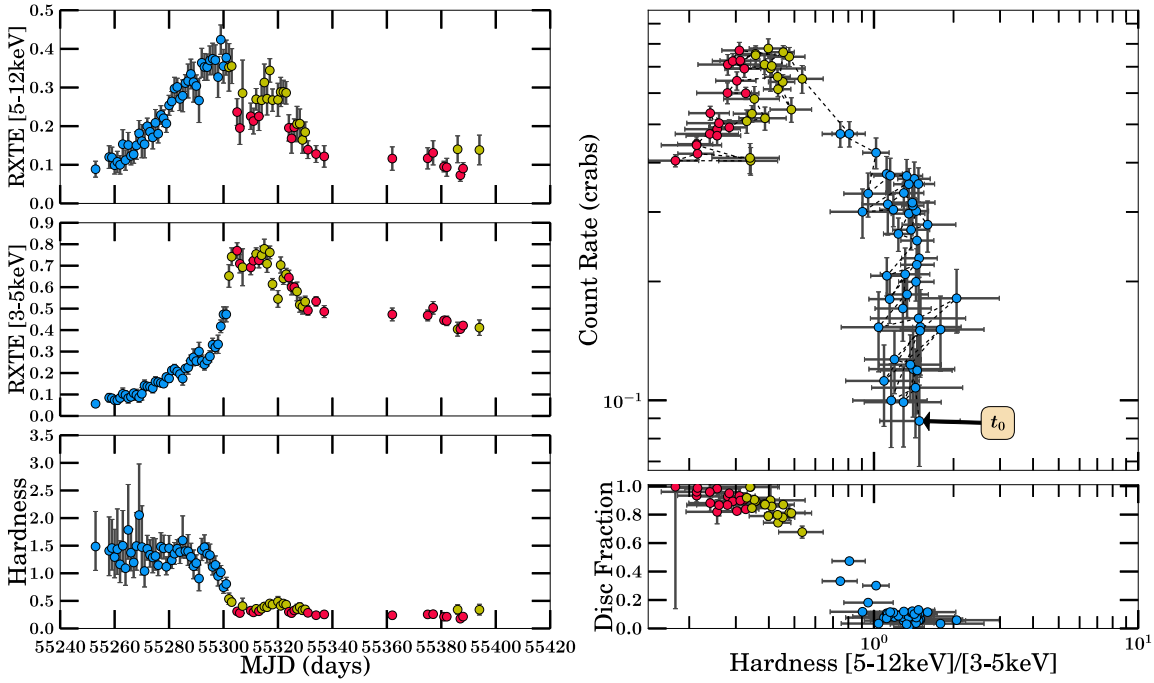

(a) 2009-2011 Outburst Analysis

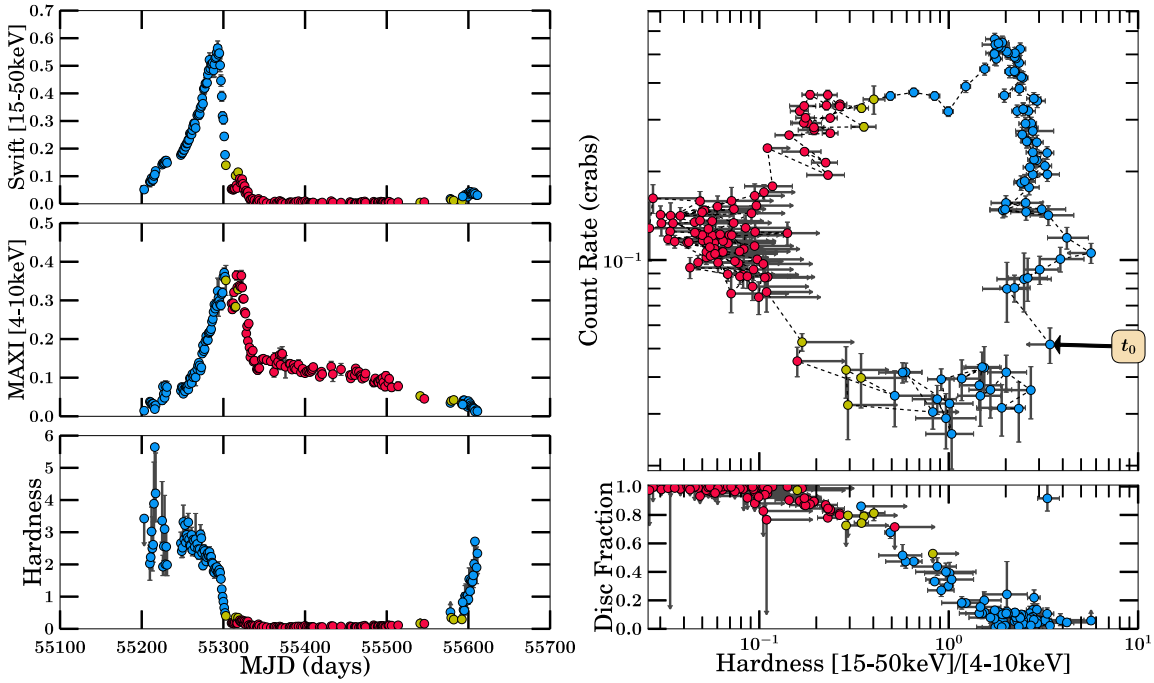

(b) 2009-2011 Outburst Analysis

Figure B.37: GX 339−4 Part 9

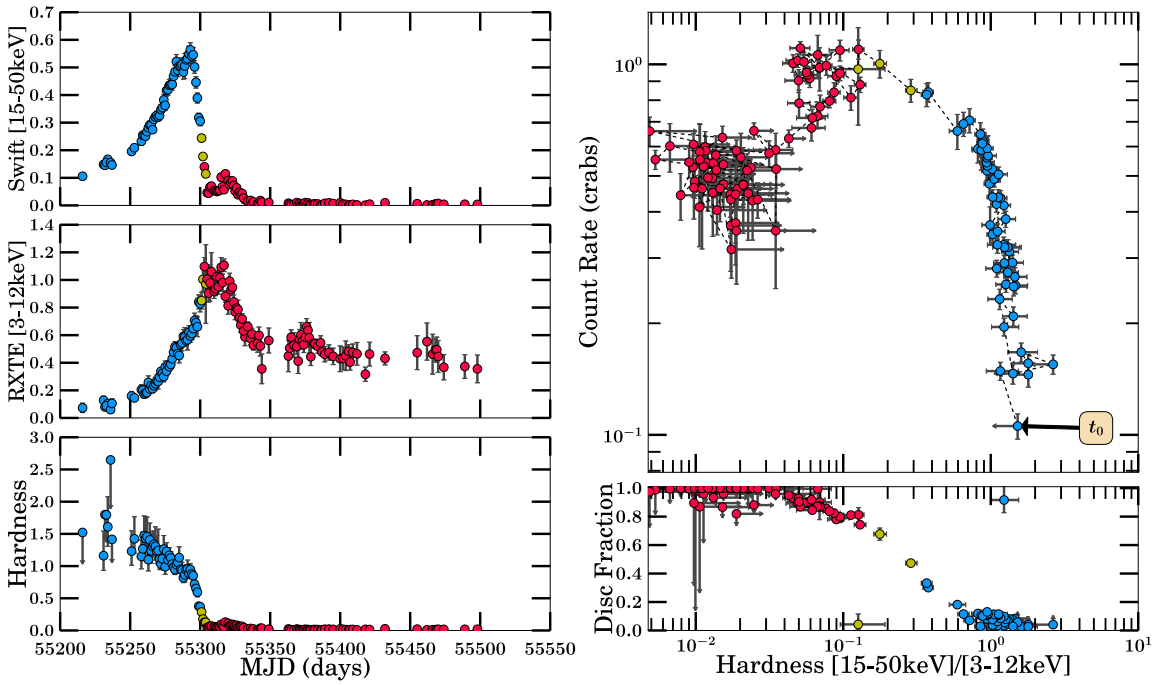

(a) 2009-2001 Outburst Analysis

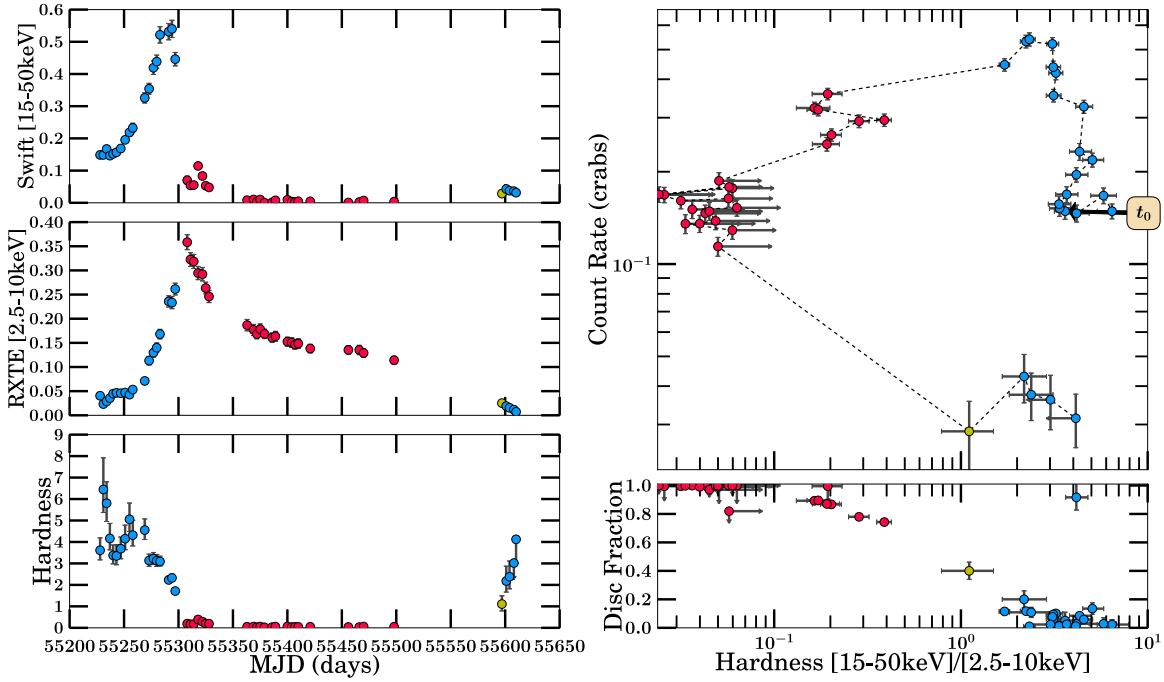

(b) 2009-2011 Outburst Analysis

Figure B.38: GX 339−4 Part 10

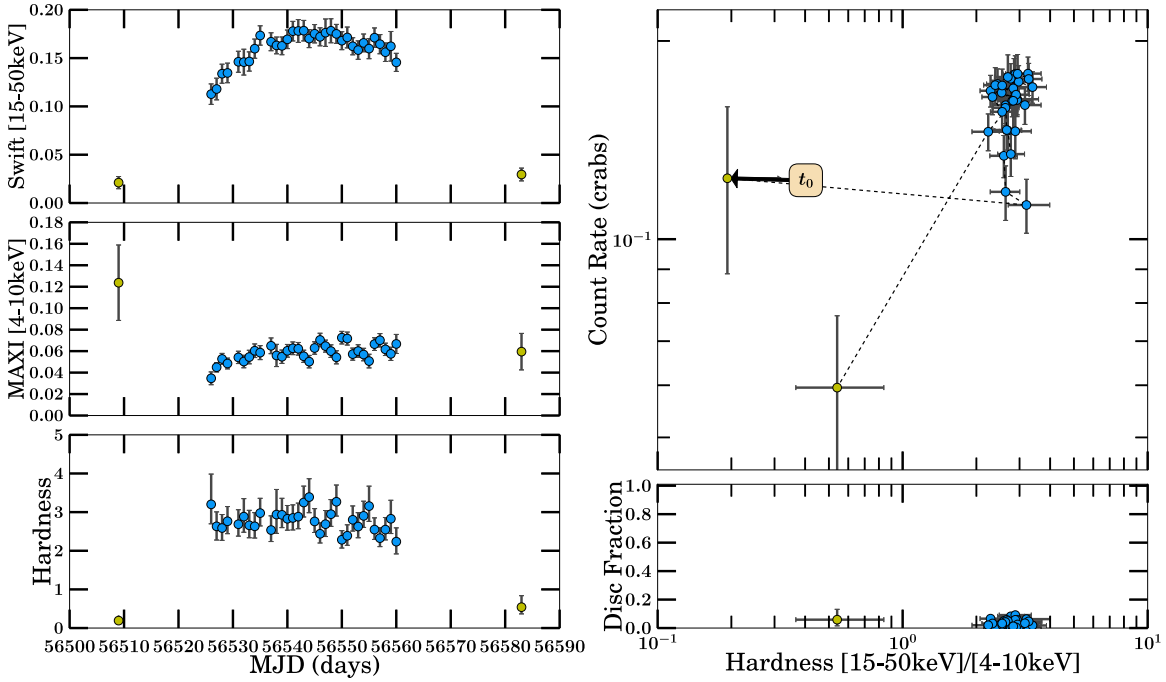

(a) 2013 Outburst Analysis

Figure B.39: GX 339−4 Part 11

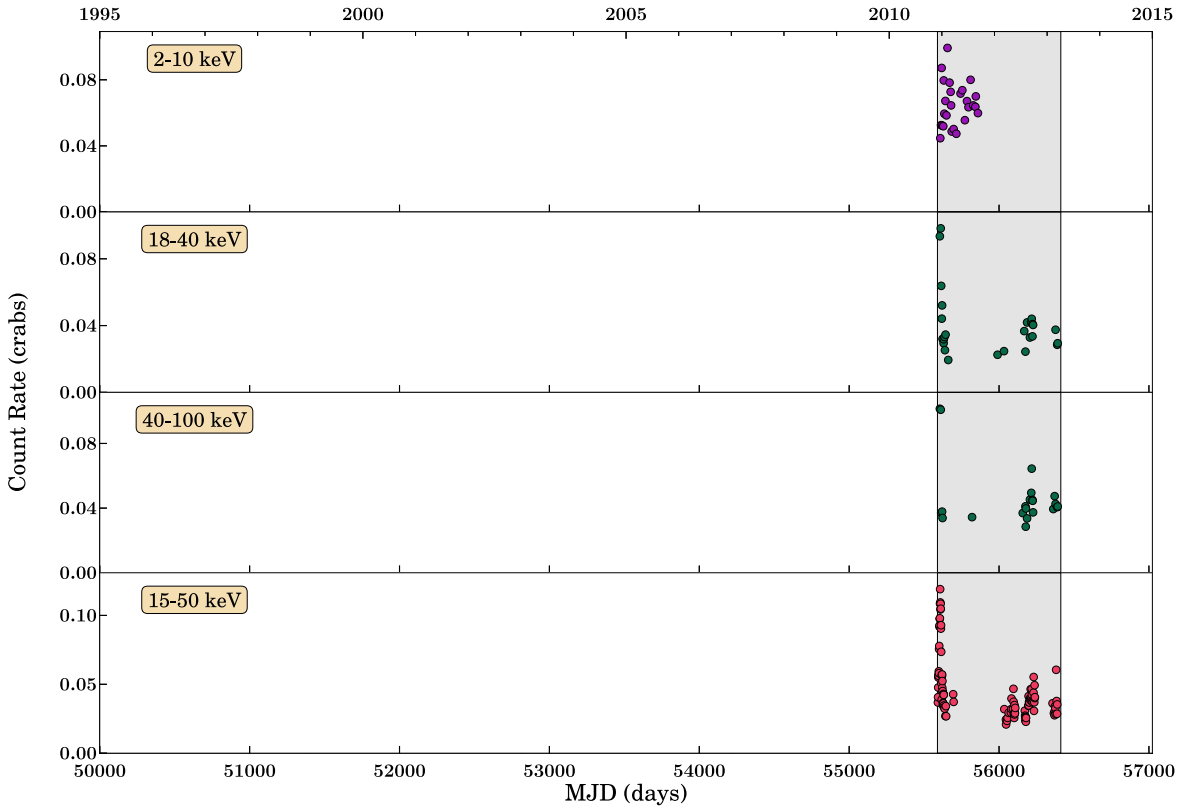

(a) Long-term Light Curve

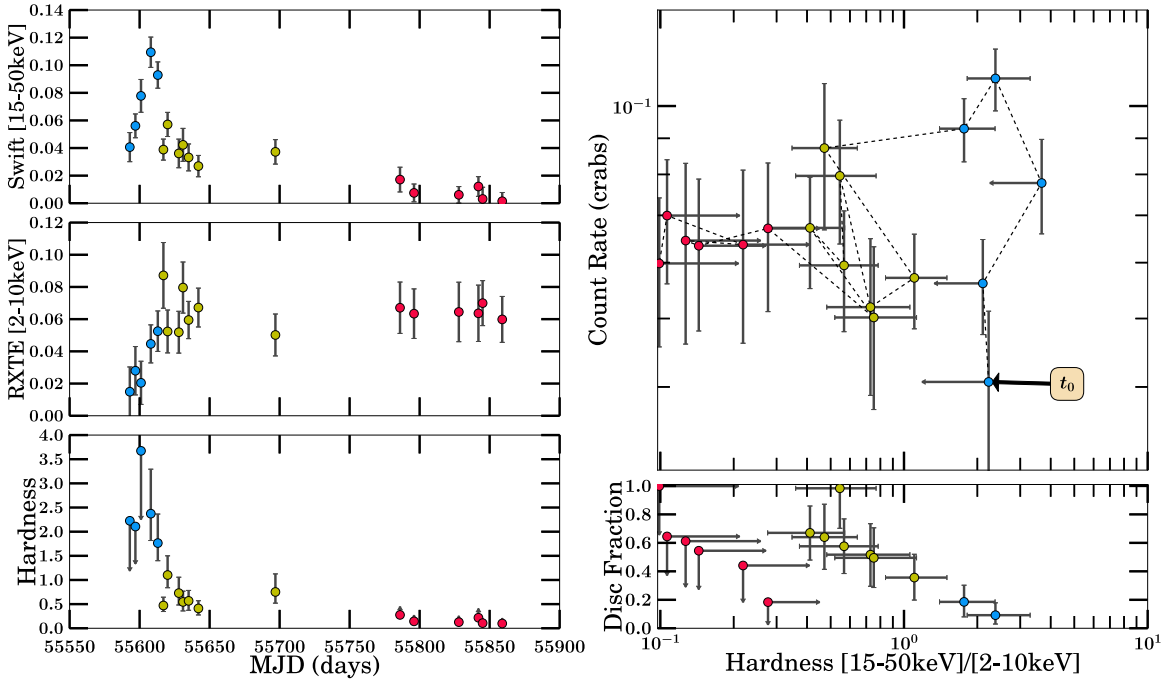

(b) 2011-2013 Outburst Analysis

Figure B.40: IGR J17091−3624

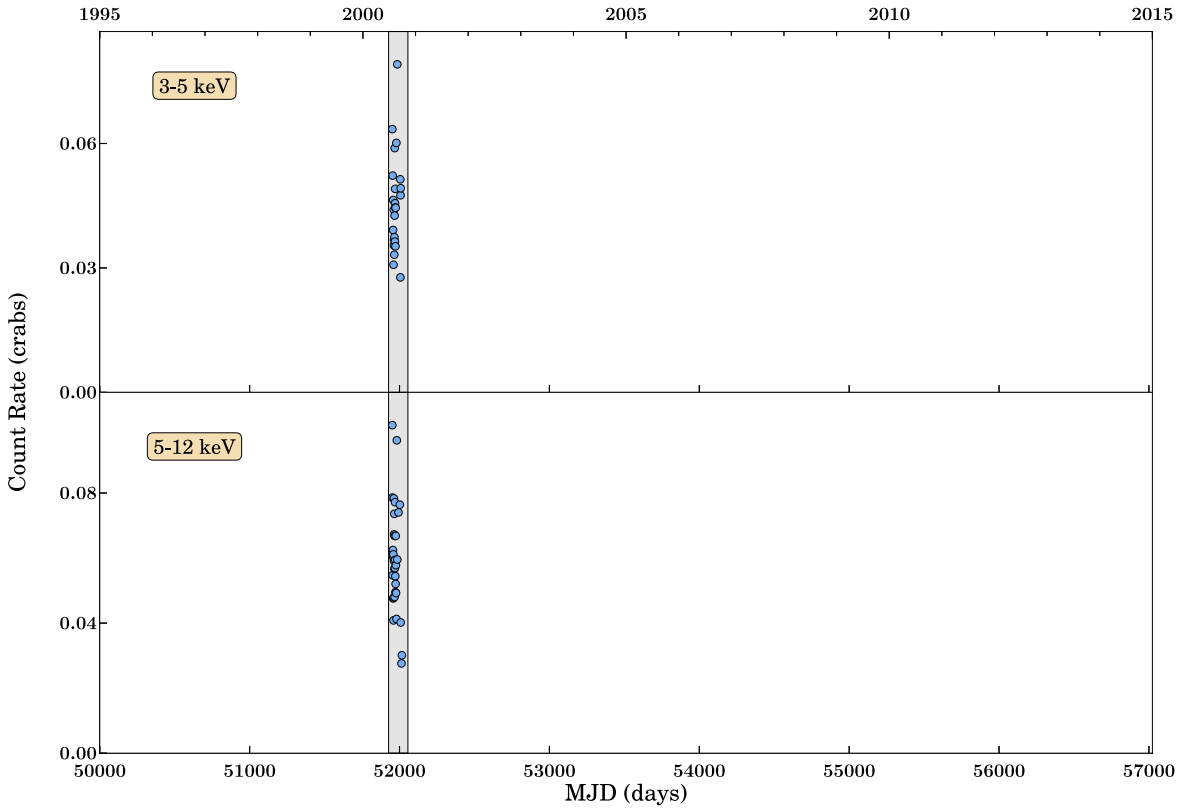

(a) Long-term Light Curve

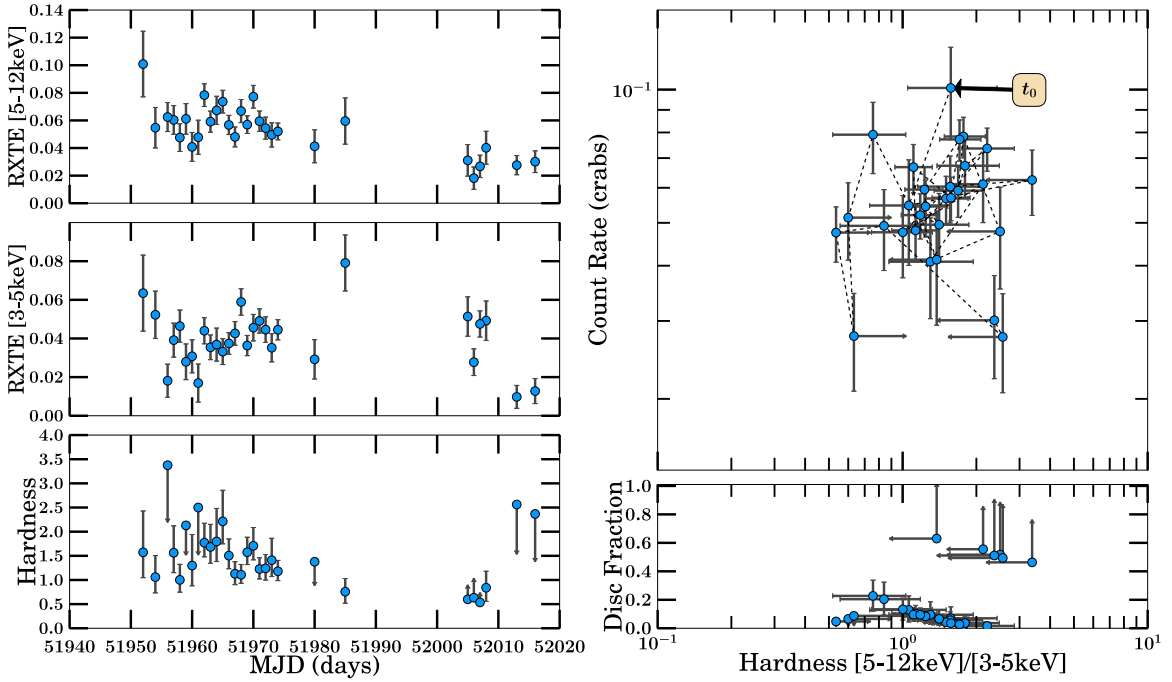

(b) 2001 Outburst Analysis

Figure B.41: SAX J1711.6−3808

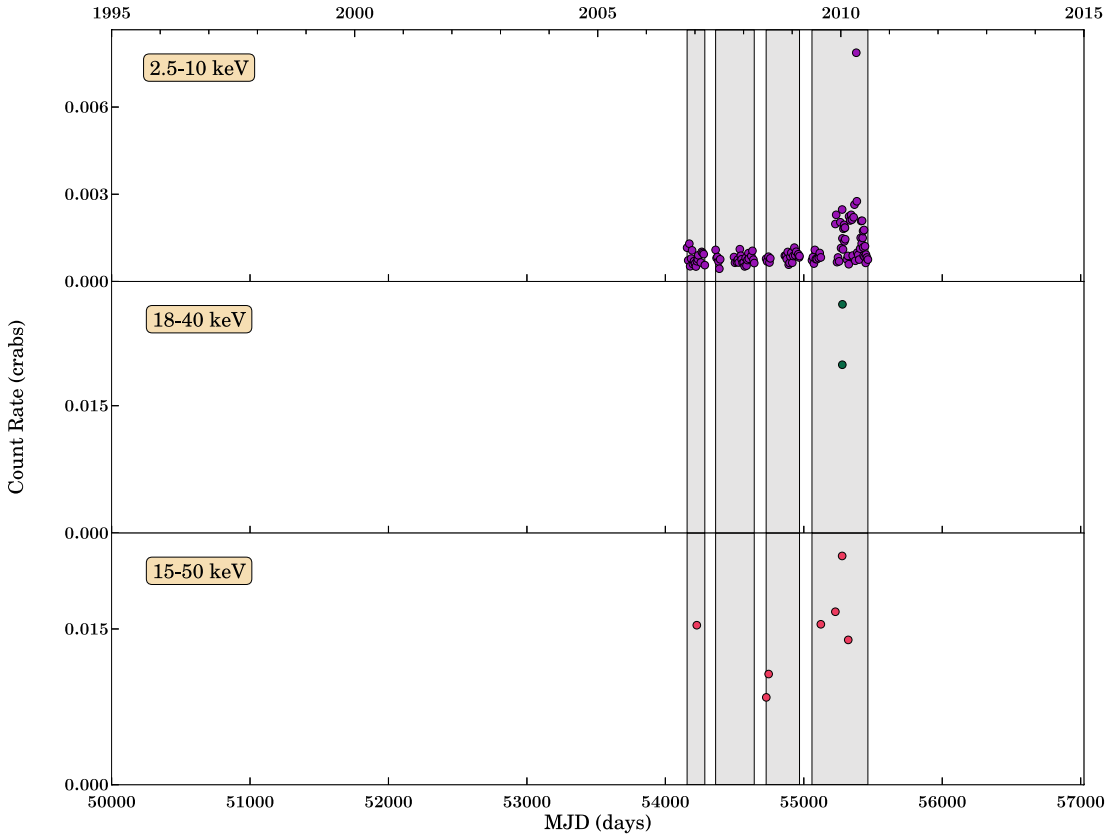

(a) Long-term Light Curve

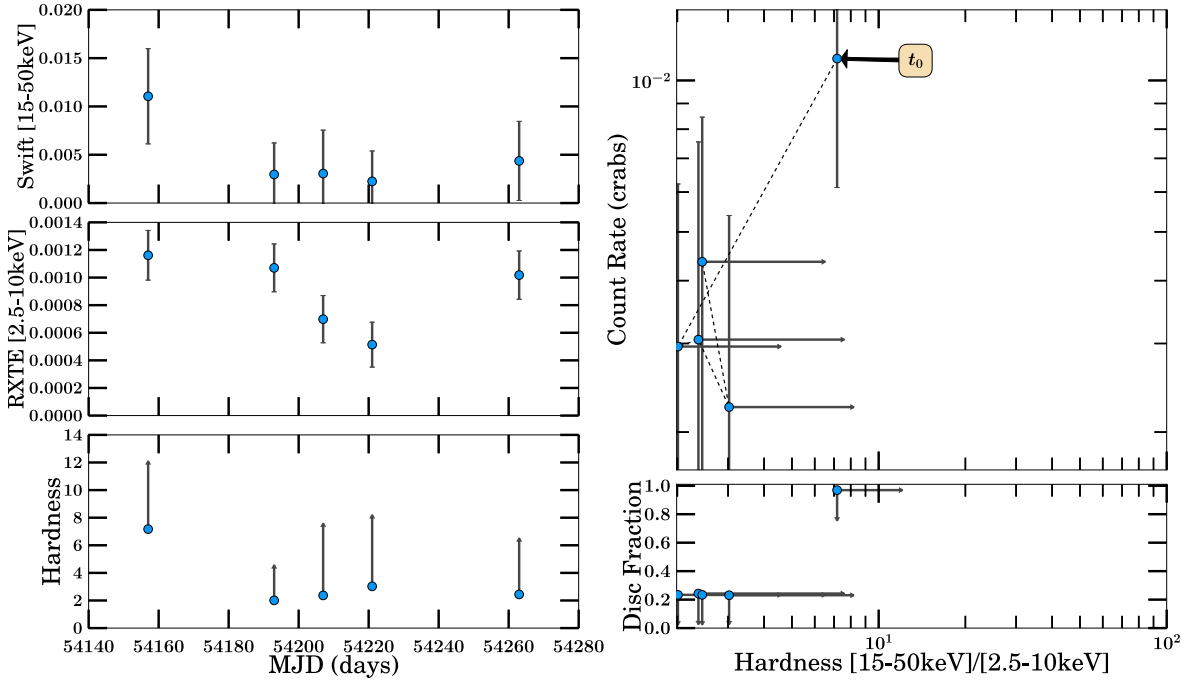

(b) 2007a Outburst Analysis

Figure B.42: XMMSL1J171900.4−353217 Part 1

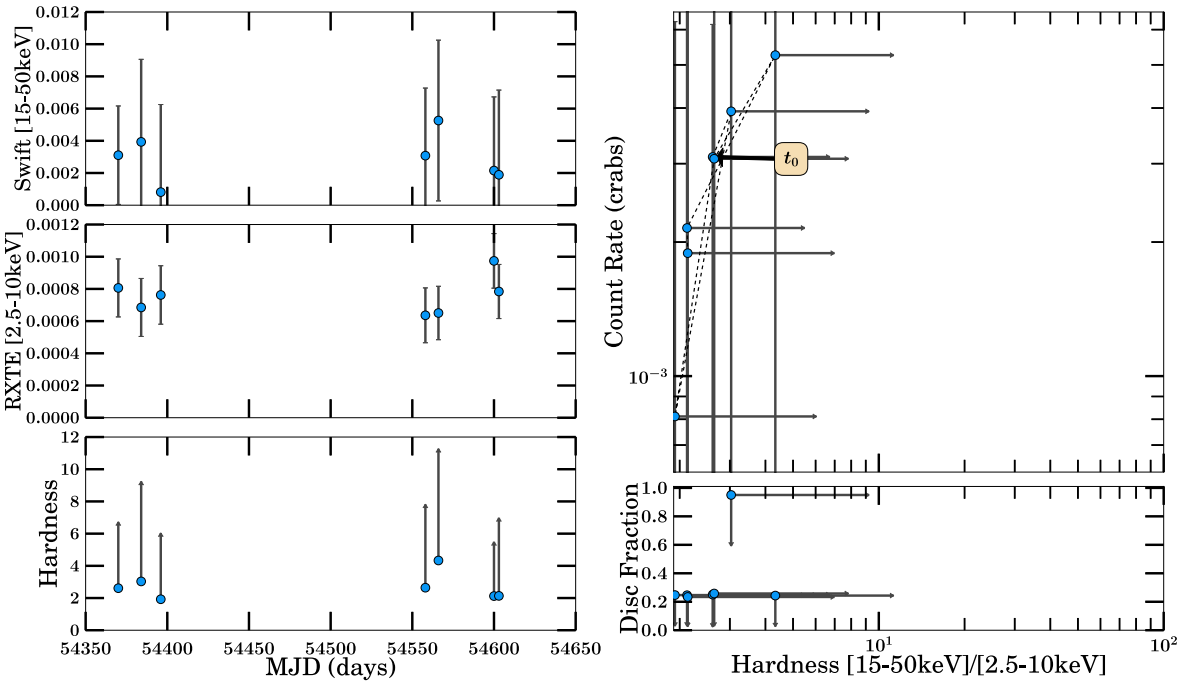

(a) 2007/2008 Outburst Analysis

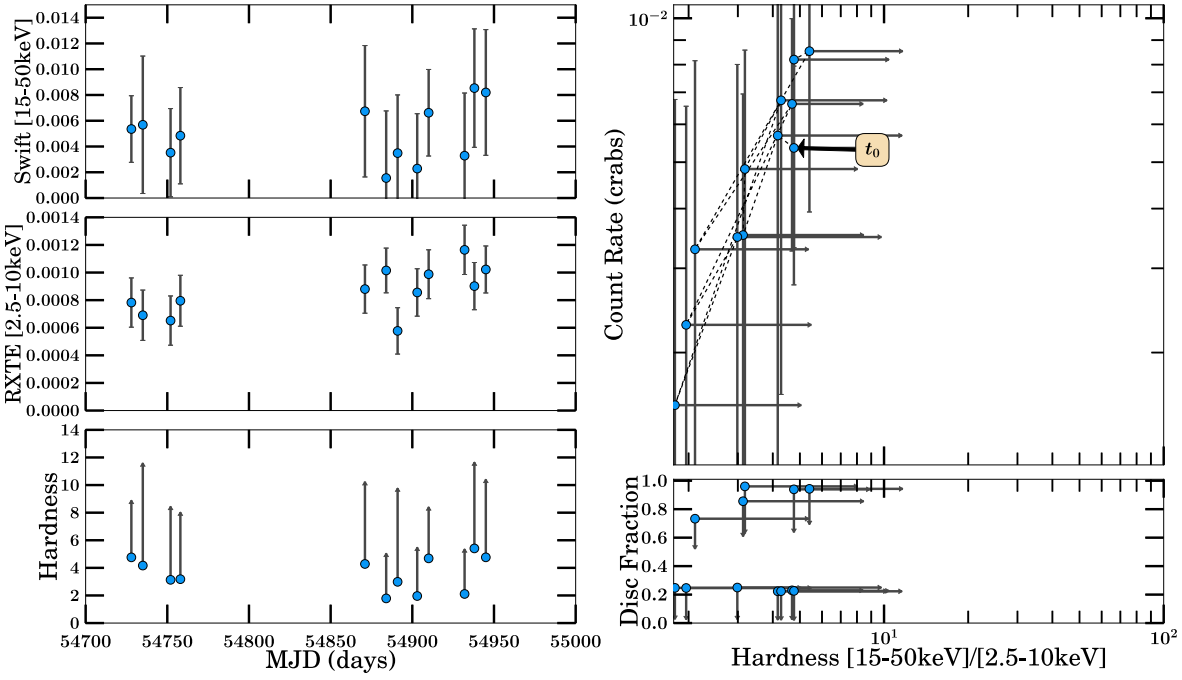

(b) 2008/2009 Outburst Analysis

Figure B.43: XMMSL1J171900.4−353217 Part 2

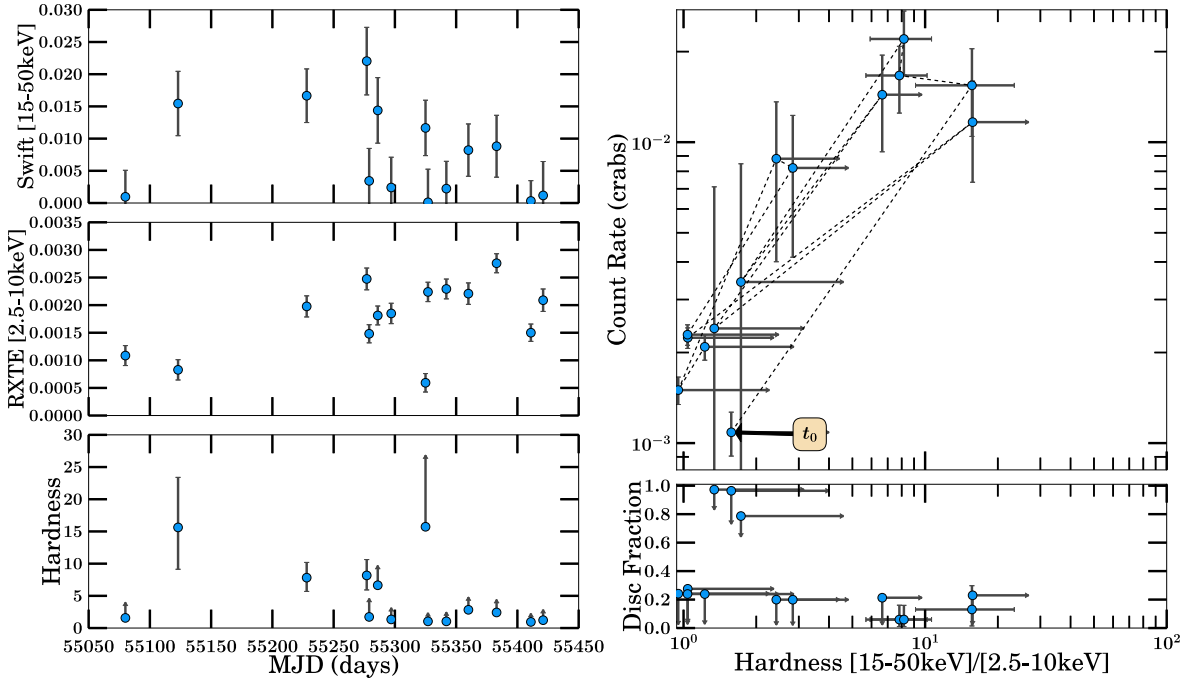

(a) 2009/2010 Outburst Analysis

Figure B.44: XMMSL1J171900.4−353217 Part 3

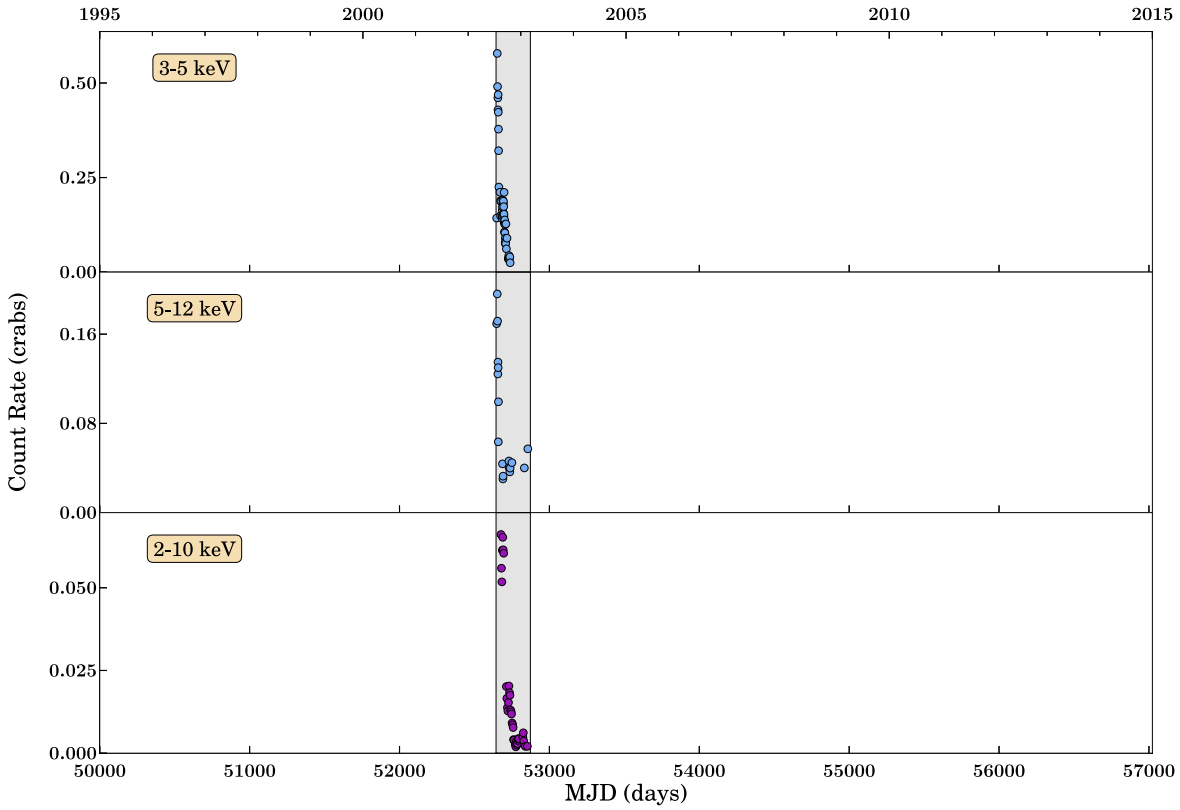

(a) Long-term Light Curve

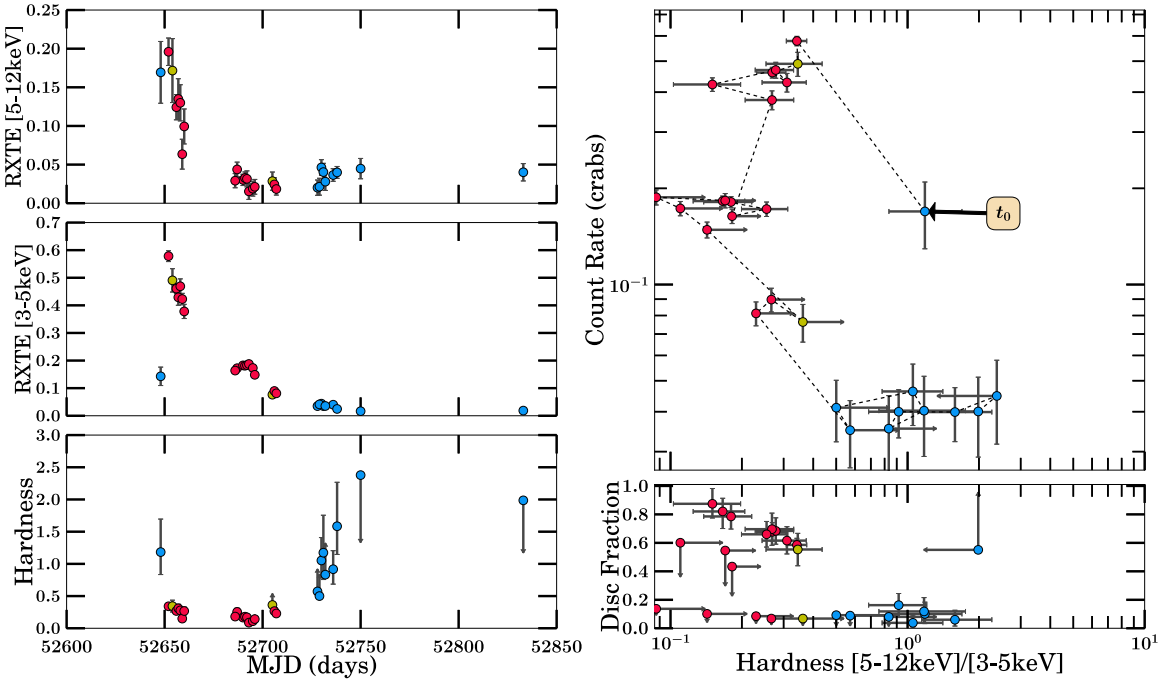

(b) 2003 Outburst Analysis

Figure B.45: XTE J1720−318

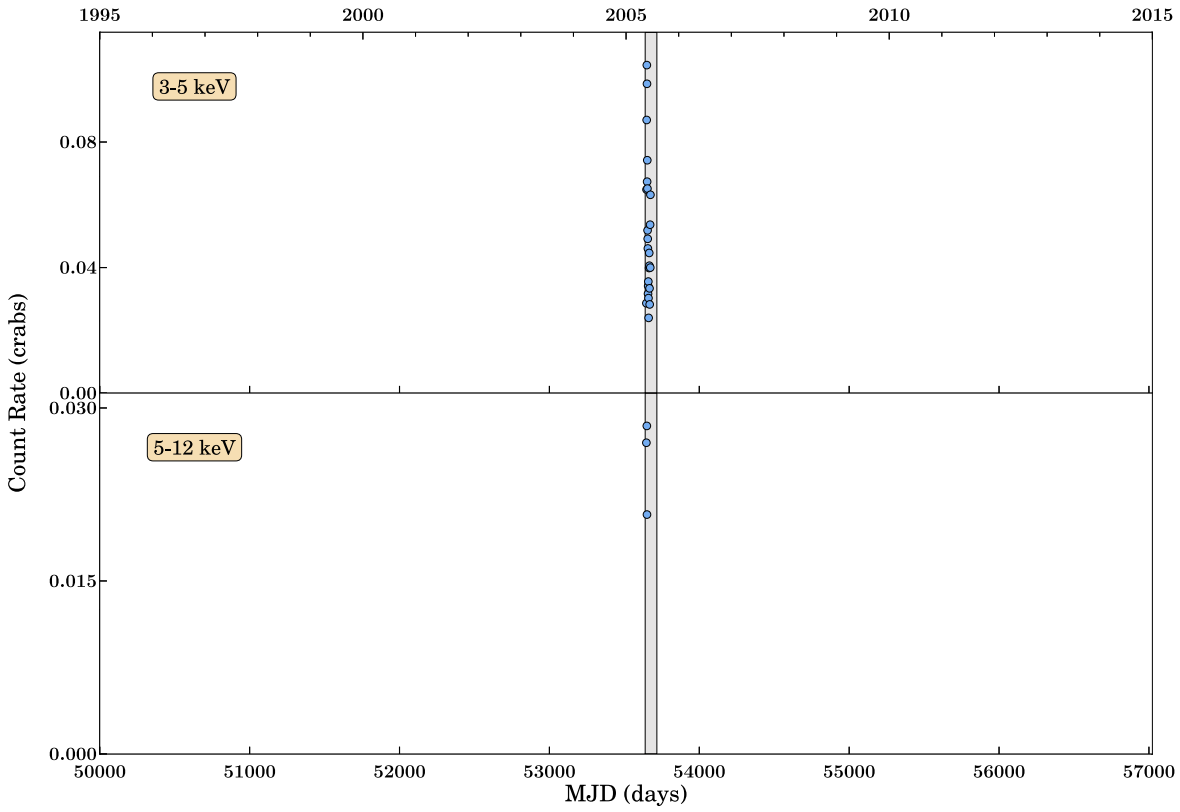

(a) Long-term Light Curve

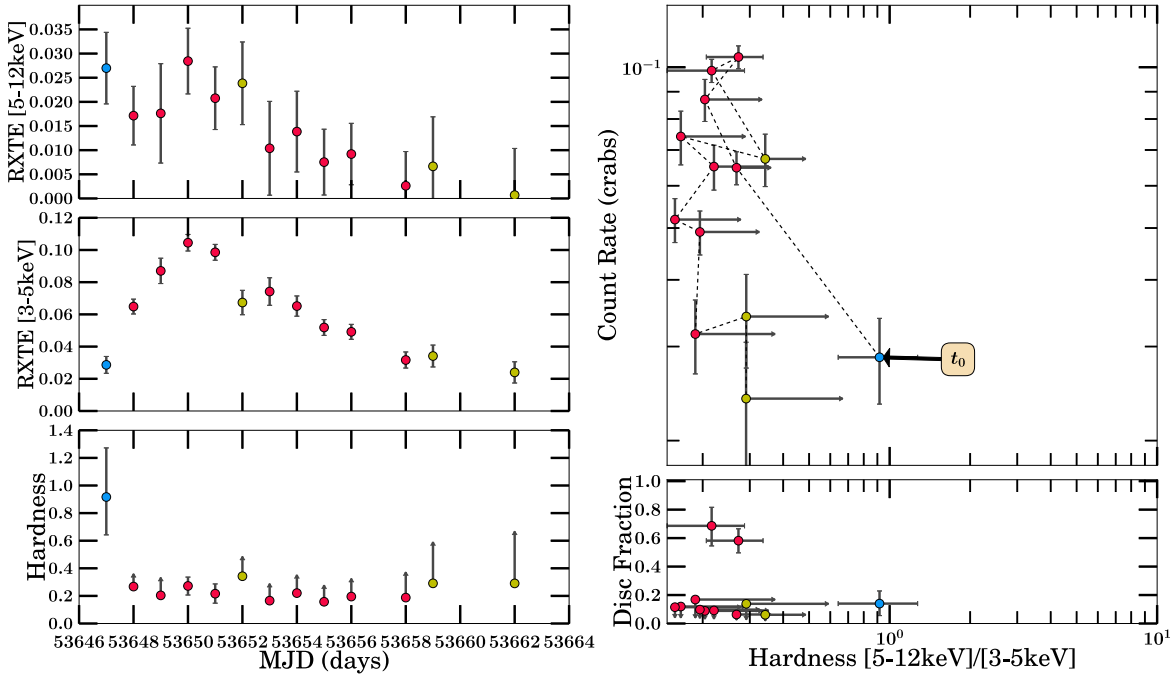

(b) 2005 Outburst Analysis

Figure B.46: XTE J1727−476

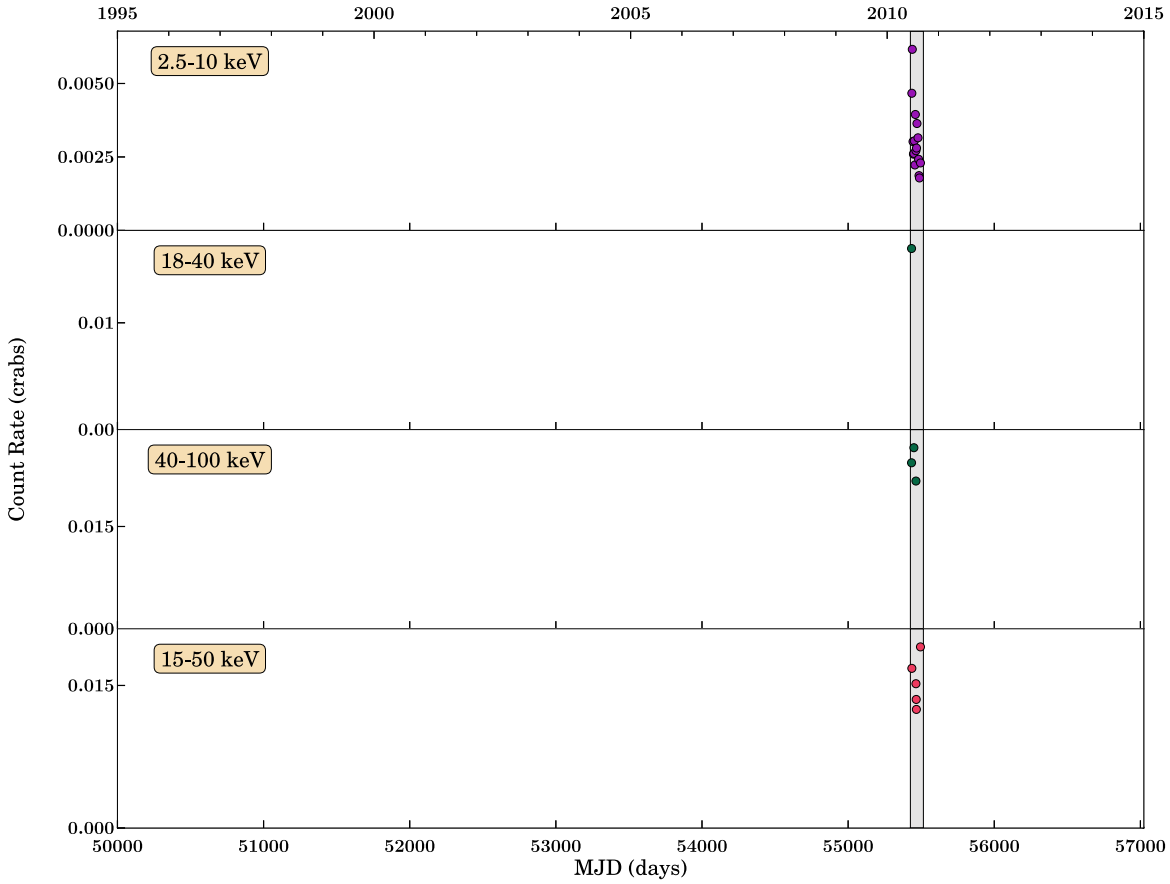

(a) Long-term Light Curve

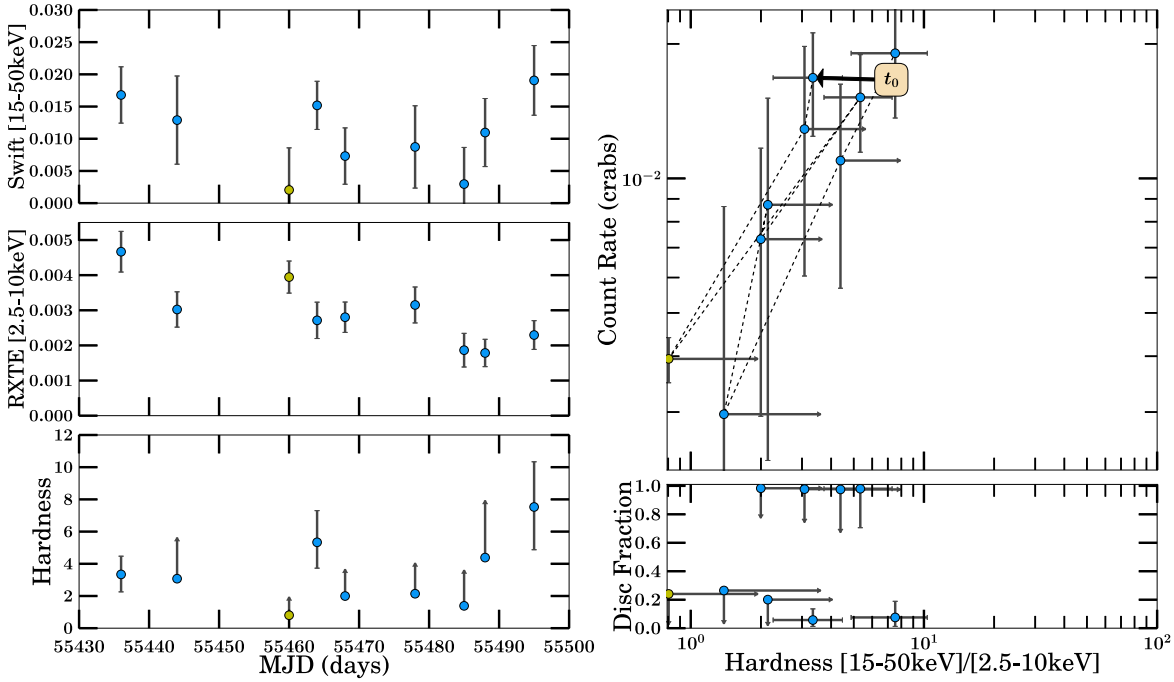

(b) 2010 Outburst Analysis

Figure B.47: IGR J17285−2922

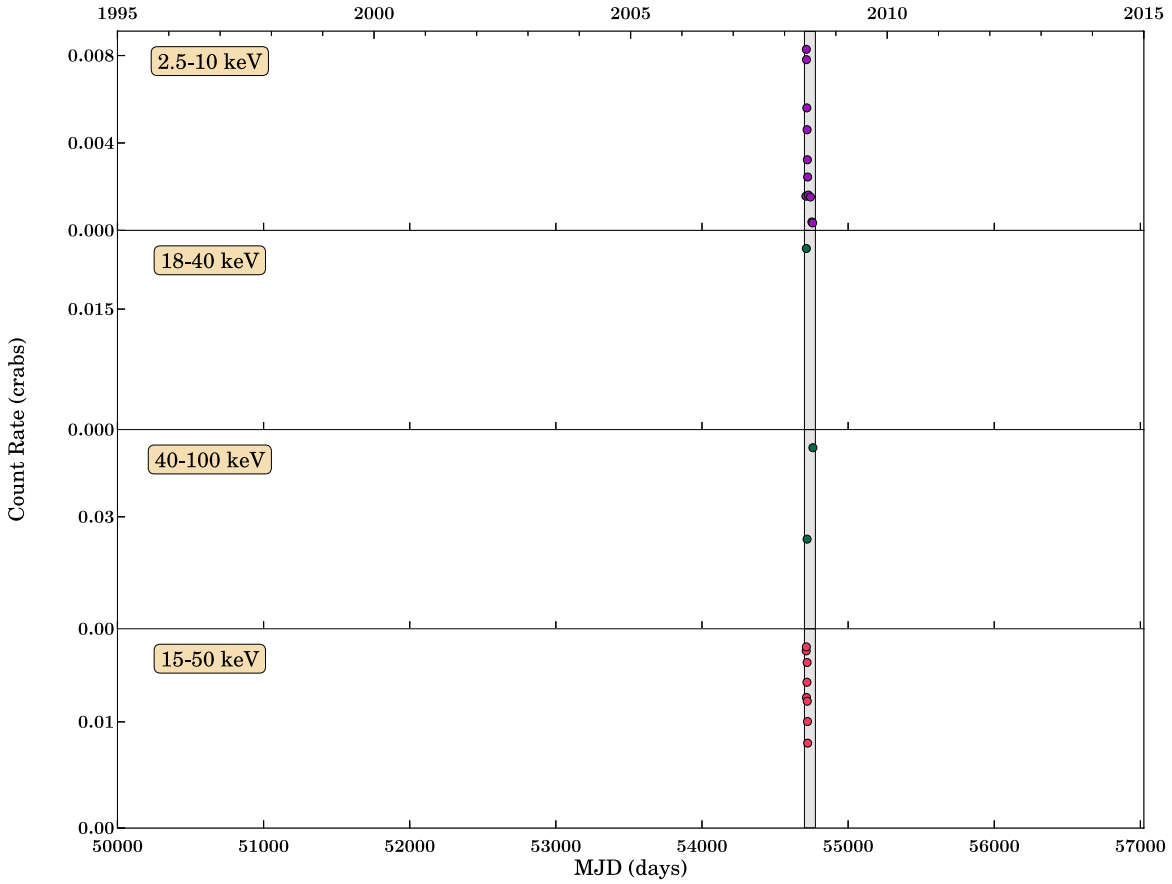

(a) Long-term Light Curve

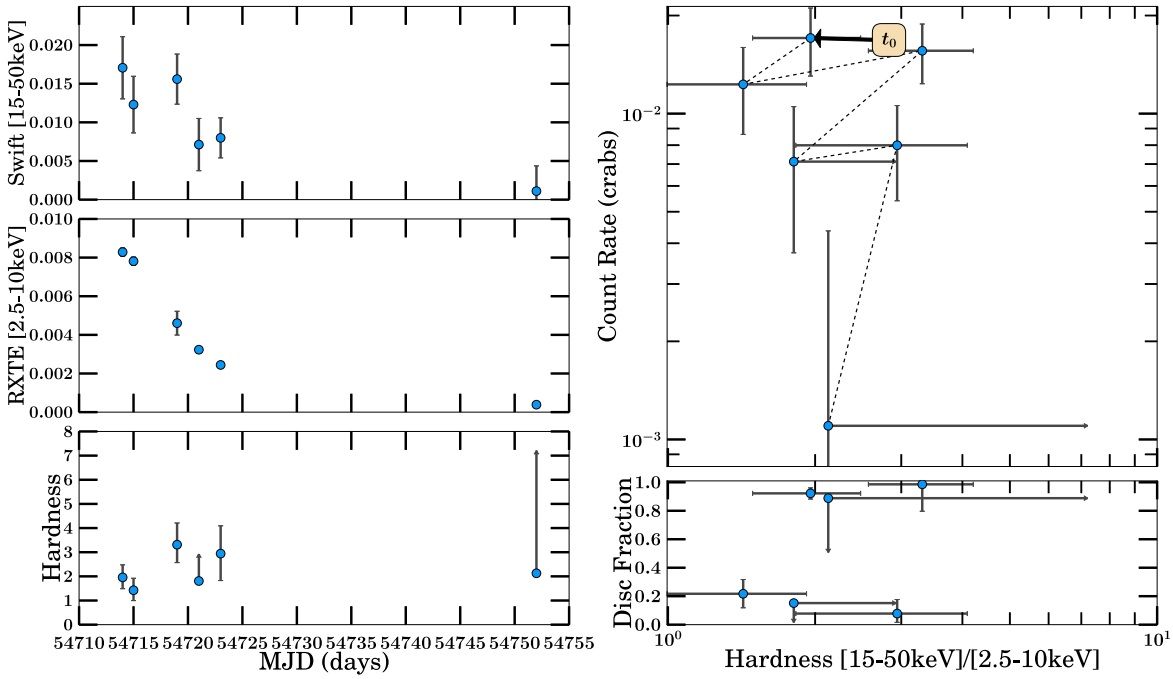

(b) 2008 Outburst Analysis

Figure B.48: IGR J17379−3747

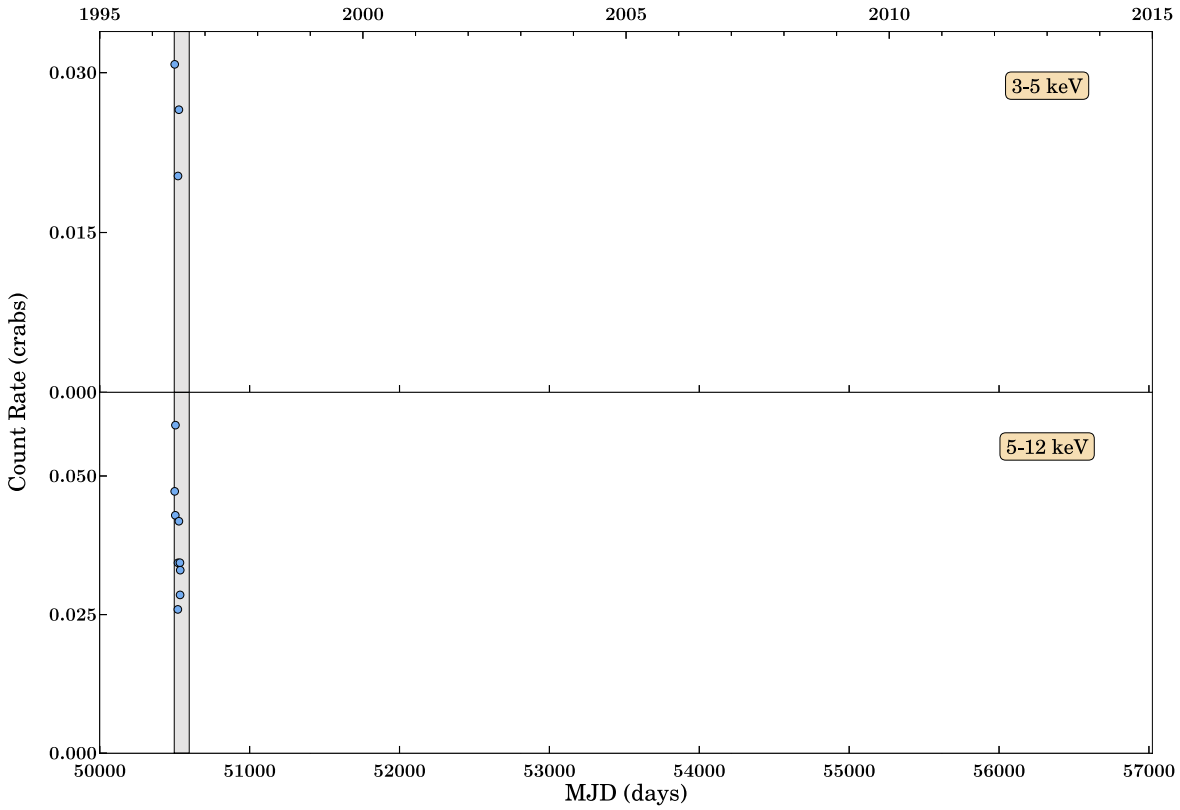

(a) Long-term Light Curve

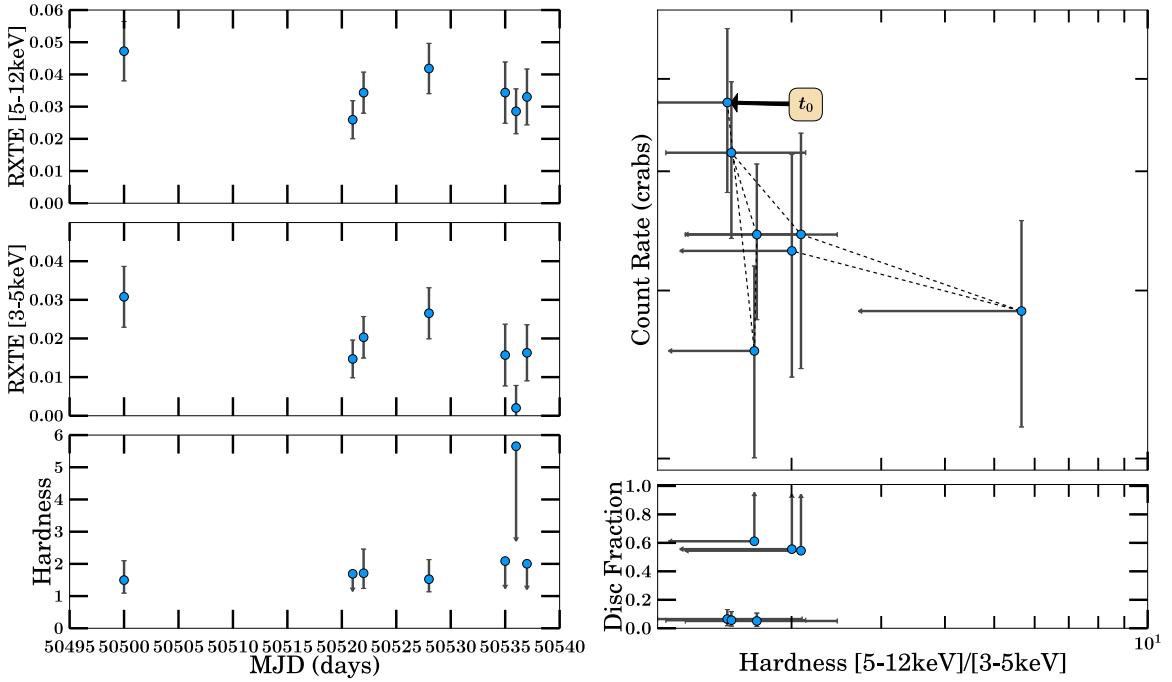

(b) 1997 Outburst Analysis

Figure B.49: GRS 1737−31

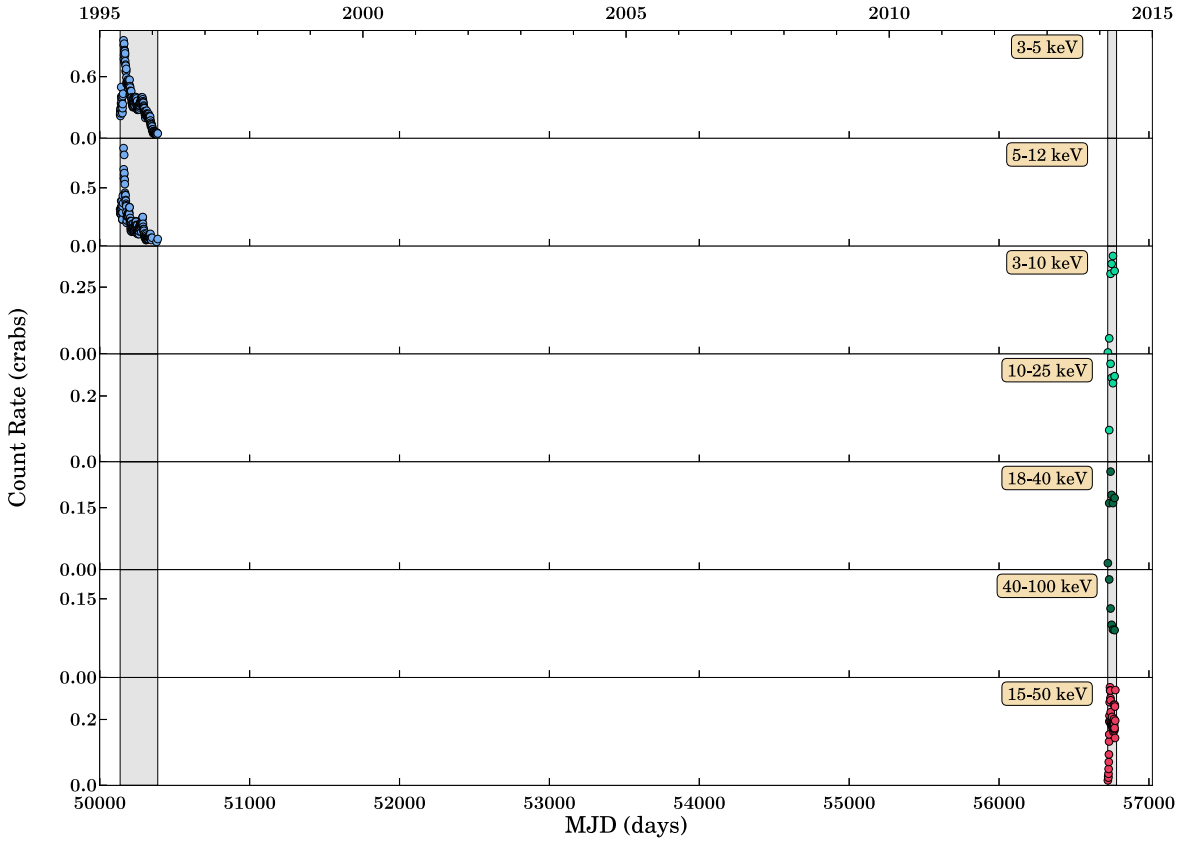

(a) Long-term Light Curve

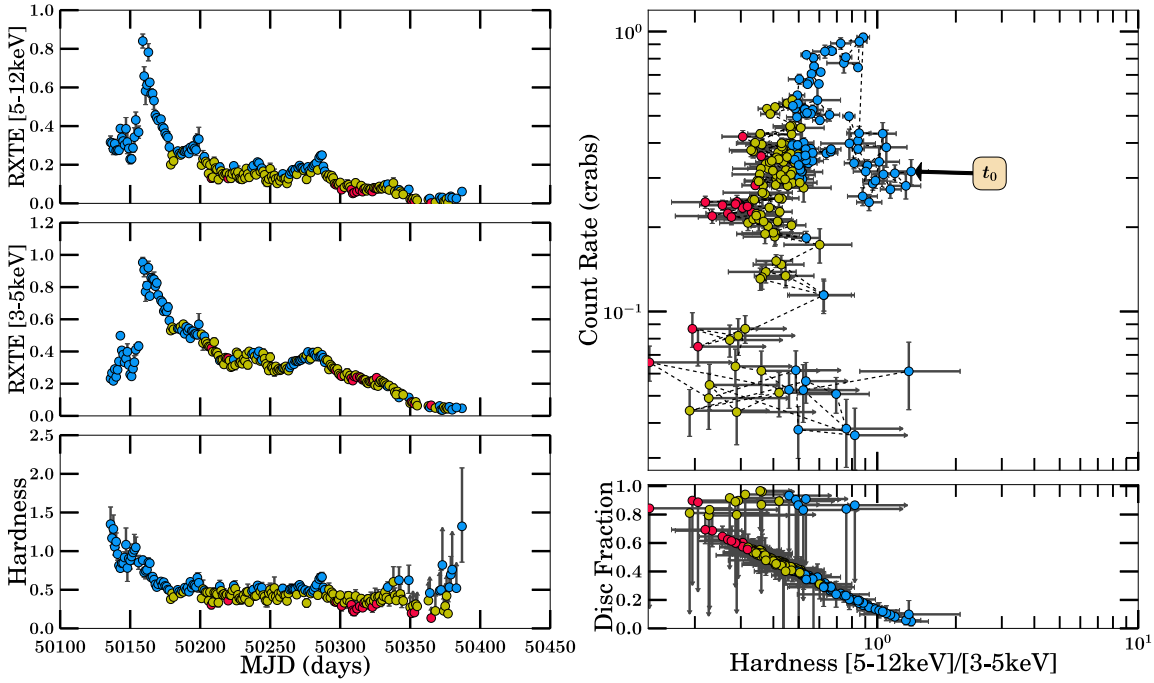

(b) 1997 Outburst Analysis

Figure B.50: GRS 1739−278 Part 1

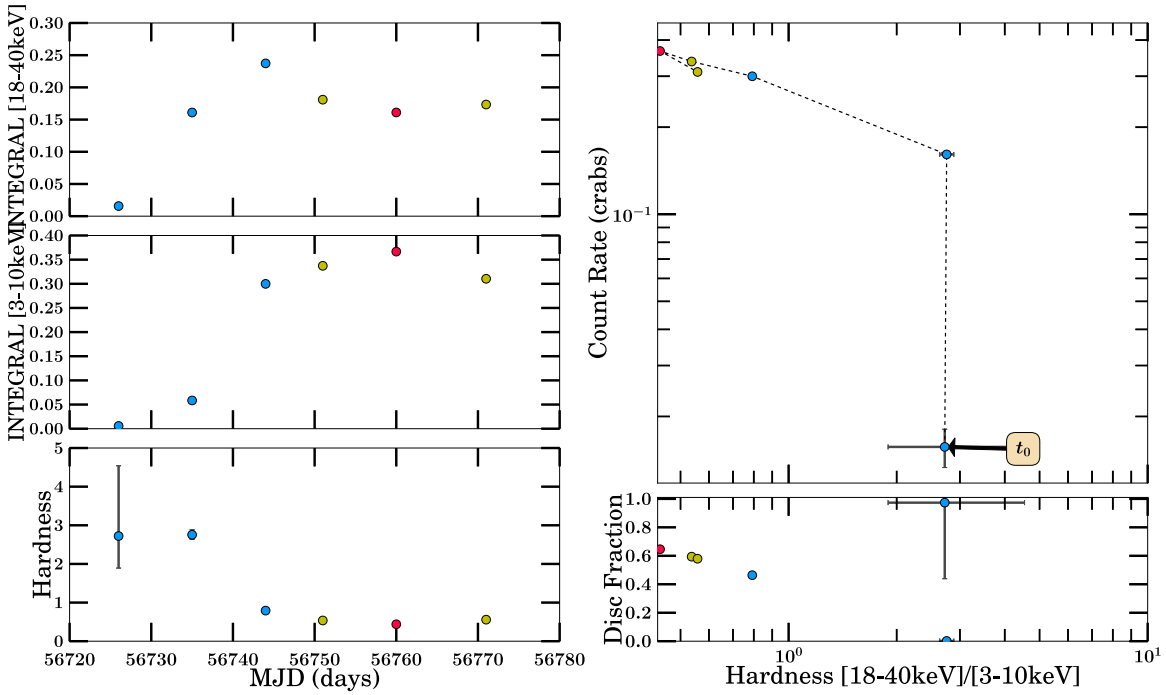

(a) 2014 Outburst Analysis

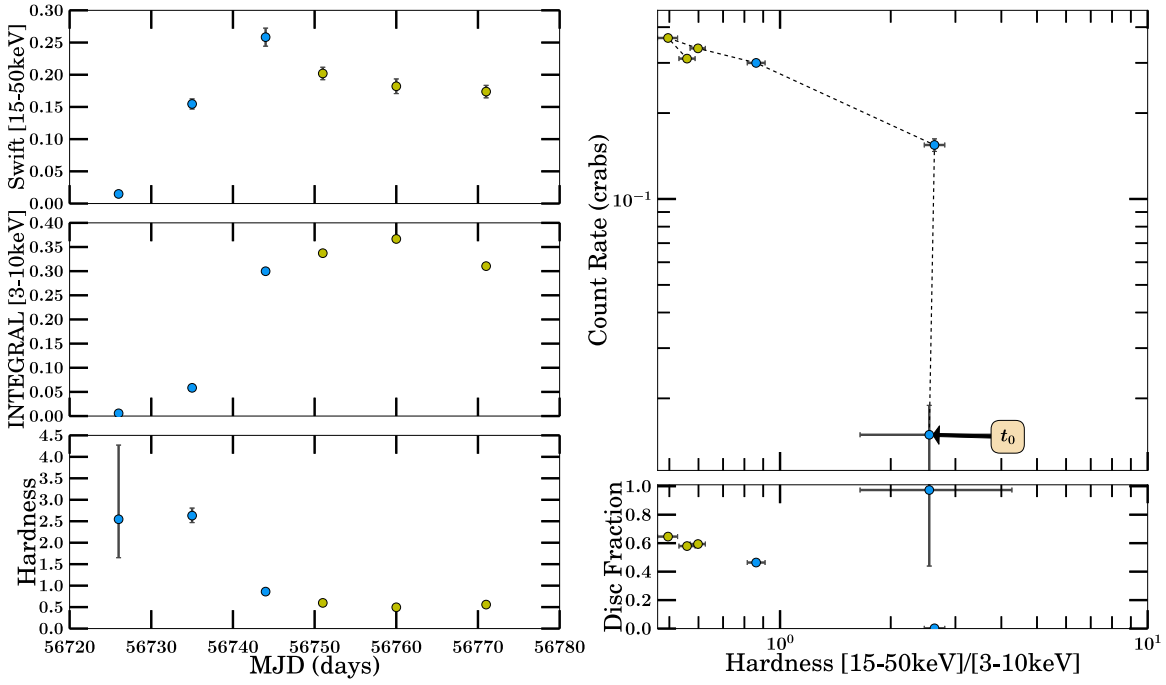

(b) 2014 Outburst Analysis

Figure B.51: GRS 1739−278 Part 2

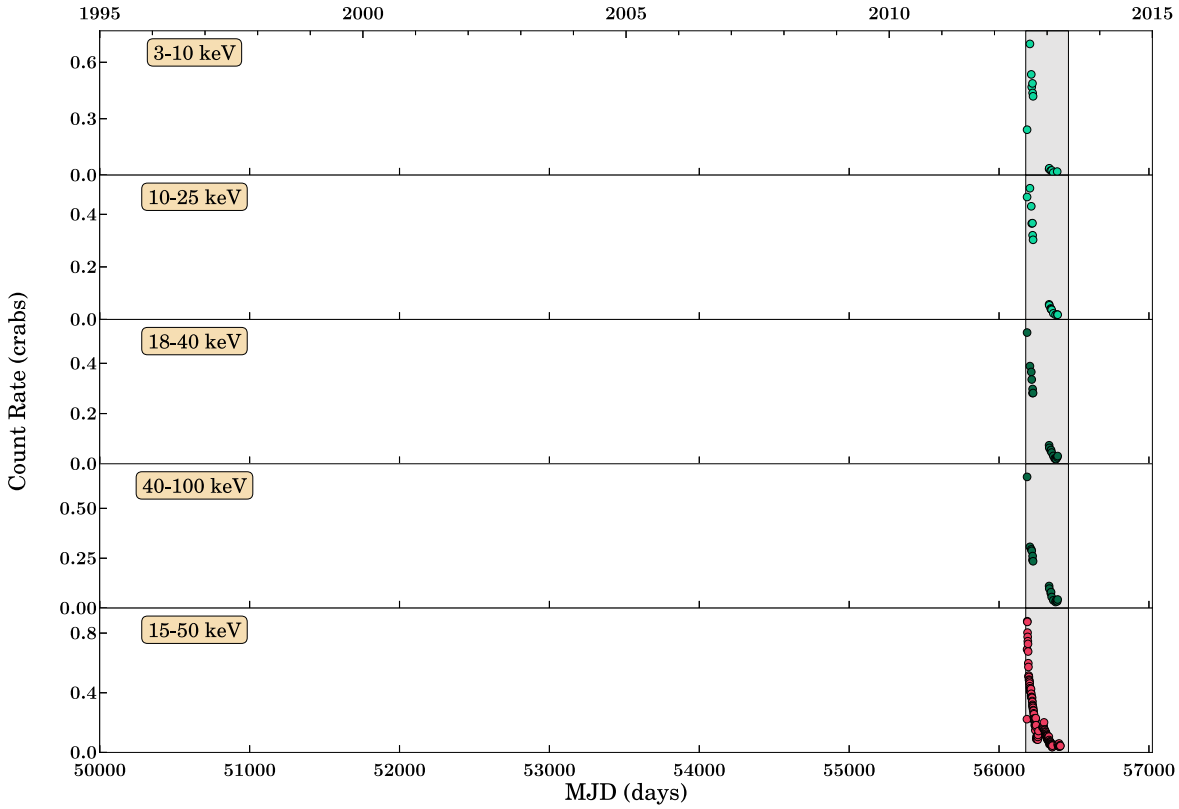

(a) Long-term Light Curve

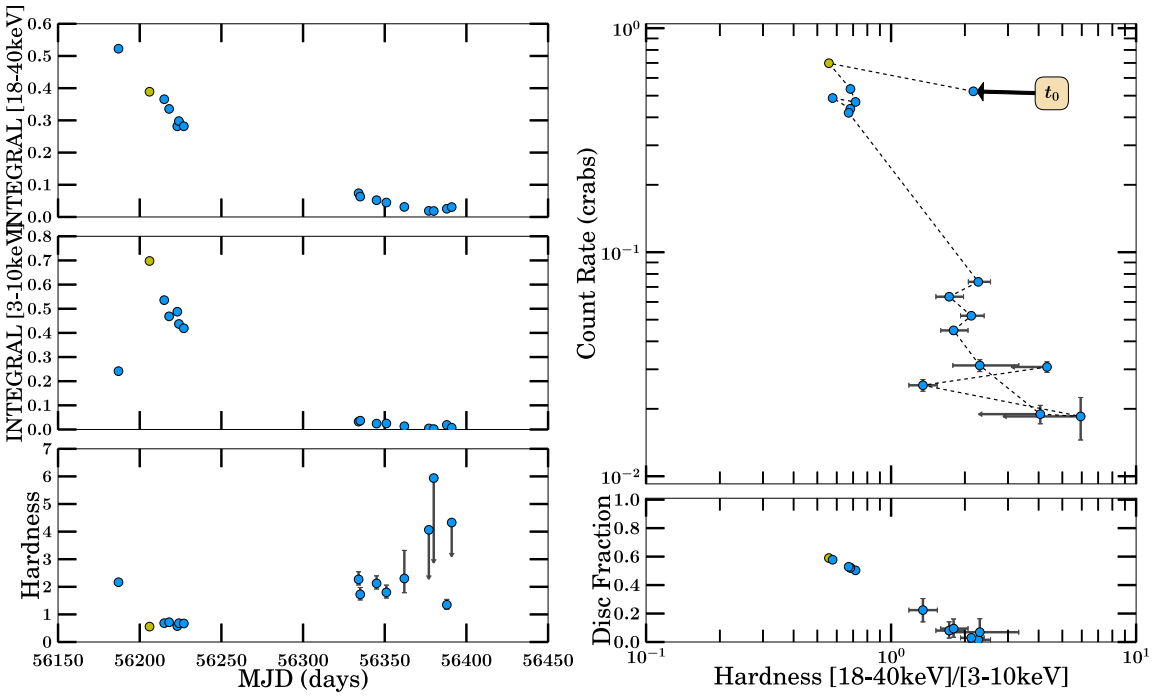

(b) 2012/2013 Outburst Analysis

Figure B.52: SWIFT J174510.8−262411 Part 1

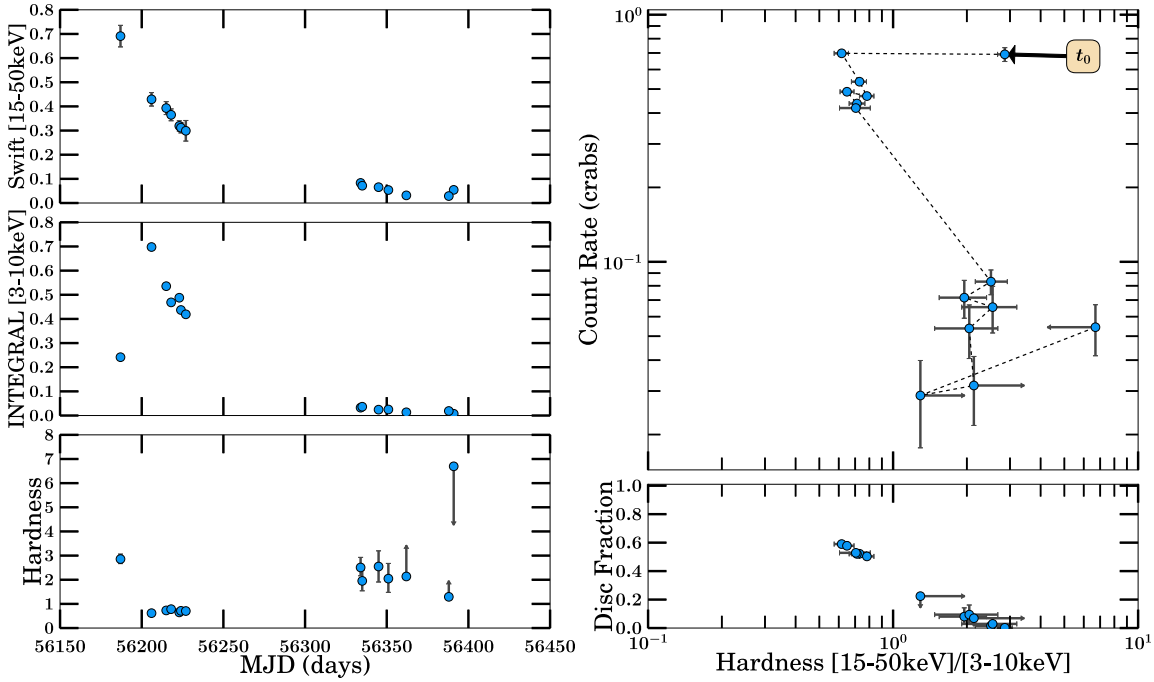

(a) 2012/2013 Outburst Analysis

Figure B.53: SWIFT J174510.8−262411 Part 2

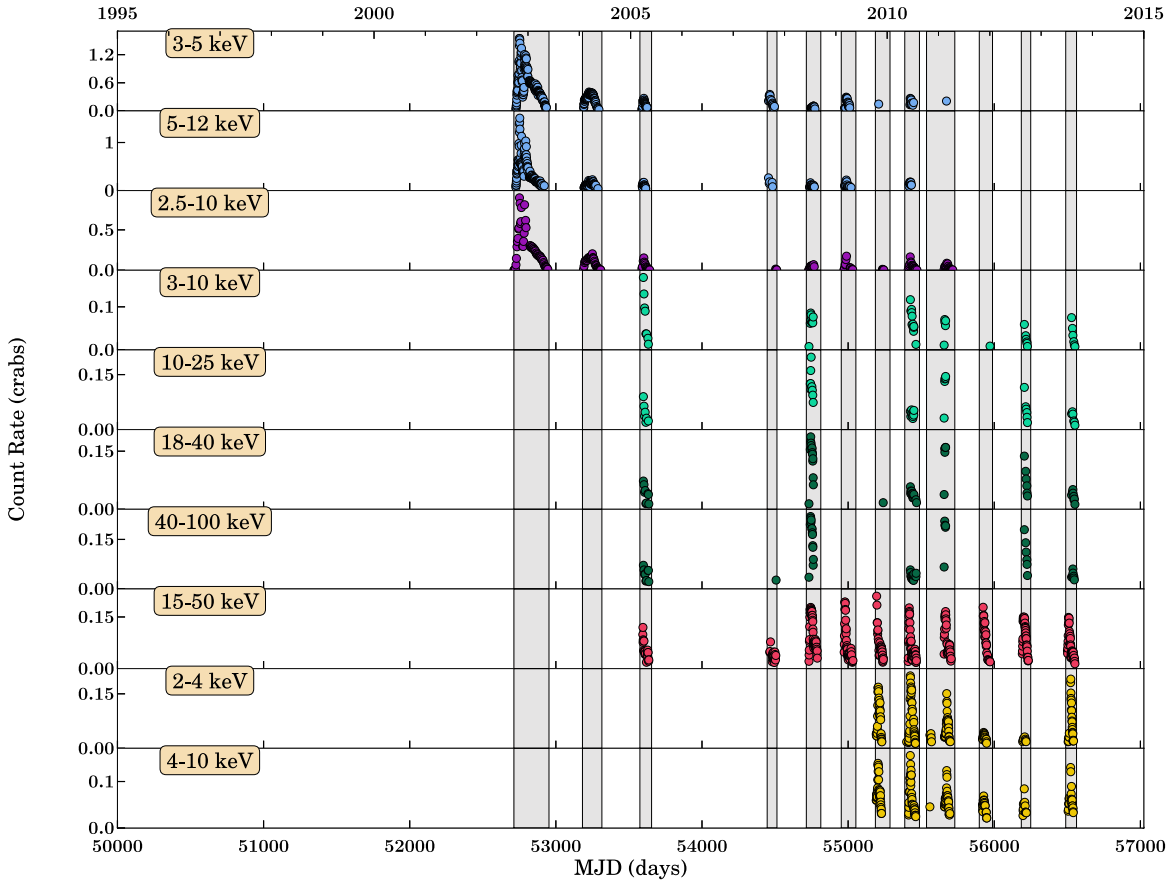

(a) Long-term Light Curve

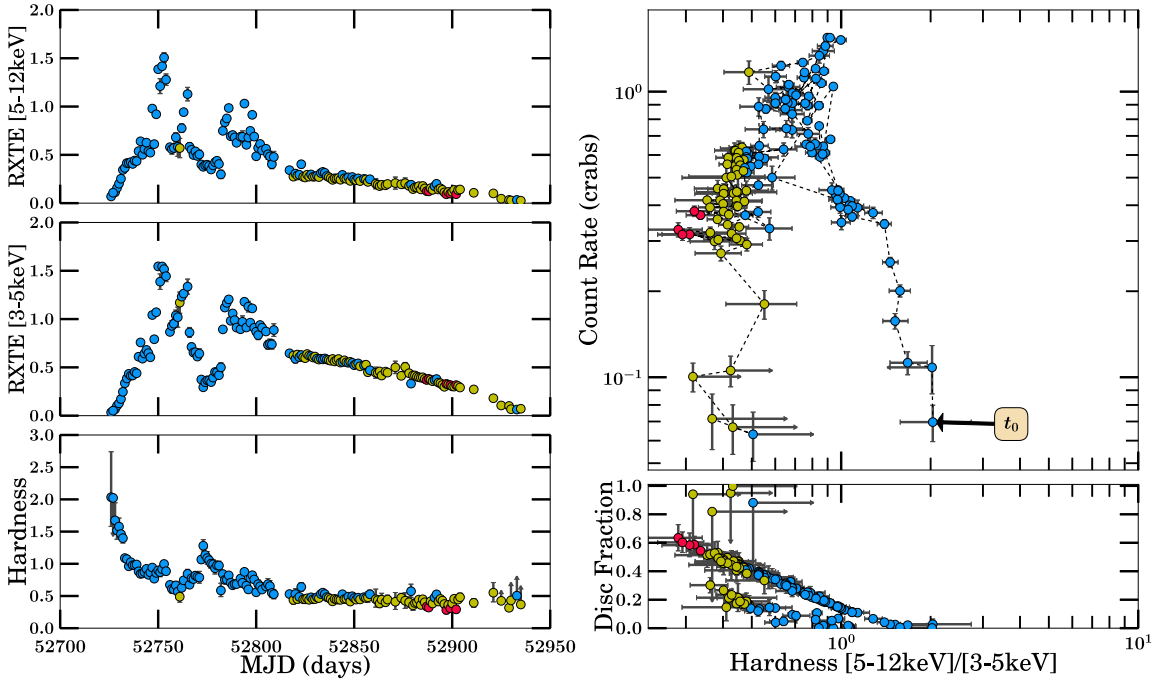

(b) 2003 Outburst Analysis

Figure B.54: H 1743−322 Part 1

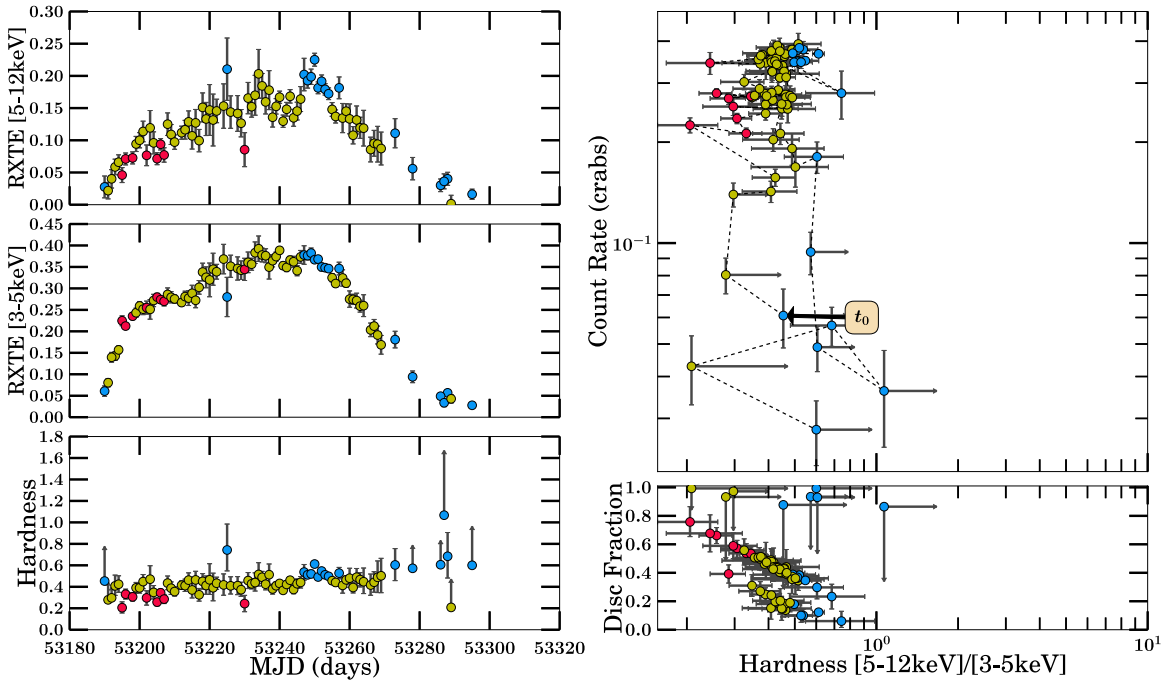

(a) 2004 Outburst Analysis

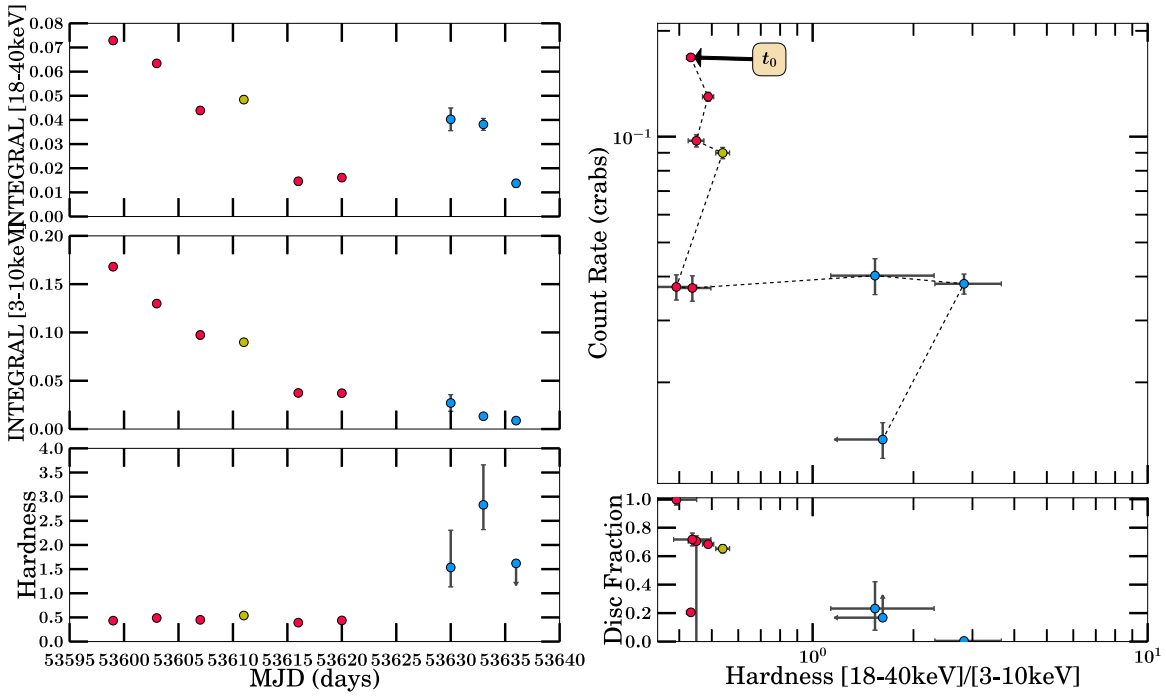

(b) 2005 Outburst Analysis

Figure B.55: H 1743−322 Part 2

Page intentionally left blank

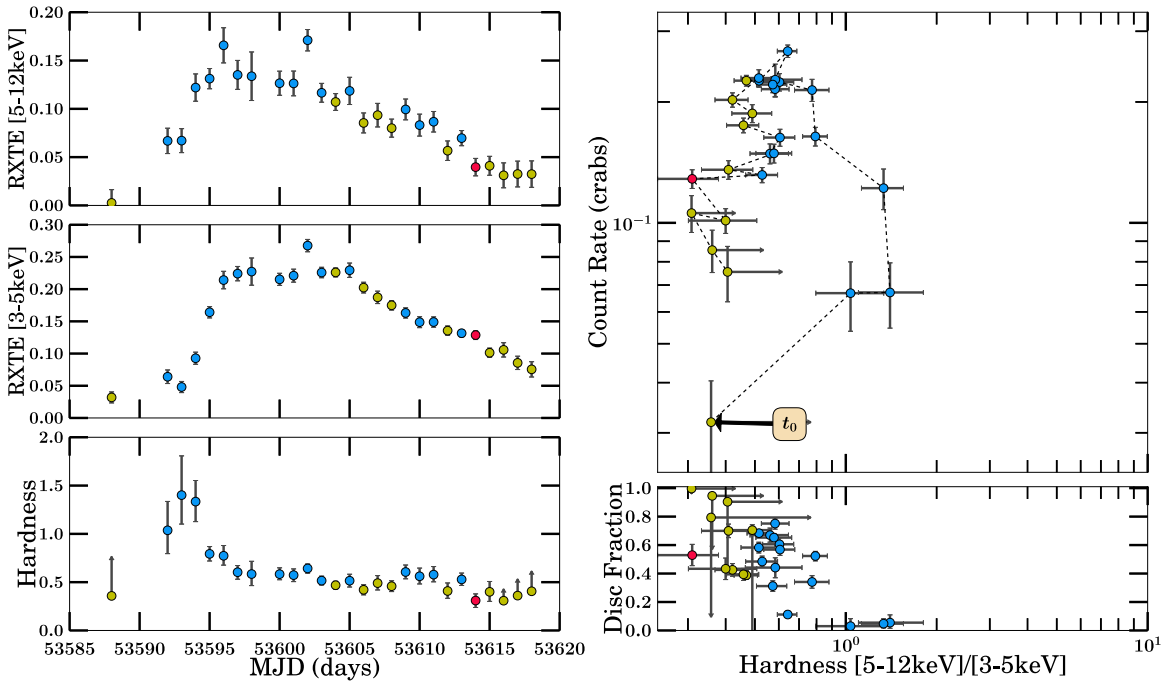

(a) 2005 Outburst Analysis

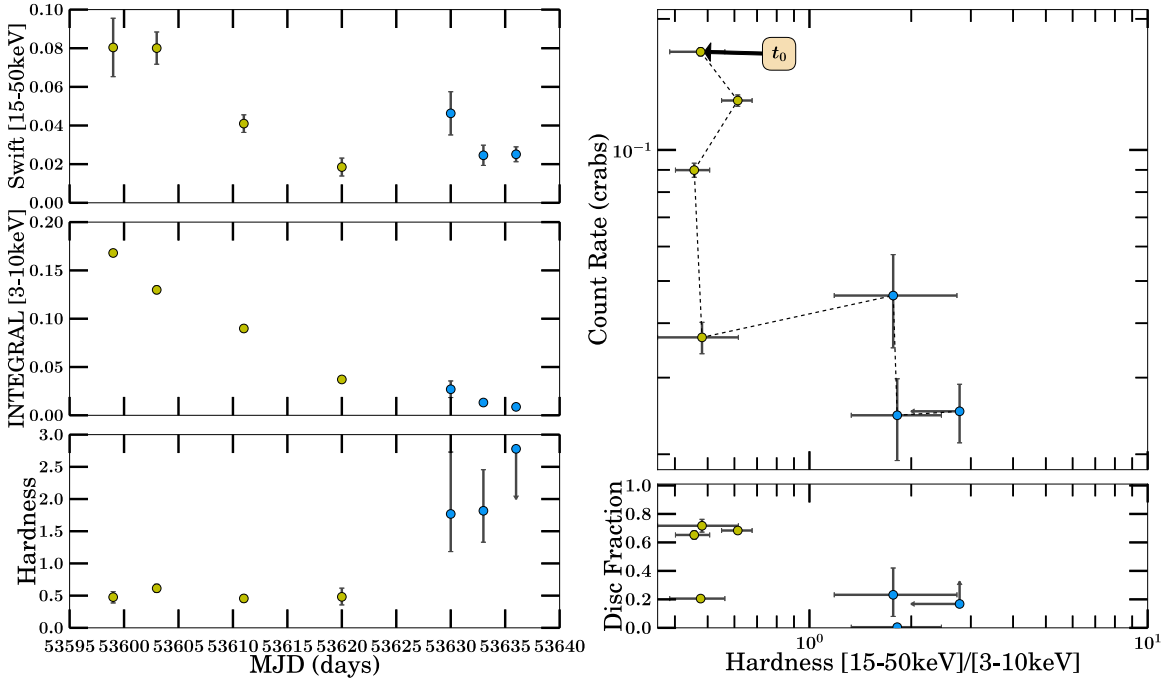

(b) 2005 Outburst Analysis

Figure B.56: H 1743−322 Part 3

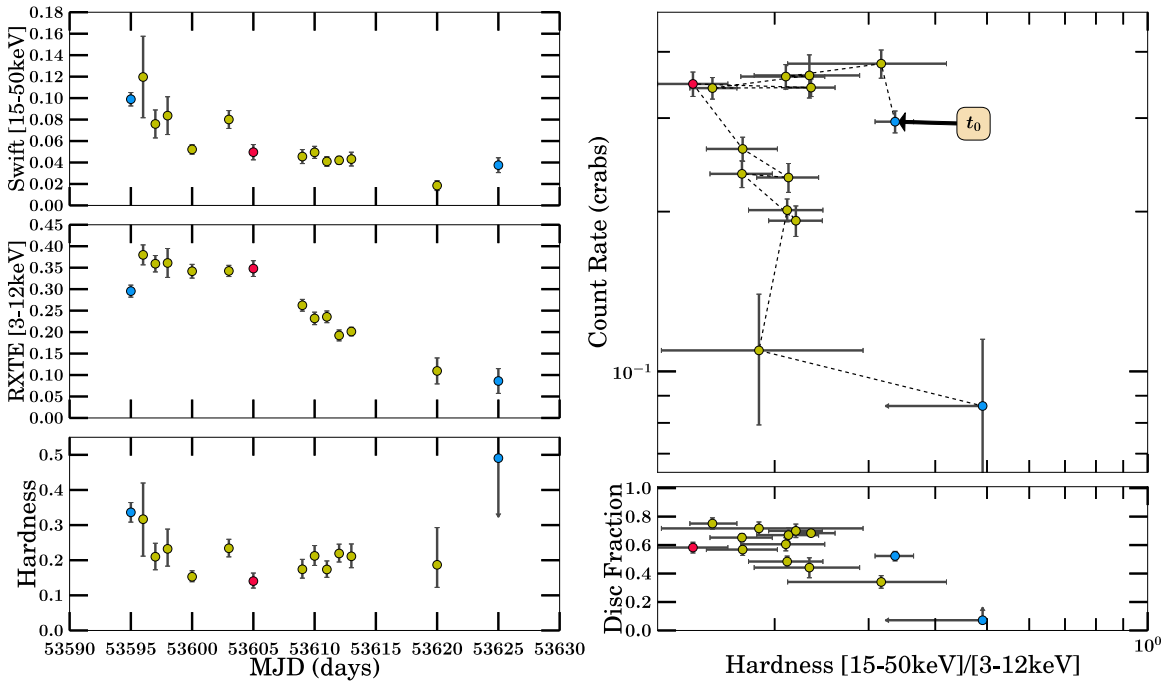

(a) 2005 Outburst Analysis

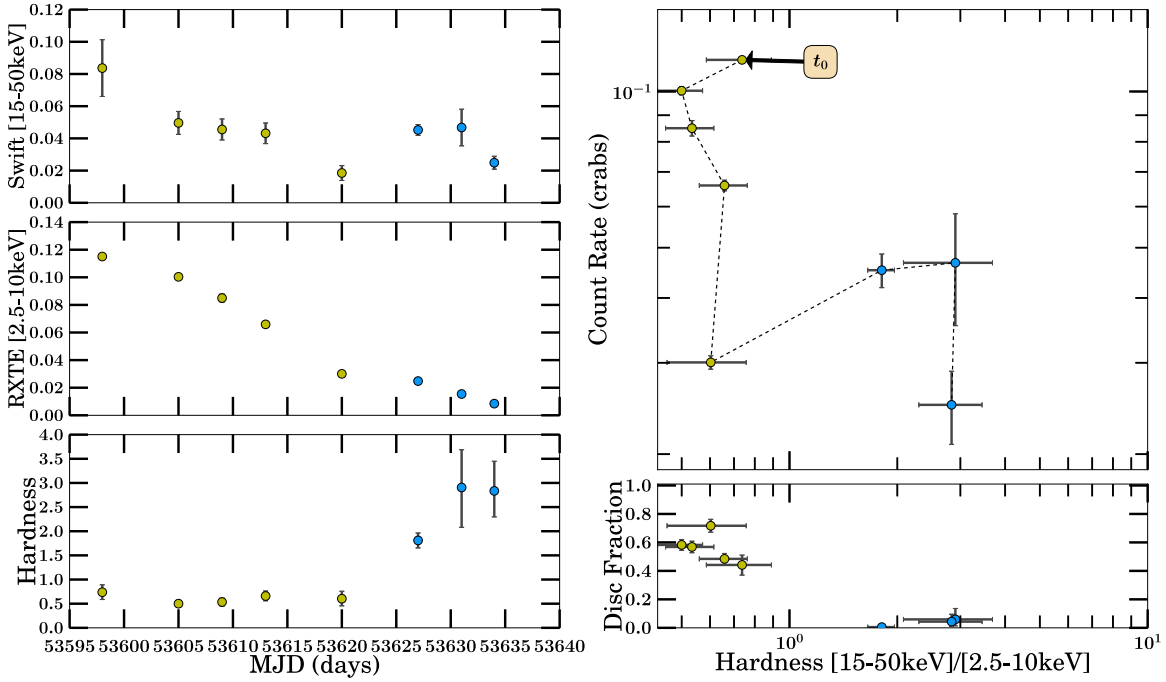

(b) 2005 Outburst Analysis

Figure B.57: H 1743−322 Part 4

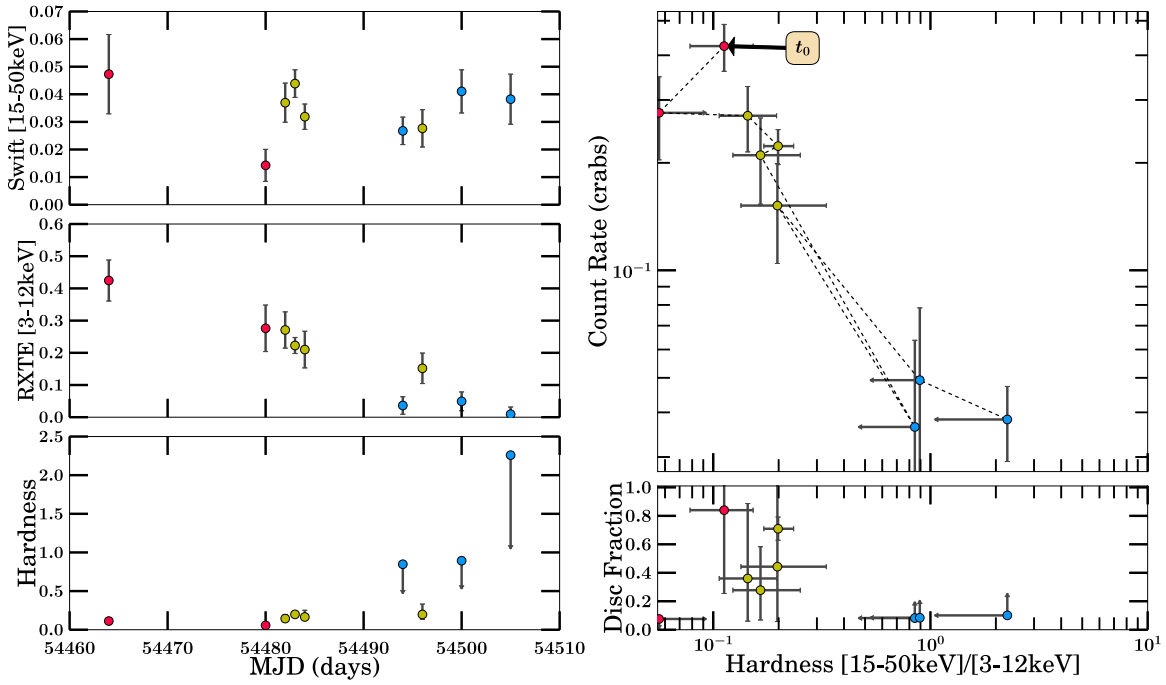

(a) 2007/2008 Outburst Analysis

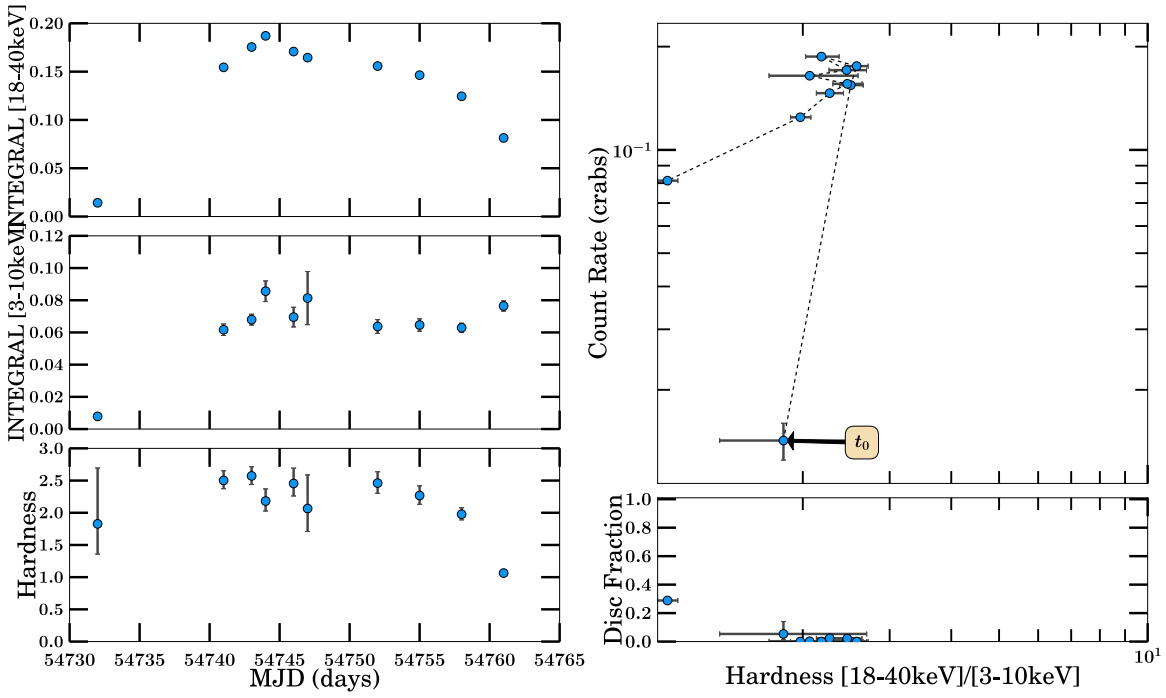

(b) 2007/2008 Outburst Analysis

Figure B.58: H 1743−322 Part 5

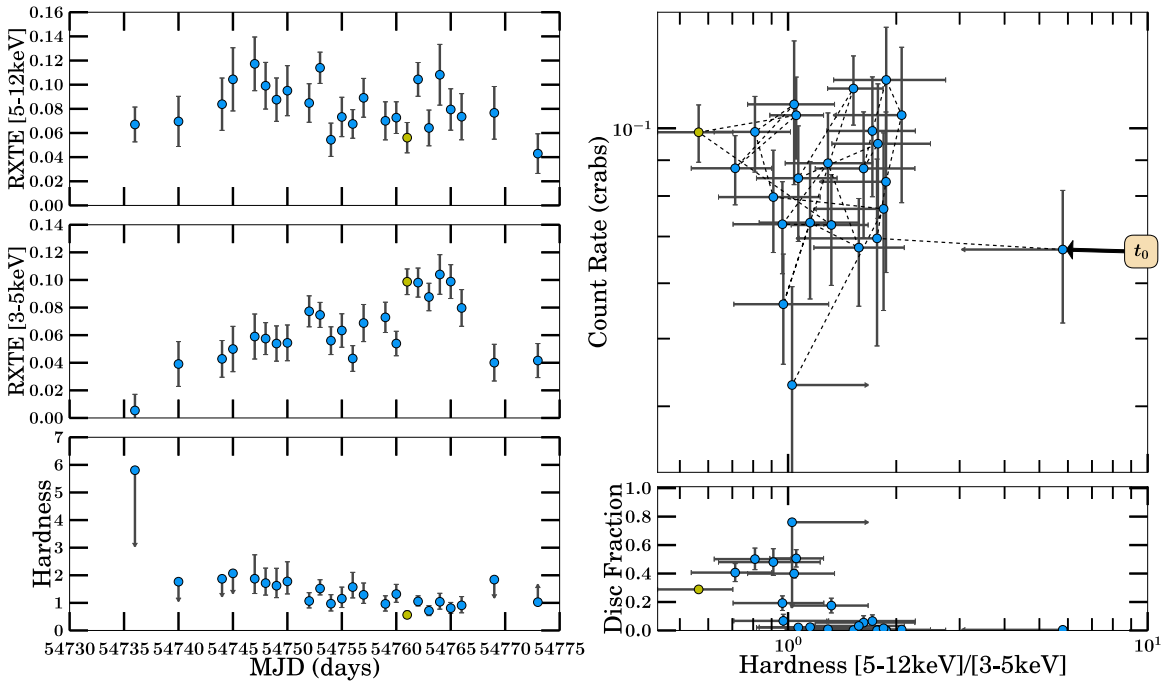

(a) 2008 Outburst Analysis

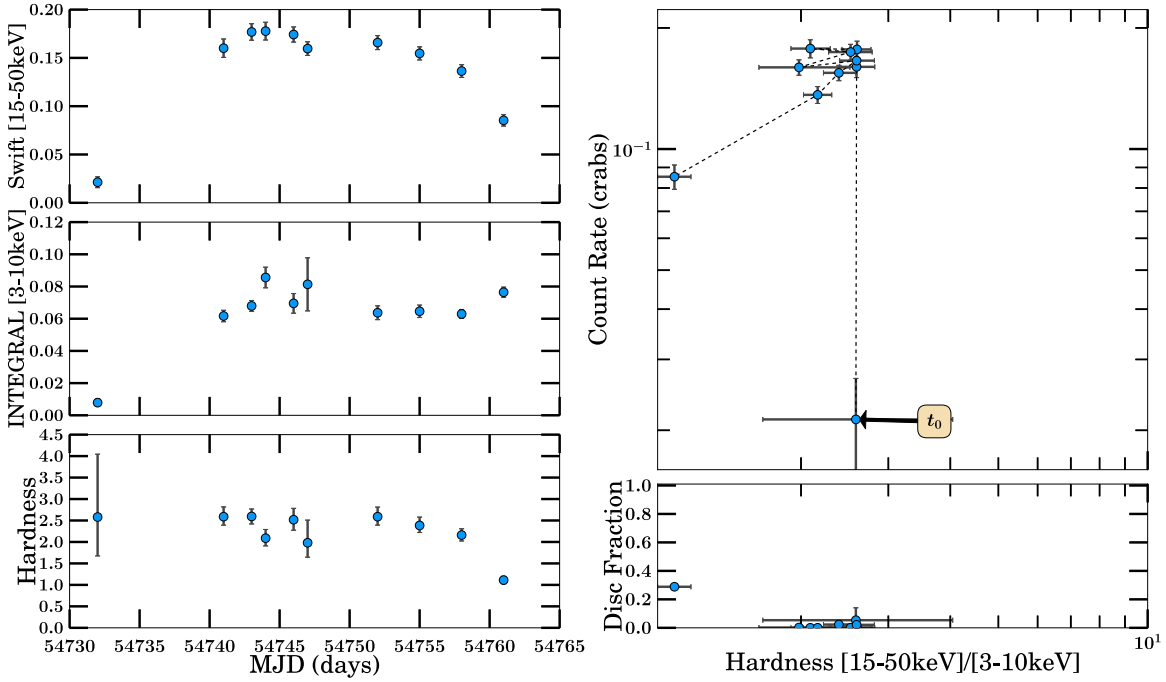

(b) 2008 Outburst Analysis

Figure B.59: H 1743−322 Part 6

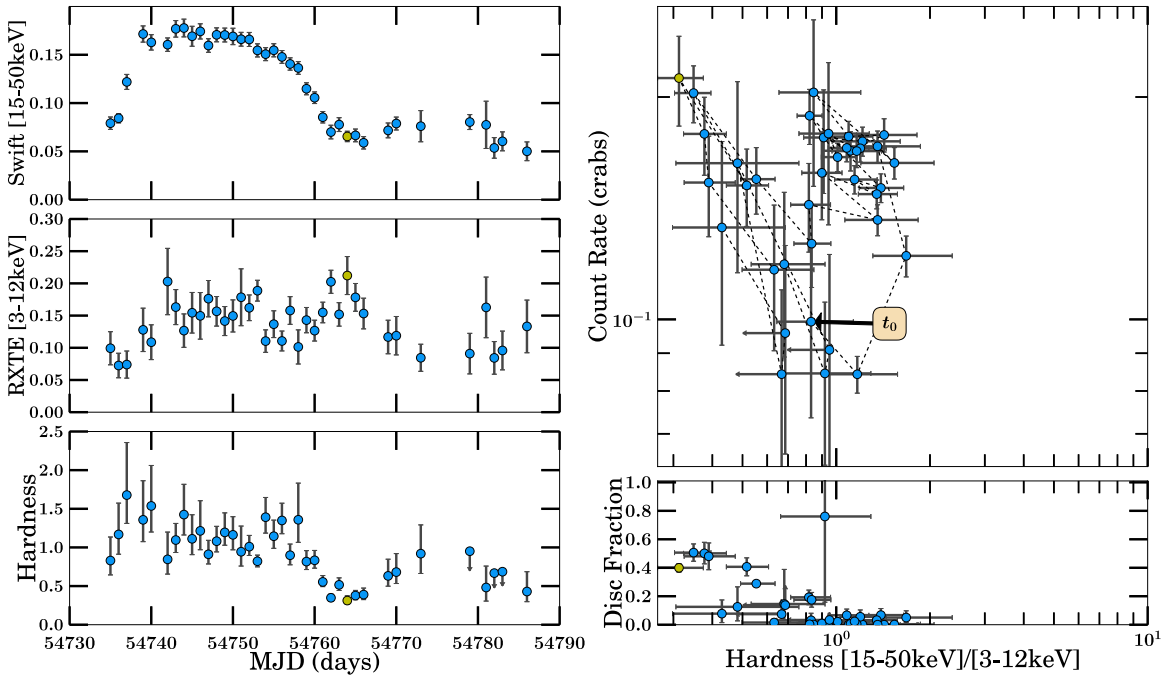

(a) 2008 Outburst Analysis

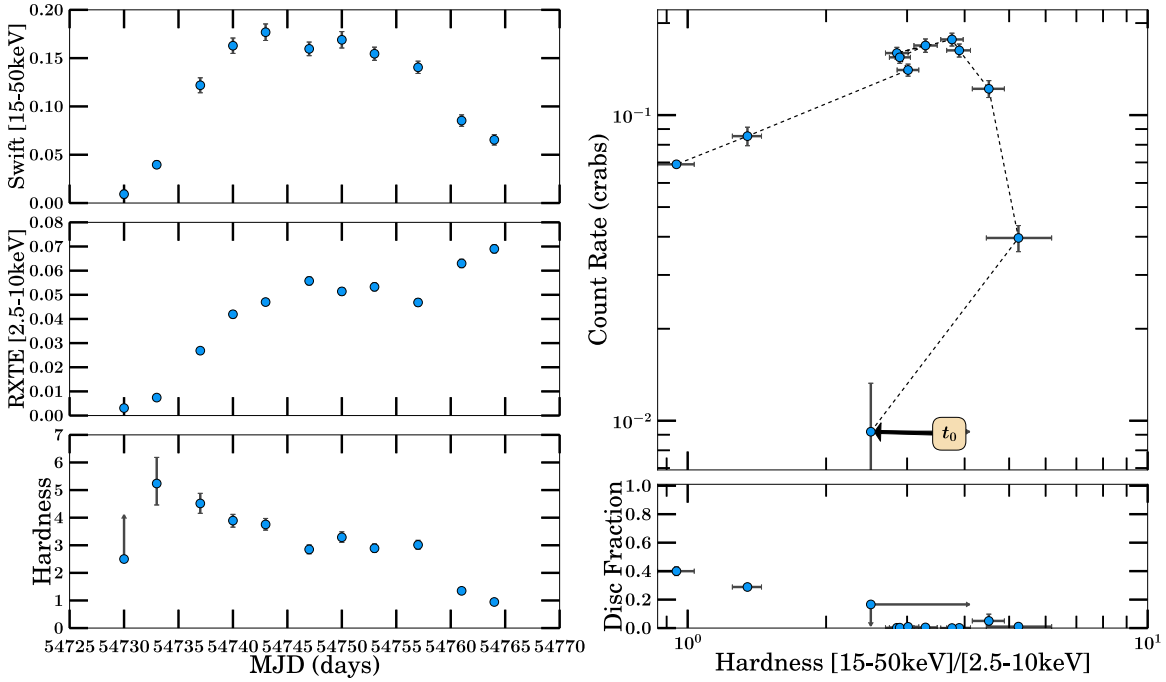

(b) 2008 Outburst Analysis

Figure B.60: H 1743−322 Part 7

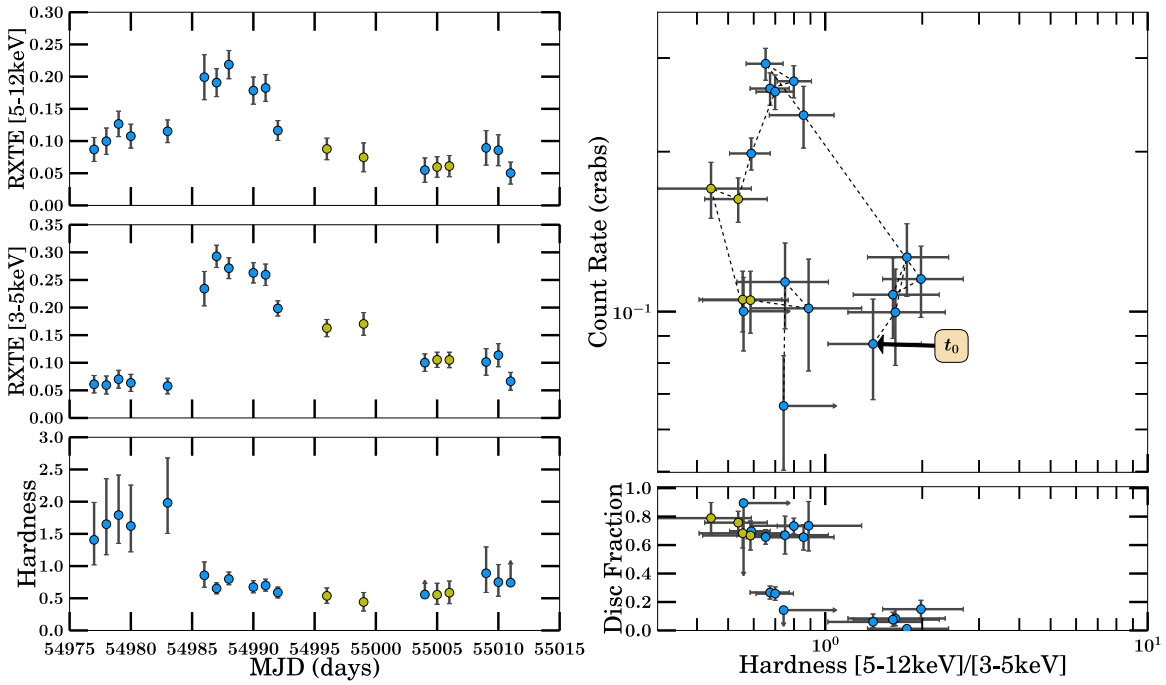

(a) 2009 Outburst Analysis

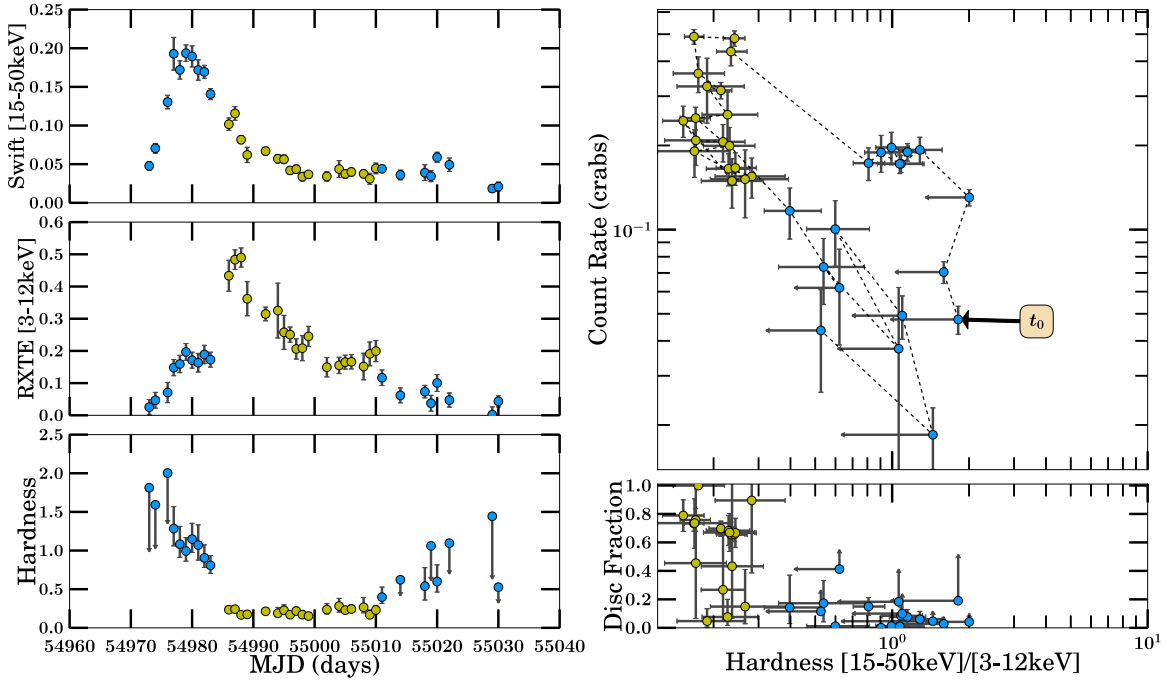

(b) 2009 Outburst Analysis

Figure B.61: H 1743−322 Part 8

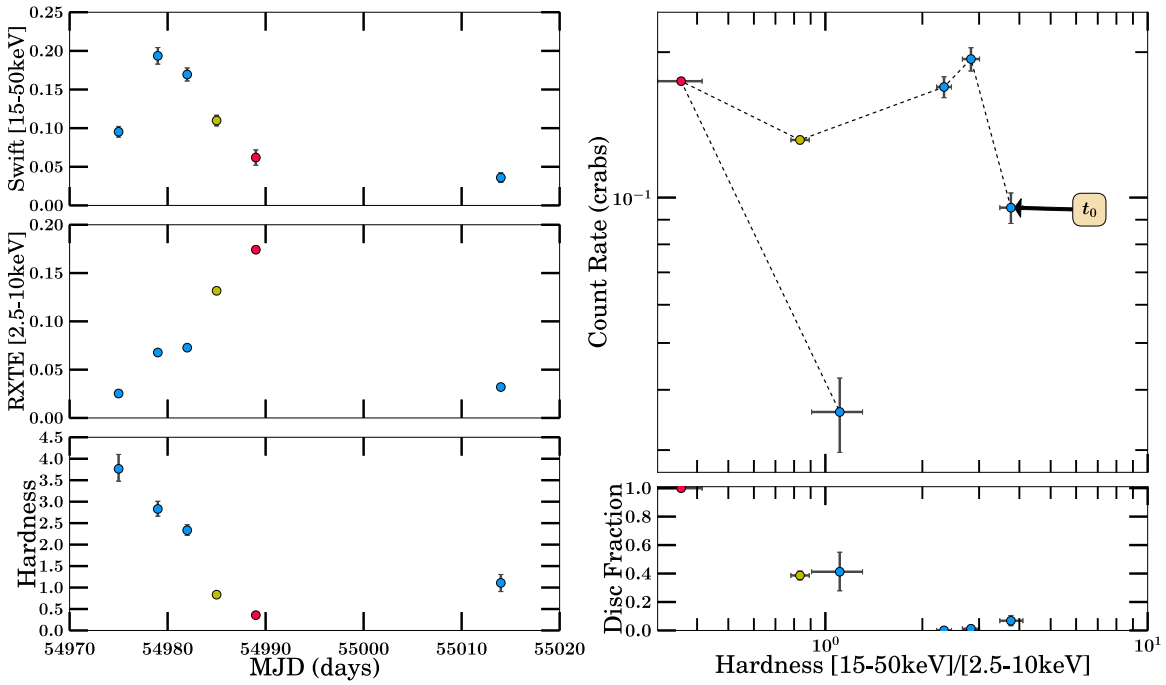

(a) 2009 Outburst Analysis

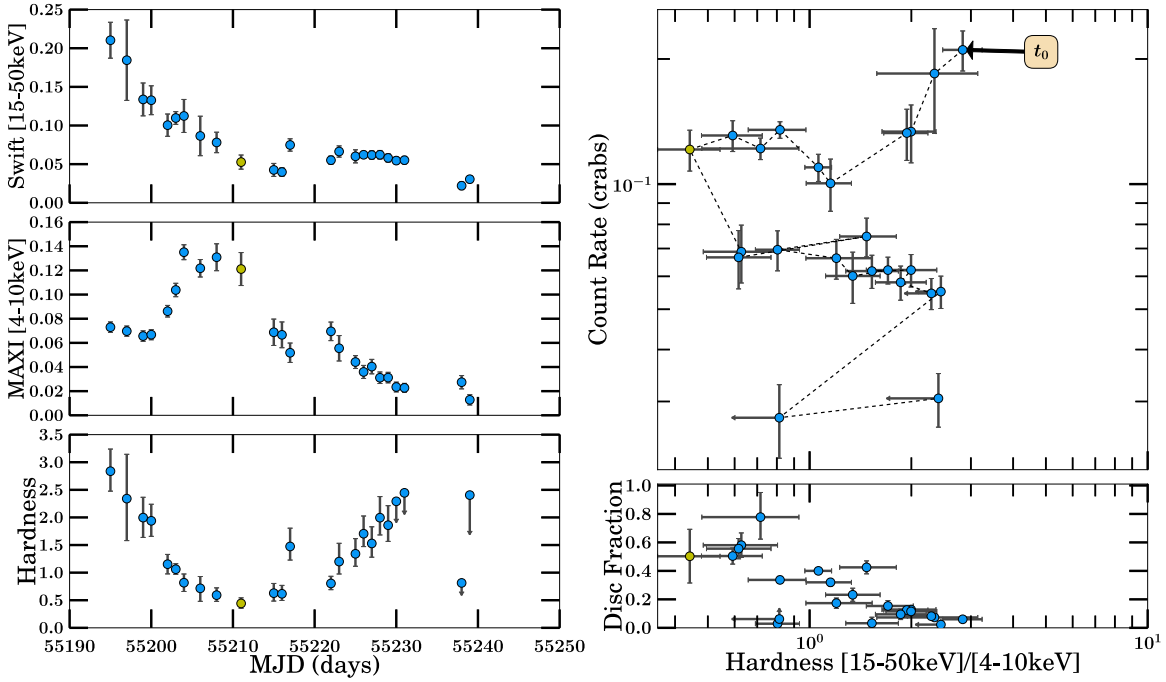

(b) 2009/2010 Outburst Analysis

Figure B.62: H 1743−322 Part 9

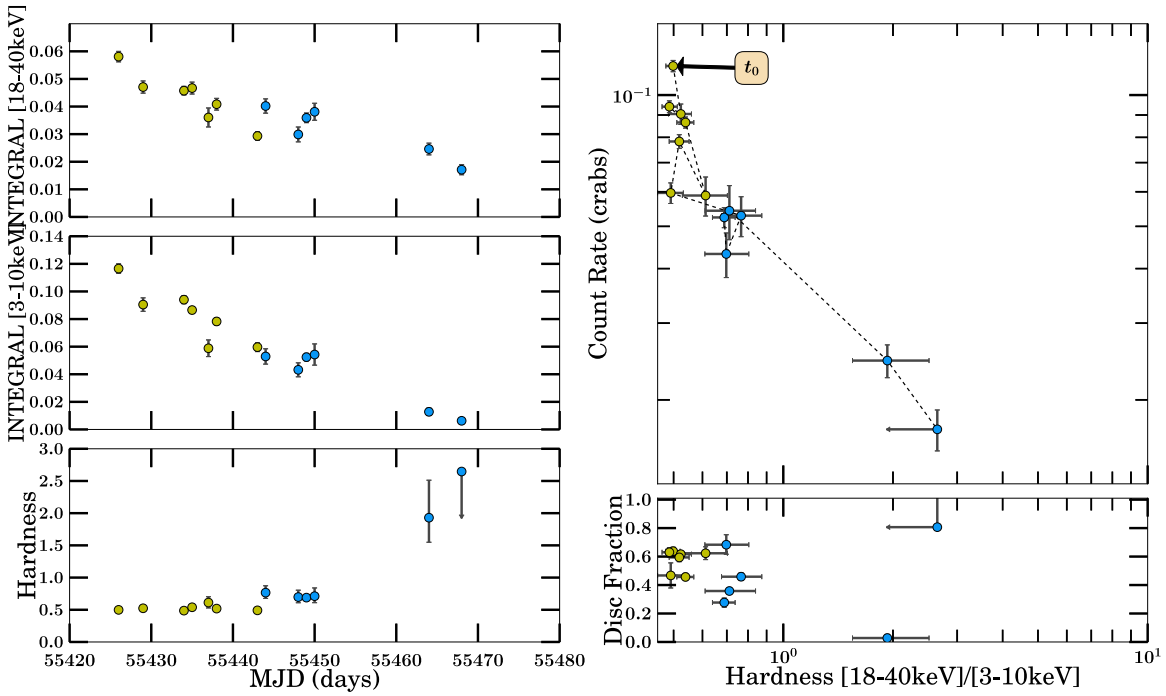

(a) 2010 Outburst Analysis

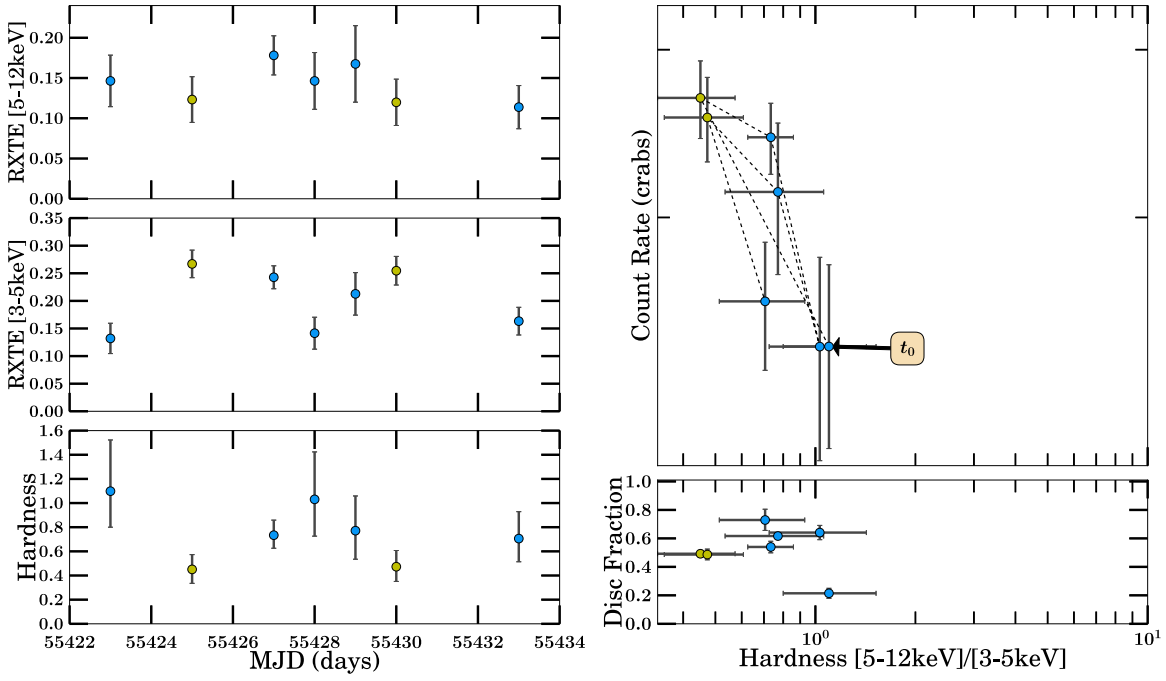

(b) 2010 Outburst Analysis

Figure B.63: H 1743−322 Part 10

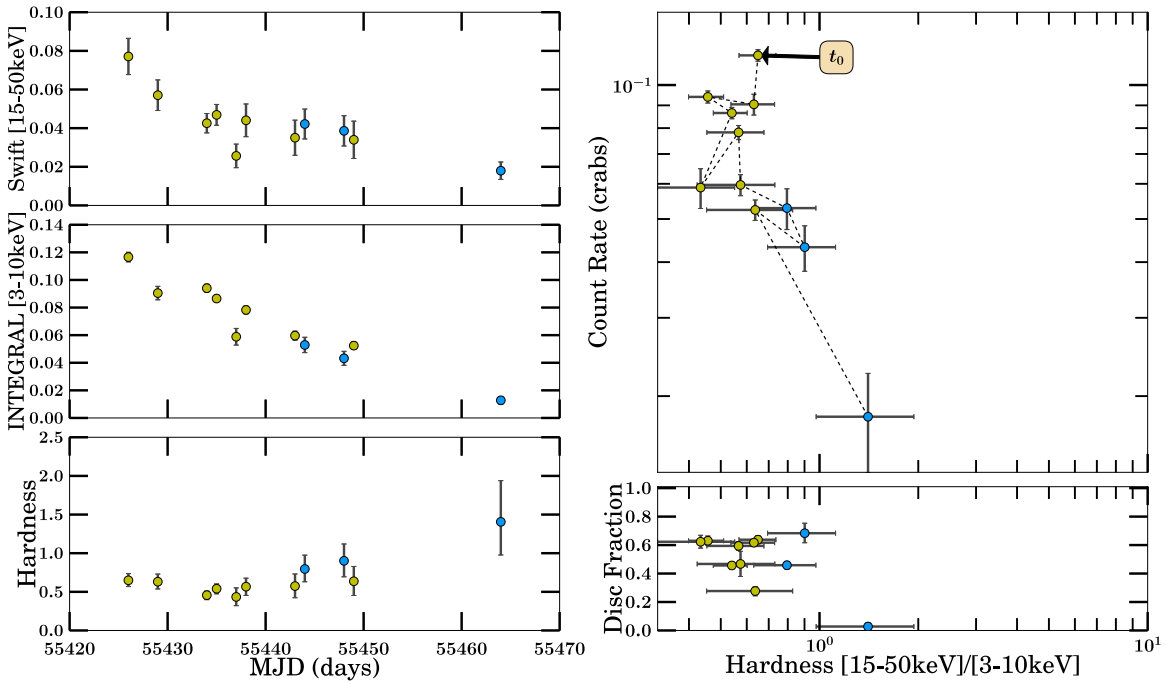

(a) 2010 Outburst Analysis

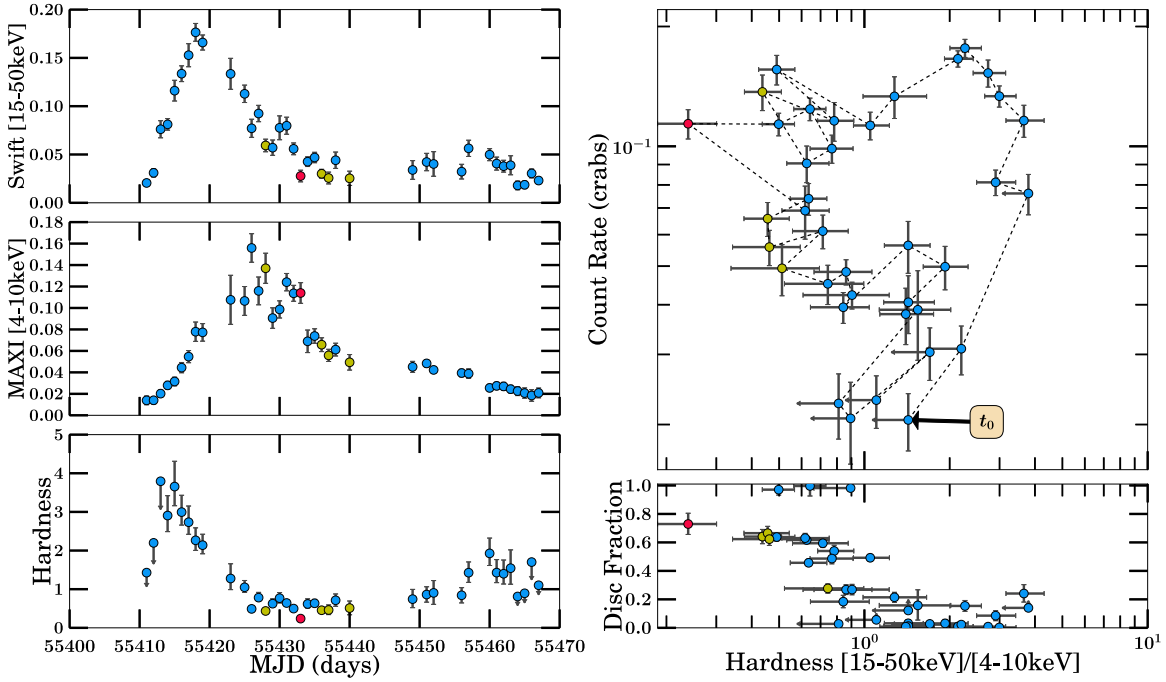

(b) 2010 Outburst Analysis

Figure B.64: H 1743−322 Part 11

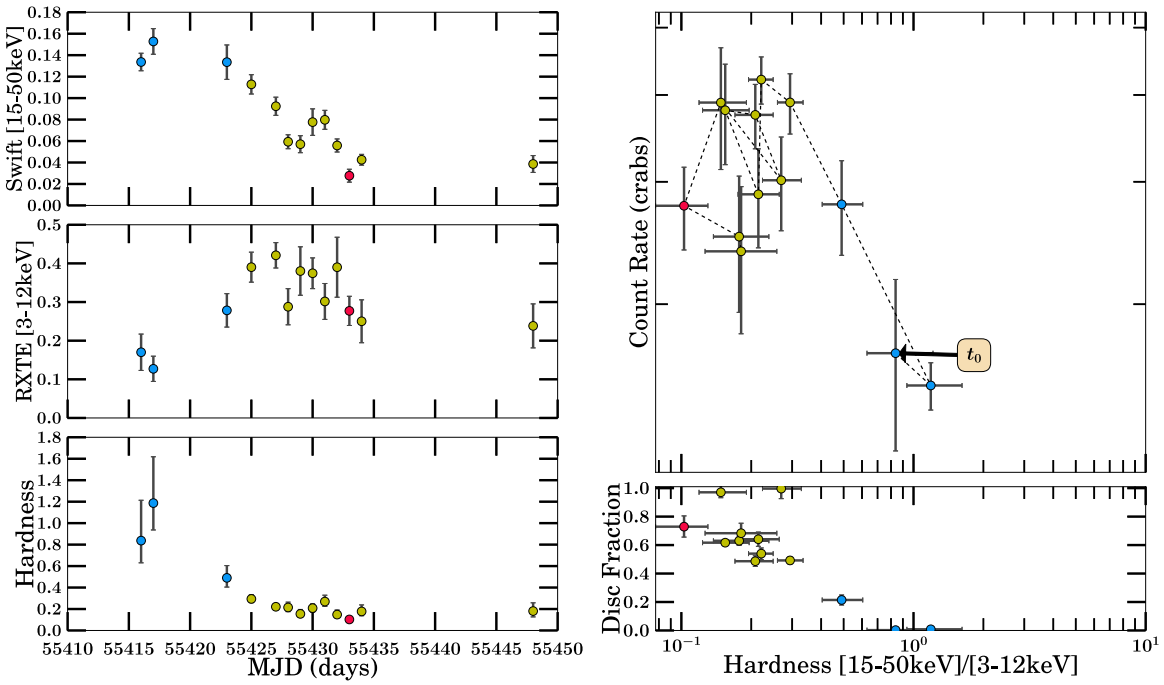

(a) 2010 Outburst Analysis

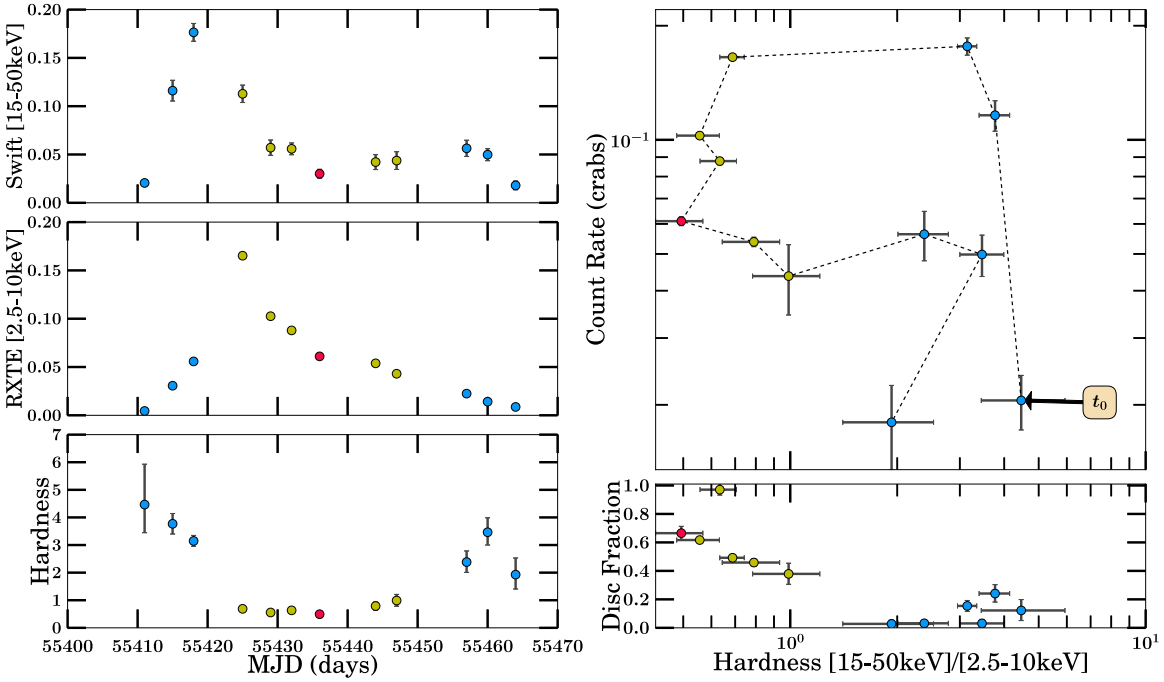

(b) 2010 Outburst Analysis

Figure B.65: H 1743−322 Part 12

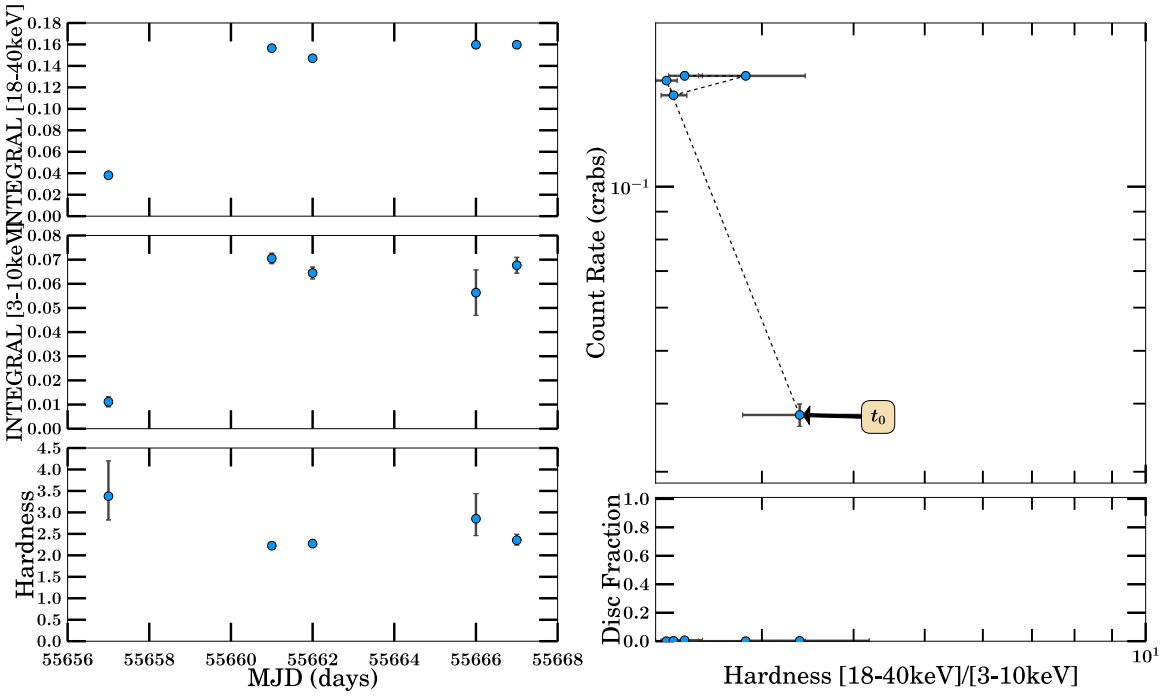

(a) 2010/2011 Outburst Analysis

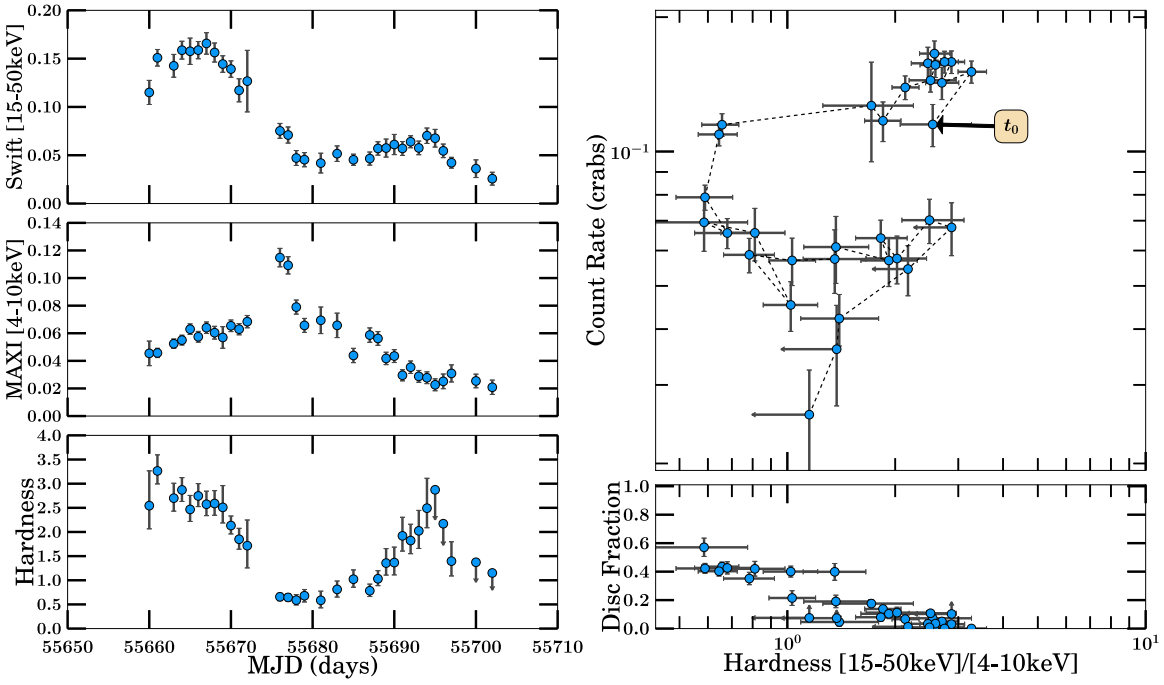

(b) 2010/2011 Outburst Analysis

Figure B.66: H 1743−322 Part 13

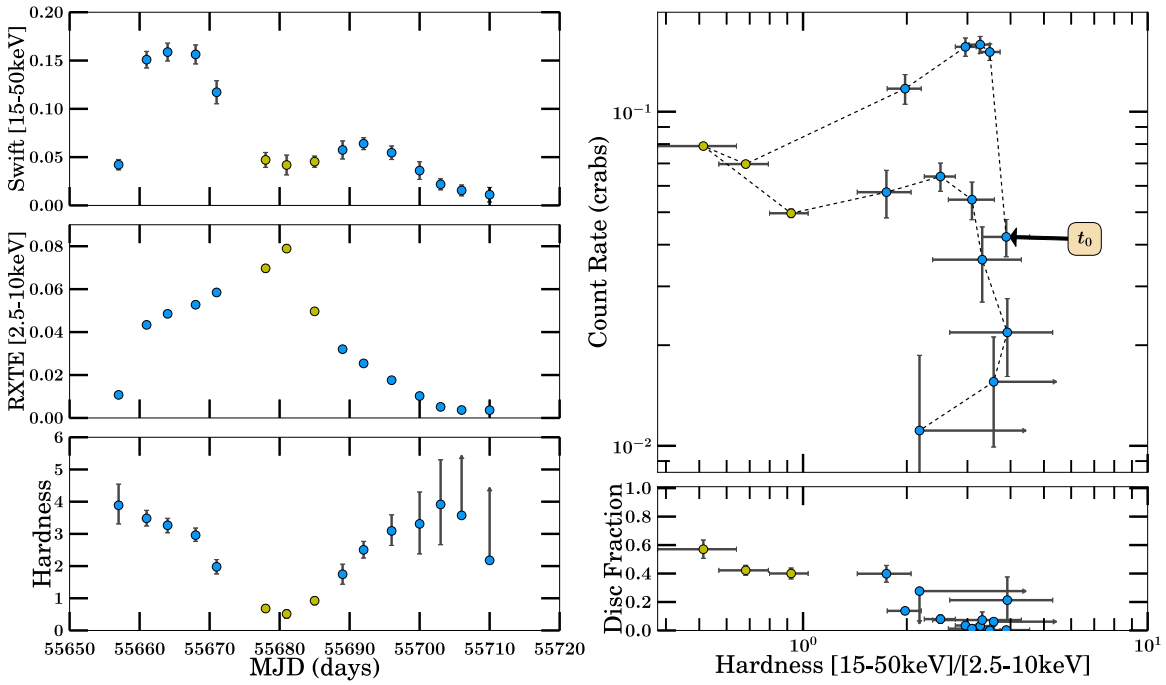

(a) 2010/2011 Outburst Analysis

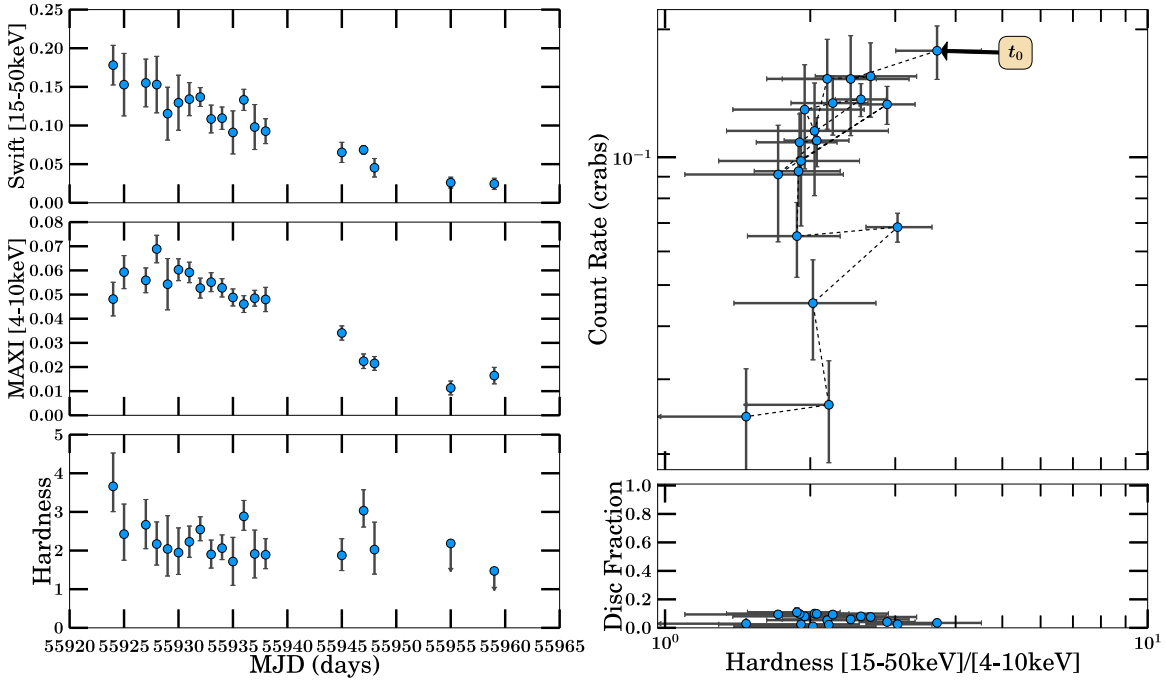

(b) 2011/2012 Outburst Analysis

Figure B.67: H 1743−322 Part 14

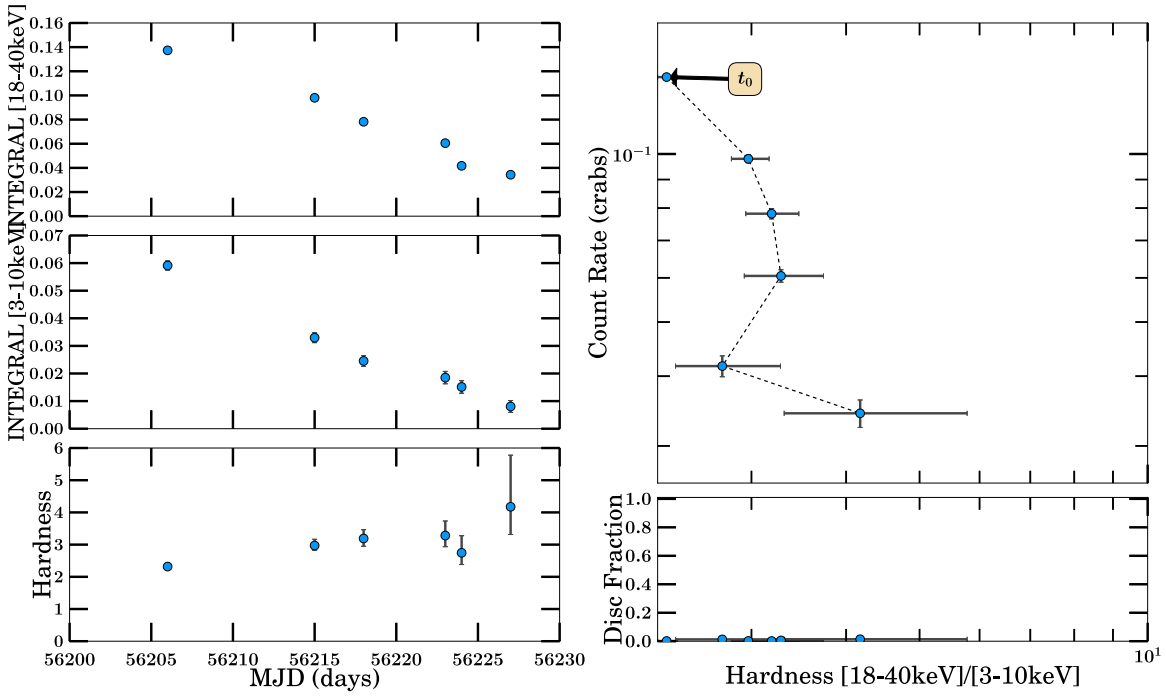

(a) 2012 Outburst Analysis

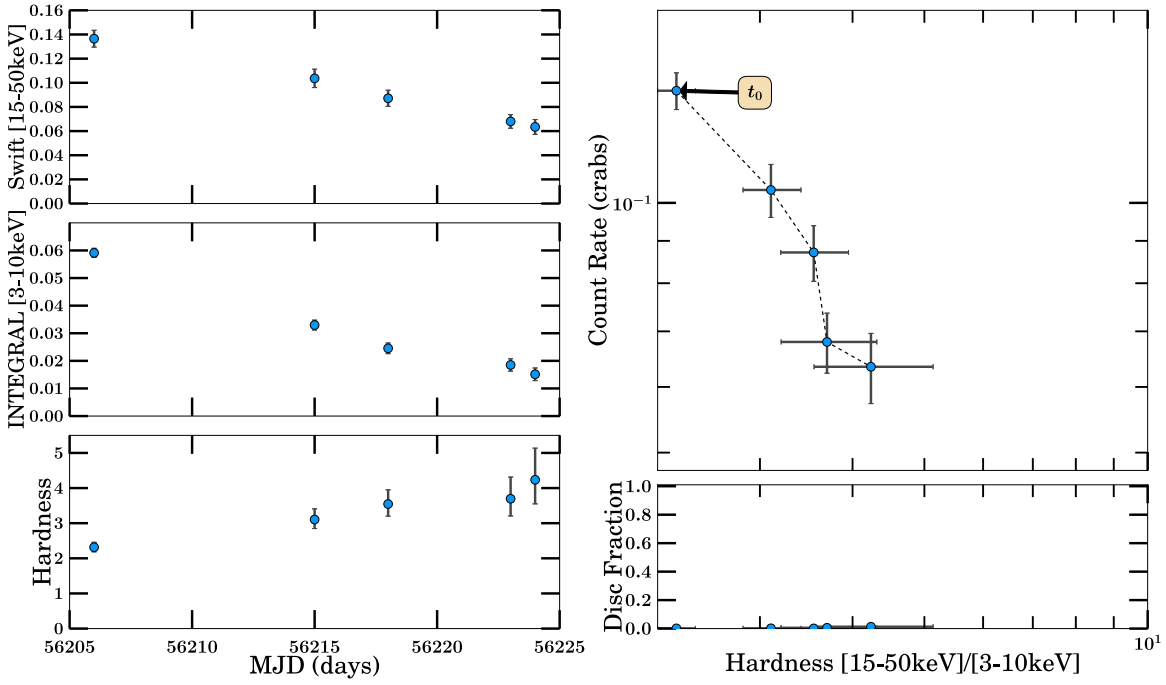

(b) 2012 Outburst Analysis

Figure B.68: H 1743−322 Part 15

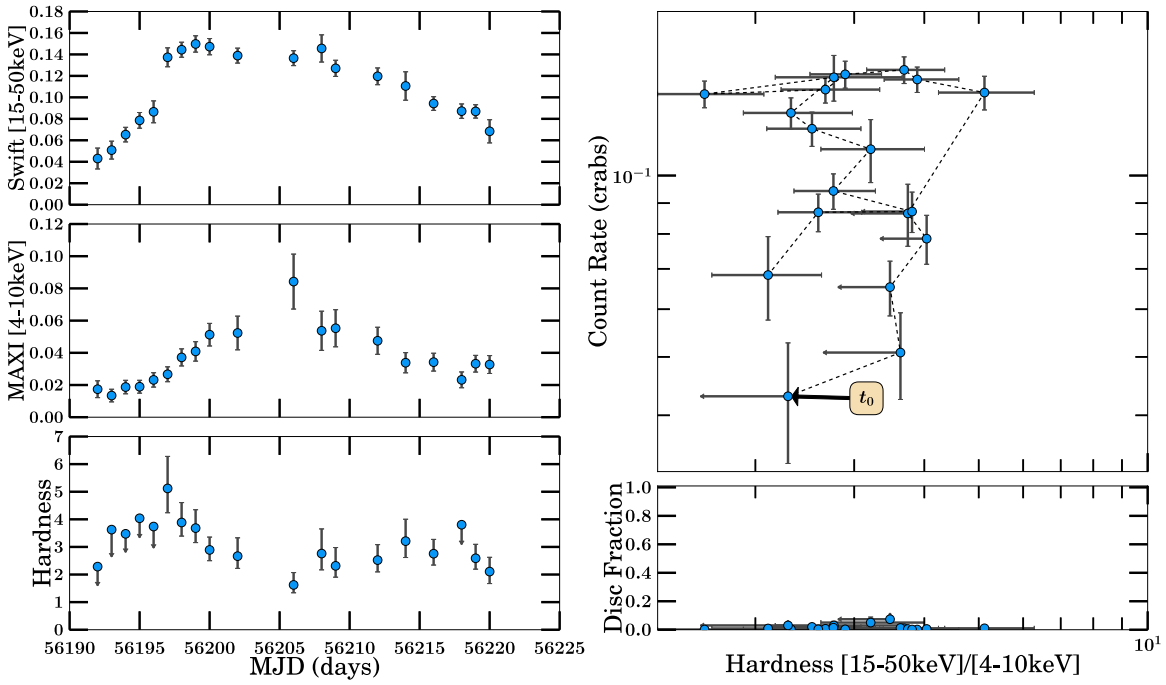

(a) 2012 Outburst Analysis

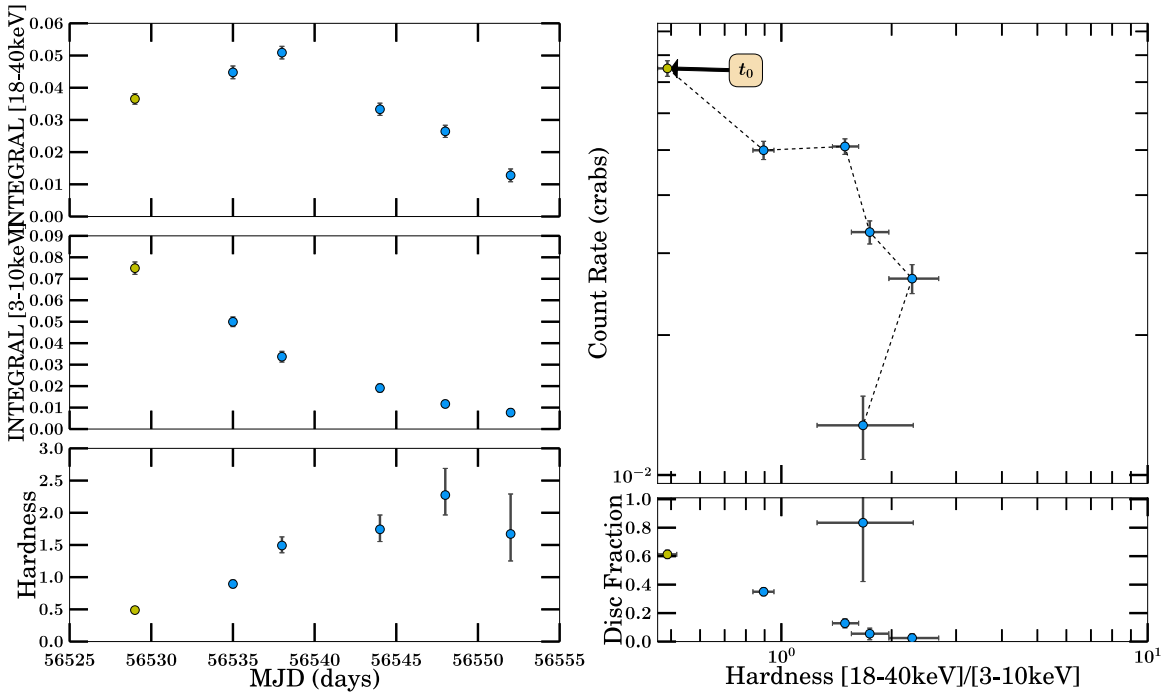

(b) 2013 Outburst Analysis

Figure B.69: H 1743−322 Part 16

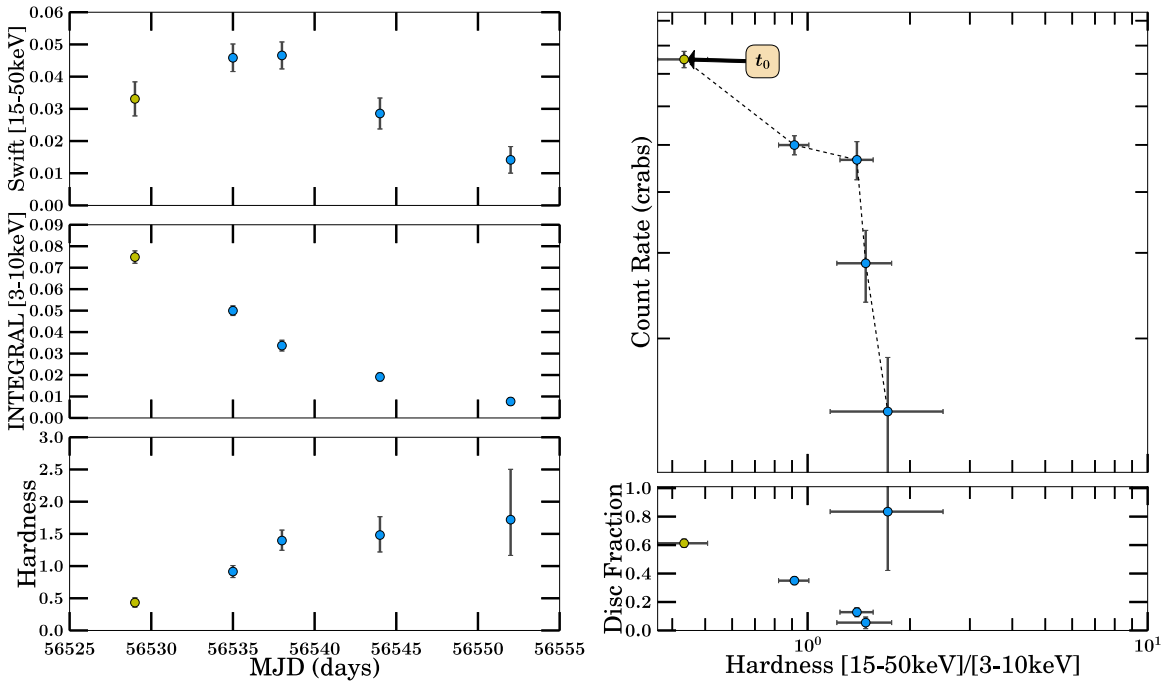

(a) 2013 Outburst Analysis

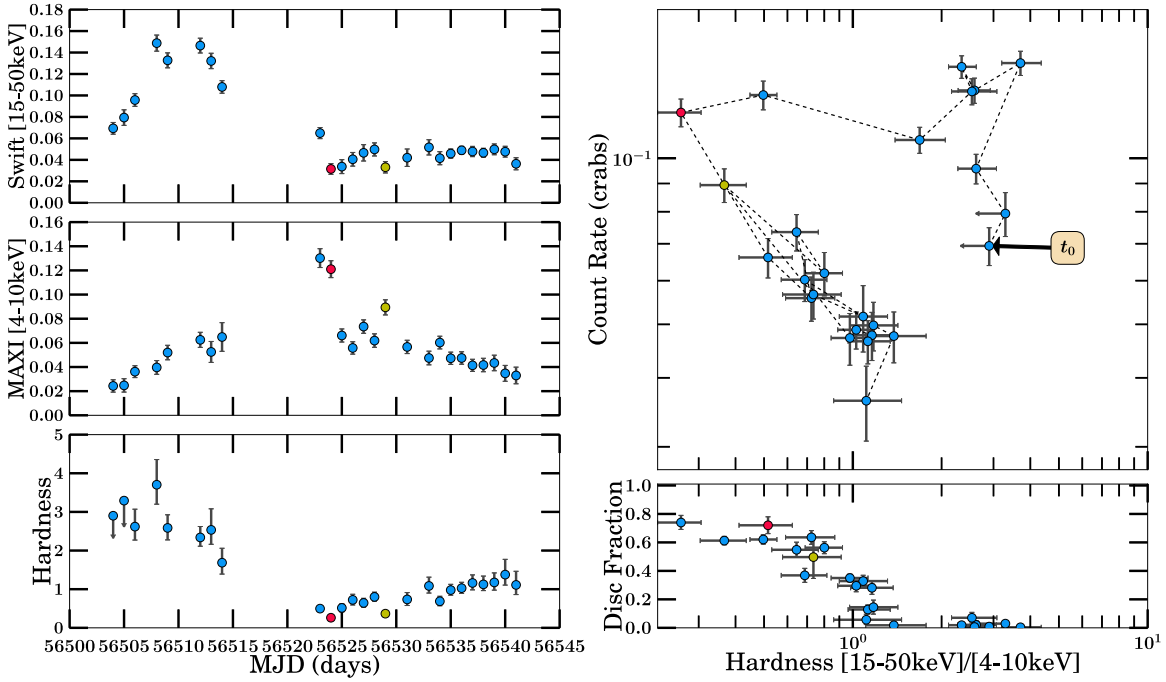

(b) 2013 Outburst Analysis

Figure B.70: H 1743−322 Part 17

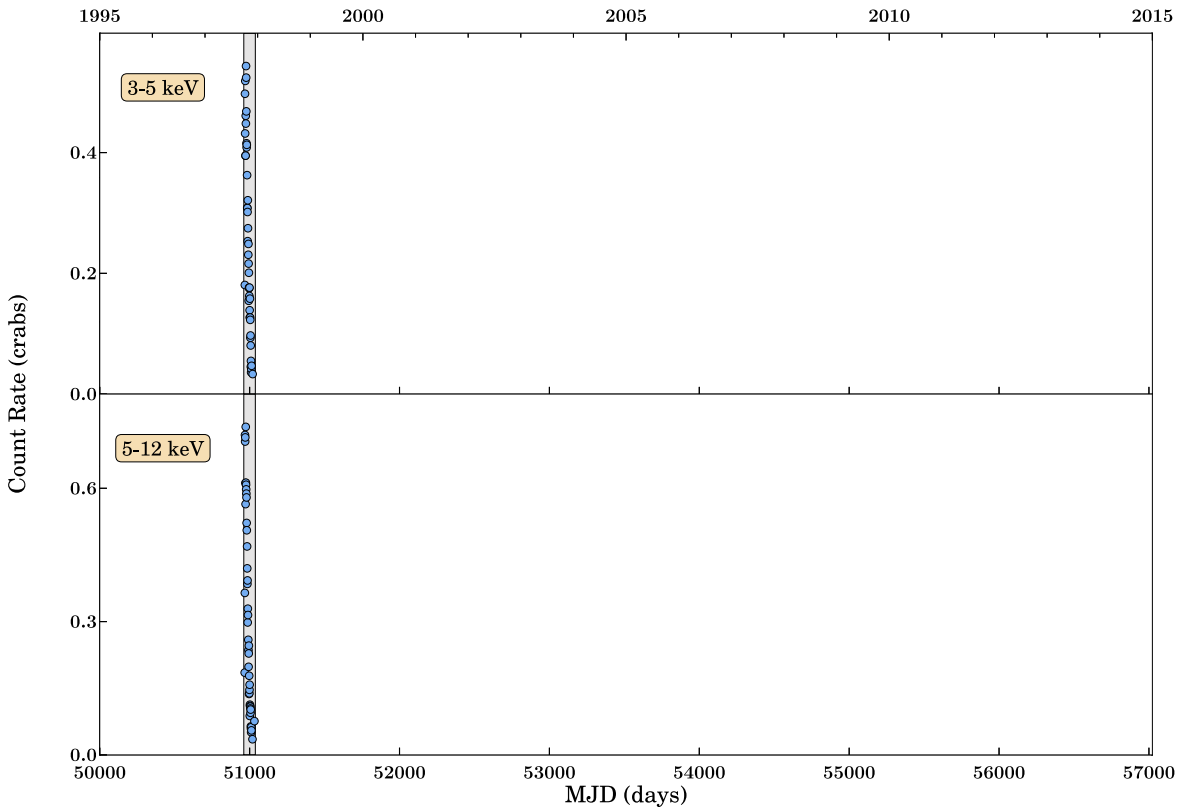

(a) Long-term Light Curve

Figure B.71: XTE J1748−288 Part 1

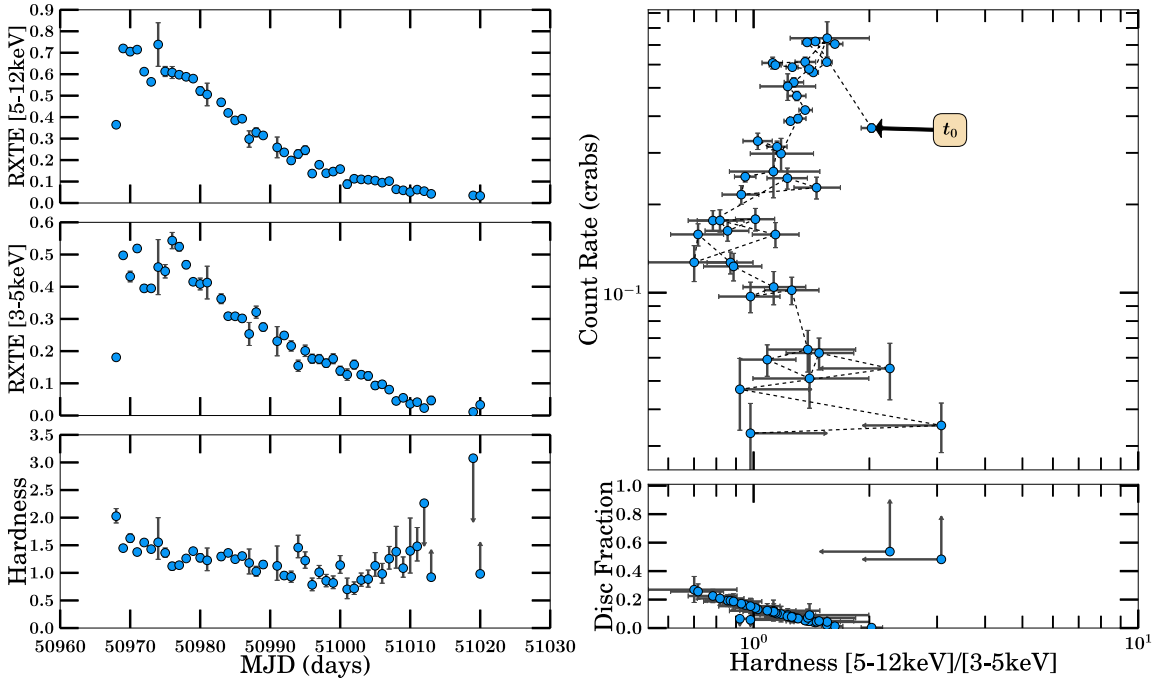

(a) 1998 Outburst Analysis

Figure B.72: XTE J1748−288 Part 2

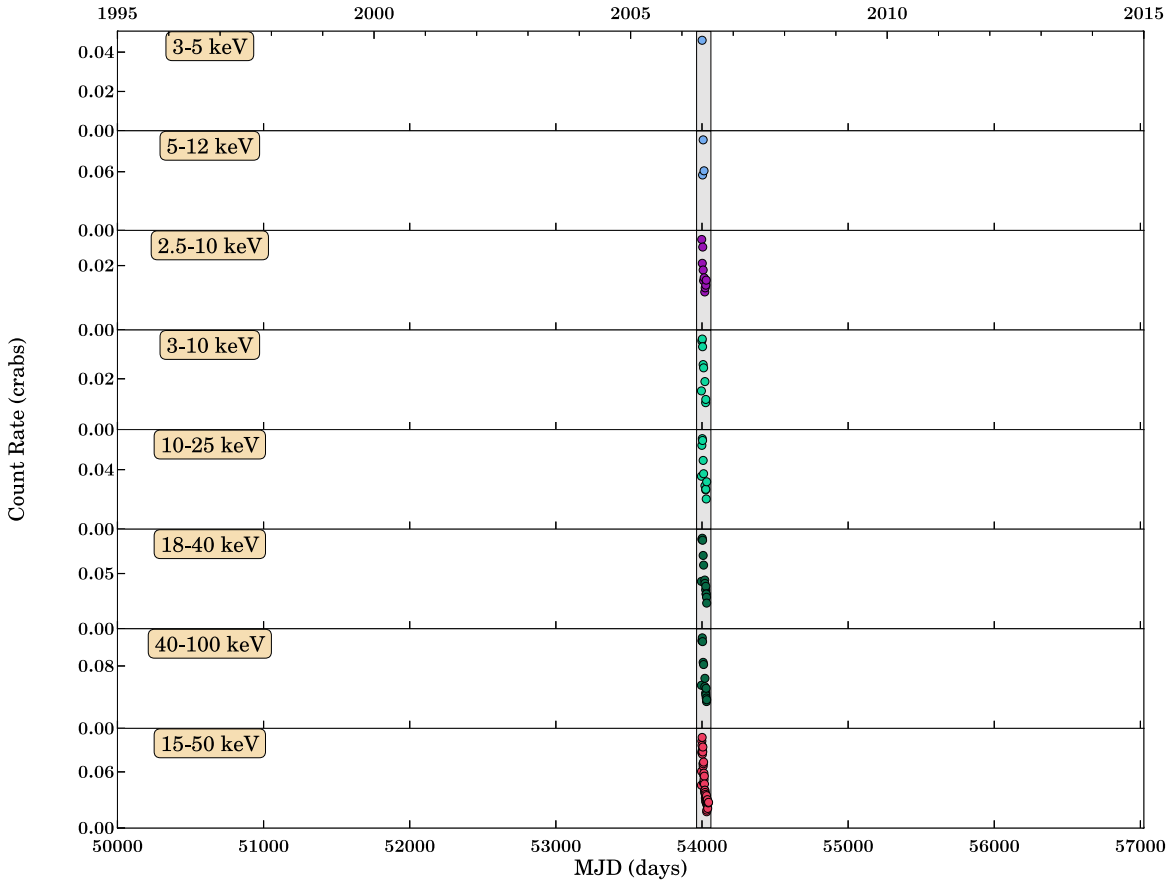

(a) Long-term Light Curve

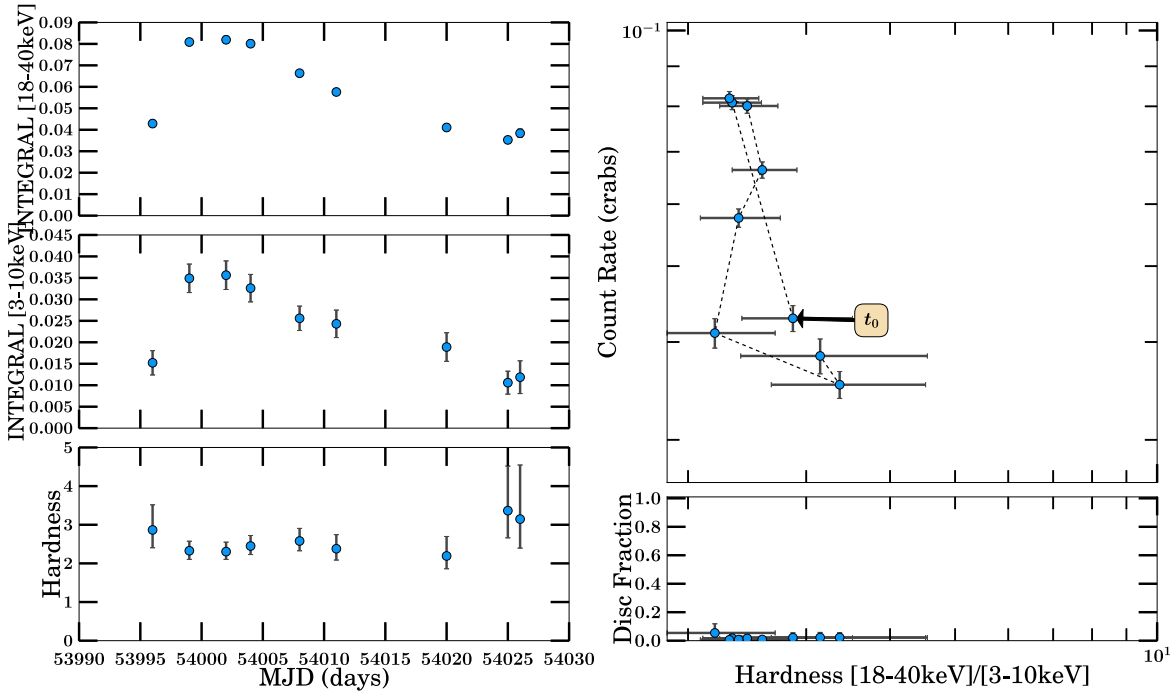

(b) 2006 Outburst Analysis

Figure B.73: IGR J17497−2821 Part 1

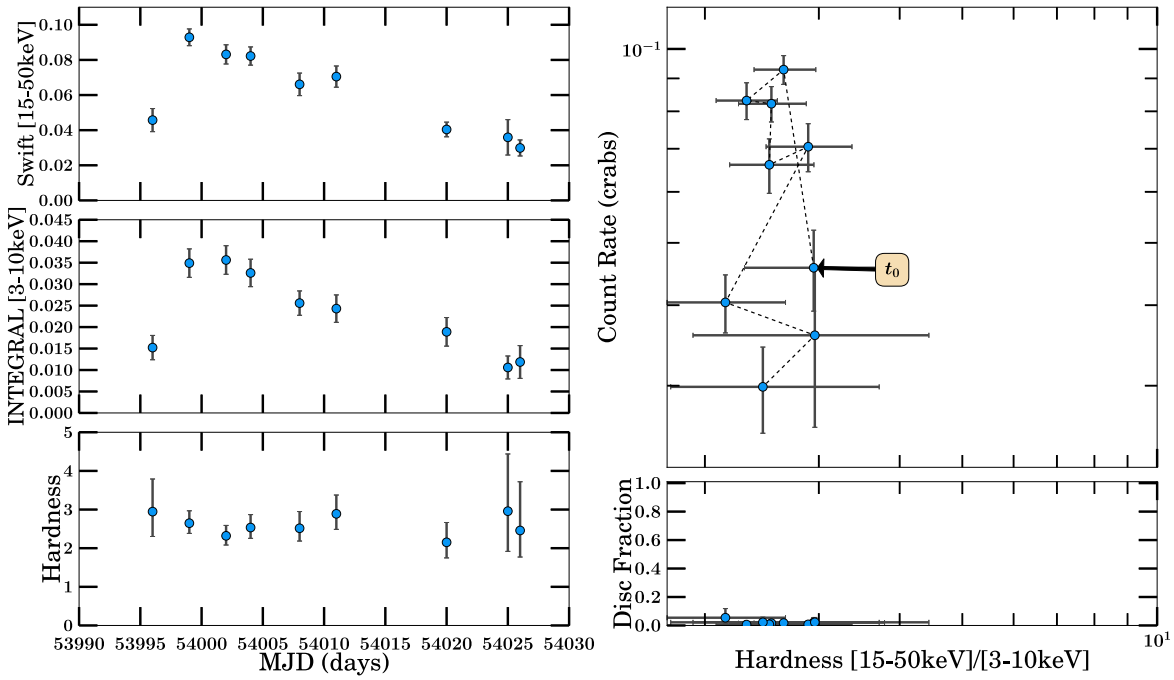

(a) 2006 Outburst Analysis

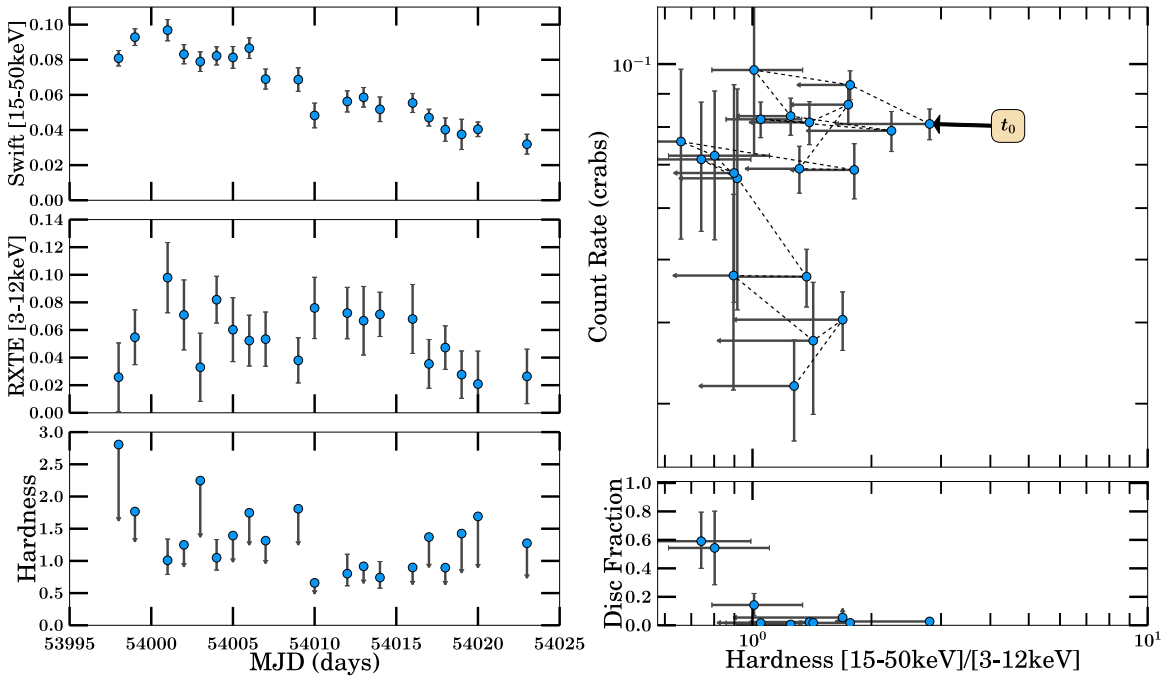

(b) 2006 Outburst Analysis

Figure B.74: IGR J17497−2821 Part 2

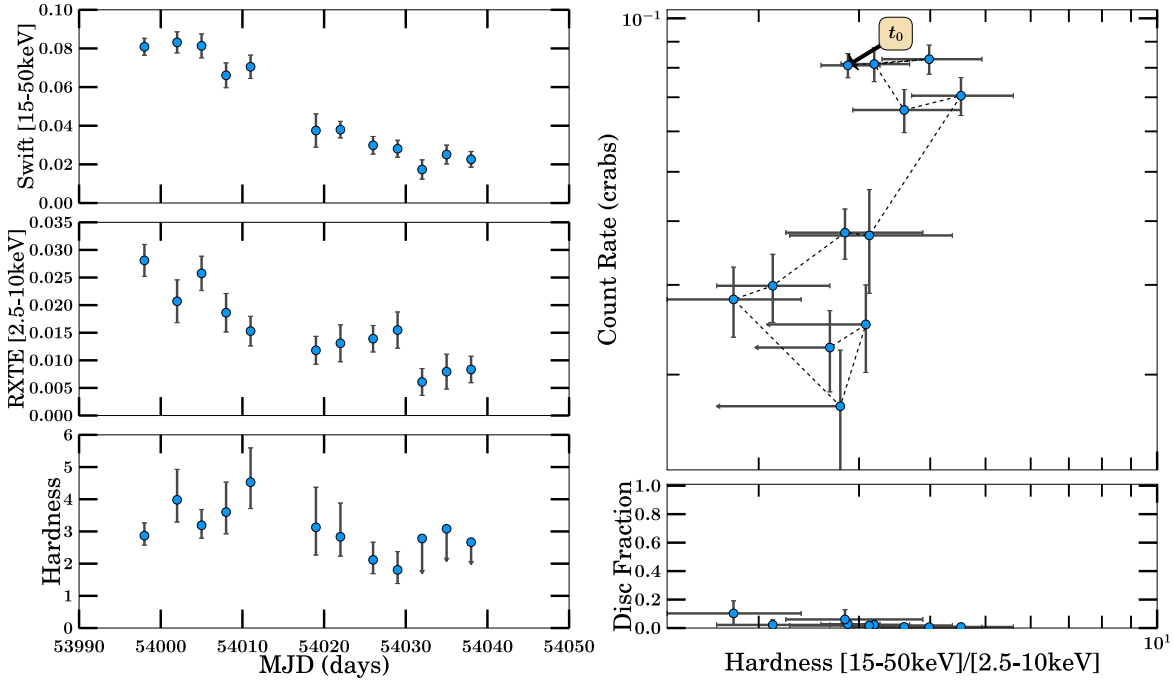

(a) 2006 Outburst Analysis

Figure B.75: IGR J17497−2821 Part 3

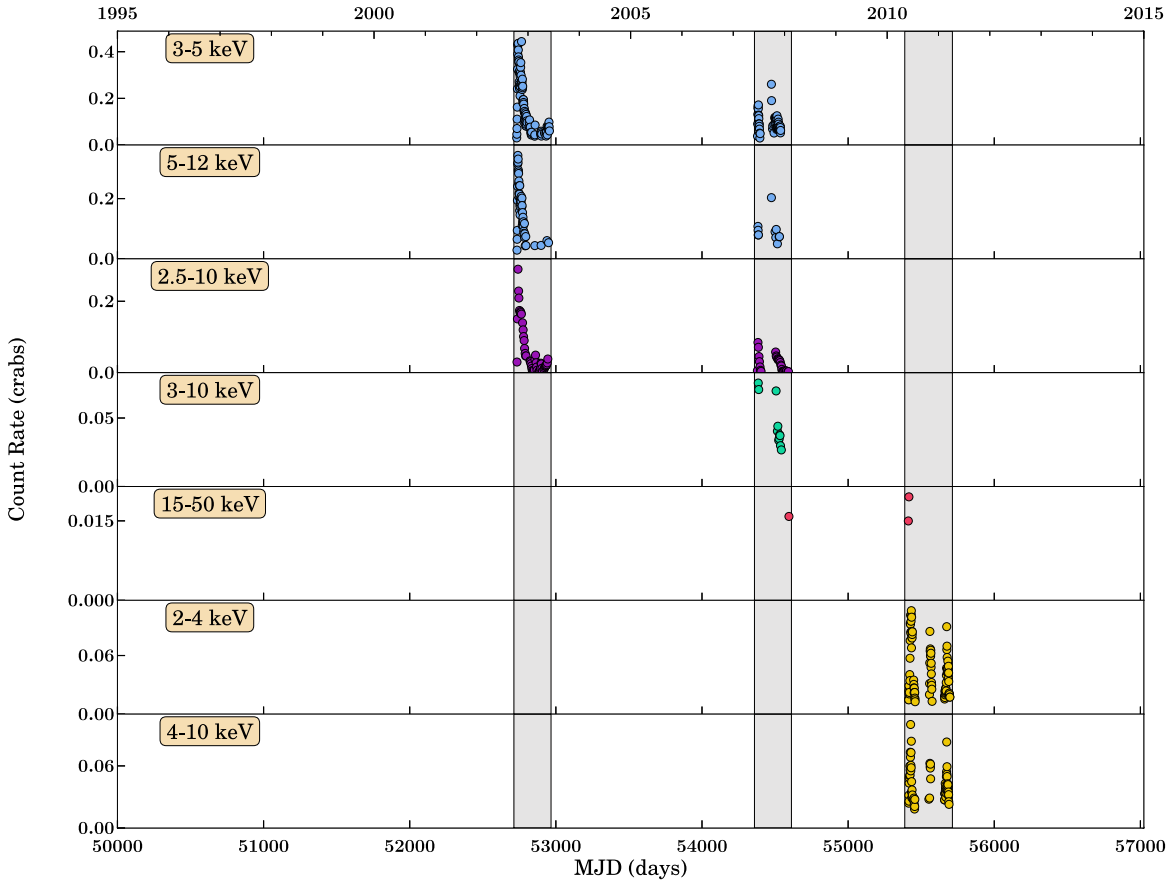

(a) Long-term Light Curve

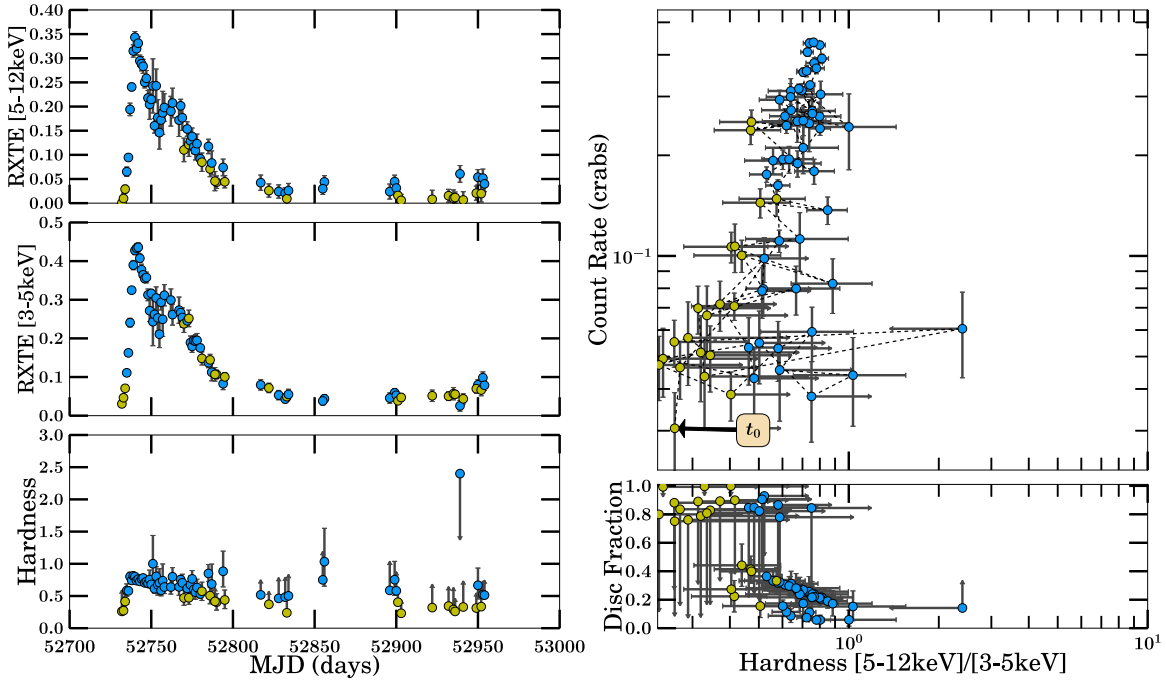

(b) 2003 Outburst Analysis

Figure B.76: SLX 1746−331 Part 1

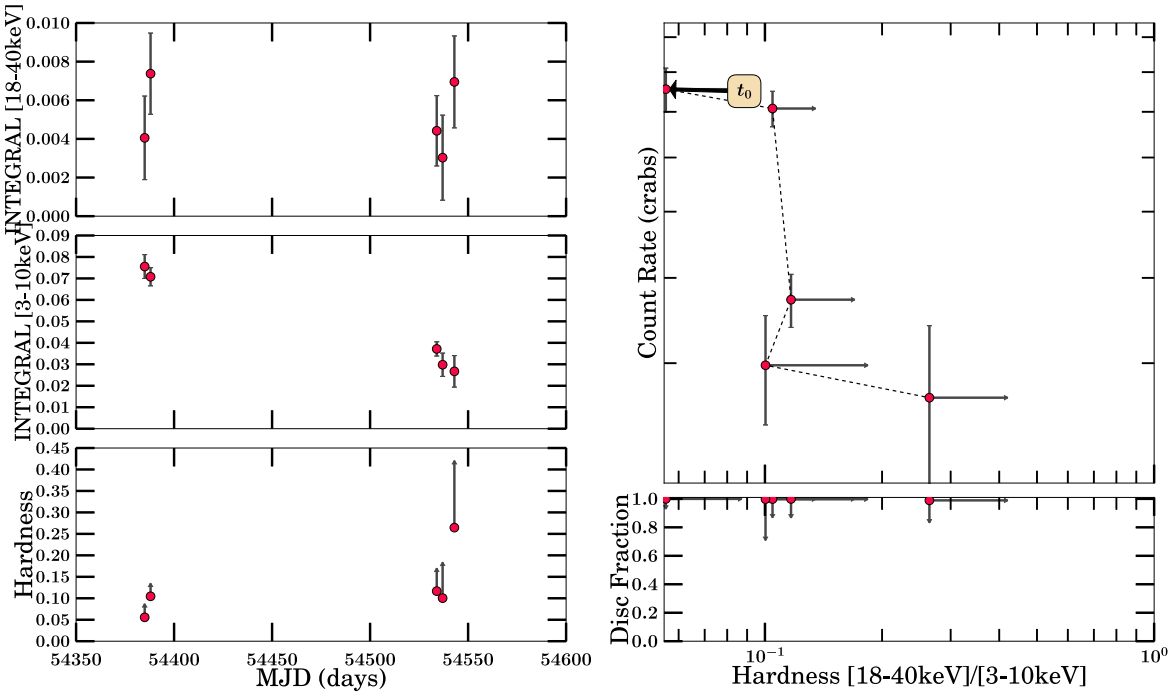

(a) 2007/2008 Outburst Analysis

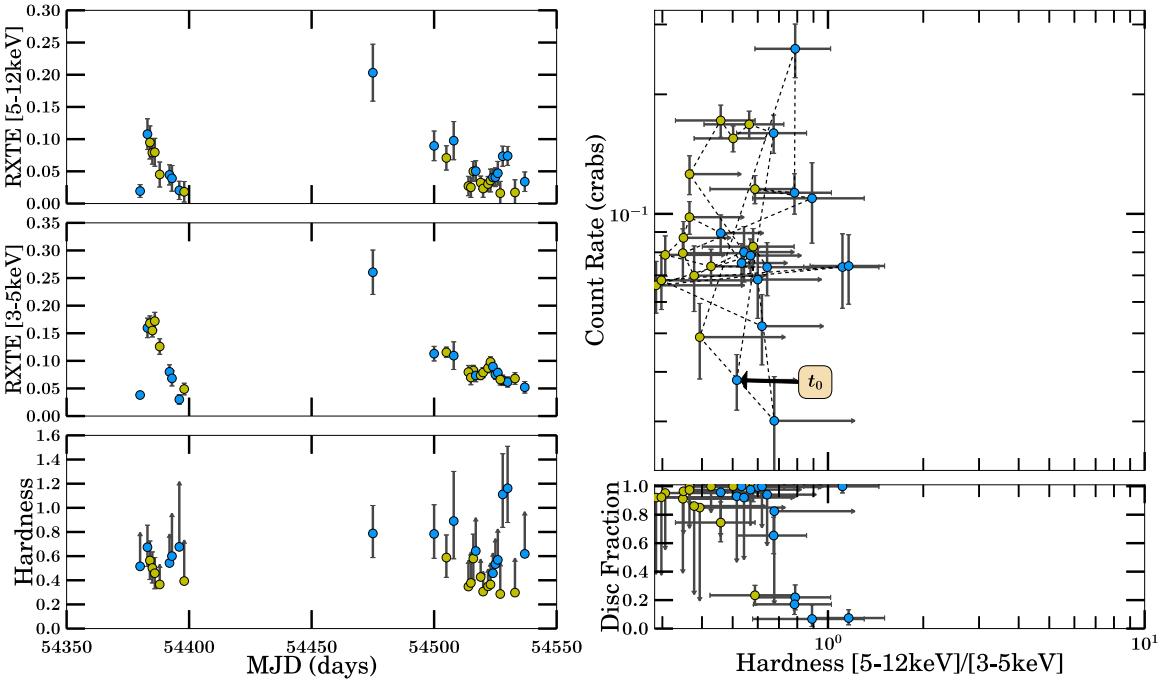

(b) 2007/2008 Outburst Analysis

Figure B.77: SLX 1746−331 Part 2

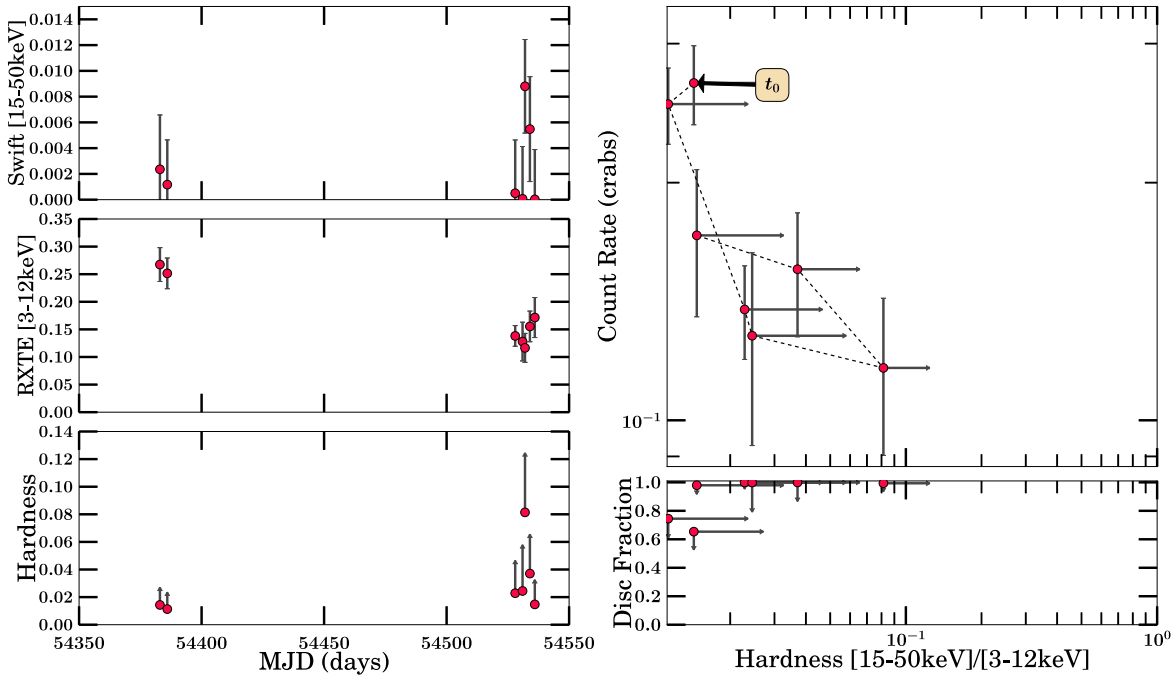

(a) 2007/2008 Outburst Analysis

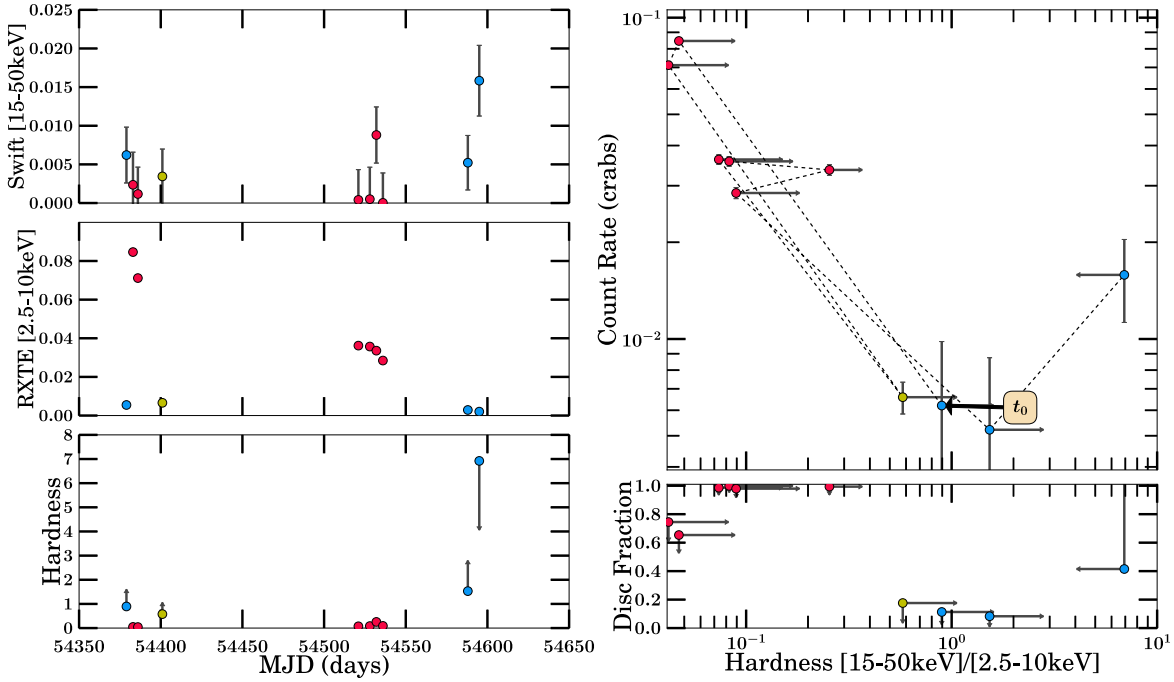

(b) 2007/2008 Outburst Analysis

Figure B.78: SLX 1746−331 Part 3

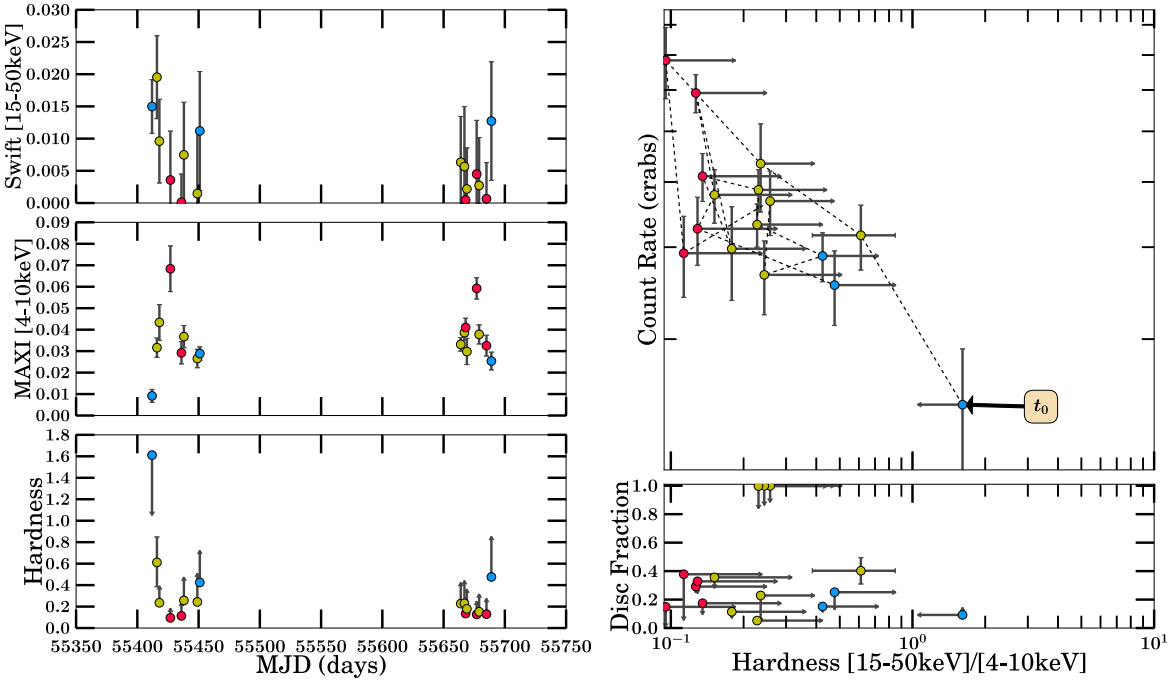

(a) 2010/2011 Outburst Analysis

Figure B.79: SLX 1746−331 Part 4

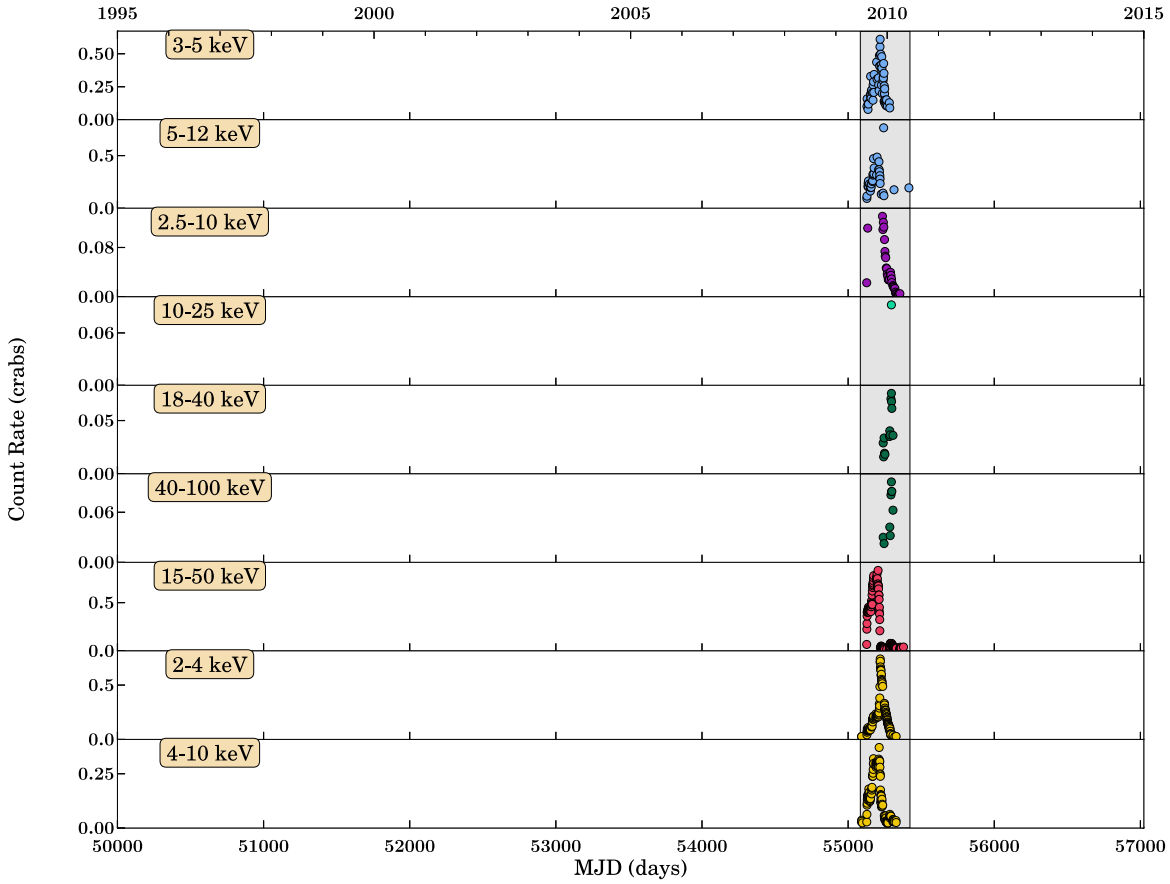

(a) Long-term Light Curve

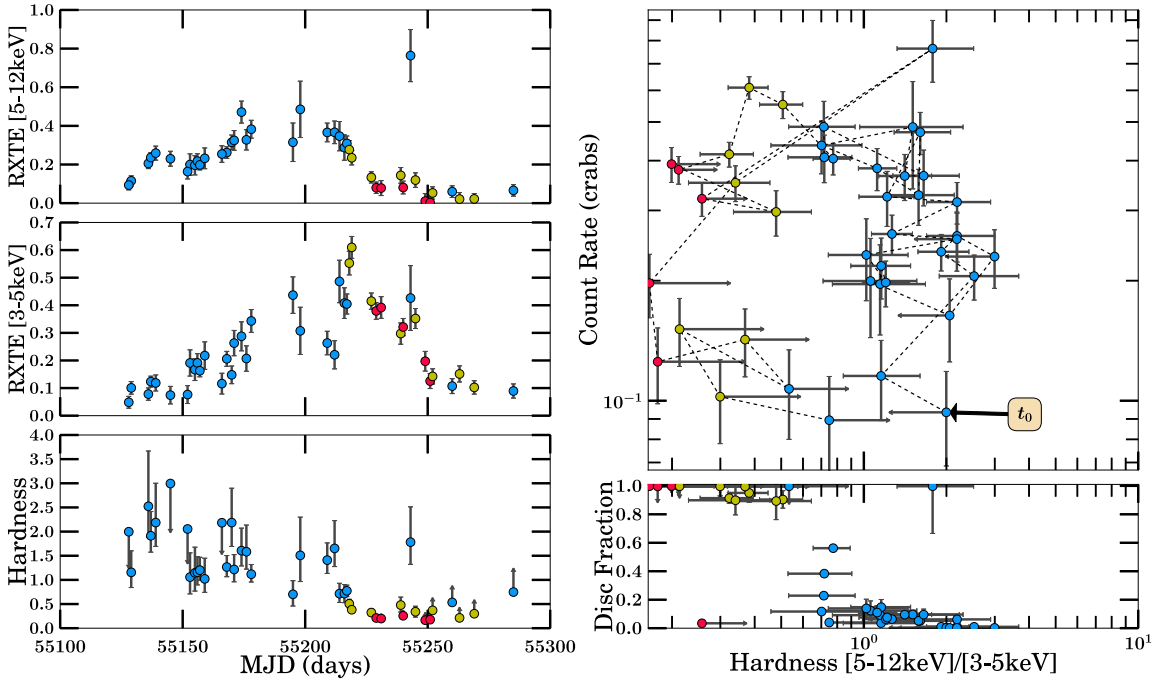

(b) 2009/2010 Outburst Analysis

Figure B.80: XTE J1752−223 Part 1

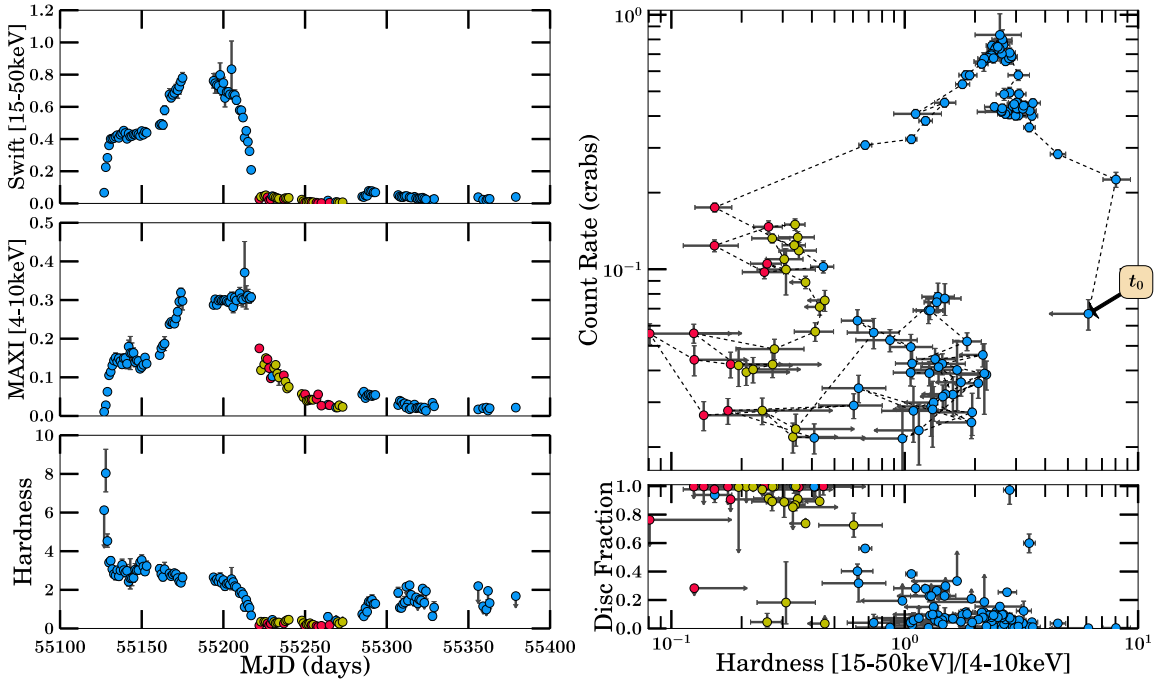

(a) 2009/2010 Outburst Analysis

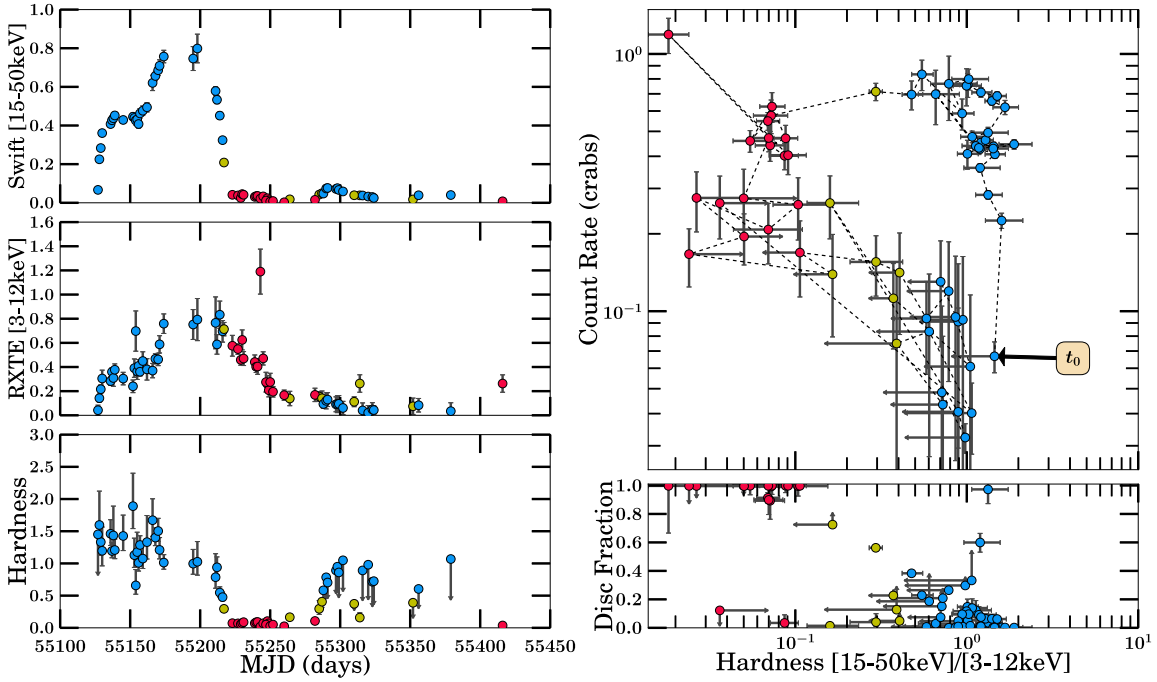

(b) 2009/2010 Outburst Analysis

Figure B.81: XTE J1752−223 Part 2

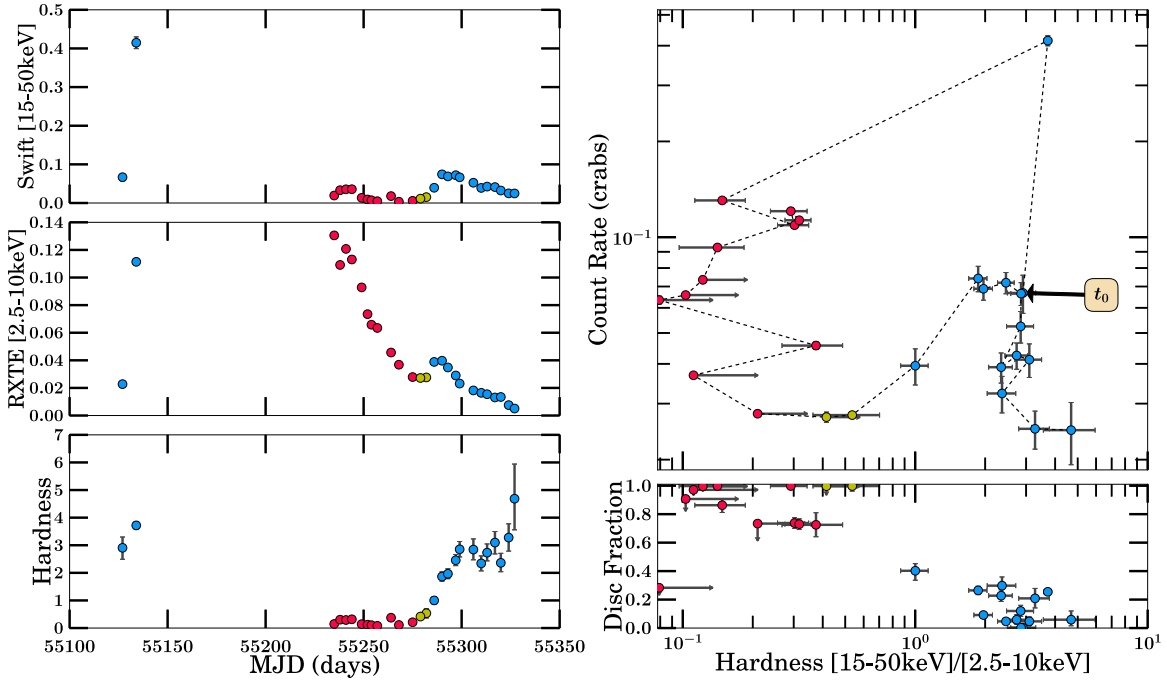

(a) 2009/2010 Outburst Analysis

Figure B.82: XTE J1752−223 Part 3

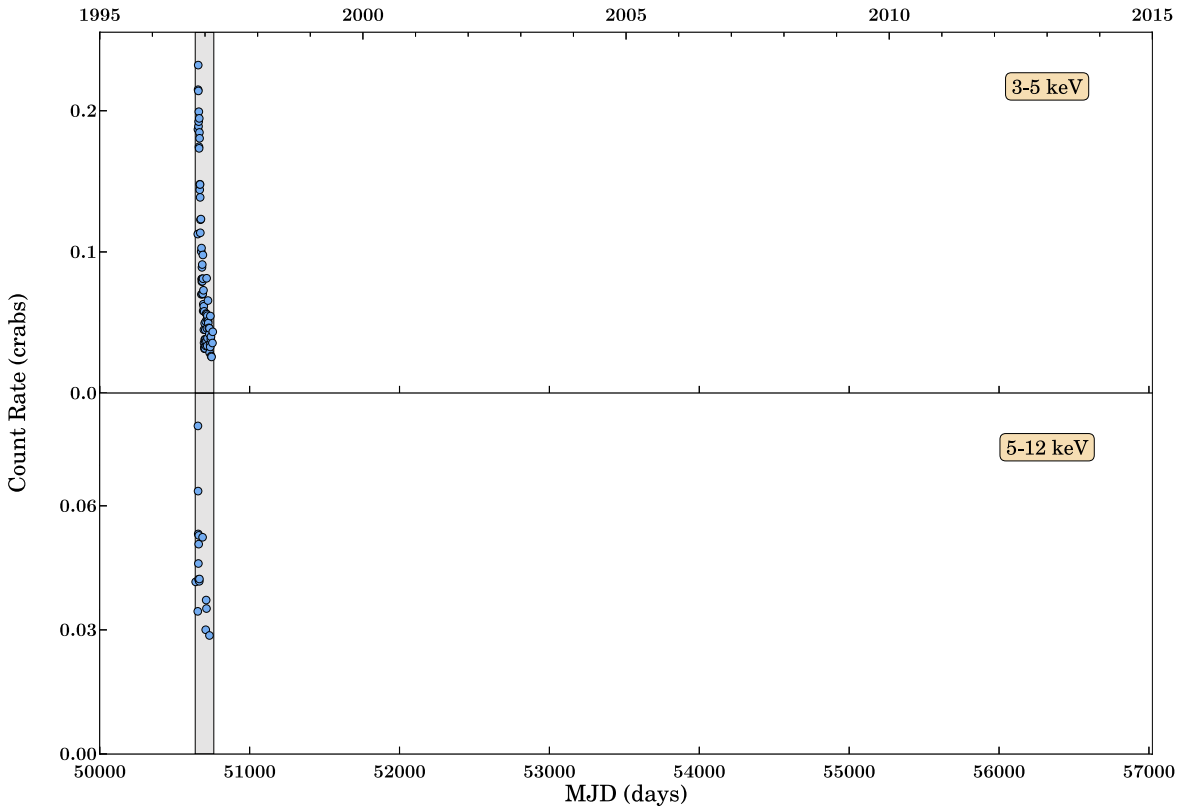

(a) Long-term Light Curve

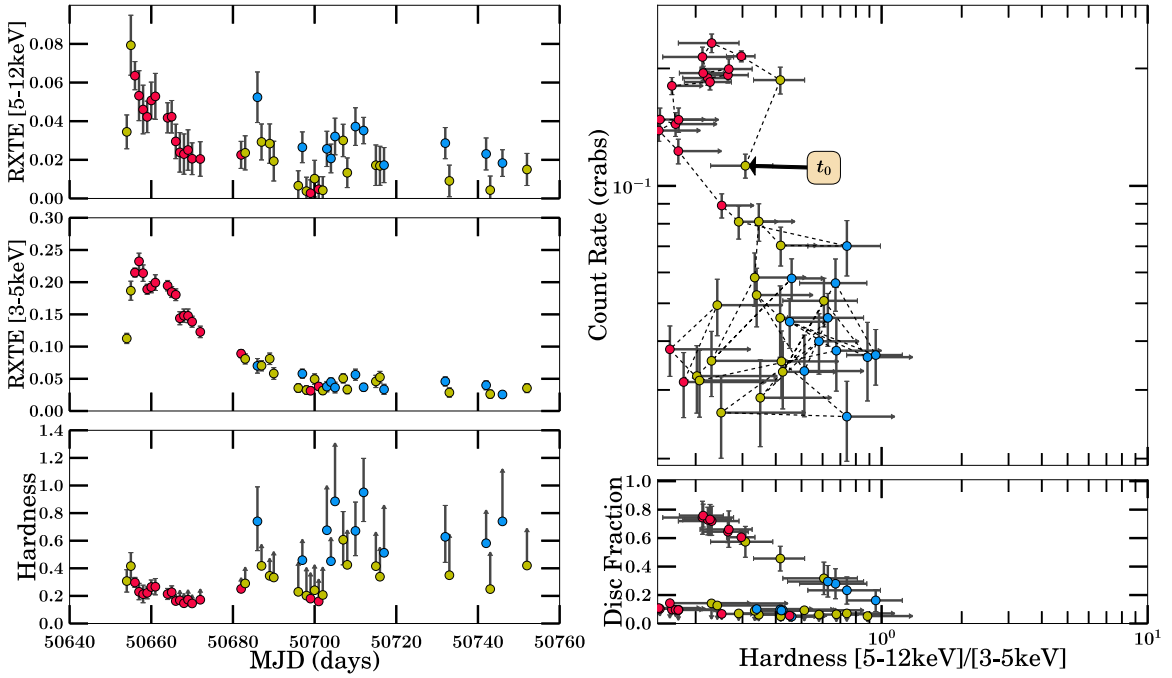

(b) 1997 Outburst Analysis

Figure B.83: XTE J1755−324

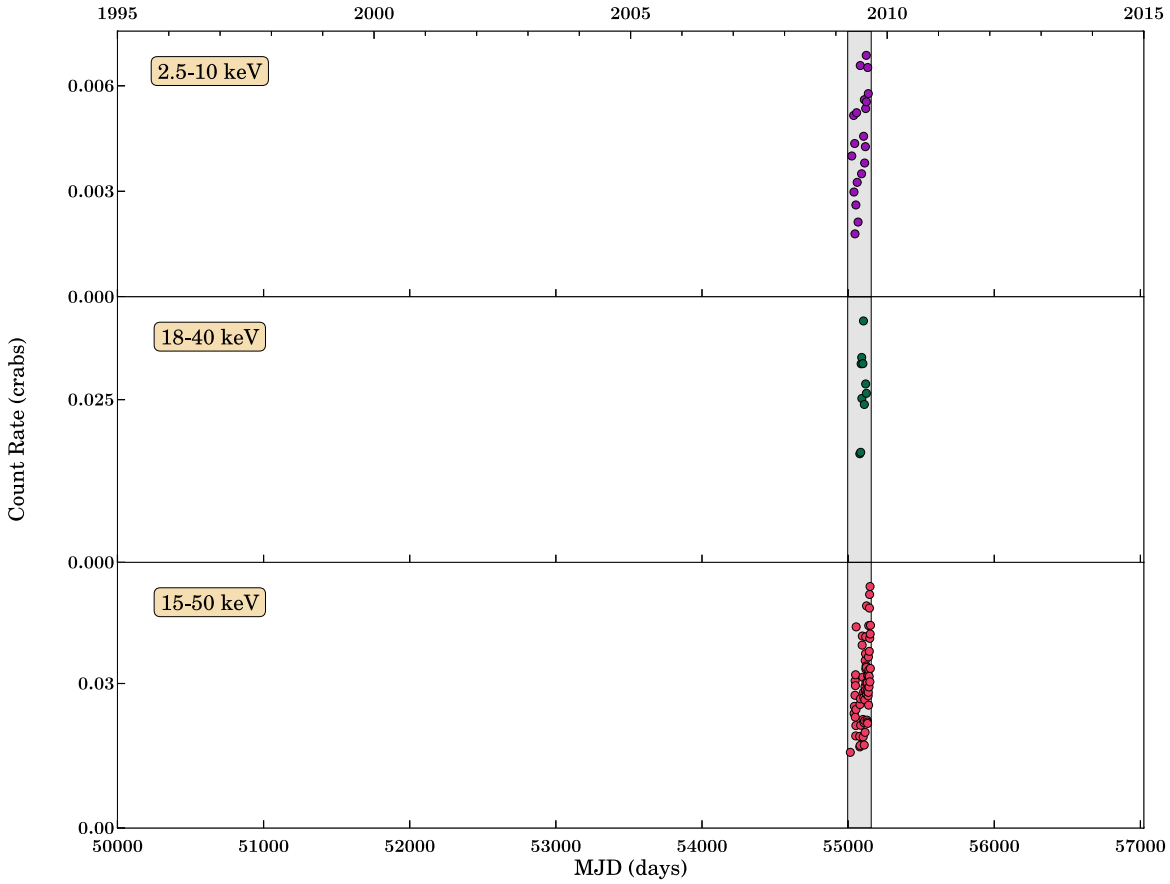

(a) Long-term Light Curve

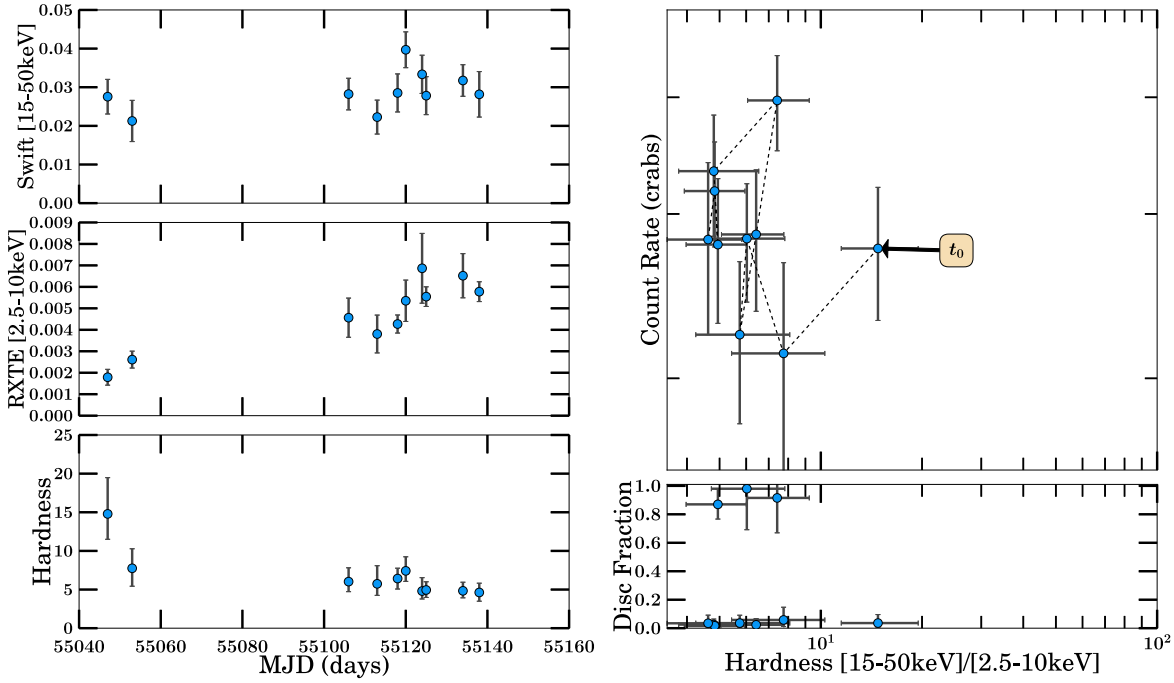

(b) 2009 Outburst Analysis

Figure B.84: IGR J17586−2129

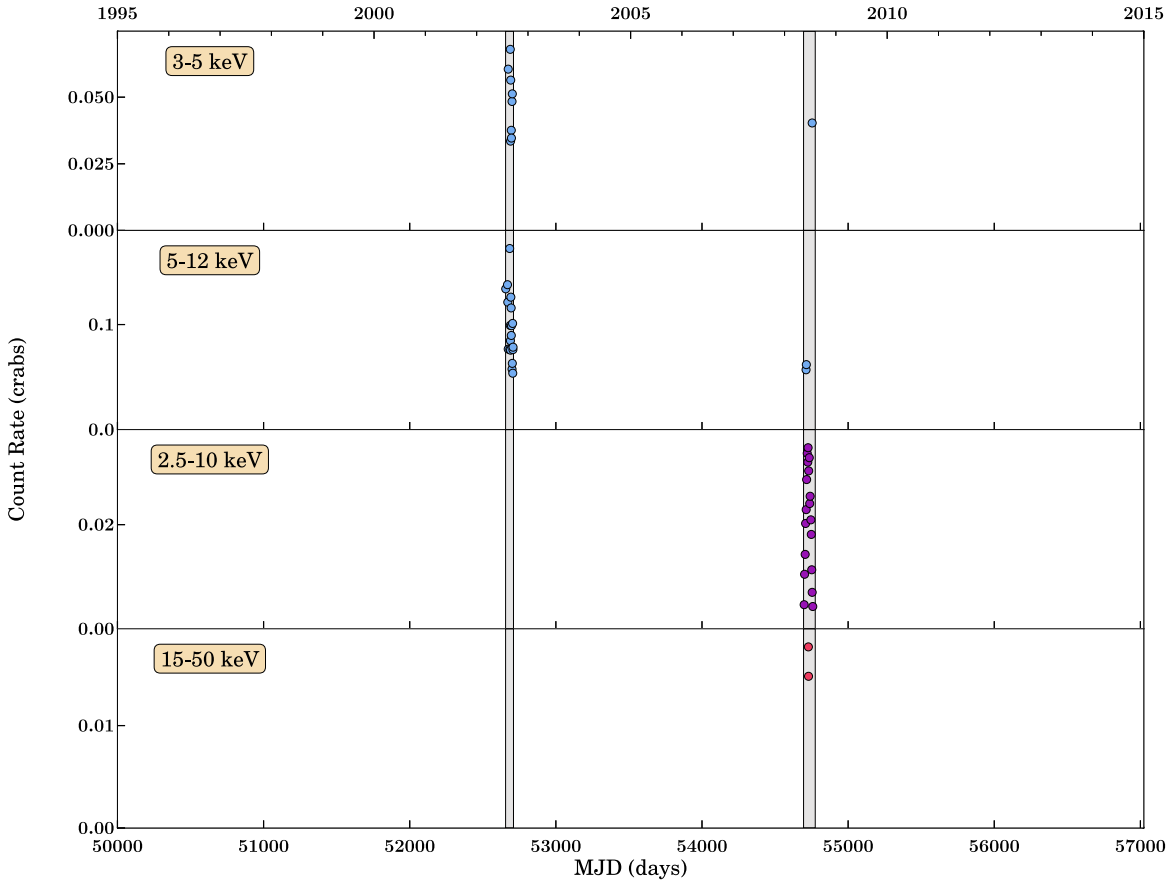

(a) Long-term Light Curve

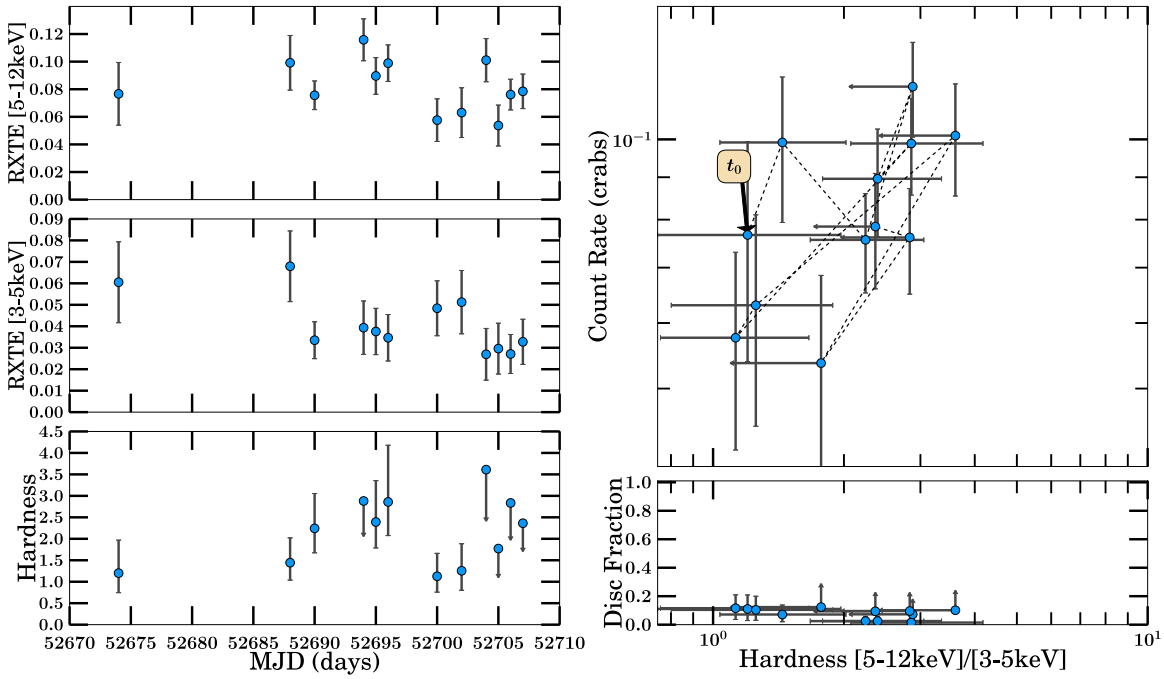

(b) 2003 Outburst Analysis

Figure B.85: XTE J1812−182 Part 1

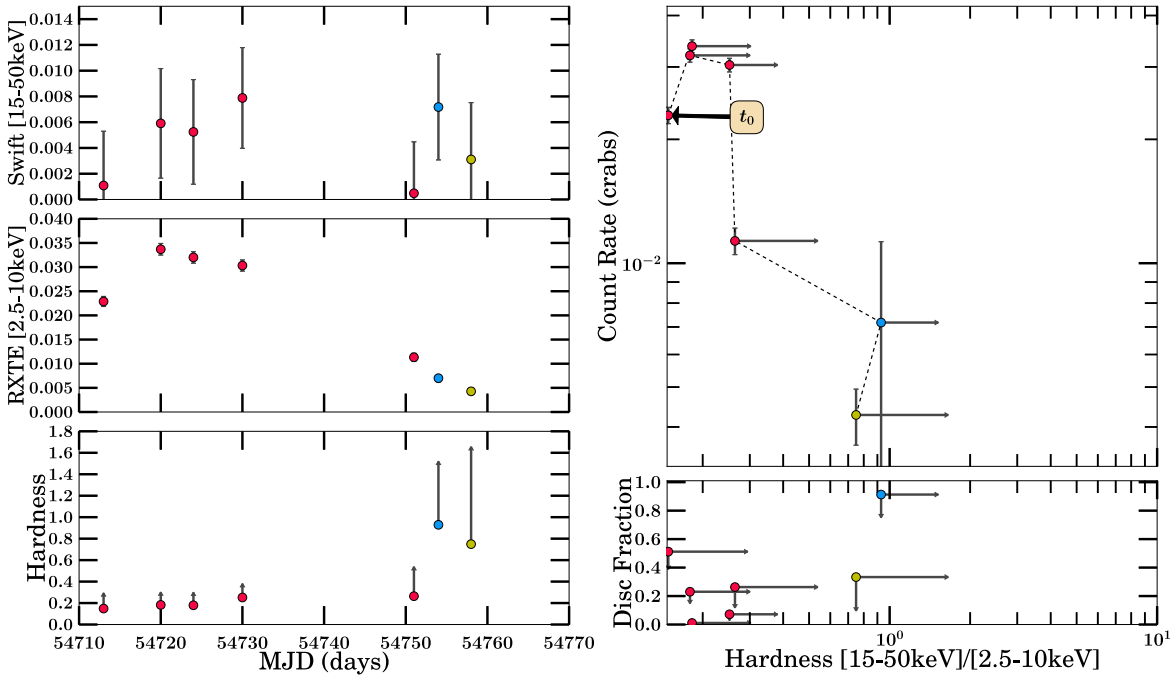

(a) 2008 Outburst Analysis

Figure B.86: XTE J1812−182 Part 2

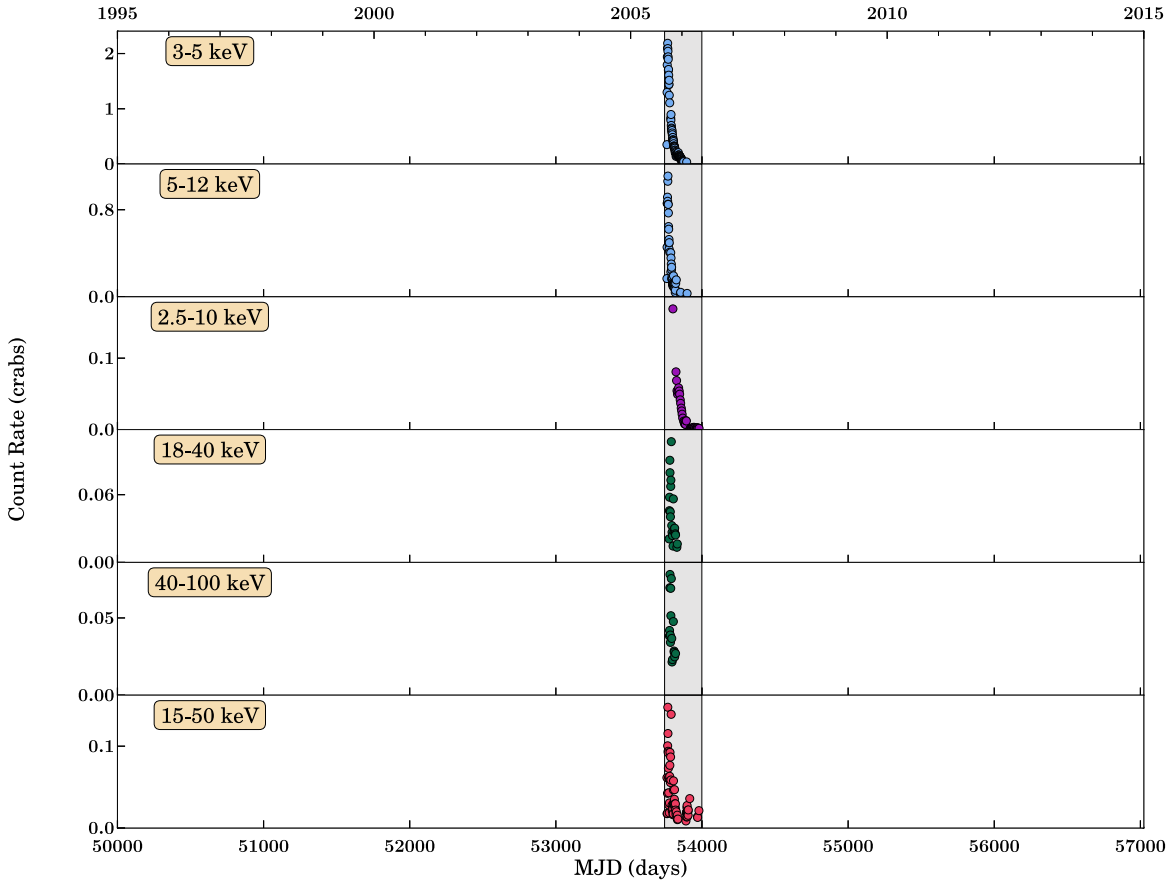

(a) Long-term Light Curve

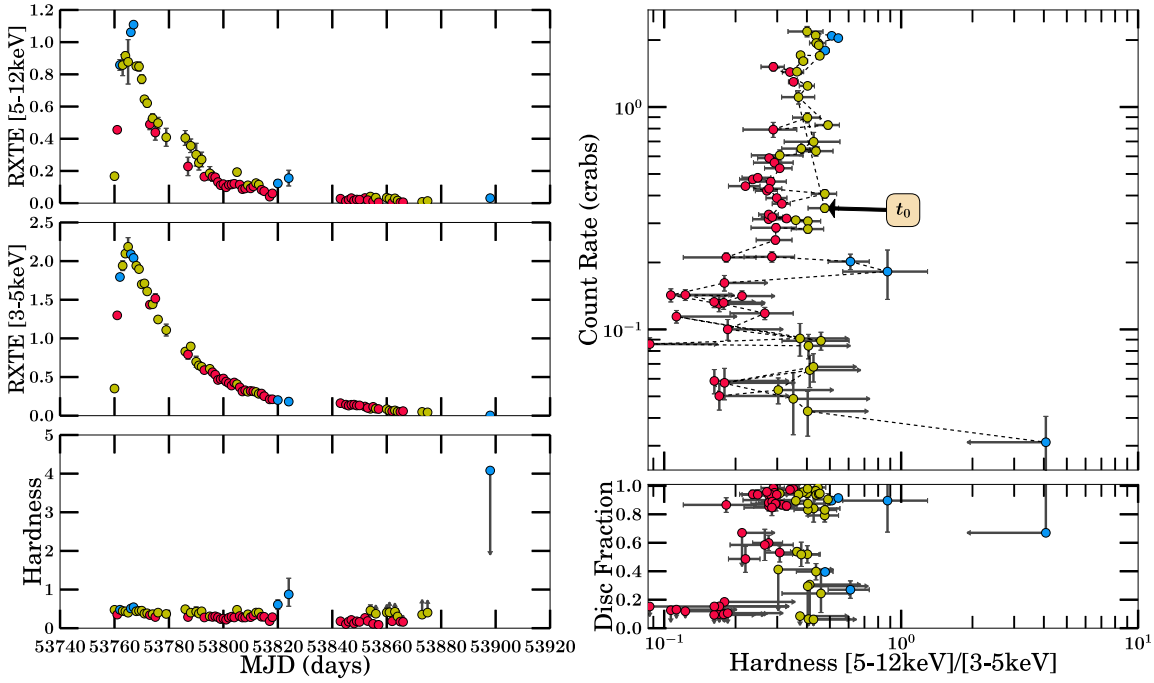

(b) 2006 Outburst Analysis

Figure B.87: XTE J1817−330 Part 1

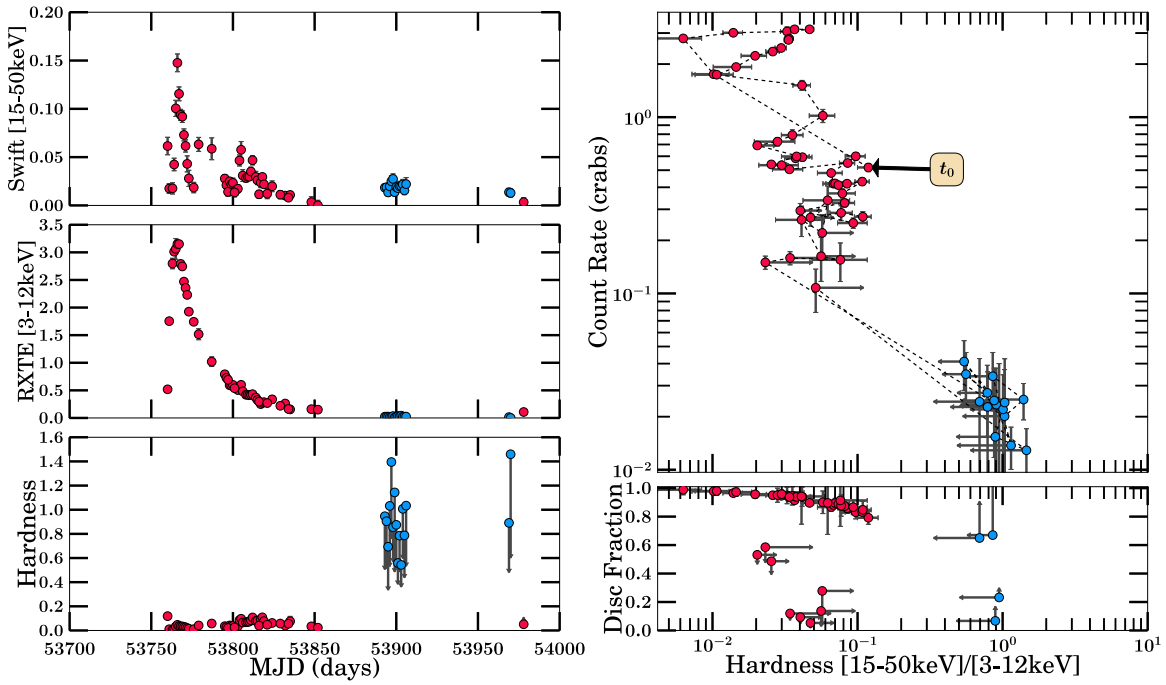

(a) 2006 Outburst Analysis

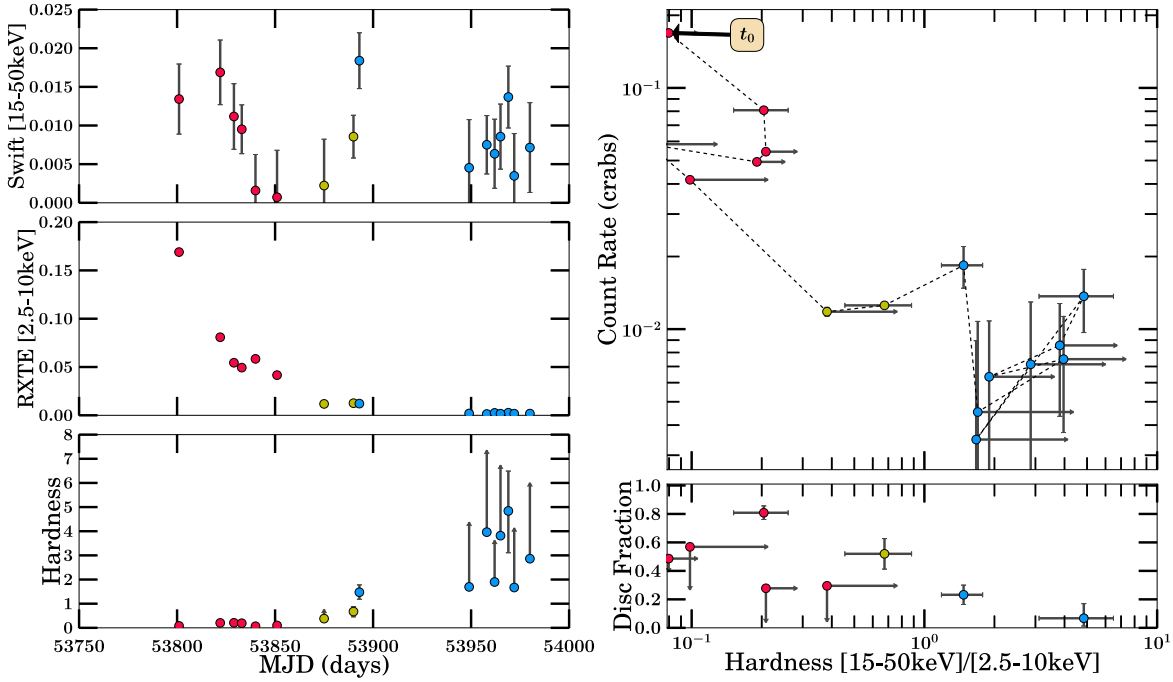

(b) 2006 Outburst Analysis

Figure B.88: XTE J1817−330 Part 2

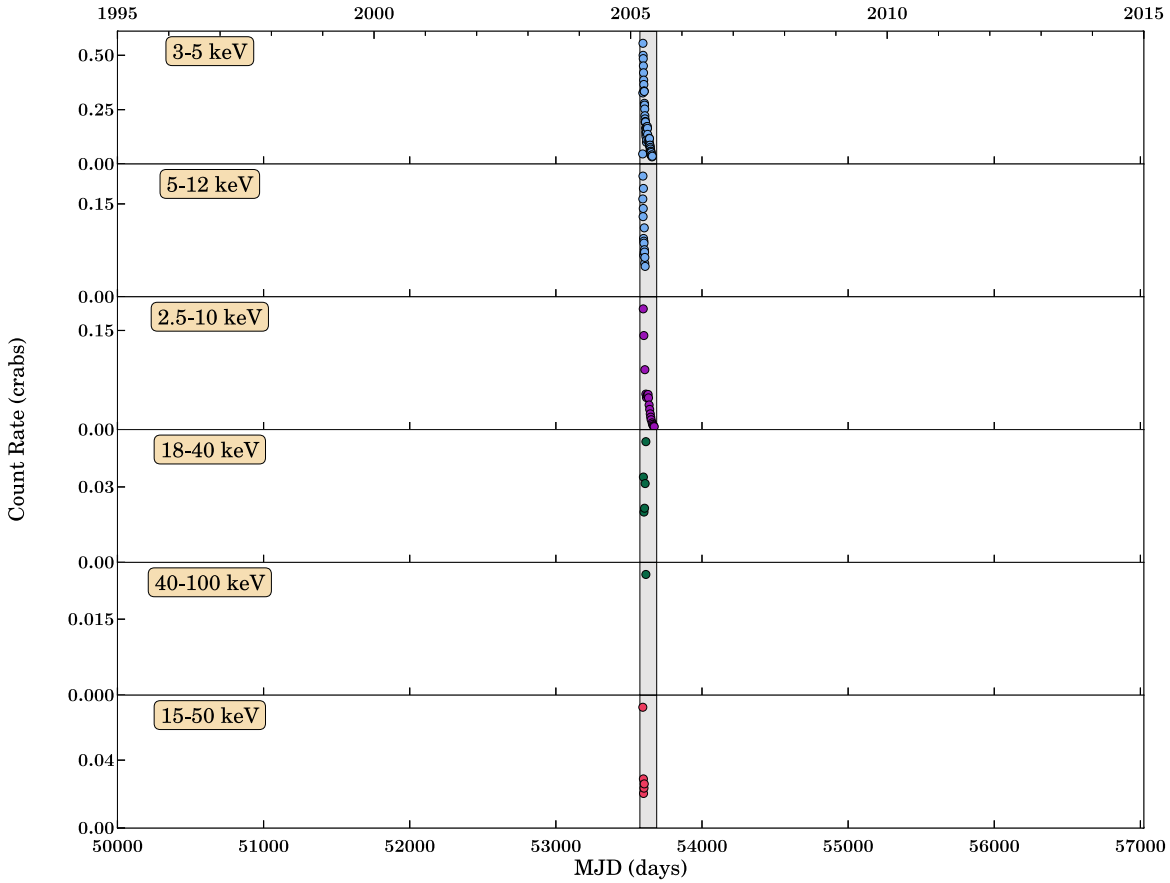

(a) Long-term Light Curve

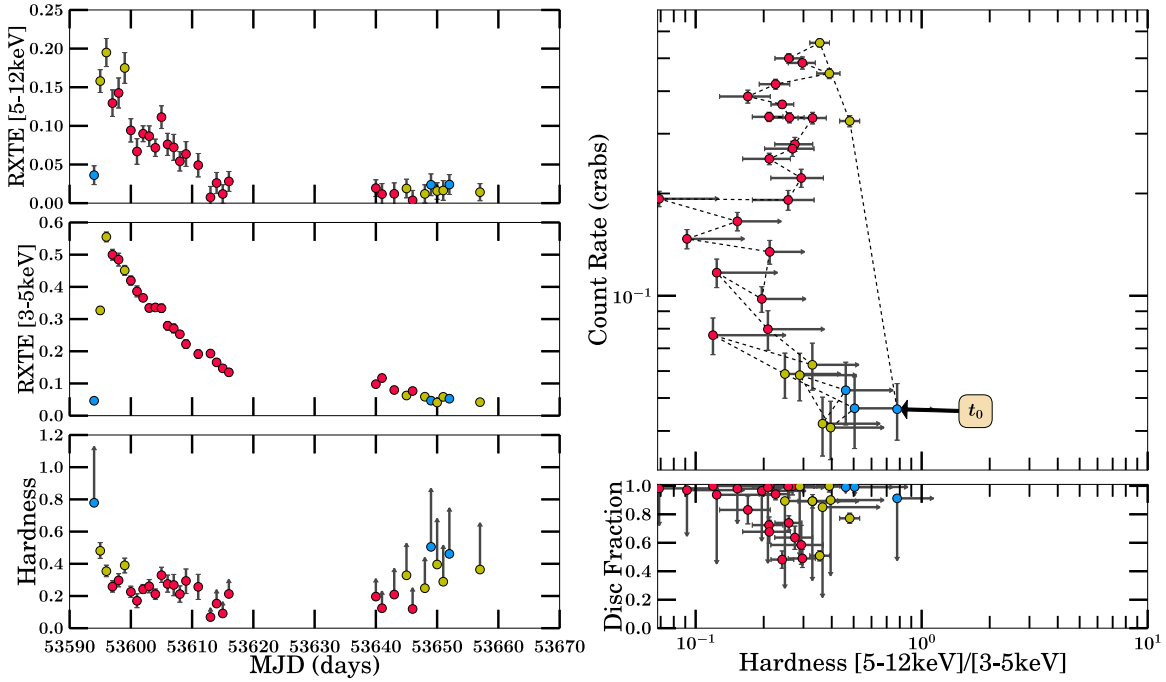

(b) 2005 Outburst Analysis

Figure B.89: XTE J1818−245 Part 1

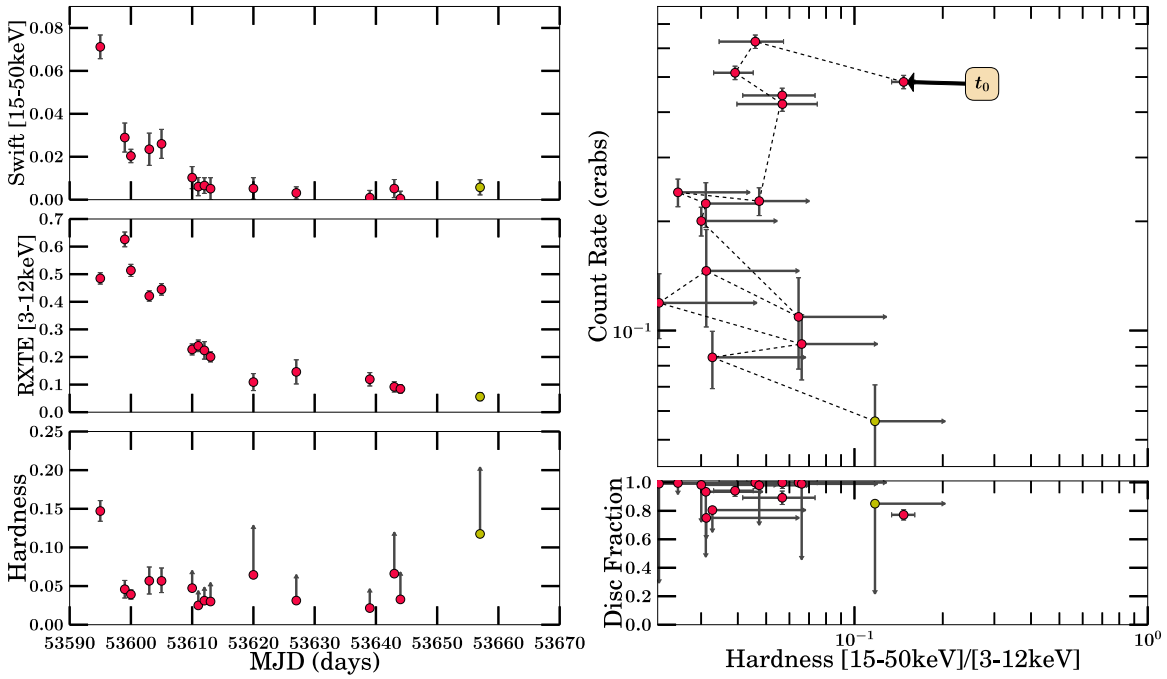

(a) 2005 Outburst Analysis

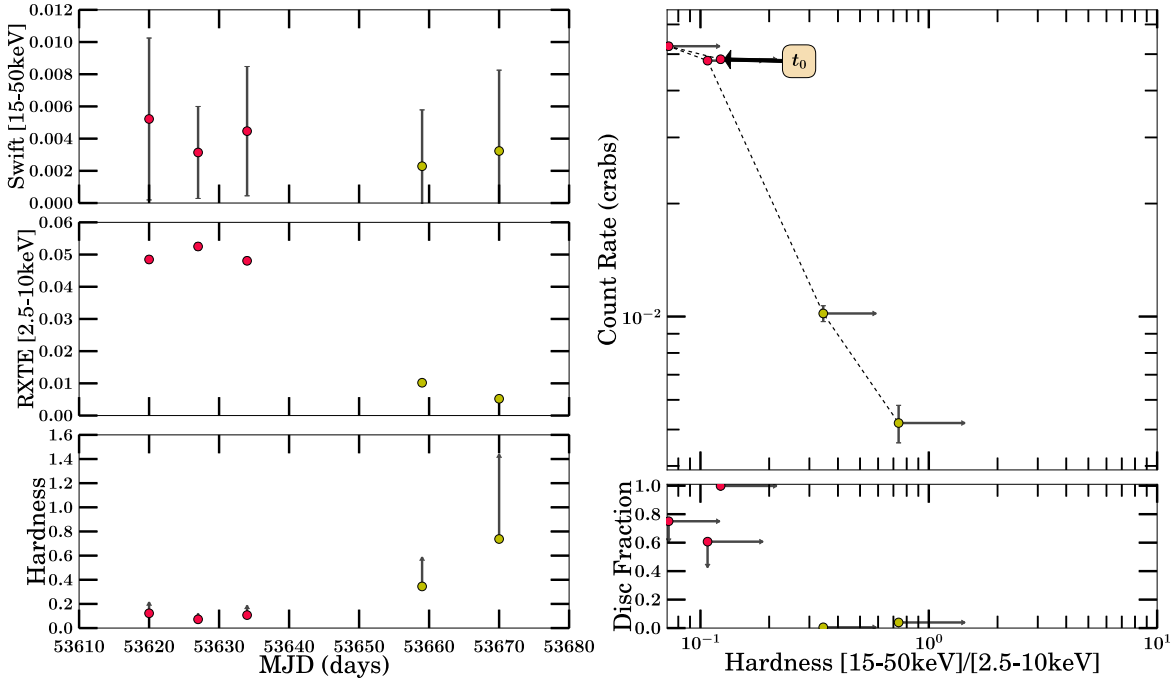

(b) 2005 Outburst Analysis

Figure B.90: XTE J1818−245 Part 2

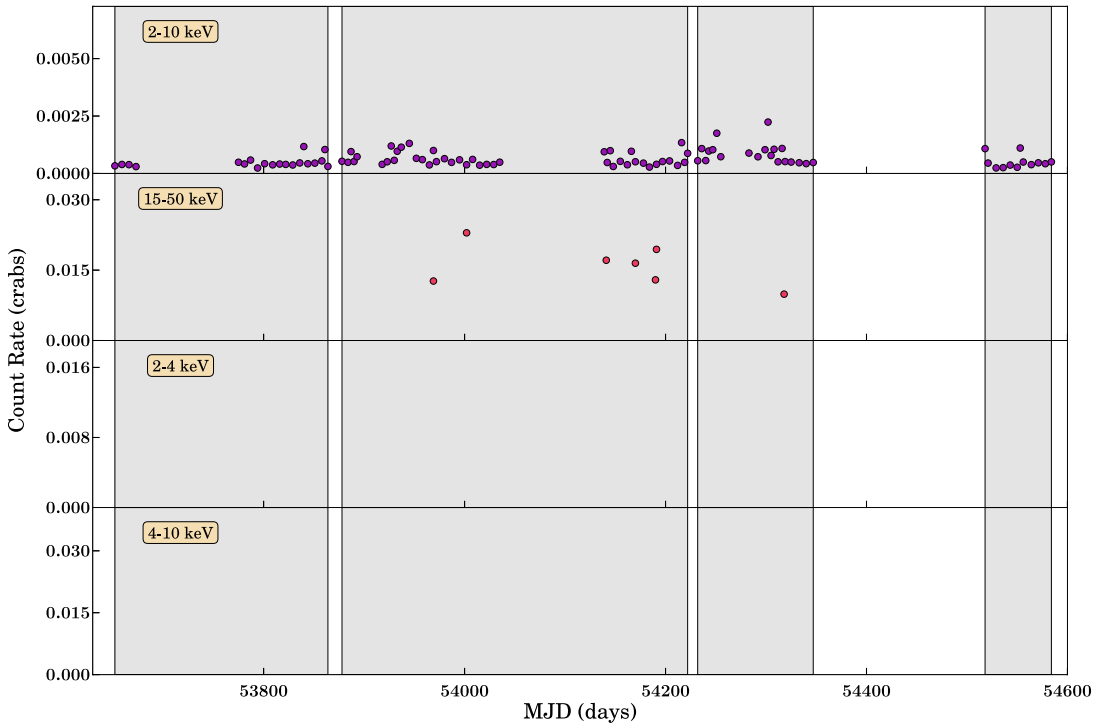

(a) Long-term Light Curve 1

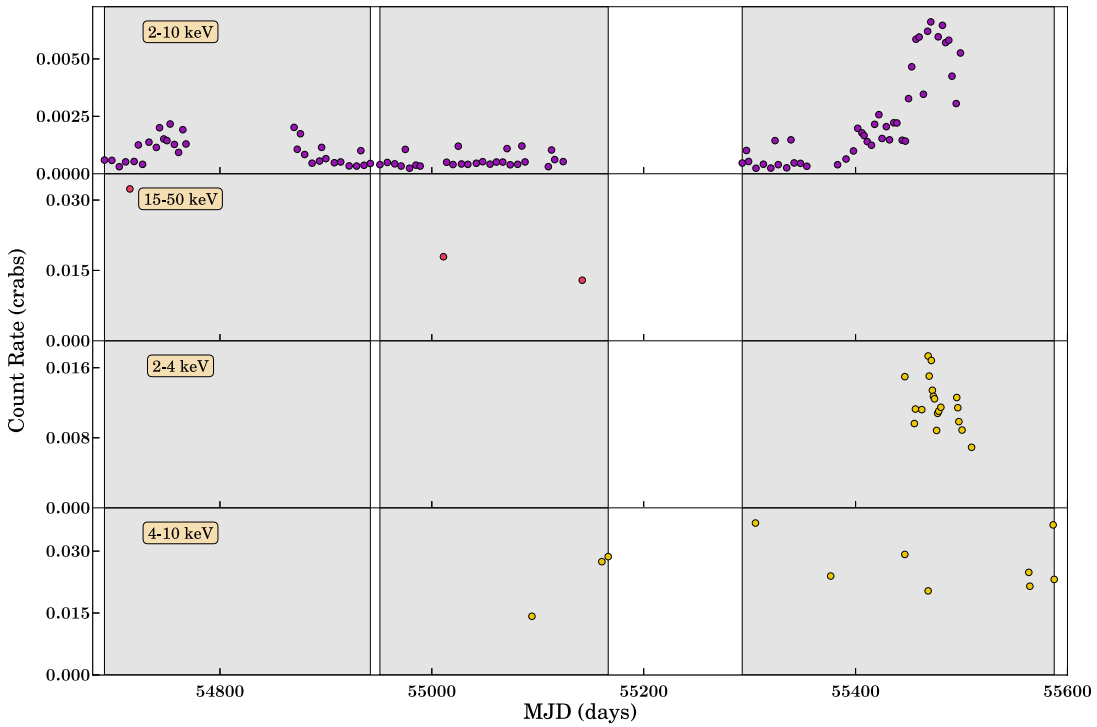

(b) Long-term Light Curve 2

Figure B.91: SAX J1819.3−2525 Part 1: Note the long term light curve has been zoomed in and split into two pieces for clarity.

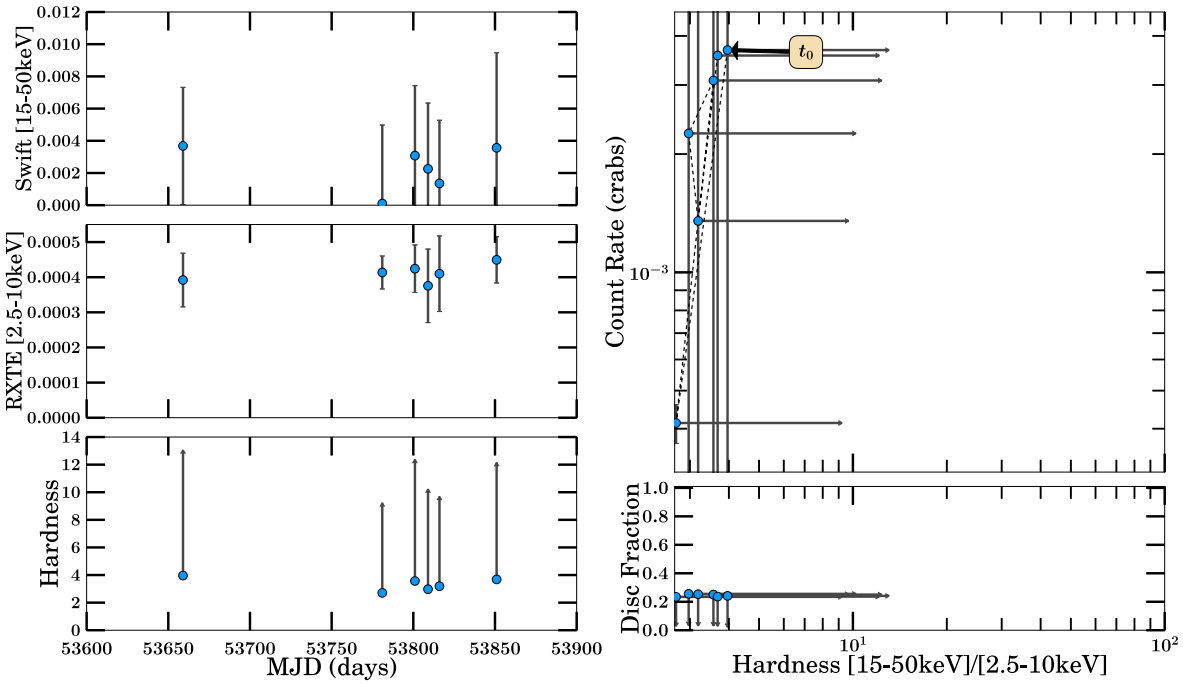

(a) 2005/2006 Outburst Analysis

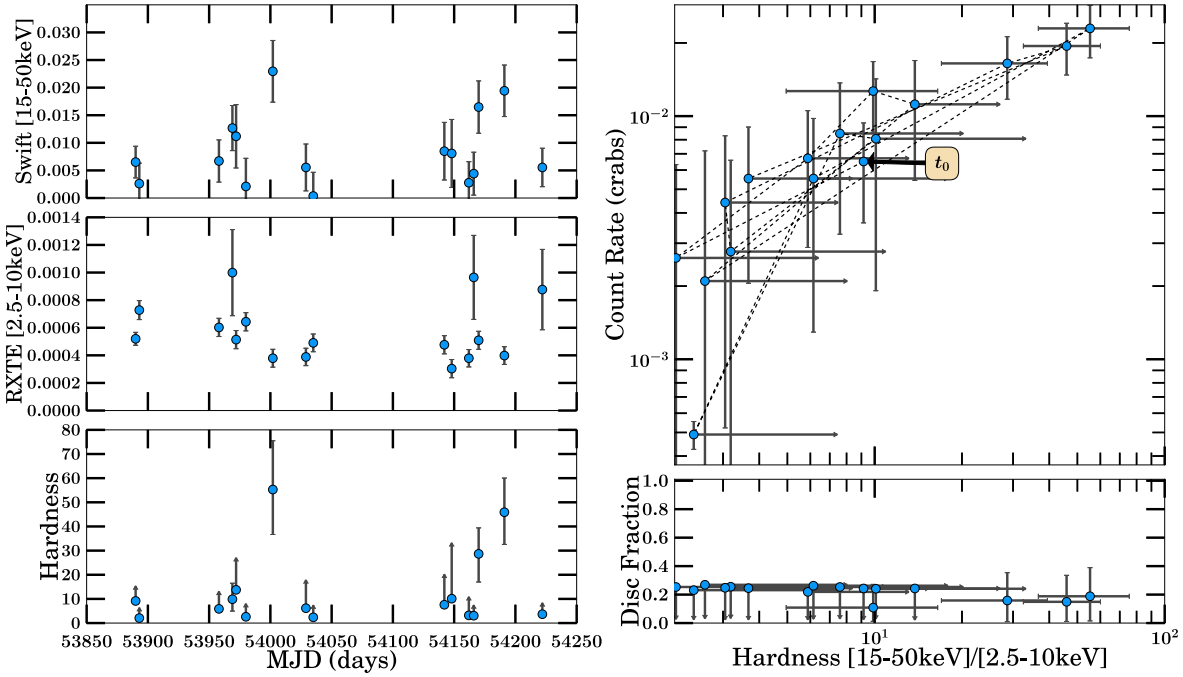

(b) 2006/2007 Outburst Analysis

Figure B.92: SAX J1819.3−2525 Part 2

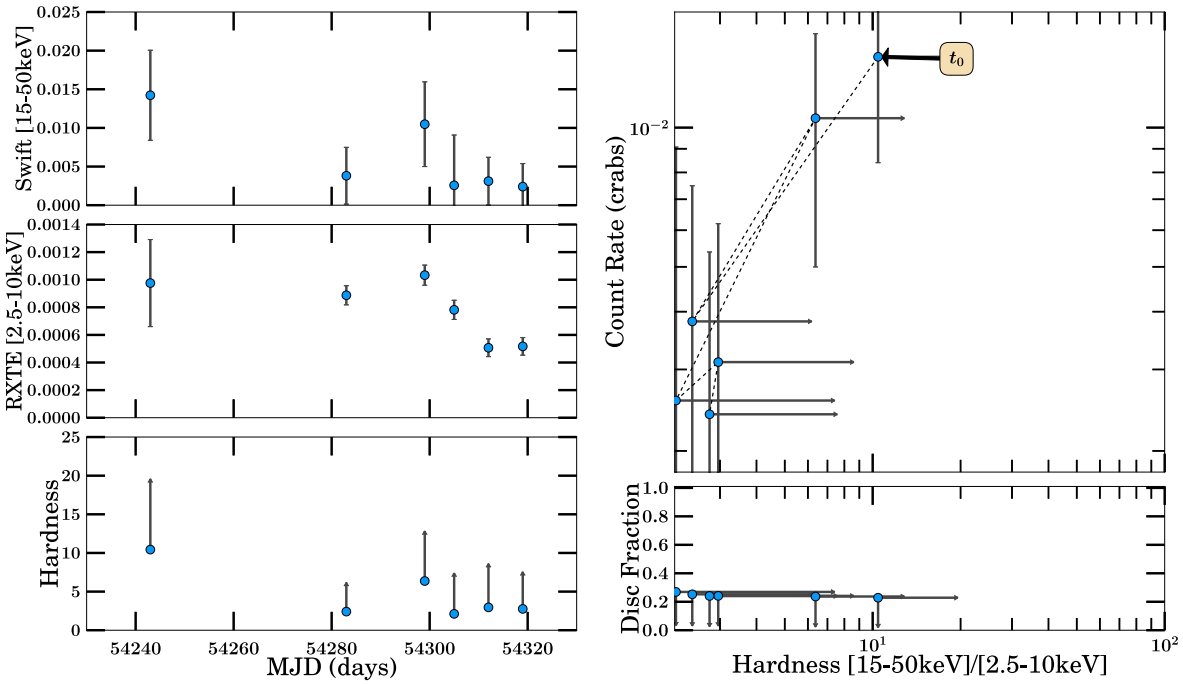

(a) 2007 Outburst Analysis

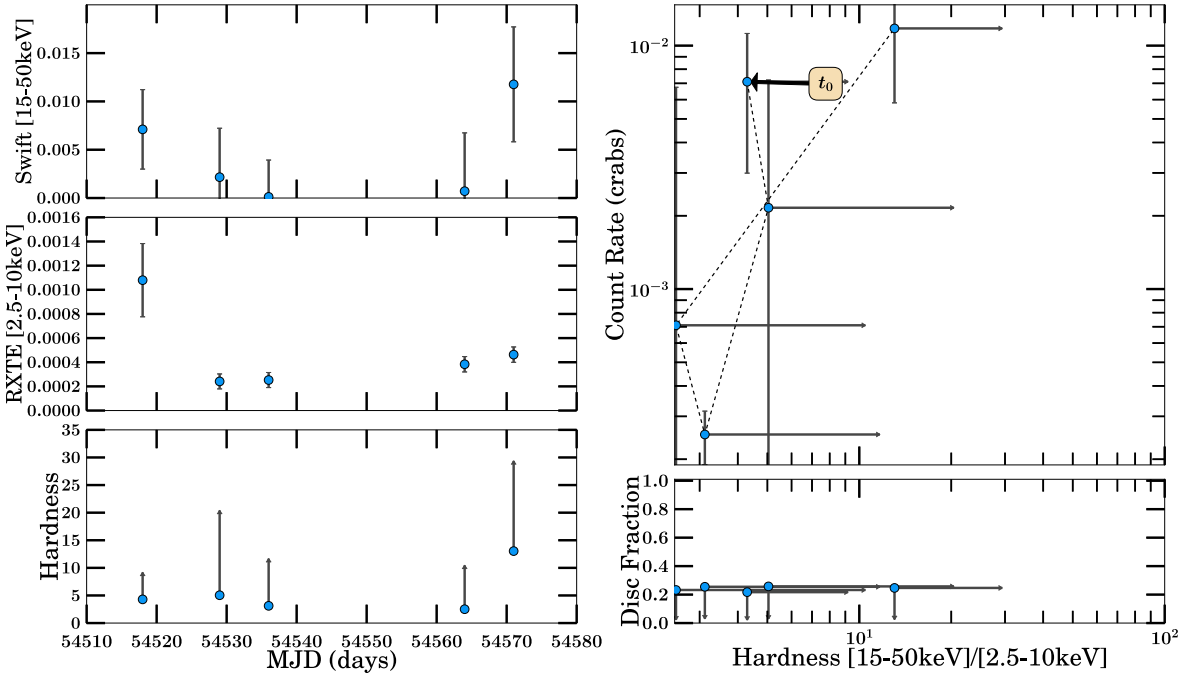

(b) 2008a Outburst Analysis

Figure B.93: SAX J1819.3−2525 Part 3

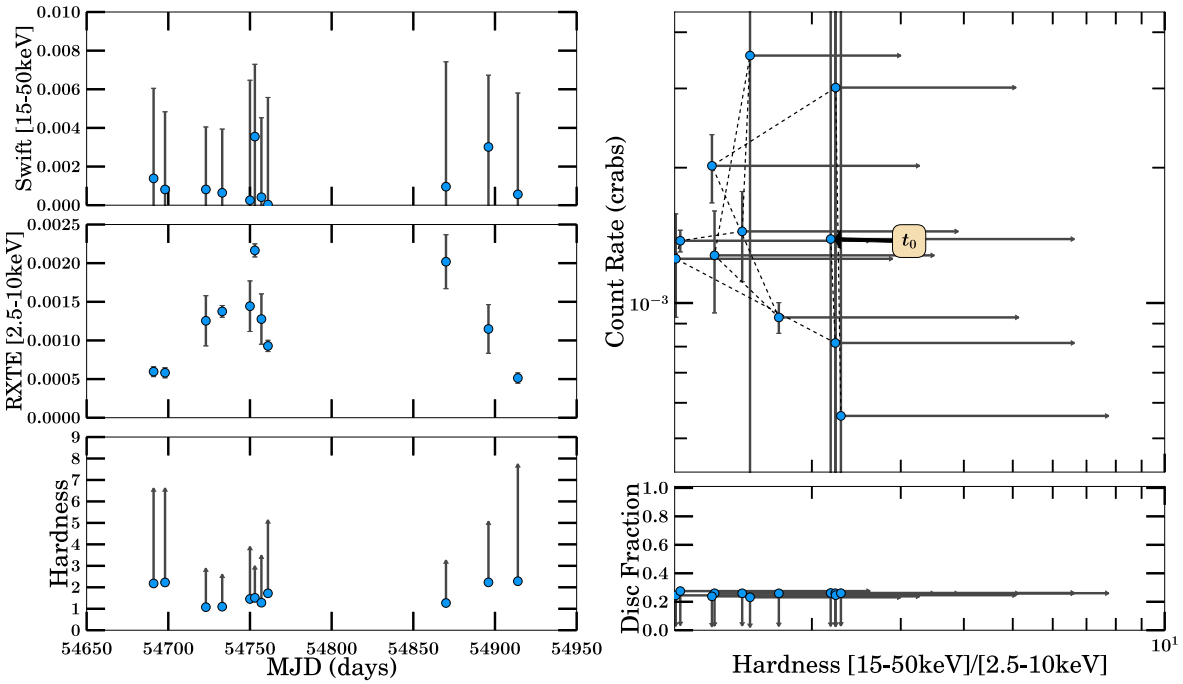

(a) 2008/2009 Outburst Analysis

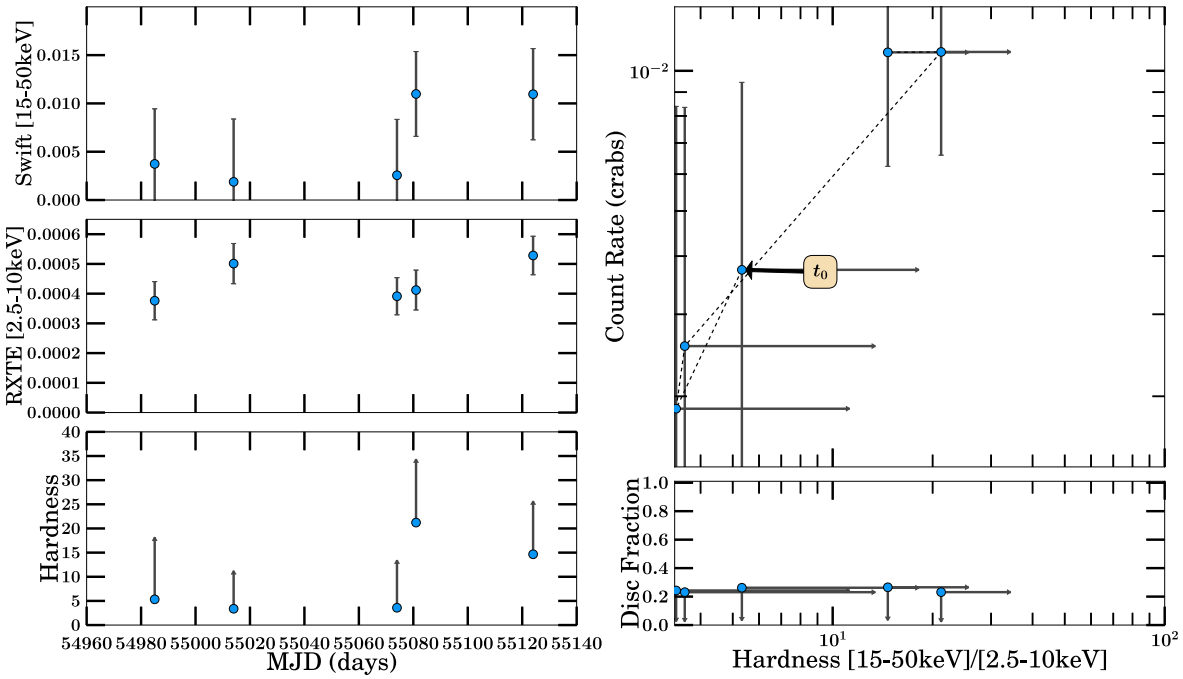

(b) 2009 Outburst Analysis

Figure B.94: SAX J1819.3−2525 Part 4

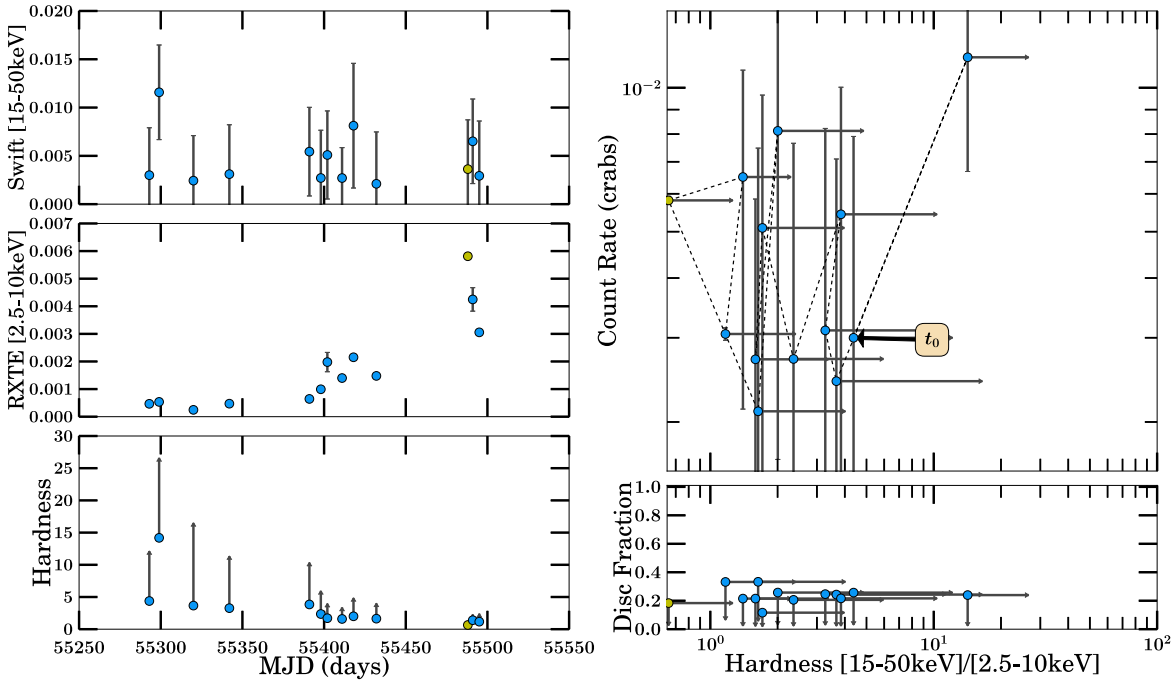

(a) 2010/2011 Outburst Analysis

Figure B.95: SAX J1819.3−2525 Part 5

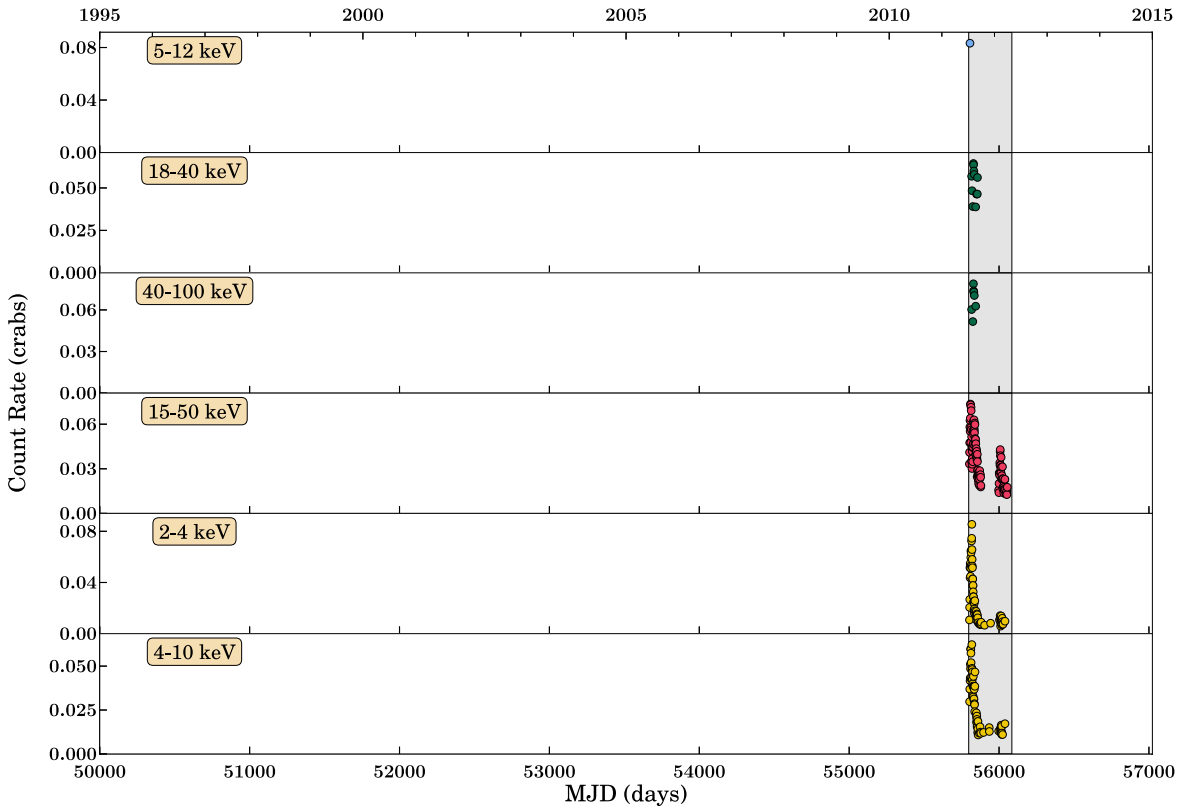

(a) Long-term Light Curve

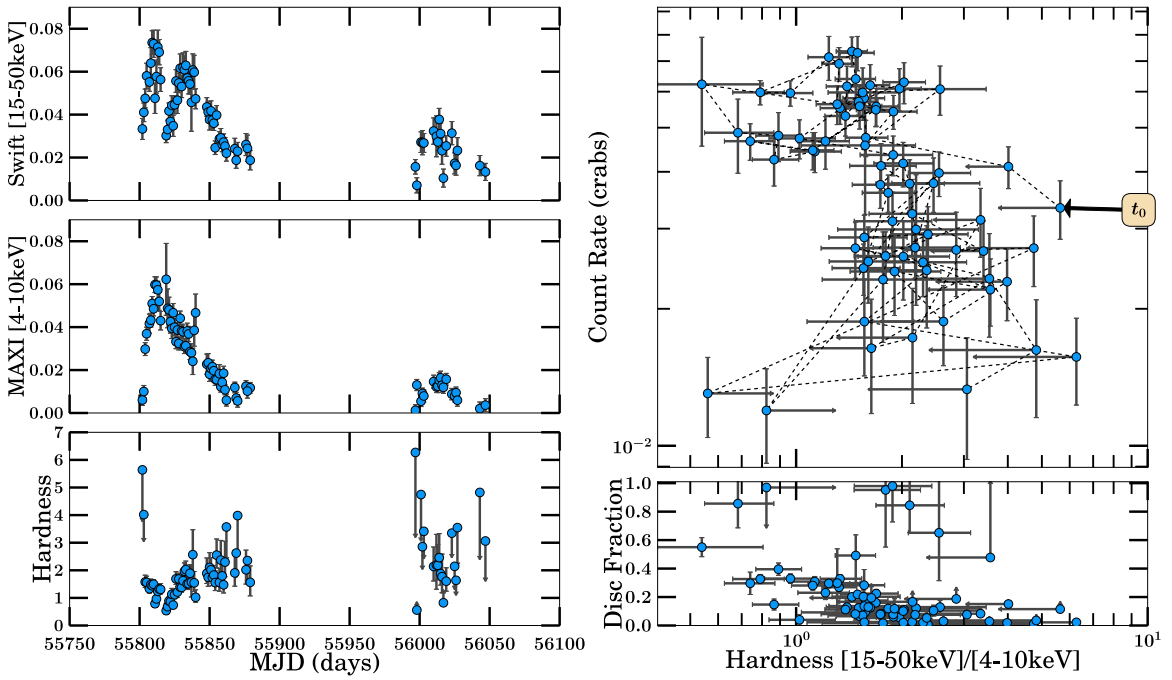

(b) 2011/2012 Outburst Analysis

Figure B.96: MAXI J1836−194

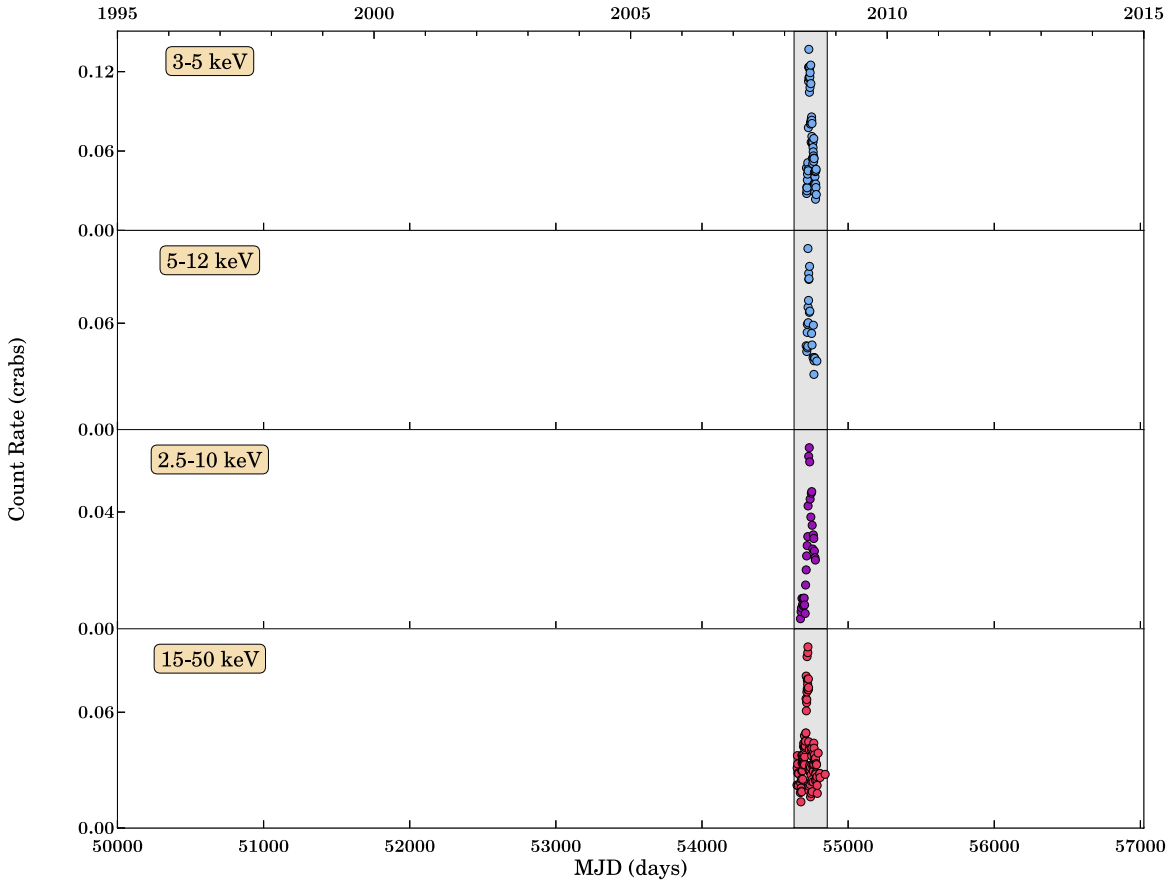

(a) Long-term Light Curve

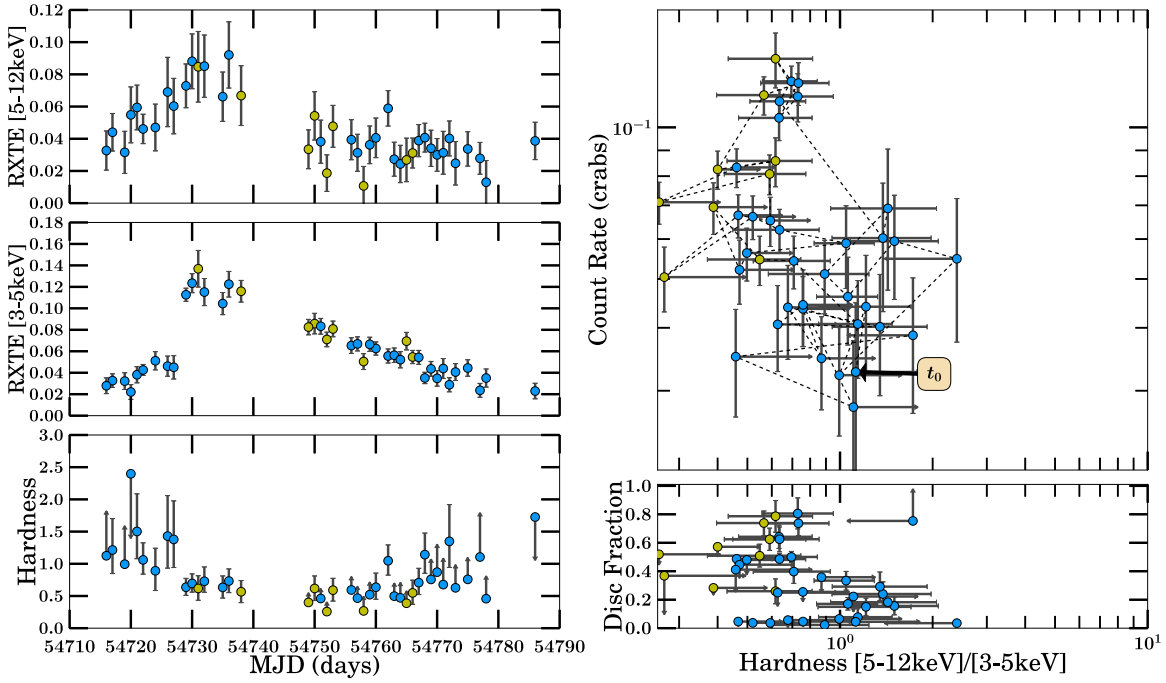

(b) 2008/2009 Outburst Analysis

Figure B.97: SWIFT J1842.5−1124 Part 1

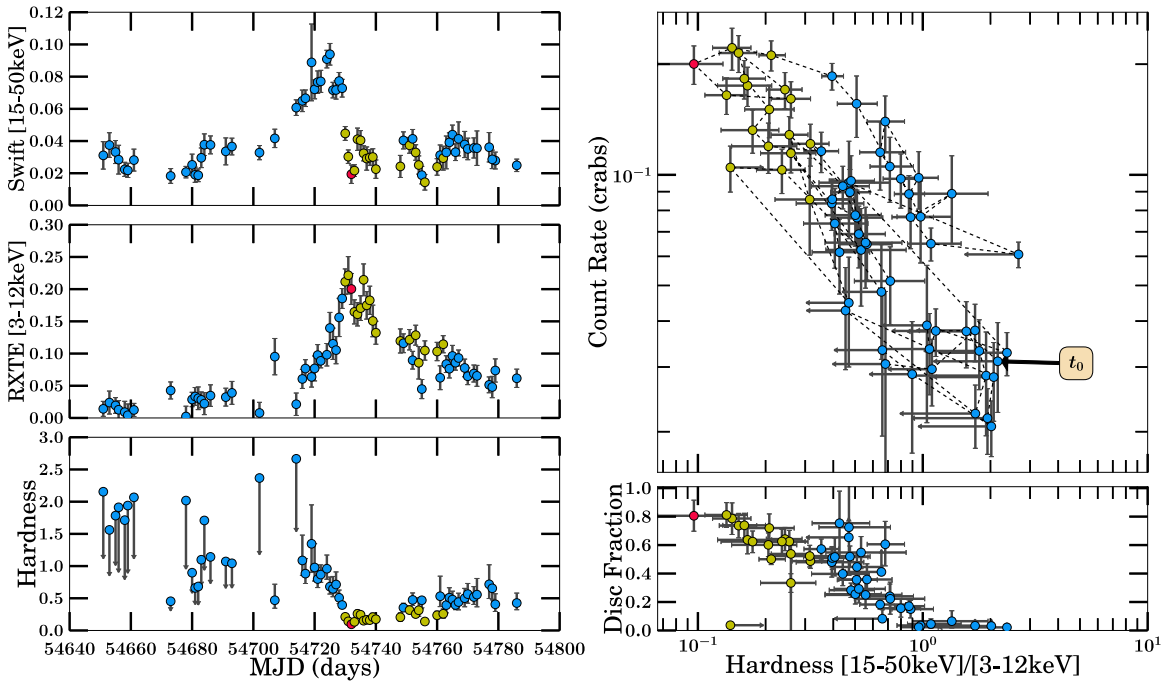

(a) 2008/2009 Outburst Analysis

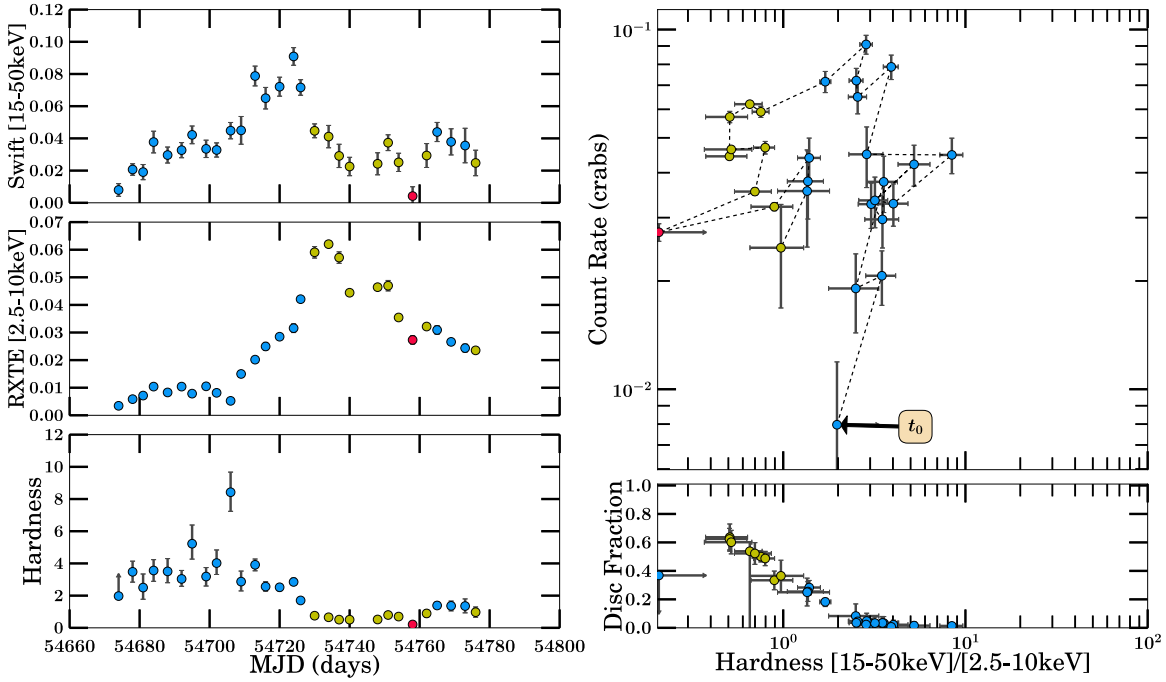

(b) 2008/2009 Outburst Analysis

Figure B.98: SWIFT J1842.5−1124 Part 2

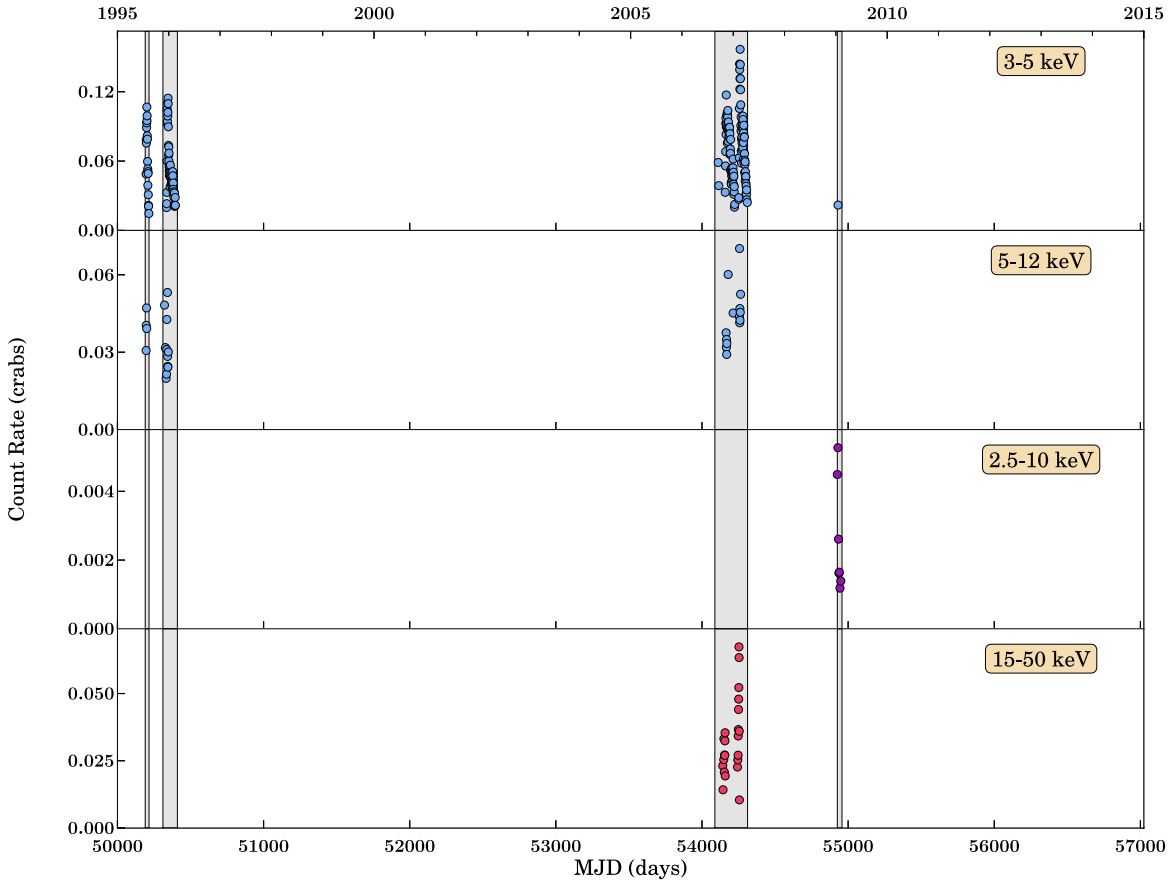

(a) Long-term Light Curve

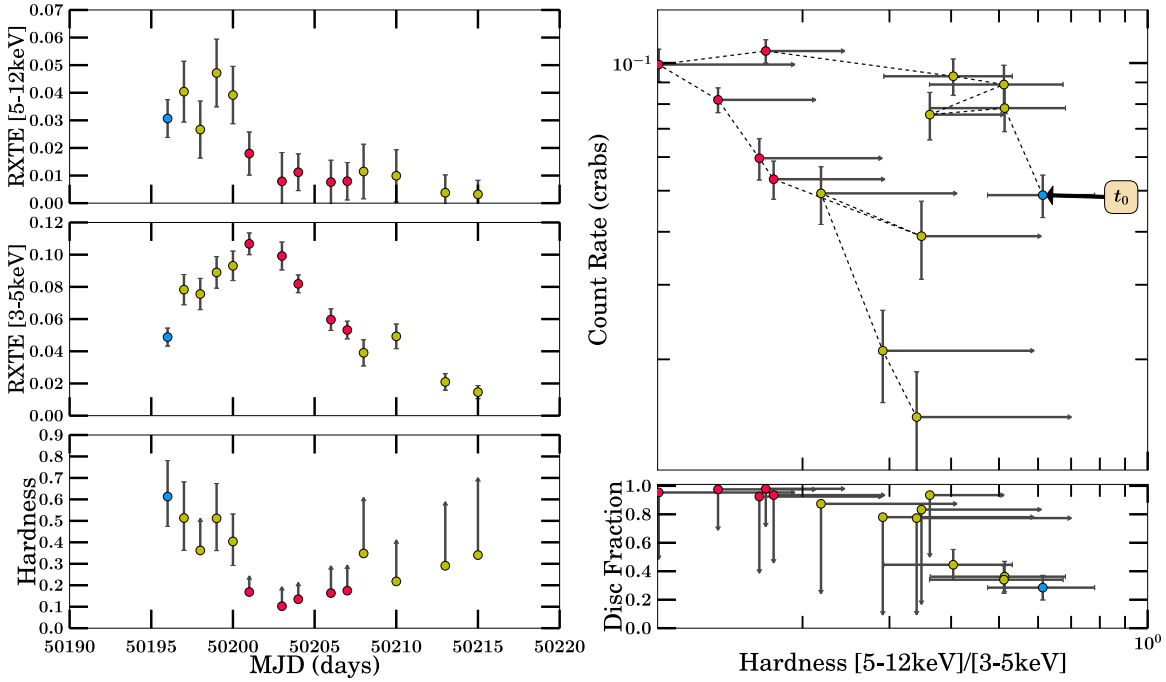

(b) 1996a Outburst Analysis

Figure B.99: XTE J1856+053 Part 1

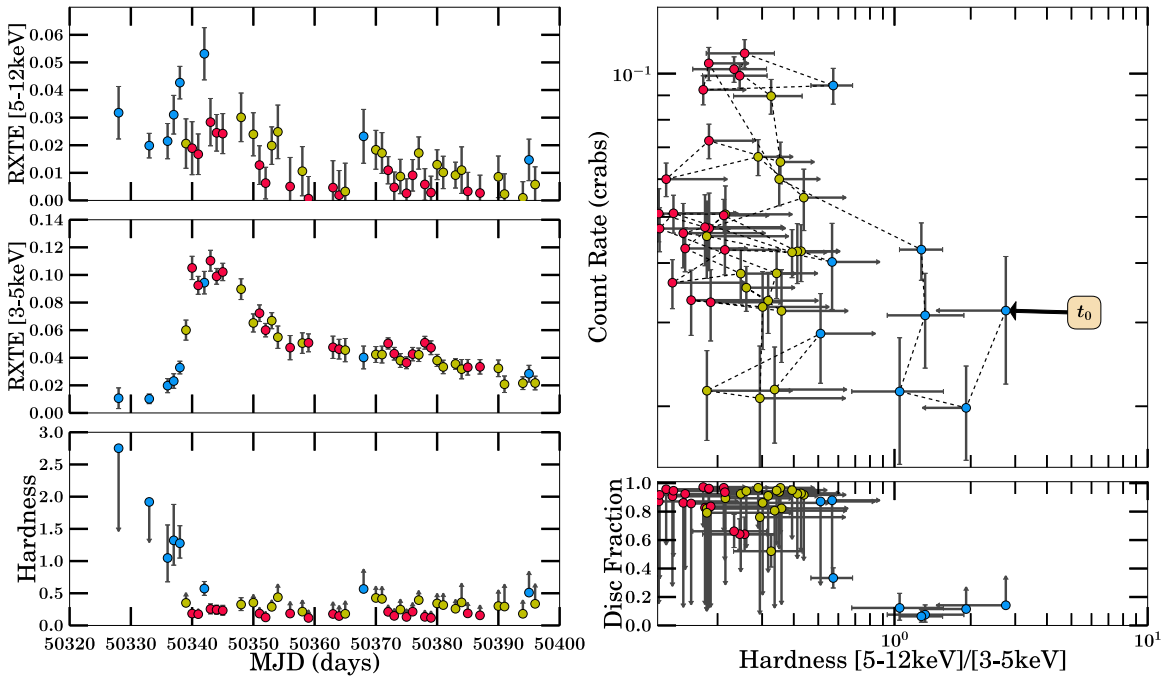

(a) 1996b Outburst Analysis

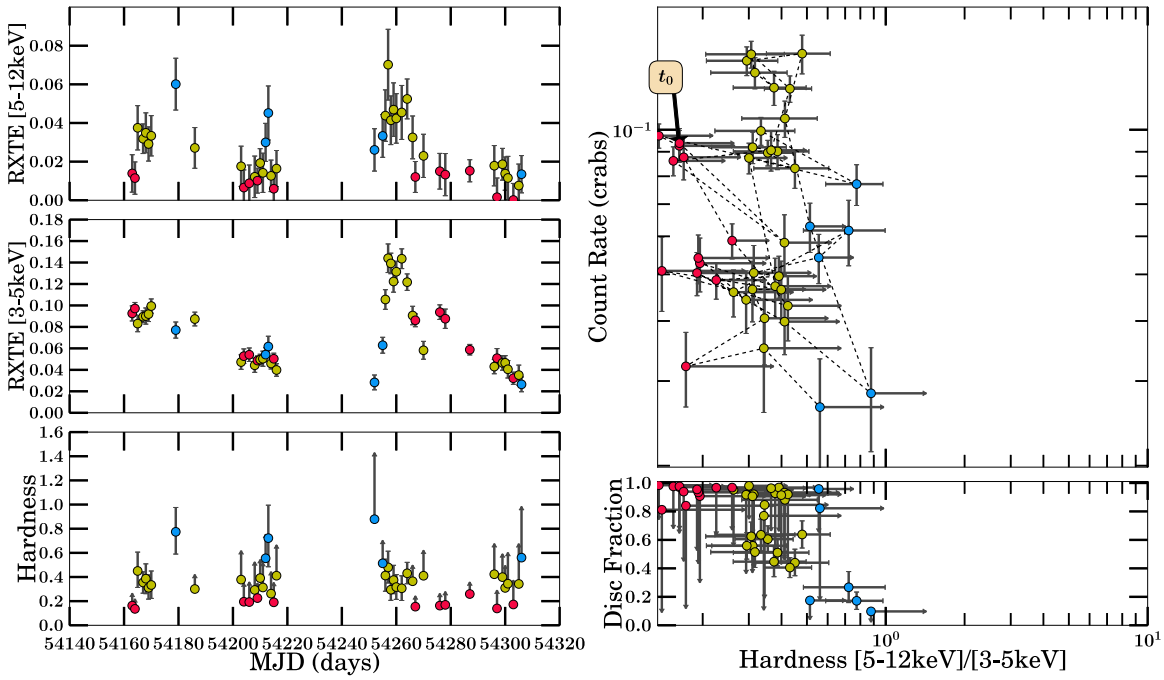

(b) 2006/2007 Outburst Analysis

Figure B.100: XTE J1856+053 Part 2

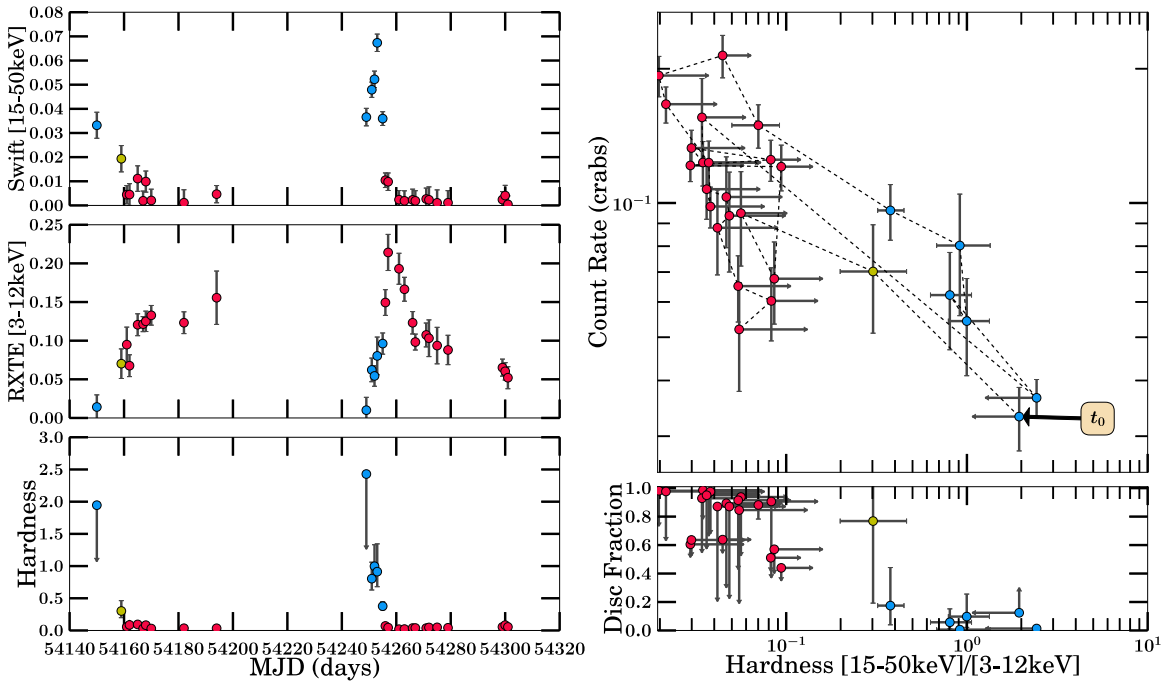

(a) 2006/2007 Outburst Analysis

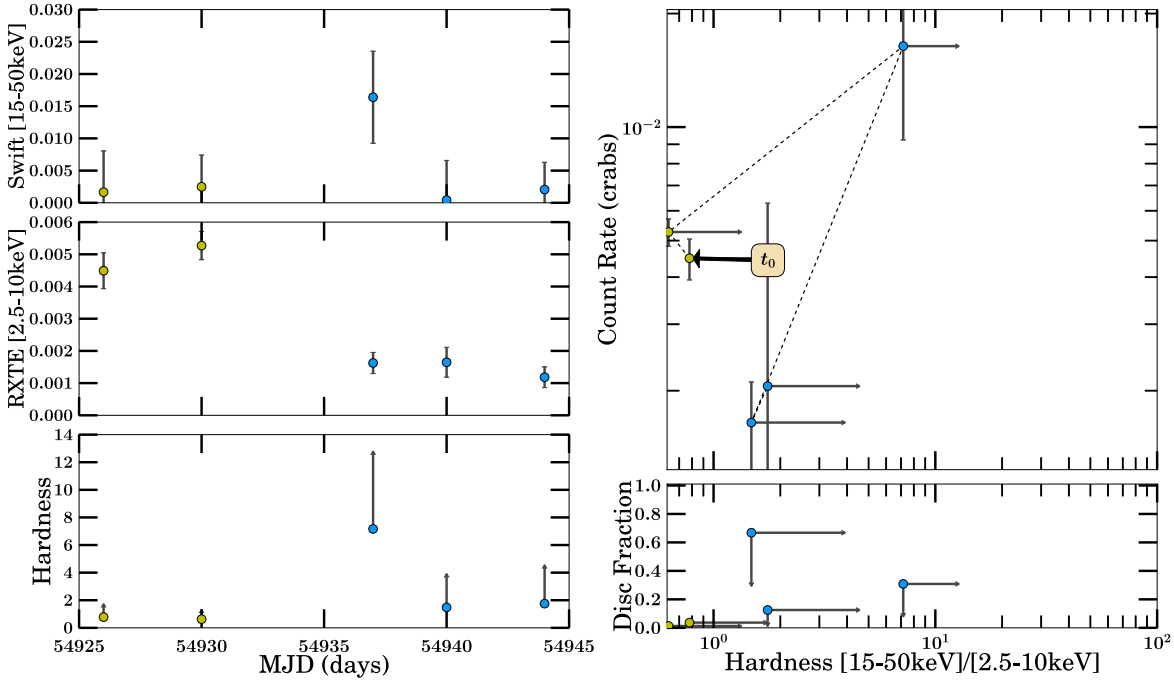

(b) 2009 Outburst Analysis

Figure B.101: XTE J1856+053 Part 3

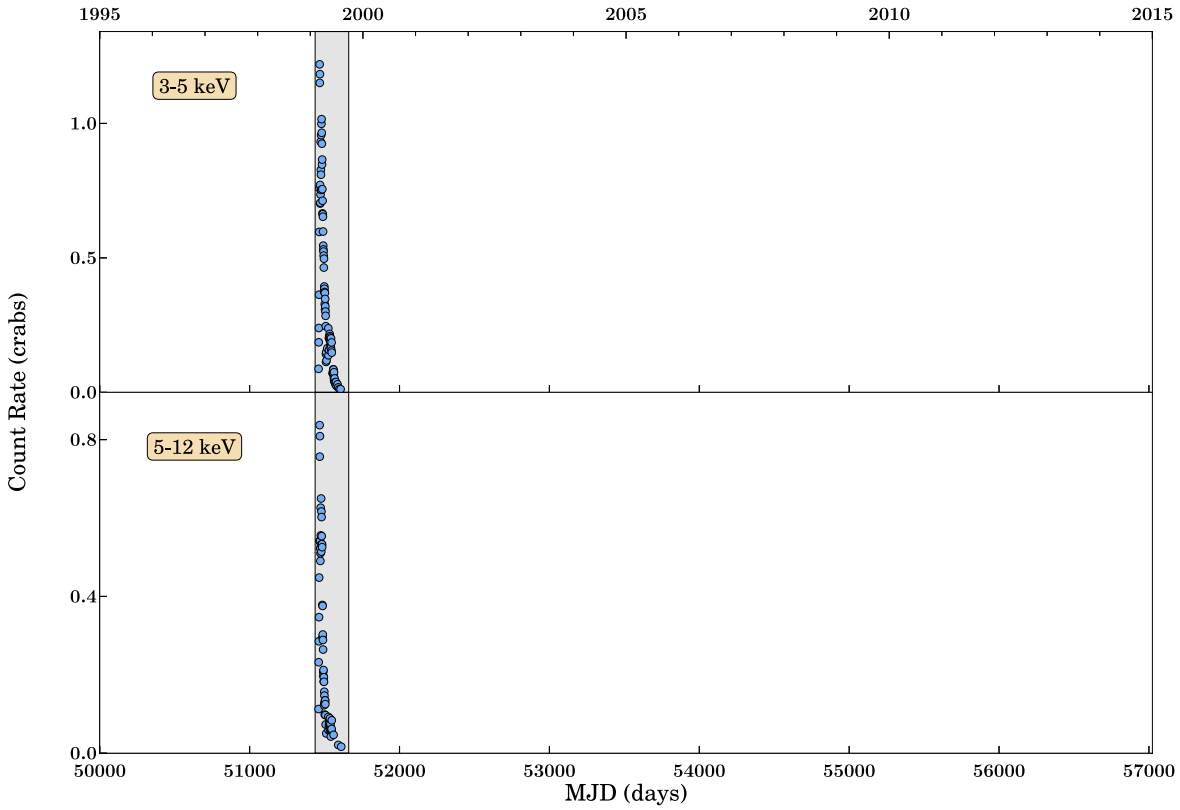

(a) Long-term Light Curve

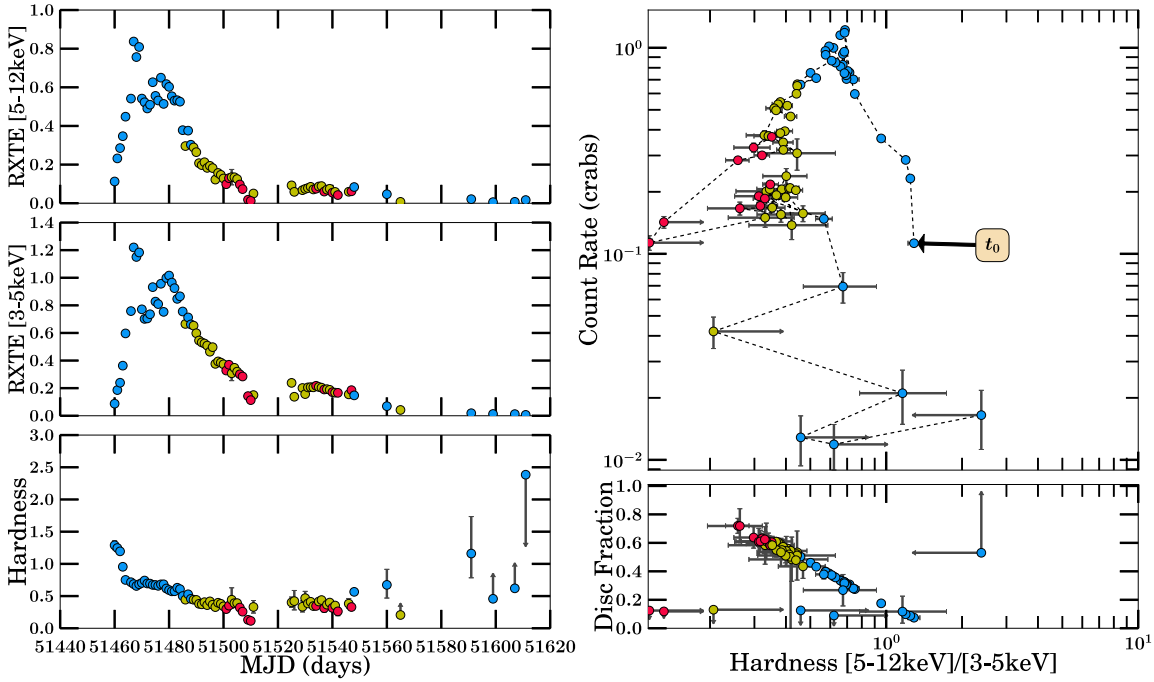

(b) 1999/2000 Outburst Analysis

Figure B.102: XTE J1859+226

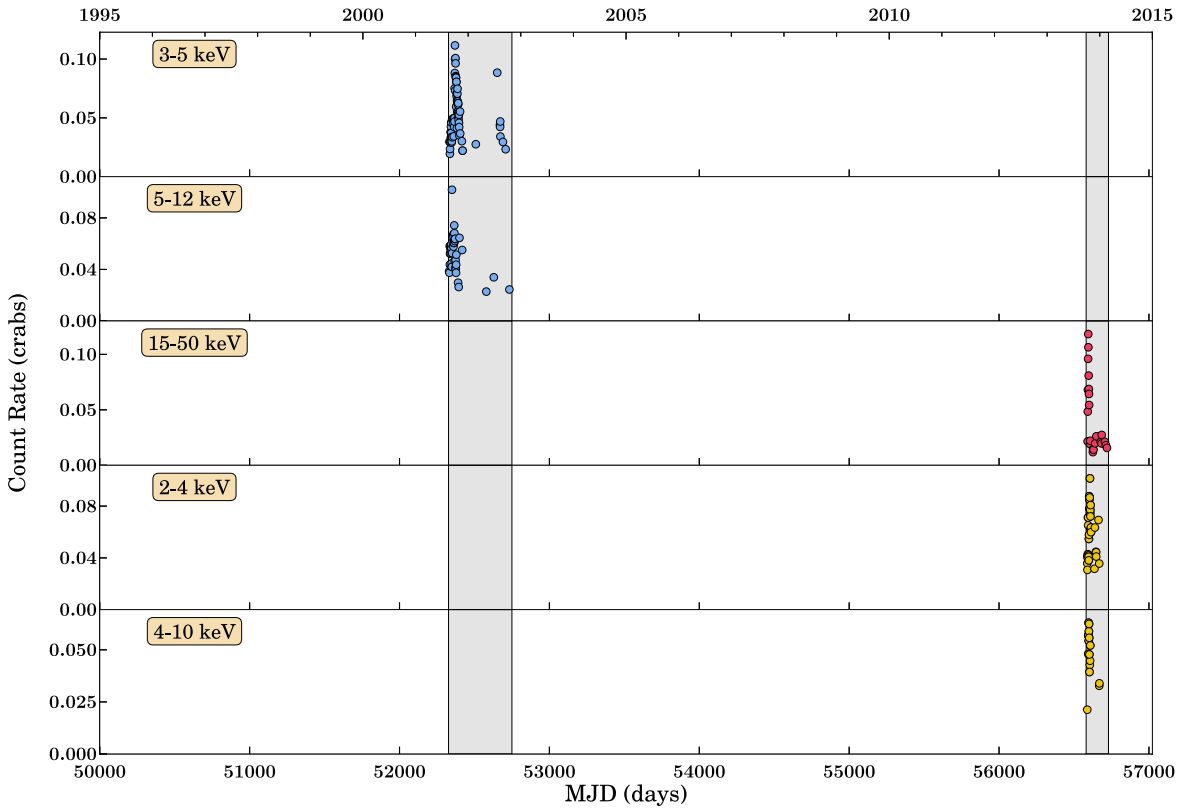

(a) Long-term Light Curve

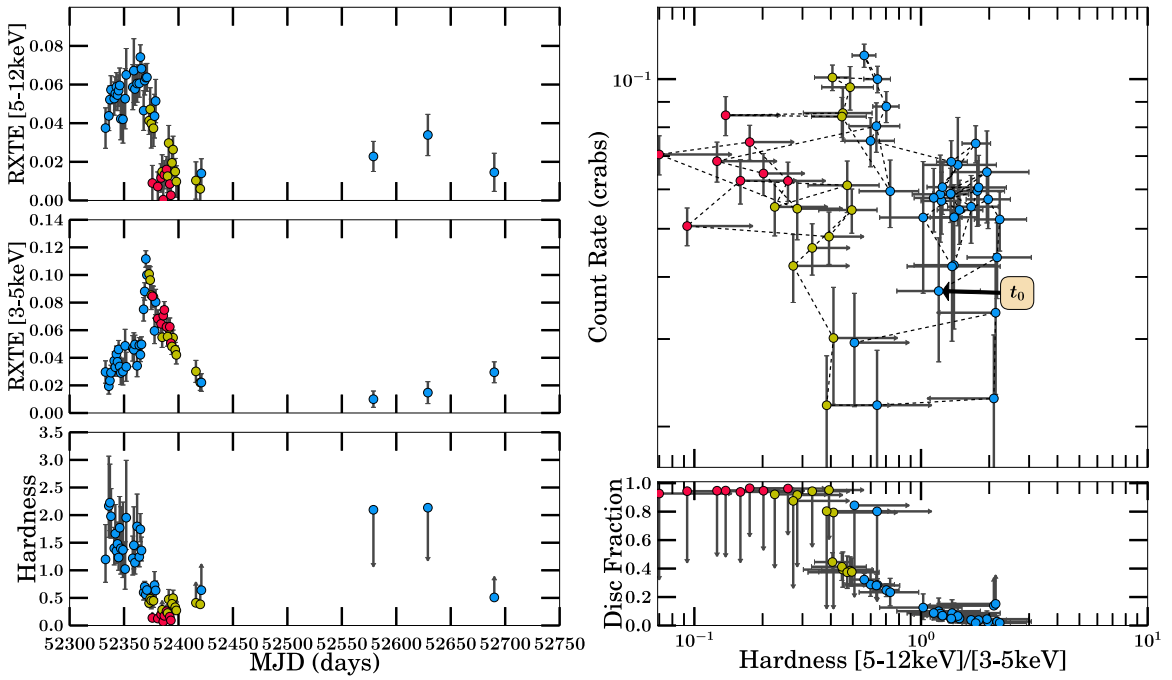

(b) 2002/2003 Outburst Analysis

Figure B.103: XTE J1908+094 Part 1

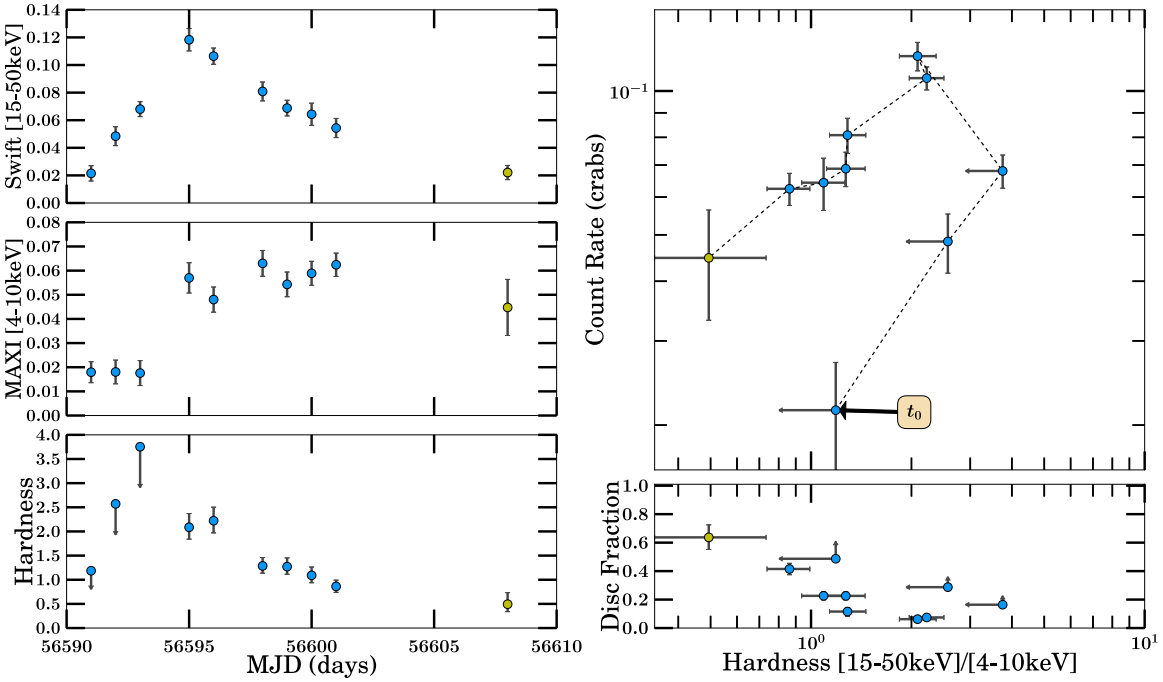

(a) 2013/2014 Outburst Analysis

Figure B.104: XTE J1908+094 Part 2

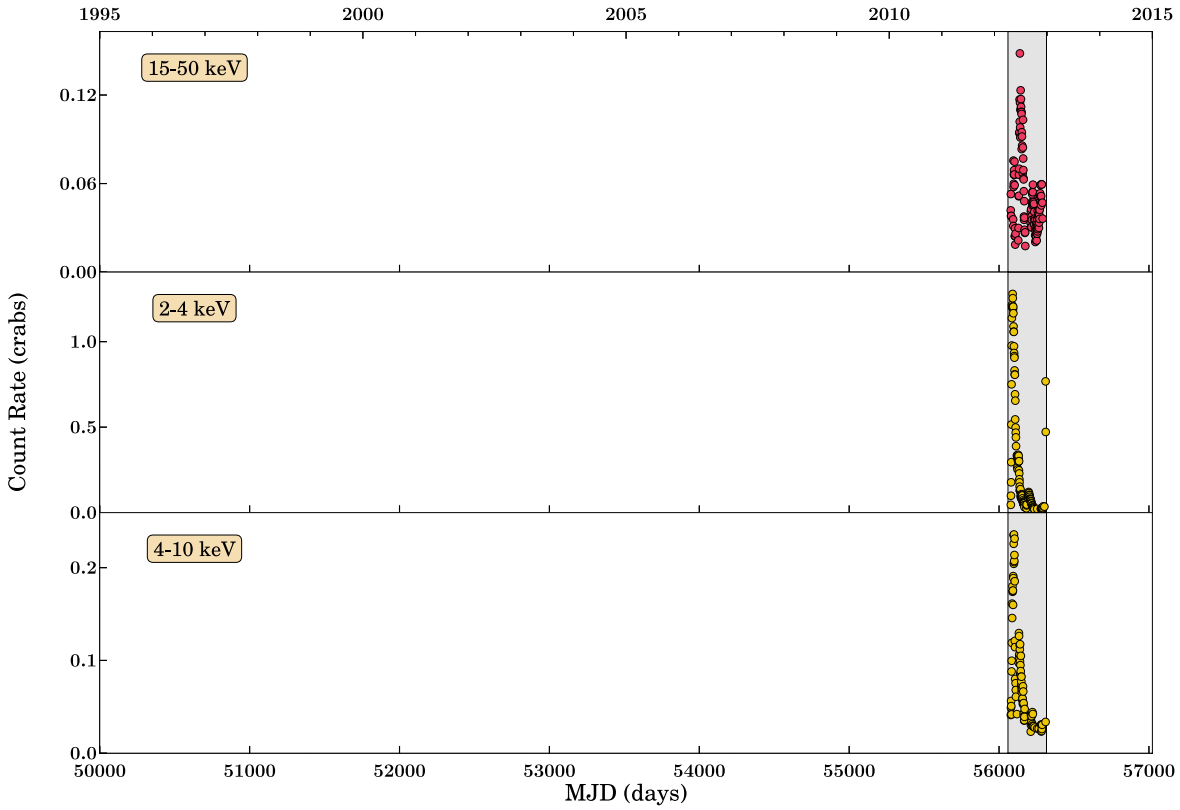

(a) Long-term Light Curve

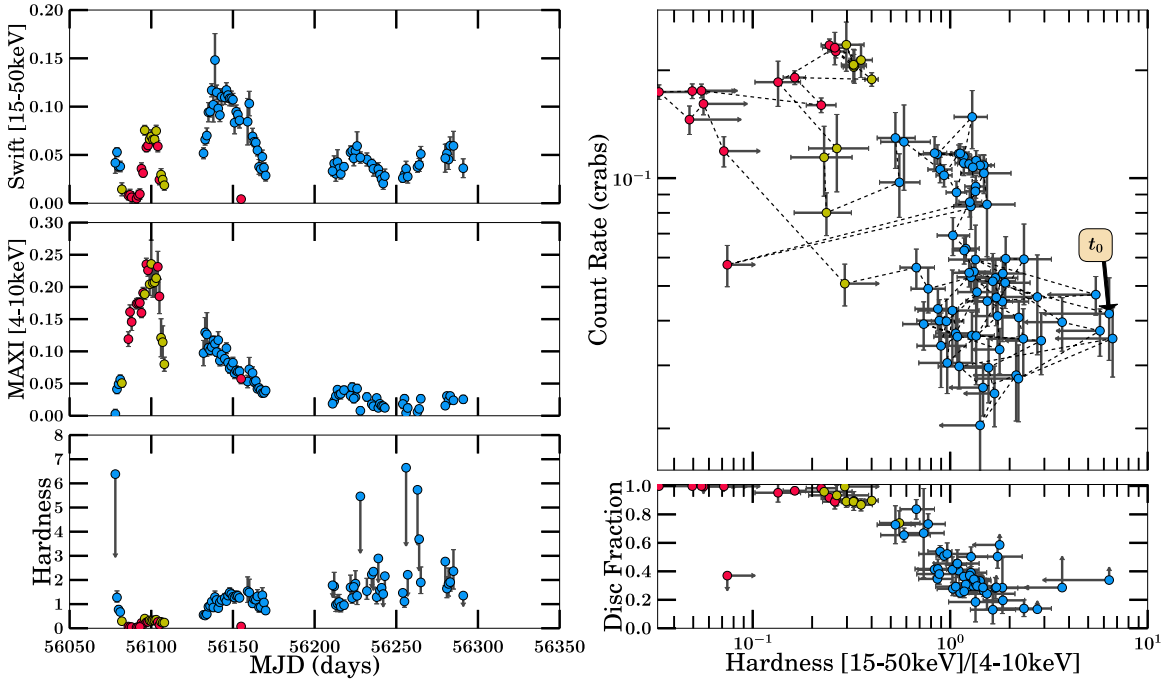

(b) 2012/2013 Outburst Analysis

Figure B.105: SWIFT J1910.2−0546

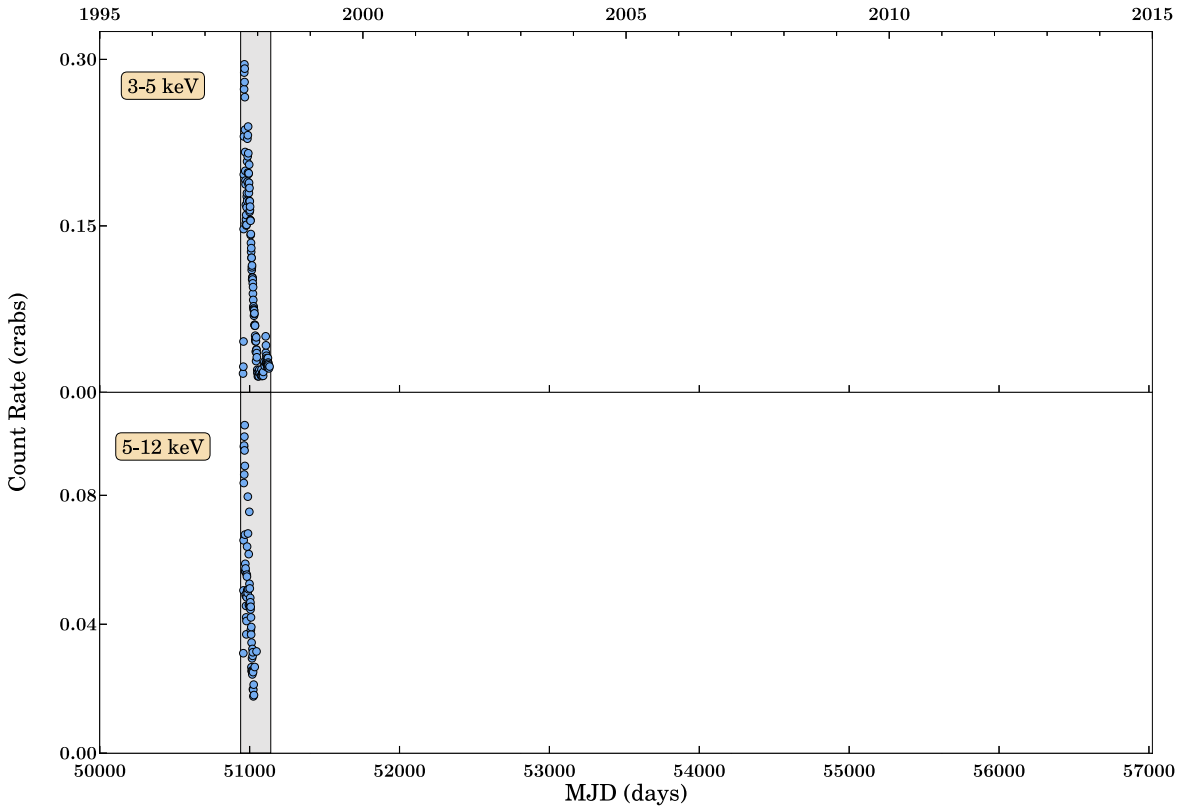

(a) Long-term Light Curve

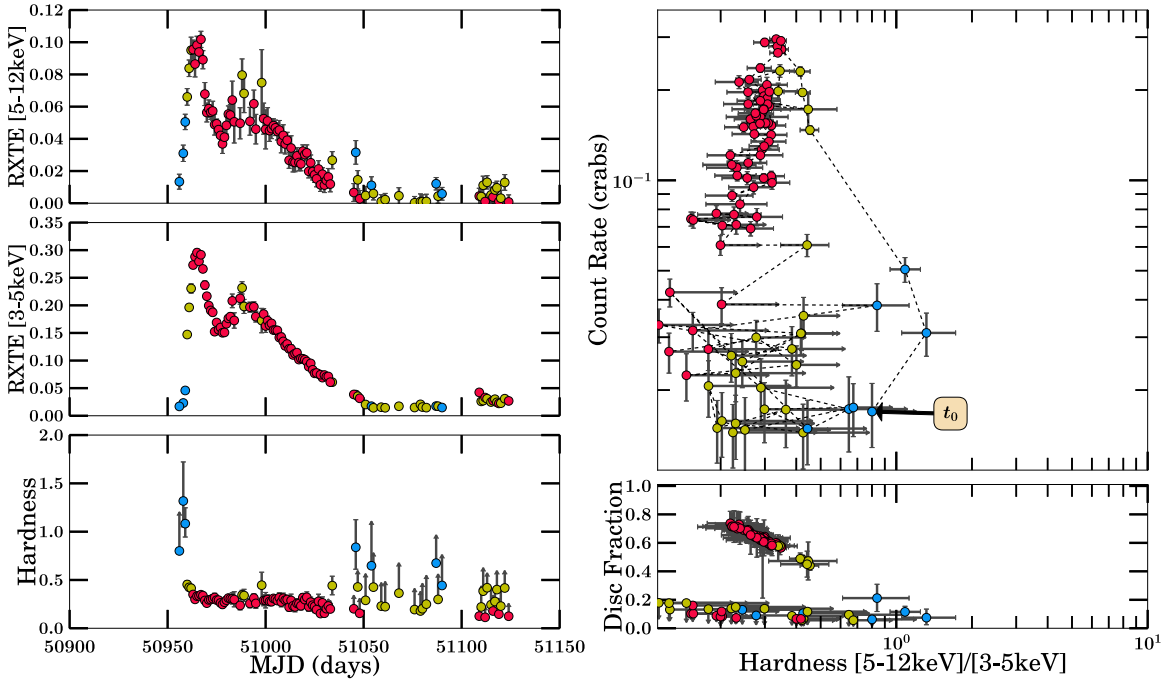

(b) 1998 Outburst Analysis

Figure B.106: XTE J2012+381

Persistent Sources - Long-term Light Curves

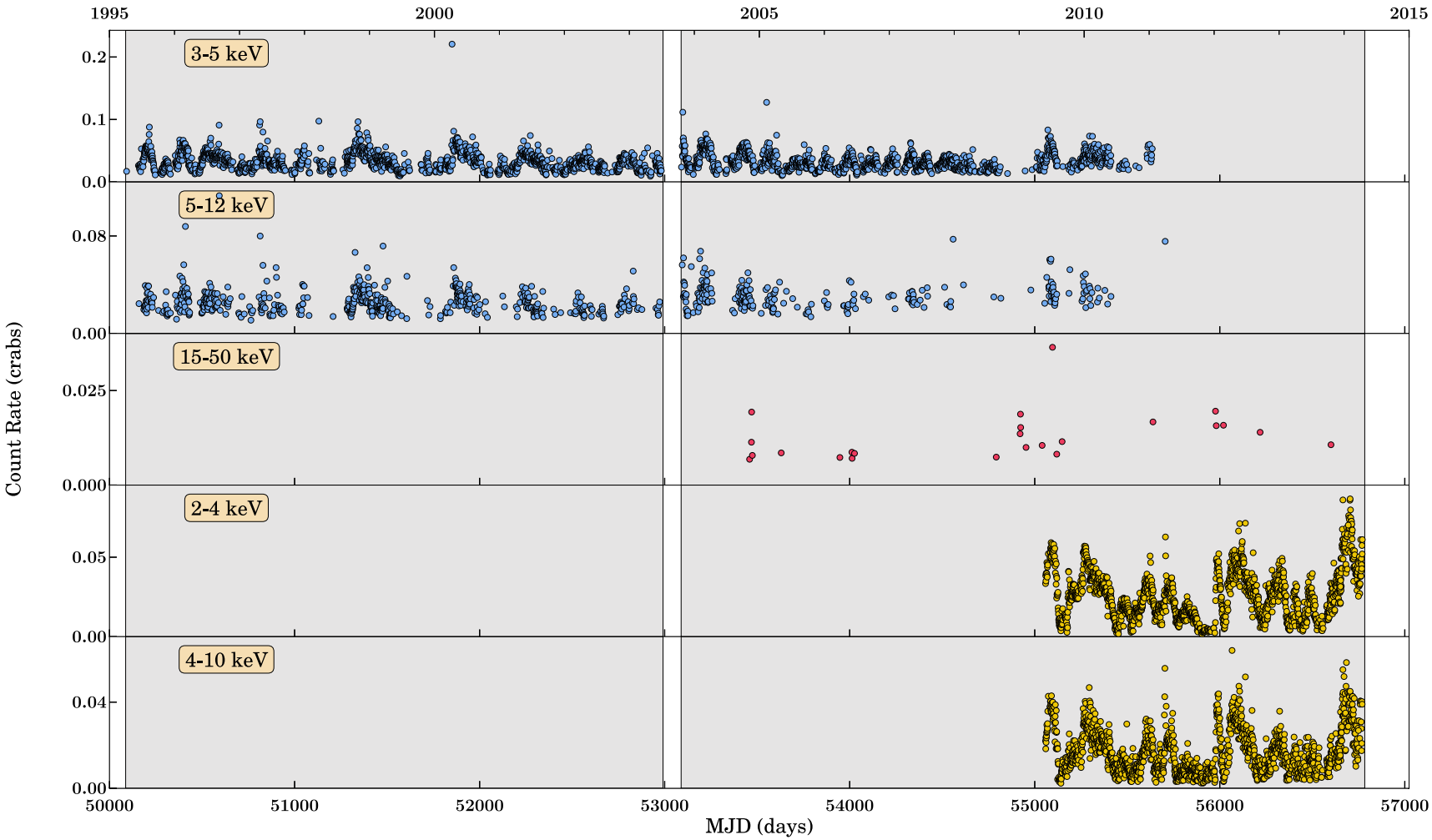

Figure B.107: 4U 0538−641 Long-term Light Curve

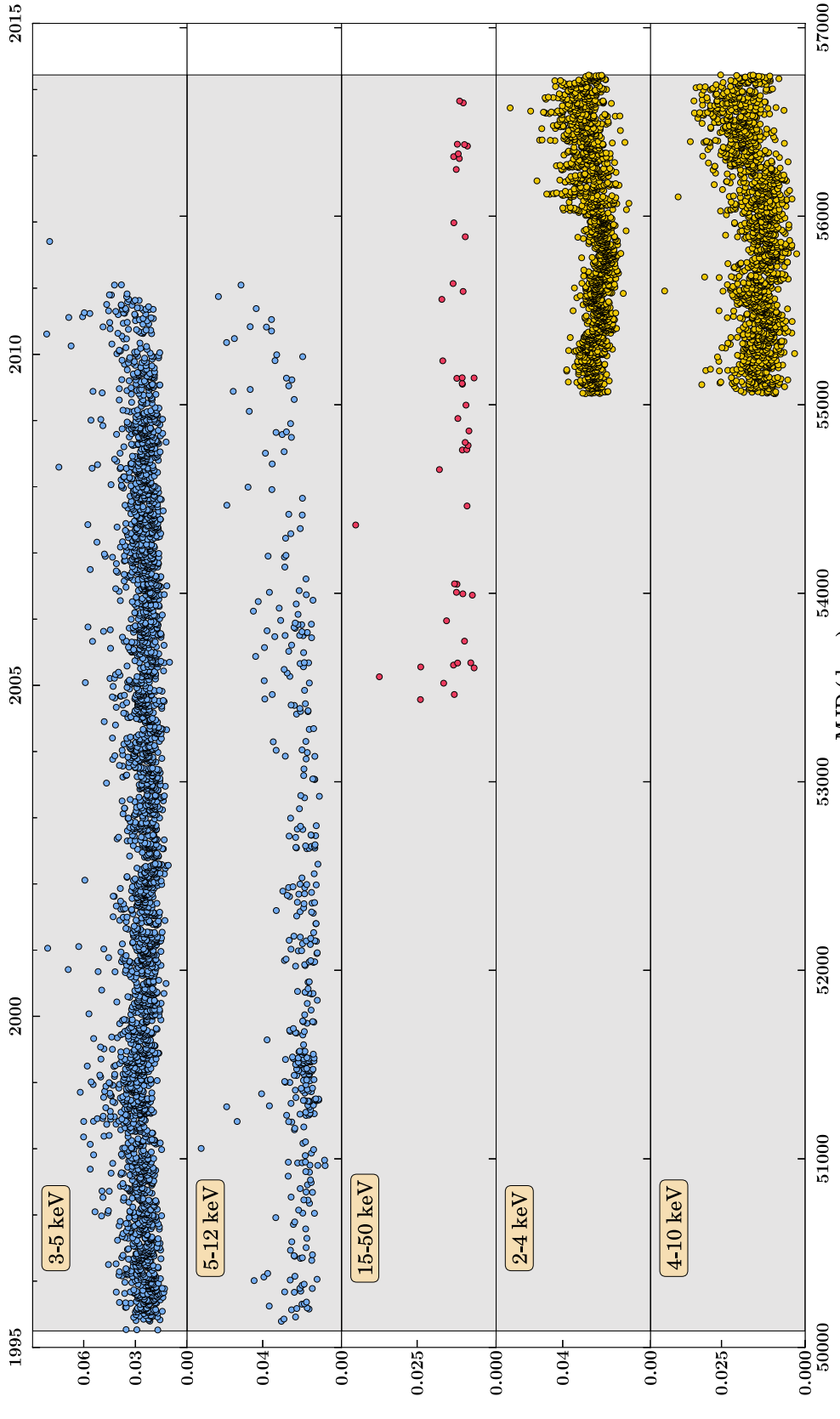

Figure B.108: 4U 0540−697 Long-term Light Curve

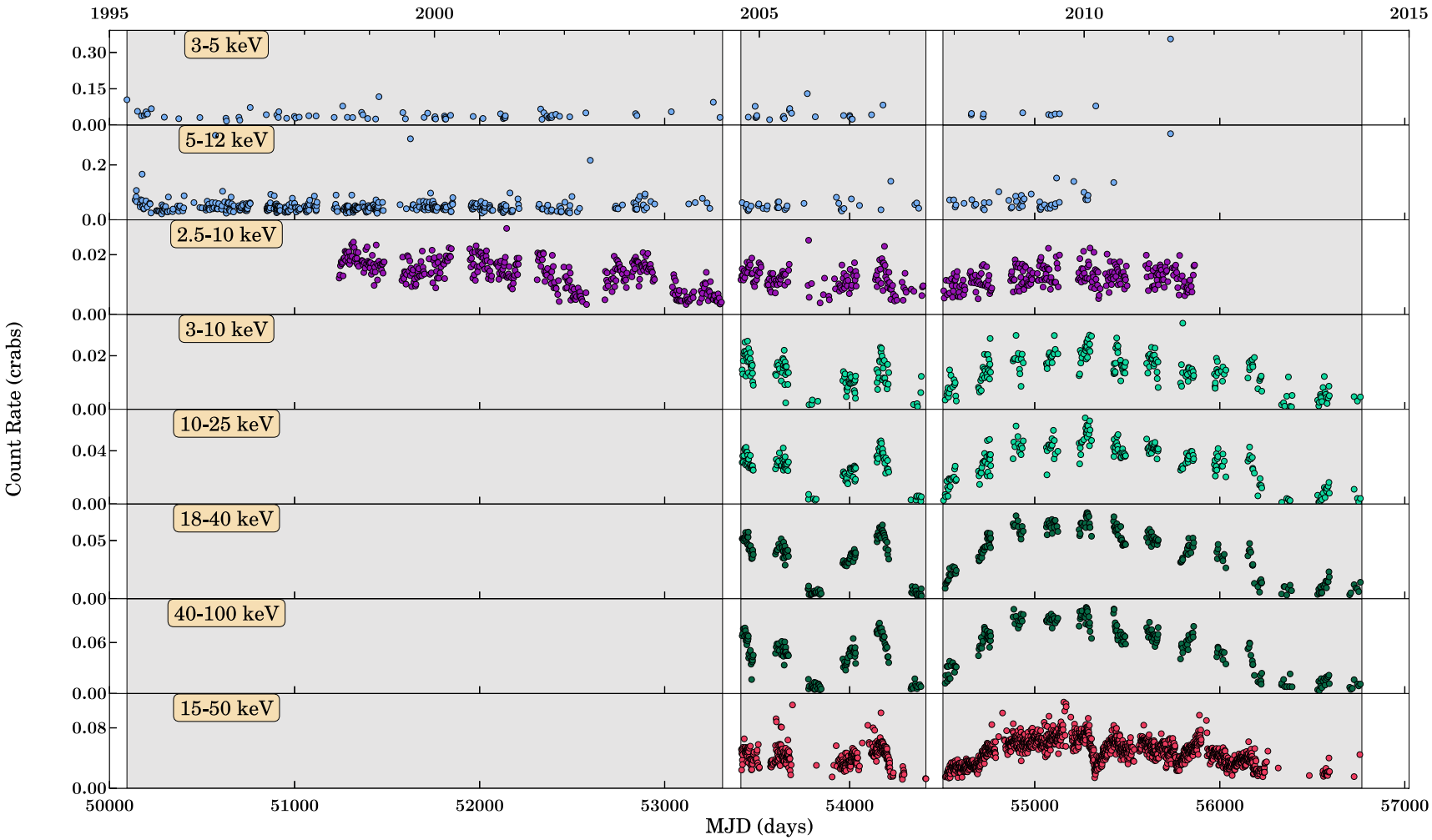

Figure B.109: 1E 1740.7−2942 Long-term Light Curve

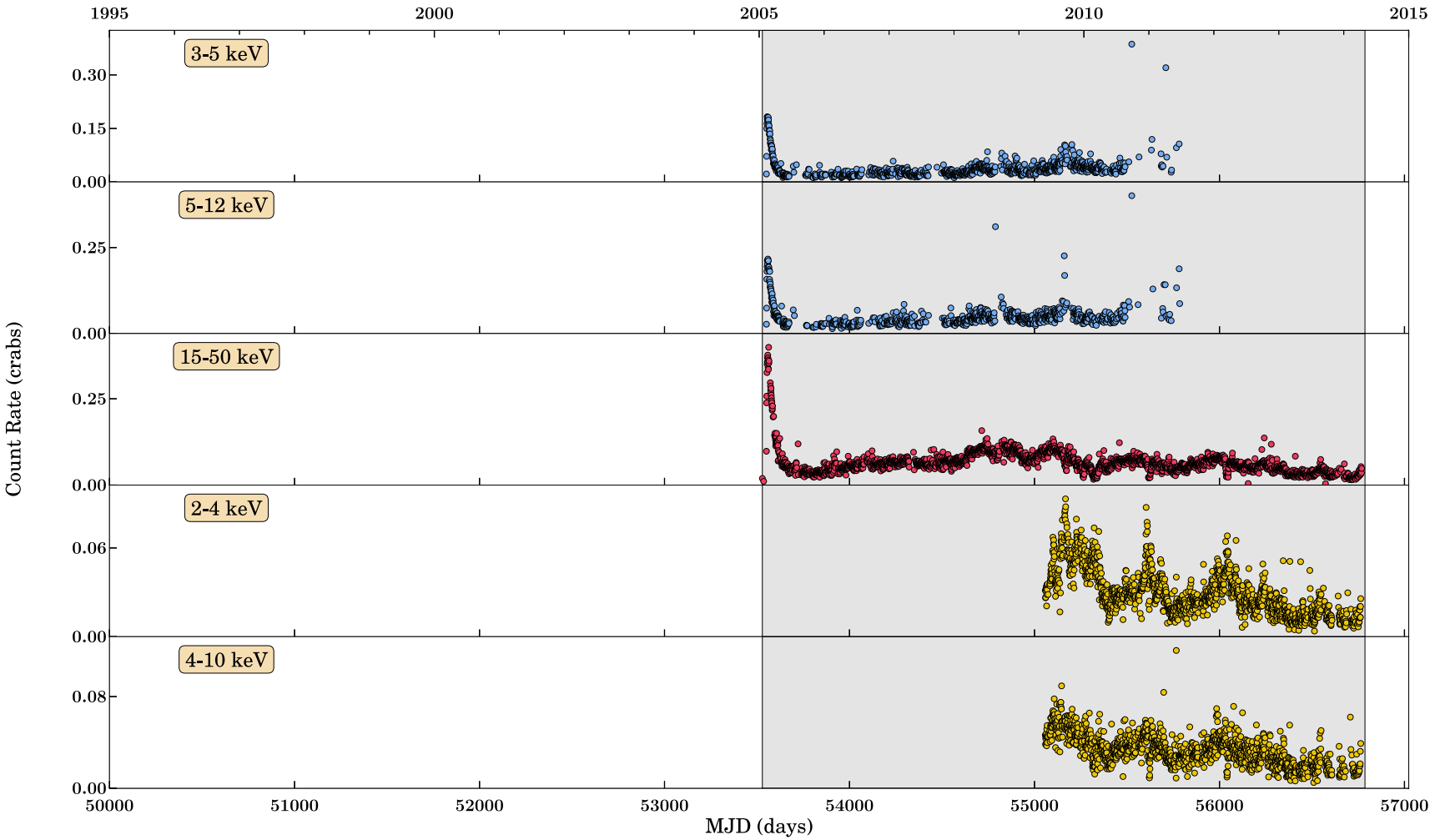

Figure B.110: Swift J1753.5−0127 Long-term Light Curve

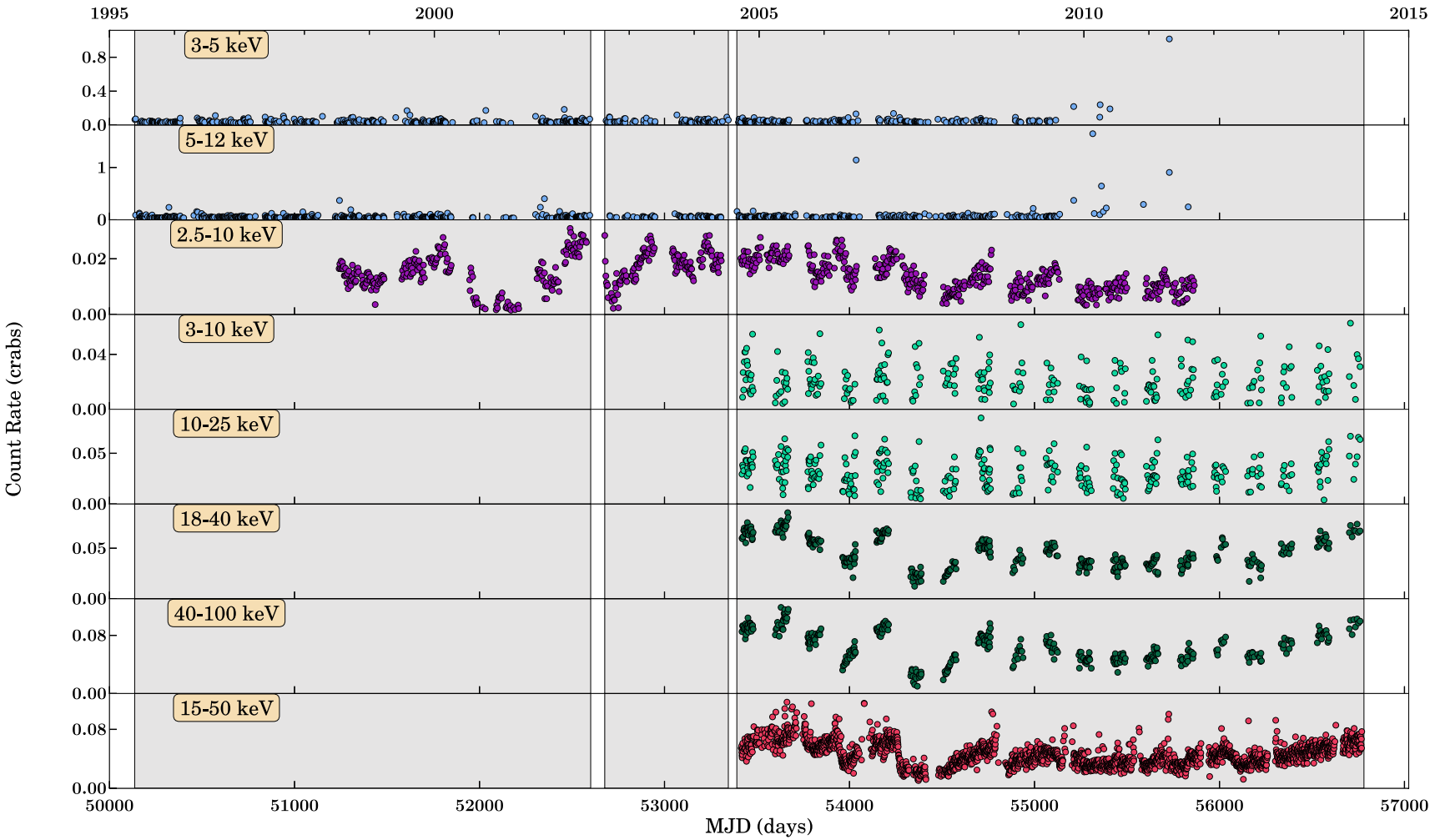

Figure B.111: GRS 1758−258 Long-term Light Curve

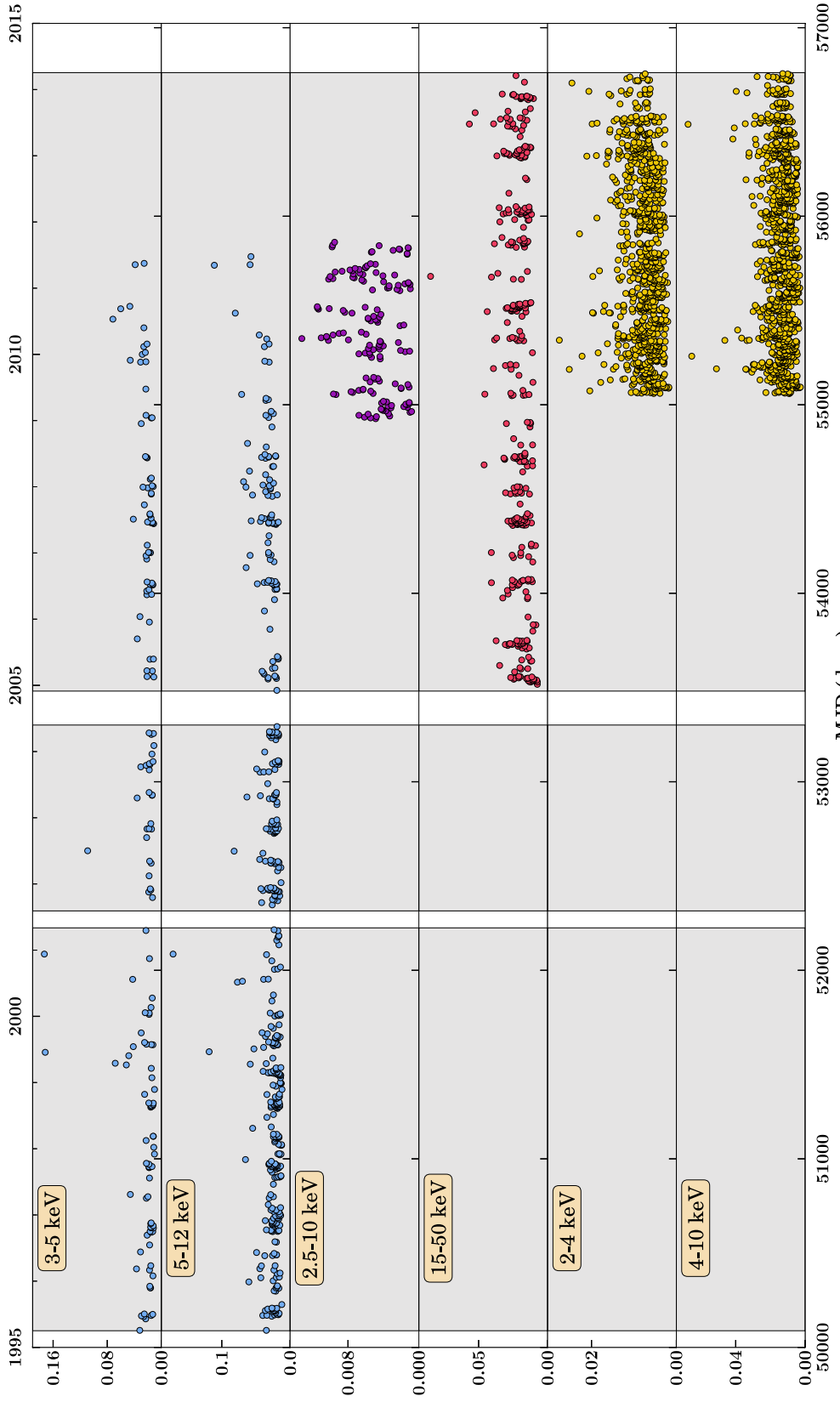

Figure B.112: SS 433 Long-term Light Curve

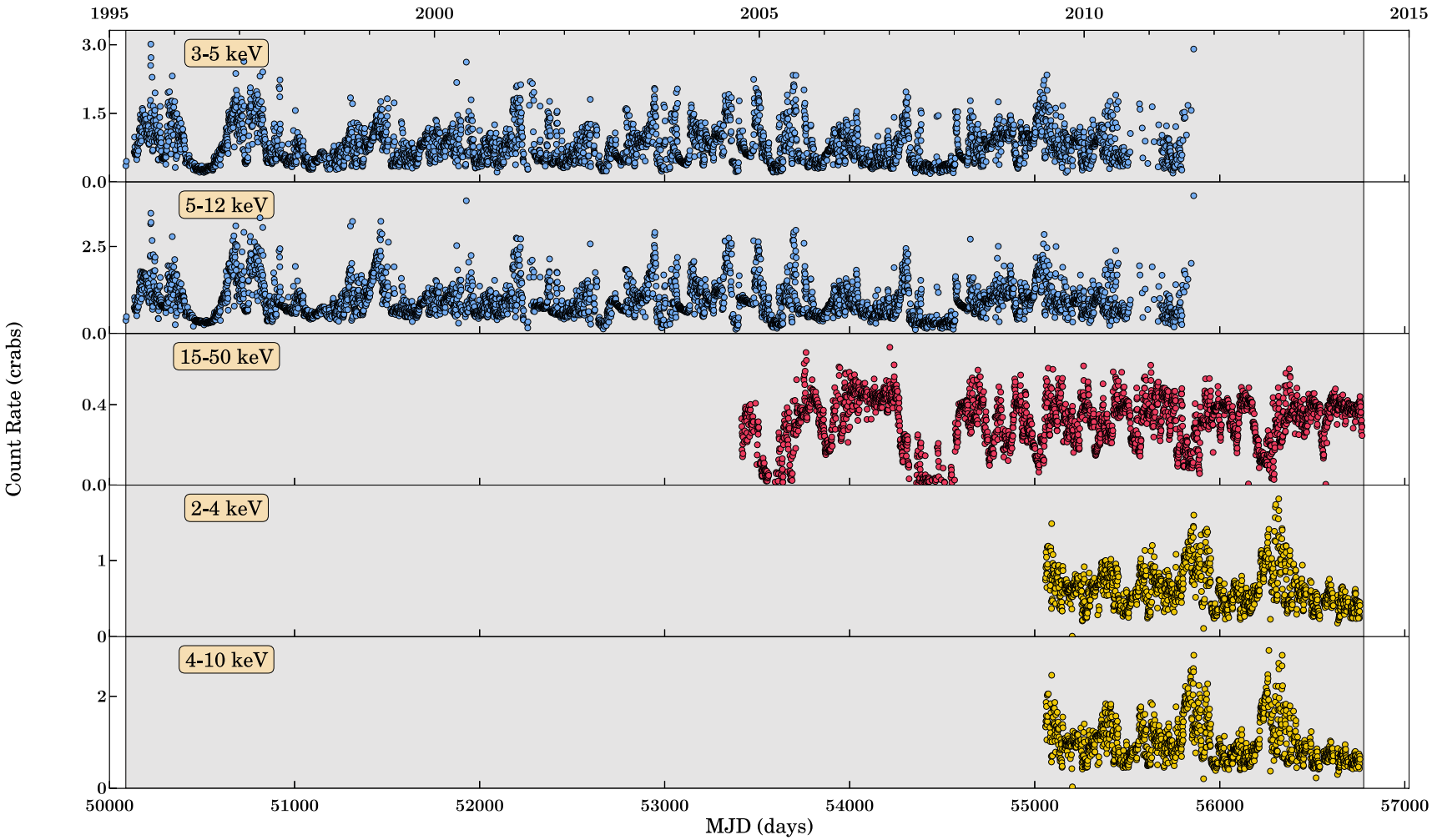

Figure B.113: GRS 1915+105 Long-term Light Curve

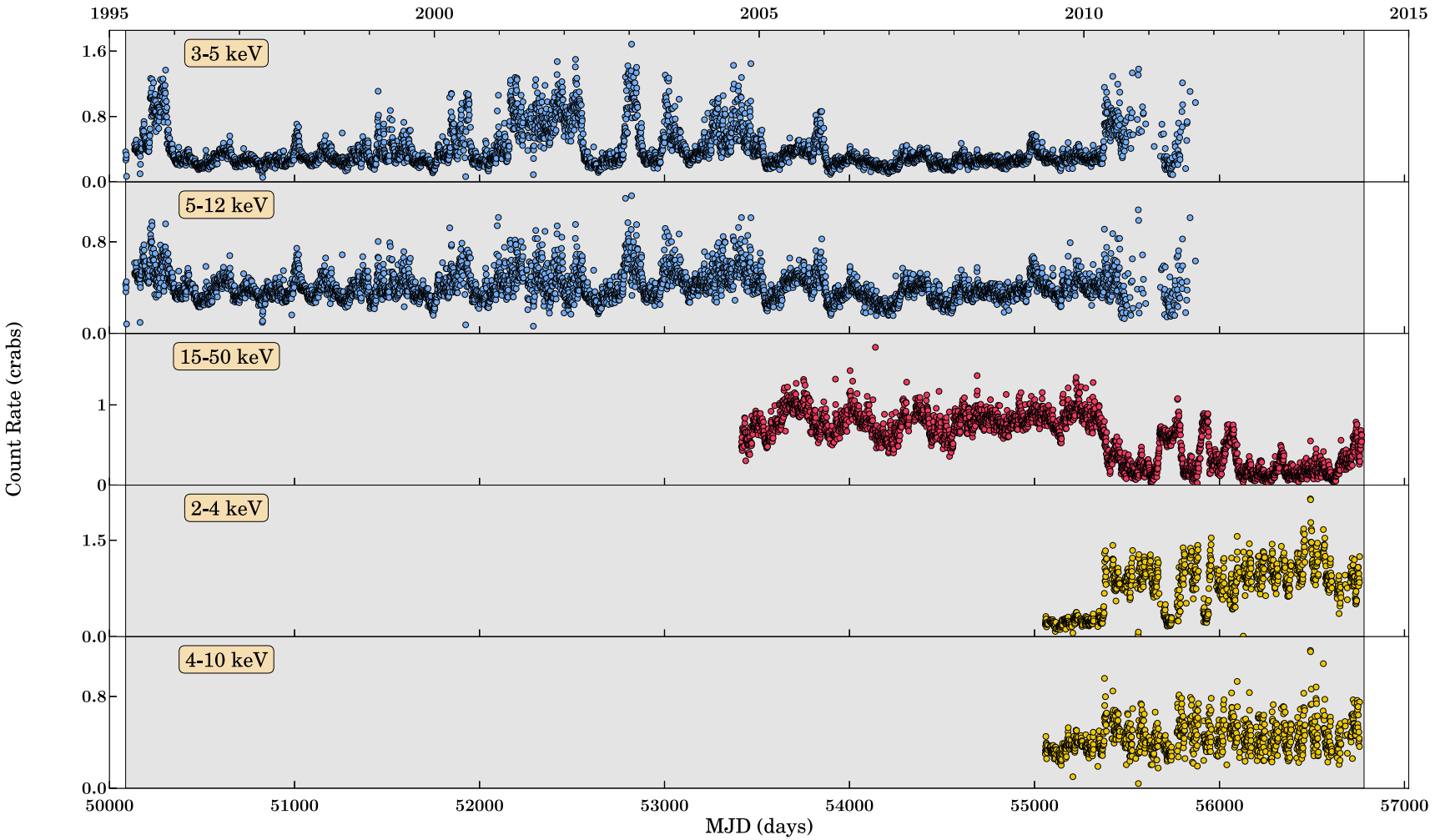

Figure B.114: 4U 1956+350 Long-term Light Curve

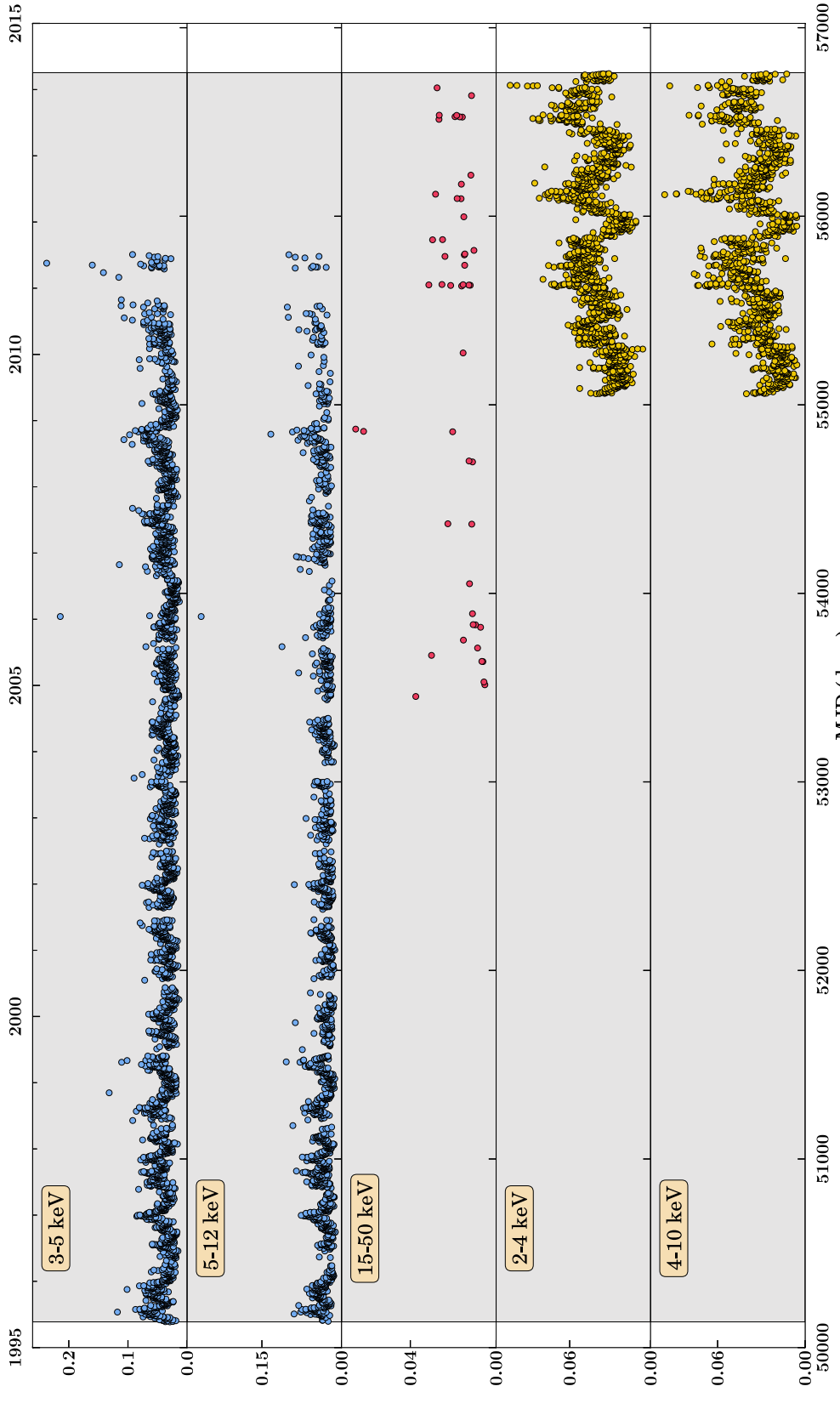

Figure B.115: 4U 1957+115 Long-term Light Curve

Persistent Sources - Outburst Analysis

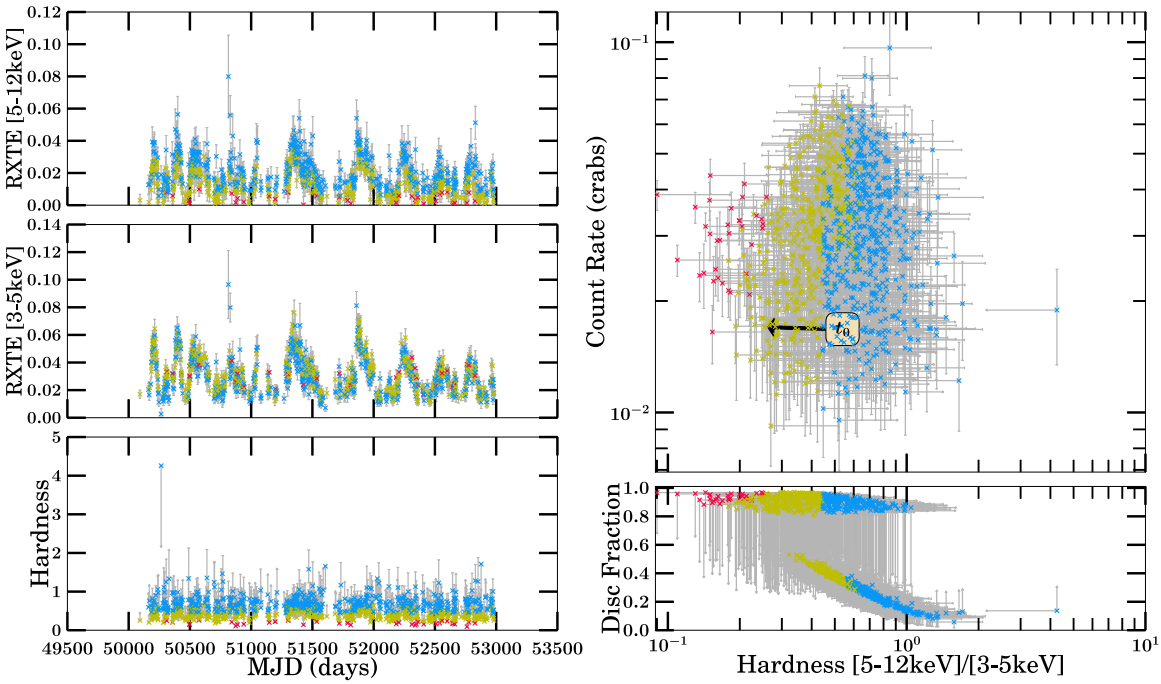

(a) 1996–2003 Outburst Analysis

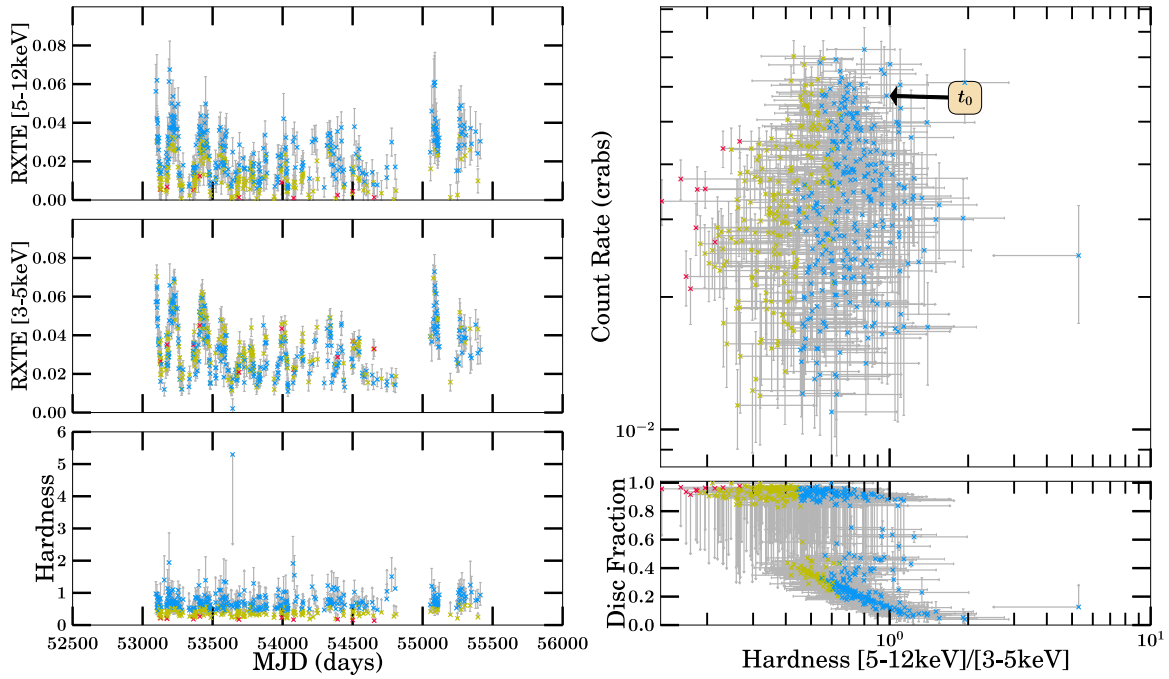

(b) 2003–2014 Outburst Analysis

Figure B.116: 4U 0538−641 Part 1

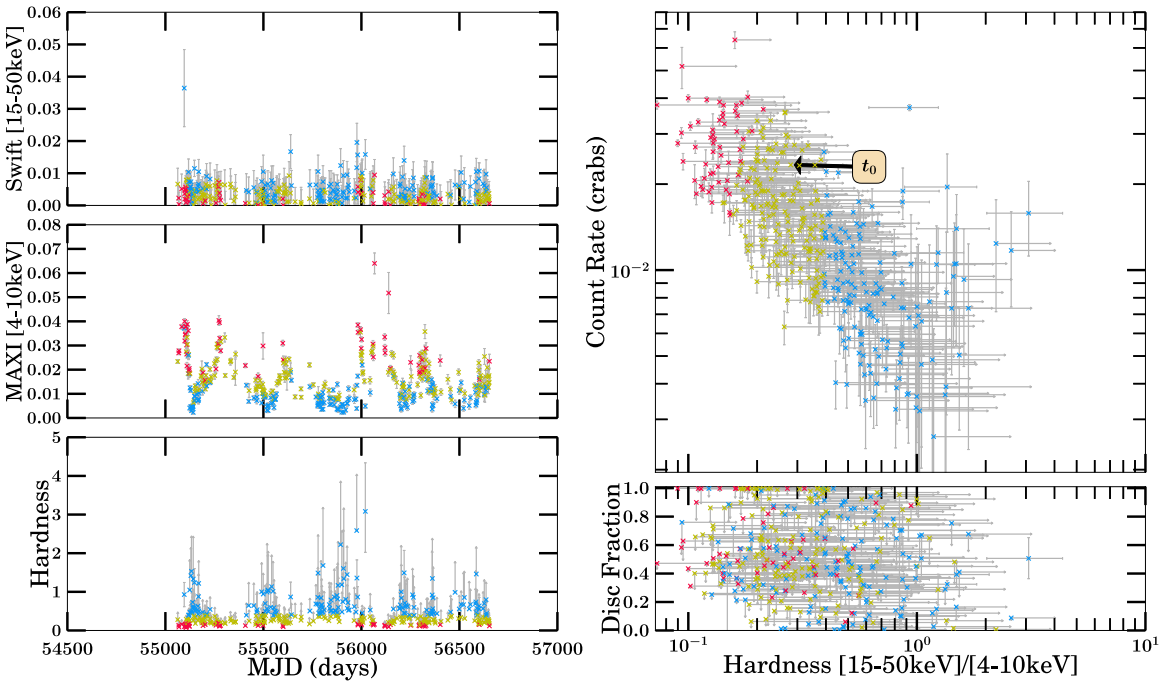

(a) 2003–2014 Outburst Analysis

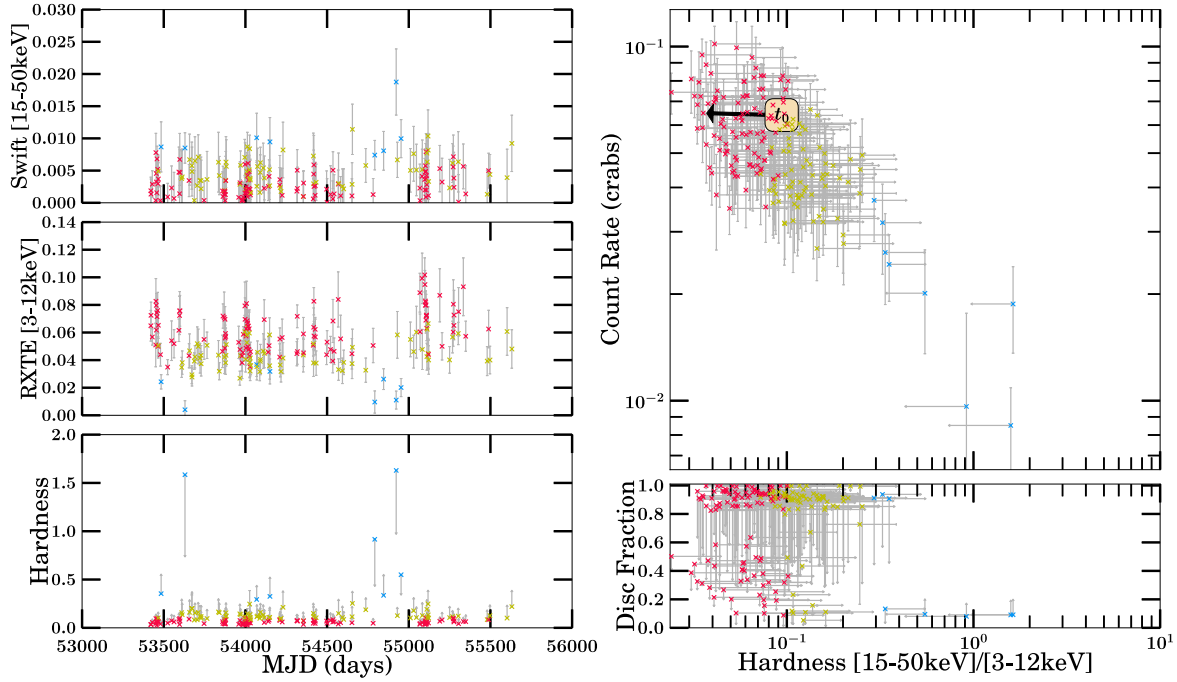

(b) 2003–2014 Outburst Analysis

Figure B.117: 4U 0538−641 Part 2

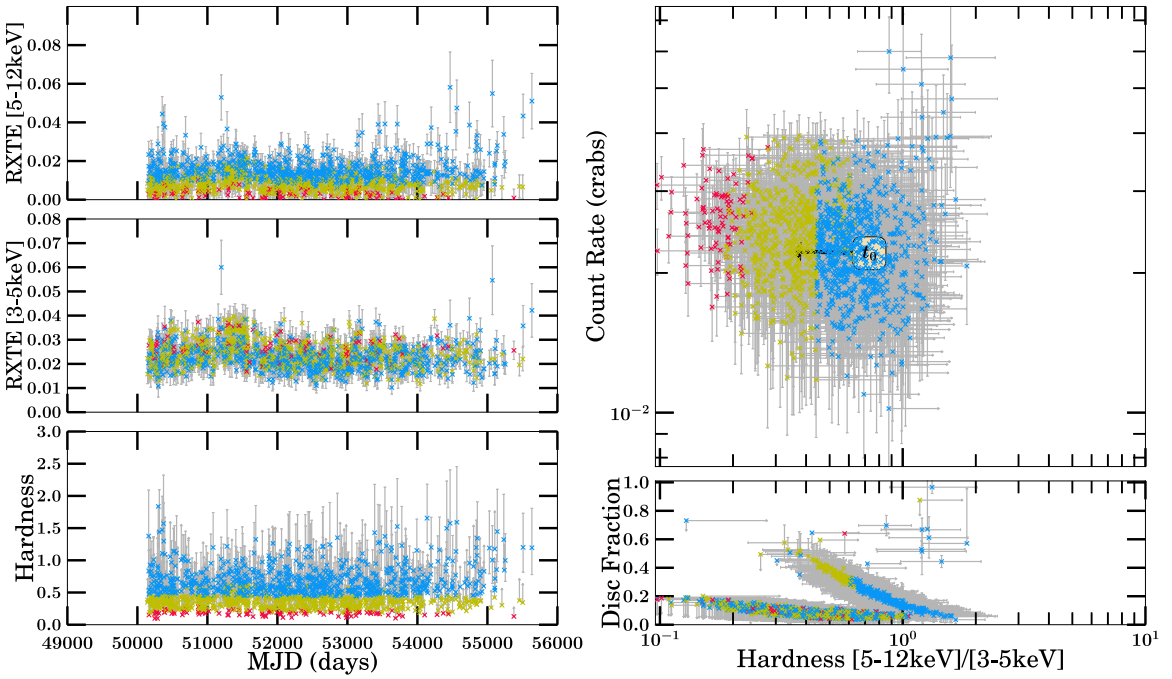

(a) 1996–2014 Outburst Analysis

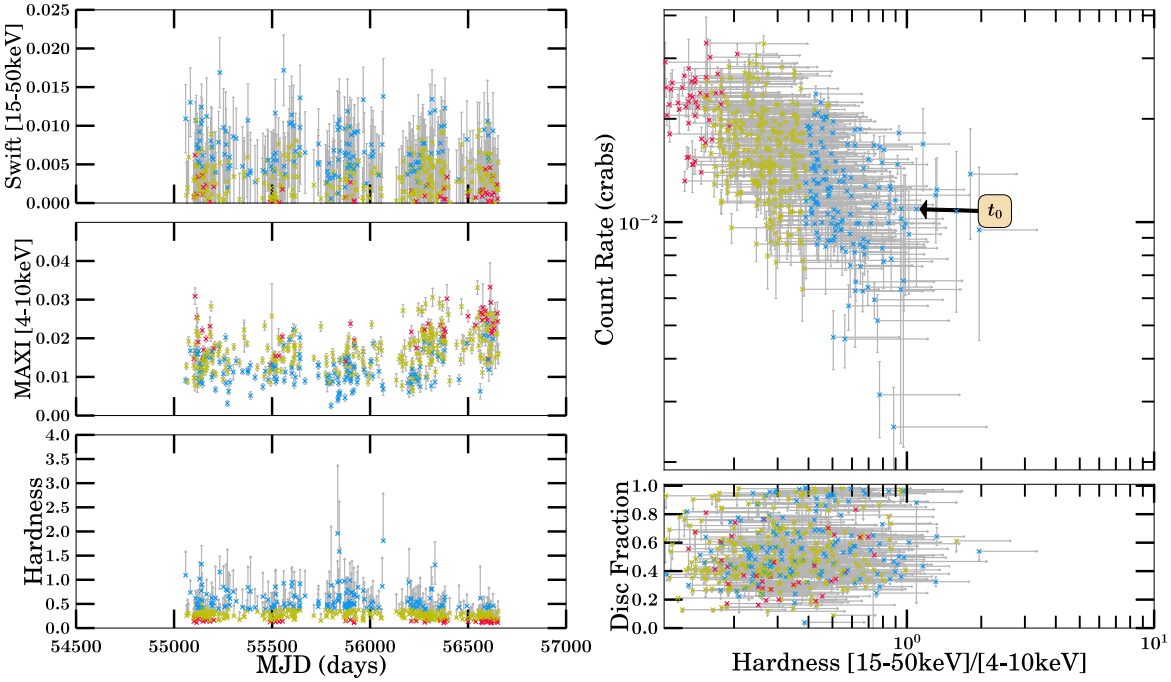

(b) 1996–2014 Outburst Analysis

Figure B.118: 4U 0540−697 Part 1

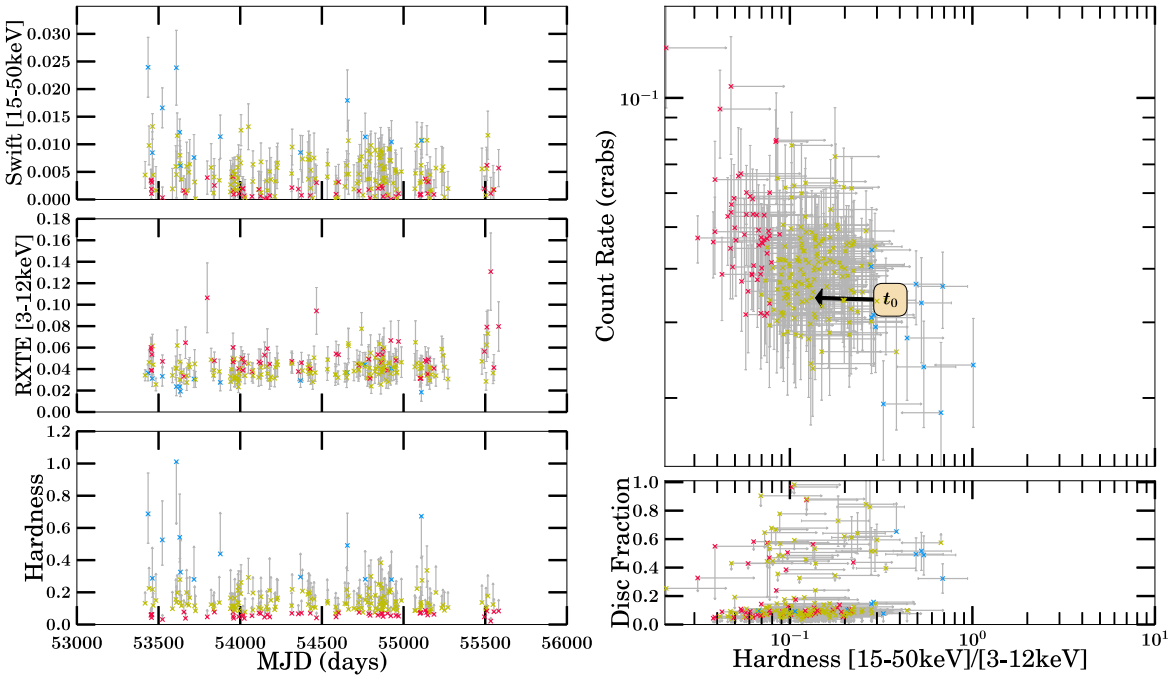

(a) 1996–2014 Outburst Analysis

Figure B.119: 4U 0540−697 Part 2

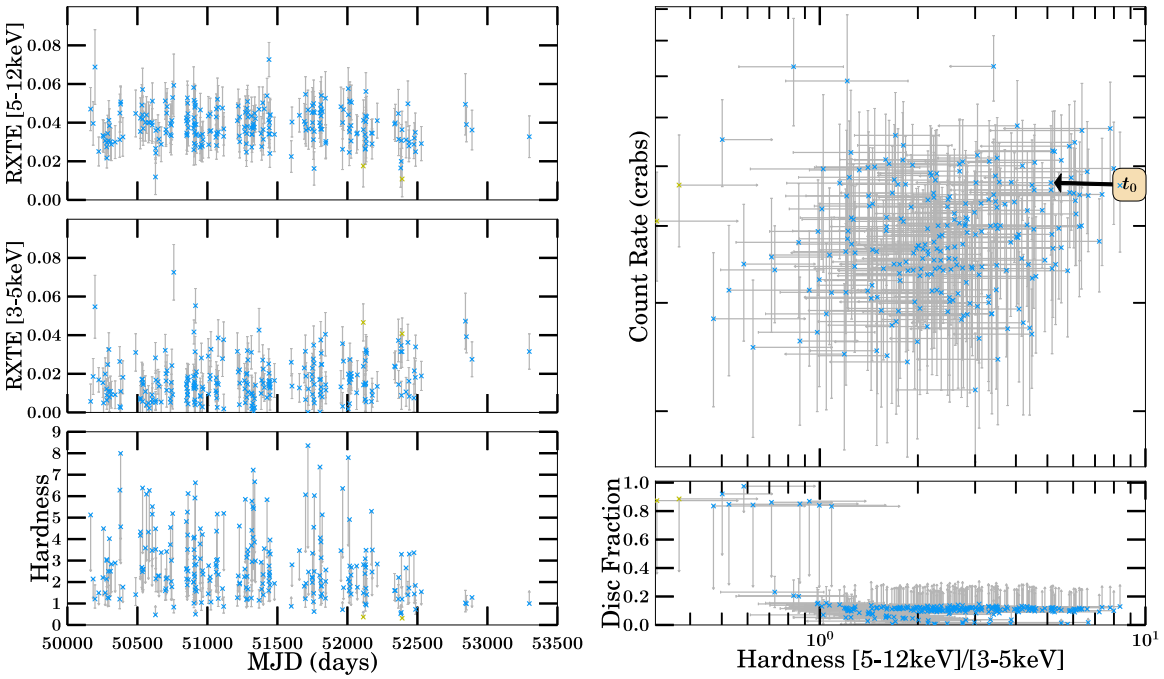

(a) 1996–2004 Outburst Analysis

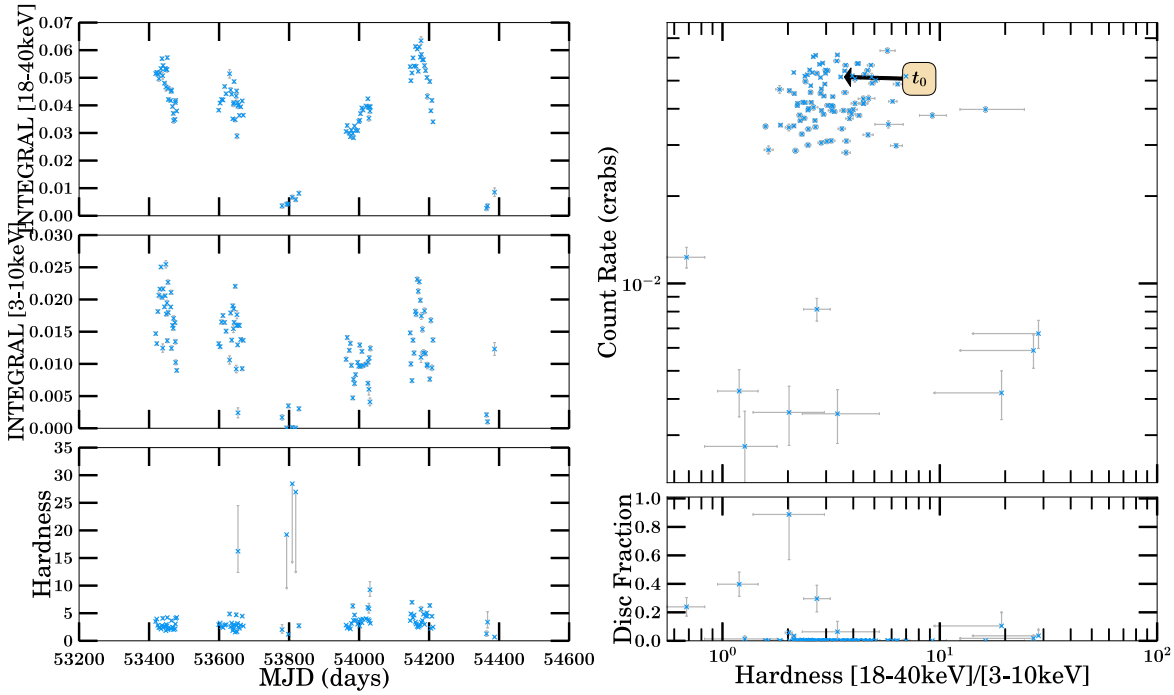

(b) 2005–2007 Outburst Analysis

Figure B.120: 1E 1740.7−2942 Part 1

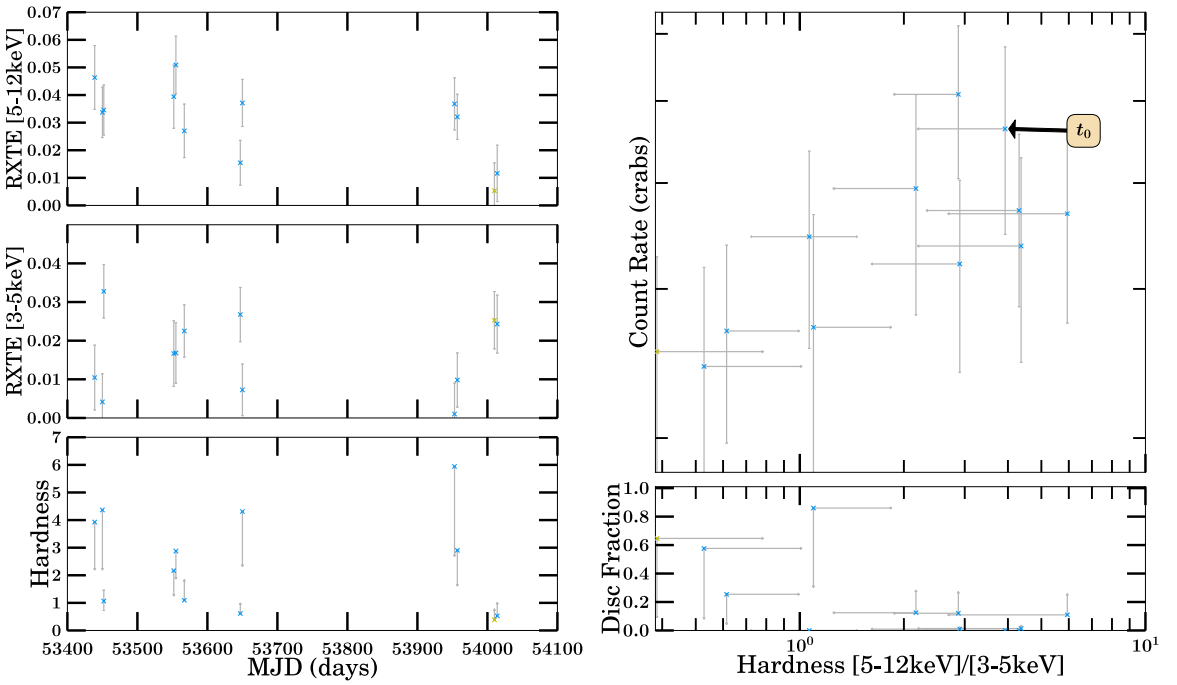

(a) 2005–2007 Outburst Analysis

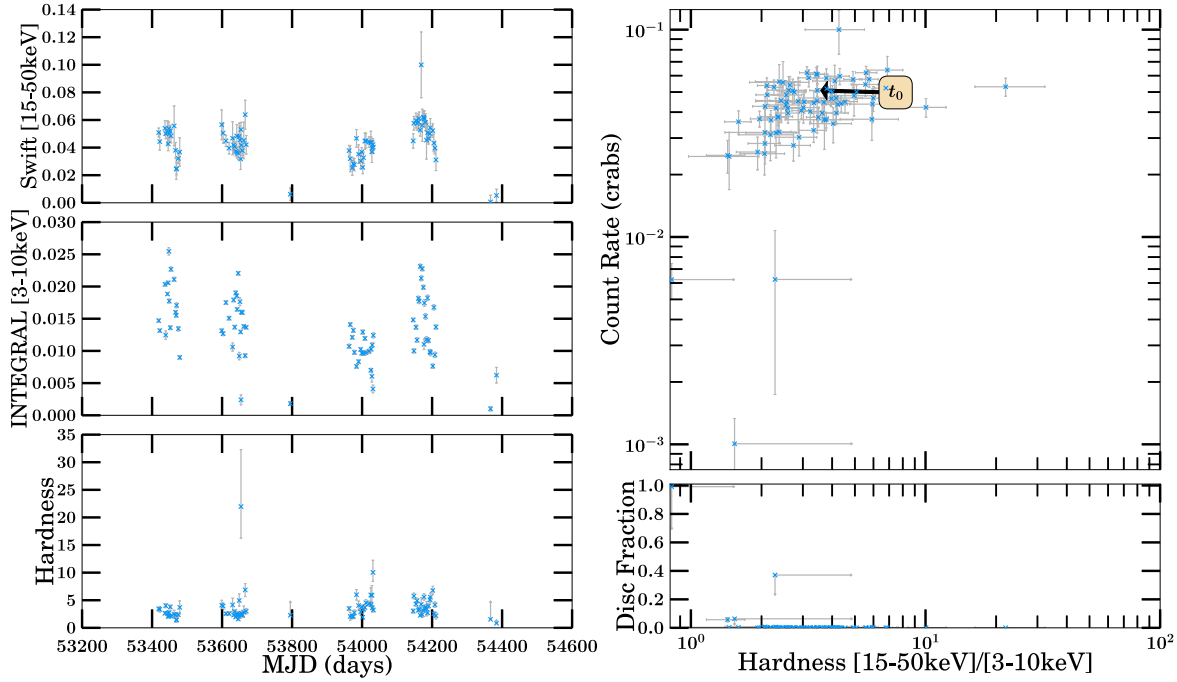

(b) 2005–2007 Outburst Analysis

Figure B.121: 1E 1740.7−2942 Part 2

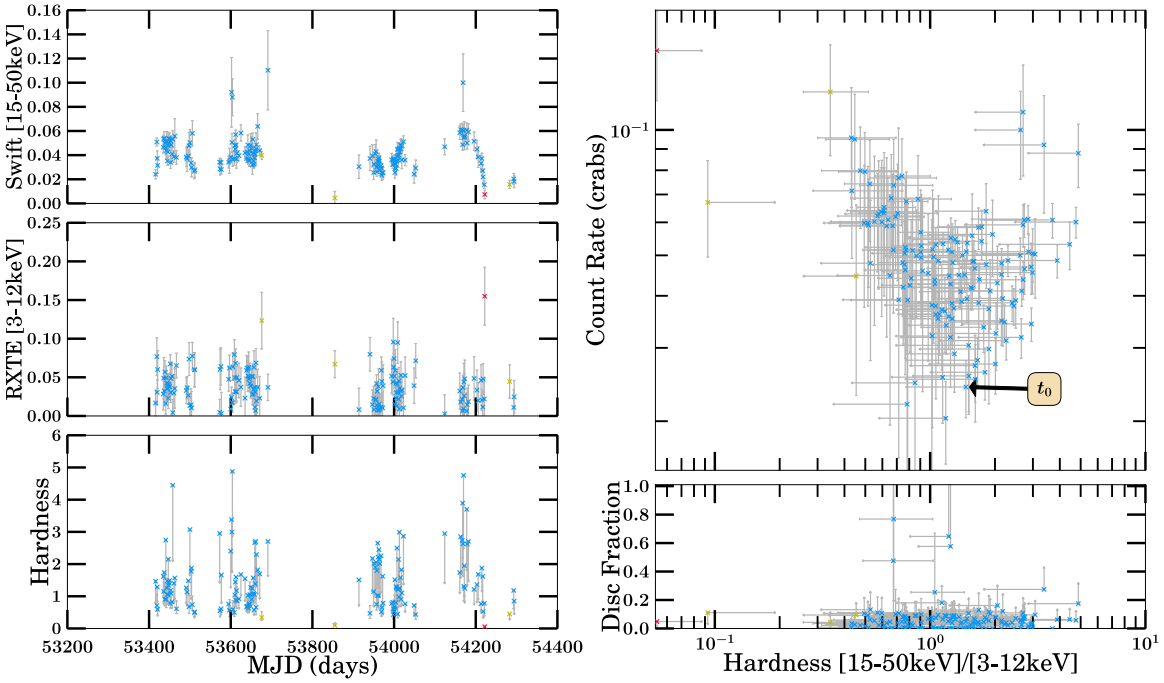

(a) 2005–2007 Outburst Analysis

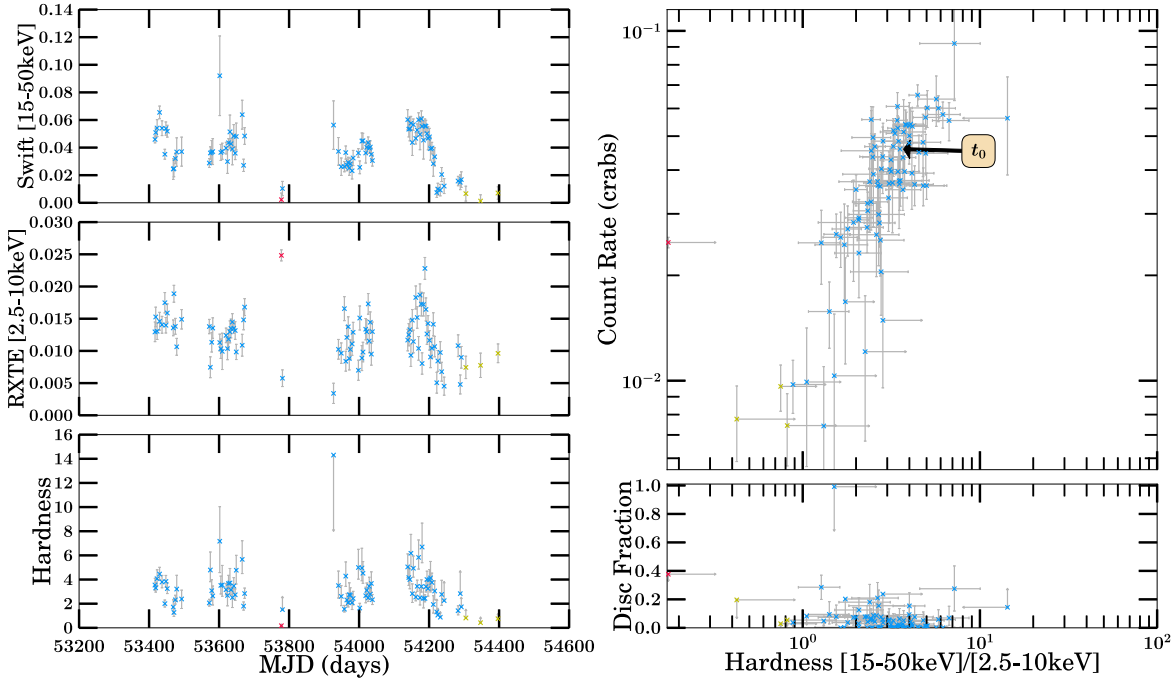

(b) 2005–2007 Outburst Analysis

Figure B.122: 1E 1740.7−2942 Part 3

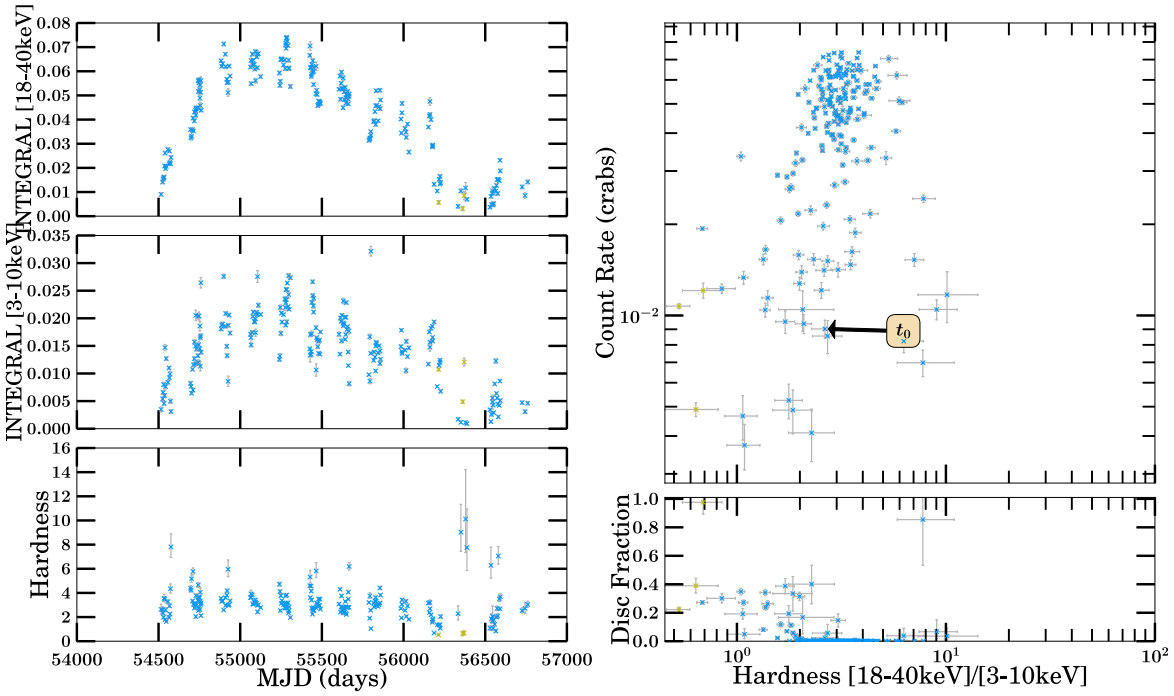

(a) 2008–2014 Outburst Analysis

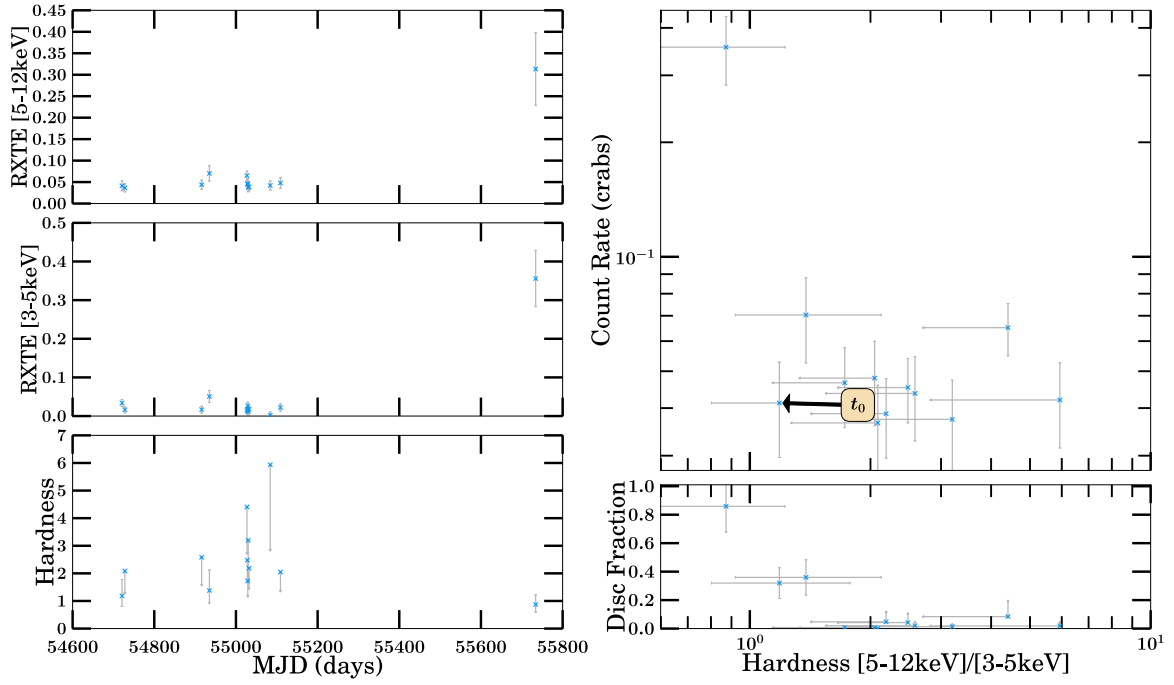

(b) 2008–2014 Outburst Analysis

Figure B.123: 1E 1740.7−2942 Part 4

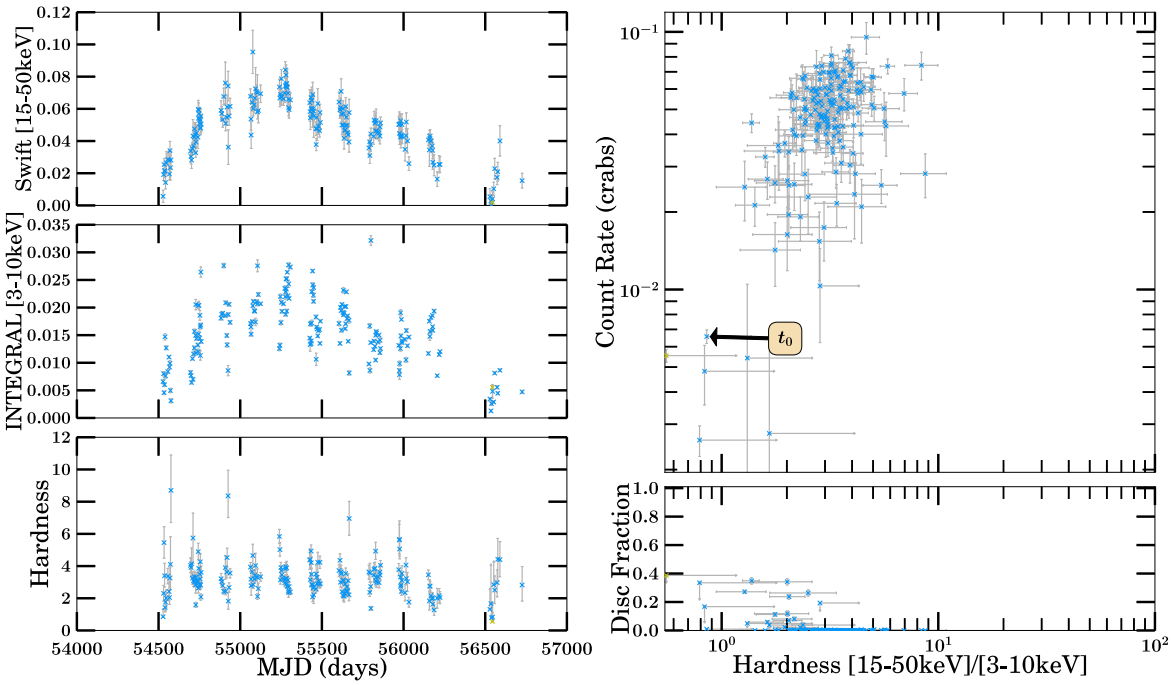

(a) 2008–2014 Outburst Analysis

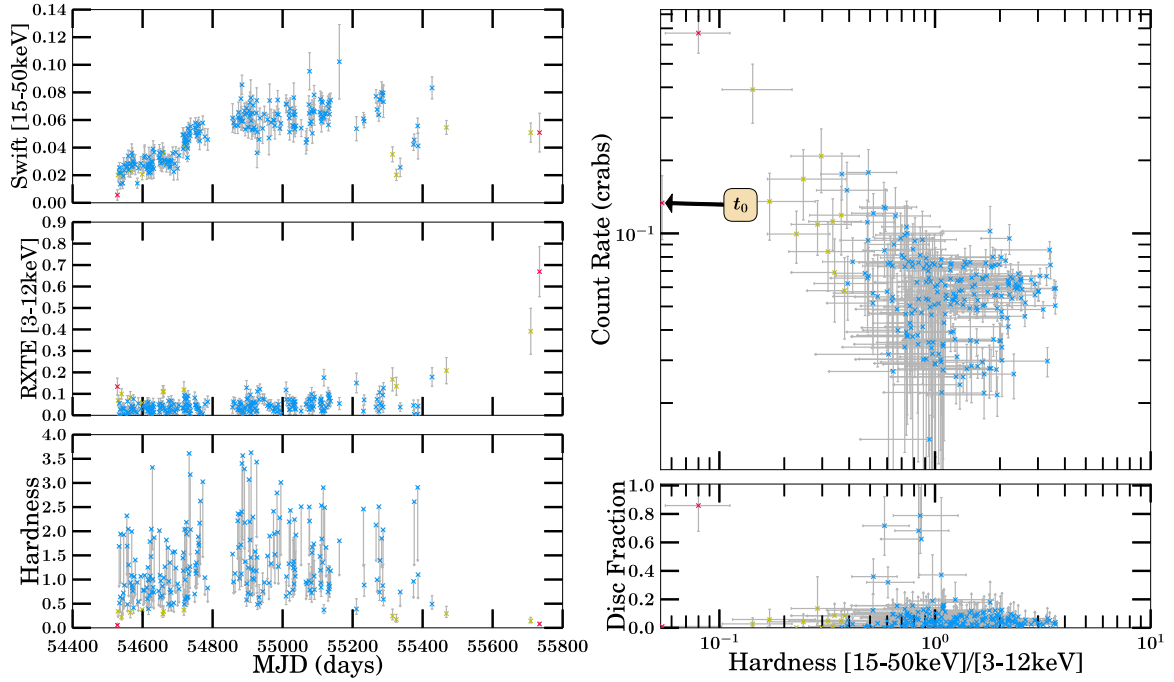

(b) 2008–2014 Outburst Analysis

Figure B.124: 1E 1740.7−2942 Part 5

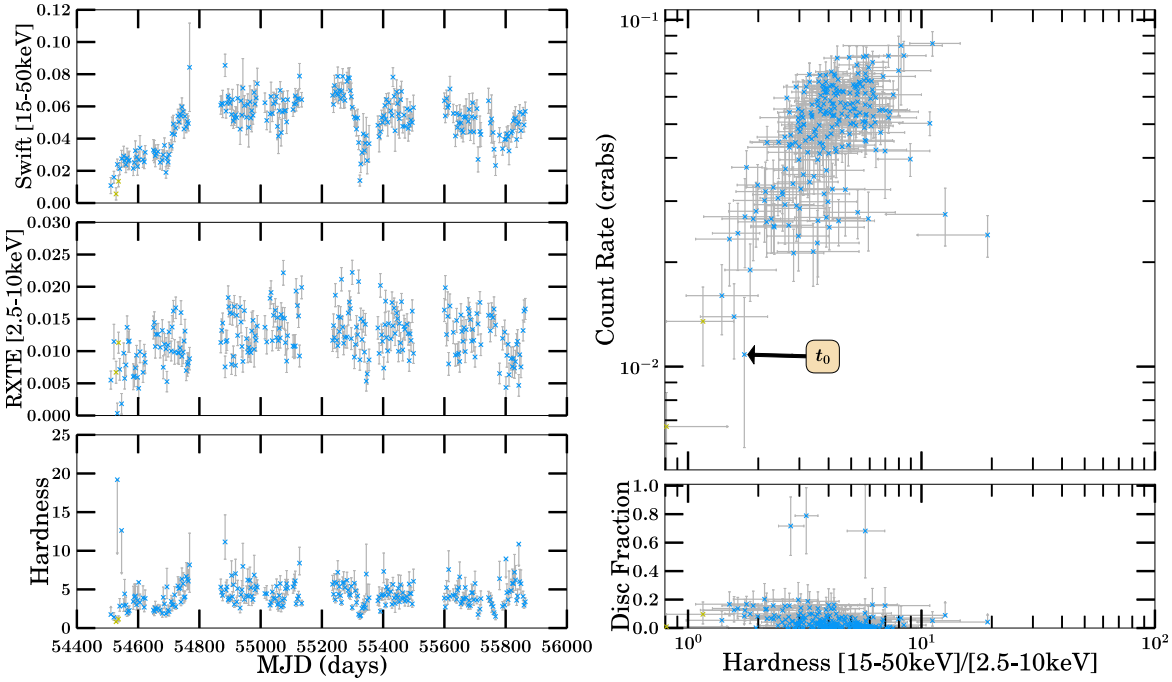

(a) 2008–2014 Outburst Analysis

Figure B.125: 1E 1740.7−2942 Part 6

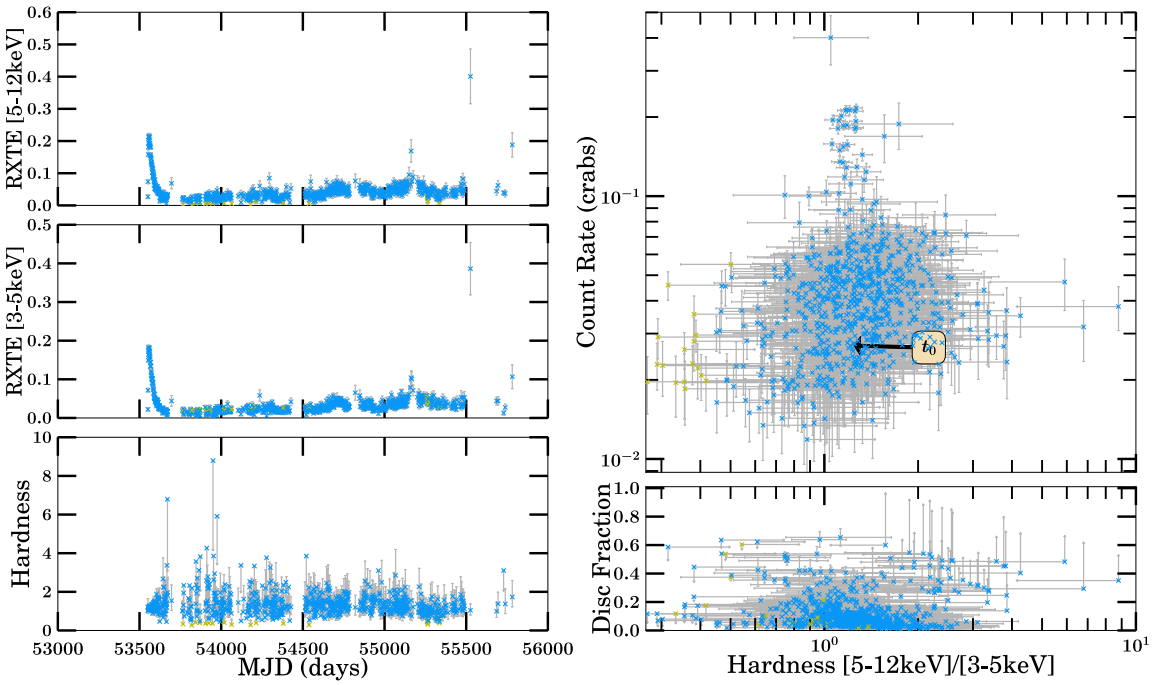

(a) 1996–2014 Outburst Analysis

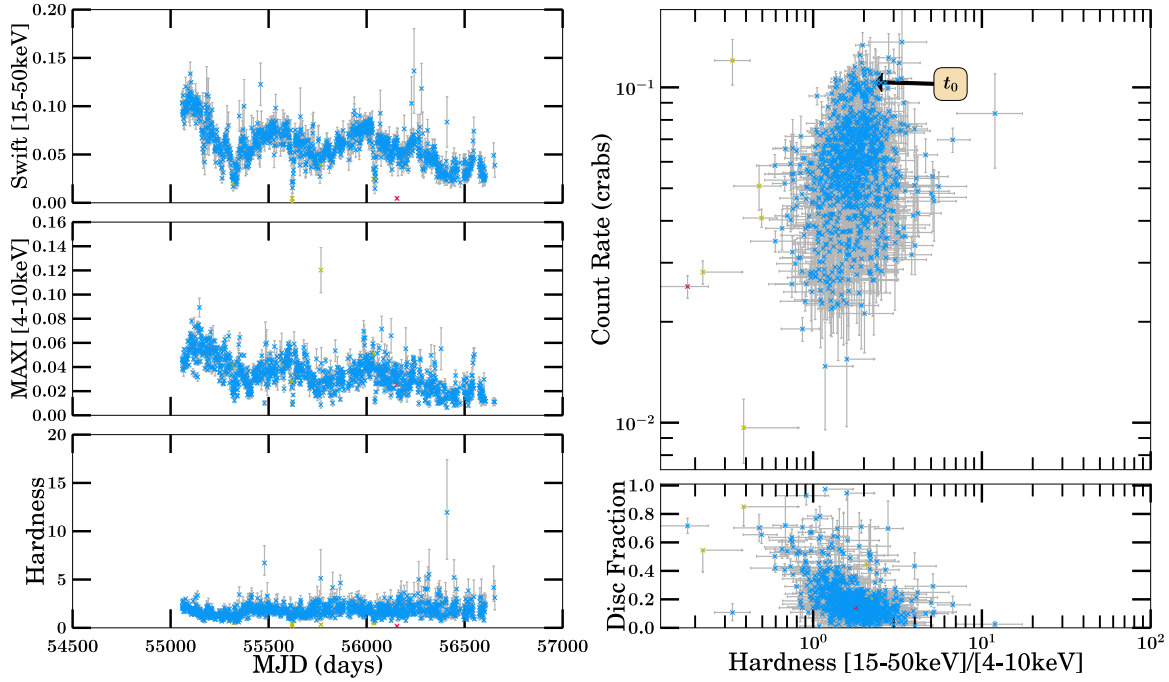

(b) 1996–2014 Outburst Analysis

Figure B.126: Swift J1753.5−0127 Part 1

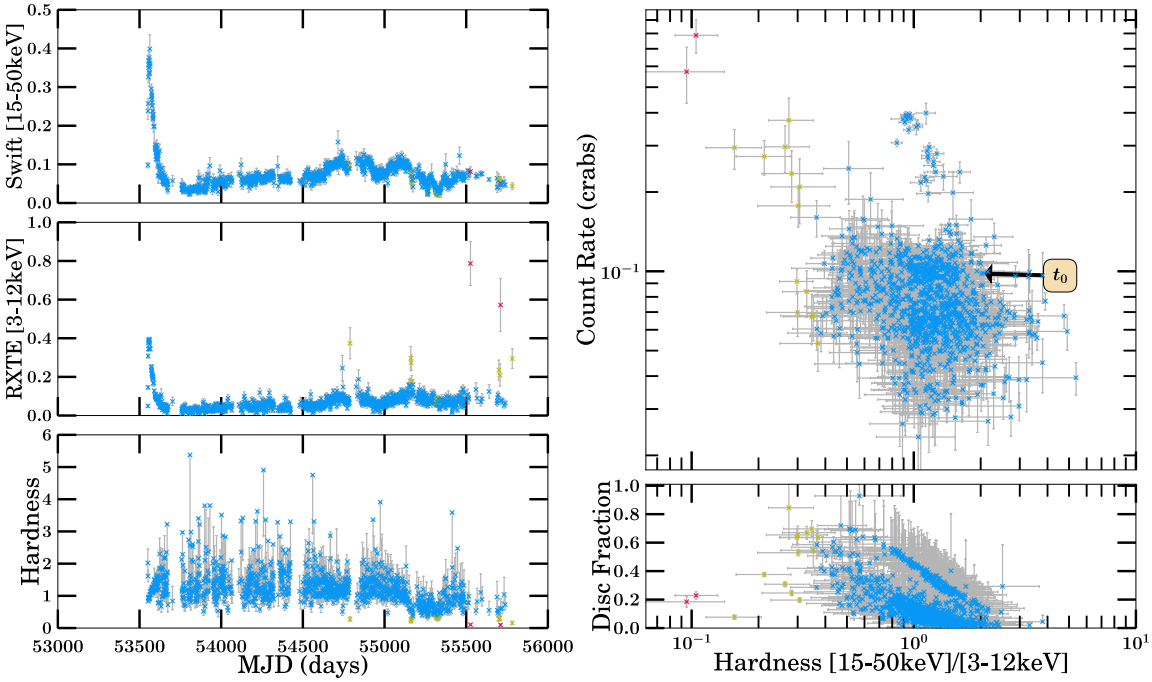

(a) 1996–2014 Outburst Analysis

Figure B.127: Swift J1753.5−0127 Part 2

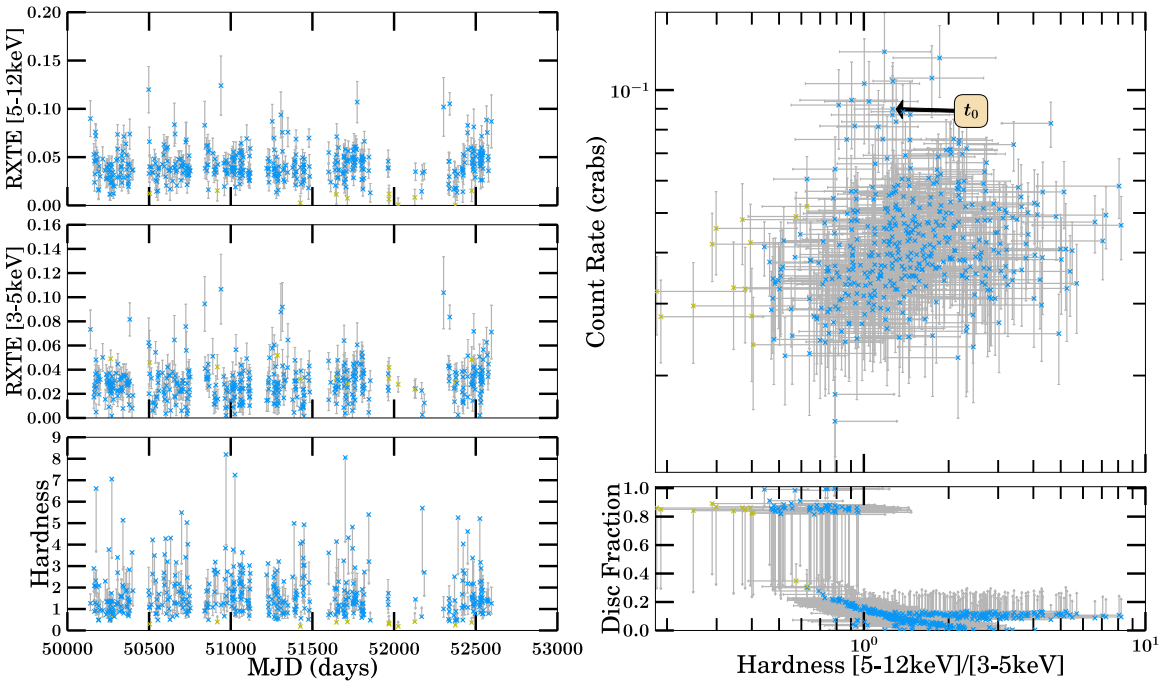

(a) 1996–2002 Outburst Analysis

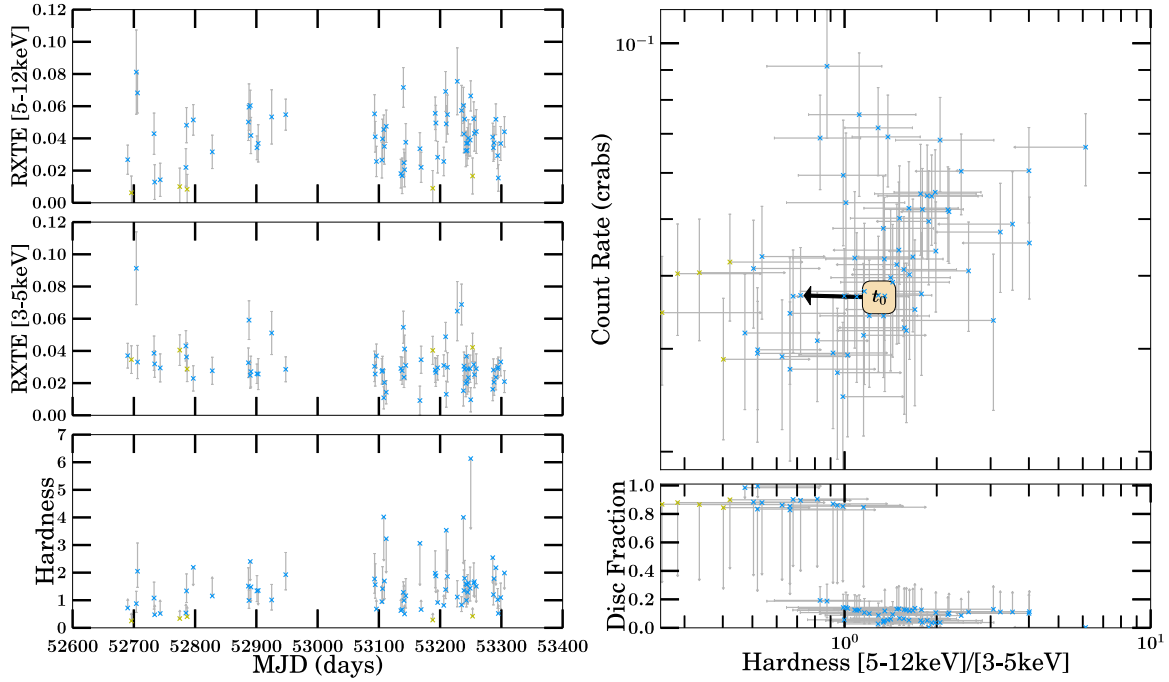

(b) 2005–2014 Outburst Analysis

Figure B.128: GRS 1758−258 Part 1

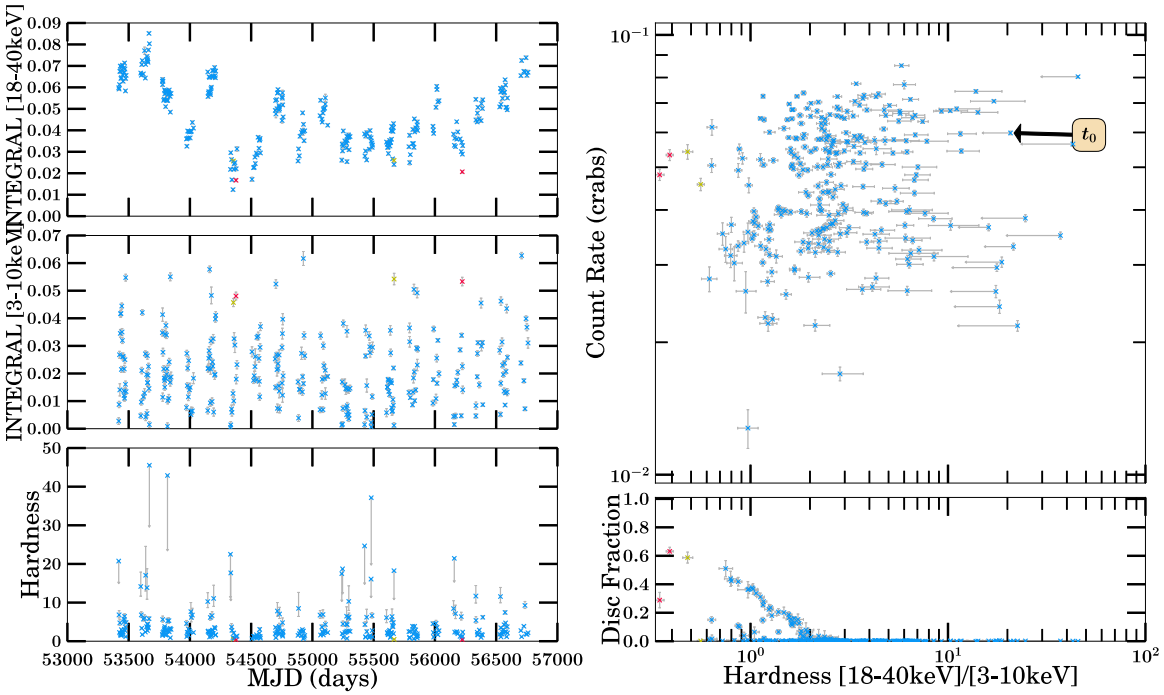

(a) 2005–2014 Outburst Analysis

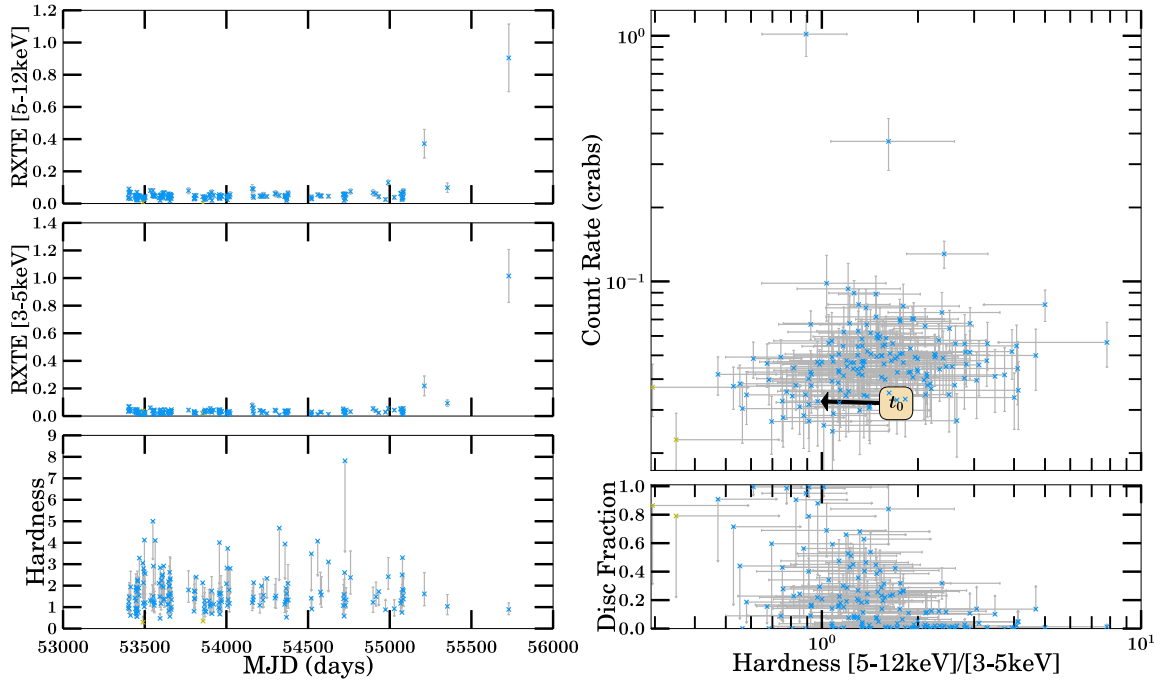

(b) 2005–2014 Outburst Analysis

Figure B.129: GRS 1758−258 Part 2

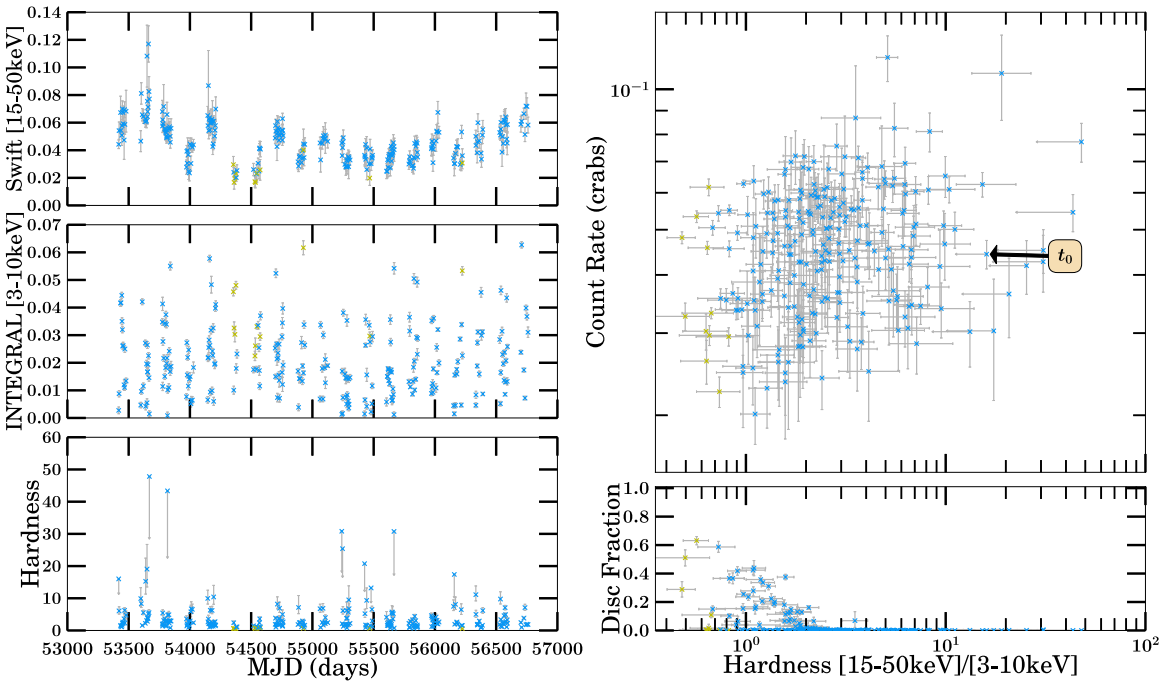

(a) 2005–2014 Outburst Analysis

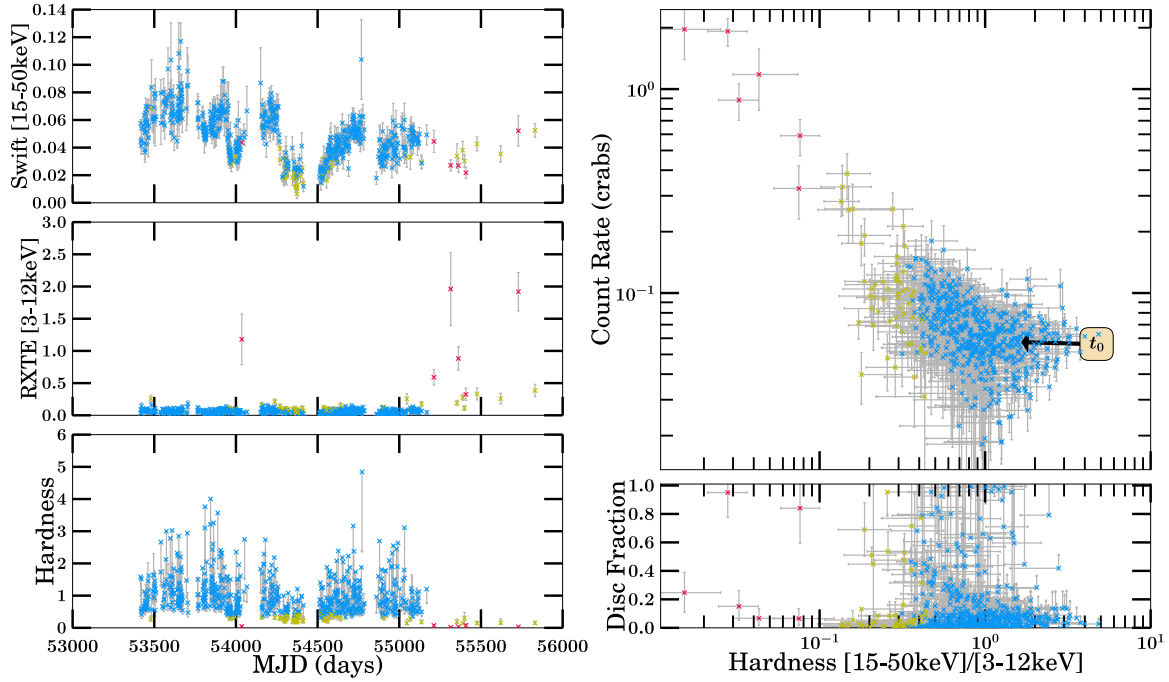

(b) 2005–2014 Outburst Analysis

Figure B.130: GRS 1758−258 Part 3

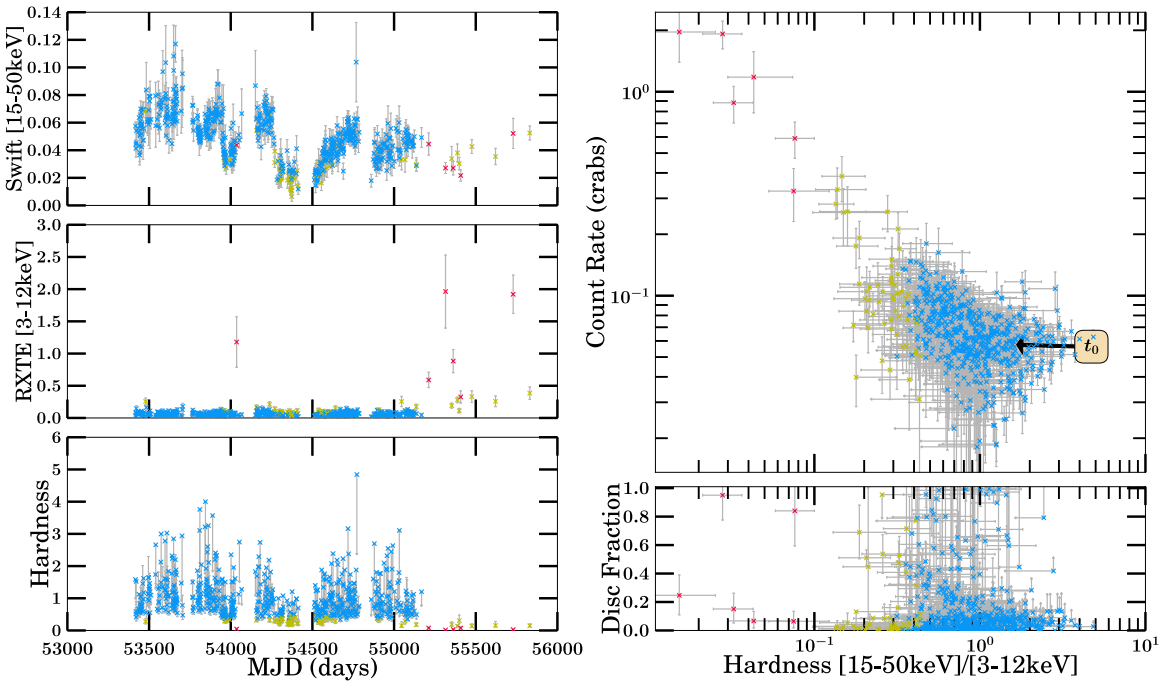

(a) 2005–2014 Outburst Analysis

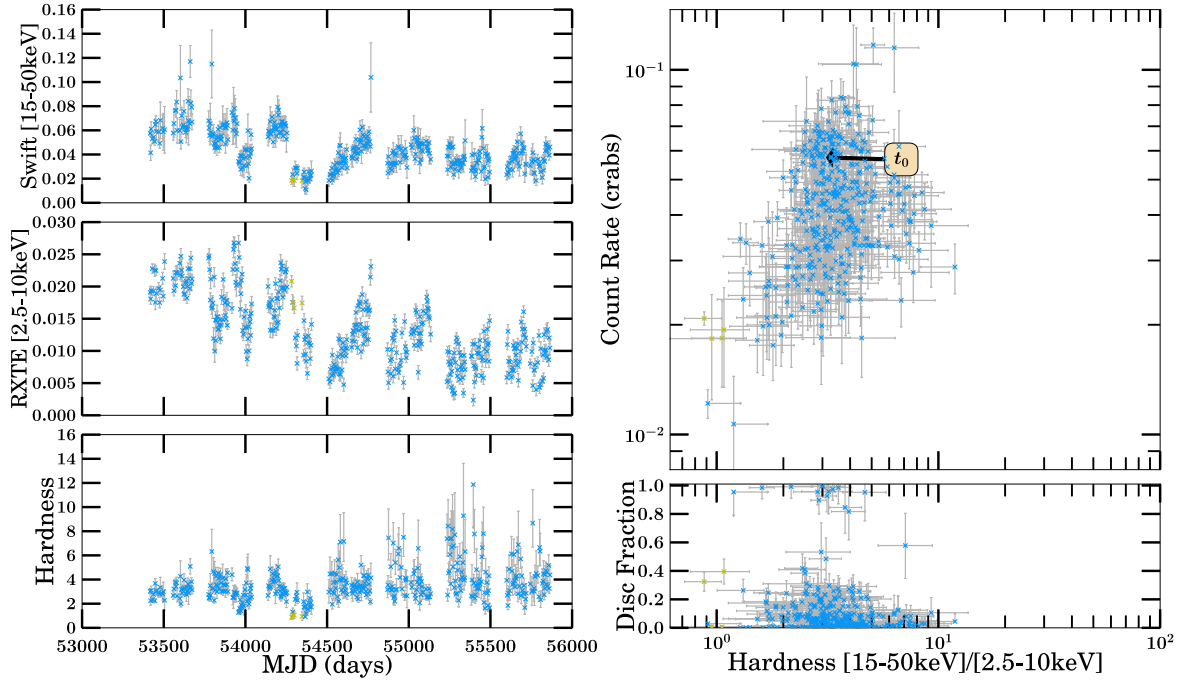

(b) 2005–2014 Outburst Analysis

Figure B.131: GRS 1758−258 Part 4

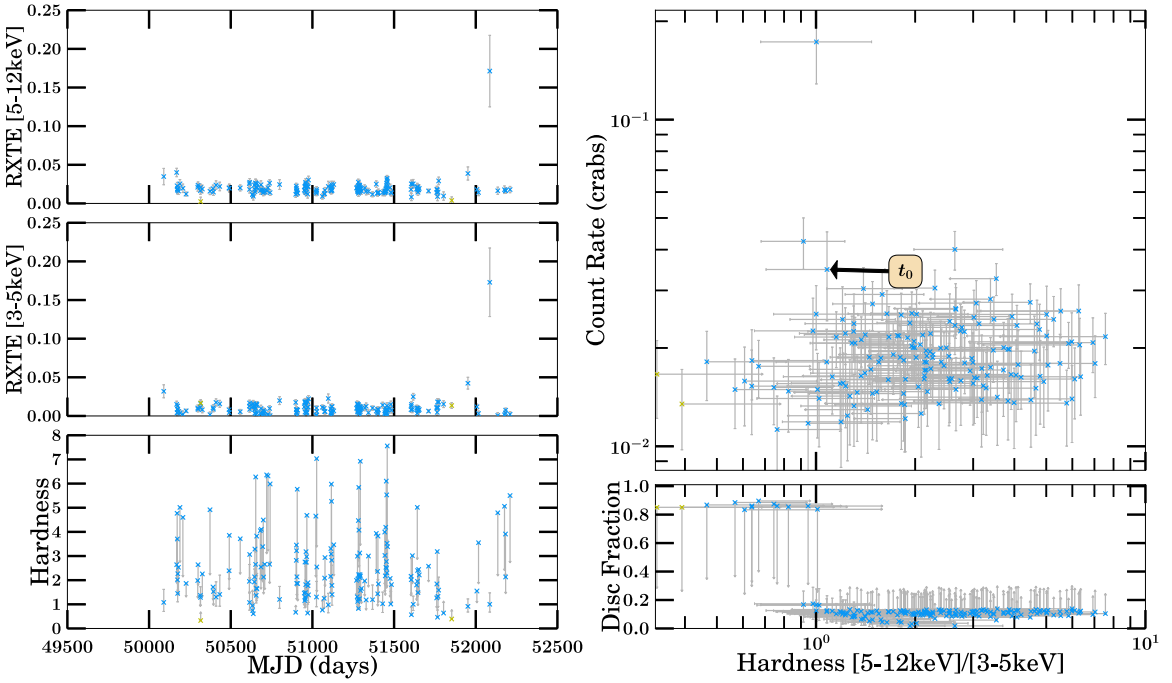

(a) 1996–2001 Outburst Analysis

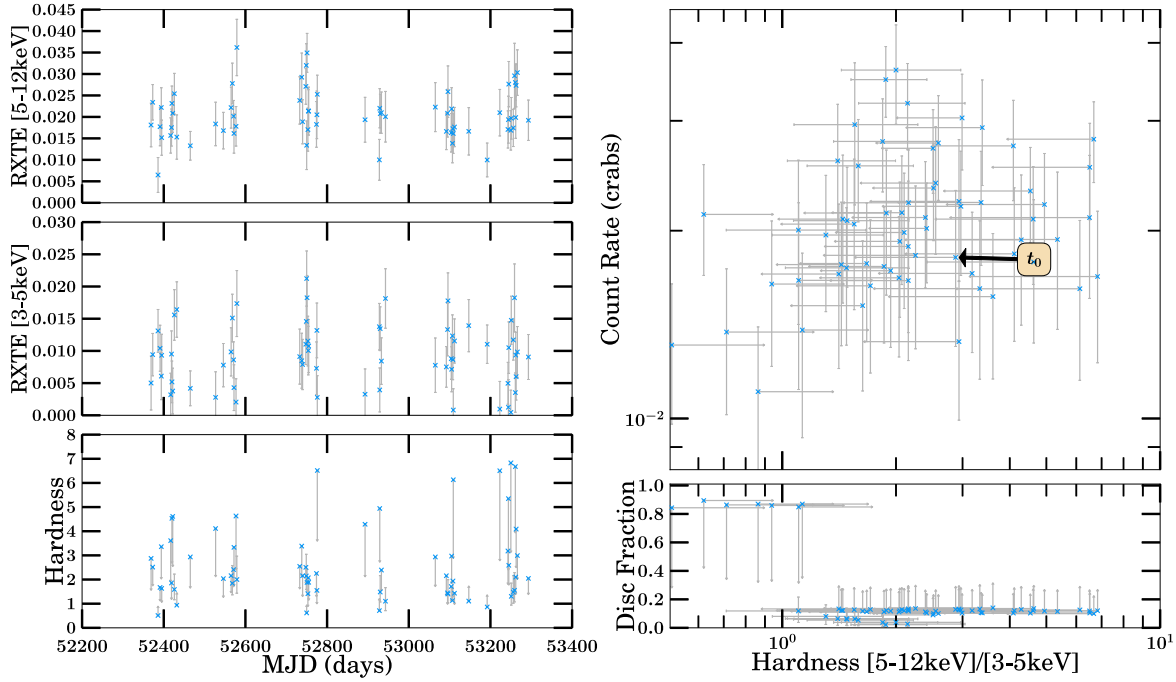

(b) 2002–2004 Outburst Analysis

Figure B.132: SS 433 Part 1

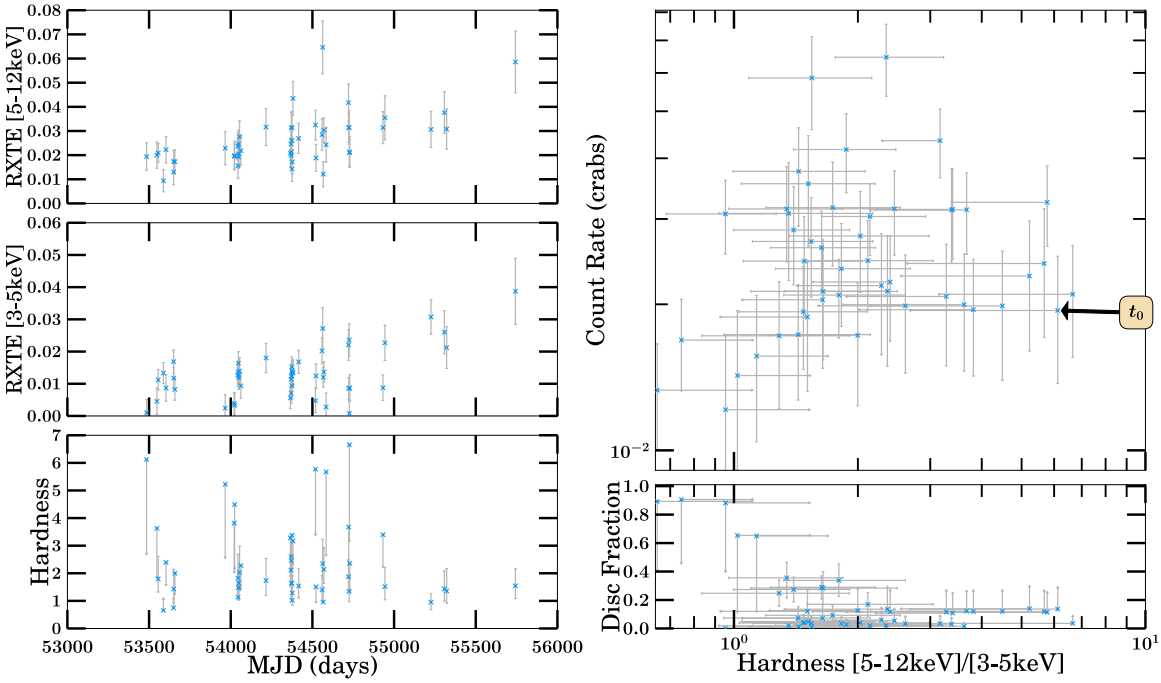

(a) 2005–2014 Outburst Analysis

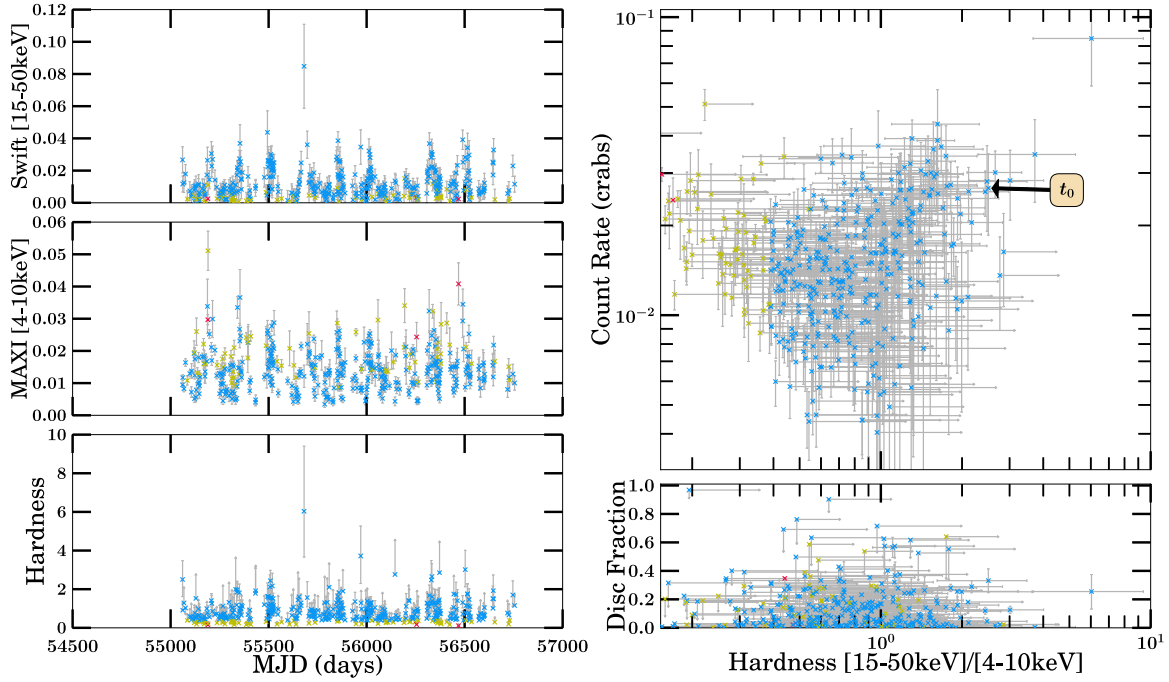

(b) 2005–2014 Outburst Analysis

Figure B.133: SS 433 Part 2

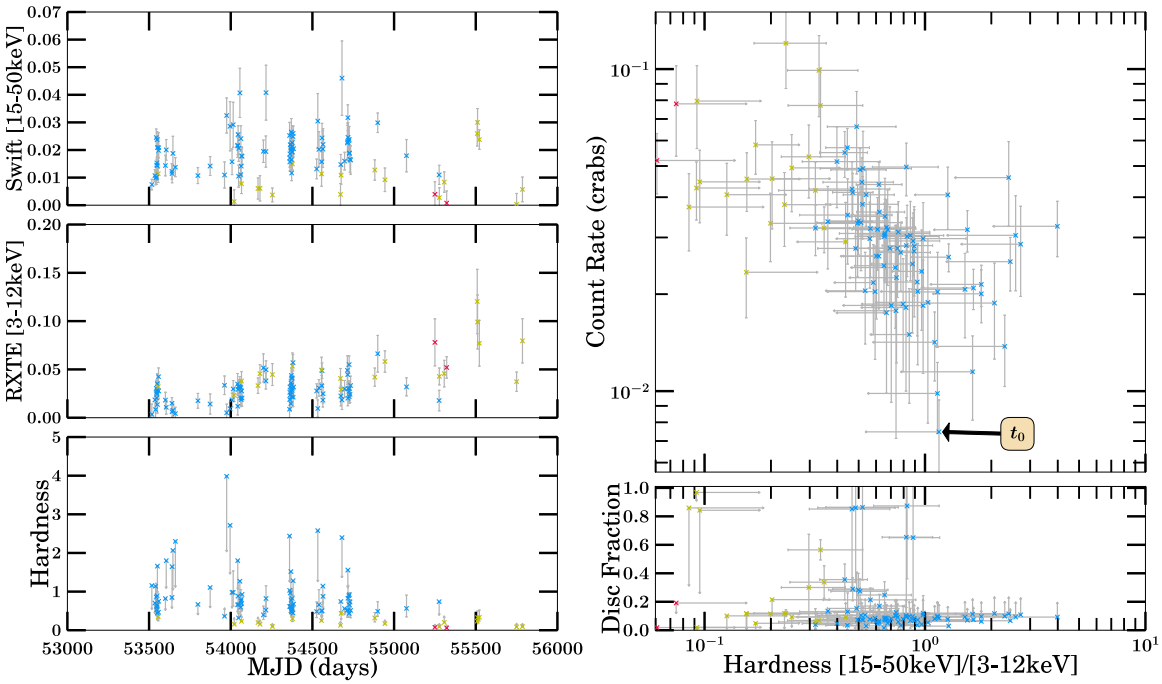

(a) 2005–2014 Outburst Analysis

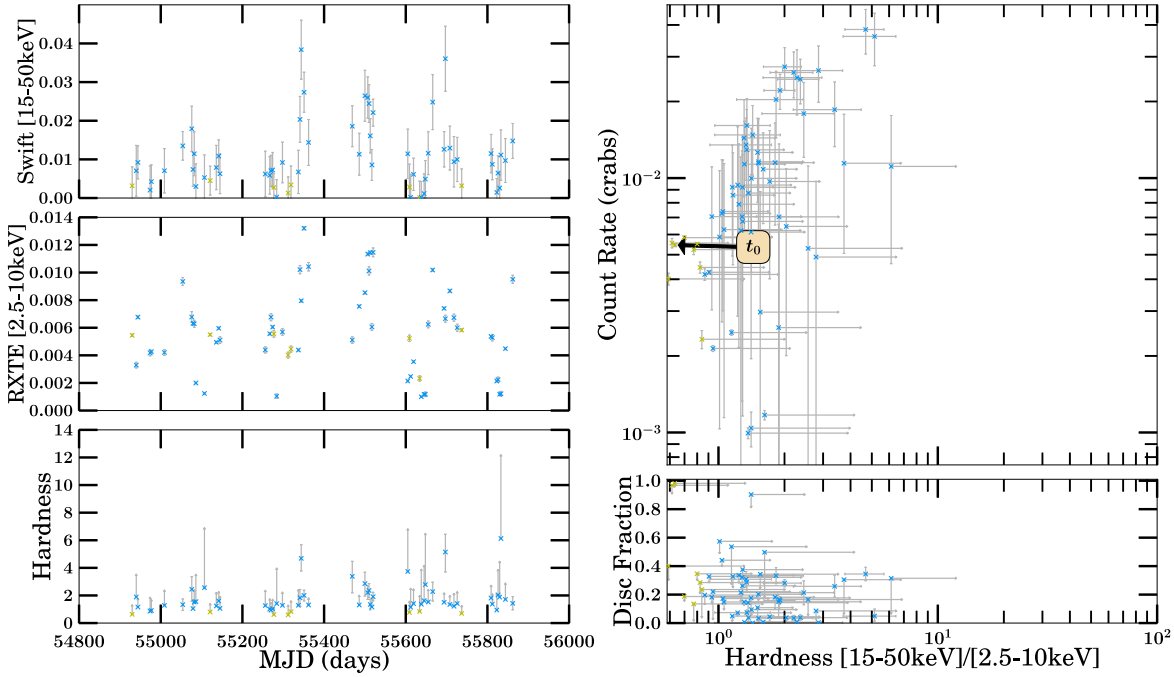

(b) 2005–2014 Outburst Analysis

Figure B.134: SS 433 Part 3

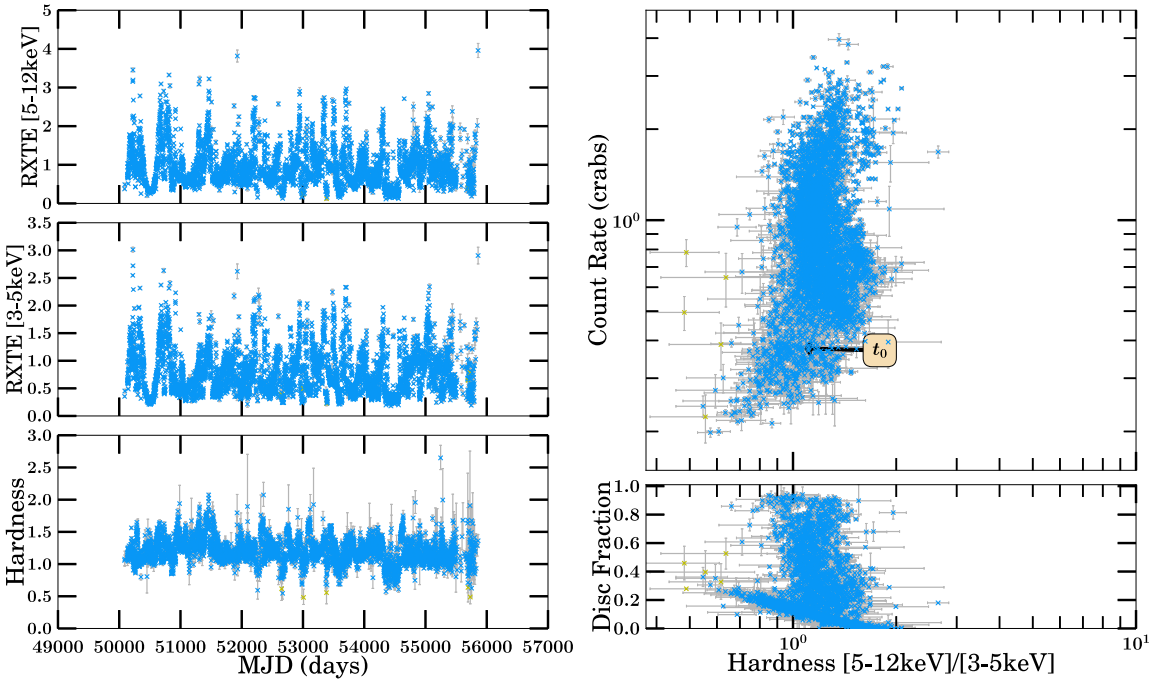

(a) 1996–2014 Outburst Analysis

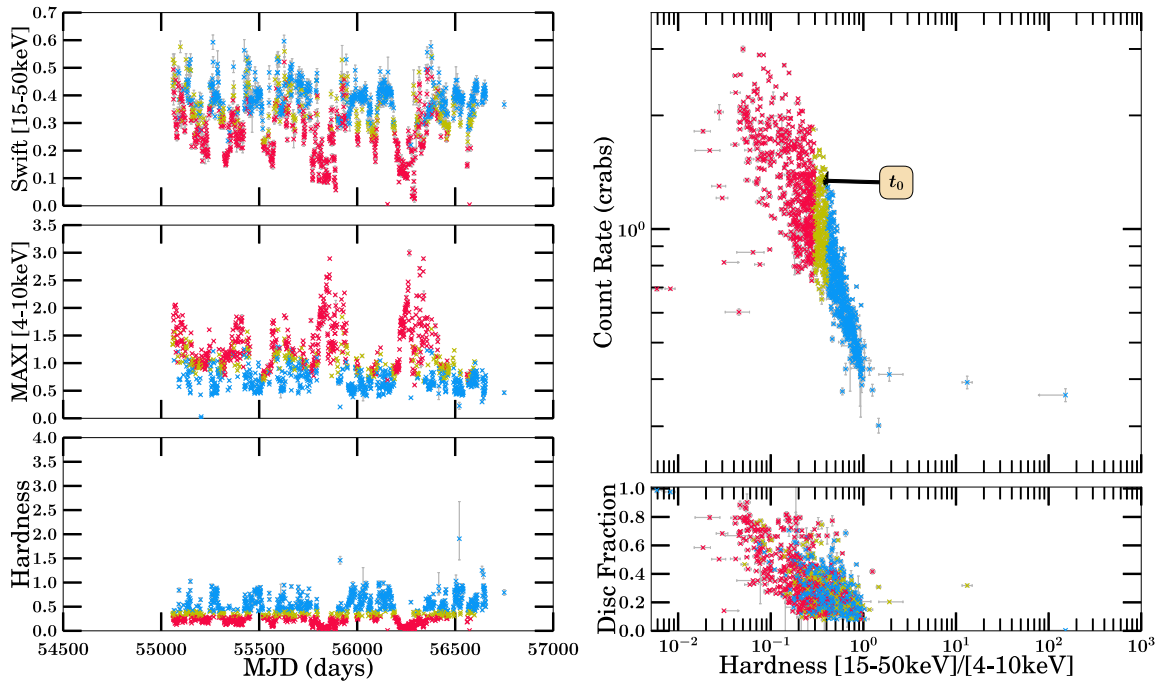

(b) 1996–2014 Outburst Analysis

Figure B.135: GRS 1915+105 Part 1

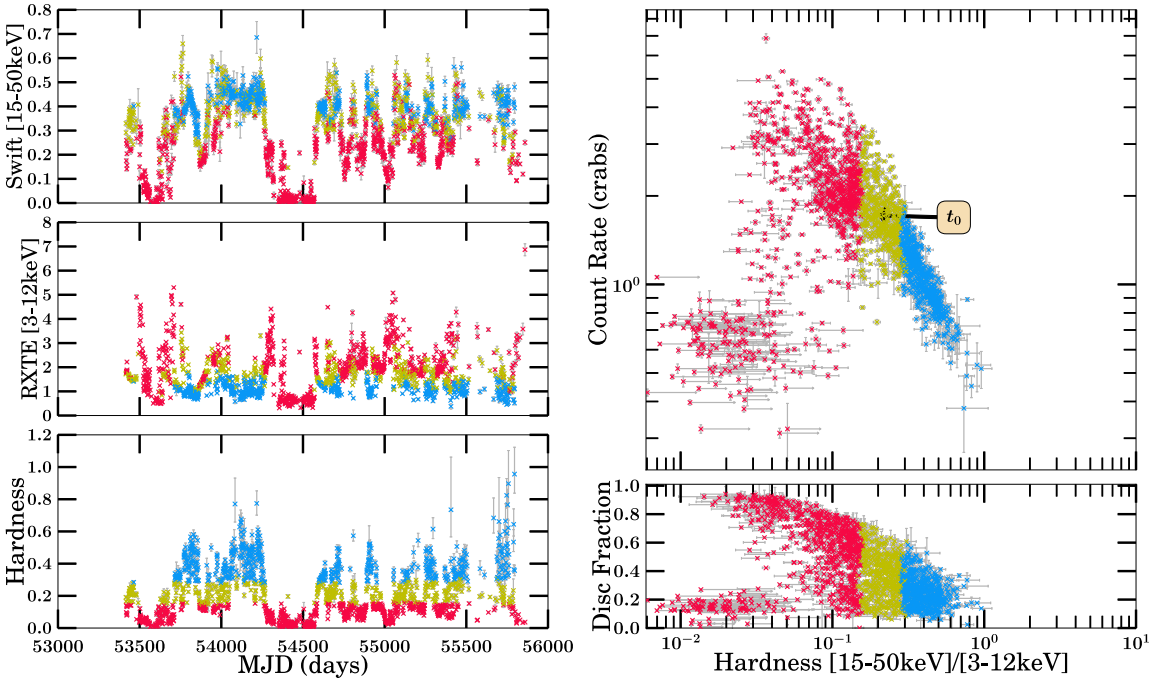

(a) 1996–2014 Outburst Analysis

Figure B.136: GRS 1915+105 Part 2

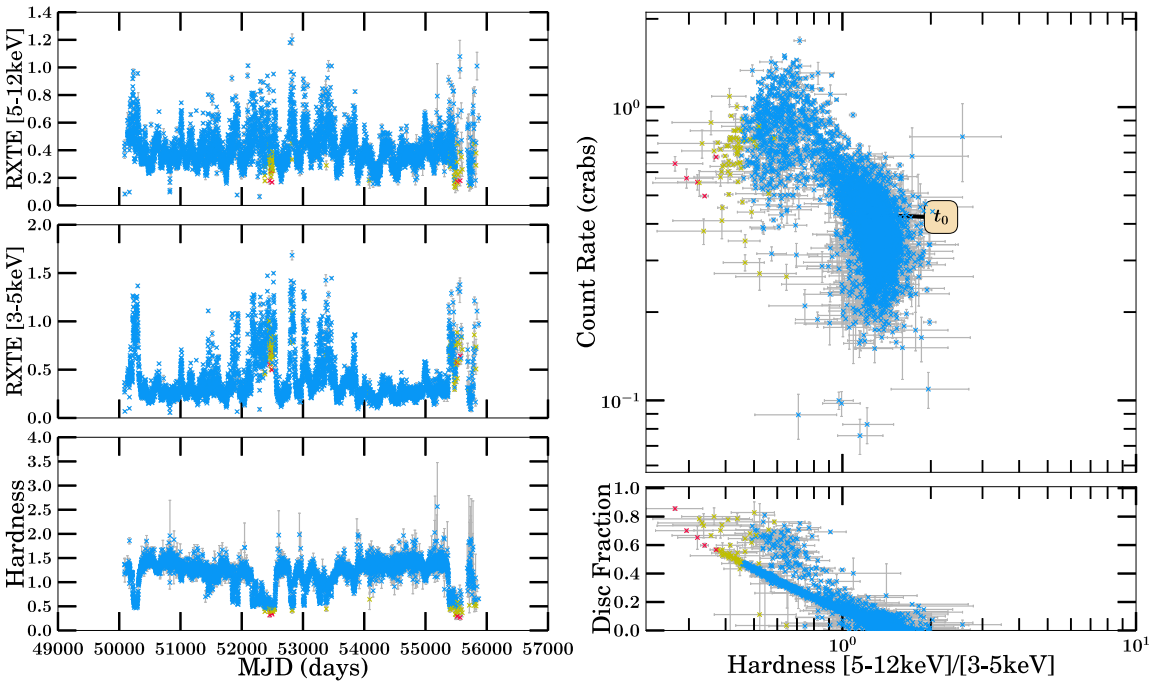

(a) 1996–2014 Outburst Analysis

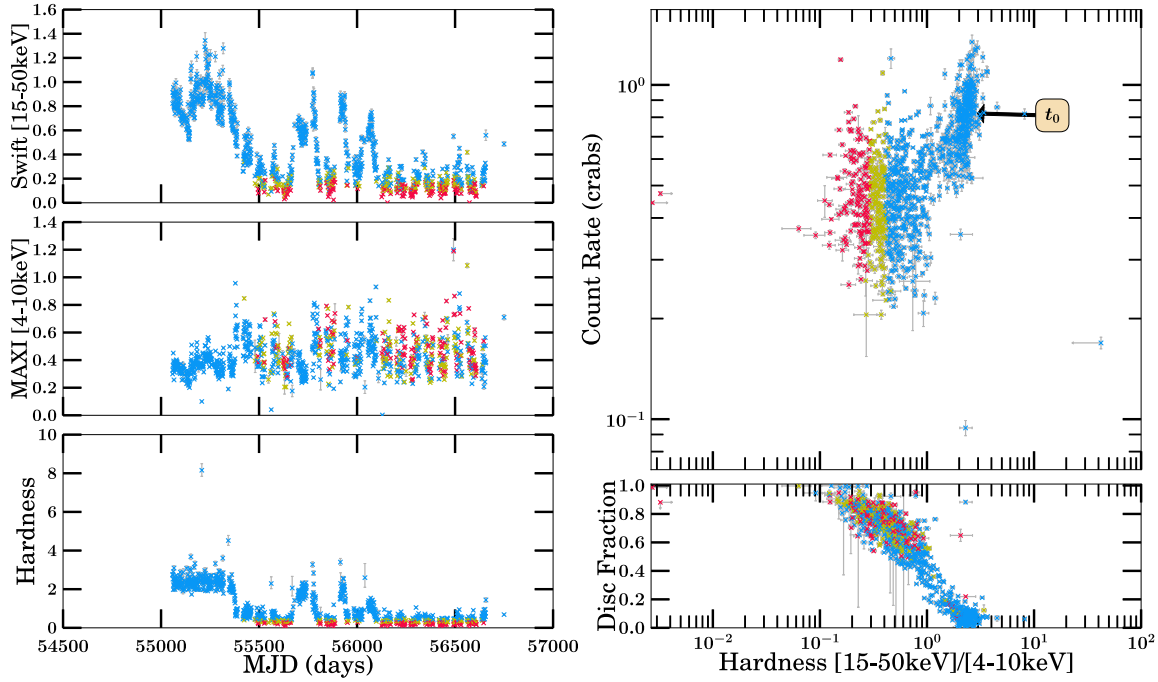

(b) 1996–2014 Outburst Analysis

Figure B.137: 4U 1956+350 Part 1

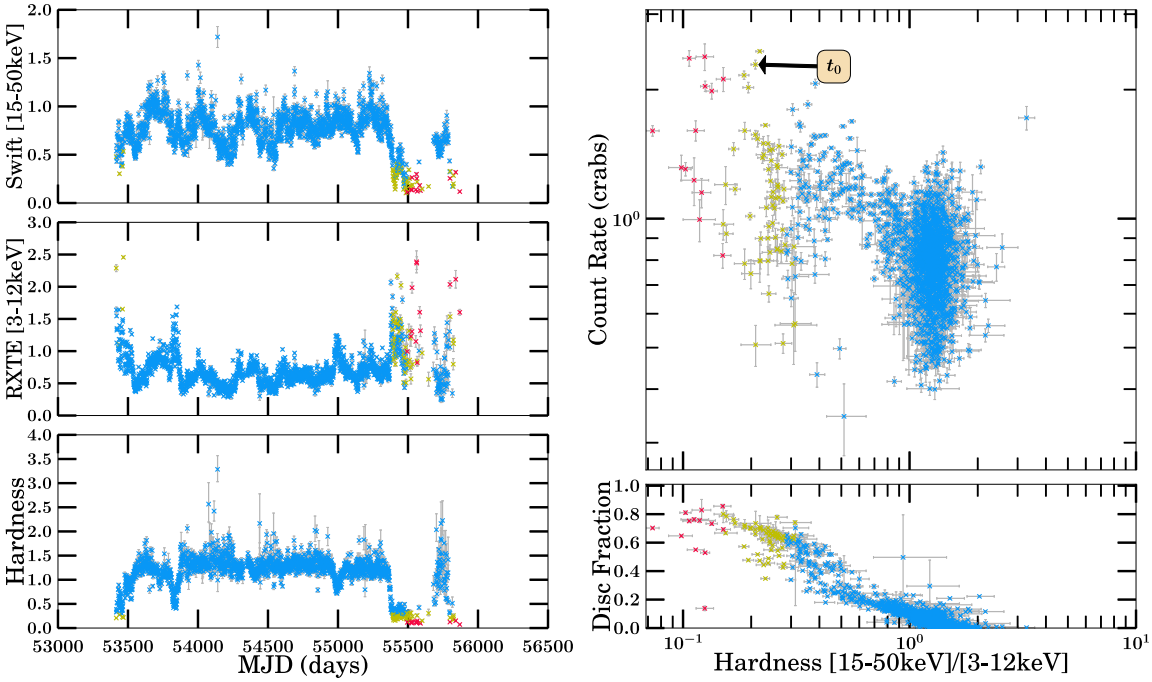

(a) 1996–2014 Outburst Analysis

Figure B.138: 4U 1956+350 Part 2

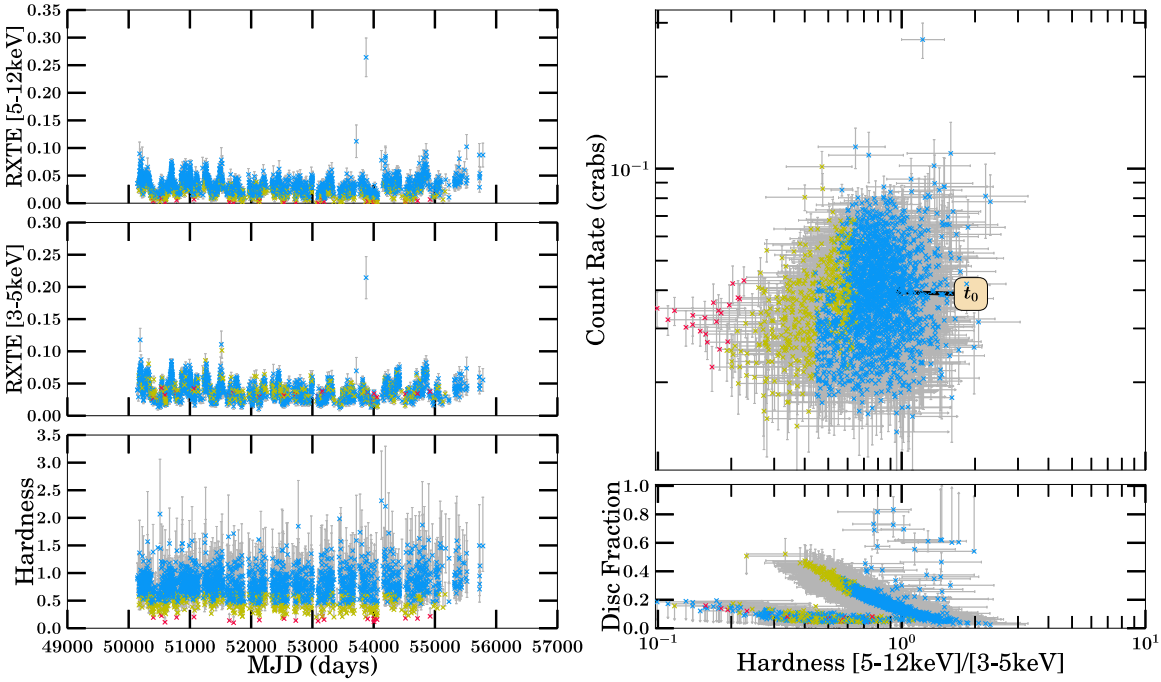

(a) 1996–2014 Outburst Analysis

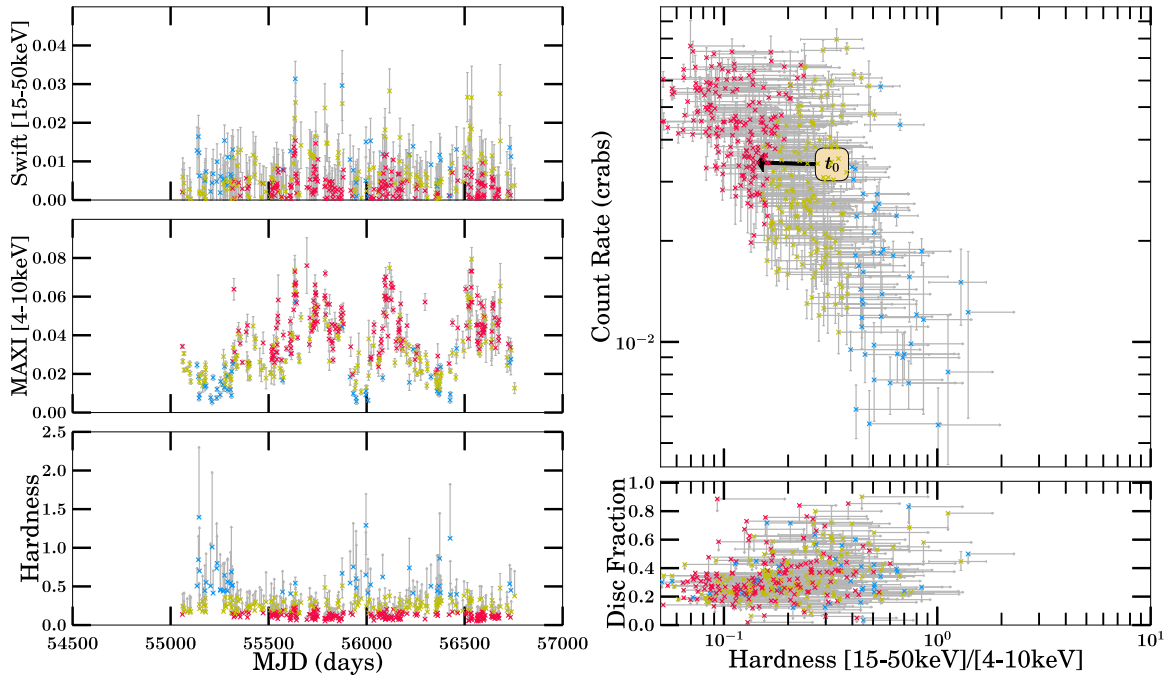

(b) 1996–2014 Outburst Analysis

Figure B.139: 4U 1957+115 Part 1

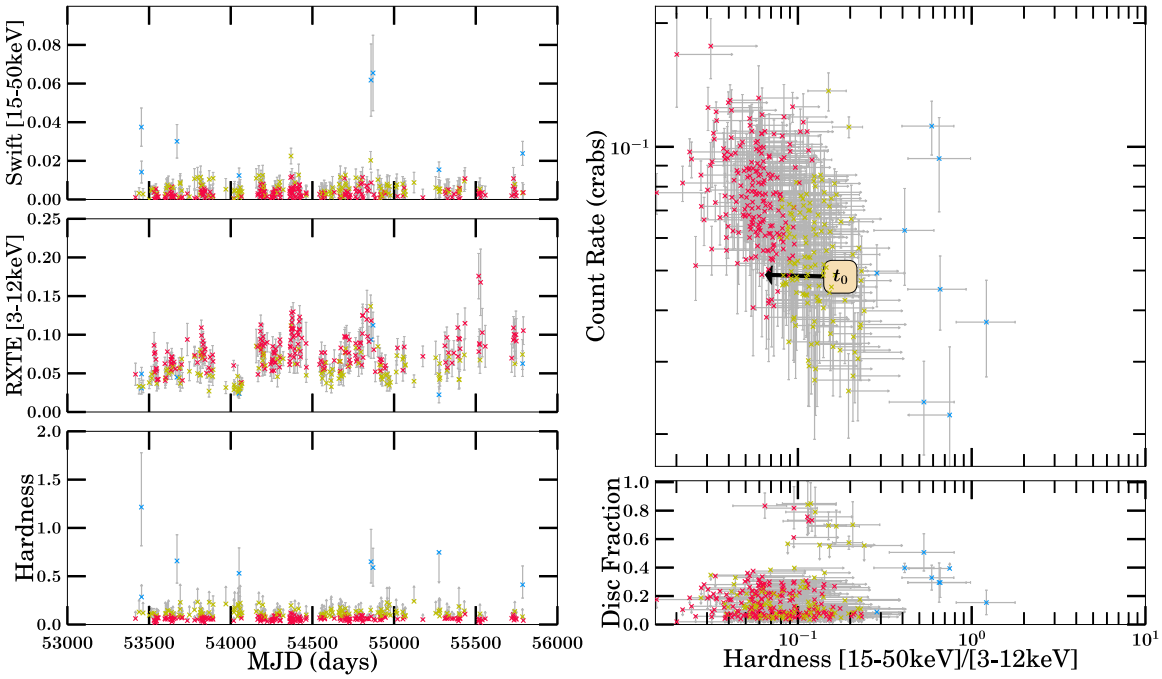

(a) 1996–2014 Outburst Analysis

Figure B.140: 4U 1957+115 Part 2

Page intentionally left blank

Bibliography

Y. Abe, Y. Fukazama, A. Kubota, D. Kasama, and K. Makishima. *PASJ*, 57:629, 2005.

G. O. Abell and B. Margon. *Nature*, 279:701, 1979.

M.A. Abramowicz and I.V. Igumenshchev. *ApJ*, 554:L53, 2001.

M.A. Abramowicz, B. Czerny, J. Lasota, and E. Szuszkiewicz. *ApJ*, 332:646, 1988.

D. Altamirano, T. Belloni, H. Krimm, P. Casella, P. Curran, J. Kennea, M. Kalamkar, M. van der Klis, R. Wijnands, M. Linares, S. Motta, T. Munoz-Darias, and H. Stiele. *ATEL*, 3230, 2011a.

D. Altamirano, T. Belloni, M. Linares, M. van der Klis, R. Wijnands, P. A. Curran, M. Kalamkar, H. Stiele, S. Motta, T. Muñoz-Darias, P. Casella, and H. Krimm. *ApJ*, 742:L17, 2011b.

D. Altamirano, M. Linares, M. van der Klis, R. Wijnands, M. Kalamkar, P. Casella, A. Watts, A. Patruno, M. Armas-Padilla, Y. Cavecchi, N. Degenaar, R. Kaur, Y. Yang, and N. Rea. *ATEL*, 3225, 2011c.

K. R. Anantharamaiah, K. S. Dwarakanath, D. Morris, W. M. Goss, and V. Radhakrishnan. *ApJ*, 410:110, 1993.

D.F. Andrews, P.J. Bickel, F.R. Hampel, W.H. Rogers, and J.W. Tukey. *Robust Estimates of Location: Survey and Advances*. Princeton University, 1972.

L. Angelini and N.E. White. *ApJ*, 586:L71, 2003.

V. A. Aref'ev, M. G. Revnivtsev, A. A. Lutovinov, and R. A. Sunyaev. *AstL*, 30: 669, 2004.

M. Armas Padilla, N. Degenaar, A. Patruno, and R. Wijnands. *ATEL*, 2656, 2010a.

M. Armas Padilla, R. Kaur, N. Degenaar, R. Wijnands, F. Lewis, and D.M. Russell. *ATEL*, 2722, 2010b.

M. Armas-Padilla, N. Degenaar, A. Patruno, D. M. Russell, M. Linares, T. J. Maccarone, J. Homan, and R. Wijnands. *MNRAS*, 417:659, 2011.

M. Armas Padilla, N. Degenaar, D. M. Russell, and R. Wijnands. *MNRAS*, 428: 3083, 2013a.

M. Armas Padilla, R. Wijnands, D. Altamirano, M. Mendez, J. M. Miller, and N. Degenaar. *arXiv:1308.4326*, 2013b.

A. M. Atoyan and F. A. Aharonian. *ApJ*, 490:L149, 1997.

T. Augusteijn, M. Coe, and P. Groot. *IAU Circ.*, 7710, 2001.

K. Ayani and T.C. Peiris. *IAU Circ.*, 7254, 1999.

C. Bailyn, D. Maitra, M. Buxton, L. Jeanty, and D. Gonzalez. *ATEL*, 171, 2003.

C.D. Bailyn and J.A. Orosz. *ApJ*, 440:L73, 1995.

C.D. Bailyn, J.A. Orosz, T.M. Girard, S. Jogee, M. Della Valle, M.C. Begam, A.S. Fruchter, R. González, P.A. Lanna, A.C. Layden, D.H. Martins, and M. Smith. *Nature*, 374:701, 1995a.

C.D. Bailyn, J.A. Orosz, J.E. McClintock, and R.A. Remillard. *Nature*, 378:157, 1995b.

S.A. Balbus. *ARA&A*, 41:555, 2003.

S.A. Balbus and J.F. Hawley. *ApJ*, 376:214, 1991.

L. Ball, M. J. Kesteven, D. Campbell-Wilson, A. J. Turtle, and R. M. Hjellming. *MNRAS*, 273:722, 1995.

J. Ballet, M. Denis, M. Gilfanov, and R. Sunyaev. *IAU Circ.*, 5874, 1993.

D.L. Band. *ApJ*, 336:937, 1989.

E. J. Barlow, A. J. Bird, D. J. Clark, R. Cornelisse, A. J. Dean, A. B. Hill, L. Moran, V. Sguera, S. E. Shaw, D. R. Willis, F. Capitanio, M. Del Santo, and L. Bassani. *A&A*, 437:L27, 2005.

P. Barr and H. van der Woerd. *ApJ*, 352:L41, 1990.

D. Barret, J. P. Roques, P. Mandrou, L. Bouchet, F. Lebrun, A. Goldwurm, P. Laurent, J. Paul, R. Sunyaev, E. Churazov, M. Gilfanov, A. Diachkov, N. Kavenson, B. Novikov, I. Chulkov, and A. Kuznetsov. *ApJ*, 392:L19, 1992.

D. Barret, C. Motch, W. Pietsch, and W. Voges. *A&A*, 296:459, 1995.

D. Barret, J. E. Grindlay, P. F. Bloser, B. A. Harmon, S. N Zhang, C. A. Wilson, C. R. Robinson, W. S. Paciesas, and C. H. Smith. *IAU Circ.*, 6519, 1996a.

D. Barret, J.E. McClintock, and J.E. Grindlay. *ApJ*, 473:963, 1996b.

E. A. Barsukova, N. V. Borisov, A. N. Burenkov, V. G. Klochkova, V. P. Goranskij, and N. V. Metlova. *ATEL*, 416, 2005.

E. S. Bartlett, J. S. Clark, M. J. Coe, M. R. Garcia, and P. Uttley. *MNRAS*, 429: 1213, 2013.

A. Bazzano, C. La Padula, P. Ubertini, and R.K. Sood. *ApJ*, 385:L17, 1992.

G. Beekman, T. Shahbaz, T. Naylor, and P. A. Charles. *MNRAS*, 281:L1, 1996.

G. Beekman, T. Shahbaz, T. Naylor, P.A. Charles, R.M. Wagner, and P. Martini. *MNRAS*, 290:303, 1997.

M.E. Beer and P. Podsiadlowski. *MNRAS*, 331:351, 2002.

T.C. Beers, K. Flynn, and K. Gebhardt. *AJ*, 100:32, 1990.

T. Belloni. *The Jet Paradigm - From Microquasars to Quasars, Lect. Notes in Phys. 794*. Springer, 2009.

T. Belloni and G. Hasinger. *A&A*, 227:L33, 1990.

T. Belloni, M. Mendez, M. van der Klis, G. Hasinger, W.H.G. Lewin, and J. van Paradijs. *ApJ*, 472:L107, 1996.

T. Belloni, M. Mendez, A. R. King, M. van der Klis, and J. van Paradijs. *ApJ*, 479: 145, 1997.

T. Belloni, S. Dieters, M. E. van den Ancker, R. P. Fender, D. W. Fox, B. A. Harmon, M. van der Klis, J. M. Kommers, W. H. G. Lewin, and J. van Paradijs. *ApJ*, 527: 345, 1999a.

T. Belloni, M. Mendez, M. van der Klis, G. Hasinger, W.H.G. Lewin, and S. Dieters. *ApJ*, 519:L159, 1999b.

T. Belloni, M. Klein-Wolt, M. Méndez, M. van der Klis, and J. van Paradijs. *A&A*, 355:271, 2000.

T. Belloni, A. P. Colombo, J. Homan, S. Campana, and M. van der Klis. *A&A*, 390: 199, 2002a.

T. Belloni, D. Psaltis, and M. van der Klis. *ApJ*, 572:392, 2002b.

T. Belloni, J. Homan, P. Casella, M. van der Klis, E. Nespoli, W.H.G. Lewin, J.M. Miller, and M. Mendez. *A&A*, 440:207, 2005.

T. Belloni, I. Parolin, M. Del Santo, J. Homan, P. Casella, R. P. Fender, W. H. G. Lewin, M. Méndez, J. M. Miller, and M. van der Klis. *MNRAS*, 367:1113, 2006.

T. Belloni, M. Cadolle Bel, P. Casella, A. Castro-Tirado, S. Corbel, M. Del Santo, E. Gallo, V. Grinberg, J. Homan, E. Kalemci, J. M. Miller, J. Miller-Jones, S. Motta, T. Munoz-Darias, M. Nowak, K. Pottschmidt, J. Rodriguez, D. Russell, J. Tomsick, and J. Wilms. *ATEL*, 4450, 2012.

T. Belloni, S. Motta, and P. Casella. *ATEL*, 5417, 2013.

T. M. Belloni and D. Altamirano. *MNRAS*, 432(10), 2013.

P.R. Bevington and D.K. Robinson. *Data Reduction and Error Analysis for the Physical Sciences*. McGraw-Hill, third edition, 2003.

J. Binney, O.E. Gerhard, A.A. Stark, J. Bally, and K.I. Uchida. *MNRAS*, 252:210, 1991.

A. J. Bird, E. J. Barlow, L. Bassani, A. Bazzano, G. Bélanger, A. Bodaghee, F. Capitanio, A. J. Dean, M. Fiocchi, A. B. Hill, F. Lebrun, A. Malizia, J. M. Mas-Hesse, M. Molina, L. Moran, M. Renaud, V. Sguera, S. E. Shaw, J. B. Stephen, R. Terrier, P. Ubertini, R. Walter, D. R. Willis, and C. Winkler. *ApJ*, 636:765, 2006.

A. J. Bird, A. Malizia, A. Bazzano, E. J. Barlow, L. Bassani, A. B. Hill, G. Belanger, F. Capitanio, D. J. Clark, A. J. Dean, M. Fiocchi, D. Gotz, F. Lebrun, M. Molina, N. Produit, M. Renaud, V. Sguera, J. B. Stephen, R. Terrier, P. Ubertini, R. Walter, C. Winkler, and J. Zurita. *ApJS*, 170:175, 2007.

A.J. Bird, A. Bazzano, L. Bassani, and F. Capitanio. *ApJS*, 186:1, 2010.

R.D. Blandford and M.C. Begelman. *MNRAS*, 303:L1, 1999.

K. Blundell, A.J. Mioduszewski, T.W.B. Muxlow, P. Podsiadlowski, and M.P. Rupen. *ApJ*, 562:L79, 2001.

K.M. Blundell and M.G. Bowler. *ApJ*, 616:L159, 2004.

A. Bodaghee, E. Bozzo, J. A. Tomsick, E. Kuulkers, J. Rodriguez, N. Barriere, V. Beckmann, M. Cadolle Bel, J. Chenevez, P. R. den Hartog, V. Grinberg, J. Kennea, R. Krivonos, A. Paizis, K. Pottschmidt, P. Romano, S. Soldi, and J. Wilms. *ATEL*, 4328, 2012.

M. Boer, J. Greiner, and C. Motch. *A&A*, 305:835, 1996.

C.T. Bolton. *ApJ*, 200:269, 1975.

A. Z. Bonanos, D. L. Massa, M. Sewilo, D. J. Lennon, N. Panagia, L. J. Smith, M. Meixner, B. L. Babler, S. Bracker, Meade, M. R., K. D. Gordon, J. L. Hora, R. Indebetouw, and B. A. Whitney. *AJ*, 138:1003, 2009.

K. Borozdin, N. Alexandrovich, V. Arefiev, R. Sunyaev, E. Churazov, M. Gilfanov, J. Ballet, and E. Jourdain. *IAU Circ.*, 6083, 1994.

K. Borozdin, N. Alexandrovich, and R. Sunyaev. *IAU Circ.*, 6350, 1996.

K. N. Borozdin, N. L. Aleksandrovich, V. A. Aref'ev, R. A. Syunyaev, and G. K. Skinner. *AstL*, 21:212, 1995.

K. N. Borozdin, M. G. Revnivtsev, S. P. Trudolyubov, N. L. Aleksandrovich, R. A. Sunyaev, and G. K. Skinner. *AstL*, 24:435, 1998.

K.N. Borozdin and S.P. Trudolyubov. *ApJ*, 533:L131, 2000.

L. Bouchet, P. Mandrou, J. P. Roques, G. Vedrenne, B. Cordier, A. Goldwurm, F. Lebrun, J. Paul, R. Sunyaev, E. Churazov, M. Gilfanov, M. Pavlinsky, S. Grebenev, G. Babalyan, I. Dekhanov, and N. Khavenson. *ApJ*, 383:L45, 1991.

L. Bouchet, M. del Santo, E. Jourdain, J. P. Roques, A. Bazzano, and G. DeCesare. *ApJ*, 693:1871, 2009.

H. Bradt. *Astrophysics Processes*. Cambridge University Press, 2008.

H. Bradt and J.E. McClintock. *ARA&A*, 21:13, 1983.

H. Bradt, V. Doxsey, and J.G. Jernigan. *X-Ray Astronomy*. Oxford, 1979.

L. L. E. Braes and G. K. Miley. *Nature*, 232:246, 1971.

L. L. E. Braes and G. K. Miley. *Nature*, 264:731, 1976.

G. Branduardi, J. C. Ives, P. W. Sanford, A. C. Brinkman, and L. Maraschi. *MNRAS*, 175:47, 2001.

W. Brinkmann, N. Kawai, and M. Matsuoka. *A&A*, 218:13, 1989.

W. Brinkmann, N. Kawai, M. Matsuoka, and H. H. Fink. *A&A*, 241:112, 1991.

C. Brocksopp, P. G. Jonker, R. P. Fender, P. J. Groot, M. van der Klis, and S. J. Tingay. *MNRAS*, 323:517, 2001.

C. Brocksopp, R. P. Fender, M. McCollough, G. G. Pooley, M. P. Rupen, R. M. Hjellming, de la Force, C. J., R. E. Spencer, T. W. B. Muxlow, S. T. Garrington, and S. Trushkin. *MNRAS*, 331:765, 2002.

C. Brocksopp, R. M. Bandyopadhyay, and R. P. Fender. *New Ast.*, 9:249, 2004.

C. Brocksopp, S. Corbel, R. P. Fender, M. Rupen, R. Sault, S. J. Tingay, D. Hannikainen, and K. O'Brien. *MNRAS*, 356:125, 2005.

C. Brocksopp, K.E. McGowan, H. Krimm, O. Godet, P. Roming, K.O. Mason, N. Gehrels, M. Still, K. Page, A. Moretti, C.R. Shrader, and S. Campana. *MNRAS*, 365:1203, 2006.

C. Brocksopp, J. C. A. Miller-Jones, R. P. Fender, and B. W. Stappers. *MNRAS*, 378:1111, 2007.

C. Brocksopp, S. Corbel, T. Tzioumis, and R. Fender. *ATEL*, 2278, 2009.

C. Brocksopp, S. Corbel, T. Tzioumis, R. Fender, and M. Coriat. *ATEL*, 2400, 2010a.

C. Brocksopp, P. G. Jonker, D. Maitra, H. A. Krimm, G. G. Pooley, G. Ramsay, and C. Zurita. *MNRAS*, 404:908, 2010b.

C. Brocksopp, S. Corbel, A. Tzioumis, J. W. Broderick, J. Rodriguez, J. Yang, R. P. Fender, and Z. Paragi. *MNRAS*, 432:931, 2013.

M. Buxton, D. Maitra, C. Bailyn, L. Jeanty, and D. Gonzalez. *ATEL*, 170, 2003.

M. Buxton, I. Hasan, E. MacPherson, and C. Bailyn. *ATEL*, 5244, 2013.

M.M. Buxton, C.D. Bailyn, H.L. Capelo, R. Chatterjee, T. Dinçer, E. Kalemci, and J.A. Tomsick. *ApJ*, 143:130, 2012.

S. M. Caballero-Nieves, D. R. Gies, C. T. Bolton, P. Hadrava, A. Herrero, T. C. Hillwig, S. B. Howell, W. Huang, L. Kaper, P. Koubsky, and M. V. McSwain. *ApJ*, 701:1895, 2009.

E. M. Cackett and J. M. Miller. *ATEL*, 1135, 2007.

E.M. Cackett, R. Wijnands, and R. Remillard. *MNRAS*, 369:1965, 2006.

M. Cadolle Bel, J. Rodriguez, P. Sizun, R. Farinelli, M. Del Santo, A. Goldwurm, P. Goldoni, S. Corbel, A. N. Parmar, E. Kuulkers, P. Ubertini, F. Capitanio, J.-P. Roques, F. Frontera, L. Amati, and N. J. Westergaard. *A&A*, 426:659, 2004.

M. Cadolle Bel, M. Ribó, J. Rodriguez, S. Chaty, S. Corbel, A. Goldwurm, F. Frontera, R. Farinelli, P. D'Avanzo, A. Tarana, P. Ubertini, P. Laurent, P. Goldoni, and I. F. Mirabel. *ApJ*, 659:549, 2007.

M. Cadolle Bel, L. Prat, J. Rodriguez, M. Ribo, L. Barragan, P. D'Avanzo, D. C. Hannikainen, E. Kuulkers, S. Campana, J. Moldon, S. Chaty, J. Zurita-Heras, A. Goldwurm, and P. Goldoni. *A&A*, 501:1, 2009.

P.J. Callanan, M.R. Garcia, J.E. McClintock, P. Zhao, R.A. Remillard, C.D. Bailyn, J.A. Orosz, B.A. Harmon, and W.S. Paciesas. *ApJ*, 441:786, 1995.

P.J. Callanan, M.R. Garcis, A.V. Filippenko, I. McLean, and H. Teplitz. *ApJ*, 470: L57, 1996.

D. E. Calvelo, T. Tzioumis, S. Corbel, C. Brocksopp, and R. P. Fender. *ATEL*, 2135, 2009.

S. Campana, L. Stella, T. Belloni, G.L. Israel, A. Santangelo, F. Frontera, M. Orlandini, and D. Dai Fiume. *A&A*, 384:163, 2001.

S. Campana, L. Stella, T. Belloni, G. L. Israel, A. Santangelo, F. Frontera, M. Orlandini, and D. Dal Fiume. *A&A*, 384:163, 2002.

D. Campbell-Wilson, V. McIntyre, R. Hunstead, A. Green, R. B. Wilson, and C. A. Wilson. *IAU Circ.*, 7010, 1998.

A.G. Cantrell, C.D. Bailyn, J.E. McClintock, and J.A. Orosz. *ApJ*, 673:L159, 2008.

A.G Cantrell, C.D. Bailyn, J.A. Orosz, J.E. McClintock, R.A. Remillard, C.S. Froning, J. Neilsen, D.M. Gelino, and L Gou. *ApJ*, 710:1127, 2010.

F. Capitanio, P. Ubertini, A. Bazzano, P. Kretschmar, A. A. Zdziarski, A. Joinet, E. J. Barlow, A. J. Bird, A. J. Dean, E. Jourdain, G. De Cesare, M. Del Santo, L. Natalucci, M. Cadolle Bel, and A. Goldwurm. *ApJ*, 622:503, 2005.

F. Capitanio, A. Bazzano, P. Ubertini, and A. J. Bird. Proceedings of the vi microquasar workshop: Microquasars and beyond. page 74, September 2006a.

F. Capitanio, A. Bazzano, P. Ubertini, A. A. Zdziarski, A. J. Bird, G. De Cesare, A. J. Dean, J. B. Stephen, and A. Tarana. *ApJ*, 643:376, 2006b.

F. Capitanio, T. Belloni, M. Del Santo, and P. Ubertini. *MNRAS*, 398:1194, 2009a.

F. Capitanio, M. Giroletti, M. Molina, A. Bazzano, A. Tarana, J. Kennea, A. J. Dean, A. B. Hill, M. Tavani, and P. Ubertini. *ApJ*, 690:1621, 2009b.

F. Capitanio, P. Ubertini, A. Bazzano, and M. Del Santo. The first year of maxi: Monitoring variable x-ray sources, poster presentations, 4th international maxi workshop. pages 14–18, 2010.

F. Capitanio, A. Tramacere, M. Del Santo, E. Bozzo, K. Watanabe, I. Caballero, J. Chenevez, A. Paizis, K. Pottschmidt, C. Sanchez-Fernandez, V. Sguera, and A. Tarana. *ATEL*, 3159, 2011.

F. Capitanio, M. Del Santo, E. Bozzo, C. Ferrigno, G. De Cesare, and A. Paizis. *MNRAS*, 422:3130, 2012.

B.W. Carroll and D.A. Ostlie. *An Introduction to Modern Astrophysics*. Addison Wesley, 2007.

T. F. Cartwright, M. C. Engel, C. O. Heinke, G. R. Sivakoff, J. J. Berger, J. C. Gladstone, and N. Ivanova. *ApJ*, 768:183, 2013.

J. Casares. Proceedings of iau symposium 238: Black holes from stars to galaxies - across the range of masses. pages 14–16. IAU, 2006.

J. Casares and P. A. Charles. *MNRAS*, 271:L5, 1994.

J. Casares, P. A. Charles, and T. Naylor. *Nature*, 355:614, 1992.

J. Casares, P. A. Charles, and T. R. Marsh. *MNRAS*, 277:L45, 1995a.

J. Casares, A.C. Martin, P. A. Charles, E.L. Martin, R. Rebolo, E.T. Harlaftis, and A.J. Castro-Tirado. *MNRAS*, 276:L35, 1995b.

J. Casares, E. L. Martín, P. A. Charles, P. Molaro, and R. Rebolo. *New Ast.*, 1:299, 1997.

J. Casares, C. Zurita, T. Shahbaz, P.A. Charles, and R.P. Fender. *ApJ*, 613:L133, 2004.

J. Casares, J. A. Orosz, C. Zurita, T. Shahbaz, J. M. Corral-Santana, J. E. McClintock, M. R. Garcia, I. G. Martínez-Pais, P. A. Charles, R. P. Fender, and R. A. Remillard. *ApJS*, 181:238, 2009.

J. Casares, M.A.P. Torres, I. Negueruela, C. Gonzalez-Fernandez, J.M. Corral-Santana, C. Zurita, and S.R. Llano. *ATEL*, 3206, 2011.

J. Casares, P. Rodriguez-Gil, C. Zurita, J.M. Corral-Santana, R. Corradi, R. Cornelisse, and P.A. Charles. *ATEL*, 4347, 2012.

J. Casares, I. Negueruela, M. Ribó, I. Ribas, J. M. Paredes, A. Herrero, and S. Simón-Díaz. *Nature*, 505:378, 2014.

P. Casella, T. Belloni, J. Homan, and L. Stella. *A&A*, 426:587, 2004.

A. J. Castro-Tirado, P. Kilmartin, A. Gilmore, O. Petterson, I. Bond, P. Yock, and C. Sanchez-Fernandez. *IAU Circ.*, 7707, 2001.

A.J. Castro-Tirado, S. Branndt, and S. Lund. *IAU Circ.*, 5590, 1992.

A.J. Castro-Tirado, S. Brandt, N. Lund, I. Lapshov, R.A. Sunyaev, A.A. Shlyapnikov, S. Guziy, and E.P. Pavlenko. *ApJS*, 92:469, 1994.

A.J. Castro-Tirado, T.R. Geballe, and N. Lund. *ApJ*, 461:L99, 1996.

A.J. Castro-Tirado, S. Ilovaisky, and H. Pederson. *IAU Circ.*, 6775, 1997.

S.K. Chakrabarti, S. Pal, A. Nandi, B. G. Anandarao, and S. Mondal. *ApJ*, 595: L45, 2003.

S.K. Chakrabarti, B. G. Anandarao, S. Pal, S. Mondal, A. Nandi, A. Bhattacharyya, S. Mandal, R. Sagar, J. C. Pandey, A. Pati, and S. K. Saha. *MNRAS*, 362:957, 2005.

D. Chakrabarty, P.G. Jonker, and C.B. Markwardt. *ATEL*, 3407, 2011.

P. A. Charles and M. J. Coe. *Compact Stellar X-Ray Sources*. Cambridge University Press, 2006.

P.A. Charles, T. Shahbaz, and T. Geballe. *IAU Circ.*, 7267, 1999.

S. Chaty, I. F. Mirabel, P. A. Duc, J. E. Wink, and L. F. Rodriguez. *A&A*, 310:825, 1996.

S. Chaty, P. A. Charles, J. Martí, I. F. Mirabel, L. F. Rodríguez, and T. Shahbaz. *MNRAS*, 343:169, 2003.

S. Chaty, R. P. Mignani, and G. L. Israel. *MNRAS*, 365:1387, 2006.

W. Chen, C.R. Shrader, and M. Livio. *ApJ*, 491:312, 1997.

Y. Chen, S. Zhang, D.F. Torres, J. Wang, J. Li, T. Li, and J. Qu. *A&A*, 522:99C, 2010.

J. Chenevez, C. Budtz-Jorgensen, N. Lund, N. J. Westergaard, P. Kretschmar, J. Rodriguez, A. Orr, and W. Hermsen. *ATEL*, 223, 2004.

C. C. Cheung. *ATEL*, 1289, 2007.

C. Chevalier and S.A. Ilovaisky. *IAU Circ.*, 5520, 1992.

C. Chevalier and S.A. Ilovaisky. *ApJ*, 269:301, 1993.

Y.Y. Chun, T. Dinçer, E. Kalemci, T. Guver, J.A. Tomsick, M.M. Buxton, C. Brocksopp, S. Corbel, and A. Cabrera-Lavers. *ApJ*, 770:10, 2013.

E. Churazov, M. Gilfanov, R. Sunyaev, M. Pavlinsky, S. Grebenev, A. Dyachkov, V. Kovtunenko, R. Kremnev, M. Niel, P. Mandrou, G. Vedrenne, J. P. Roques, A. Cordier, B.a nd Goldwurm, F. Lebrun, and J. Paul. *ApJ*, 407:752, 1993.

E. Churazov, M. Gilfanov, J. Ballet, and E. Jourdain. *IAU Circ.*, 6083, 1994.

M.J. Church and M. Balucinska-Church. *A&A*, 317:L47, 1997.

J. S. Clark, A. S. Miroshnichenko, V. M. Larionov, V. M. Lyuty, R. I. Hynes, G. G. Pooley, M. J. Coe, M. McCollough, S. Dieters, Yu. S. Efimov, J. Fabregat, V. P. Goranskii, C. A. Haswell, N. V. Metlova, E. L. Robinson, P. Roche, V. I. Shenavrin, and W. F. Welsh. *A&A*, 356:50, 2000.

B. A. Cooke, A. M. Levine, F. L. Lang, F. A. Primini, and W. H. G. Lewin. *ApJ*, 285:258, 1984.

S. Corbel, R. P. Fender, A. K. Tzioumis, M. Nowak, V. McIntyre, P. Durouchoux, and R. Sood. *A&A*, 359:251, 2000.

S. Corbel, R. P. Fender, A. K. Tzioumis, J. A. Tomsick, J. A. Orosz, J. M. Miller, R. Wijnands, and P. Kaaret. *Science*, 298:196, 2002.

S. Corbel, M.A. Nowak, R. P. Fender, A. K. Tzioumis, and S. Markoff. *A&A*, 400: 1007, 2003.

S. Corbel, R. P. Fender, J. A. Tomsick, A. K. Tzioumis, and S. Tingay. *ApJ*, 617: 1272, 2004.

S. Corbel, P. Kaaret, R. P. Fender, A. K. Tzioumis, J. A. Tomsick, and J. A. Orosz. *ApJ*, 632:504, 2005.

S. Corbel, J. Rodriguez, T. Tzioumis, and J. Tomsick. *ATEL*, 3167, 2011.

S. Corbel, P. Edwards, T. Tzioumis, M. Coriat, R. Fender, and C. Brocksopp. *ATEL*, 4410, 2012.

S. Corbel, M. Coriat, C. Brocksopp, A.K. Tzioumis, R.P. Fender, J.A. Tomsick, M.M. Buxton, and C.D. Bailyn. *MNRAS*, 428:2500, 2013.

B. Cordier, J. Paul, J. Ballet, A. Goldwurm, L. Bouchet, J. P. Roques, P. Mandrou, G. Vedrenne, E. Churazov, M. Gilfanov, R. Sunyaev, B. Novikov, I. Chulkov, N. Kuleshova, I. Tserenin, and A. Sheikhet. *A&A*, 275:1, 1993.

B. Cordier, J. Paul, and J-M. Hameury. *ApJS*, 92:401, 1994.

M. Coriat and J. Rodriguez. *ATEL*, 2219, 2009.

M. Coriat, S. Corbel, L. Prat, J. C. A. Miller-Jones, D. Cseh, A. K. Tzioumis, C. Brocksopp, J. Rodriguez, R. P. Fender, and G. R. Sivakoff. *MNRAS*, 414:677, 2011.

M. Coriat, P. Edwards, R. Fender, S. Corbel, T. Tzioumis, J. Miller-Jones, P. Curran, and R. Armstrong. *ATEL*, 4760, 2013a.

M. Coriat, T. Tzioumis, S. Corbel, and R. Fender. *ATEL*, 5575, 2013b.

J. M. Corral-Santana, J. Casares, T. Shahbaz, C. Zurita, I. G. Martínez-Pais, and P. Rodríguez-Gil. *MNRAS*, 413:L15, 2011.

J. M. Corral-Santana, J. Casares, T. Muñoz-Darias, P. Rodríguez-Gil, T. Shahbaz, M. A. P. Torres, C. Zurita, and A. A. Tyndall. *Science*, 339:1048, 2013.

A. P. Cowley, D. Crampton, J. B. Hutchings, R. Remillard, and J. E. Penfold. *ApJ*, 272:118, 1983.

A. P. Cowley, D. Crampton, and J. B. Hutchings. *ApJ*, 333:906, 1988.

A. P. Cowley, P. C. Schmidtke, A. L. Anderson, and T. K. McGrath. *PASP*, 107: 145, 1995.

A.P. Cowley. *ARA&A*, 30:287, 1992.

D. Crampton and J. B. Hutchings. *ApJ*, 251:604, 1987.

W. Cui, W. A. Heindl, J. H. Swank, D. M. Smith, E. H. Morgan, R. Remillard, and F. E. Marshall. *ApJ*, 487:73, 1997a.

W. Cui, E. H. Morgan, W. A. Heindl, J. H. Swank, and D. M. Smith. *IAU Circ.*, 6604, 1997b.

W. Cui, S.N. Zhang, W. Chen, and E.H. Morgan. *ApJ*, 512:L443, 1999.

W. Cui, C.R. Shrader, C.A. Haswell, and R.I. Hynes. *ApJ*, 525:L123, 2000.

J. R. Cummings, C. Gronwall, D. Grupe, H. A. Krimm, C. B. Markwardt, D. M. Palmer, B. Sbarufatti, and M. Stamatikos. *GCN*, 13774, 2012.

P. A. Curran and S. Chaty. *A&A*, 557:45, 2013.

P. A. Curran, P. A. Evans, M. Still, C. Brocksopp, and C. Done. *ATEL*, 2424, 2010.

P. A. Curran, T. J. Maccarone, P. Casella, P. A. Evans, W. Landsman, H. A. Krimm, C. Brocksopp, and M. Still. *MNRAS*, 410:541, 2011.

P. A. Curran, M. Coriat, J. C. A. Miller-Jones, R. P. Armstrong, P. G. Edwards, G. R. Sivakoff, P. Woudt, D. Altamirano, T. M. Belloni, S. Corbel, R. P. Fender, E. G. Körding, H. A. Krimm, S. Markoff, S. Migliari, D. M. Russell, J. Stevens, and T. Tzioumis. *MNRAS*, 437:3265, 2014.

R. M. Cutri, M. F. Skrutskie, S. van Dyk, C. A. Beichman, J. M. Carpenter, T. Chester, L. Cambresy, T. Evans, J. Fowler, J. Gizis, E. Howard, J. Huchra, T. Jarrett, E. L. Kopan, J. D. Kirkpatrick, R. M. Light, K. A. Marsh, H. McCallon, S. Schneider, R. Stiening, M. Sykes, M. Weinberg, W. A. Wheaton, S. Wheelock, and N. Zacarias. 2mass all-sky catalog of point sources,vizier on-line data catalog: Ii/246, 2003.

R. D. Davies, D. Walsh, I. W. A. Browne, M. R. Edwards, and R. G. Noble. *Nature*, 261:476, 1976.

R. J. Davis, M. R. Edwards, J. Morison, and R. E. Spencer. *Nature*, 257:659, 1975.

A. de Ugarte Postigo, H. Flores, K. Wiersema, C. C. Thoene, J. P. U. Fynbo, and P. Goldoni. *GCN*, 11307, 2010.

D. Debnath, S.K. Chakrabarti, and A. Nandi. *AdSpR*, 52:2143, 2013a.

D. Debnath, S. Mondal, and S.K. Chakrabarti. *arXiv:1306.3745v1*, 2013b.

N. Degenaar and R. Wijnands. *ATEL*, 1541, 2008.

N. Degenaar, D. Altamirano, M. Klein-Wolt, and R. Wijnands. *ATEL*, 1451, 2008a.

N. Degenaar, D. Altamirano, and R. Wijnands. *ATEL*, 1467, 2008b.

M. del Santo, A. Bazzano, A. A. Zdziarski, D. M. Smith, N. Bezayiff, R. Farinelli, G. De Cesare, P. Ubertini, A. J. Bird, M. Cadolle Bel, F. Capitanio, A. Goldwurm, A. Malizia, I. F. Mirabel, L. Natalucci, and C. Winkler. *A&A*, 433:613, 2004.

M. Del Santo, J. Malzac, E. Jourdain, T. Belloni, and P. Ubertini. *MNRAS*, 390: 227, 2008.

M. Del Santo, E. Kuulkers, E. Bozzo, F. Capitanio, J. Alfonso-Garzon, V. Beckmann, T. Bird, S. Brandt, J. Chenevez, T. Courvoisier, A. Domingo, K. Ebisawa, P. Jonker, P. Kretschmar, C. Markwardt, T. Oosterbroek, A. Paizis, K. Pottschmidt, C. Sanchez-Fernandez, and R. Wijnands. *ATEL*, 3203, 2011.

M. della Valle and S. Benetti. *IAU Circ.*, 5890, 1993.

M. della Valle, B.J. Jarvis, and R.M. West. *A&A*, 247:L33, 1991.

M. della Valle, I. F. Mirabel, and L. F. Rodriguez. *A&A*, 290:803, 1994.

M. della Valle, S. Benetti, E. Cappellaro, and C. Wheeler. *A&A*, 318:179, 1997.

M. della Valle, N. Massetti, and A. Bianchini. *A&A*, 329:606, 1998.

V. Dhawan, I. F. Mirabel, and L. F. Rodríguez. *ApJ*, 543:373, 2000.

M. Diaz Trigo, L. Boirin, E. Costantini, M. Mendez, and A. Parmar. *A&A*, 528: A150, 2011.

M. Díaz Trigo, J.C.A. Miller-Jones, S. Migliari, J.W. Broderick, and T. Tzioumis. *Nature*, 504:260, 2013.

S. W. Dieters, T. Belloni, E. Kuulkers, P. Woods, W. Cui, S. N. Zhang, W. Chen, M. van der Klis, J. van Paradijs, J. Swank, W. H. G. Lewin, and C. Kouveliotou. *ApJ*, 538:307, 2000.

S. G. Djorgovski, R. R. Gal, A. Mahabal, T. Galama, J. Bloom, R. Rutledge, S. Kulkarni, and F. Harrison. *ATEL*, 44, 1999.

S. D'Odorico, T. Oosterloo, T. Zwitter, and M. Calvani. *Nature*, 353:329, 1991.

S. Doebereiner, J. Englhauser, W. Pietsch, C. Reppin, J. Truemper, E. Kendziorra, M. Maisack, B. Mony, R. Staubert, and V. V. Efremov. The 23rd eslab symposium on two topics in x ray astronomy: X ray binaries. volume 1, pages 387–392. ESA, 1989.

J. F. Dolan, C. J. Crannell, B. R. Dennis, K. J. Frost, and L. E. Orwig. *ApJ*, 230: 551, 1979.

C. Done. *XXI Canary Islands Winter School of Astrophysics*. Cambridge University Press, 2010.

C. Done and A. Kubota. *MNRAS*, 371:1216, 2006.

C. Done, G. Wardzinski, , and M. Gierlinski. *MNRAS*, 349:393, 2004.

C. Done, M. Gierlinski, and A. Kubota. *ARA&A*, 15:1, 2007.

R.A. Downes, R.F. Webbink, M.M. Shara, H. Ritter, U. Kolb, and H.W. Duerbeck. *PASJ*, 113:764, 2001.

H. Doxsey, G. Bradt, and R. Fabbiano. *IAU Circ.*, 3113, 1977.

G. M. Dubner, M. Holdaway, W. M. Goss, and I. F. Mirabel. *AJ*, 116:1842, 1998.

M. L. Duldig, J. G. Greenhill, R. M. Thomas, R. F. Haynes, L. W. J. Simons, and P. G. Murdin. *MNRAS*, 187:567, 1979.

R. J. H. Dunn, R. P. Fender, E. G. Körding, T. Belloni, and C. Cabanac. *MNRAS*, 403:61, 2009.

P. Durouchoux, I. A. Smith, K. Hurley, A. S. B. Schultz, L. B. F. M. Waters, J. van Paradijs, P. Wallyn, R. M. Hjellming, M. P. Rupen, J. Marti, F. Mirabel, and L. F. Rodriguez. *IAU Circ.*, 6383, 1996.

L.J. Eachus, E.L. Wright, and W. Liller. *ApJ*, 203:L17, 1976.

K. Ebisawa, F. Makino, K. Mitsuda, T. Belloni, A.P. Cowley, P.C. Schmidtke, and A. Treves. *ApJ*, 403:684, 1993.

K. Ebisawa, M. Ogawa, T. Aoki, T. Dotani, M. Takizawa, Y. Tanaka, K. Yoshida, S. Miyamoto, S. Iga, K. Hayashida, S. Kitamoto, and K. Terada. *PASJ*, 46:375, 1994.

K. Ebisawa, G. Bourban, A. Bodaghee, N. Mowlavi, and T. J.-L. Courvoisier. *A&A*, 411:L59, 2003.

P.P Eggleton. *ApJ*, 268:368, 1983.

S. S. Eikenberry, E. Fischer, W. J.a nd Egami, and S. G. Djorgovski. *ApJ*, 556:1, 2001.

S.S. Eikenberry, K. Matthews, E.H. Morgan, R.A. Remillard, and R.W. Nelson. *ApJ*, 494:L61, 1998.

M. Elvis, C. G. Page, K. A. Pounds, M. J. Ricketts, and M. J. L. Turner. *Nature*, 257:656, 1975.

A. N. Emelyanov, N. L. Aleksandrovich, and R. A. Sunyaev. *AstL*, 26:297, 2000.

C. J. Eyles, G. K. Skinner, A. P. Willmore, and F. D. Rosenberg. *Nature*, 257:291, 1975.

A.C. Fabian and M.J. Rees. *MNRAS*, 187:13P, 1979.

S.N. Fabrika and L.V. Bychkova. *A&A*, 240:L5, 1990.

H. Falke, E. Kording, and S. Markoff. *A&A*, 414:895, 2004.

R. Farinelli, L. Amati, N. Shaposhnikov, F. Frontera, N. Masetti, E. Palazzi, R. Landi, C. Lombardi, M. Orlandini, and C. Brocksopp. *MNRAS*, 428:3295, 2013.

I. Fejes, R.T. Schilizzi, and R.C. Vermeulen. *A&A*, 189:124, 1988.

R. Fender. *Compact Stellar X-Ray Sources*. Cambridge University Press, 2006.

R. Fender and E. Gallo. *arXiv:1407.3674*, 2014.

R. Fender, S. Corbel, T. Tzioumis, V. McIntyre, D. Campbell-Wilson, M. Nowak, R. Sood, R. Hunstead, A. Harmon, P. Durouchoux, and W. Heindl. *ApJ*, 519: L165, 1999a.

R. Fender, D. Rayner, R. Norris, R. J. Sault, and G. Pooley. *ApJ*, 530:L29, 2000a.

R. Fender, S. Garrington, and T. Muxlow. *ATEL*, 558, 2005.

R. P. Fender and G. G. Pooley. *MNRAS*, 300:573, 1998.

R. P. Fender, G. G. Pooley, C. Brocksopp, and S. J. Newell. *MNRAS*, 290:L65, 1997a.

R. P. Fender, R. E. Spencer, S. J. Newell, and A. K. Tzioumis. *MNRAS*, 286:L29, 1997b.

R. P. Fender, S.J. Tingay, J. Higdon, R. Wark, and M. Wieringa. *IAU Circ.*, 6779, 1997c.

R. P. Fender, S. T. Garrington, D. J. McKay, T. W. B. Muxlow, G. G. Pooley, R. E. Spencer, A. M. Stirling, and E. B. Waltman. *MNRAS*, 304:865, 1999b.

R. P. Fender, G. G. Pooley, P. Durouchoux, R. P. J. Tilanus, and C. Brocksopp. *MNRAS*, 312:853, 2000b.

R. P. Fender, R. M. Hjellming, R. P. J. Tilanus, G. G. Pooley, J. R. Deane, R. N. Ogley, and R. E. Spencer. *MNRAS*, 322:L23, 2001.

R. P. Fender, D. Rayner, D. G. McCormick, T. W. B. Muxlow, G. G. Pooley, R. J. Sault, and R. E. Spencer. *MNRAS*, 336:39, 2002.

R. P. Fender, A. M. Stirling, R. E. Spencer, I. Brown, G. G. Pooley, T. W. B. Muxlow, and J. C. A. Miller-Jones. *MNRAS*, 369:603, 2006.

R. P. Fender, J. Homan, and T.M. Belloni. *MNRAS*, 396:1370, 2009.

R.P. Fender. *The Jet Paradigm - From Microquasars to Quasars, Lect. Notes in Phys. 794*. Springer, 2009.

R.P. Fender and T.M. Belloni. *ARA&A*, 42:317, 2004.

R.P. Fender, B.W. Stappers, M. Wieringa, and R. Wark. *IAU Circ.*, 6937, 1998.

R.P. Fender, T.M. Belloni, and E. Gallo. *MNRAS*, 355:1105, 2004.

C. Ferrigno, E. Bozzo, M. Del Santo, and F. Capitanio. *A&A*, 537:L7, 2011.

A. V. Filippenko and R. Chornock. *IAU Circ.*, 7644, 2001.

A. V. Filippenko, T. Matheson, D. C. Leonard, A. J. Barth, and S. D. van Dyk. *PASP*, 109:461, 1997.

A. V. Filippenko, D.C. Leonard, T. Matheson, W. Li, E.C. Moran, and A.G. Riess. *PASP*, 111:969, 1999.

A.V. Filippenko, R.W. Romani, W.L.W. Sargent, and R.D. Blandford. *AJ*, 96:242, 1988.

A.V. Filippenko, T. Matheson, and L.C. Ho. *ApJ*, 455:614, 1995.

E. Filippova, E. Kuulkers, N. M. Skådt, J. Alfonso-Garzon, V. Beckmann, A. J. Bird, S. Brandt, J. Chenevez, M. Del Santo, A. Domingo, K. Ebisawa, P. G. Jonker, P. Kretschmar, C. B. Markwardt, T. Oosterbroek, A. Paizis, K. Pottschmidt, C. Sanchez-Fernandez, R. Wijnands, E. Bozzo, and C. Ferrigno. *ATEL*, 5991, 2014.

E. V. Filippova, S. S. Tsygankov, A. A. Lutovinov, and R. A. Sunyaev. *AstL*, 31: 729, 2005.

W. B. Focke, C. B. Markwardt, J. H. Swank, and R. E. Taam. Rossi2000. In *Astrophysics with the Rossi X-ray Timing Explorer*. NASA's Goddard Space Flight Center, March 2000.

D. Foreman-Mackey, D.W. Hogg, D. Lang, and J. Goodman. *arXiv:1202.365v4*, 2012.

R. S. Foster, E. B. Waltman, M. Tavani, B. A. Harmon, S. N. Zhang, W. S. Paciesas, and F. D. Ghigo. *ApJ*, 467:L81, 1996.

D. Fox and W. Lewin. *IAU Circ.*, 6964, 1998.

R.J. Francey. *Nature Phys. Sci.*, 229:228, 1971.

J. Frank, A. King, and D. Raine. *Accretion Power in Astrophysics*. Cambridge University Press, 2002.

G.W. Fraser. *Detectors in X-ray Astronomy*. Cambridge University Press, 2009.

W.L. Freedman, B.F. Madore, B.K. Gibson, L. Ferrarese, D.D. Kelson, S. Sakai, J.R. Mould, R.C. Kennicutt, H.C. Ford, J.A. Graham, J.P. Huchra, S.M.G. Hughes, G.D. Illingworth, L.M. Macri, and P.B. Stetson. *ApJ*, 553:47, 2001.

V.P. Frolov and A. Zelnikov. *Introduction to Black Hole Physics*. Oxford University Press, 2011.

C.S. Froning and E.L. Robinson. *AJ*, 121:2212, 2001.

C.S. Froning, T.J. Maccarone, K. France, L. Winter, E.L. Robinson, R.I. Hynes, and F. Lewis. *ApJ*, 780:48, 2014.

F. Frontera, M. Orlandini, L. Amati, D. dal Fiume, N. Masetti, A. Orr, A. N. Parmar, E. Brocato, G. Raimondo, A. Piersimoni, M. Tavani, and R. A. Remillard. *A&A*, 339:L69, 1998.

F. Frontera, A. A. Zdziarski, L. Amati, J. Mikolajewska, T. Belloni, S. Del Sordo, F. Haardt, E. Kuulkers, N. Masetti, M. Orlandini, E. Palazzi, A. N. Parmar, R. A. Remillard, A. Santangelo, and L. Stella. *ApJ*, 561:1006, 2001.

B. Fuhrmeister and J.H.M.M. Schmitt. *A&A*, 403:247, 2003.

E. Gallo and R. P. Fender. *MNRAS*, 337:869, 2002.

E. Gallo, R. P. Fender, and R. I. Hynes. *MNRAS*, 356:1017, 2005.

E. Gallo, R. P. Fender, J. C. A. Miller-Jones, A. Merloni, P. G. Jonker, S. Heinz, T. J. Maccarone, and M. van der Klis. *MNRAS*, 370:1351, 2006.

P. M. Garnavich and J. Quinn. *IAU Circ.*, 7388, 2000.

P. M. Garnavich, K. Z. Stanek, and P. Berlind. *IAU Circ.*, 7276, 1999.

N. Gehrels. *ApJ*, 303:336, 1986.

B. J. Geldzahler. *ApJ*, 264:L49, 1983.

D.M. Gelino. PhD thesis, New Mexico State University, 2001.

D.M. Gelino and T.E. Harrison. *ApJ*, 599:1254, 2003.

D.M. Gelino, T.E. Harrison, and B.J. McNamara. *AJ*, 122:971, 2001a.

D.M. Gelino, T.E. Harrison, and J.A. Orosz. *AJ*, 122:2668, 2001b.

D.M. Gelino, S. Balman, U. Kzloglu, A. Ylmaz, E. Kalemci, and J.A. Tomsick. *ApJ*, 642:438, 2006.

D.M. Gelino, C.R. Gelino, and T.E. Harrison. *ApJ*, 718:1, 2010.

T.E. Gelino, D.M. Harrison. *BAAS*, 34:654, 2002.

R. Giacconi, S. Murray, H. Gursky, E. Kellogg, E. Schreier, T. Matilsky, D. Koch, and H. Tananbaum. *ApJ*, 27:37, 1974.

M. Gierlinski and J. Newton. *MNRAS*, 370:837, 2006.

M. Gierlinski, A.A. Zdziarski, C. Done, W.N. Johnson, K. Ebisawa, Y. Ueda, F. Haardt, and B.F. Phlips. *MNRAS*, 288:958, 1997.

M. Gierlinski, C. Done, and K. Page. *MNRAS*, 388:753, 2008.

M. Gierlinski, C. Done, and K. Page. *MNRAS*, 392:1106, 2009.

M. Gierlinski, A.A. Zdziarski, and C. Done. *arXiv:1011.5840*, 2010.

D. R. Gies and C. T. Bolton. *ApJ*, 260:240, 1982.

D. R. Gies and C. T. Bolton. *ApJ*, 304:371, 1986.

D. R. Gies, M. V. McSwain, R. L. Riddle, Z. Wang, P. J. Wiita, and D. W. Wingert. *ApJ*, 566:1069, 2002.

M. Gilfanov. *The Jet Paradigm - From Microquasars to Quasars, Lect. Notes in Phys. 794*. Springer, 2009.

M. Gilfanov, E. Churazov, R. Sunyaev, N. Khavenson, B. Novikov, A. Dyachkov, R. Kremnev, K. Sukhanov, L. Bouchet, P. Mandrou, J. P. Roques, G. Vedrenne, B. Cordier, A. Goldwurm, P. Laurent, and J. Paul. *ApJ*, 418:844, 1993.

M. Gilfanov, E. Churazov, and M. Revnivtsev. *ApJ*, 352:182, 1999.

T. Gleissner, J. Wilms, G. G. Pooley, M. A. Nowak, K. Pottschmidt, S. Markoff, S. Heinz, M. Klein-Wolt, R. P. Fender, and R. Staubert. *A&A*, 425:1061, 2004.

E. Gogus, M.H. Finger, C. Kouveliotou, P.M. Woods, S.K. Patel, J.H. Rupen, M.a nd Swank, C.B. Markwardt, and M. van der Klis. *ApJ*, 609:977, 2004.

P. Goldoni, M. Vargas, A. Goldwurm, J. Paul, V. Borrel, E. Jourdain, L. Bouchet, J.-P. Roques, M. Revnivtsev, E. Churazov, M. Gilfanov, R. Sunyaev, A. Dyachkov, N. Khavenson, I. Tserenin, and N. Kuleshova. *ApJ*, 511:847, 1999.

J.I. Gonzalez Hernandez, R. Rebolo, G. Israelian, A.V. Filippenko, R. Chornock, N. Tominaga, H. Umeda, and K. Nomoto. *ApJ*, 679:732, 2008.

A. Goodman. Ism and star formation online book: For harvard university astronomy, 2011.

J. Goodman and J. Weare. *Comm. App. Math. Comp. Sci.*, 5:65, 2010.

S. A. Grebenev and R. A. Sunyaev. *AstL*, 31:672, 2005.

S. A. Grebenev and R. A. Sunyaev. *ATEL*, 4401, 2012.

S. A. Grebenev, S. V. Molkov, M. G. Revnivtsev, and R. A. Sunyaev. *ATEL*, 447, 2005a.

S. A. Grebenev, S. V. Molkov, and R. A. Sunyaev. *ATEL*, 444, 2005b.

S. A. Grebenev, S. V. Molkov, M. G. Revnivtsev, and R. A. Sunyaev. The obscured universe: Proceedings of the vi integral workshop. 2007.

J. Greene, C.D. Bailyn, and J.A. Orosz. *ApJ*, 554:1290, 2001.

J. Greiner and N. Reid. *IAU Circ.*, 5786, 1993.

J. Greiner, S. Snowden, B. A. Harmon, C. Kouveliotou, and W. Paciesas. Aip conference proceddings 304, the second compton symposium. page 260, 1994.

J. Greiner, E.H. Morgan, and R.A. Remillard. *ApJ*, 473:L107, 1996.

J. Greiner, K. Dennerl, and P. Predehl. *A&A*, 314:L21, 1997.

J. Greiner, J. G. Cuby, and M. J. McCaughrean. *Nature*, 414:522, 2001a.

J. Greiner, J. G. Cuby, M. J. McCaughrean, A. J. Castro-Tirado, and R. E. Mennickent. *A&A*, 373:L37, 2001b.

J. Greiner, G. Sla, and T. Kruehler. *ATEL*, 1577, 2008.

J. Greiner, A. Rau, and P. Schady. *ATEL*, 4030, 2012.

R. Griffiths, M. Johnston, R. Doxsey, G. Fabbiano, D. Schwartz, J. Schwarz, H. Friedman, A. Longmore, R. Cannon, P. Murdin, D. Malin, M. Smith, A. Boksenberg, and W. Liller. *IAU Circ.*, 3110, 1977.

R. E. Griffiths, H. Bradt, R. Doxsey, H. Friedman, H. Gursky, M. Johnston, A. Longmore, D. F. Malin, P. Murdin, D. A. Schwartz, and J. Schwarz. *ApJ*, 221:L63, 1978.

H.J. Grimm, M. Gilfanov, , and R Sunyaev. *A&A*, 391:923, 2002.

V. Grinberg, N. Hell, K. Pottschmidt, M. Böck, M. A. Nowak, J. Rodriguez, A. Bodaghee, M. Cadolle Bel, G. L. Case, M. Hanke, M. Kühnel, S. B. Markoff, G. G. Pooley, R. E. Rothschild, J. A. Tomsick, C. A. Wilson-Hodge, and J. Wilms. *A&A*, 554:88, 2013.

V. Grinberg, K. Pottschmidt, M. Böck, C. Schmid, M. A. Nowak, P. Uttley, J. A. Tomsick, J. Rodriguez, N. Hell, A. Markowitz, A. Bodaghee, M. Cadolle Bel, R. E. Rothschild, and J. Wilms. *A&A*, 565:1, 2014.

J. E. Grindlay, D. Band, F. Seward, D. Leahy, M. C. Weisskopf, and F. E. Marshall. *ApJ*, 277:286, 1984.

P. Groot, S. Tingay, A. Udalski, and J. Miller. *IAU Circ.*, 7708, 2001.

F. Haardt, M. R. Galli, A. Treves, L. Chiappetti, D. Dal Fiume, A. Corongiu, T. Belloni, F. Frontera, E. Kuulkers, and L. Stella. *ApJS*, 133:187, 2001.

P.J. Hakala, P. Muhli, and G. Dubus. *MNRAS*, 306:701, 1999.

J. P. Halpern. *ATEL*, 549, 2005.

J. P. Halpern and S. Tyagi. *ATEL*, 682, 2005.

P. Han, J. Qu, S. Zhang, J. Wang, L. Song, G. Ding, S. Yan, and Y. Lu. *MNRAS*, 413:1072, 1999.

P. Han, J. Qu, S. Zhang, J. Wang, L. Song, G. Ding, S. Yan, and Y. Lu. *MNRAS*, 413:1072, 2011.

X. Han and R. M. Hjellming. *ApJ*, 400:304, 1992.

D. Hannikainen, D. Campbell-Wilson, R. Hunstead, V. McIntyre, J. Lovell, J. Reynolds, T. Tzioumis, and K. Wu. *ApSS*, 276:45, 2001.

D. C. Hannikainen, R. W. Hunstead, D. Campbell-Wilson, and R. K. Sood. *A&A*, 337:460, 1998.

D. C. Hannikainen, J. Rodriguez, O. Vilhu, L. Hjalmarsdotter, A. A. Zdziarski, T. Belloni, J. Poutanen, K. Wu, S. E. Shaw, V. Beckmann, R. W. Hunstead, G. G. Pooley, N. J. Westergaard, I. F. Mirabel, P. Hakala, A. Castro-Tirado, and Ph. Durouchoux. *A&A*, 435:995, 2005.

E. Harlaftis, S. Collier, K. Horne, and A.V. Filippenko. *A&A*, 341:491, 1999.

E. T. Harlaftis and J. Greiner. *A&A*, 413:L13, 2004.

E.T. Harlaftis, K. Horne, and A.V. Filippenko. *PASP*, 108:762, 1996.

E.T. Harlaftis, D. Steeghs, K. Horne, and A.V. Filippenko. *AJ*, 114:1170, 1997.

E.T. Harlaftis, V.S. Dhillion, and A. Castro-Tirado. *A&A*, 369:210, 2001.

B. A. Harmon, S. N. Zhang, G. J. Fishman, and C. A. Wilson. *IAU Circ.*, 5890, 1993a.

B. A. Harmon, W. S. Paciesas, and G. J. Fishman. *IAU Circ.*, 5619, 1994a.

B. A. Harmon, C. A. Wilson, W. S. Paciesas, G. N. Pendleton, M. S. Briggs, B. C. Rubin, M. H. Finger, G. J. Fishman, M. N. Brock, R. B. Wilson, and C. A. Meegan. *ApJ*, 425:L17, 1994b.

B. A. Harmon, C. A. Wilson, S. N. Zhang, W. S. Paciesas, G. J. Fishman, R. M. Hjellming, M. P. Rupen, D. M. Scott, M. S. Briggs, and B. C. Rubin. *Nature*, 374: 703, 1995.

B. A. Harmon, K. J. Deal, W. S. Paciesas, S. N. Zhang, C. R. Robinson, E. Gerard, L. F. Rodríguez, and I. F. Mirabel. *ApJ*, 471:85, 1997.

B. A. Harmon, M. L. McCollough, C. A. Wilson, S. N. Zhang, and W. S. Paciesas. *IAU Circ.*, 6933, 1998.

B.A. Harmon, R.B. Wilson, and M.H. Finger. *IAU Circ.*, 5504, 1992.

B.A. Harmon, S.N. Zhang, W.S. Paciesas, and G.J. Fishman. *IAU Circ.*, 5900, 1993b.

C.A. Haswell, E.I. Robinson, K. Horne, R.F. Steining, and T.M.C. Abbott. *ApJ*, 411:802, 1993.

C.A. Haswell, A.R. King, J.R. Murray, and P.A. Charles. *MNRAS*, 321:475, 2001.

W. A. Heindl and D. M. Smith. *ApJ*, 578:L125, 2002.

W.A. Heindl, T.A. Prince, and J.M. Grunsfeld. *ApJ*, 430:829, 1994.

J. Heise. *IAU Circ.*, 6606, 1997.

P. Hertz and J.E. Grindlay. *ApJ*, 278:137, 1984.

B. Hiemstra, M. Mendez, C. Done, Díaz T.M., D. Altamirano, and P. Casella. *MNRAS*, 411:137, 2011.

R. M. Hjellming. *ApJ*, 182:L29, 1973.

R. M. Hjellming and X.-H. Han. *IAU Circ.*, 4796, 1989.

R. M. Hjellming and K.J. Johnson. *ApJ*, 236:L141, 1981.

R. M. Hjellming and C. M. Wade. *ApJ*, 168:L21, 1971.

R. M. Hjellming, T. A. Calovini, X.H. Han, and F. A. Cordova. *ApJ*, 335:L75, 1988.

R. M. Hjellming, M. P. Rupen, C. R. Shrader, D. Campbell-Wilson, R. W. Hunstead, and D. J. McKay. *ApJ*, 470:L105, 1996a.

R. M. Hjellming, A. J. Mioduszewski, Y. Ueda, M. Ishida, H. Inoue, T. Dotani, W. H. G. Lewin, and J. Greiner. *IAU Circ.*, 6872, 1998a.

R. M. Hjellming, M. P. Rupen, F. Ghigo, E. B. Waltman, A. J. Mioduszewski, R. P. Fender, B. W. Stappers, M. Wieringa, R. Wark, and D. W. E. Green. *IAU Circ.*, 6937, 1998b.

R. M. Hjellming, M. P. Rupen, R. W. Hunstead, D. Campbell-Wilson, A. J. Mioduszewski, B. M. Gaensler, D. A. Smith, R. J. Sault, R. P. Fender, R. E. Spencer, C. J. de la Force, A. M. S. Richards, S. T. Garrington, S. A. Trushkin, F. D. Ghigo, E. B. Waltman, and M. McCollough. *ApJ*, 544:977, 1999a.

R. M. Hjellming, M. P. Rupen, A. J. Mioduszewski, E. Kuulkers, M. McCollough, B. A. Harmon, M. Buxton, R. Sood, A. Tzioumis, D. Rayner, S. Dieters, and P. Durouchoux. *ApJ*, 514:383, 1999b.

R. M. Hjellming, M. P. Rupen, R. W. Hunstead, D. Campbell-Wilson, A. J. Mioduszewski, B. M. Gaensler, D. A. Smith, R. J. Sault, R. P. Fender, R. E. Spencer, C. J. de la Force, A. M. S. Richards, S. T. Garrington, S. A. Trushkin, F. D. Ghigo, E. B. Waltman, and M. McCollough. *ApJ*, 544:977, 2000.

R.M. Hjellming. *ATEL*, 61, 2000.

R.M. Hjellming and M.P. Rupen. *Nature*, 375:464, 1995.

R.M. Hjellming, M. P. Rupen, J. Marti, F. Mirabel, and L.F. Rodriguez. *IAU Circ.*, 6383, 1996b.

R.M. Hjellming, M.P. Rupen, and A.J. Mioduszewski. *IAU Circ.*, 6934, 1998c.

R.M. Hjellming, M.P. Rupen, and A.J. Mioduszewski. *IAU Circ.*, 6924, 1998d.

R.M. Hjellming, M.P. Rupen, and A.J. Mioduszewski. *IAU Circ.*, 7254, 1999c.

R.M. Hjellming, M.P. Rupen, and A.J. Mioduszewski. *IAU Circ.*, 7265, 1999d.

Rupen M. P. Mioduszewski A. J. Smith D. A. Hjellming, R. M., B. A. Harmon, E. B. Waltman, F. D. Ghigo, and G. G. Pooley. *BAAS*, 193, 1998e.

M.P. Hobson, G. Efstathiou, , and A.N. Lasenby. *General Relativity: An Introduction for Physicists*. Cmbridge University Press, 2006.

D.W. Hog, J. Bovy, and D. Lang. *arXiv:1008.4686v1*, 2010.

E. Hog, C. Fabricius, V. V. Makarov, S. Urban, T. Corbin, G. Wycoff, U. Bastian, P. Schwekendiek, and A. Wicenec. *A&A*, 355:L27, 2000a.

E. Hog, C. Fabricius, V. V. Makarov, S. Urban, T. Corbin, G. Wycoff, U. Bastian, P. Schwekendiek, and A. Wicenec. *A&A*, 355:27, 2000b.

S.S. Holt, L.J. Kaluzienski, E.A. Boldt, and P.J. Serlemitsos. *ApJ*, 233:334, 1979.

J. Homan. *ATEL*, 2387, 2010.

J. Homan and T. Belloni. *Ap&SS*, 300:107, 2005.

J. Homan and R. Wijnands. *ATEL*, 169, 2003.

J. Homan, R. Wijnands, M. van der Klis, T. Belloni, J. van Paradijs, M. Klein-Wolt, R. Fender, and M. Méndez. *ApJS*, 132:377, 2001.

J. Homan, M. Klein-Wolt, S. Rossi, J.M. Miller, R. Wijnands, T. Belloni, M. van der Klis, and W.H.G. Lewin. *ApJ*, 586:1262, 2003a.

J. Homan, J. M. Miller, R. Wijnands, D. Steeghs, T. Belloni, M. van der Klis, and W. H. G. Lewin. *ATEL*, 162, 2003b.

J. Homan, M. Buxton, S. Markoff, C.D. Bailyn, E. Nespoli, and T. Belloni. *ApJ*, 624:295, 2005.

J. Homan, J.M. Miller, and R. Wijnands. *ATEL*, 752, 2006a.

J. Homan, R. Wijnands, A. Kong, J.M. Miller, S. Rossi, T. Belloni, and W.H.G. Lewin. *MNRAS*, 366:235, 2006b.

X-M. Hua, L. Titarchuk, and Y. Lyubarskij. *ApJ*, 449:188, 1995.

R.W. Hunstead and J. Webb. *IAU Circ.*, 7925, 2002.

J. B. Hutchings, D. Crampton, and A. P. Cowley. *ApJ*, 275:L43, 1983.

J. B. Hutchings, D. Crampton, A. P. Cowley, L. Bianchi, and I. B. Thompson. *AJ*, 94:340, 1987.

R. I. Hynes. *ApJ*, 623:1026, 2005.

R. I. Hynes, C. A. Haswell, S. Chaty, C. R. Shrader, and W. Cui. *MNRAS*, 331:169, 2000a.

R. I. Hynes, C. W. Mauche, C. A. Haswell, C. R. Shrader, W. Cui, and S. Chaty. *ApJ*, 539:L37, 2000b.

R. I. Hynes, C. Zurita, C. A. Haswell, J. Casares, P. A. Charles, E. P. Pavlenko, S. Yu. Shugarov, and D. A. Lott. *MNRAS*, 330:1009, 2002.

R. I. Hynes, D. Steeghs, J. Casares, P. A. Charles, and K. O'Brien. *ApJ*, 593:L95, 2003.

R. I. Hynes, D. Steeghs, J. Casares, P. A. Charles, and K. O'Brien. *ApJ*, 609:317, 2004.

R. I. Hynes, E.L. Robinson, and M. Bitner. *ApJ*, 630:405, 2005.

R.I. Hynes, P. Rocher, P.A. Charles, and M.J. Coe. *MNRAS*, 305:L49, 1999.

S. Ichimaru. *ApJ*, 217:840, 1977.

J. in 't Zand, J. Heise, A. Bazzano, M. Cocchi, L. di Ciolo, and J. M. Muller. *IAU Circ.*, 7119, 1999.

J. J. M. in 't Zand, J. Heise, A. C. Brinkman, R. Jager, G. K. Skinner, T. G. Patterson, H.-C. Pan, M. R. Nottingham, A. P. Willmore, and O. Al-Emam. *AdSpR*, 11:187, 1991.

J. J. M. in 't Zand, H. C. Pan, J. A. M. Bleeker, G. K. Skinner, M. R. Gil'Fanov, and R. A. Siuniaev. *A&A*, 266:283, 1992.

J. J. M. in 't Zand, R. G. Kaptein, and J. Heise. *IAU Circ.*, 7582, 2001.

J. J. M. in't Zand, E. Kuulkers, A. Bazzano, R. Cornelisse, M. Cocchi, J. Heise, J. M. Muller, L. Natalucci, M. J. S. Smith, and P. Ubertini. *A&A*, 357:520, 2000.

J. J. M. in't Zand, M. Capalbi, and M. Perri. *IAU Circ.*, 7873, 2002a.

J. J. M. in't Zand, C. B. Markwardt, A. Bazzano, M. Cocchi, R. Cornelisse, J. Heise, E. Kuulkers, L. Natalucci, M. Santos-Lleo, J. Swank, and P. Ubertini. *A&A*, 390: 587, 2002b.

J. J. M. in't Zand, J. M. Miller, T. Oosterbroek, and A. N. Parmar. *A&A*, 394:553, 2002c.

J. J. M. in't Zand, J. Heise, P. Lowes, and P. Ubertini. *ATEL*, 160, 2003.

Z. Ioannou, E. L. Robinson, W. F. Welsh, and C. A. Haswell. *AJ*, 127:481, 2004.

W. Ishibashi, E. Bozzo, R. Terrier, S. Mereghetti, A. Paizis, L. Ducci, D. Gotz, A. Bazzano, M. Fiocchi, A. de Rosa, A. Tarana, M. Del Santo, L. Natalucci, F. Panessa, F. Capitanio, V. Sguera, V. Bianchin, K. Watanabe, L. Kuiper, L. Barragan, J. Chenevez, I. Caballero, C. Shrader, A. Bird, G. Puehlhofer, C. Sanchez-Fernandez, G. Skinner, P. R. D. Hartog, K. Pottschmidt, I. Negueruela, and L. Prat. *ATEL*, 2803, 2010.

M. Ishida, K. Morio, and Y. Ueda. *ApJ*, 601:1088, 2004.

K. Jahoda, A. Swank, J. an Giles, M. Stark, T. Strohmayer, W. Zhang, and E. Morgan. Spie conference series. In O.H. Siegmund and M.A. Gummin, editors, *X-Ray,*

and Gamma-Ray Instrumentation for Astronomy VII, volume 2808, pages 59–70, 1996.

R.K. Jain, C.D. Bailyn, J.A. Orosz, R.A. Remillard, and J.E. McClintock. *ApJ*, 517: L131, 1999.

C. Jones. *ApJ*, 214:856, 1977.

C. Jones, W. Forman, H. Tananbaum, and M. J. L. Turner. *ApJ*, 210:L9, 1976.

P. G. Jonker, E. Gallo, V. Dhawan, M. Rupen, R. P. Fender, and G. Dubus. *MNRAS*, 351:1359, 2004.

P. G. Jonker, J. Miller-Jones, J. Homan, E. Gallo, M. Rupen, J. Tomsick, R. P. Fender, P. Kaaret, D. T. H. Steeghs, M. A. P. Torres, R. Wijnands, S. Markoff, and W. H. G. Lewin. *MNRAS*, 401:1255, 2010.

G. V. Jung, D. J. Kurfess, W. N. Johnson, R. L. Kinzer, J. E. Grove, M. S. Strickman, W. R. Purcell, D. A. Grabelsky, and M. P. Ulmer. *A&A*, 295:23, 1995.

P. Kaaret, S. Corbel, J. A. Tomsick, R. Fender, J. M. Miller, J. A. Orosz, A. K. Tzioumis, and R. Wijnands. *ApJ*, 582:945, 2003.

P. Kaaret, S. Corbel, J. A. Tomsick, J. Lazendic, A. K. Tzioumis, Y. Butt, and R. Wijnands. *ApJ*, 641:410, 2006.

M. Kalamkar, J. Homan, D. Altamirano, M. van der Klis, P. Casella, and M. Linares. *ApJ*, 731:L2, 2011.

E. Kalemci, J. A. Tomsick, R. E. Rothschild, K. Pottschmidt, and P. Kaaret. *ApJ*, 563:239, 2001.

E. Kalemci, J. A. Tomsick, R. E. Rothschild, K. Pottschmidt, S. Corbel, R. Wijnands, J.M. Miller, and P. Kaaret. *ApJ*, 586:419, 2003.

E. Kalemci, J. A. Tomsick, M. M. Buxton, R. E. Rothschild, K. Pottschmidt, S. Corbel, C. Brocksopp, and P. Kaaret. *ApJ*, 622:508, 2005.

E. Kalemci, J. A. Tomsick, R. E. Rothschild, K. Pottschmidt, S. Corbel, and P. Kaaret. *ApJ*, 639:340, 2006.

E. Kalemci, J. A. Tomsick, K. Yamaoka, and Y. Ueda. *ATEL*, 1348, 2008.

T. R. Kallman, M. A. Bautista, S. Goriely, C. Mendoza, J.M. Miller, P. Palmeri, P. Quinet, and J. Raymond. *ApJ*, 701:865, 2009.

V. Kalogera and G. Baym. *ApJ*, 470:L61, 1996.

L. J. Kaluzienski and S. S. Holt. *IAU Circ.*, 3104, 1977.

L. J. Kaluzienski, S. S. Holt, E. A. Boldt, P. J. Serlemitsos, G. Eadie, K. A. Pounds, M. J. Ricketts, and M. Watson. *ApJ*, 201:L121, 1975.

L. J. Kaluzienski, S. S. Holt, J. H. Swank, E. A. Boldt, and P. J. Serlemitsos. *BAAS*, 9:592, 1977.

A. Kaniovsky, K. Borozdin, and R. Sunyaev. *IAU Circ.*, 5878, 1993.

G.H. Kaplin, V.V. Kallarakl, R.S. Harrington, K.J. Johnston, and J.H. Spencer. *ApJ*, 85:1, 1980.

D. I. Karasev, A. A. Lutovinov, and S. A. Grebenev. *AstL*, 33:159, 2007.

D. I. Karasev, A. A. Lutovinov, and R. A. Burenin. *AstL*, 34:753, 2008.

R. Kaur, L. Kaper, L.E. Ellerbroek, D.M. Russell, D. Altamirano, R. Wijnands, Y. Yang, P. D'Avanzo, A. de Ugarte Postigo, H. Flores, J.P.U. Fynbo, P. Goldoni, C.C. Thöne, A. van der Horst, M. van der Klis, C. Kouveliotou, K. Wiersema, and E. Kuulkers. *ApJ*, 746:L23, 2012.

J. C. Kemp, G. D. Henson, D. J. Kraus, L. C. Carroll, I. S. Beardsley, K. Takagishi, J. Jugaku, M. Matsuoka, E. M. Leibowitz, T. Mazeh, and H. Mendelson. *ApJ*, 305:805, 1986.

J. Kennea, J. M. Miller, A. Beardmore, N. Degenaar, and M. T. Reynolds. *ATEL*, 4071, 2012a.

J. A. Kennea and G. K. Skinner. *PASJ*, 48:117, 1996.

J. A. Kennea, H. Krimm, V. Mangano, P. Curran, P. Romano, P. Evans, and D. N. Burrows. *ATEL*, 2877, 2010.

J. A. Kennea, E. A. Hoversten, M. H. Siegel, P. A. Evans, H. A. Krimm, P. Romano, V. Mangano, P. Curran, K. Yamaoka, and H. Negoro. *ATEL*, 3613, 2011a.

J. A. Kennea, P. Romano, V. Mangano, A. P. Beardmore, P. A. Evans, P. A. Curran, H. A. Krimm, C. B. Markwardt, and K. Yamaoka. *ApJ*, 736:22, 2011b.

J. A. Kennea, D. Altamirano, P. A. Evans, H. A. Krimm, P. Romano, V. Mangano, P. Curran, K. Yamaoka, and H. Negoro. *ATEL*, 4034, 2012b.

J. A. Kennea, H. A. Krimm, S. T. Holland, S. D. Barthelmy, W. Baumgartner, J. Cummings, N. Gehrels, C. B. Markwardt, D. Palmer, T. Sakamoto, G. Skinner, M. Stamatikos, J. Tueller, and T. Ukwatta. *ATEL*, 4145, 2012c.

J. A. Kennea, Y. J. Yang, D. Altamirano, P. A. Evans, H. A. Krimm, P. Romano, V. Mangano, P. Curran, K. Yamaoka, and H. Negoro. *ATEL*, 4044, 2012d.

J.A. Kennea, D. Palmer, D. Burrows, and N. Gehrels. *ATEL*, 626, 2005.

J.A. Kennea, D. Steeghs, M.A.P. Torres, J. Homan, and J.M. Miller. *ATEL*, 1237, 2007.

M. Kimura, H. Tomida, S. Nakahira, H. Negoro, S. Ueno, M. Ishikawa, T. Mihara, M. Serino, M. Sugizaki, T. Yamamoto, J. Sugimoto, M. Matsuoka, N. Kawai, M. Morii, R. Usui, K. Ishikawa, M. Nakajima, M. Asada, H. Sakakibara, N. Serita, A. Yoshida, H. Tsunemi, Y. Ueda, K. Hiroi, M. Shidatsu, R. Sato, M. Yamauchi, Y. Nishimura, T. Hanayama, K. Yoshidome, Y. Tsuboi, M. Higa, and K. Yamaoka. *ATEL*, 4198, 2012.

A. King. *X-Ray Binaries*. Cambridge University Press, 1995.

A. L. King, J.E Pringle, and M. Livio. *MNRAS*, 376:1740, 2007.

A. L. King, J. M. Miller, N. Degenaar, M. Reynolds, and R. Reis. *ATEL*, 4295, 2012.

A. R. King and H. Ritter. *MNRAS*, 293:42, 1998.

M. G. Kirsch, U. G. Briel, D. Burrows, S. Campana, G. Cusumano, K. Ebisawa, M. J. Freyberg, M. Guainazzi, F. Haberl, K. Jahoda, J. Kaastra, P. Kretschmar, S. Larsson, P. Lubinski, K. Mori, P. Plucinsky, A. M. Pollock, R. Rothschild, S. Sembay, J. Wilms, and M. Yamamoto. Proceedings of the spie. In O.H.W. Siegmund, editor, *UV, X-Ray, and Gamma-Ray Space Instrumentation for Astronomy XIV*, volume 5898, pages 22–23, 2005.

S. Kitamoto, S. Miyamoto, and H. Tsunemi. *PASJ*, 36:799, 1984.

S. Kitamoto, H. Tsunemi, S. Miyamoto, K. Yamashita, and S. Mizobuchi. *Nature*, 342:518, 1989.

S. Kitamoto, K. Takahashi, and K. Yamashita. *PASJ*, 42:85, 1990a.

S. Kitamoto, H. Tsunemi, H. Pedersen, S.A. Ilovaisky, and M. van der Klis. *ApJ*, 361:590, 1990b.

S. Kitamoto, H. Tsunemi, S. Miyamoto, and K. Hyashida. *ApJ*, 394:609, 1992.

M. Klein-Wolt, R.P. Fender, G.G. Pooley, T. Belloni, S. Migliari, E. H. Morgan, and M. van der Klis. *MNRAS*, 331:745, 2002.

G. Knevitt, G. A. Wynn, S. Vaughan, and M. G. Watson. *MNRAS*, 437:3087, 2014.

A. K. H. Kong. *ApJ*, 760:L127, 2012.

A. K. H. Kong, C.-C. Lin, Y.-T. Chen, P. A. Price, E. Magnier, K. Chambers, N. Kaiser, J. Morgan, W. Burgett, J. Heasley, W. Sweeney, C. Waters, H. Flewelling, and J. Tonry. *ATEL*, 2976, 2010a.

A. K. H. Kong, P. A. Price, E. Magnier, K. Chambers, N. Kaiser, J. Morgan, W. Burgett, W. Heasley, J.a nd Sweeney, C. Waters, and J. Flewelling, H.a nd Tonry. *ATEL*, 3011, 2010b.

A.K.H. Kong. *ATEL*, 625, 2005.

A.K.H. Kong, P.A. Charles, E. Kuulkers, and S. Kitamoto. *MNRAS*, 329:588, 2002.

T. Kotani, N. Kawai, T. Aoki, J. Doty, M. Matsuoka, K. Mitsuda, F. Nagase, G. Ricker, and N.E. White. *PASJ*, 46:L147, 1994.

T. Kotani, N. Kawai, F. Nagase, M. Namiki, M. Sakano, T. Takeshima, Y. Ueda, K. Yamaoka, and R. M. Hjellming. *ApJ*, 543:L133, 2000.

L. Kreidberg, C.D. Bailyn, W.M. Farr, and V. Kalogera. *ApJ*, 757:36, 2012.

H. A. Krimm and J. A. Kennea. *ATEL*, 3148, 2011.

H. A. Krimm, S. D. Barthelmy, W. Baumgartner, J. Cummings, E. Fenimore, N. Gehrels, C. B. Markwardt, D. Palmer, A. Parsons, T. Sakamoto, G. Sato, G. Skinner, M. Stamatikos, and J. Tueller. *ATEL*, 1855, 2008a.

H. A. Krimm, N. Gehrels, E. A. Hoversten, J. Mao, J. P. Osborne, J. L. Racusin, M. Stamatikos, G. Tagliaferri, E. Troja, and L. Vetere. *GCN Circ.*, 8200, 2008b.

H. A. Krimm, J. Kennea, S. D. Barthelmy, W. Baumgartner, J. Cummings, E. Fenimore, N. Gehrels, C. B. Markwardt, D. Palmer, A. Parsons, T. Sakamoto, G. Sato, G. Skinner, M. Stamatikos, and J. Tueller. *ATEL*, 1610, 2008c.

H. A. Krimm, J. A. Kennea, P. A. Evans, and C. B. Markwardt. *ATEL*, 1714, 2008d.

H. A. Krimm, J. A. Kennea, S. D. Barthelmy, W. Baumgartner, J. Cummings, E. Fenimore, N. Gehrels, C. B. Markwardt, D. Palmer, A. Parsons, T. Sakamoto, G. Skinner, J. Tueller, and T. Ukwatta. *ATEL*, 2156, 2009a.

H. A. Krimm, T. E. Strohmayer, J. H. Swank, S. D. Barthelmy, W. Baumgartner, J. Cummings, E. Fenimore, N. Gehrels, C. B. Markwardt, D. Palmer, T. Sakamoto, G. Skinner, M. Stamatikos, J. Tueller, and T. Ukwatta. *ATEL*, 2300, 2009b.

H. A. Krimm, P. Romano, S. Vercellone, S. D. Barthelmy, W. Baumgartner, J. Cummings, E. Fenimore, N. Gehrels, C. B. Markwardt, D. Palmer, T. Sakamoto, G. Skinner, M. Stamatikos, J. Tueller, and T. Ukwatta. *ATEL*, 2375, 2010.

H. A. Krimm, S. D. Barthelmy, W. Baumgartner, J. Cummings, E. Fenimore, N. Gehrels, C. B. Markwardt, D. Palmer, T. Sakamoto, G. Skinner, M. Stamatikos, J. Tueller, and T. Ukwatta. *ATEL*, 3138, 2011a.

H. A. Krimm, J. A. Tomsick, C. B. Markwardt, C. Brocksopp, F. Grise, P. Kaaret, and P. Romano. *ApJ*, 735:104, 2011b.

H. A. Krimm, S. D. Barthelmy, W. Baumgartner, J. Cummings, E. Fenimore, N. Gehrels, C. B. Markwardt, D. Palmer, T. Sakamoto, G. Skinner, M. Stamatikos, J. Tueller, and T. Ukwatta. *ATEL*, 4139, 2012.

H. A. Krimm, S. D. Barthelmy, W. Baumgartner, J. Cummings, N. Gehrels, A. Y. Lien, C. B. Markwardt, D. Palmer, T. Sakamoto, M. Stamatikos, and T. Ukwatta. *ATEL*, 5523, 2013a.

H. A. Krimm, S. T. Holland, R. H. D. Corbet, A. B. Pearlman, P. Romano, J. A. Kennea, J. S. Bloom, S. D. Barthelmy, W. H. Baumgartner, J. R. Cummings, N. Gehrels, A. Y. Lien, C. B. Markwardt, D. M. Palmer, T. Sakamoto, and and Ukwatta T. N. Stamatikos, M. *ApJSS*, 209:14, 2013b.

H. A. Krimm, S. D. Barthelmy, W. Baumgartner, J. Cummings, N. Gehrels, A. Y. Lien, C. B. Markwardt, and Sakamoto T. Palmer, D., M. Stamatikos, and T. Ukwatta. *ATEL*, 5986, 2014.

H.A. Krimm, J.L. Racusin, and C.B. Markwardt. *ATEL*, 1706, 2008e.

H.A. Krimm, J.A. Kennea, and S.T. Holland. *ATEL*, 3142, 2011c.

H.A. Krimm, J.A. Kennea, and S.T. Holland. *ATEL*, 5529, 2013c.

R. Krivonos, S. Molkov, M. Revnivtsev, S. Grebenev, R. Sunyaev, and A. Paizis. *ATEL*, 545, 2005.

A. Kubota and K. Makishima. *ApJ*, 601:428, 2004.

A. Kubota, Y. Tanaka, K. Makishima, Y. Ueda, T. Dotani, H. Inoue, and K. Yamaoka. *PASJ*, 50:667, 1998.

A. Kubota, K. Makishima, and Ebisawa K. *ApJ*, 560:L147, 2001.

L. Kuiper, J. van Paradijs, and M. van der Klis. *A&A*, 203:79, 1988.

E. Kuulkers, A. N. Parmar, S. Kitamoto, L. R. Cominsky, and R. K. Sood. *MNRAS*, 291:81, 1997a.

E. Kuulkers, M. van der Klis, and A.N. Parmar. *ApJ*, 474:L47, 1997b.

E. Kuulkers, R. P. Fender, R.E. Spencer, R.J. Davis, and I. Morison. *MNRAS*, 306: 919, 1999.

E. Kuulkers, A. Lutovinov, A. Parmar, F. Capitanio, N. Mowlavi, and W. Hermsen. *ATEL*, 149, 2003.

E. Kuulkers, J. Chenevez, S. Shaw, D. Brandt, T. Courvoisier, A. Domingo Garau, K. Ebisawa, P. Kretschmar, C. Markwardt, N. Mowlavi, T. Oosterbroek, A. Paizis, D. Risquez Oneca, C. Sanchez-Fernandez, and R. Wijnands. *ATEL*, 888, 2006a.

E. Kuulkers, S. Shaw, A. Paizis, A. Gros, J. Chenevez, C. Sanchez-Fernandez, S. Brandt, T. J.-L. Courvoisier, A.D. Garau, K. Ebisawa, P. Kretschmar, C. Markwardt, N. Mowlavi, T. Oosterbroek, A. Orr, D.R. Oneca, and R. Wijnands. *ATEL*, 874, 2006b.

E. Kuulkers, S. E. Shaw, A. Paizis, J. Chenevez, S. Brandt, T. J.-L. Courvoisier, A. Domingo, K. Ebisawa, P. Kretschmar, C. B. Markwardt, N. Mowlavi, T. Oosterbroek, A. Orr, D. Rísquez, C. Sanchez-Fernandez, and R. Wijnands. *A&A*, 466: 595, 2007.

E. Kuulkers, V. Beckmann, S. Shaw, S. Brandt, J. Chenevez, T. J.-L. Courvoisier, A. Domingo, K. Ebisawa, P. Jonker, P. Kretschmar, C. Markwardt, T. Oosterbroek, A. Paizis, D. Risquez, C. Sanchez-Fernandez, and R. Wijnands. *ATEL*, 1385, 2008.

E. Kuulkers, A. Ibarra, A. Pollock, A. Parmar, J. Chenevez, C. Kouveliotou, A. J. van der Horst, Z. Paragi, J. Granot, and G. B. Taylor. *ATEL*, 2912, 2010.

E. Kuulkers, C. Kouveliotou, T. Belloni, M. Cadolle Bel, J. Chenevez, M. Díaz Trigo, J. Homan, A. Ibarra, J. A. Kennea, T. Munoz-Darias, J.-U. Ness, A. N. Parmar, A. M. T. Pollock, E. P. J. van den Heuvel, and A. J. van der Horst. *A&A*, 552: 32, 2013.

S. I. Kuznetsov, M. R. Gilfanov, E. M. Churazov, R. A. Sunyaev, A. V. D'Yachkov, N. G. Khavenson, B. S. Novikov, R. S. Kremnev, P. Goldoni, A. Goldwurm, P. Laurent, J. Paul, J.-P. Roques, E. Jourdain, L. Bouchet, and G. Vedrenne. *AstL*, 25: 351, 1999.

S. Kwok. *Physics and Chemistry of the Interstellar Medium.* University Science Books, California, 2007.

I. Lapshov, S. Sazonov, and R. Sunyaev. *IAU Circ.*, 5864, 1993.

J.P. Lasota. *NewAR*, 45:449, 2001.

J. C. Lee, C. S. Reynolds, R. Remillard, N.S. Schulz, E.G. Blackman, and A.C. Fabian. *ApJ*, 567:1102, 2002.

E.M. Leibowitz, S. Hemar, and M. Orio. *MNRAS*, 300:463, 1998.

C. Leong, E. Kellogg, H. Gursky, H. Tananbaum, and R. Giacconi. *ApJ*, 170:67, 1971.

A. M. Levine and R. A. Remillard. *ATEL*, 1024, 2007.

A.M. Levine, H. Bradt, W. Cui, J. G. Jernigan, E. H. Morgan, R. Remillard, R.E. Shirey, and D.A. Smith. *ApJ*, 469:L33, 1996.

A.M. Levine, D. Lin, and R.A. Remillard. *ATEL*, 623, 2005a.

A.M. Levine, J.H. Swank, D. Lin, and R.A. Remillard. *ATEL*, 578, 2005b.

W. Liller. *ATEL*, 7254, 1999.

D. Lin, I.A. Smith, E.P. Liang, T. Bridgman, D. M. Smith, J. Martí, Ph. Durouchoux, I. F. Mirabel, and L. F. Rodríguez. *ApJ*, 532:548, 2000.

M. Linares, M. van der Klis, and R. Wijnands. *ApJ*, 660:595, 2007.

J. C. Ling, W. A. Mahoney, Wm. A. Wheaton, and A. S. Jacobson. *ApJ*, 321:L117, 1987.

J.C. Ling, W.A. Mahoney, W.A. Wheaton, A.S. Jacobson, and L. Kaluzienski. *ApJ*, 275:307, 1983.

B. F. Liu, W. Yuan, F. Meyer, E. Meyer-Hofmeister, and G. Z. Xie. *ApJ*, 527:L17, 1999.

J. Liu, Q. Z. ad van Paradijs and E. P. J. van den Heuvel. *A&A*, 469:807, 2007.

Q. Z. Liu, J. van Paradijs, and E. P. J. van den Heuvel. *A&A*, 147:25, 2000.

Q. Z. Liu, J. van Paradijs, and E. P. J. van den Heuvel. *A&A*, 368:1021, 2001.

Q. Z. Liu, J. van Paradijs, and E. P. J. van den Heuvel. *A&A*, 455:1165, 2006.

C. Lloyd, A. Oksanen, P. Starr, G. Darlington, and R. Pickard. *ATEL*, 4246, 2012.

M. Longair. *High Energy Astrophysics*. Cambridge University Press, New York, 2011.

A. Longmore, R. Cannon, P. Murdin, and D. Malin. *IAU Circ.*, 3110, 1977.

N. Lundt and S. Brandt. *IAU Circ.*, 5161, 1991.

A. Lutovinov, P. RKretschmar, C. Budtz-Joergensen, A. Domingo, V. Schoenfelder, G. Palumbo, and C. Winkler. *ATEL*, 145, 2003a.

A. Lutovinov, J. Rodriguez, N. Produit, N. Lund, W. Hermsen, and R. Much. *ATEL*, 151, 2003b.

A. A. Lutovinov and M. G. Revnivtsev. *AstL*, 29:719, 2003.

T.J. Maccarone. *MNRAS*, 360:68, 2005.

R.K.D. MacDonald, C. D. Bailyn, and A. G. Cantrell. Bulletin of the american astronomical society - meeting abstracts #217. volume 43. American Astronomical Society, 2011.

D.J.C. Mackay. *Information Theory, Inference, and Learning Algorithms*. Cambridge University Press, 2003.

Y. Maeda, K. Koyama, M. Sakano, T. Takeshima, and S. Yamauchi. *PASJ*, 48:417, 1996.

D. S. Main, D. M. Smith, W. A. Heindl, J. Swank, M. Leventhal, I. F. Mirabel, and L. F. Rodríguez. *ApJ*, 525:901, 1999.

D. Maitra and C.D. Bailyn. *ApJ*, 637:992, 2006.

D. Maitra, B. Cobb, C. Bailyn, J. Nelan, and D. Gonzalez. *ATEL*, 628, 2005.

D. Maitra, J.M. Miller, M.T. Reynolds, R. Reis, and M. Nowak. *arXiv:1306.4365*, 2013.

F. Makino. *IAU Circ.*, 4342, 1987.

F. Makino. *IAU Circ.*, 4571, 1988.

F. Makino. *IAU Circ.*, 4782, 1989.

F. Makino and the Ginga Team. *IAU Circ.*, 5161.

K. Makishima, Y. Maejima, K. Mitsuda, H. V. Bradt, R. A. Remillard, I. R. Tuohy, R. Hoshi, and M. Nakagawa. *ApJ*, 308:635, 1986.

P. Mandrou. *IAU Circ.*, 5032, 1990.

V. Mangano, W. H. Baumgartner, J. R. Cummings, N. Gehrels, E. A. Hoversten, C. B. Markwardt, and B. Sbarufatti. *GCN*, 11294, 2010a.

V. Mangano, E. A. Hoversten, C. B. Markwardt, B. Sbarufatti, R. L. C. Starling, and T. N. Ukwatta. *GCN*, 11296, 2010b.

B. Margon. Procedding of the texas symposium on relativistic astrophysics. pages 550–565, Munich, West Germany, December 1978.

B. Margon. *ARA&A*, 22:507, 1984.

B. Margon and S.F. Anderson. *ApJ*, 347:448, 1989.

B. Margon, J.R. Thorstensen, and S. Bowyer. *ApJ*, 221:907, 1978.

H. Mark, R. Price, R. Rodrigues, F. D. Seward, and C. D. Swift. *ApJ*, 155:L143, 1969.

T. H. Markert, C. R. Canizares, G. W. Clark, W. H. G. Lewin, H. W. Schnopper, and G. F. Sprott. *ApJ*, 184:L67, 1973.

T. H. Markert, F. N. Laird, G. W. Clark, D. R. Hearn, G. F. Sprott, F. K. Li, H. V. Bradt, W. H. G. Lewin, H. W. Schnopper, and P. F. Winkler. *ApJS*, 39:573, 1979.

S. Markoff, M. Nowak, S. Corbel, R. Fender, and H. Falcke. *A&A*, 397:645, 2003.

C. B. Markwardt. *Ap&SS*, 276:209, 2001.

C. B. Markwardt. *ATEL*, 143, 2003a.

C. B. Markwardt. *ATEL*, 115, 2003b.

C. B. Markwardt and A.P. Beardmore. *ATEL*, 2120, 2009.

C. B. Markwardt and J. H. Swank. *ATEL*, 133, 2003.

C. B. Markwardt and J. H. Swank. *ATEL*, 1235, 2007.

C. B. Markwardt and J. H. Swank. *ATEL*, 1442, 2008.

C. B. Markwardt and J. H. Swank. *ATEL*, 2108, 2009.

C. B. Markwardt and J. H. Swank. *ATEL*, 2823, 2010.

C. B. Markwardt, F. E. Marshall, and J. H. Swank. *IAU Circ.*, 7274, 1999a.

C. B. Markwardt, J. H. Swank, and F. E. Marshall. *IAU Circ.*, 7120, 1999b.

C. B. Markwardt, J. H. Swank, and E. Smith. *IAU Circ.*, 7707, 2001.

C. B. Markwardt, T.E. Strohmayer, J. H. Swank, and A.M. Levine. *ATEL*, 579, 2005.

C. B. Markwardt, M. Klein-Wolt, J. H. Swank, and R. Wijnands. *ATEL*, 1249, 2007.

C. B. Markwardt, J. P. Halpern, S. T. Holland, J. A. Kennea, H. A. Krimm, and J. H. Swank. *ATEL*, 1716, 2008a.

C. B. Markwardt, H. Krimm, R. Wijnands, and J. H. Swank. *ATEL*, 1709, 2008b.

C. B. Markwardt, D. Pereira, and J. H. Swank. *ATEL*, 1699, 2008c.

C. B. Markwardt, D. Pereira, and J. H. Swank. *ATEL*, 1685, 2008d.

C. B. Markwardt, S. D. Barthelmy, P. A. Evans, and J. H. Swank. *ATEL*, 2261, 2009a.

C. B. Markwardt, J. H. Swank, S. D. Barthelmy, W. H. Baumgartner, D. N. Burrows, P. A. Evans, S. T. Holland, E. A. Hoversten, and K. L. Page. *ATEL*, 2258, 2009b.

C. B. Markwardt, J. H. Swank, H. A. Krimm, D. Pereira, and T. E. Strohmayer. *ATEL*, 2107, 2009c.

C. B. Markwardt, T. E. Strohmayer, and J. H. Swank. *ATEL*, 2615, 2010.

T.R. Marsh, E.I. Robinson, and Wood J.H. *MNRAS*, 266:137, 1994.

F. E. Marshall and D. M. Smith. *IAU Circ.*, 6603, 1997.

F. E. Marshall, J. H. Swank, E. A. Boldt, S. S. Holt, and P. J. Serlemitsos. *ApJ*, 230:L45, 1979.

F. E. Marshall, R. F. Mushotzky, R. Petre, and P. J. Serlemitsos. *ApJ*, 419:301, 1993.

F. E. Marshall, K. Ebisawa, R. Remillard, and A. Valinia. *IAU Circ.*, 6504, 1996.

H.L. Marshall, C.R. Canizares, and N.S. Schulz. *ApJ*, 564:941, 2002.

J. Marti, I. F. Mirabel, P.-A. Duc, and L. F. Rodriguez. *A&A*, 323:158, 1997.

J. Marti, S. Mereghetti, S. Chaty, I. F. Mirabel, P. Goldoni, and L. F. Rodriguez. *A&A*, 338:L95, 1998.

J. Marti, I.F. Mirabel, S. Chaty, and L.F. Rodriguez. *A&A*, 363:184, 2000a.

J. Marti, I.F. Mirabel, S. Chaty, and L.F. Rodriguez. *A&A*, 56:943, 2000b.

J. Martí, I. F. Mirabel, L. F. Rodríguez, and I. A. Smith. *A&A*, 386:571, 2002.

J. Marti, P. L. Luque-Escamilla, J. R. Sanchez-Sutil, A. J. Munoz-Arjonilla, E. Sanchez-Ayaso, J. A. Combi, and M. T. García-Hernandez. *ApJ*, 721:L126, 2010.

A.C. Martin, J. Casares, P.A. Charles, F. van der Hooft, and J. van Paradijs. *MNRAS*, 274:L46, 1995.

N. Masetti, A. Bianchini, J. Bonibaker, M. della Valle, and R. Vio. *A&A*, 314:123, 1996.

K. O. Mason, A. N. Parmar, and N. E. White. *MNRAS*, 216:1033, 1985.

T. A. Matilsky, R. Giacconi, H. Gursky, E. M. Kellogg, and H. D. Tananbaum. *ApJ*, 174:L53, 1972.

M. Matsuoka, K. Kawasaki, S. Ueno, H Tomida, M. Kohama, M. Suzuki, Y. Adachi, M. Ishikawa, T. Mihara, M. Sugizaki, N. Isobe, Y. Nakagawa, H. Tsunemi, E. Miyata, N. Kawai, J. Kataoka, M. Morii, A. Yoshida, H. Negoro, M. Nakajima, Y. Ueda, H. Chujo, K. Yamaoka, O. Yamazaki, S. Nakahira, T. You, R. Ishiwata, S. Miyoshi, S. Eguchi, K. Hiroi, H. Katayama, and K. Ebisawa. *PASJ*, 61: 999, 2009.

M. Mayer and J.E. Pringle. *MNRAS*, 376:435, 2007.

J. McClintock, C. Canizares, and L. Petro. *IAU Circ.*, 3251, 1978.

J. E. McClintock and R. A. Remillard. *ApJ*, 308:110, 1986.

J. E. McClintock, M. R. Garcia, N. Caldwell, E. E. Falco, P. M. Garnavich, and P. Zhao. *ApJ*, 551:L147, 2001a.

J. E. McClintock, C. A. Haswell, M. R. Garcia, J. J. Drake, R. I. Hynes, H. L. Marshall, M. P. Muno, S. Chaty, P. M. Garnavich, P. J. Groot, W. H. G. Lewin, C. W. Mauche, J. M. Miller, G. G. Pooley, C. R. Shrader, and S. D. Vrtilek. *ApJ*, 555:477, 2001b.

J.E. McClintock and R.A. Remillard. *Compact Stellar X-Ray Sources*. Cambridge University Press, 2006.

J.E. McClintock, R.A. Remillard, M.P. Rupen, M. A. P. Torres, D. Steeghs, A.M. Levine, and J.A. Orosz. *ApJ*, 698:1398, 2009.

M.L. McCollough and C.A. Wilson. *IAU Circ.*, 7282, 1999.

R.E. McCrosky. *IAU Circ.*, 5597, 1992.

D.L. Meier. *Ap&SS*, 300:55, 2005.

S. Mereghetti, T. Belloni, and A. Goldwurm. *ApJ*, 433:L21, 1994.

S. Mereghetti, D.I. Cremonesi, F. Haardt, T. Murakami, T. Belloni, and A. Goldwurm. *ApJ*, 476:829, 1997.

E. Meyer-Hofmeister. *A&A*, 423:321, 2004.

T. Mihara, M. Nakajima, M. Sugizaki, M. Serino, M. Matsuoka, M. Kohama, K. Kawasaki, H. Tomida, S. Ueno, N. Kawai, J. Kataoka, M. Morii, A. Yoshida, K. Yamaoka, S. Nakahira, H. Negoro, N. Isobe, M. Yamauchi, and I. Sakurai. *PASJ*, 63:623, 2011.

M. Milgrom. *A&A*, 76:L3, 1979.

J. M. Miller. *arXiv:0609447v1*, 2006.

J. M. Miller, D. W. Fox, T. Di Matteo, R. Wijnands, T. Belloni, D. Pooley, C. Kouveliotou, and W. H. G. Lewin. *ApJ*, 546:1055, 2001a.

J. M. Miller, R. Wijnands, J. Homan, T. Belloni, D. Pooley, S. Corbel, C. Kouveliotou, M. van der Klis, and W. H. G. Lewin. *ApJ*, 563:928, 2001b.

J. M. Miller, J. Raymond, A. C. Fabian, J. Homan, M. A. Nowak, R. Wijnands, M. van der Klis, T. Belloni, J. A. Tomsick, D. M. Smith, P. A. Charles, and W. H. G. Lewin. *ApJ*, 601:450, 2004.

J. M. Miller, J. Homan, and G. Miniutti. *ApJ*, 652:113, 2006a.

J. M. Miller, J. Homan, D. Steeghs, M. Rupen, R. W. Hunstead, R. Wijnands, P. A. Charles, and A. C. Fabian. *ApJ*, 653:525, 2006b.

J. M. Miller, J. Raymond, A. Fabian, D. Steeghs, J. Homan, C. Reynolds, M. van der Klis, and R. Wijnands. *Nature*, 441:953, 2006c.

J. M. Miller, J. Raymond, J. Homan, A. C. Fabian, D. Steeghs, R. Wijnands, M. Rupen, P. Charles, M. van der Klis, and W. H. G. Lewin. *ApJ*, 646:394, 2006d.

J. M. Miller, J. Raymond, C. S. Reynolds, A. C. Fabian, T. R. Kallman, and J. Homan. *ApJ*, 680:1359, 2008.

J. M. Miller, A. Beardmore, J. Kennea, M. T. Reynolds, A. L. King, A. C. Fabian, C. S. Reynolds, and J. Raymond. *ATEL*, 4070, 2012a.

J. M. Miller, J. Raymond, J. Kennea, A. Beardmore, M. T. Reynolds, D. Maitra, N. Degenaar, E. M. Cackett, A. C. Fabian, and C. S. Reynolds. *ATEL*, 4191, 2012b.

J. C. A. Miller-Jones and G. R. Sivakoff. *ATEL*, 4394, 2012.

J. C. A. Miller-Jones, D. G. McCormick, R. P. Fender, R. E. Spencer, T. W. B. Muxlow, and G. G. Pooley. *MNRAS*, 363:867, 2005.

J. C. A. Miller-Jones, E. Gallo, M. P. Rupen, A. J. Mioduszewski, W. Brisken, R. P. Fender, P. G. Jonker, and T. J. Maccarone. *MNRAS*, 388:1751, 2008.

J. C. A. Miller-Jones, P. G. Jonker, V. Dhawan, W. Brisken, M. P. Rupen, G. Nelemans, and E. Gallo. *ApJ*, 706:L230, 2009.

J. C. A. Miller-Jones, O. K. Madej, P. G. Jonker, J. Homan, E. M. Ratti, and M. A. P. Torres. *ATEL*, 3358, 2011a.

J. C. A. Miller-Jones, G. R. Sivakoff, M. Rupen, and D. Altamirano. *ATEL*, 3628, 2011b.

J. C. A. Miller-Jones, G. R. Sivakoff, D. Altamirano, M. Coriat, S. Corbel, V. Dhawan, H. A. Krimm, R. A. Remillard, M. P. Rupen, D. M. Russell, R. P. Fender, S. Heinz, E. G. Körding, D. Maitra, S. Markoff, S. Migliari, C. L. Sarazin, and V. Tudose. *MNRAS*, 421:468, 2012.

J. C. A. Miller-Jones, G. R. Sivakoff, and H.A. Krimm. *ATEL*, 5530, 2013.

J.C.A. Miller-Jones, A.K. Tzioumis, P.G. Jonker, G.R. Sivakoff, T.J. Maccarone, and G. Nelemans. *ATEL*, 3364, 2011c.

S. Mineshige, M. Hirose, and Y. Osaki. *PASJ*, 44:L15, 1992.

A.J. Mioduszewski and M.P. Rupen. *ApJ*, 614:432, 2004.

I. F. Mirabel and L. F. Rodríguez. *Nature*, 371:46, 1994.

I. F. Mirabel, L. F. Rodriguez, B. Cordier, J. Paul, and F. Lebrun. *Nature*, 358:215, 1992.

I. F. Mirabel, L. F. Rodriguez, J. Marti, R. Teyssier, J. Paul, and M. Auriere. *IAU Circ.*, 5773, 1993.

I. F. Mirabel, R. Bandyopadhyay, P. A. Charles, T. Shahbaz, and L. F. Rodríguez. *ApJ*, 477:L45, 1997.

K. Mitsuda, H. Inoue, K. Koyama, K. Makishima, M. Matsuoka, Y. Ogawara, K. Suzuki, Y. Tanaka, N. Shibazaki, and T. Hirano. *PASJ*, 36:741, 1984.

S. Miyamoto and S. Kitamoto. *Nature*, 342:773, 1989.

S. Miyamoto, K. Kimura, and S. Kitamoto. *ApJ*, 383:807, 1991.

S. Miyamoto, S. Kitamoto, S. Iga, H. Negoro, and K. Terada. *ApJ*, 391:L21, 1992.

S. Miyamoto, S. Kitamoto, S. Iga, Y. Kamodo, K. Hayashida, K. Terada, and H. Negoro. Fourth international toki conference on plasma physics. pages 353–357, Japan, 1993. ESA.

E. Morgan, J. Swank, C. Markwardt, and N. Gehrels. *ATEL*, 550, 2005.

E. H. Morgan, R. A. Remillard, and J. Greiner. *ApJ*, 482:993, 1997.

K. Morihana, M. Sugizaki, S. Nakahira, M. Shidatsu, Y. Ueda, M. Serino, T. Mihara, M. Matsuoka, H. Negoro, and K. Nobuyuki. *PASJ*, 65:L10, 2013.

R. Mostafa, M. Mendez, B. Hiemstra, P. Soleri, T. Belloni, A.I. Ibrahim, and M.N. Yasein. *MNRAS*, 431:2341, 2013.

F. Mostellar and J.W. Tukey. *Data Analysis and Regression.* Addison Wesley, Reading, MA, 1977.

C. Motch, S. A. Ilovaisky, C. Chevalier, and P. Angebault. *SSRv*, 40:219, 1985.

C. Motch, P. Guillout, F. Haberl, J. Krautter, M. W. Pakull, W. Pietsch, K. Reinsch, W. Voges, and F.-J. Zickgraf. *A&AS*, 132:341, 1998.

S. Motta, T. Belloni, and J. Homan. *MNRAS*, 400:1603, 2009.

S. Motta, T. Muñoz-Darias, and T. Belloni. *MNRAS*, 408:1796, 2010.

S. Motta, J. Homan, T. Muñoz Darias, P. Casella, T. M. Belloni, B. Hiemstra, and M. Méndez. *MNRAS*, 427:595, 2012.

T. Munoz-Darias, S. Motta, D. Pawar, T. M. Belloni, S. Campana, and D. Bhattacharya. *MNRAS*, 404:L94, 2010.

T. Munoz-Darias, S. Motta, H. Stiele, and T. Belloni. *ATEL*, 3341, 2011.

T. Muñoz-Darias, S. Motta, H. Stiele, and T. M. Belloni. *MNRAS*, 415:292, 2011.

T. Muñoz-Darias, A. de Ugarte Postigo, D. M. Russell, S. Guziy, J. Gorosabel, J. Casares, M. Armas Padilla, P. A. Charles, R. P. Fender, T. M. Belloni, F. Lewis,

S. Motta, A. Castro-Tirado, C. G. Mundell, R. Sánchez-Ramírez, and C. C. Thöne. *MNRAS*, 432:1133, 2013.

T. Muñoz-Darias, R. P. Fender, S. E. Motta, and T. M. Belloni. *arXiv1407.1318*, 2014.

P. Murdin, R. E. Griffiths, K. A. Pounds, M. G. Watson, and A. J. Longmore. *MNRAS*, 178:27, 1977.

S. Nakahira, H. Negoro, K. Yamaoka, M. Matsuoka, Y. Ueda, H. Tomida, M. Sugizaki, M. Nakajima, N. Kawai, A. Yoshida, and T. Mihara. *ATEL*, 2259, 2009.

S. Nakahira, K. Yamaoka, M. Sugizaki, Y. Ueda, H. Negoro, K. Ebisawa, N. Kawai, M. Matsuoka, H. Tsunemi, A. Daikyuji, S. Eguchi, K. Hiroi, M. Ishikawa, R. Ishiwata, N. Isobe, K. Kawasaki, M. Kimura, and Mihara T. Kohama, M., S. Miyoshi, M. Morii, and Nakajima M. Nakagawa, Y.E., H. Ozawa, T. Sootome, K. Sugimori, M. Suzuki, H. Tomida, S. Ueno, T. Yamamoto, A. Yoshida, and Maxi Team. *PASJ*, 62:L27, 2010.

S. Nakahira, H. Negoro, T. Mihara, M. Sugizaki, M. Serino, T. Yamamoto, T. Sootome, M. Matsuoka, M. Nakajima, M. Asada, F. Suwa, H. Sakakibara, S. Ueno, H. Tomida, M. Kohama, M. Ishikawa, N. Kawai, M. Morii, K. Sugimori, R. Usui, T. Toizumi, Y. Aoki, S. Song, A. Yoshida, K. Yamaoka, H. Tsunemi, M. Kimura, H. Kitayama, Y. Ueda, K. Hiroi, M. Shidatsu, Y. Tsuboi, T. Matsumura, K. Yamazaki, M. Yamauchi, Y. Nishimura, and T. Hanayama. *ATEL*, 3830, 2011.

S. Nakahira, S. Koyama, K. Ueda, Y.a nd Yamaoka, M. Sugizaki, T. Mihara, M. Matsuoka, A. Yoshida, K. Makishima, K. Ebisawa, A. Kubota, S. Yamada, H. Negoro, K. Hiroi, M. Ishikawa, N. Kawai, M. Kimura, H. Kitayama, M. Kohama, T. Matsumura, M. Morii, M. Nakajima, M. Serino, M. Shidatsu, T. Sootome, K. Sugimori, F. Suwa, H. Tomida, Y. Tsuboi, H. Tsunemi, S. Ueno, R. Usui, T. Yamamoto, K. Yamazaki, M.S. Tashiro, Y. Terada, and H. Seta. *PASJ*, 64:13, 2012a.

S. Nakahira, Y. Ueda, T. Takagi, T. Mihara, M. Sugizaki, M. Serino, T. Yamamoto, J. Sugimoto, M. Matsuoka, S. Ueno, H. Tomida, M. Ishikawa, N. Kawai, M. Morii, R. Usui, K. Ishikawa, T. Yoshii, H. Negoro, M. Nakajima, M. Asada, H. Sakakibara, N. Serita, A. Yoshida, H. Tsunemi, M. Kimura, K. Hiroi, M. Shidatsu, R. Sato, Y. Tsuboi, M. Yamauchi, Higa M., Y. Nishimura, T. Hanayama, K. Yoshidome, and K. Yamaoka. *ATEL*, 4273, 2012b.

S. Nakahira, J. Sugimoto, M. Serino, T. Mihara, H. Negoro, M. Sugizaki, M. Morii, T. Yamamoto, T. Takagi, M. Matsuoka, S. Ueno, H. Tomida, M. Kimura, M. Ishikawa, Y. Nakagawa, N. Kawai, R. Usui, K. Ishikawa, T. Yoshii, A. Yoshida, T. Sakamoto, Y. Nakano, Y. Kawakubo, H. Tsunemi, M. Sasaki, M. Nakajima, K. Fukushima, T. Onodera, K. Suzuki, Y. Ueda, M. Shidatsu, T. Kawamuro, Y. Tsuboi, M. Higa, M. Yamauchi, K. Yoshidome, H. Yamada, Y. Ogawa, and K. Yamaoka. *ATEL*, 5241, 2013.

M. Namiki, N. Kawai, T. Kotani, and K. Makishima. *PASJ*, 55:281, 2003.

A. Nandi, S.K. Chakrabarti, T. Belloni, and P Goldoni. *MNRAS*, 359:629, 2005.

R. Narayan and I. Yi. *ApJ*, 452:710, 1994.

L. Natalucci, J.A. Tomsick, A. Bazzano, D.M. Smith, M. Bachetti, D. Barret, S.E. Boggs, F.E. Christensen, W.W. Craig, M. Fiocchi, F. Fürst, B.W. Grefenstette, C.J. Hailey, F.A. Harrison, R. Krivonos, E. Kuulkers, J.M. Miller, K. Pottschmidt, D. Stern, P. Ubertini, D.J. Walton, and W.W. Zhang. *ApJ*, 780:63, 2014.

H. Negoro, K. Yamaoka, S. Nakahira, K. Kawasaki, S. Ueno, H. Tomida, and Ishikawa M. Kohama, M., T. Mihara, Y. E. Nakagawa, M. Sugizaki, M. Serino, T. Yamamoto, T. Sootome, M. Matsuoka, N. Kawai, M. Morii, K. Sugimori, R. Usui, A. Yoshida, H. Tsunemi, M. Kimura, M. Nakajima, H. Ozawa, F. Suwa, Y. Ueda, N. Isobe, S. Eguchi, K. Hiroi, A. Daikyuji, Y.K. Uzawa, and K. Matsumura. *ATEL*, 2873, 2010.

H. Negoro, S. Nakahira, Y. Ueda, T. Mihara, M. Sugizaki, M. Serino, T. Yamamoto, T. Sootome, M. Matsuoka, S. Ueno, H. Tomida, M. Kohama, M. Ishikawa,

N. Kawai, M. Morii, K. Sugimori, R. Usui, T. Toizumi, A. Yoshida, K. Yamaoka, H. Tsunemi, M. Kimura, H. Kitayama, M. Nakajima, F. Suwa, M. Asada, H. Sakakibara, K. Hiroi, M. Shidatsu, Y. Tsuboi, T. Matsumura, and K. Yamazaki. *ATEL*, 3330, 2011a.

H. Negoro, M. Nakajima, S. Nakahira, M. Morii, H. A. Krimm, D. M. Palmer, J. A. Kennea, T. Mihara, M. Sugizaki, M. Serino, T. Yamamoto, T. Sootome, M. Matsuoka, S. Ueno, H. Tomida, M. Kohama, M. Ishikawa, N. Kawai, K. Sugimori, R. Usui, T. Toizumi, A. Yoshida, K. Yamaoka, H. Tsunemi, M. Kimura, H. Kitayama, F. Suwa, M. Asada, H. Sakakibara, Y. Ueda, K. Hiroi, M. Shidatsu, Y. Tsuboi, T. Matsumura, and K. Yamazaki. *ATEL*, 3611, 2011b.

H. Negoro, N. Kawai, S. Nakahira, T. Mihara, M. Sugizaki, M. Serino, T. Yamamoto, T. Sootome, M. Matsuoka, and Tomida H. Ueno, S., M. Kohama, M. Ishikawa, M. Morii, K. Sugimori, R. Usui, T. Toizumi, Y. Aoki, S. Song, A. Yoshida, K. Yamaoka, H. Tsunemi, M. Kimura, H. Kitayama, M. Nakajima, F. Suwa, M. Asada, H. Sakakibara, and Hiroi K. Ueda, Y., M. Shidatsu, Y. Tsuboi, T. Matsumura, K. Yamazaki, M. Yamauchi, Y. Nishimura, and T. Hanayama. *ATEL*, 3842, 2012a.

H. Negoro, N. Kawai, K. Yamaoka, and MAXI Team. Aip conference proceedings: Suzaku 2011 - exploring the x-ray universe suzaku and beyond. volume 1427, pages 314–315, Japan, 2012b.

E.T. Neil, C.D. Bailyn, and B.E. Cobb. *AJ*, 657:409, 2007.

J. Neilsen and J.C. Lee. *Nature*, 458:481, 2009.

J. Neilsen, S.D. Steeghs, and S.D. Vrtilek. *MNRAS*, 384:849, 2008.

J. Neilsen, R.A. Remillard, and J.C. Lee. *ApJ*, 737:69, 2011.

J. Neilsen, M. Coriat, R. Fender, J.C. Lee, G. Ponti, A.K. Tzioumis, P.G. Edwards, and J.W. Broderick. *ApJ*, 784:L5, 2014.

Z. Ninkov, G.A.H. Walker, and S. Yang. *ApJ*, 321:425, 1987.

P. L. Nolan and J. L. Matteson. *ApJ*, 265:389, 1983.

P. L. Nolan, D. E. Gruber, F. K. Knight, J. L. Matteson, R. E. Rothschild, F. E. Marshall, A. M. Levine, and F. A. Primini. *Nature*, 293:275, 1983.

M. A. Nowak, J. Wilms, W. A. Heindl, K. Pottschmidt, J. B. Dove, and M. C. Begelman. *MNRAS*, 320:316, 2001.

M. A. Nowak, J. Wilms, and K. Pottschmidt. *ApJ*, 744:107, 2012.

M.A. Nowak and J. Wilms. *ApJ*, 522:476, 1999.

M.A. Nowak, A. Juett, J. Homan, Y. Yao, J. Wilms, and and Canizares C.R. Schulz, N.S. *ApJ*, 689:1199, 2008.

K. O'Brien, F. Clarke, R.P. Fender, C. Brocksopp, D. Steeghs, R. Hynes, and P. Charles. *ATEL*, 117, 2003.

G.I. Ogilvie and G. Dubus. *MNRAS*, 320:485, 2001.

R. N. Ogley, T. D. C. Ash, and R. P. Fender. *IAU Circ.*, 6726, 1997.

S. Okamura and T. Noguchi. *IAU Circ.*, 4589, 1988.

A. Okazaki and I. Negueruela. *A&A*, 377:161, 2001.

J. B. Oke. *ApJ*, 217:181, 1977.

T. Oosterbroek, M. van der Klis, J. van Paradijs, B. Vaughan, R. Rutledge, W. H. G. Lewin, Y. Tanaka, F. Nagase, T. Dotani, K. Mitsuda, and S. Miyamoto. *A&A*, 321:776, 1997.

T. Oosterbroek, A. N. Parmar, E. Kuulkers, T. Belloni, M. van der Klis, F. Frontera, and A. Santangelo. *ApJ*, 340:431, 1998.

M. Orlandini, A. N. Parmar, F. Frontera, N. Masetti, D. Dal Fiume, A. Orr, A. Piccioni, G. Raimondo, A. Santangelo, G. Valentini, and T. Belloni. *ApJ*, 356:163, 2000.

J. A. Orosz, E. J. Polisensky, C. D. Bailyn, S. W. Tourtellotte, J. E. McClintock, and R. A. Remillard. Bulletin of the american astronomical society - meeting #201. volume 34, page 1124. American Astonomical Society.

J.A. Orosz. Iau symposium: A massive star odyssey, from main sequence to supernova. volume 212, page 365, 2003.

J.A. Orosz and C.D. Bailyn. *ApJ*, 446:L59, 1995.

J.A. Orosz and C.D. Bailyn. *ApJ*, 477:876, 1997.

J.A. Orosz, C.D. Bailyn, J.E. McClintock, and R.A. Remillard. *ApJ*, 468:380, 1996.

J.A. Orosz, C. Bailyn, and R. Jain. *IAU Circ.*, 7009, 1998a.

J.A. Orosz, R.K. Jain, C.D. Bailyn, J.E. McClintock, and R.A. Remillard. *ApJ*, 499: 375, 1998b.

J.A. Orosz, E. Kuulkers, M. van der Klis, J.E. McClintock, M.R. Garcia, P.J. Callanan, C.D. Bailyn, R.K. Jain, and R.A. Remillard. *ApJ*, 555:489, 2001.

J.A. Orosz, P.J. Groot, M. van der Klis, J.E. McClintock, M.R. Garcia, P. Zhao, R.K. Jain, C.D. Bailyn, and R.A. Remillard. *ApJ*, 568:845, 2002.

J.A. Orosz, J.E. McClintock, R.A. Remillard, and S. Corbel. *ApJ*, 616:376, 2004.

J.A. Orosz, D. Steeghs, J.E. McClintock, M.A.P. Torres, I. Bochkov, L. Gou, R. Narayan, M. Blaschak, A.M. Levine, R.A. Remillard, C.D. Bailyn, M.M. Dwyer, and M. Buxton. *ApJ*, 697:573, 2009.

J.A. Orosz, J.E. McClintock, J.P. Aufdenberg, R.A. Remillard, M.J. Reid, R. Narayan, and L. Gou. *ApJ*, 742:84, 2011a.

J.A. Orosz, J.F. Steiner, J.E. McClintock, M.A.P. Torres, R.A. Remillard, C.D. Bailyn, and J.M. Miller. *ApJ*, 730:75, 2011b.

J.A. Orosz, J.F. Steiner, J.E. McClintock, M.M. Buxton, C.D. Bailyn, D. Steeghs, A. Guberman, and M.A.P. Torres. *arXiv:1402.0085*, 2014.

F. N. Owen, T. J. Balonek, J. Dickey, Y. Terzian, and S. T. Gottesman. *ApJ*, 203: L15, 1976.

H. Ozawa, F. Suwa, H. Negoro, M. Serino, S. Ueno, H. Tomida, M. Kohama, M. Ishikawa, T. Mihara, M. Sugizaki, and Yamamoto T. Nakagawa, Y. E., T. Saotome, M. Matsuoka, N. Kawai, M. Morii, K. Sugimori, R. Usui, A. Yoshida, K. Yamaoka, S. Nakahira, H. Tsunemi, M. Kimura, H. Kitayama, M. Nakajima, Y. Ueda, N. Isobe, S. Eguchi, K. Hiroi, M. Shidatsu, A. Daikyuji, Y. Tsuboi, Uzawa, T. Matsumura, and K. Yamazaki. *ATEL*, 3098, 2011.

F. Ozel, D. Psaltis, R. Narayan, and J.E. McClintock. *ApJ*, 725:1918, 2010.

W. S. Paciesas, M. S. Briggs, B. A. Harmon, R. B. Wilson, and M. H. Finger. *IAU Circ.*, 5580, 1992.

B. Paczynski. *A&A*, 9:183, 1971.

B. Paczynski. *A&A*, 34:161, 1974.

A. Paizis, V. Beckmann, D. Gotz, L. Sidoli, A. Bazzano, G. Belanger, M. Cadolle-Bel, J. Chenevez, A. de Rosa, E. Kuulkers, M. Falanga, M. Fiocchi, L. Kuiper, J. C. Leyder, S. Mereghetti, S. Piraino, K. Pottschmidt, S. Shaw, J. Tomsick, K. Watanabe, R. Walter, and G. Weidenspointner. *ATEL*, 1248.

A. Paizis, M. A. Nowak, S. Chaty, J. Rodriguez, T. J.-L. Courvoisier, M. Del Santo, K. Ebisawa, R. Farinelli, P. Ubertini, and J. Wilms. *ApJ*, 657:L109, 2007.

A. Paizis, K. Ebisawa, H. Takahashi, T. Dotani, T. Kohmura, M. Kokubun, J. Rodriguez, Y. Ueda, R. Walter, S. Yamada, K. Yamaoka, and T. Yuasa. *PASJ*, 61: 107, 2009.

D. M. Palmer, S. D. Barthelmey, J. R. Cummings, N. Gehrels, H. A. Krimm, C. B. Markwardt, T. Sakamoto, and J. Tueller. *ATEL*, 546, 2005.

H.C. Pan, G.K. Skinner, R.A. Sunyaev, and K.N. Borozdn. *MNRAS*, 274:L15, 1995.

M. Pandey, A. P. Rao, C. H. Ishwara-Chandra, P. Durouchoux, and R. K. Manchanda. *A&A*, 463:567, 2007.

M. D. Pandey, Ph. Durouchoux, R. K. Manchanda, A. P. Rao, C. H. Ishwara-Chandra, and G. Pooley. *astro-ph/0509645*, 2005.

S. Q. Park, J. M. Miller, J. E. McClintock, R. A. Remillard, J. A. Orosz, C. R. Shrader, R. W. Hunstead, D. Campbell-Wilson, C. H. Ishwara-Chandra, A. P. Rao, and M. P. Rupen. *ApJ*, 610:378, 2004.

S.Q. Park, J.M. Miller, J.E. McClintock, and S.S. Murray. *ApJ*, 618:L45, 2005.

A.N. Parmar and N.E. White. *IAU Circ.*, 4051, 1985.

A.N. Parmar, L. Stella, and N.E. White. *ApJ*, 304:664, 1986.

A.N. Parmar, L. Angelini, P. Roche, and N.E. White. *A&A*, 279:179, 1993.

A.N. Parmar, L. Angelini, and N.E. White. *ApJ*, 452:L129, 1995.

A.N. Parmar, O.R. Williams, E. Kuulkers, L. Angelini, and N.E. White. *A&A*, 319: 855, 1997.

B. Paul, P. C. Agrawal, A. R. Rao, M. N. Vahia, J. S. Yadav, T. M. K. Marar, S. Seetha, and K. Kasturirangan. *A&A*, 320:37, 1997.

B. Paul, P. C. Agrawal, A. R. Rao, M. N. Vahia, J. S. Yadav, S. Seetha, and K. Kasturirangan. *ApJ*, 492:63, 1998.

J. Paul, B. Cordier, A. Goldwurm, F. Lebrun, P. Mandrou, J. P. Roques, and Bouchet L. Vedrenne, G., E. Churazov, and M. Gilfanov. Gamma ray line astrophysics. New York, 1991. AIP.

J. Paul, L. Bouchet, E. Churazov, and R. Sunyaev. *IAU Circ.*, 6348, 1996.

H. Pederson. *The Messenger*, 34:21, 1983.

P. Podsiadlowski, S. Rappaport, and E. Pfahl. *ApJ*, 565:1107, 2002.

G. Ponti, R. P. Fender, M. C. Begelman, R. J. H. Dunn, J. Neilsen, and M. Coriat. *MNRAS*, 422:11, 2012.

G. Pooley. *ATEL*, 385, 2005.

G. G. Pooley and R. P. Fender. *MNRAS*, 222:925, 1997.

G. G. Pooley and E.M. Waldram. *IAU Circ.*, 7390, 2000.

S.F. Portegies Zwart, J. Dewi, and T. Maccarone. *MNRAS*, 355:413, 2004.

K. Pottschmidt, J. Wilms, M. A. Nowak, G. G. Pooley, T. Gleissner, W. A. Heindl, D. M. Smith, R. Remillard, and R. Staubert. *A&A*, 407:1039, 2003.

K. Pottschmidt, M. Chernyakova, A. A. Zdziarski, P. Lubinski, D. M. Smith, and N. Bezayiff. *A&A*, 452:285, 2006.

K.A. Pounds. *IAU Circ.*, 2729, 1974.

W. Priedhorsky. *Ap&SS*, 126:89, 1986.

W. C. Priedhorsky, J. Terrell, and S. S. Holt. *ApJ*, 270:233, 1983.

J.E. Pringle. *ARA&A*, 19:137, 1981.

D. Psaltis. *Compact Stellar X-Ray Sources*. Cambridge University Press, 2006.

J. L. Racusin, P. A. Evans, D. Grupe, E. A. Hoversten, H. A. Krimm, C. B. Markwardt, C. Pagani, K. L. Page, D. M. Palmer, M. Stamatikos, M. C. Stroh, and L. Vetere. *GCN Circ.*, 8199, 2008.

A. Rau, J. Greiner, J. Elliott, and Olivares E.F. *ATEL*, 3365, 2011a.

A. Rau, J. Greiner, and R. Filgas. *ATEL*, 3140, 2011b.

A. Rau, J. Greiner, and P. Schady. *ATEL*, 4144, 2012a.

A. Rau, F. Knust, D.A. Kann, and J. Greiner. *ATEL*, 4380, 2012b.

A.M. Read, R.D. Saxton, and P. Esquej. *ATEL*, 2607, 2010a.

A.M. Read, R.D. Saxton, P. Esquej, and P.A. Evans. *ATEL*, 2627, 2010b.

M. J. Rees, M. C. Begelman, R. D. Blandford, and E. S. Phinney. *Nature*, 295:17, 1982.

W. Reich and R. Schlickeiser. *A&A*, 256:408, 1992.

M.J Reid, J.E. McClintock, R. Narayan, L. Gou, and and Orosz J.A. Remillard, R.A. *ApJ*, 742:83, 2011.

P. Reig. *Ap&SS*, 332:1, 2011.

P. Reig, T. Belloni, and M. van der Klis. *A&A*, 412:229, 2003.

P. Reig, A. Zezas, and L. Gkouvelis. *A&A*, 522:107, 2010.

R. C. Reis, J. M. Miller, and Cackett E. M. Fabian, A. C., and Reynolds C. S. Maitra, D., M. Rupen, D. T. H. Steeghs, and R. Wijnands. *MNRAS*, 410:2497, 2011.

R. C. Reis, J. M. Miller, M. T. Reynolds, and and Walton D. J. Fabian, A. C. *ApJ*, 751:34, 2012.

R. C. Reis, M. T. Reynolds, J. M. Miller, D. J. Walton, D. Maitra, A. King, and N. Degenaar. *ApJ*, 778:155, 2013.

R. Remillard. *Mem. S.A. It.*, 70:881, 1999.

R. Remillard. *IAU Circ.*, 7707, 2001.

R. Remillard and D. Smith. *ATEL*, 88, 2002.

R. Remillard, and Swank J. Levine, A., and T. Strohmayer. *IAU Circ.*, 6710, 1997.

R. Remillard, A. Levine, A. Wood, and Starrfield S. Wagner, R. M., and and Bowell E. and Skiff B. and Koehn B. Shrader, C. *IAU Circ.*, 6920, 1998.

R. Remillard, E. Morgan, D. Smith, and E. Smith. *IAU Circ.*, 7389, 2000.

R. Remillard, and Torres M. A. P. Garcia, M., D. Steeghs, and GSFC ASM Team at MIT. *ATEL*, 384, 2005.

R. Remillard, A. M. Levine, and Markwardt C. B. Morgan, E. H., and J. H. Swank. *ATEL*, 714, 2006.

R. A. Remillard and ASM Team at MIT. *ATEL*, 2265, 2009.

R.A. Remillard and A.M. Levine. *ATEL*, 144, 2003.

R.A. Remillard and J.E. McClintock. *ARA&A*, 44:49, 2006.

R.A. Remillard and and McClintock J.E. and Bailyn C.D. Orosz, J.A. *ApJ*, 459:226, 1996.

R.A. Remillard, J.E. McClintock, and C.D. Bailyn. *ApJ*, 399:L145, 1992.

R.A. Remillard, J.E. McClintock, and Bailyn C.D. Sobczak, G.J., J.A. Orosz, E.H. Morgan, and A.M. Levine. *ApJ*, 517:L127, 1999a.

R.A. Remillard, and McClintock J.E. Morgan, E.H., C.D. Bailyn, and J.A. Orosz. *ApJ*, 522:397, 1999b.

R.A. Remillard, G.J. Sobczak, M.P. Muno, and J.E. McClintock. *ApJ*, 564:962, 2002.

R.A. Remillard, A.M. Levine, E.H. Morgan, E. Smith, and J. Swank. *IAU Circ.*, 8050, 2003.

M. Revnivtsev. *A&A*, 410(865), 2003.

M. Revnivtsev and R. Sunyaev. *IAU Circ.*, 7715, 2001.

M. Revnivtsev, M. Gilfanov, and E. Churazov. *A&A*, 339:483, 1998a.

M. Revnivtsev, M. Gilfanov, E. Churazov, R. Sunyaev, K. Borozdin, N. Alexandrovich, N. Khavenson, I. Chulkov, A. Goldwurm, J. Ballet, M. Denis, P. Laurent, J.-P. Roques, V. Borrel, and and Jourdain E. Bouchet, L. *A&A*, 331:557, 1998b.

M. Revnivtsev, R. Sunyaev, and K. Borozdin. *A&A*, 361:37, 2000a.

M. Revnivtsev, M. Gilfanov, E. Churazov, and R. Sunyaev. *A&A*, 391:1013, 2002.

M. Revnivtsev, M. Gilfanov, E. Churazov, and R. Sunyaev. *ATEL*, 150, 2003.

M. G. Revnivtsev, S. P. Trudolyubov, and K. N. Borozdin. *MNRAS*, 312:151, 2000b.

M.G. Revnivtsev, K.N. Borozdin, W.C. Priedhorsky, and A. Vikhlinin. *ApJ*, 530: 955, 2000c.

A. P. Reynolds, A. N. Parmar, P. J. Hakala, A. M. T. Pollock, O. R. Williams, A. Peacock, and B. G. Taylor. *A&AS*, 134:287, 1999.

M. Reynolds, P. Callanan, and T. Nagayama. *ATEL*, 2125, 2009.

M.T. Reynolds, P.J. Callanan, and A.V. Filippenko. *MNRAS*, 374:657, 2007.

D. Ricci, G.I. Israel, and L. Stella. *A&A*, 299:731, 1995.

G.A. Richer. *IBVS*, 3362, 1987.

M. J. Ricketts, K. A. Pounds, and M. J. L. Turner. *Nature*, 257:658, 1975.

M. J. Ricketts, R. Hall, C. G. Page, K. A. Pounds, and M. R. Sims. *Vistas in Astronomy*, 25:71, 1981.

M. S. E. Roberts, P. F. Michelson, L. R. Cominsky, F. E. Marshall, R. H. D. Corbet, and E. A. Smith. *IAU Circ.*, 6302, 1996.

E.L. Robinson, I.I. Ivans, and W.F. Welsh. *ApJ*, 565:1169, 2002.

E.L. Robinson, A. J. Bayless, P. A. Mason, and P. Robertson. American astronomical society meeting abstracts. volume 219. American Astonomical Society, 2012.

and Corbel S. Rodriguez, J., E. Kalemci, J. A. Tomsick, and M. Tagger. *ApJ*, 612: 1018, 2004.

J. Rodriguez, S. Corbel, and J. A. Tomsick. *ApJ*, 595:1032, 2003.

J. Rodriguez, M. Cadolle Bel, J.A. Tomsick, S. Corbel, C. Brocksopp, A. Paizis, S.E. Shaw, and A. Bodaghee. *ApJ*, 655:L97, 2007.

J. Rodriguez, S. Corbel, I. Caballero, J. A. Tomsick, T. Tzioumis, A. Paizis, M. Cadolle Bel, and E. Kuulkers. *A&A*, 533:L4, 2011a.

J. Rodriguez, S. Corbel, J. A. Tomsick, A. Paizis, and E. Kuulkers. *ATEL*, 3168, 2011b.

L. F. Rodriguez and I. F. Mirabel. *A&A*, 101:173, 1998.

L. F. Rodriguez, I. F. Mirabel, and J. Marti. *ApJ*, 401:L15, 1992.

L. F. Rodriguez, E. Gerard, I. F. Mirabel, Y. Gomez, and A. Velazquez. *ApJS*, 101: 173, 1995.

L.F. Rodríguez and I.F. Mirabel. *ApJ*, 474:L123, 1997.

A. F. Rojas, N. Masetti, and D. Minniti. *ATEL*, 3372, 2011.

S. Rossi, J. Homan, J. M. Miller, and T. Belloni. *NuPhS*, 132:416, 2004.

D. M. Rothstein, S. S. Eikenberry, S. Chatterjee, E. Egami, S. G. Djorgovski, and W. A. Heindl. *ApJ*, 580:L61, 2002.

J. Roy, P. C. Agrawal, B. Paul, and K. Duorah. *MNRAS*, 412:1011, 2011.

A. Rozanaska and B. Czerny. *A&A*, 360:1170, 2000.

B. C. Rubin, B. A. Harmon, W. S. Paciesas, C. R. Robinson, S. N. Zhang, and G. J. Fishman. *ApJ*, 492:L67, 1998.

M. P. Rupen, R. M. Hjellming, and A. J. Mioduszewski. *IAU Circ.*, 6938, 1998.

M. P. Rupen, V. Dhawan, and A. J. Mioduszewski. *IAU Circ.*, 7874, 2002.

M. P. Rupen, C. Brocksopp, A. J. Mioduszewski, V. Dhawan, and Fender R. Sault, R., and S. Corbel. *IAU Circ.*, 8054, 2003a.

M. P. Rupen, A. J. Mioduszewski, and V. Dhawan. *ATEL*, 137, 2003b.

M. P. Rupen, A. J. Mioduszewski, and V. Dhawan. *BAAS*, 36:937, 2004.

M. P. Rupen, V. Dhawan, and A. J. Mioduszewski. *ATEL*, 589, 2005a.

M. P. Rupen, A. J. Mioduszewski, and V. Dhawan. *ATEL*, 490, 2005b.

M.P. Rupen, V. Dhawan, and A.J. Mioduszewski. *ATEL*, 210, 2003c.

M.P. Rupen, A.J. Mioduszewski, and V. Dhawan. *ATEL*, 172, 2003d.

M.P. Rupen, A.J. Mioduszewski, and V. Dhawan. *ATEL*, 152, 2003e.

M.P. Rupen, V. Dhawan, and A.J. Mioduszewski. *ATEL*, 419, 2005c.

M.P. Rupen, V. Dhawan, and A.J. Mioduszewski. *ATEL*, 489, 2005d.

M.P. Rupen, A.J. Mioduszewski, and V. Dhawan. *ATEL*, 434, 2005e.

M.P. Rupin, V. Dhawan, and A.J. Mioduszewski. *ATEL*, 717, 2006a.

M.P. Rupin, V. Dhawan, and A.J. Mioduszewski. *ATEL*, 721, 2006b.

D. M. Russell, Y. J. Yang, A. Patruno, N. Degenaar, and Wijnands R. Altamirano, D., and F. Lewis. *ATEL*, 2827, 2010.

D. M. Russell, F. Lewis, P. Roche, and D. Altamirano. *ATEL*, 3359, 2011a.

D. M. Russell, J. C. A. Miller-Jones, T. J. Maccarone, Y. J. Yang, R. P. Fender, and F. Lewis. *ApJ*, 739:L19, 2011b.

D. M. Russell, S. Markoff, P. Casella, A. G. Cantrell, R. Chatterjee, R. P. Fender, E. Gallo, P. Gandhi, J. Homan, D. Maitra, and O'Brien K. Miller-Jones, J. C. A., and T. Shahbaz. *MNRAS*, 429:815, 2012.

D. M. Russell, T. D. Russell, J. C. A. Miller-Jones, K. O'Brien, R. Soria, G. R. Sivakoff, T. Slaven-Blair, F. Lewis, S. Markoff, J. Homan, D. Altamirano, P. A. Curran, M. P. Rupen, T. M. Belloni, M. Cadolle Bel, P. Casella, S. Corbel, V. Dhawan, R. P. Fender, E. Gallo, P. Gandhi, S. Heinz, E. G. Körding, H. A. Krimm, D. Maitra, S. Migliari, R. A. Remillard, C. L. Sarazin, T. Shahbaz, and V. Tudose. *ApJ*, 768:L35, 2013.

T. D. Russell, R. Soria, J. C. A. Miller-Jones, P. A. Curran, S. Markoff, D. M. Russell, and G. R. Sivakoff. *MNRAS*, 439:1390, 2014a.

T. D. Russell, R. Soria, C. Motch, M. W. Pakull, M. A. P. Torres, P. A. Curran, P. G. Jonker, and J. C. A. Miller-Jones. *MNRAS*, 439:1381, 2014b.

G.B. Rybicki and A.P. Lightman. *Radiative Processes in Astrophysics*. Wiley-VCH, Berlin, 1985.

K. Saito, K. Yamaoka, M. Fukuyama, T. G. Miyakawa, A. Yoshida, and J. Homan. Proceedings of the vi microquasar workshop: Microquasars and beyond. page 93.1, Como, Italy, September 2006.

G. Sala, J. Greiner, M. Ajello, E. Bottacini, and F. Haberl. *A&A*, 473:561, 2007.

G. Sala, J. Greiner, M. Ajello, and N. Primak. *A&A*, 489:1239, 2008.

N. N. Samus, M. Hazen, D. Williams, B. Welther, G. V. Williams, and D. Hoffleit. *IAU Circ.*, 7277, 1999.

C. Sanchez-Fernandez, C. Zurita, J. Casares, T. Shahbaz, and A. Castro-Tirado. *IAU Circ.*, 7506, 2000.

C. Sanchez-Fernandez, E. Kuulkers, A. J. Bird, C. Ferrigno, G. Belanger, A. Bazzano, M. Del Santo, L. Natalucci, P. Ubertini, P. R. den Hartog, D. Gotz, L. Prat, J.-C. Leyder, A. Lohfink, T. Oosterbroek, S. Piraino, K. Pottschmidt, and K. Watanebe. *ATEL*, 2194, 2009.

D. Sanwal, E. L. Robinson, E. Zhang, C. Colome, P. M. Harvey, T. F. Ramseyer, C. Hellier, and J.H. Wood. *ApJ*, 460:437, 1996.

R. Sato, M. Serino, S. Nakahira, S. Ueno, H. Tomida, M. Ishikawa, T. Mihara, M. Sugizaki, T. Yamamoto, M. Matsuoka, N. Kawai, M. Morii, R. Usui, A. Yoshida, H. Tsunemi, M. Kimura, H. Negoro, M. Nakajima, M. Asada, H. Sakakibara, Y. Ueda, K. Hiroi, M. Shidatsu, Y. Yamauchi, Tsuboi M., Y. Nishimura, T. Hanayama, and K. Yamaoka. *ATEL*, 4024, 2012.

B. Sbarufatti, J. A. Kennea, M. C. Stroh, D. N. Burrows, P. A. Evans, A. P. Beardmore, H. A. Krimm, and N. Gehrels. *ATEL*, 4782, 2013.

F. D. Seward, C. G. Page, M. J. L. Turner, and K. A. Pounds. *MNRAS*, 175:39, 1986.

F.D. Seward. *Allen's Astrophysical Quantities*. Springer-Verlag, New York, 4 edition, 2000.

V. Sguera, E. J. Barlow, A. J. Bird, D. J. Clark, A. J. Dean, A. B. Hill, L. Moran, S. E. Shaw, D. R. Willis, A. Bazzano, P. Ubertini, and A. Malizia. *A&A*, 444:221, 2005.

V. Sguera, A. Bazzano, A. J. Bird, A. J. Dean, P. Ubertini, E. J. Barlow, L. Bassani, D. J. Clark, A. B. Hill, A. Malizia, M. Molina, and J. B. Stephen. *ApJ*, 646:452, 2006.

V. Sguera, A. Bazzano, A. J. Bird, A. B. Hill, A. J. Dean, L. Bassani, A. Malizia, and P. Ubertini. *A&A*, 468:L21, 2007.

V. Sguera, S. P. Drave, A. J. Bird, A. Bazzano, R. Landi, and P. Ubertini. *MNRAS*, 417:573, 2011.

T. Shahbaz, T. Naylor, and P. A. Charles. *MNRAS*, 268:756, 1994a.

T. Shahbaz, F. A. Ringwald, J. C. Bunn, T. Naylor, P. A. Charles, and J. Casares. *MNRAS*, 271:L10, 1994b.

T. Shahbaz, A. P. Smale, T. Naylor, P. A. Charles, J. van Paradijs, B. J. M. Hassall, and P. Callanan. *MNRAS*, 282:1437, 1996a.

T. Shahbaz, F. van der Hooft, P. A. Charles, J. Casares, and J. van Paradijs. *MNRAS*, 282:L47, 1996b.

T. Shahbaz, P.A. Charles, and A.R. King. *MNRAS*, 301:382, 1998.

T. Shahbaz, F. van der Hooft, J. Casares, P. A. Charles, and J. van Paradijs. *MNRAS*, 306:89, 1999.

T. Shahbaz, R. Fender, and P.A. Charles. *A&A*, 376:L17, 2001.

T. Shahbaz, D. M. Russell, C. Zurita, J. Casares, J. M. Corral-Santana, V. S. Dhillon, and T. R. Marsh. *MNRAS*, 434:2696, 2013.

N.I. Shakura and R.A. Sunyaev. Proceedings of iau symposium 55. page 155, Madrid, 1972.

S.L. Shapiro, A.P. Lightman, and D.M. Eardley. *ApJ*, 445:780, 1976.

N. Shaposhnikov. *ATEL*, 2391, 2010.

N. Shaposhnikov and L. Titarchuk. *ApJ*, 699:453, 2009.

N. Shaposhnikov, J. Swank, C. R. Shrader, M. Rupen, V. Beckmann, C. B. Markwardt, and D. A. Smith. *ApJ*, 655:434, 2007.

N. Shaposhnikov, C. B. Markwardt, and J. H. Swank. *ATEL*, 2269, 2009.

N. Shaposhnikov, C. Markwardt, J. Swank, and H. Krimm. *ApJ*, 723:1817, 2010.

N. Shaposhnikov, J.H. Swank, C. Markwardt, and H. Krimm. The first year of maxi: Monitoring variable x-ray sources - 4th international maxi workshop. page 51, 2012.

A. W. Shaw, P. A. Charles, A. J. Bird, R. Cornelisse, J. Casares, F. Lewis, T. Muñoz-Darias, D. M. Russell, and C. Zurita. *MNRAS*, 433:740, 2013.

S. Shaw, E. Kuulkers, C. B. Markwardt, and R. Galis. *ATEL*, 1711, 2008.

M. Shidatsu, H. Negoro, S. Nakahira, T. Mihara, S. Ueno, H. Tomida, M. Ishikawa, M. Sugizaki, M. Serino, T. Yamamoto, J. Sugimoto, M. Matsuoka, N. Kawai, M. Morii, R. Usui, K. Ishikawa, A. Yoshida, H. Tsunemi, M. Kimura, M. Nakajima, M. Asada, H. Sakakibara, N. Serita, Y. Ueda, K. Hiroi, R. Sato, T. Kawamuro, Y. Tsuboi, M. Higa, M. Yamauchi, Y. Nishimura, T. Hanayama, K. Yoshidome, and K. Yamaoka. *ATEL*, 4419, 2012.

M. Shidatsu, Y. Ueda, S. Nakahira, C. Done, K. Morihana, M. Sugizaki, T. Mihara, T. Hori, H. Negoro, N. Kawai, K. Yamaoka, K. Ebisawa, M. Matsuoka, M. Serino, T. Yoshikawa, T. Nagayama, and N. Matsunaga. *ApJ*, 779:26, 2013.

C. R. Shrader, R.M. Wagner, R. M. Hjellming, X. H. Han, and S. G. Starrfield. *ApJ*, 434:698, 1994.

C. R. Shrader, R. M. Wagner, P. A. Charles, E. T. Harlaftis, and T. Naylor. *ApJ*, 487:858, 1997.

L. Sidoli, S. Mereghetti, G. L. Israel, L. Chiappetti, A. Treves, and M. Orlandini. *ApJ*, 525:215, 1999.

L. Sidoli, A. Paizis, S. Mereghetti, D. Gotz, and M. Del Santo. *MNRAS*, 415:2373, 2011.

V. Simon, C. Bartolini, A. Piccioni, and A. Guarenieri. *MNRAS*, 369:355, 2006.

K.P. Singh, K.M.V. Apparao, and R.P. Kraft. *ApJ*, 421:753, 1994.

G.R. Sivakoff, J.C.A. Miller-Jones, and H.A. Krimm. *ATEL*, 3147, 2011.

G. K. Skinner, A. P. Willmore, C. J. Eyles, D. Bertram, and M. J. Church. *Nature*, 330:544, 1987.

G. K. Skinner, A. J. Foster, A. P. Willmore, and C. J. Eyles. *MNRAS*, 243:72, 1990.

G. K. Skinner, H. C. Pan, M. Maisack, R. Staubert, K. N. Borozdin, A. C. Brinkman, J. Englhauser, M. R. Gilfanov, A. C. Kaniovsky, W. Pietsch, R. A. Sunyaev, and J. J. M. in 't Zand. *A&A*, 252:172, 1991.

A.P. Smale and P.T. Boyd. *ApJ*, 756:146, 2012.

D. Smith, R. Remillard, J. Swank, T. Takeshima, and E. Smith. *IAU Circ.*, 6855, 1998a.

D. A. Smith. *IAU Circ.*, 7008, 1998.

D. A. Smith, A. Levine, and A. Wood. *IAU Circ.*, 6932, 1998b.

D. A. Smith, A. Levine, and E.H. Morgan. *IAU Circ.*, 7523, 1999a.

D. A. Smith, A. Levine, and E.H. Morgan. *ATEL*, 143, 1999b.

D. M. Smith, M. Leventhal, R. Cavallo, N. Gehrels, J. Tueller, and G. Fishman. *ApJ*, 458:576, 1996.

D. M. Smith, W. A. Heindl, C. B. Markwardt, and J. H. Swank. *ApJ*, 554:41, 2001.

D. M. Smith, W. A. Heindl, and J. H. Swank. *ApJ*, 578:L129, 2002a.

D. M. Smith, W. A. Heindl, and J. H. Swank. *ApJ*, 569:362, 2002b.

D.M. Smith, W.A. Heindl, J. Swank, M. Leventhal, I.F. Mirabel, and L.F. Rodriguez. *ApJ*, 489:L51, 1997.

G.J. Sobczak, J.E. McClintock, R.A. Remillard, C.D. Bailyn, and J.A. Orosz. *ApJ*, 520:776, 1999.

G.J. Sobczak, J.E. McClintock, R.A. Remillard, W. Cui, A.M. Levine, E.H. Morgan, J.A. Orosz, and C.D. Bailyn. *ApJ*, 544:993, 2000.

S. Soldi, R. Walter, D. Eckert, S. Balman, A. Bazzano, V. Beckmann, and Boggs S. Belloni, T., F. Capitanio, J. Chenevez, M. Del Santo, R. Diehl, I. Donnarumma, P. Goldoni, D. Gotz, J.-C. Leyder, S. Mereghetti, A. Paizis, K. Pottschmidt, L. Sidoli, A. Tarana, J. Tueller, K. Watanabe, and G. Weidenspointner. *ATEL*, 885, 2006.

P. Soleri, T. Muñoz-Darias, S. Motta, T. Belloni, P. Casella, M. Méndez, D. Altamirano, M. Linares, R. Wijnands, R. Fender, and M. van der Klis. *MNRAS*, 429: 1244, 2012.

R.K. Sood and D. Cambell-Wilson. *IAU Circ.*, 6006, 1994.

R. Soria, M.S. Bessell, and P. Wood. *IAU Circ.*, 6732, 1997.

H. Spruit. *Accretion Processes in Astrophysics*. Cambridge University Press, 2014.

K. Sriram, A. R. Rao, and C. S. Choi. *A&A*, 541:6, 2013a.

K. Sriram, A. R. Rao, and C. S. Choi. *A&A*, 775:28, 2013b.

R. Starling, P. Evans, and R. Wijnands. *ATEL*, 1704, 2008.

D. Steeghs, J.M. Miller, D. Kaplan, and M. Rupen. *ATEL*, 146, 2003.

D. Steeghs, M. A. P. Torres, P. G. Jonker, H. Chen, P. Green, J. Miller, and M. R. Garcia. *ATEL*, 494, 2005a.

D. Steeghs, M. A. P. Torres, W. Pych, and I. Thompson. *ATEL*, 585, 2005b.

J.F. Steiner, J.E. McClintock, J.A. Orosz, M.M. Buxton, C.D. Bailyn, R.A. Remillard, and E. Kara. *ApJ*, 783:101, 2014.

J. B. Stephen, L. Bassani, M. Molina, A. Malizia, A. Bazzano, P. Ubertini, A. J. Dean, A. J. Bird, F. Lebrun, R. Much, and R. Walter. *A&A*, 432:L49, 2005.

H. Stiele, T. Munoz-Darias, S. Motta, and T. Belloni. *arXiv:1103.4312*, 2011.

H. Stiele, T. Munoz-Darias, S. Motta, and T. M. Belloni. *MNRAS*, 422:679, 2012.

M. Still, N. Hehrels, D. Steeghs, M.A.P. Torres, O. Godet, and C. Brocksopp. *ATEL*, 588, 2005a.

M. Still, P. Roming, C. Brocksopp, and C.B. Markwardt. *ATEL*, 553, 2005b.

A. M. Stirling, R. E. Spencer, C. J. de la Force, M. A. Garrett, R. P. Fender, and R. N. Ogley. *MNRAS*, 327:1273, 2001.

T. E. Strohmayer and E. A. Smith. *ATEL*, 3618, 2011.

R. Stubbings. *IAU Circ.*, 7523, 1999.

R. Stubbings and A. Pearce. *IAU Circ.*, 7253, 1999.

S. J. Sturner and C. R. Shrader. *ApJ*, 625:923, 2005.

R. Sunyaev and M. Revnivtsev. *A&A*, 358:617, 2000.

R. Sunyaev, E. Churazov, M. Gilfanov, M. Pavlinsky, S. Grebenev, G. Babalyan, I. Dekhanov, N. Khavenson, L. Bouchet, P. Mandrou, J. P. Roques, G. Vedrenne, B. Cordier, A. Goldwurm, F. Lebrun, and J. Paul. *ApJ*, 383:L49, 1991a.

R. Sunyaev, E. Churazov, M. Gilfanov, M. Pavlinsky, S. Grebenev, G. Babalyan, I. Dekhanov, N. Yamburenko, L. Bouchet, M. Niel, J. P. Roques, P. Mandrou, A. Goldwurm, B. Cordier, Ph. Laurent, and J. Paul. *ApJ*, 247:L29, 1991b.

R. Sunyaev, M. Gilfanov, E. Churazov, M. Pavlinsky, G. Babalyan, I. Dekhanov, A. Kuznetsov, S. Grebenev, S. Yunin, N. Yaburenko, B. Cordier, F. Lebrun, P. Laurent, J. Ballet, P. Mandrou, J. P. Roques, and G. Vedrenne. *SvAL*, 17: 50, 1991c.

R. Sunyaev, E. Churazov, M. Gilfanov, A. Dyachkov, N. Khavenson, S. Grebenev, R. Kremnev, K. Sukhanov, A. Goldwurm, J. Ballet, B. Cordier, J. Paul, M. Denis, G. Vedrenne, M. Niel, and E. Jourdain. *ApJ*, 389:L75, 1992.

R. Sunyaev, E. Churazov, M. Revnivtsev, S. Trudolyubov, M. Vargas, J. Paul, J.-P. Roques, E. Jourdain, and GRANAT/SIGMA Team. *IAU Circ.*, 6599, 1997.

R. A. Sunyaev and J. Truemper. *Nature*, 279:506, 1979.

R. A. Sunyaev, K. N. Borozdin, N. L. Aleksandrovich, V. A. Arefev, A. S. Kaniovskii, V. V. Efremov, M. Maisack, C. Reppin, and J. K. Skinner. *AstL*, 20:777, 1994.

F. Suwa, H. Negoro, S. Nakahira, M. Serino, T. Mihara, N. Kawai, S. Ueno, H. Tomida, M. Ishikawa, M. Sugizaki, T. Yamamoto, M. Matsuoka, M. Morii, R. Usui, A. Yoshida, H. Tsunemi, M. Kimura, M. Nakajima, M. Asada, H. Sakakibara, N. Serita, Y. Ueda, K. Hiroi, M. Shidatsu, R. Sato, Y. Tsuboi, M. Yamauchi, Higa M., Y. Nishimura, T. Hanayama, and K. Yamaoka. *ATEL*, 4035, 2012.

J. Swank. Proceedings of the symposium the active x-ray sky: Results from bepposax and rossi-xte. In L. Scarsi, H. Bradt, P. Giommi, and F. Fiore, editors, *Nuclear Physics B Proceedings Supplements*, Rome, Italy, October 1997. astro–ph/9802188.

J. Swank. *ATEL*, 295, 2004.

J. Swank and C. Markwardt. Asp conference proceedings: New century of x-ray astronomy. volume 251, page 94, San Francisco, 2001.

J. Swank and C. Markwardt. *ATEL*, 390, 2005.

J. Swank, E. Smith, and C. Markwardt. *IAU Circ.*, 7792, 2002.

Y. Tachibana, T. Takagi, M. Serino, M. Morii, S. Nakahira, H. Negoro, S. Ueno, H. Tomida, M. Kimura, M. Ishikawa, Y. E. Nakagawa, T. Mihara, M. Sugizaki, J. Sugimoto, A. Yoshikawa, M. Matsuoka, N. Kawai, R. Usui, T. Yoshii, A. Yoshida, T. Sakamoto, Y. Nakano, Y. Kawakubo, H. Ohtsuki, H. Tsunemi, M. Sasaki, M. Nakajima, K. Fukushima, T. Onodera, K. Suzuki, Y. Ueda, M. Shidatsu, T. Kawamuro, T. Hori, Y. Tsuboi, M. Higa, M. Yamauchi, K. Yoshidome, Y. Ogawa, H. Yamada, and K. Yamaoka. *ATEL*, 5803, 2014.

T. Takeshima, J. K. Cannizzo, R. Corbet, and F. E. Marshall. *IAU Circ.*, 6390, 1996.

Y. Tanaka and W.H.G. Lewin. *X-Ray Binaries*. Cambridge University Press, 1995.

Y. Tanaka and N. Shibazaki. *ARA&A*, 34:607, 1996.

H. Tananbaum, H. Gursky, E. Kellogg, and R. Giacconi. *ApJ*, 177:L5, 1972.

T.M. Tauris and E.P.J. van den Heuval. *Compact Stellar X-Ray Sources*. Cambridge University Press, 2006.

M. Tavani, A. Fruchter, S. N. Zhang, B. A. Harmon, R. N. Hjellming, M. P. Rupen, C. Bailyn, and M. Livio. *ApJ*, 473:L103, 1996.

J.R. Thorstensen. *ApJ*, 312:739, 1987.

S. P. Tigelaar, R. P. Fender, R. P. J. Tilanus, E. Gallo, and G. G. Pooley. *MNRAS*, 352:1015, 2004.

S. J. Tingay, D. L. Jauncey, R. A. Preston, J. E. Reynolds, D. L. Meier, D. W. Murphy, A. K. Tzioumis, D. J. McKay, M. J. Kesteven, J. E. J. Lovell, D. Campbell-Wilson, S. P. Ellingsen, R. Gough, R. W. Hunstead, D. L. Jonos, P. M. McCulloch, V. Migenes, J. Quick, M. W. Sinclair, and D. Smits. *Nature*, 374:141, 1995.

L. Titarchuk. *ApJ*, 434:313, 1994.

L. Titarchuk and Y. Lyubarskij. *ApJ*, 450:876, 1995.

H. Tomida, H. Negoro, T. Mihara, M. Kohama, Y. E. Nakagawa, M. Sugizaki, T. Yamamoto, M. Matsuoka, K. Kawasaki, S. Ueno, M. Ishikawa, M. Suzuki, N. Kawai, M. Morii, K. Sugimori, A. Yoshida, K. Yamaoka, S. Nakahira, H. Tsunemi, M. Kimura, M. Nakajima, S. Miyoshi, H. Ozawa, R. Ishiwata, Y. Ueda, N. Isobe, S. Eguchi, K. Hiroi, and A. Daikyuji. *ATEL*, 2363, 2009.

J. A. Tomsick, E. Smith, J. Swank, R. Wijnands, and J. Homan. *IAU Circ.*, 7575, 2001a.

J. A. Tomsick, M. Del Santo, and T. Belloni. *ATEL*, 4393, 2012.

J.A. Tomsick. *ATEL*, 675, 2005.

J.A. Tomsick and P. Kaaret. *ApJ*, 537:448, 2000.

J.A. Tomsick, P. Kaaret, R.A. Kroeger, and R.A. Remillard. *ApJ*, 512:892, 1999.

J.A. Tomsick, S. Corbel, and P. Kaaret. *ApJ*, 563:229, 2001b.

J.A. Tomsick, S. Corbel, R. Fender, J.M. Miller, J.A. Orosz, T. Tzioumis, R. Wijnands, and P. Kaaret. *ApJ*, 582:933, 2003.

J.A. Tomsick, E. Kalemci, and P. Kaaret. *ApJ*, 601:439, 2004.

J.A. Tomsick, S. Corbel, A. Goldwurm, and P. Kaaret. *ApJ*, 630:413, 2005.

J.A. Tomsick, S. Chaty, J. Rodriguez, R. Walter, and P. Kaaret. *ATEL*, 959, 2006.

J.A. Tomsick, S. Chaty, J. Rodriguez, R. Walter, and P. Kaaret. *ApJ*, 701:811, 2009.

A. Toor and F. D. Seward. *AJ*, 79:995, 1974.

M. A. P. Torres, D. Steeghs, C. Blake, P. G. Jonker, M. R. Garcia, J. E. McClintock, J. Miller, P. Zhao, M. Calkins, P. Berlind, E. Falco, J. Bloom, P. Callanan, and P. Rodriguez-Gil. *ATEL*, 566, 2005.

M. A. P. Torres, D. Steeghs, P. G. Jonker, K. Luhman, J. E. McClintock, and M. R. Garcia. *ATEL*, 733, 2006.

M. A. P. Torres, D. Steeghs, P. G. Jonker, J. E. Greene, and K. N. Hainline. *ATEL*, 1720, 2008a.

M. A. P. Torres, D. Steeghs, J.A. Kennea, J. Homan, and J.M. Miller. *ATEL*, 1696, 2008b.

M. A. P. Torres, P. G. Jonker, D. Steeghs, H.-W. Chen, S. A. Shectman, and D. J. E. Floyd. *ATEL*, 1958, 2009a.

M. A. P. Torres, P. G. Jonker, D. Steeghs, H. Yan, J. Huang, and A. M. Soderberg. *ATEL*, 2263, 2009b.

M. A. P. Torres, D. Steeghs, P. G. Jonker, J.E. McClintock, N. Morrell, and M. Roth. *ATEL*, 2190, 2009c.

M. A. P. Torres, D. Steeghs, P. G. Jonker, I. Thompson, and A. M. Soderberg. *ATEL*, 2269, 2009d.

M. A. P. Torres, D. Steeghs, P. G. Jonker, and N. R. Ross. *ATEL*, 2870, 2010.

M. A. P. Torres, P. G. Jonker, D. Steeghs, and J.S. Mulchaey. *ATEL*, 3150, 2011.

A. Treves, T. Belloni, L. Chiappetti, L. Maraschi, L. Stella, E. G. Tanzi, and M. van der Klis. *ApJ*, 325:119, 1988.

V. Trimble, W.K. Rose, and J. Weber. *ApJ*, 162:1P, 1973.

S. Trudolyubov, E. Churazov, M. Gilfanov, M. Revnivtsev, R. Sunyaev, N. Khavenson, A. Dyachkov, I. Tserenin, M. Vargas, P. Goldoni, P. Laurent, J. Paul, E. Jourdain, J.-P. Roques, P. Mandrou, and G. Vedrenne. *A&A*, 342:496, 1997.

S. Trudolyubov, M. Gilfanov, E. Churazov, R. Sunyaev, N. Khavenson, A. Dyachkov, I. Tserenin, K. Sukhanov, P. Laurent, J. Ballet, J. Goldoni, P. an Paul, J.-P. Roques, V. Borrel, L. Bouchet, and E. Jourdain. *A&A*, 334:895, 1998.

S. Trudolyubov, E. Churazov, M. Gilfanov, M. Revnivtsev, R. Sunyaev, N. Khavenson, A. Dyachkov, I. Tserenin, M. Vargas, P. Goldoni, P. Laurent, J. Paul, E. Jourdain, J.-P. Roques, P. Mandrou, and G. Vedrenne. *A&A*, 342:496, 1999.

S.P. Trudolyubov, K.N. Borozdin, and W.C. Priedhorsky. *MNRAS*, 322:309, 2001.

S. A. Trushkin, N. A. Nizhelskij, and G. V. Zhekanis. *ATEL*, 3656, 2011.

H. Tsunemi, S. Kitamoto, S. Okamura, and D. Roussel-Dupre. *ApJ*, 337:L81, 1989.

M. Turler, M. Cadolle Bel, R. Diehl, N.-J. Westergaard, B. McBreen, O. R. Williams, S. A. Grebenev, and A. Lutovinov. *ATEL*, 624, 2005a.

M. Turler, S. Paltani, and N. Mowlavi. *ATEL*, 631, 2005b.

M. Turler, C. Kuulkers, E. Ferrigno, J. Alfonso-Garzon, V. Beckmann, T. Bird, S. Brandt, L. Chenevez, T. Courvoisier, A. Domingo, K. Ebisawa, P. Jonker, P. Kretschmar, C. Markwardt, T. Oosterbroek, A. Paizis, C. Sanchez-Fernandez, and R. Wijnands. *ATEL*, 2825, 2010.

P. Ubertini, A. Bazzano, C. La Padula, R.K. manchanda, and V.F. Polcaro. *ApJ*, 383:262, 1991a.

P. Ubertini, A. Bazzano, F. Perotti, E. Quadrini, and Dean A.J. Court, A., N. Dipper, R. Lewis, and and Stephen J.B. Bassani, L. *ApJ*, 366:544, 1991b.

Y. Ueda, T. Dotani, S. Uno, H. Inoue, and Maeda Y. Nagase, F., M. Sakano, and and Swank J. H. Durouchoux, P. *IAU Circ.*, 6627, 1997.

M. Uemura, T. Kato, and Yamaoka H. and Takamizawa K. Matsumoto, K., Y. Sano, K. Haseda, L.M. Cook, D. Buczynski, and G. Masi. *PASJ*, 52:L15, 2000a.

M. Uemura, T. Kato, and Buczynski D. Yamaoka, H., K. Takamizawa, O. Trondal, G. G. Pooley, E. M. Waldram, and and McCollough M. L. Wilson, C. A. *IAU Circ.*, 7390, 2000b.

M. Uemura, T. Kato, R. Ishioka, K. Tanabe, and Santallo R. Torii, K., B. Monard, C.B. Markwardt, J.H. Swank, and Macquart J. Sault, R.J., and Kiyota S. and Stubbings R. and Nelson P. Linnolt, M., and Bailyn C. Richards, T., D. West, G. Masi, A. Miyashita, and and Scarmato T. Sano, Y. *PASJ*, 56:61, 2004.

R. Usui, and Tomida H. Nakahira, S., H. Negoro, M. Morii, and Ishikawa K. and Ueno S. and Ishikawa M. and Mihara T. Kawai, N., M. Sugizaki, M. Serino, T. Yamamoto, M. Matsuoka, A. Yoshida, H. Tsunemi, M. Kimura, and Asada M. Nakajima, M., and Serita N. Sakakibara, H., Y. Ueda, K. Hiroi, M. Shidatsu, R. Sato, Y. Tsuboi, M. Yamauchi, Higa M., Y. Nishimura, T. Hanayama, and and Yamaoka K. Yoshidome, K. *ATEL*, 4140, 2012.

F. van der Hooft, C. Kouveliotou, J. van Paradijs, B. C. Rubin, D. J. Crary, M. H. Finger, B. A. Harmon, M. van der Klis, W. H. G. Lewin, J. P. Norris, and G. J. Fishman. *ApJ*, 458:L75, 1996.

F. van der Hooft, C. Kouveliotou, J. van Paradijs, W. S. Paciesas, and van der Klis M. Lewin, W. H. G., D. J. Crary, M. H. Finger, B. A. Harmon, and S. N. Zhang. *ApJ*, 519:332, 1999a.

F. van der Hooft, C. Kouveliotou, J. van Paradijs, W. S. Paciesas, W. H. G. Lewin, M. van der Klis, D. J. Crary, M. H. Finger, B. A. Harmon, and S. N. Zhang. *ApJ*, 513:477, 1999b.

A. J. van der Horst, J. Granot, Z. Paragi, C. Kouveliotou, R. A. M. J. Wijers, and E. Ramirez-Ruiz. *ATEL*, 2874, 2010.

M. van der Klis. *Compact Stellar X-Ray Sources*. Cambridge University Press, 2006.

F. van Leeuwen. *A&A*, 474:653, 2007.

J. van Paradijs. *ApJ*, 464:L139, 1996.

J. van Paradijs and J.E. McClintock. *X-Ray Binaries*. Cambridge University Press, 1995.

J. van Paradijs and F. Verbunt. Aip conference proceedings. volume 115, pages 49–62, 1984.

M. Vargas, A. Goldwurm, J. Paul, M. Denis, V. Borrel, L. Bouchet, J. P. Roques, E. Jourdain, S. Trudolyubov, M. Gilfanov, E. Churazov, R. Sunyaev, N. Khavenson, B. Dyachkov, and I. Chulkov. *A&A*, 313:828, 1996.

M. Vargas, A. Goldwurm, P. Laurent, J. Paul, E. Jourdain, J.-P. Roques, V. Borrel, L. Bouchet, R. Sunyaev, E. Churazov, M. Gilfanov, B. Novikov, A. Dyachkov, N. Khavenson, K. Sukhanov, and N. Kuleshova. *A&A*, 476:23, 1997.

L. Vasiliev, S. Trudolyubov, and M. Revnivtsev. *A&A*, 362:L53, 2000.

R. C. Vermeulen, V. Icke, R. T. Schilizzi, I. Fejes, and R. E. Spencer. *Nature*, 328: 309, 1987.

R. C. Vermeulen, R. T. Schilizzi, R. E. Spencer, J.D. Romney, and I. Feyes. *A&A*, 270:177, 1993.

D. A. Verner, G. J. Ferland, K. T. Korista, and D. G. Yakovlev. *ApJ*, 465:487, 1996.

A. Vikhlinin, E. Churazov, M. Gilfanov, R. Sunyaev, A. Dyachkov, N. Khavenson, R. Kremnev, K. Sukhanov, J. Ballet, P. Laurent, L. Salotti, A. Claret, J. F. Olive, M. Denis, P. Mandrou, and J. P. Roques. *ApJ*, 424:395, 1994.

W. Voges, B. Aschenbach, Th. Boller, H. Bräuninger, U. Briel, W. Burkert, K. Dennerl, J. Englhauser, R. Gruber, F. Haberl, G. Hartner, G. Hasinger, M. Kürster, E. Pfeffermann, W. Pietsch, P. Predehl, C. Rosso, J. H. M. M. Schmitt, J. Trümper, and H. U. Zimmermann. *A&A*, 349:389, 1999.

I. Vovk, C. Ferrigno, E. Drave, Bozzo S. P., C. Sanchez, E. Kuulkers, A. Bazzano, M. Del Santo, M. Fiocchi, L. Natalucci, A. Tarana, I. Caballero, D. Goetz, J. Chenevez, P. den Hartog, L. Kuiper, and K. Watanabe. *ATEL*, 4381, 2012.

S. Wachter and A.P. Smale. *ApJ*, 496:L21, 1998.

R.A. Wade and K. Horne. *ApJ*, 424:411, 1998.

R. M. Wagner, S. G. Starrfield, A. Cassatella, G. M. Hurst, M. Mobberley, and B. G. Marsden. *IAU Circ.*, 4783, 1989.

R. M. Wagner, T. J. Kreidl, S. B. Howell, and S. G. Starrfield. *ApJ*, 401:L97, 1992.

R.M. Wagner, C. B. Foltz, T. Shahbaz, J. Casares, P. A. Charles, S. G. Starrfield, and P. Hewett. *ApJ*, 556:42, 2001.

R. Walter, A. Bodaghee, E. J. Barlow, A. J. Bird, A. Dean, A. B. Hill, S. Shaw, A. Bazzano, P. Ubertini, L. Bassani, A. Malizia, J. B. Stephen, G. Belanger, F. Lebrun, and R. Terrier. *ATEL*, 229, 2004.

R. Walter, P. Lubinski, S. Paltani, N. Produit, J. Zurita, E. Kuulkers, V. Beckmann, N. Gehrels, A. Blecha, F. Carrier, and M. Cherix. *A&A*, 461:L17, 2007.

M. G. Watson, G. C. Stewart, A. R. King, and W. Brinkmann. *MNRAS*, 222:261, 1986.

M.G. Watson, M.J. Ricketts, and R.E. Griffiths. *ApJ*, 221:L69, 1978.

N. A. Webb, T. Naylor, Z. Ioannou, P. A. Charles, and T. Shahbaz. *MNRAS*, 317: 528, 2000.

N. E. White and J. van Paradijs. *ApJ*, 473:L25, 1996.

N.E. White and F.E. Marshall. *ApJ*, 281:354, 1984.

N.E. White and J.H. Swank. *ApJ*, 253:61, 1982.

N.E. White, A.N. Parmar, M. Sztajno, H.U. Zimmermann, K.O. Mason, and S.M. Kahn. *ApJ*, 283:L9, 1984.

N.E. White, L. Stella, and A.N. Parmar. *ApJ*, 324:363, 1988.

N.E. White, F. Nagase, and A.N. Parmar. *X-Ray Binaries*. Cambridge University Press, 1995.

N.E. White, Y. Ueda, T. Dotani, and F. Nagase. *IAU Circ.*, 6927, 1998.

R. Wijnands and J.M. Miller. *ApJ*, 564:974, 2002.

R. Wijnands and M. van der Klis. *ApJ*, 528:L93, 1999.

R. Wijnands and M. van der Klis. *ApJ*, 528:L93, 2000.

R. Wijnands, J.M. Miller, and W.H.G. Lewin. *IAU Circ.*, 7715, 2001.

R. Wijnands, J.M. Miller, and M. van der Klis. *MNRAS*, 331:60, 2002.

R. Wijnands, J. J. M. in't Zand, M. Rupen, T. Maccarone, J. Homan, R. Cornelisse, R. Fender, J. Grindlay, M. van der Klis, E. Kuulkers, C. B. Markwardt, J. C. A. Miller-Jones, and Q. D. Wang. *MNRAS*, 449:1117, 2006.

R. Wijnands, M. Linares, N. Degenaar, and C.B. Markwardt. *ATEL*, 1700, 2008.

J. Wilms, M.A. Nowak, J.B. Dove, R.P. Fender, and T. Di Matteo. *ApJ*, 522:460, 1999.

J. Wilms, A. Allen, and R. McCray. *ApJ*, 542:914, 2000.

J. Wilms, M. A. Nowak, K. Pottschmidt, W. A. Heindl, J. B. Dove, and M. C. Begelman. *MNRAS*, 320:327, 2001.

J. Wilms, M. A. Nowak, K. Pottschmidt, G. G. Pooley, and S. Fritz. *A&A*, 447:245, 2006.

J. Wilms, K. Pottschmidt, G.G. Pooley, S. Markoff, M.A. Nowak, I. Kreykenbohm, and R.E. Rothschild. *ApJ*, 663:L97, 2007.

C.K. Wilson and R.E. Rothschild. *ApJ*, 274:717, 1983.

C. Wilson-Hodge, M. L. Cherry, G. L. Case, W. Baumgartner, E. Beklen, P. N. Bhat, M. S. Briggs, A. Camero-Arranz, V. Chaplin, V. Connaughton, M. H. Finger, N. Gehrels, J. Greiner, K. Jahoda, P. Jenke, R. M. Kippen, C. Kouveliotou, H. A. Krimm, E. Kuulkers, N. Lund, C. A. Meegan, L. Natalucci, W. S. Paciesas, R. Preece, J. C. Rodi, N. Shaposhnikov, G. K. Skinner, D. Swartz, A. von Kienlin, R. Diehl, and X. L. Zhang. Proceedings of the 8th integral workshop - the restless gamma-ray universe. Dublin, Ireland, September 2010.

C. Winkler, T. J.-L. Courvoisier, G. Di Cocco, N. Gehrels, A. Gimenez, S. Grebenev, W. Hermsen, J. M. Mas-Hesse, F. Lebrun, N. Lund, G. G. C. Palumbo, J. Paul, J.-P. Roques, H. Schnopper, V. Schönfelder, R. Sunyaev, B. Teegarden, P. Ubertini, G. Vedrenne, and A. J. Dean. *A&A*, 411:L1, 2003.

A. Wood, D. A. Smith, F. E. Marshall, and J. Swank. *IAU Circ.*, 7274, 1999.

P. M. Woods, C. Kouveliotou, M. H. Finger, E. Gogus, J. Swank, C. Markwardt, and T. Strohmayer. *IAU Circ.*, 7856, 2002.

J. Wren and T. McKay. *IAU Circ.*, 7394, 2000.

Y. X. Wu, W. Yu, T. P. Li, T. J. Maccarone, and X. D. Li. *ApJ*, 718:620, 2010.

K. Yamaoka and S. Nakahira. *ATEL*, 2785, 2010.

K. Yamaoka, J. Homan, and M. Uemura. *ATEL*, 1796, 2008.

K. Yamaoka, S. Nakahira, and J.A. Tomsick. *ATEL*, 2892, 2010a.

K. Yamaoka, S. Nakahira, J.A. Tomsick, and S.A. Trushkin. *ATEL*, 2832, 2010b.

K. Yamaoka, R. Allured, P. Kaaret, J. Kennea, T. Kawaguchi, P. Gandhi, N. Shaposhnikov, Y. Ueda, S. Nakahira, T. Kotani, H. Negoro, I. Takahashi, A. Yoshida, N. Kawai, and S. Sugita. *PASJ*, 64:32, 2012.

S. Yamauchi and K. Koyama. *PASJ*, 42:L83, 1990.

S. Yamauchi and E. Nakamura. *PASJ*, 56:803, 2004.

J. Yang, Z. Paragi, S. Corbel, L. I. Gurvits, R. M. Campbell, and C. Brocksopp. *MNRAS*, 418:L25, 2011.

Y.J. Yang, C. Brocksopp, S. Corbel, Z. Paragi, T. Tzioumis, and R.P. Fender. *MNRAS*, 409:L64, 2010a.

Y.J. Yang, A. Patruno, N. Degenaar, D.M. Russell, D. Altamirano, and R. Wijnands. *ATEL*, 2824, 2010b.

Y. Yao, Q.D. Wang, and S.N. Zhang. *MNRAS*, 362:229, 2005.

T. Yaqoob, K. Ebisawa, and K. Mitsuda. *MNRAS*, 264:411, 1993.

I. Yi. Astrophysical discs - an ec summer school, astronomical society of the pacific, conference series. volume 160, page 279, 1999.

W. Yuan. *MNRAS*, 324:119, 2001.

W. Yuan, N. Kawai, W. Brinkmann, and M. Matsuoka. *A&A*, 297:451, 1995.

A.A. Zdziarski, J. Poutanen, J. Mikolajewska, M. Gierlinski, K. Ebisawa, and W.N. Johnson. *MNRAS*, 301:435, 1998.

A.A. Zdziarski, J. Poutanen, W.S. Paciesas, and L. Wen. *ApJ*, 578:357, 2002.

A.A. Zdziarski, M. Gierlinski, J. Mikolajewska, G. Wardzinski, D.M. Smith, A.B. Harmon, and S. Kitamoto. *MNRAS*, 351:791, 2004.

S. N. Zhang, C. A. Wilson, B. A. Harmon, G. J. Fishman, R. B. Wilson, W. S. Paciesas, M. Scott, and B. C. Rubin. *IAU Circ.*, 6046, 1994.

S. N. Zhang, K. Ebisawa, R. Sunyaev, Y. Ueda, B. A. Harmon, S. Sazonov, G. J. Fishman, H. Inoue, W. S. Paciesas, and T. Takahashi. *ApJ*, 479:381, 1997.

J.N. Zhou, Q.Z. Liu, Y.P. Chen, J. Li, J.L. Qu, S. Zhang, H.Q. Gao, and Z. Zhang. *MNRAS*, 421:2285, 2013.

C. Zurita, C. Sánchez-Fernández, J. Casares, P. A. Charles, T. M. Abbott, P. Hakala, P. Rodríguez-Gil, S. Bernabei, A. Piccioni, A. Guarnieri, C. Bartolini, N. Masetti, T. Shahbaz, A. Castro-Tirado, and A. Henden. *MNRAS*, 334:999, 2002.

C. Zurita, D. Rodríguez, P. Rodríguez-Gil, J. Casares, T. Shahbaz, J. Acosta, G. Gómez-Velarde, C. Abajas, and T. Muñoz-Darias. *ATEL*, 383, 2005.

C. Zurita, M. A. P. Torres, D. Steeghs, P. Rodríguez-Gil, T. Muñoz-Darias, J. Casares, T. Shahbaz, I. G. Martínez-Pais, P. Zhao, M. R. Garcia, A. Piccioni, C. Bartolini, A. Guarnieri, J. S. Bloom, C. H. Blake, E. E. Falco, A. Szentgyorgyi, and M. Skrutskie. *ApJ*, 644:432, 2006.

C. Zurita, M. Durant, M. A. P. Torres, T. Shahbaz, J. Casares, and D. Steeghs. *ApJ*, 681:1458, 2008.

J. A. Zurita Heras, S. Chaty, M. Cadolle Bel, and L. Prat. *MNRAS*, 413:235, 2011.

T. Zwitter and M. Calvani. *MNRAS*, 236:581, 1989.

P.T. Zycki, C. Done, and D.A. Smith. *MNRAS*, 309:561, 1999.